ngineering Center
University of Wisconsin-Madison

The Technical Proceedings of

The Second International TOVS Study Conference

A REPORT from the

Cooperative Institute for Meteorological Satellite Studies

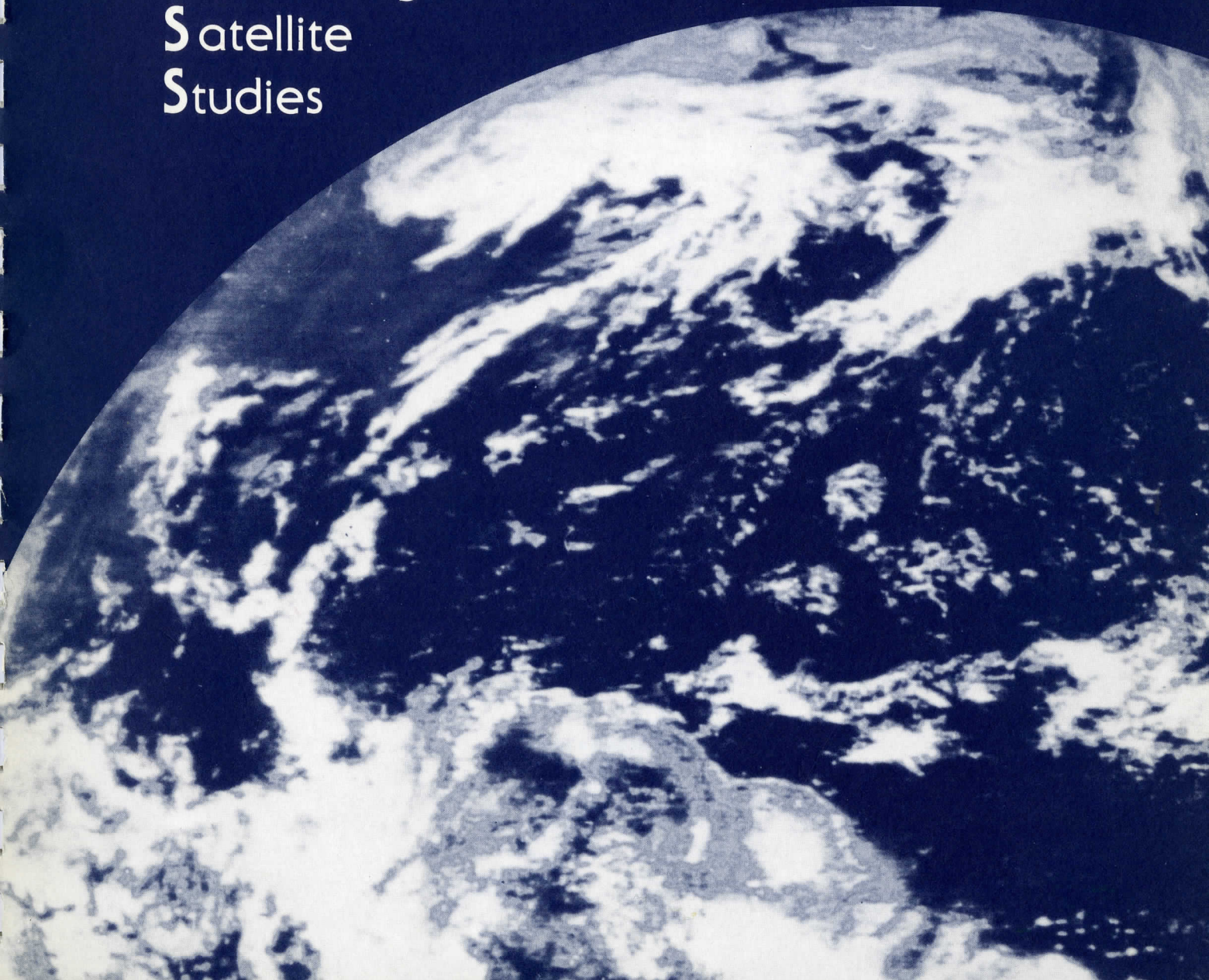

The Technical Proceedings of

The Second International TOVS Study Conference

Igls, Austria

February 18 - 22, 1985

Edited by

W. P. Menzel

Cooperative Institute for Meteorological Satellite Studies
Space Science and Engineering Center
University of Wisconsin
1225 West Dayton Street
Madison, Wisconsin 53706
(608)262-0544

September 1985

FORWARD

These Technical Proceedings detail the scientific presentations at the Second International TOVS Study Conference (ITSC-II) held in Igls, Austria, 18-22 February, 1985. A summary of the conference objectives, conclusions, and plans for future action is contained in a separate document titled A Report on ITSC-II available from the CIMSS, University of Wisconsin-Madison.

The Technical Proceedings contains the paper by Le Marshall which provides a statistical analysis of the soundings produced by various ITSC working group members using their retrieval algorithms on the TOVS data sets provided for an international comparison of results. New developments in the technique for calculating temperature and water vapor profiles from TOVS radiance data are also presented. In particular, a new "simultaneous" retrieval methodology is described in papers by Chedin, et al., Smith et al., and Svensson. With this methodology, temperature and water vapor profiles, surface and cloud temperatures, and the concentration of other optically active gases (i.e., ozone) are calculated directly and simultaneously from the complete set of TOVS radiances. Papers by Aoki, Hayden et al., Lloyd et al., and Taylor et al., detail procedures for using the 1 km resolution AVHRR data to improve the "cloud clearing" in TOVS profile retrievals. These two advances, simultaneous retrieval and the incorporation of AVHRR, represent important steps toward defining an optimal procedure for TOVS profile retrieval that can become a standard for international use. Several papers deal with the objective analysis of TOVS retrieval results, an important step in achieving improvement in numerical weather predictions. The Technical Proceedings also include papers on the development of a low cost microcomputer system for TOVS processing and NOAA's plan for future improvements in the satellite instrumentation and their operational processing procedures.

In summary, these technical proceedings describe the most recent advancements of the ITSC working group members in achieving its central objective of defining an optimal approach for TOVS profile retrieval. The results presented indicate that this objective has been nearly achieved. Technical work is now being focused on the "cloud clearing" problem with special emphasis on retrieving cloud parameters for their use in synoptic weather practice and the international cloud climatology program. The results of these efforts and those resulting from further refinements of TOVS temperature and water vapor profiling algorithms are to be presented at the Third International TOVS Study Conference to be held during August, 1986 at Madison, Wisconsin (USA).

William L. Smith, Chairman
Second International TOVS Study Conference

ACKNOWLEDGEMENTS

The publication of these proceedings has been possible through the financial support from the National Oceanic and Atmospheric Administration to the Cooperative Institute for Meteorological Satellite Studies in Madison, Wisconsin.

The careful retyping of several of the edited manuscripts was accomplished by Laura Beckett and the production was handed by Sue Pfefferkorn. We thank them for the quality work.

A special thank you goes to Dr. John LeMarshall of the Bureau of Meteorology Research Centre in Melbourne, Australia. His diligent efforts produced the quantitative intercomparison of the TOVS retrieved temperature and moisture fields that will help bring us closer to a universally accepted method of processing TOVS data.

TABLE OF CONTENTS

ADDITIONAL PAPERS RELEVANT TO ITSC-II

CHARACTERISTICS OF ERRORS IN RETRIEVED VERTICAL TEMPERATURE

Tadao Aoki

Meteorological Satellite Center
Nakakiyoto, Kiyose, Tokyo 204, Japan

1. INTRODUCTION

It is important to know the characteristics of errors in vertical temperature sounding for the future improvement of the data processing sytem. In this work we study the dependence of errors on the cloud amount and scan angle.

2. EFFECT OF CLOUD

The observed radiance I of a HIRS channel is written as

$$I = (1 - n)R + nI_c$$
$$= R + n(I_c - R), \qquad (1)$$

where R is the clear radiance, n the cloud amount and I_c the cloudy radiance. In MSC the method for the clear radiance retrieval is stochastic using the initial values for R and $Q = n(I_c - R)$, and the error statistics of the measured quantities I and initial guesses of R and Q. The cloud amount of a HIRS spot is known by counting the cloudy pixels of AVHRR contained within it and Q is estimated from AVHRR radiance data. The clear radiances of HIRS channels are determined from adjacent four spots of HIRS assuming the clear radiance is constant in the area of these four spots (Aoki, 1982a).

It is expected that for the better estimation of clear radiances the cloud amount in the four HIRS spots concerned are desired to be greatly different with each other. From this point of view, a quality index to the retrieved clear radiance has been defined as

$$\gamma = (1 - \bar{n})^2 + n_{max} - n_{min}, \qquad (2)$$

where $\bar{n}$ is the average cloud amount for four HIRS spots concerned, n_{max} the maximum cloud amount and n_{min} the minimum cloud amount. We call 'clear case' when $\gamma \geq \gamma_c$ and 'cloudy case' when $\gamma < \gamma_c$ ($\gamma_c = 0.4$).

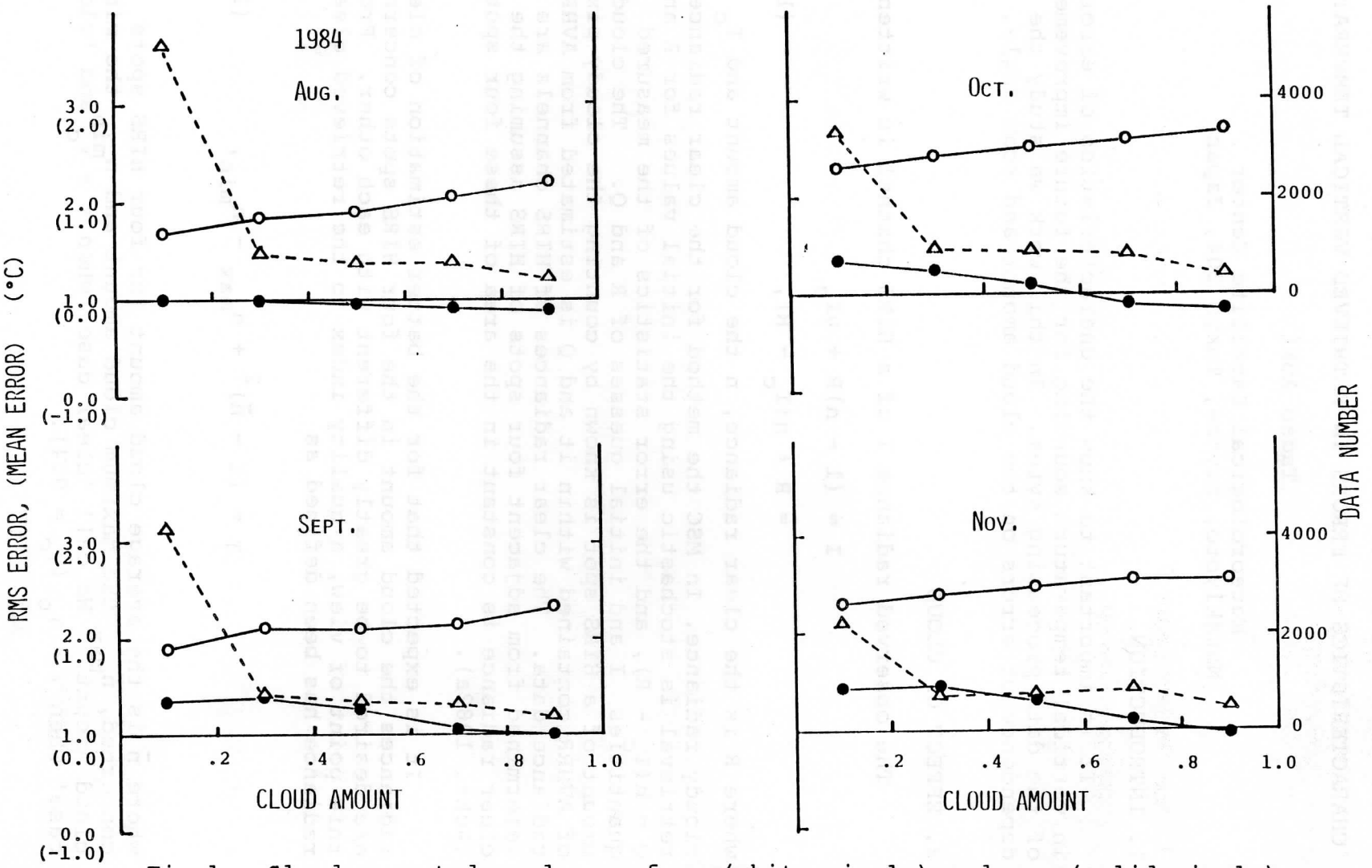

Fig.1 Cloud amount dependence of rms(white circle) and mean(solid circle) errors of retrieved vertical temperature averaged over 14 standard pressure levels. Data number(triangle) are also shown.

Fig.1 shows the dependence of the error of the vertical temperature on the average cloud amount $\bar{n}$ in 'clear case'. The rms and mean errors are averages for 14 standard pressure levels from 20 to 1000 mb. It can be seen that errors are slightly dependent on cloud amount. Positive values of bias error especially for small cloud amount may be explained by the fact that in the season examined here regression coefficients are determined from the data of warmer season preceding the time when the coefficients are used. It seems, however, this effect does not influence in the case of higher cloud amount. The reason is not clear at this stage.

3. EFFECT OF ANGULAR CORRECTION

In MSC the effect of the scan angle θ are corrected by fully empirical procedure. The correction is made to the regression coefficient rather than to the radiance. The temperature T is obtained by the equation

$$T = C(\mu)R(\mu), \tag{3}$$

where C is the regression coefficient and $\mu = 1/\cos\theta$.

The regression coefficient C at $\mu = \mu$ and j-th height z_j is obtained by

$$C_{ji}(\mu, z_j) = C^{\circ}_{ji}(\mu^{\circ}, z_j + \delta)$$

$$\delta = \eta_i \Delta\mu \tag{4}$$

$$\Delta\mu = \mu - \mu^{\circ}$$

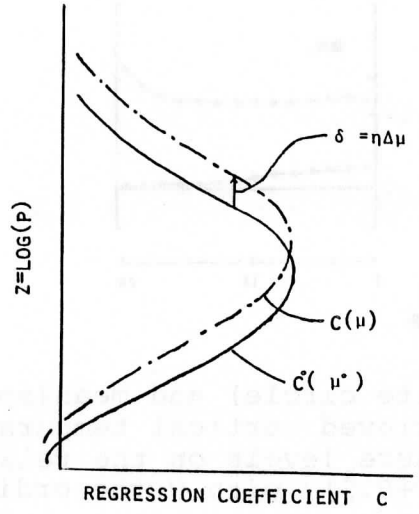

Fig.2 Relationship between the curves $C(\mu,z)$ and $C^{\circ}(\mu^{\circ},z)$.

where η_i is constant for the i-th channel and $\mu°$ is the at a reference scan angle. C° and η are empirically determined (Aoki, 1982b). The procedure of this angle correction is illustrated in Fig.2.

Fig.3 shows the angular dependence of the rms and mean error of the retrieved vertical temperature averaged over all pressure levels as in Fig.1. Somewhat large error especially in September may be suggesting that it is difficult to apply the angular correction mentioned above over full range of scan angle θ(about 0 - 60°degree). Thus coefficients C° and η were seperately determined for two angle ranges, about 0 - 30 and 30 - 60°degree. The errors for this two angle range method are shown in Fig.4 being compared with single angle range method. It can be seen a significant improvement of accuracy is retained by the two angle range method.

4. REFERENCES

Aoki, T., 1982a: An improved method to retrieve the clear column radiance from partially cloudy spots of radiometer on board satellite, J. Met. Soc. Japan, 60, 758-764.

_____, 1982b: Theoretical background of the vertical sounding from TIROS-N satellite seriese, Met. Satellite Center Tech. note, 5, 25-32.

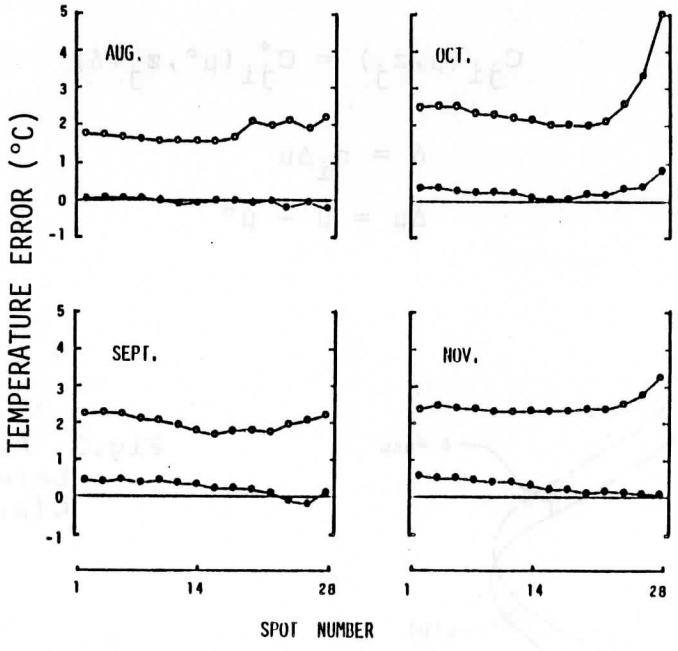

Fig.3 Dependence of rms(white circle) and mean(solid circle) errors of retrieved vertical temperature averaged over 14 pressure levels on the relative spot number, [|N-28.5|+0.5], with N the ordinary HIRS scan spot number.

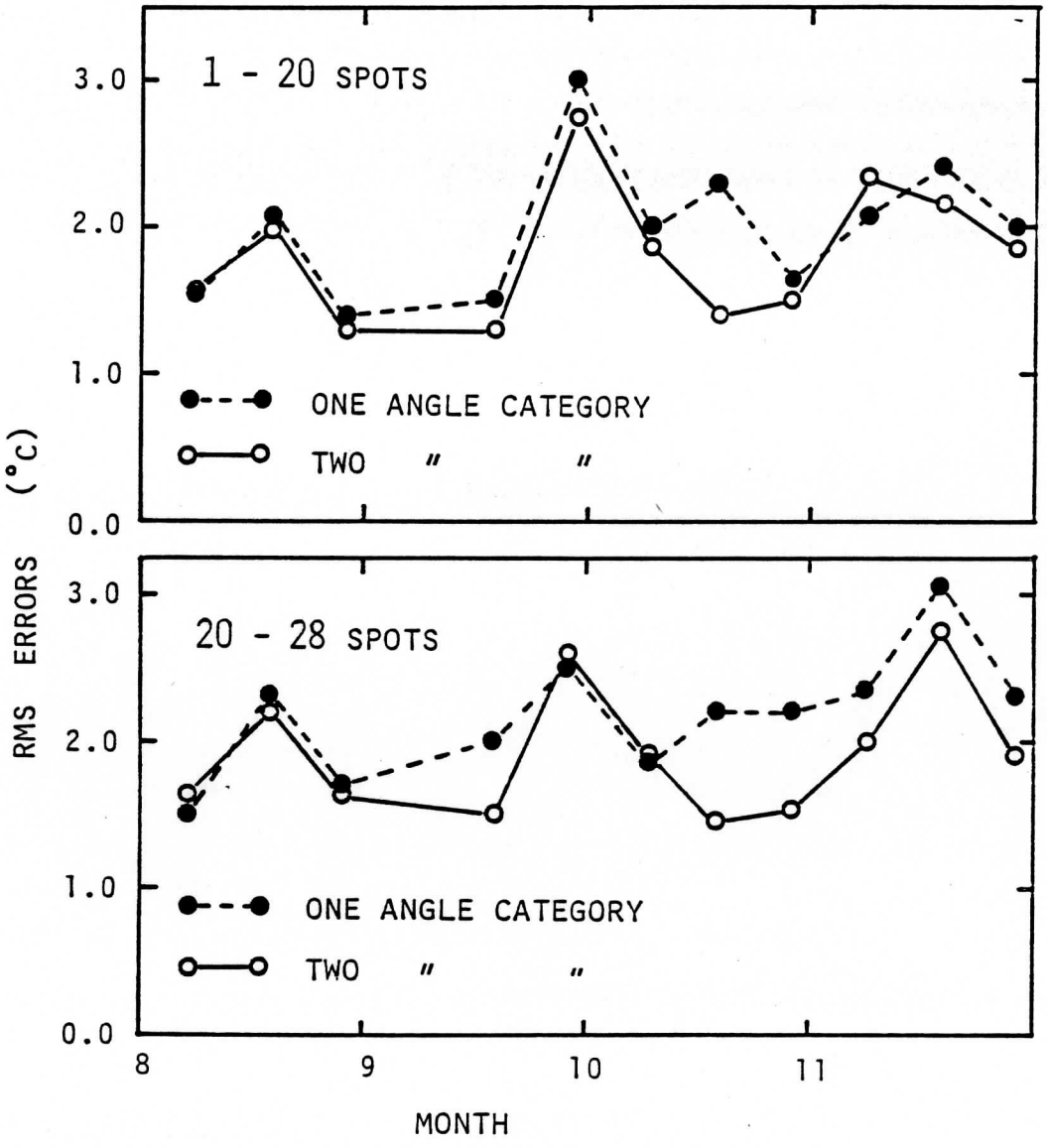

Fig.4 Comparison of rms errors for one and two angle categories. Upper part is for HIRS relative spot number 1-20 and lower is for 20-28.

INITIAL PROCESSING OF TOVS DATA BY USING MICROCOMPUTER MERA-60

Leslaw Baranski
Krzysztof Rosemski
Institute of Meteorology and Water Management
Krakow, Poland

1. INTRODUCTION

In 1984 at the Institute of Meteorology and Water Management in Krakow, the information system support on the microcomputer MERA-60 (with DEC software) was completed and put into operation for retrieval of the vertical temperature and moisture profiles.

Computing power of the microcomputer limited our calculations to one atmospheric sounding only for a selected area. Processing of the TOVS data will be done in two stages. The first stage is the initial data processing. The hardware and software supporting this stage was completed in 1984. Initial processing of TOVS data include all the information transmitted by the Direct Sounder Broadcast system during one satellite pass extending to the radio horizon of the Krakow TIP receiving station. The main goal of the initial processing is as follows:

- reception of the TOVS data,
- extraction and reorganization of HIRS, MSU data for a selected area,
- detection and elimination of transmission errors,
- formation of a file of the calibration coefficients, and
- formation of files containing the auxiliary data for improvement of subsequent processing.

The second processing stage (planned to be finished in 1985) involves selection of the HIRS and MSU data nearest to a selected geographical point. The temperature and moisture profile computed above this point is the final result of the second processing stage.

A summary of the processing software is presented below.

2. CONTROL OF RECEIVING TOVS DATA

The macroassembler program was completed for registration of the raw TIP data on the magnetic tape. This program is also used for providing the input data into the automatic tracking antenna device. This data specifies the instantaneous positions of antenna (in azimuth and elevation). The antenna position is calculated every 20 seconds, just before beginning of the transmission by using data contained in the APT Predict Bulletin.

3. EXTRACTION AND DECOMPOSITION OF TOVS DATA

A macroassembler program was written for decomposition of succeeding TIP minor frames and extraction of HIRS, MSU and organization data important for future processing. Those data are recorded on a magnetic

disk with a format which makes it easy for identification and future processing on FORTRAN level. This program also controls the parity of the frames and meritorical correctness of the received TOVS data (numeration of frames and elements). The frames with erroneous numeration are not registered.

4. EXTRACTION OF THE PRINCIPAL INFORMATION OF TOVS DATA TRANSMISSION

The TIP data transmission is not continuous; breaks due to disturbances are observed. Those disturbances are especially frequent during the beginning and the end of transmission and for low satellite orbits. It has been observed that for elevation angles above 5 degrees, the received data are useful for future processing. Errors in receiving and registering the data are also observed. The time values of TIP major frames and numeration are very important for geographical location and for MSU data identification.

In this regard, it was necessary to develop auxiliary program to deliver information of transmission and detected errors as well as reading and correcting of TIP major frames times. This program and also the next programs are written in FORTRAN-IV language.

5. FORMATTING THE MSU DATA

MSU data in contrast to HIRS data are unequally distributed in TIP minor frames. For efficiency of programs using MSU data it is convenient to assemble these data in records which contain all data from a single MSU line. The time of TIP minor frame is used to identify the MSU words. The program also calculates start times of MSU lines.

6. CALIBRATION OF TOVS DATA

The relationship between instrument counts and radiance (or brightness temperature) can be written in the form:

$$R_H = G_H N_H + I_H \quad \text{for HIRS} \tag{1}$$

$$T_M = G_M f(N_M) + I_M \quad \text{for MSU} \tag{2}$$

where:
- R_H - the radiance measured in a HIRS channel
- N_H - HIRS output counts
- T_M - brightness temperature for a MSU channel
- N_M - MSU output counts
- G_H, I_H - calibration coefficients for HIRS
- G_M, I_M - calibration coefficients for MSU
- f - function of nonlinearity correction for MSU

Calibration coefficients are calculated according to the algorithm published by L. Lauritson et al. (1979). During initial processing, the radiances (brightness temperatures) are not calculated for all HIRS and MSU IFOVs, because determination of the single temperature profile only requires the radiometric data from the surrounding area of the sounding point.

Calculation of the brightness temperatures for HIRS and MSU channels will be performed in the second stage of the processing. It was assumed that the necessary coefficients will be calculated for each transmission.

7. GEOGRAPHICAL LOCATION OF TOVS MEASUREMENTS

The radiometric data from these IFOVs nearest to the selected area center are necessary for determination of the temperature and moisture profile over this area. Hence, it is necessary to find such an IFOV which is located as near as possible from considered earth point. The method of finding this field by locating all IFOVs seems to be too expensive, because calculation is complex and the processor is slow. Therefore, a method of searching succeeding areas composed of five HIRS lines was applied for finding the desired point in the HIRS area. An approximate searching method is used for finding the number of line and element situated as near as possible from this point.

8. CONCLUSION

In the Institute of Meteorology and Water Management in Poland, the receiving station for DSB TIP data and microcomputer support system was completed. This instrumentation is designed for preprocessing of TOVS data and vertical sounding calculations. At the end of 1984, the software for initial processing was completed. The retrieval of the first temperature and moisture profile is planned in 1985 from the NOAA-9 satellite, after obtaining the appropriate coefficients from NESDIS.

IAMAP ACTIVITIES

H. J. Bolle

Institut fur Meteorologie und Geophysik
Universitat Innsbruck
Innsbruck, AUSTRIA

1. BACKGROUND

The International Association for Meteorology and Atmospheric Physics represents the individual scientists working in the broad field of atmospheric sciences. The IAMAP activities are organized by its ten commissions of which the Radiation Commission is responsible for all problems concerned with radiative properties of the atmosphere and the earth surface, radiative transfer and remote sensing. Through its commissions, IAMAP is promoting atmospheric research in general as well as the development of new techniques for operational application. In close cooperation with WMO, IAMAP furthers the exchange of research results by means of symposia, workshops, and the publication of the conclusions of working groups. In the area of remote sensing, IAMAP also works closely with COSPAR which was responsible for the development of the satellite component for FGGE and is now a basis for the WWW.

With respect to this operational observing system the question arose whether the products of TOVS meets the specifications defined by the meteorological community. The question of quality control for these products had to be addressed and a calibration and validation procedure had to be established. It is precisely this question which was addressed by the IRC Working Group on Inversion Procedures.

Consequently, IAMAP very much supports the activities of this Working Group which not only organizes the International TOVS Study Conferences but also contributes to the Nowcasting Conferences organized primarily by IAMAP's Commission on Cloud Physics. The financial contributions which IAMAP can make to individual activities are extremely small and therefore one of its tasks is to stimulate potential sponsors to support the scientific activities. Thus, in the case of the two TOVS conferences, IAMAP is very grateful to the efforts undertaken by the Cooperative Institute for Meteorological Satellite Studies to organize these conferences and for the support received from WMO. It now seems to be appropriate that those organizations which are benefitting from the application of these new scientific developments, such as national weather services and research institutions running mesoscale models, should provide the financial basis jointly with WMO, IAMAP, and COSPAR for the future exchange of basic information to improve the routine application of TOVS data.

2. NEW ACTIVITIES

New research goals are presently defined by ICSU and WMO within the World Climate Research Program in which TOVS data also start to

play an important role. One major problem within the WCRP is the assessment of data over the oceans which is needed for climate modeling. The International Satellite Cloud Climatology Project is also a major research program. The potential contributions of TOVS and VAS data to this project are not yet fully developed: cloud retrieval algorithms are currently based mainly upon bispectral imagery. Within the International Satellite Land Surface Climatology Project, which was recently initiated by COSPAR, IAMAP and UNEP and which is also supported by WMO, the HIRS data have already taken their place for the generation of global skin temperature data sets. But furthermore there is the potential to use TOVS retrievals for the correction of infrared images obtained from other satellites. TOVS data may also contribute substantially to the determination of the radiative budget at the surface which is strongly needed for the computation of evaporation.

There remains one very important and so far unsolved problem to which TOVS may contribute: the early detection of climate change. The increasing amount of CO_2 in the atmosphere should increase the temperature at the surface and within the troposphere but should cool the stratosphere. It would be very important for climatic studies to detect as early as possible any trends which appear. Thus, very accurate and reliable measurements are necessary over long time periods to assess changes of temperature to within a few decidegrees and perhaps to note small changes in the water vapor content of the atmosphere as well as the geographical distribution of these quantities.

Such applications of temperature and water vapor soundings enter new fields of research to which IAMAP Commissions may address themselves in the future. The Joint Scientific Committee for the WCRP is currently inviting nations and international organizations to participate in the WCRP projects which are defined in the Scientific Plan for the WCRP (ICSU-WMO WCRP Publications Series No. 2, 1984; WMO TD-No. 6). IAMAP is ready to respond to this challenge and to join with WMO in stimulating and coordinating the necessary efforts.

4/STAFF/17

THE "3I" PROCEDURE APPLIED TO THE RETRIEVAL OF METEOROLOGICAL PARAMETERS FROM NOAA-7 AND NOAA-8

A. Chedin, N. A. Scott, C. Wahiche, P. Moulinier and N. Husson
Laboratoire de Météorologie Dynamique du CNRS
Ecole Polytechnique, 91128 Palaiseau Cedex, France

G. Rochard, J. Quéré and M. Derrien
Météorologie Nationale, Centre de Météorologie Spatiale
22302 Lannion, France

1. INTRODUCTION

The 3I (Improved Initialization Inversion) method has been designed for retrieving meteorological or climatic parameters from satellite vertical sounders and first applied to NOAA-7, the third of the TIROS-N operational weather satellites series. The 3I algorithm has already been described in some details in several publications : Chedin and Scott (1984), Chedin et al. (1985), Scott et al. (1984 a), Wahiche et al. (1984). This approach to the radiative transfer equation problem directly pertains to pattern recognition theory as it has been shown by Chedin and Scott (1985). The first purpose of the present paper is to present an overview of the 3I method : initialization of the inversion problem including cloud detection and cloud clearing, atmospheric temperatures retrieval, cloud parameters retrieval, atmospheric water vapor retrieval and surface temperatures retrieval. The second purpose of this paper is to discuss the results of two applications of the algorithm, one to NOAA-7 for the March 4-5, 1982 ALPEX (ALPine EXperiment) IOP (Intensive Observing Period) and the other to NOAA-8 (cyclogenesis over the United States, June 7, 1984). From the latter case, an interesting meteorological event, actually a "cold pool", has been detected along 90° longitude and between latitudes 35° to 40° (Section 4.2).

2. SURVEY OF THE 3I METHOD

The 3I procedure is a physico-statistical type method. It is a physical type method since it requires a theoretical simulation of atmospheric transmittances which directly enter the inversion process itself. It is a statistical type method since it relies upon an a priori knowledge of the observations (the brightness temperatures in each channel of the vertical sounder) as well as of the parameters (the atmospheric structure). This a priori knowledge is contained in a large data set, the TIGR (TOVS Initial Guess Retrieval) data set, created once and for all, and comprising for all possible observing conditions (viewing angle, surface pressure, surface emissivity) and for about 1200 atmospheric situations covering the whole globe, the transmittance profiles and associated brightness temperatures for each of the TOVS channels and the partial derivatives of these brightness temperatures with respect to such or such atmospheric parameter. Provided the observed brightness temperatures correspond to clear areas or have been properly "cleared", the 3I procedure follows two principal steps :

a) Retrieval of the initial guess solution : the observed clear column radiances are first used to retrieve the "best" initial guess solution in a statistical sense. The procedure makes use of the "TIGR" data set. The selected set of observed brightness temperatures is "compared" to each of the computed sets of brightness temperatures and the "closest" is retained. The distance between two sets is calculated in the axis system defined by the eigenvectors of the normalized brightness temperatures covariance matrix. This search for the closest archived situation may be carried out by considering either all the HIRS-2 and MSU channels or more restricted brightness temperature sets emphasizing such or such property in the atmosphere, for example: a set of channels almost insensitive to clouds.

b) The basis for the retrieval of the "exact" solution is a maximum probability estimation procedure aimed at minimizing the differences between the brightness temperatures associated with the initial guess and the observed ones. Use is made of the Jacobian associated with the retrieved initial guess, in the "TIGR" data set.

At present, the spatial resolution of the 3I algorithm is a compromise between the spatial resolutions of the two major sounders on board the NOAA's : HIRS-2 and MSU. Retrievals are made for boxes of 4 to 2 (according to the viewing angle) HIRS-2 spots by 3 HIRS-2 spots along the sub-orbital track. Such boxes approximately represent a surface of 100x100 km^2. However, in order to increase the density and check the coherence of the results, an oversampling is introduced along the sub-orbital track and one retrieval is produced every 100x30 km^2, two consecutive boxes sharing two scan lines (see, for example, Chedin and Scott, 1984).

A brief review of the essential aspects of the 3I method is presented in the following sections. References are made to existing publications when available.

2.1 Cloud detection

The cloud detection algorithm has been described by C. Wahiche et al. (1984, 1985). No modifications have been made to these presentations.

2.2 Initialization of the inversion problem

This important problem, at the basis of the 3I algorithm, has been discussed in details in Chedin and Scott (1984), Chedin et al. (1985) and Chedin and Scott (1985). In the latter reference, initialization of the retrieval process from the 3I method is presented and discussed within the frame of pattern recognition theory, an approach allowing important features of an observation to be simply detected and classified. In this reference, comparisons have been made between initialization fields (for example thickness iso-contours) and "final" fields resulting from the inversion process, displaying a remarkable agreement.

2.3 Cloud clearing

The procedure for retrieving the initial guess solution in the proper sub-set of the TIGR data set (the one corresponding to the observation conditions : viewing angle, surface pressure and emissivity) is

direct in case of clear areas, while two steps are required for not clear areas (see Chedin et al., 1985). In the first step, comparisons are made between the observations and the archived brightness temperatures on the basis of a restricted set of channels, in principle insensitive to clouds. Operational forecasts of the temperature at the lowest level are also included in this proximity search. From this preliminary initial guess is started the cloud clearing algorithm based upon the so-called "ψ-method" (Chedin and Scott, 1984 ; Chedin et al., 1985). Following this method, a cleared infrared brightness temperature is obtained by adding to the initial guess value of the channel considered, the difference between the observed and the initial guess values of a microwave channel, almost insensitive to clouds and peaking approximately at the same level. The ψ-method is applied to channels 3, 4, 5, 6, 14 and 15. Contrary to the well known N^* method (Smith,1968), which used at least two spots to eliminate the effects of the clouds, the Ψ-method only uses one spot and consequently avoids the assumption that the difference in radiance for a given channel in the two spots is only due to a variation of the amount of clouds of the same type (same height in particular). The result is that the N^* method is subject to noise when this assumption does not hold.

The strong correlation between the initialization of the inversion process and the cloud clearing technique must also be pointed out : the quality of the initialization and that of the cleared brightness temperatures are directly connected.

2.4 Temperature inversion algorithm

Three important characteristics of the inversion scheme must be recalled :

1) The basis for the retrieval of the "exact" solution is a maximum probability estimation procedure aiming at finding the solution the most likely consistent with the observations. Use is made of the Jacobian associated with the retrieved initial guess, in the "TIGR" data set. See Chedin et al. (1985).

2) Since it starts from an optimum initial guess, which is the situation the closest to the observed situation among those archived in the TIGR data set, the 3I method aims at estimating the difference between the parameters and their values for the closest situation rather than the parameters themselves (or the difference between the parameters and their mean or climatological values).

3) The 3I procedure produces an initial guess solution of high quality which may start a physical type inversion method requiring only one iteration (one matrix inversion) to get an accurate final solution. To the best of our knowledge, this method, developed in 1983 (see Chedin and Scott, 1984), has been the first single-iteration - or direct - physical method.

2.5 Cloud parameters retrieval : the "coherence of effective cloud amounts" method

Considering a partially cloudy field of view (cloud amount N), the radiance measured by the satellite in channel i can be expressed as (Smith, 1968) :

$$I_{m_i} = (1 - N\,\varepsilon_i)\, I_{Cl_i} + N\,\varepsilon_i\, I_{Cd_i}(p_c) \qquad (1)$$

where I_{Cl_i} is the clear radiance, $I_{Cd_i}(p_c)$ the radiance arising from a black cloud at level p_c and ε_i the cloud emissivity. $N\varepsilon_i$ is called the "effective cloud amount" in channel i. From Eq. (1), N and ε_i cannot be reached separately. The use of Eq. (1) (written for several channels) to determine $N\varepsilon_i$ and p_c requires knowledge of I_{Cl_i} and the function $I_{Cd_i}(p_c)$. These values can be reached from the TIGR data set. More precisely, the TIGR data set provides an estimation of I_{Cl_i} and of $I_{Cd_i}(p_c)$ in all HIRS/2 channels, for a set of cloud levels p_c (23 values from the surface to 200 mb) and for all the possible conditions of observations.

The method is based upon the consideration of a plausible variation of the cloud emissivity $\varepsilon_c(\nu)$ with frequency. From the conclusions of a study by Yamamoto et al. (1970), we assume that $\varepsilon_c(\nu)$ is roughly constant in the longwave region (5 channels : 4 to 8) and in the shortwave region (5 channels : 13, 14, 15, 18, 19), and, moreover, that the shortwave value is slightly lower than the longwave one. The algorithm can be divided into two steps :

1) Selection, among the initial set of 23 pressure levels, of a sub-set of plausible cloud top levels.

A level is plausible if the following test is verified : we consider the function :

$$S(p_c) = \sum_{(i,j)} \left[\left(\frac{I_{m_i} - I^{\circ}_{Cl_i}}{I_{m_j} - I^{\circ}_{Cl_j}} \right) - \left(\frac{I^{\circ}_{Cd_i}(p_c) - I^{\circ}_{Cl_i}}{I^{\circ}_{Cd_j}(p_c) - I^{\circ}_{Cl_j}} \right) \right]^2 \qquad (2)$$

for (i,j) = (4,5), (5,6), (6,7)

where $I^{\circ}_{Cl_k}$ and $I^{\circ}_{Cd_k}(p_c)$ are respectively the estimations of I_{Cl_k} and $I_{Cd_k}(p_c)$. Eq. (2) derives from Eq. (1), written for each pair of channels considered, after $N\varepsilon_i$ has been eliminated.

The test consists in verifying that $S(p_c)$ is close to its minimum value S_{min}. In the pairs of adjacent channels technique, the cloud top level p_c would be the one for which $S(p_c) = S_{min}$. Here the test limit is : $S(p_c) / S_{min} \leqslant 5$.

2) Tests on the coherence of effective cloud amounts.

For each plausible cloud level p_c, corresponding values of $N\varepsilon_i$ are computed in each channel from Eq. (1). This step is itself divided into two parts :

. Elimination of obviously impossible levels : various tests are carried out, in each spectral region, to make sure that the individual values $N\varepsilon_i$ are not too much scattered, and that both mean values (respectively $N\varepsilon_{LW}$ and $N\varepsilon_{SW}$ for the longwave and the shortwave region) are comprised between 0 and 1, and that $N\varepsilon_{SW}$ is slightly lower than $N\varepsilon_{LW}$.

. Choice of the final cloud top level : the ratio of the standard deviation of the effective cloud amounts $N\varepsilon_i$ by the mean value $N\varepsilon_{LW}$ in the longwave region must be minimum, which ensures the smallest scattering.

For daylight observations, shortwave channels cannot be used because of their contamination by reflected solar radiation. In that case, a simplified algorithm is applied, in which all tests using shortwave channels are excluded.

The algorithm has been validated on synthetic data and compared, favourably in particular for low clouds, to those obtained by Wielicky and Coakley (1981) with the pair of adjacent channels technique . Knowledge of the cloud parameters makes it possible to "clear" all the channels influenced by the clouds and not corrected by the ψ-method. More details are given in Wahiche et al. (1985).

2.6 Water vapor and surface temperature retrievals

Retrievals of water vapor amounts are made for three layers delimited by the levels 1000 mb, 800 mb, 500 mb and 300 mb in addition to the total amount of precipitable water vapor. Following the temperature profile retrieval, the brightness temperatures associated with the initial guess are corrected for the deviations between the initial temperature profile and the final solution giving rise to the initial guess for water vapor and surface temperature retrievals.

Because of the difficulty in retrieving accurate water vapor amounts from TOVS, two different methodologies are presently experienced. The first one is a simultaneous physical inversion of the water vapor amounts and of the surface temperature. The second relies upon regressions obtained from the TIGR data set which main interest is to comprise all possible conditions of observations (viewing angle, surface parameters, ..) as well as a large representative sample of atmospheric situations.

1) Simultaneous physical inversion of water vapor and surface temperature.

Four HIRS/2 channels are presently used : 8, 10, 11 and 12 for the day-time observations and 18, 10, 11, 12 for night-time observations. A ridge type estimation procedure is used :

$$\Delta\beta = (X'X + \gamma I)^{-1} X' \Delta Y$$

where X (X', transpose of X) is the matrix of the partial derivatives of the brightness temperatures with respect to relative humidities and surface temperature, ΔY the difference between observed (cleared) brightness temperatures and the initial guess (corrected as explained above), $\Delta\beta$ the difference between the final and initial values of the parameters considered, γ a smoothing parameter (Lagrangian parameter).

2) Regressions from the TIGR data set.

Regressions for the relative humidities of the three above mentioned layers and for the surface temperature are derived from the TIGR data set. The sets of channels used to predict the relative humidities for the layers 300-500 mb, 500-800 mb and 800-1000 mb are respectively : 4, 5, 6, 11, 12 and 15 for the first layer ; 5, 6, 7, 10, 11, 12 and 15 for the second ; 5, 6, 7, 10, 11, 14 and 15 for the third one. The surface temperature is predicted from three regressions using the sets of channels : 8, 10, 11, MSU2, MSU3 for the first one ; 8, 10, 18 and MSU2 for the second one ; 8, 10, 11, 19, MSU2 and MSU3 for the last one. If we denote respectively by T(8), T(18) and T(19) the three values provided by these regressions, the surface temperature is obtained from T(8) for day time observations and from 0.5 T(8) + 0.25 T(18) + 0.25 T(19) for night time observations. More details are given in Wahiche (1984).

2.7 Microwave surface emissivity

Microwave surface emissivity is an important parameter bearing information on the type of the surface (ice monitoring in particular). It is directly extracted from the measurements in the first channel of the microwave sounding unit, a window channel (see Wahiche, 1984).

3. APPLICATION OF THE 3I ALGORITHM TO NOAA-7

The 3I procedure briefly described in the preceding sections was first applied to the ALPEX (ALPine EXperiment) IOP for March 4-5,1982. Satellite data were prepared by NOAA/NESDIS Development Laboratory, Madison (USA). They represent 4 satellite passes : March 4, orbits Nbs. 3586 and 3587 at 12h00 and 13h45 respectively ; March 5, orbits Nbs. 3594 and 3595 at 2h05 and 3h45 respectively. Each pass is made of approximately 70 to 80 scan lines. Forecasts data were obtained, for the same period, from ECMWF, Reading (GB). Results have been reported in the references already quoted. They were obtained from the first version of the TIGR data set, comprising at that time 398 atmospheric situations of middle latitude type. The new version of the TIGR data set, rapidly described in Section 2, comprises 1207 atmospheric situations, distributed in 525 polar, 545 mid-latitude and 137 tropical situations. A significant improvement over previous results has been obtained as shown in the next section.

3.1 Comparison between the 3I results and conventional data

For the period considered, a preliminary assessement of the quality of the 3I procedure can be made by comparing retrievals to the available radiosounding measurements. These data were obtained from ECMWF. Results of this comparison between radiosondes and retrievals are illustrated on Fig. 1.

On this figure, we have used the standard levels stratification for the sake of simplicity in comparing with other algorithms. One of the most salient features of this figure is the good quality of the retrievals in the lower part of the troposphere (500-1000 mb). The agreement

is significantly better than what we obtained from the first version of TIGR. The peak at about 250 mb for the clear boxes with the new TIGR, also noted by other authors (see Smith, 1984) is under investigation. The most striking point is the decrease of the number of boxes automatically rejected by the inversion algorithm : 32 boxes for the first TIGR and only 16 now, over a total of 171 radiosondes available. The improvement issuing from the new TIGR is also illustrated on Figures 2-5 presenting geopotential thicknesses and thermal winds derived from the retrieved thermal structure, with the first TIGR data set (Figs. 2 and 4) and with the new TIGR data set (Figs. 3 and 5). The spatial coherence appears greater on the latter two and the number of rejections is clearly smaller. The quality of the initialization is illustrated by comparisons between the initial and final thickness iso-contours fields. Fig. 6 presents the thickness iso-contours field obtained from the retrieved solutions (that of Fig. 3) and may be directly compared to Fig. 7 which presents the same field derived from the initial guess solutions.

The general appearance of the initialization field of Fig. 7 is already remarkably close to that of Fig. 6.

A similar conclusion comes from Figs. 8 and 9 which present the same type of results for the two night-time passes and for the atmospheric layer comprised between 850 mb and 700 mb, a layer much thinner than the vertical resolution associated with an infrared sounder. Fig. 8 is for the retrieved field when Fig. 9 is for the initialized field.

Results illustrated on Figs. 2-9 have been obtained using as a proximity criterion for selecting the initial guess solution among the situations archived in the TIGR data set an average minimum distance classifier as explained in Chedin and Scott (1985).

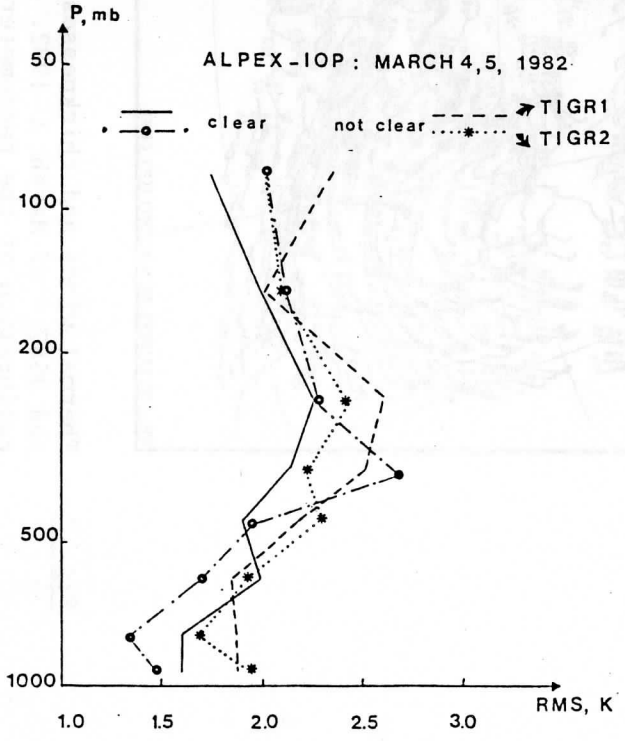

Figure 1

RMS error of retrieved mean layer temperature (standard levels) compared to collocated radiosondes for the ALPEX IOP, March 4-5, 1982.

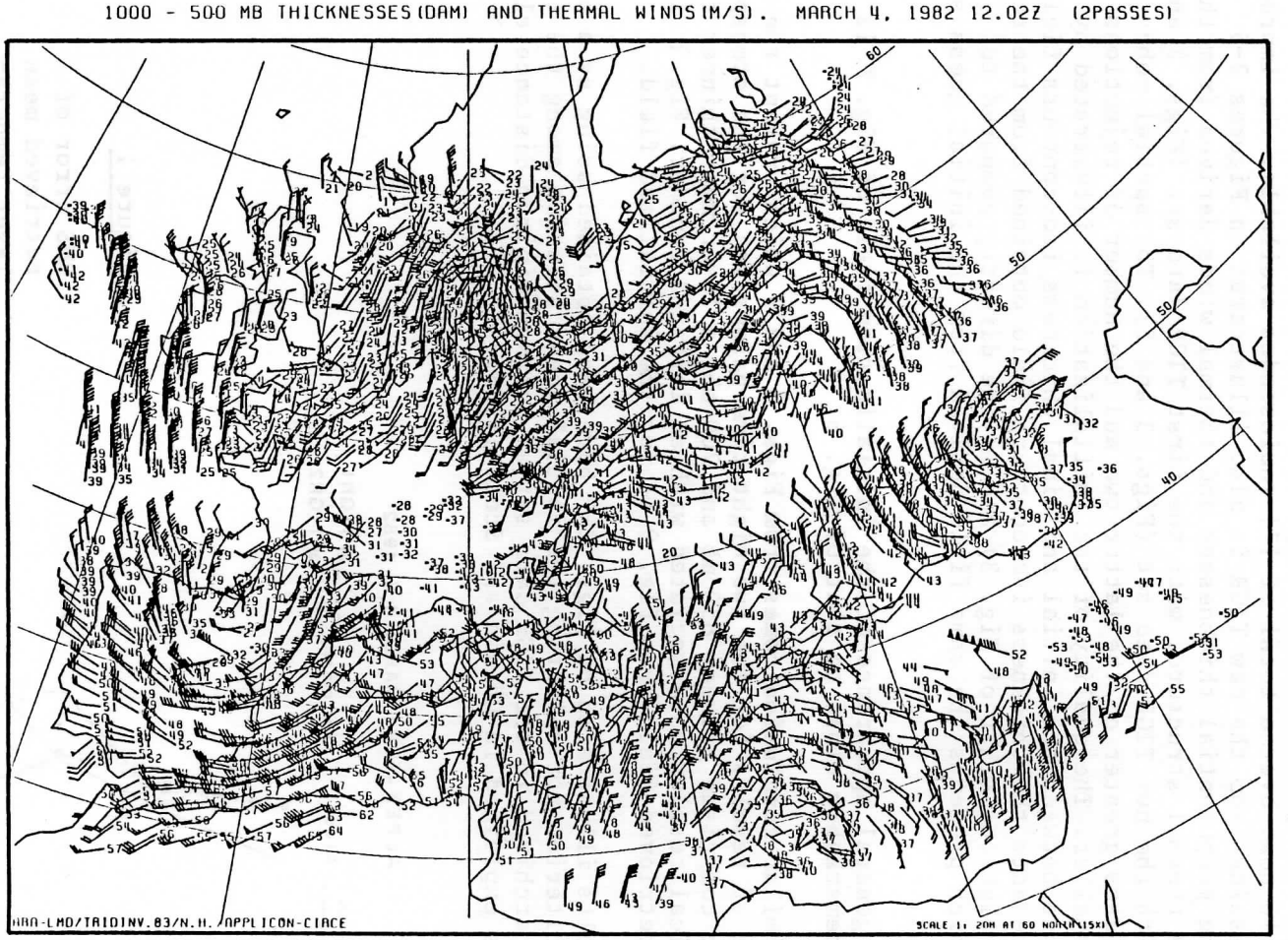

Fig. 2 Thermal winds and thicknesses betwen 1000 and 500 mb for the two day-passes - orbits 3586 and 3587 - of March 4 1982. Areas where data are missing are either regions where the calibration of the radiometer occurred or regions where the rejection tests have a significant impact. Winds are in m/s. ; thicknesses are in dam minus 500. "Old" TIGR data set.

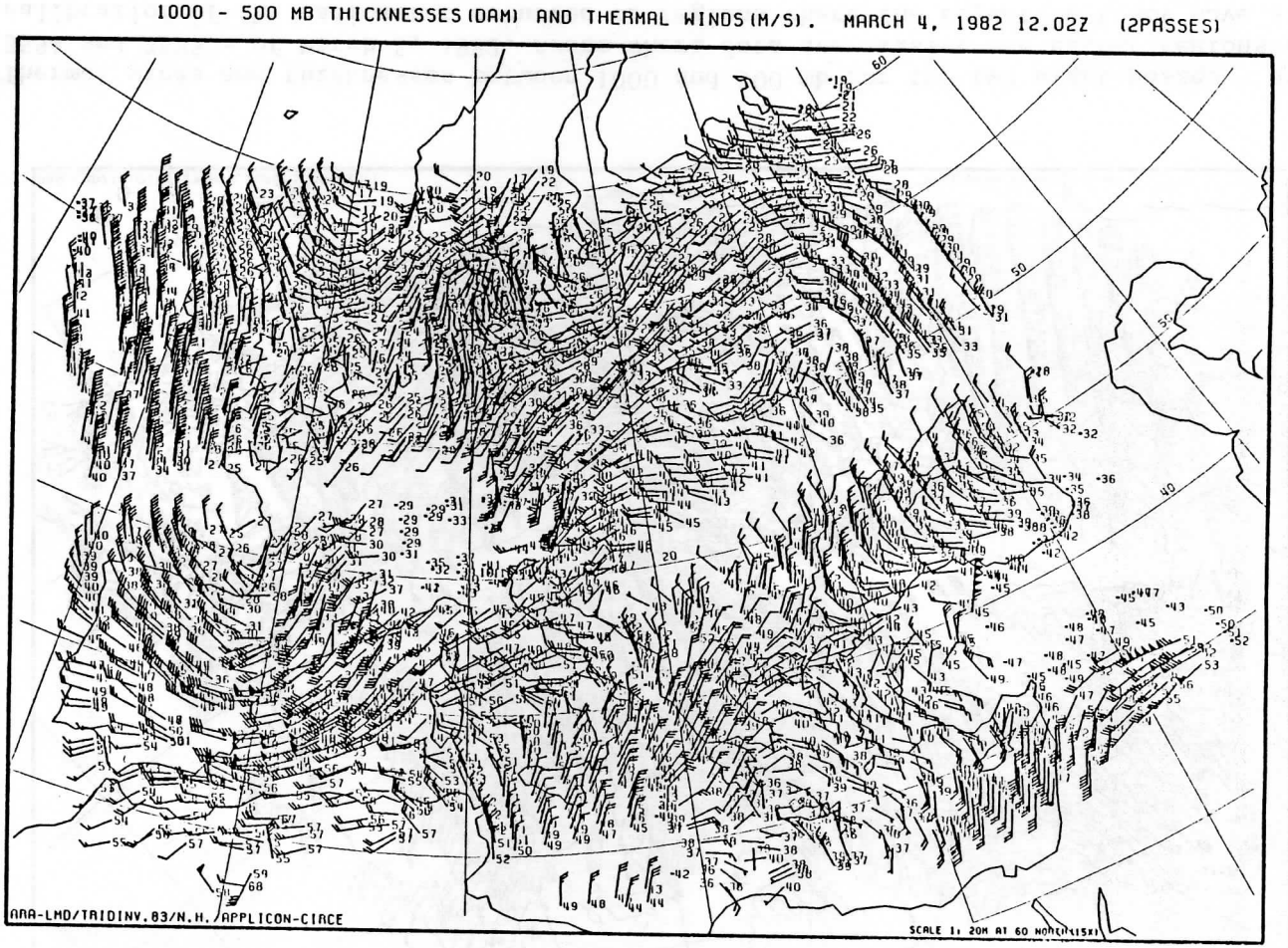

Fig. 3 Thermal winds and thicknesses between 1000 and 500 mb for the two day passes - orbits 3586 and 3587 - of March 4 1982. Areas where data are missing are either regions where the calibration of the radiometer occurred or regions where the rejection tests have a significant impact. Winds are in m/s. ; thicknesses are in dam minus 500. "New" TIGR data set.

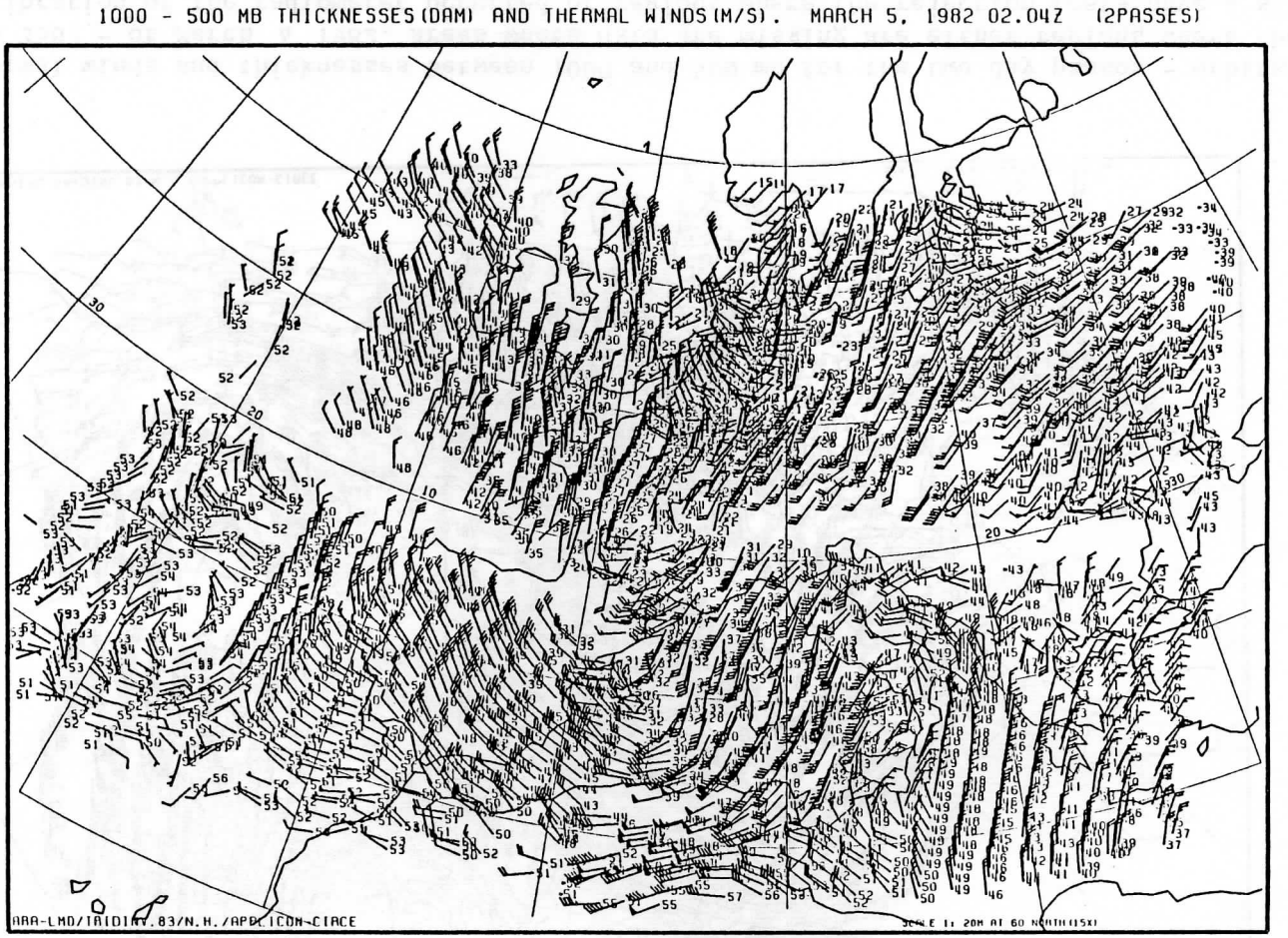

Fig. 4 Thermal winds and thicknesses between 1000 and 500 mb for the two night passes - orbits 3594 and 3595 - of March 5, 1982. Areas where data are missing are either regions where the calibration of the radiometer occurred or regions where the rejection tests have a significant impact. Winds are in m/s. ; thicknesses are in dam minus 500. "Old" TIGR data set.

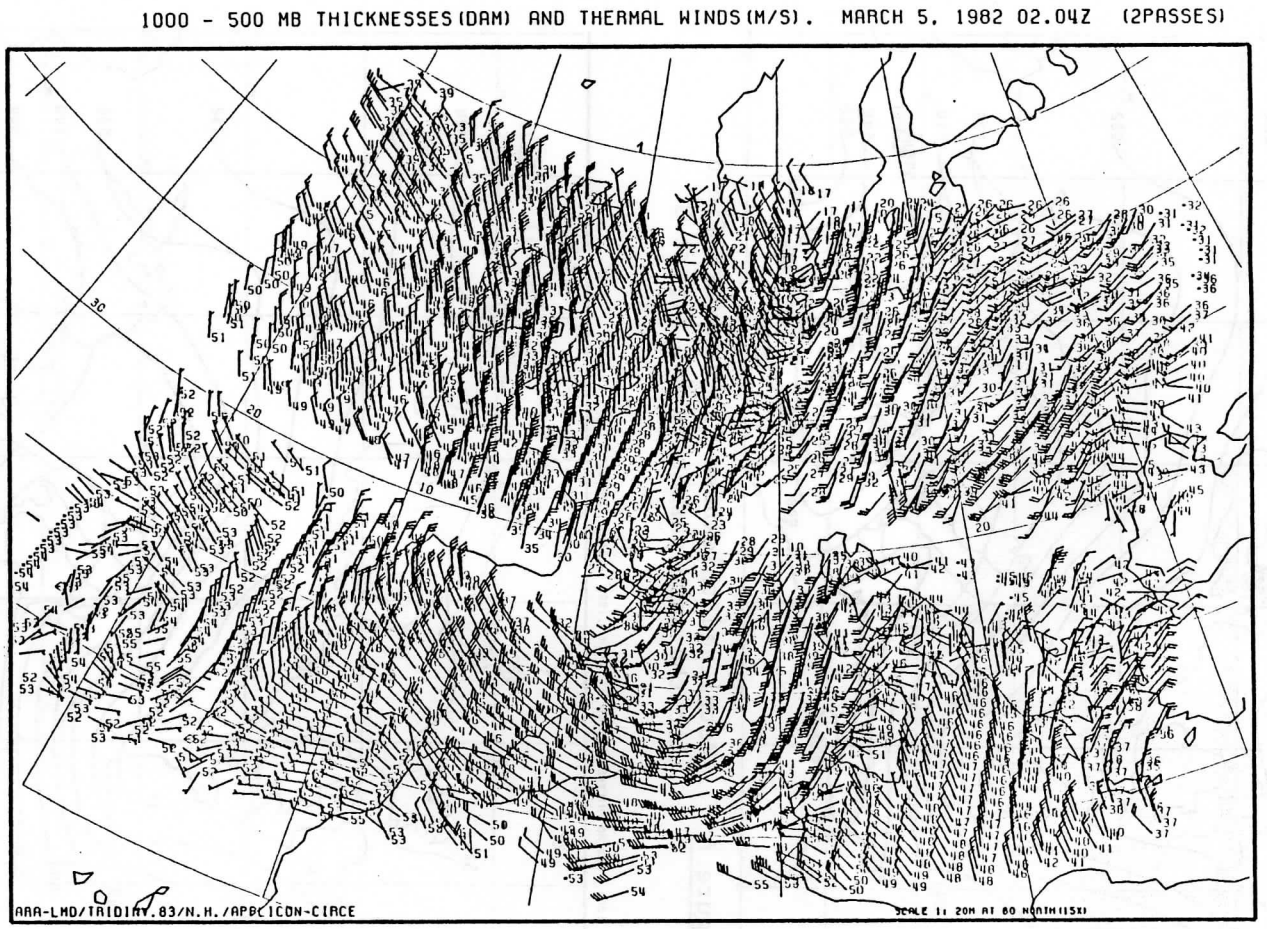

Fig. 5 Thermal winds and thicknesses between 1000 and 500 mb for the two night passes - orbits 3594 and 3595 - of March 5, 1982. Areas where data are missing are either regions where the calibration of the radiometer occurred or regions where the rejection tests have a significant impact. Winds are in m/s. ; thicknesses are in dam minus 500. "New" TIGR data set.

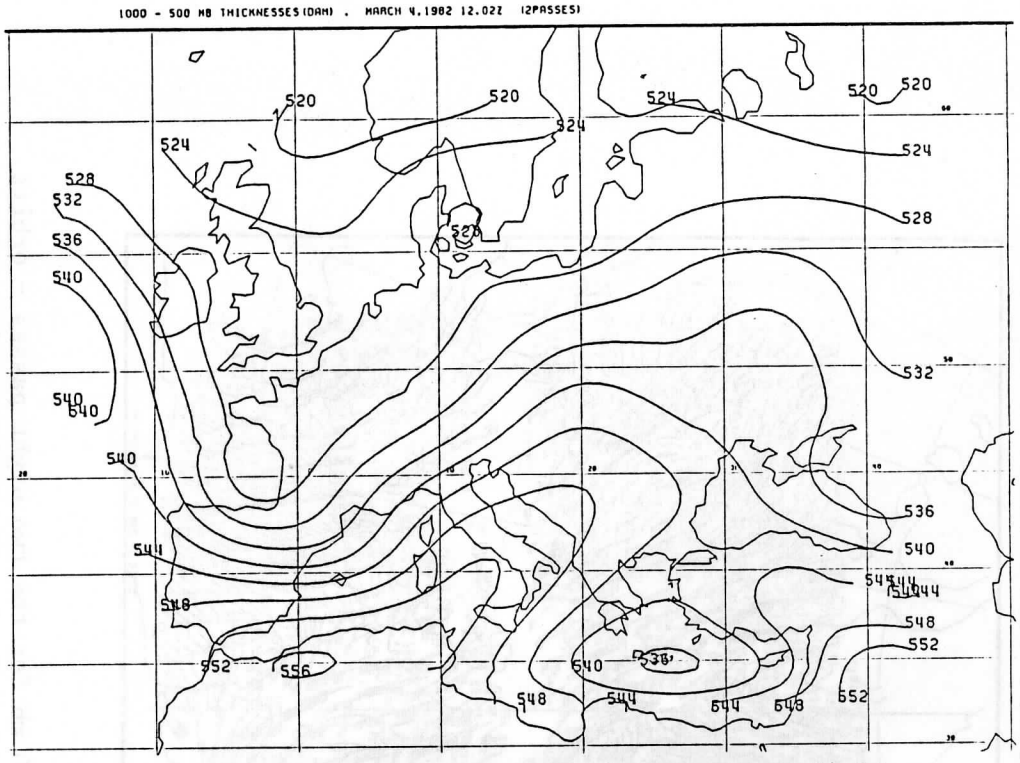

Figure 6 Retrieved thickness iso-contours field for the same passes as for Figure 3.

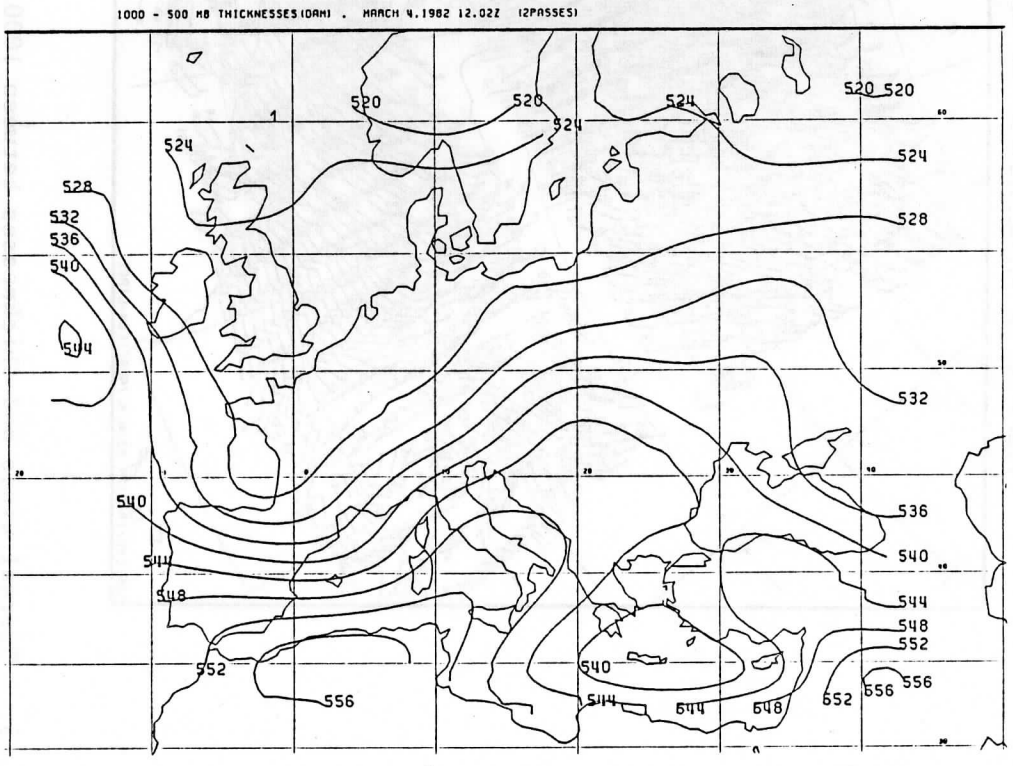

Figure 7 Thickness iso-contours field corresponding to the initial guess solution for the same passes as for Figure 3.

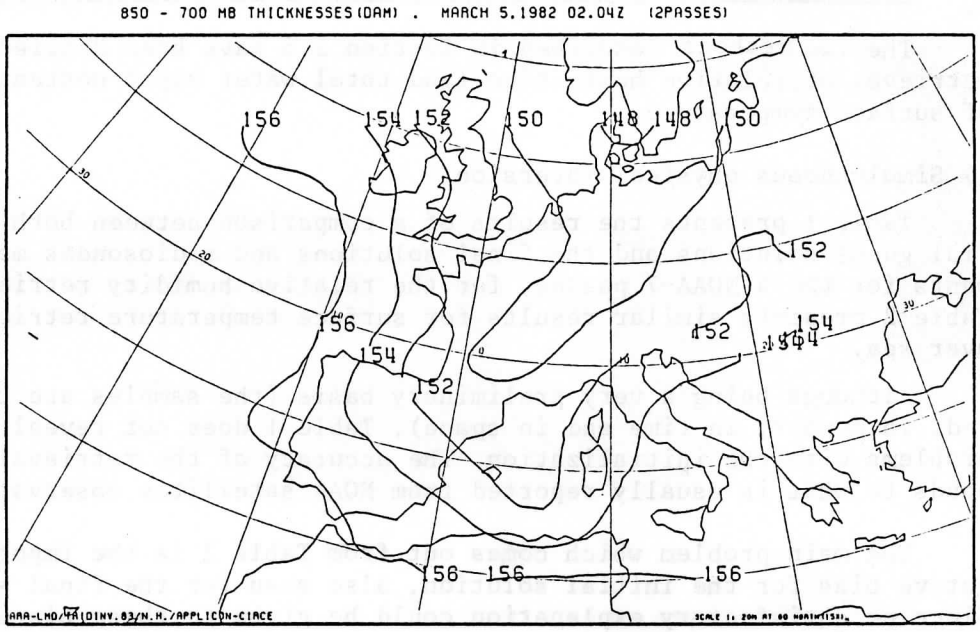

Figure 8 Retrieved thicknesses for the two night-time passes (in dam) and for the layer 850-700 mb.

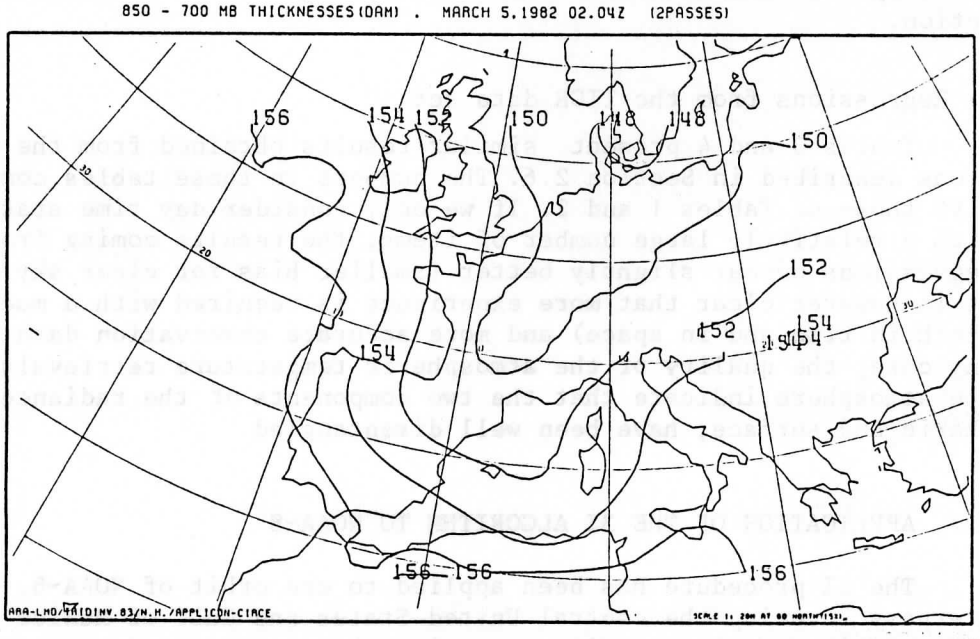

Figure 9 Initialized thicknesses for the same passes as for Figure 8.

3.2 Results for the relative humidities and surface temperatures

The two methods described in Section 2.6 have been applied to the retrieval of relative humidities (and total water vapor contents) and of surface temperature.

1) Simultaneous physical inversion

Table 1 presents the results of a comparison between both the initial guess solutions and the final solutions and radiosondes measurements for the 4 NOAA-7 passes, for the relative humidity retrievals. Table 2 presents similar results for surface temperature retrievals over sea.

Although being a very preliminary basis (the samples are too limited, in number, in time and in space), Table 1 does not reveal important problems with the initialization. The accuracy of the retrievals corresponds to what is usually reported from NOAA satellites observations.

The main problem which comes out from Table 2 is the important negative bias for the initial solution, also seen for the final solution. Since no satisfactory explanation could be given to these biases, we have compared these results to those obtained for one pass (March 4) by the French Meteorological Office from AVHRR observations (Personal Communication, July 1984, T. Phulpin and P. Leborgne, CMS Lannion, France). These results show the same bias, even a little larger, which could find its origin in the bata base (archived by ECMWF, Reading, GB) itself. The encouraging result is the standard deviation decrease from the initial guess to the final solution. If the latter is satisfactory, the former is acceptable and does not reveal a very big problem with the initialization.

2) Regressions from the TIGR data set

Tables 3 and 4 present similar results obtained from the regressions described in Section 2.6. The numbers in these tables compare well with those of Tables 1 and 2. If we only consider day time statistics with a relatively large number of items, the results coming from the regressions appear slightly better (smaller bias for clear sky conditions). It is however clear that more experience is required with a much larger (both in time and in space) and more accurate observation data base. In any case, the quality of the atmospheric temperature retrievals low in the atmosphere indicate that the two components of the radiances, atmospheric and surface, have been well disentangled.

4. APPLICATION OF THE 3I ALGORITHM TO NOAA-8

The 3I procedure has been applied to one orbit of NOAA-8, a morning overpass covering the central United States and Gulf of Mexico on June 7, 1984. It is very interesting to notice that a tornado devastated Barneveld (Wisconsin) later in the evening. Satellite data have been prepared by CIMSS, Madison, and comprise approximately 80 scan lines. For the same period , the LFM (Limited Finemesh Model) predicts have also been obtained from CIMSS.

Table 1 Water vapor inversion : statistics for the initial solutions and the retrievals compared to radiosondes measurements (ALPEX IOP, March 1982). Clear areas and partially cloudy areas (up to 50%) are considered

		Initial solution			Retrieval		
		Mean (o-c)	s.d.	n_{stat}	Mean (o-c)	s.d.	n_{stat}
$RH_{300-500mb}$	[1]	-0.11	0.20	53	-0.07	0.16	52
$RH_{500-800mb}$	[1]	-0.12	0.22	54	-0.10	0.15	51
$RH_{800-1000mb}$	[1]	0.04	0.16	51	-0.07	0.17	52
U_{total}	[2]	-0.03	0.27	54	-0.08	0.22	50

[1] Percent relative humidities.
[2] In $g.cm^{-2}$. Mean over the sample : 0.9 $g.cm^{-2}$.

Table 2 Surface temperature inversion over sea : statistics for the initial guess solutions and the retrievals, compared to ships of opportunity measurements (ALPEX IOP, March 1982). Not clear areas include up to 50% cloud amounts.

		Clear			Clear + Not clear		
		Mean (c-o)	s.d.	n_{stat}	Mean (c-o)	s.d.	n_{stat}
Initial solution	Night	-2.9	1.9	11	-2.9	2.2	16
	Day	-3.5	2.1	71	-2.9	2.4	97
Retrievals	Night	-1.3	1.2	12	-1.4	1.3	17
	Day	-1.6	1.2	72	-0.5	2.2	97

Table 3 Water vapor regressions : statistics for the retrievals compared to radiosonde measurements (ALPEX IOP, March 1982).

		Mean (o-c)	s.d.	n_{stat}
$RH_{200-500mb}$	1	-0.07	0.16	55
$RH_{500-800mb}$	1	-0.07	0.18	54
$RH_{800-1000mb}$	1	-0.008	0.14	54
U_{total}	2	-0.006	0.21	56

1 Percent relative humidities
2 In $g.cm^{-2}$. Mean over the sample : 0.9 $g.cm^{-2}$

Table 4 Surface temperature regressions over sea : statistics for the retrievals compared to ships of opportunity measurements (ECMWF Reading archives ; ALPEX IOP, March 1982).

	Clear			Clear + Not clear		
	Mean (c-o)	s.d.	n_{stat}	Mean (c-o)	s.d.	n_{stat}
Night	-1.1	1.0	11	-0.94	1.00	16
Day	-0.1	1.4	72	-0.60	2.30	99

4.1 Validation of the transmittance/radiance model

Accurate computation of transmittances and radiances (brightness temperatures) for the TOVS channels and the atmospheric situations in TIGR are an essential condition to correctly retrieving meteorological parameters from the 3I method.

Use is made of the fast line-by-line model "4A" (Automatized Atmospheric Absorption Atlas ; Scott and Chedin, 1981), properly validated against TOVS - radiosonde matched data for the satellite of interest, here NOAA-8. Two types of matched data have been considered. The first file was extracted from the NOAA/NESDIS DSDV files : 240 matchups covering the periods Summer 1983 and Winter 1983-1984 corresponding to night time observations over land or sea for polar, middle and tropical latitudes. The second file was produced by CMS/Lannion : 16 situations (over sea ; day and night ; middle latitudes ; winter) with an accurate estimation of the surface temperature, a parameter essential to an accurate validation of transparent channels. Radiances originally produced by 4A were transformed owing to the γ-δ procedure (see, for example, Scott et al., 1984a) to constrain the biases between observations and computations to zero. The mean values of the γ and δ factors are, respectively, 1.02 and -0.3. Their standard deviations are 0.03 and 0.5. The TIGR data set (1207 situations) for NOAA-8 is based upon these results.

4.2 Geopotential thicknesses and thermal winds for NOAA-8 observations over Central United States and Gulf of Mexico (June 4, 1984).

Figure 10 presents geopotential thicknesses and thermal winds for the NOAA-8 orbit considered and for the layer 1000-500 mb. Over a total of 1254 possible retrievals, 1080 were declared acceptable, the rejections representing 8.6 %, a relatively small fraction if one considers the meteorological situation characterized by an extended and relatively heavy cloudiness (see Fig. 11 which reproduces the corresponding channel 2 AVHRR picture). Figure 12 presents the associated thickness iso-contours field. Figures 13 to 24 present similar results for other atmospheric layers. The quality of the initialization is illustrated on Figures 25 and 26 which display thermal winds and thickness iso-contours for the layer 1000-500 mb and for the initialization field, which may be directly compared to Figs. 10 and 12.

With the a priori knowledge of the fact that a tornado devastated some areas in the state of Wisconsin (Barneveld, in particular), these results appear interesting since they seem to bring into evidence a cold pool along 90° longitude and between latitudes 35° and 40° . This phenomenon appears on both the thermal wind charts (Fig. 10, for example) and on the iso-contours field of Fig. 12 (minimum at 570 dam): the almost symmetrical isotherms about the low center are characteristical. The forecast of the violent meteorological event which occured a few hours after the satellite pass could have benefited from the results of the inversion algorithm.

Figure 11 AVHRR (channel 2) picture for NOAA-8, June 7, 1984 over Central United States (morning overpass).

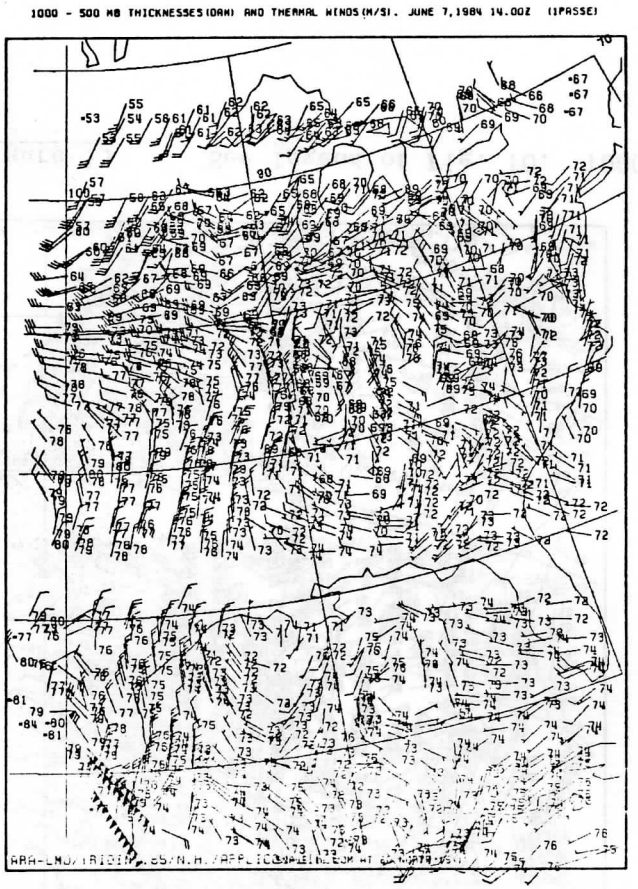

Figure 10

Thermal winds and thicknesses between 1000 and 500 mb, for the June 7, 1984, NOAA-8 pass over Central U.S.

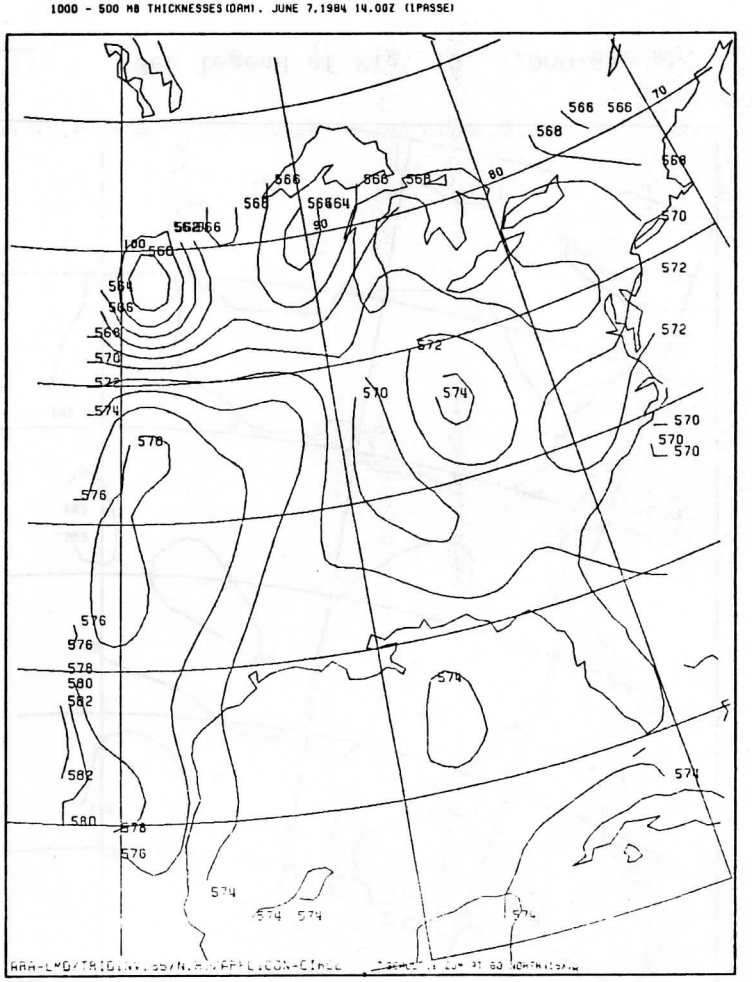

Figure 12

Retrieved thickness iso-contours field for the same pass as for Fig. 10.

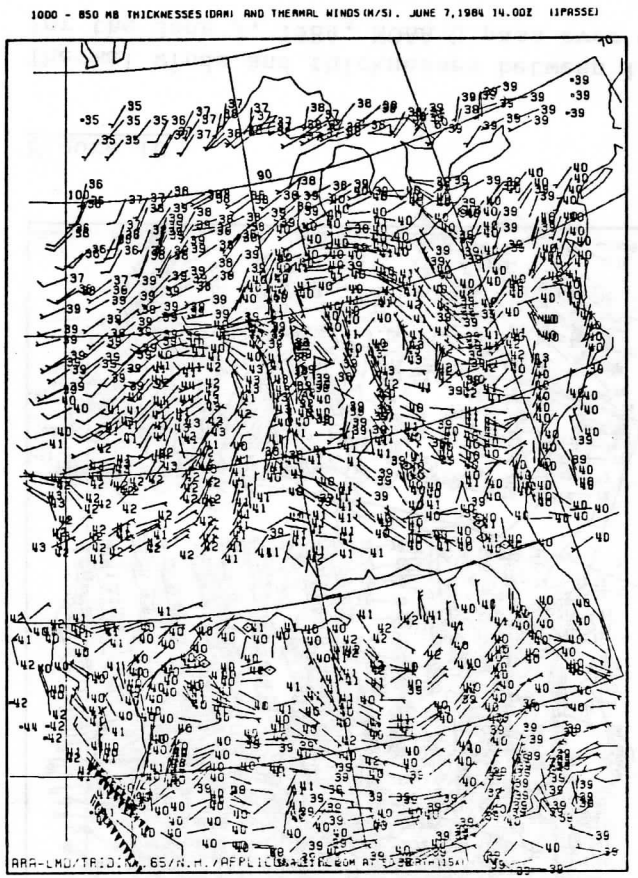

Figure 13 See legend of Fig. 10. 1000-850 mb.

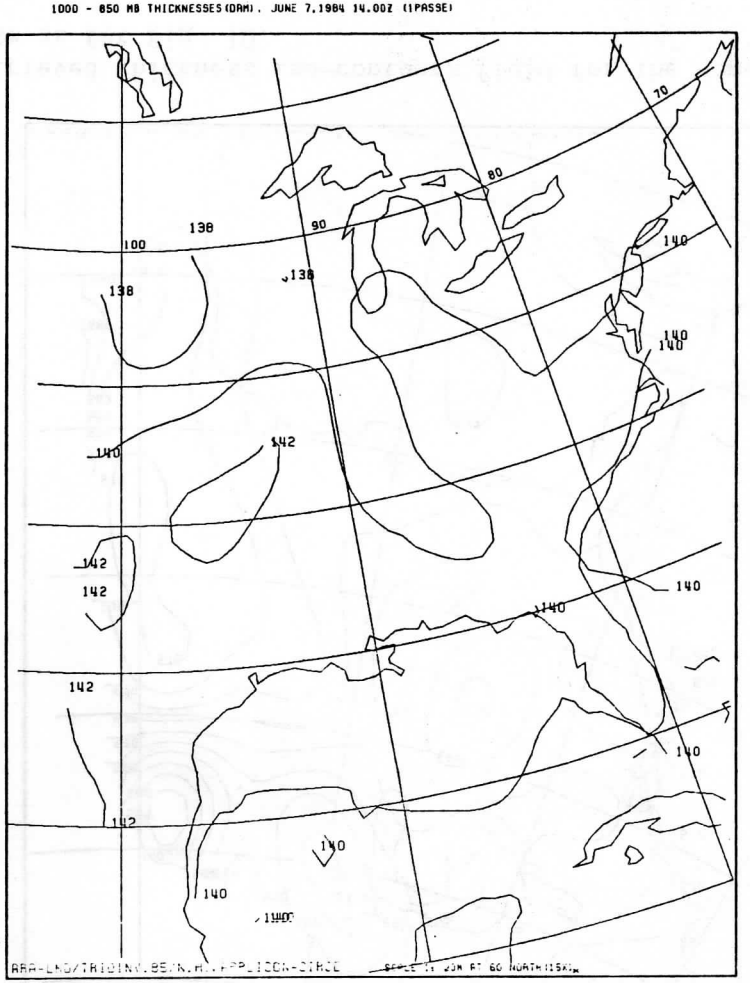

Figure 14 See legend of Fig. 12. 1000-850 mb.

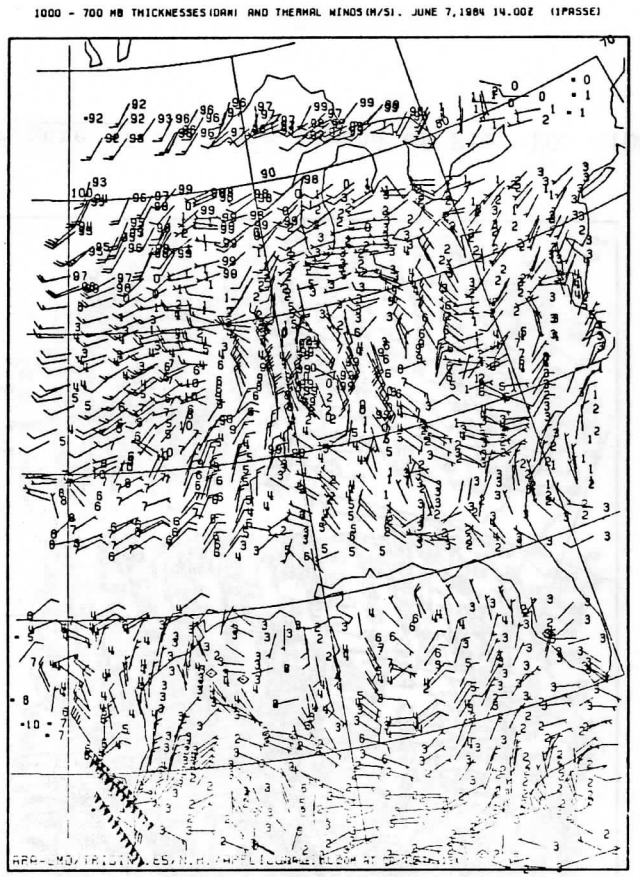

Figure 15 See legend of Fig. 10. 1000-700 mb.

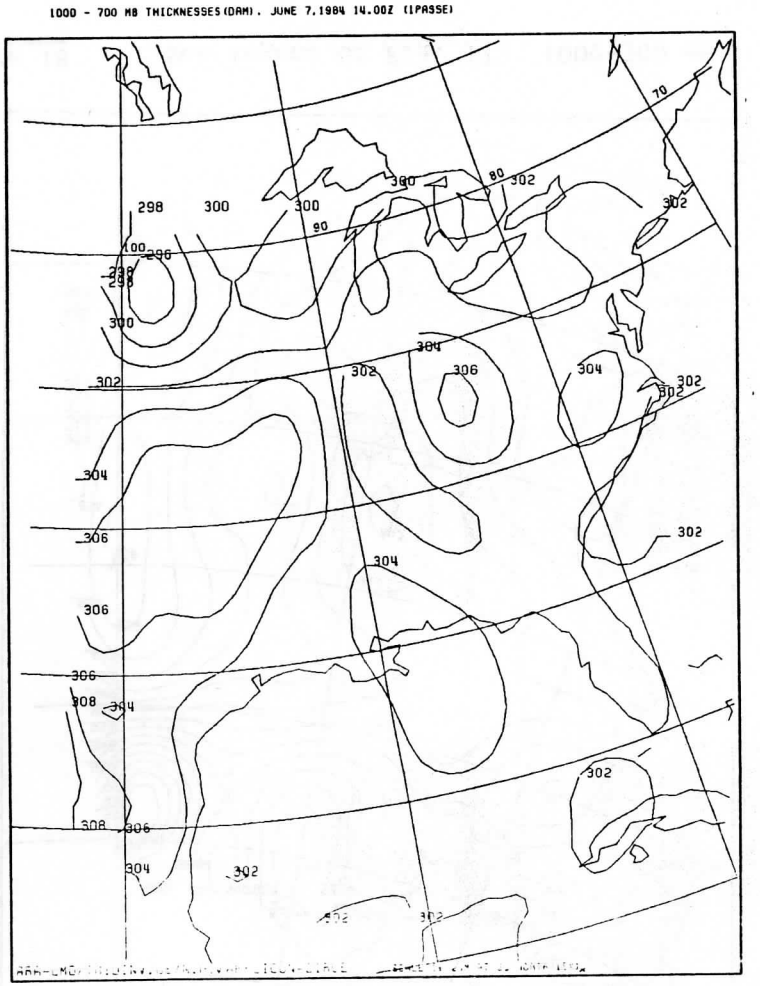

Figure 16 See legend of Fig. 12. 1000-700 mb.

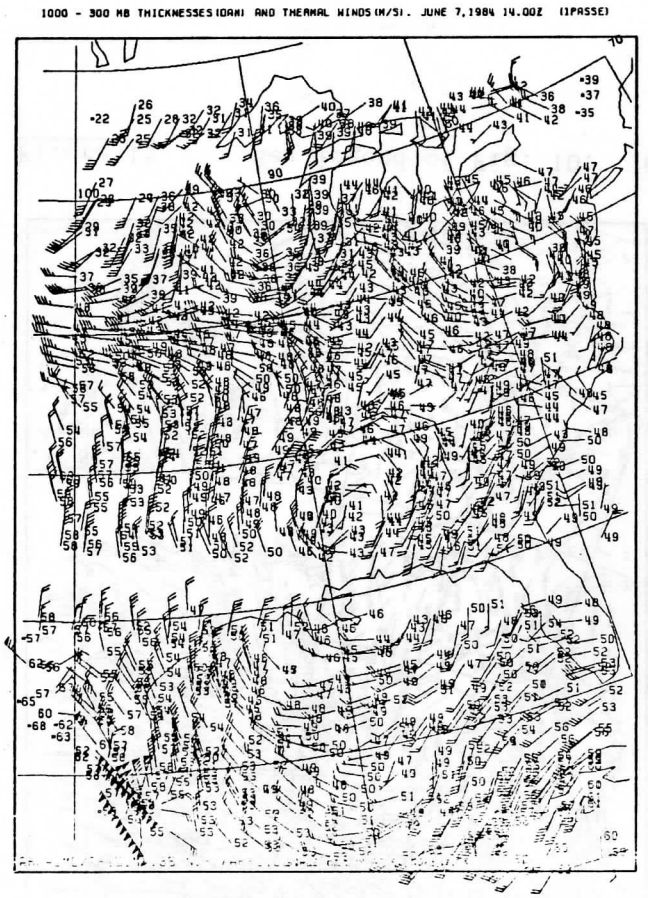

Figure 17 See legend of Fig. 10. 1000-300 mb.

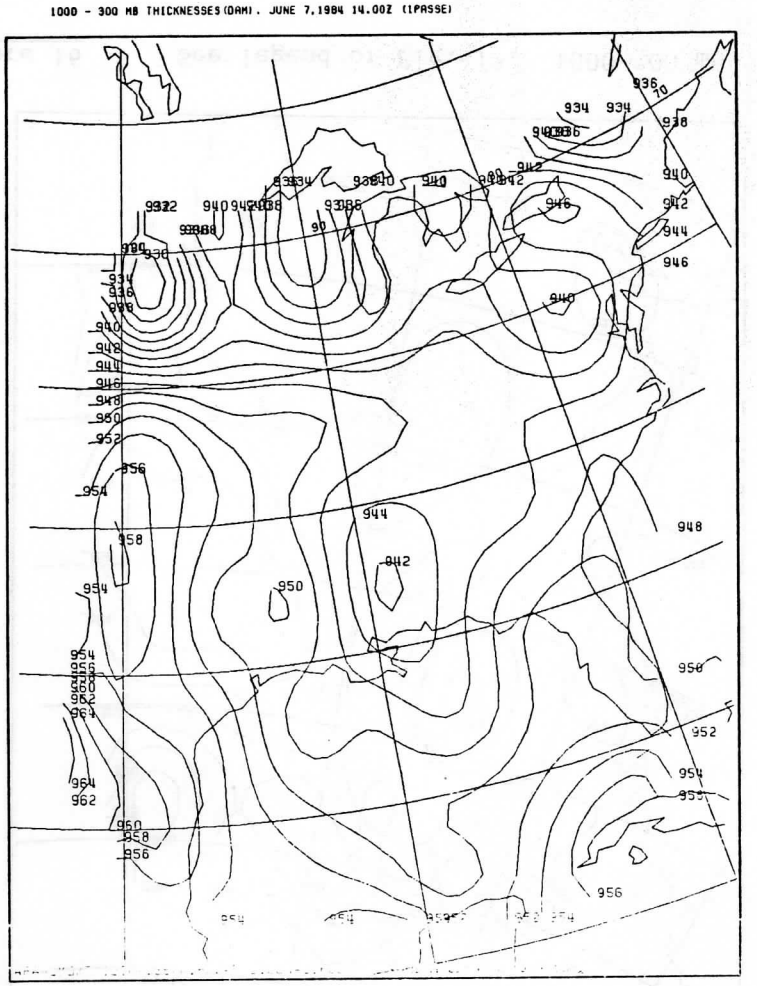

Figure 18 See legend of Fig. 12. 1000-300 mb.

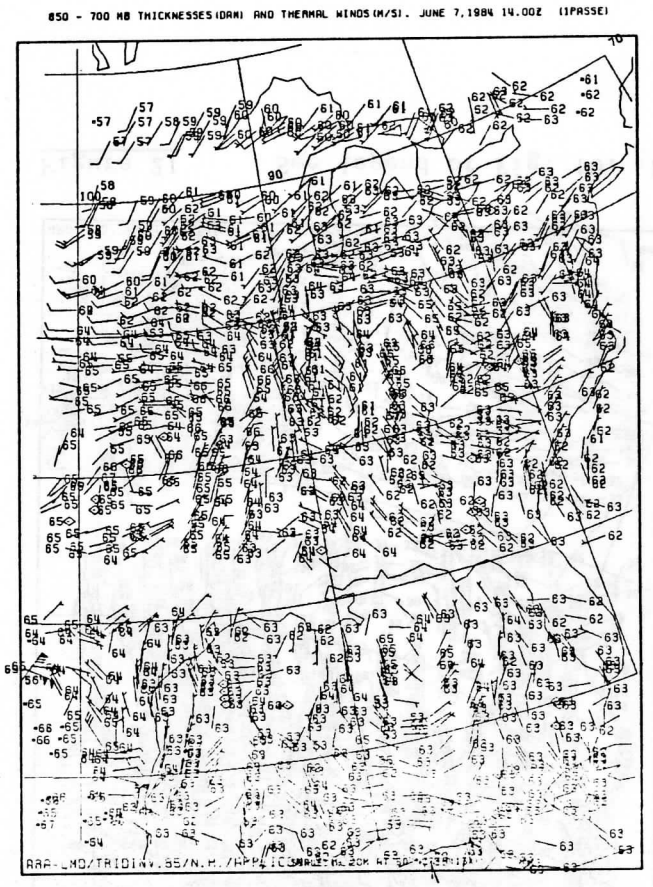

Figure 19 See legend of Fig. 10. 850-700 mb.

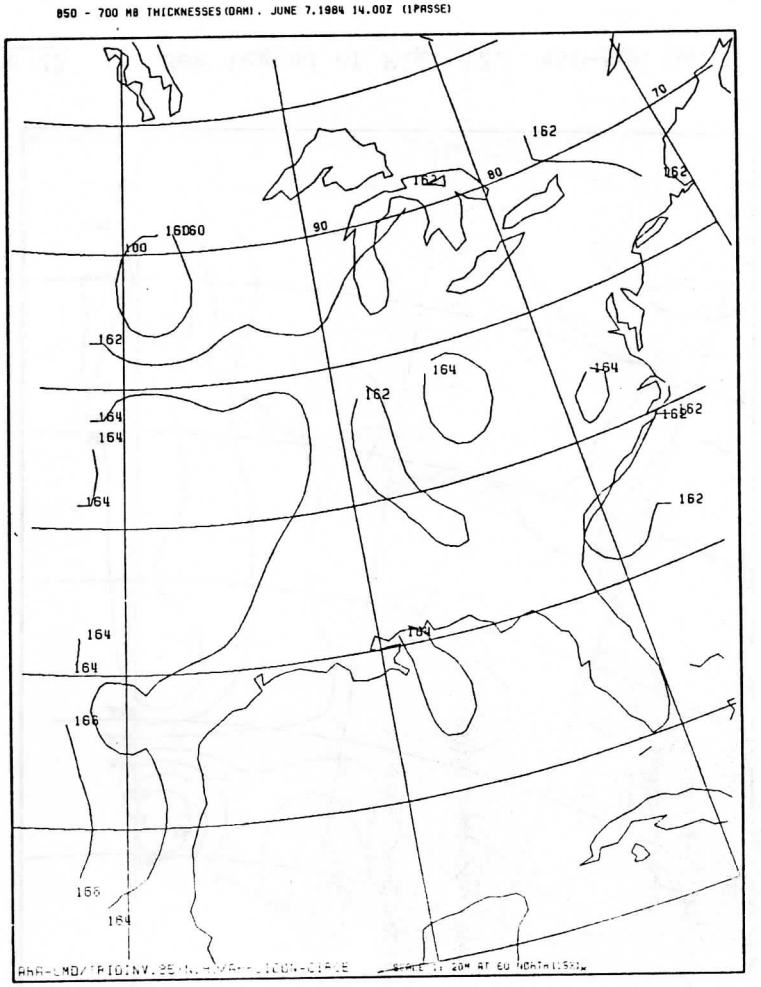

Figure 20 See legend of Fig. 12. 850-700 mb.

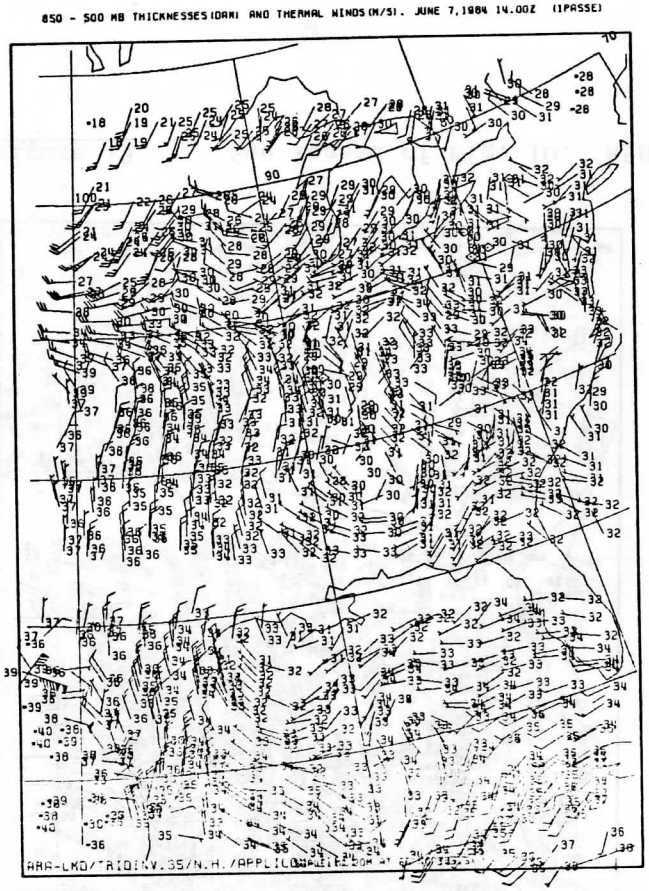

Figure 21 See legend of Fig. 10. 850-500 mb.

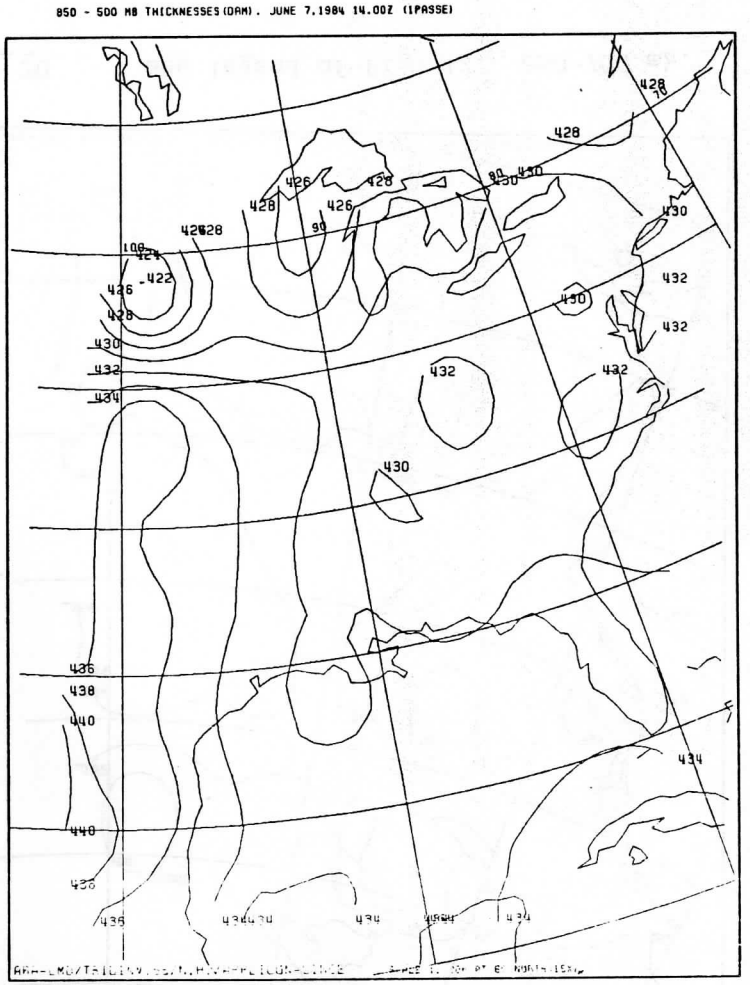

Figure 22 See legend of Fig. 12. 850-500 mb.

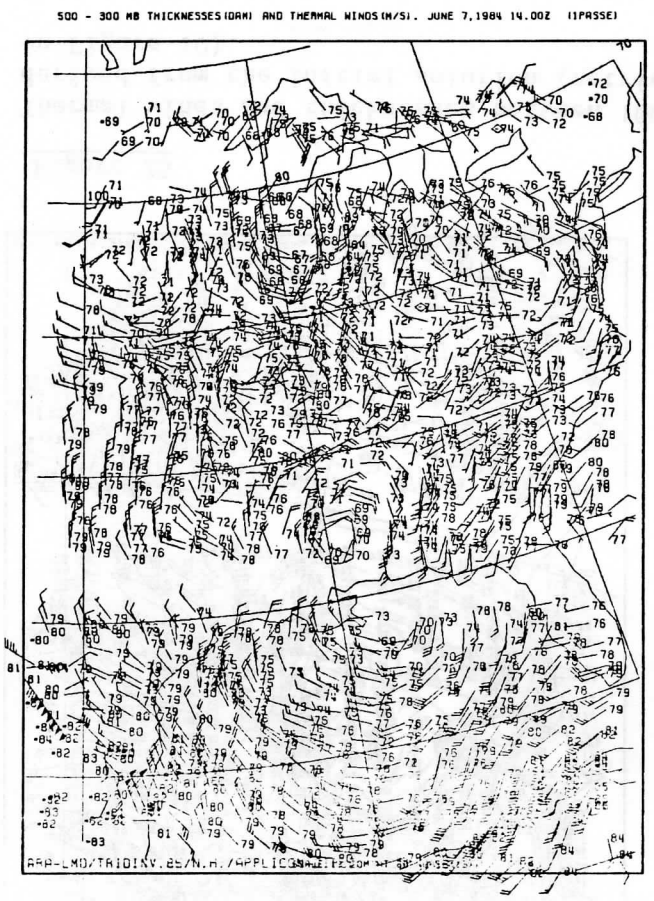

Figure 23 See legend of Fig. 10. 500-300 mb.

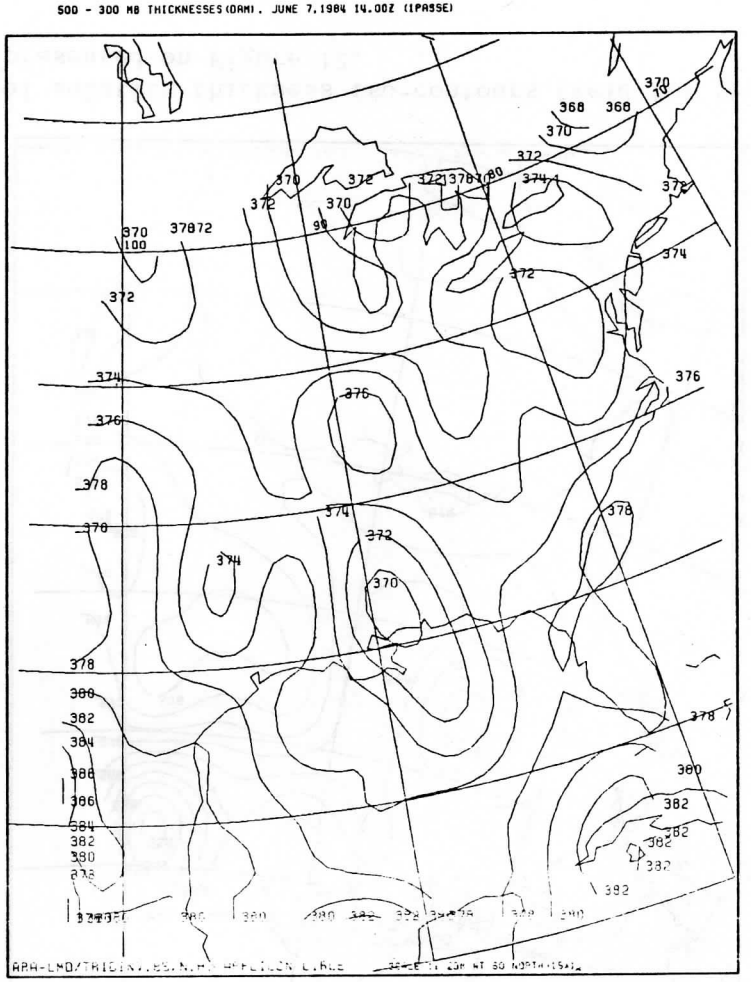

Figure 24 See legend of Fig. 12. 500-300 mb.

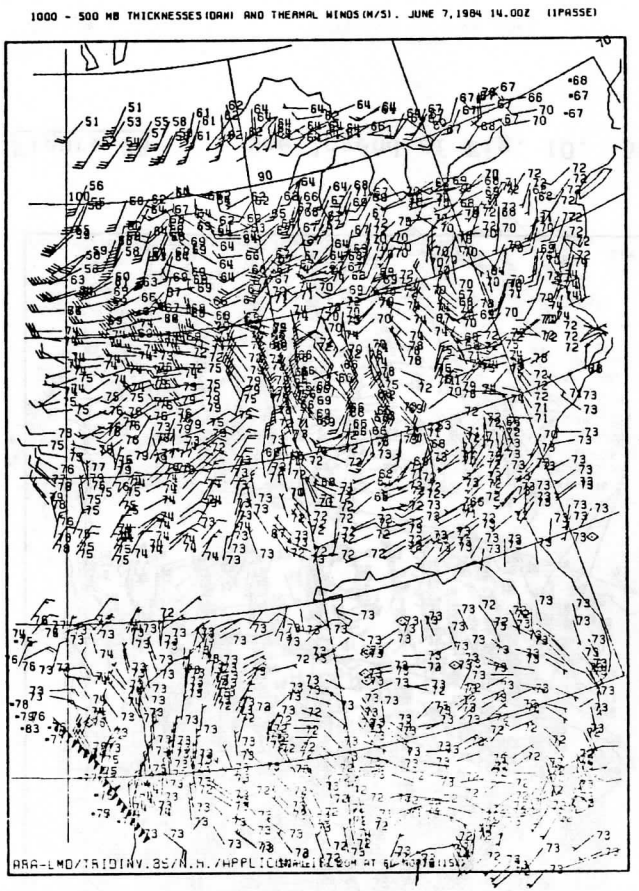

Figure 25

Thermal winds and thicknesses between 1000 and 500 mb derived from the initial solution (retrieved solution on Figure 10).

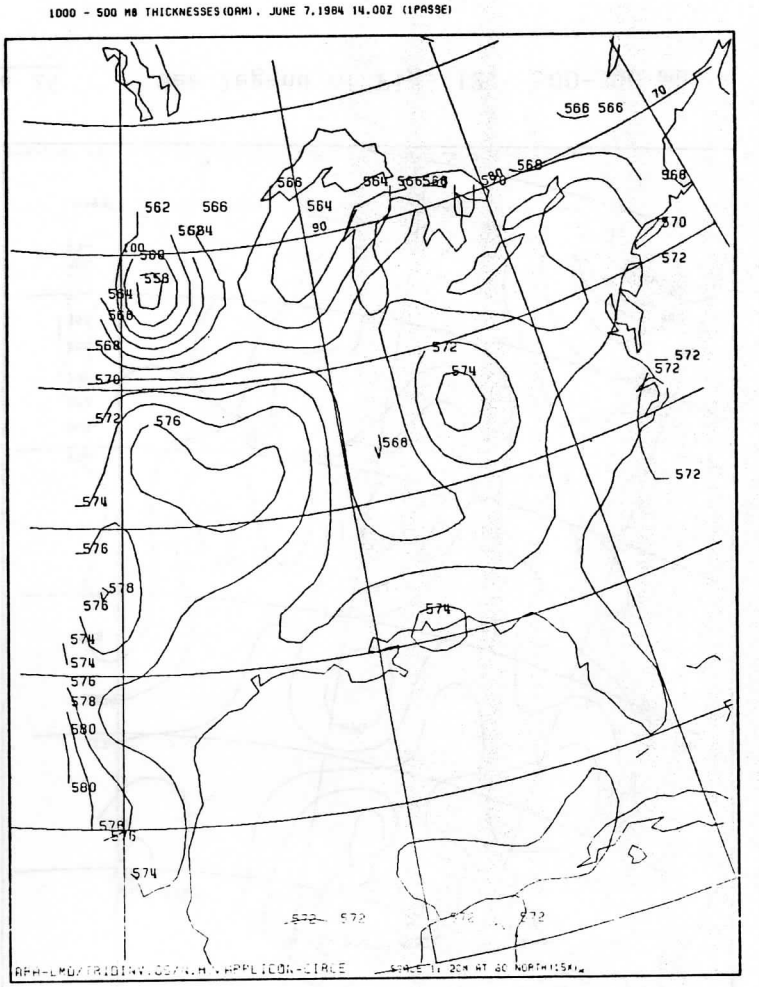

Figure 26

Initial solution thickness iso-contours field for the case presented on Figure 12.

5. CONCLUSION

For both the ALPEX case (NOAA-7) and the Central US overpass by NOAA-8, the 3I algorithm has demonstrated its capability to retrieve quite accurately large scale features as well as small scale events. The spatial resolution of the 3I method combined with a small number of rejections (bad retrievals) even for relatively cloudy situations lead to a high density of retrievals. The strong coupling of physics and statistics, from an "educated" data set - the "TIGR" data set -, ensures a good spatial coherence.

The next step, recently started, will consist in merging as far as possible the AVHRR data, currently processed by the CMS Lannion, to the TOVS data,resulting for clear and partly cloudy areas,in an important improvement in the spatial resolution. This is the principal aim of the "4I" method : Improved Initialization Inversion with Imagery.

REFERENCES

Chedin, A., N.A. Scott, 1984 : Improved Initialization Inversion Procedure. Proc. of the 1st Int. TOVS Study Conference. Igls, Austria. August 1983. A report from the CIMSS, Ed. P. Menzel, p.14-79.

Chedin, A., N.A. Scott, 1985 : Initialization of the radiative transfer equation inversion problem from a pattern recognition type approach. Applications to the satellites of the TIROS-N series. Advances in Remote Sensing Retrieval Methods, Academic Press, A. Deepak Ed. To be published.

Chedin, A., N.A. Scott, C. Wahiche, P. Moulinier, 1985 : The Improved Initialization Inversion method : a high resolution physical method for temperature retrievals from the TIROS-N series. Accepted to J. Clim. Appl. Meteor.

Scott, N.A., and A. Chedin, 1981 : A fast line-by-line method for atmospheric absorption computations : the Automatized Atmospheric Absorption Atlas. J. Appl. Meteor. 20, 802-812.

Scott, N.A., A. Chedin, E. Devedeux, C. Wahiche, N. Husson and I. Cohen-Hallaleh, 1984b : Validation of a fast line-by-line transmittance and radiance algorithm against observations from the satellites of the TIROS-N series. Intern. Radiat. Symp., August 21-29, Perugia, Italy. To be published by Academic Press, A. Deepak Ed.

Scott, N.A., A. Chedin, C. Wahiche, P. Moulinier, 1984a : Geopotential thicknesses and thermal winds retrieved from the satellites of the TIROS-N series through the "3I" method. Intern. Radiat. Symp., August 21-29, Perugia, Italy. To be published by Academic Press, A. Deepak Ed.

Smith, W.L., 1968 : An improved method for calculating tropospheric temperature and moisture from satellite radiometer measurements. Mon. Wea. Rev. 96, 387-396.

Wahiche, C., 1984 : Contribution au problème de la détermination de paramètres météorologiques à partir des données fournies par les satellites de la série TIROS-N. Impact de la couverture nuageuse. Thesis. Paris. November 1984. 207 pages.

Wahiche, C., N.A. Scott and A. Chedin, 1984 : Cloud parameters retrievals from the satellites of the TIROS-N series. Intern. Radiat. Symp., August 21-29, Perugia, Italy. To be published by Academic Press, A. Deepak Ed.

Wahiche, C., N.A. Scott and A. Chedin, 1985 : Cloud detection and cloud parameters retrieval from the satellites of the TIROS-N series. Submitted to Annales Geophysicae.

Yamamoto, G., M. Tanaka and S. Asano, 1970 : Radiative transfer in water clouds in the infrared region. J. Atmos. Sci. 27, 282-292.

DEVELOPMENTS OF A MESOSCALE ANALYSIS USING RAW SATELLITE DATA

Y. Durand and R. Juvanon du Vachat

Centre de Recherche en Meteorologie Dynamique
2 Avenue Rapp
75007 Paris
FRANCE

1. INTRODUCTION

A mesoscale analysis has been developed in the French Weather Service to provide the initial conditions for a short-range numerical weather prediction model over France (mesh size = 35 Km, PERIDOT project cf. R. Juvanon du Vachat, 1983). Since we lack of classical data in the upper layers of the atmosphere, we make use of TOVS data whose resolution is approximately the mesh size of the model and we insert them directly in the analysis, without retrieval procedures.

In the First TOVS Study Conference the humidity analysis was presented by Durand and Juvanon du Vachat (1983). So in this report we recall general principle used to insert directly radiances in the analysis with emphasis on temperature and wind fields. In the paragraph 4, we also report some results on tests on the impact of this satellite radiance information on the forecast fields.

2. ANALYSIS SCHEME

The analysis is directly performed on the prognostic variables of the forecast PERIDOT model : the horizontal wind, u, v, the temperature T, the surface pressure ps. In Fig. 1 we can see the horizontal domain, with a grid-mesh equal to 35 Km. In Fig. 2 is given the vertical structure with the 15 irregular σ-layers (σ = p/ps, ps pressure) with high resolution in the lower atmosphere.

The analysis scheme is a tridimensional optimum interpolation method which uses as first guess field a six-hour large scale forecast field interpolated in the PERIDOT fine-mesh grid.

It uses the following classical observations :

SYNOP, SHIP, DRIBU, TEMP (with characteristic levels), PILOT, AIREP, SATOB, and the following observed parameters : geopotential, temperature, wind.

It also uses thermal wind deduced from TEMP observations, to prevent a separability between an analysis of wind field only performed with wind observations and an analysis of temperature only performed with temperature observations.

Concerning the satellite observations, it uses clear sky HIRS-2 radiances in the 19 channels. The clear sky radiances are discriminated (i) by using AVHRR information (Esther data bank provided by CMS/Lannion, see Phulpin et al. (1983)), or if not available (ii) by comparison of radiances in different channels, in adjacent pixels, and a comparison between radiances in the window channels (8, 18, 19) and forecast surface temperature. If the radiance is suspected to be cloudy, it is rejected.

3. STATISTICAL MODEL

The analysis is performed by using the multivariate optimum interpolation method, whose principle is briefly recalled.

A first guess field X^f (provided by a large-scale forecast valid at the hour of the analysis) is modified by a linear combination of residuals (observed fields X^o minus forecast fields X^f) so the analysed field at the grid point k is :

$$X_k^a = X_k^f + \sum_{i=1}^{n} \lambda_i (X_i^o - X_i^f)$$

and the λ_i are solutions of the equations that minimize the analysis error variance. We notice that the field appearing under the summation needs not to be the same as the analysed one. In particular even radiance data may be used to analyse wind and temperature field, provided one knows the forecast and observation error correlation between radiances in different channels and between radiances and wind and temperature. To evaluate radiance residuals we use the NOAA program (TOVS Export Package) which determines synthetic radiances from classical meteorological parameters. This is done in the following procedure.

We assume that all the statistics on εZ^f (= forecast error on the geopotential) and εr^f (r = mixing ratio) have been evaluated before. It allows to know the statistics on εT^f and εr^f, by using the hydrostatic law (Durand, 1983). Then we use a sample of 200 quality-controlled radiosonde observations which are representative of the area to be analysed. For each radiosonde observation we use the preceding NOAA program to compute the radiance from the observed profile : $(T^t, r^t) \longrightarrow R^t$ (t like true). By choosing a random set of 10 profiles in εT, εr which is in agreement with the preceding statistics on $\overline{\varepsilon Z^f \varepsilon Z^f}$, $\overline{\varepsilon Z^f \varepsilon r^f}$, $\overline{\varepsilon r^f \varepsilon r^f}$ by hydrostatic law, we get 10 erroneous profiles $T^e = T^t + \varepsilon T$, $r^e = r^t + \varepsilon r$, and 10 erroneous radiances with the NOAA program : $(T^e, r^e) \longrightarrow R^e$. This creates a set of 2000 radiance residuals : $R^e - R^t$ which is used to calculate all the required forecast error statistics $\overline{\varepsilon R^f \varepsilon R^f}$ $\overline{\varepsilon R^f \varepsilon T^f}$ and $\overline{\varepsilon R^f \varepsilon Z^f}$.

These statistics are given in the Tables 1, 2, 3. We report here the standard deviations of radiance forecast errors in the 19 channels (in °K) :

1.44, 1.65, 1.41, 1.05, 1.02, 1.37, 3.27,
8.70, 0.32, 6.54, 2.84, 3.96, 5.28, 2.64,
1.00, 1.07, 1.52, 9.33, 9.11.

The whole statistical model of this analysis mainly based on the geopotential field and separability (horizontal, vertical) hypotheses (see Appendix 1). From statistics on the geopotential forecast error we get statistics on temperature forecast error, by using the hydrostatic law, statistics on wind forecast error, by using the geostrophic law, and statistics on thermal wind forecast error by using the classical relation. From this basis statistical model, all correlations involving wind, temperature, or thermal wind, together with radiances can be deduced with a little algebra.

For example the following error correlations between quantities defined in the points 1 and 3 (cf. Sketch) are computed as :

$$\text{Corr}(\varepsilon_{R_1}, \varepsilon_{x_3}) = \text{Corr}(\varepsilon_{R_1}, \varepsilon_{Z_2}) \times \text{Corr}(\varepsilon_{Z_2}, \varepsilon_{x_3})$$

with x being the geopotential or the horizontal wind components.
Similarly we have :

$$\text{Corr}(\varepsilon_{R_1}, \varepsilon_{y_3}) = \text{Corr}(\varepsilon_{R_1}, \varepsilon_{T_2}) \times \text{Corr}(\varepsilon_{Z_2}, \varepsilon_{y_3})$$

with y being the temperature or the thermal wind components.

So we only need to know the additionnal correlations involving radiances :

$$\text{Corr}\left(\varepsilon_{R_1^f}, \varepsilon_{Z_2^f}\right) \text{ and } \text{Corr}\left(\varepsilon_{R_1^f}, \varepsilon_{T_2^f}\right)$$

for 19 channels and some isobaric levels.

The full covariance forecast error matrix is given in the Appendix 2.

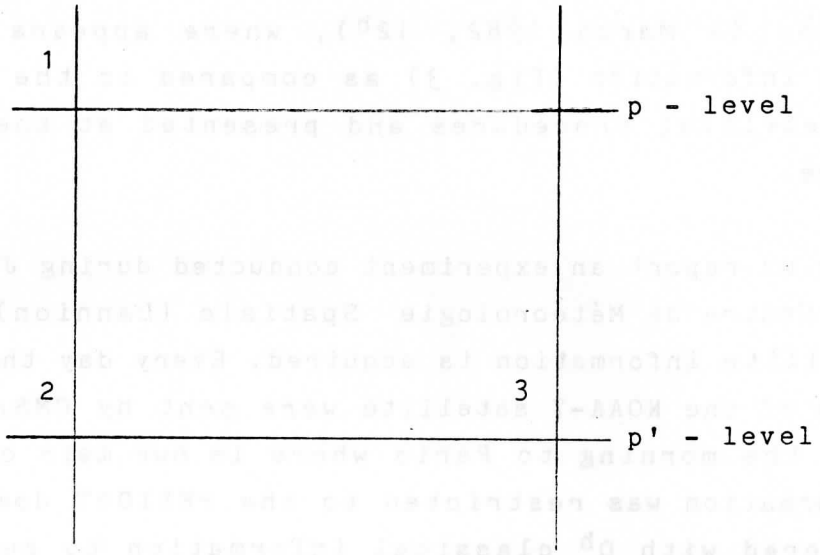

The evaluation of the radiance observational error statistics is made by using a sample of collocated radiance and radiosonding. The observation error variances are (in $(°K)^2$)

0.3 0.4 0.2 0.1 0.1 0.4 0.3 10. 200.
10. 1.5 2. 10. 1.5 1. 1. 5. 10.
10.

The horizontal distances where the correlation between radiance observation errors drops to 0, are (in km) :

1000. 1000. 1000. 800. 700. 500. 500. 600.
600. 700. 800. 800. 500. 600. 600. 700.
1200. 600. 600.

The full covariance matrix of radiance observations errors for the 19 HIRS-2 channels is given in Table 4.

4. RESULTS

As a complement for TOVS-1 proceedings, we present the 1000-500 mbar thicknesses produced by this analysis on the Alpex Case (4 March 1982, 12^h), where appears a very fine-mesh information (Fig. 3) as compared to the results got by retrieval procedures and presented at the TOVS-1 Conference.

Then we report an experiment conducted during June 1984 with the Centre de Météorologie Spatiale (Lannion), where the satellite information is acquired. Every day the HIRS-2 radiances of the NOAA-7 satellite were sent by CMS/Lannion early in the morning to Paris where is our main computer. This information was restricted to the PERIDOT domain and was gathered with 0^h classical information to get the 0^h fine-mesh analysis.

Our objective was twofold :

1) to compare the fine-mesh analysis without(A) and with (B) the satellite information (11 cases).

2) to run the forecast model and compare the predicted fields when the initial state is defined by A or B (4 cases).
We notice that only clear-sky radiances were inserted in the analysis, discriminated by (ii) procedure (cf. 2 §).

Concerning the objective 1, many local differences are observed on the temperature field, the order of magnitude of these differences is about 1°C, with a maximum difference of 2 or 3°C. It is difficult to say which analysis is the best, due to the lack of reference observation at this scale (35 km). On the Table 5 the horizontally averaged temperature difference in the 15 vertical levels is reported. A positive bias appears on the mean error.

We don't notice any significant differences on the wind analysis, which seems to indicate that radiance data have no impact on the wind field, probably due to the fact that the analysis scheme is not enough multivariate.

The relative humidity analysis with satellite data has more details especially above 700 mbar, with differences often larger than 10 %. The Figure 4 shows the humidity analysis at 500 and 850 mbar with (B) or without satellite data (A). By comparing A and B, we notice a change in the isoline pattern near Britanny (see 70, 80 isolines at 500 mbar and 90 at 850 mbar), and the Figure B appears coherent with the clear-cloudy contrast observed on the NOAA-7 picture.

Concerning the objective 2, we have observed a positive impact on precipitation forecasts over the Center of France in two cases (5, 6 June 1984). See the Figure 5 for the case 5 June 1984. This impact indeed is small but has been verified by SYNOP Stations observing showers. On the 7 June case, some differences are observed on the cloudiness and precipitation forecast maps, but it is impossible to say which forecast is the best one. And on the 13 June case no significant impact is found on any map : this could be due to the meteorological situation which corresponds to a fine weather without any precipitation on the model area.

The impact of satellite data on fine-mesh forecasts is limited to the following meteorological fields : cloudiness, precipitation, humidity and surface fields. No significant impact has been found on upper-air mass and wind fields.

In summary the impact of radiance data on the forecast fields appears small but significant. But these results only are preliminary since the whole PERIDOT forecast system was not completely tuned at the time of these experiences.

5. FUTURE

We now are preparing a new experiment with NOAA-9 Satellite data along the same principle as the preceding one (June 1984). The CMS/Lannion will send each day HIRS-2 radiances data acquired from the early morning passes of NOAA-9, that will be used for the 0^h analysis. Since supplementary information related to nebulosity (deduced from 11μm AVHRR channel) will also be sent simultaneoulsy so that we will use cloudy radiances as well as clear sky ones in the analysis scheme.

We are happy to acknowledge people from CMS/Lannion who makes possible the June 1984 experiment, reported in this paper. Patricia Audouard is acknowledged for expertly typing this manuscript.

6. REFERENCES

Durand Y., Juvanon du Vachat R., 1983 : Mesoscale Analysis using satellite information. Technical Proceedings of the First International Conference (Igls, September 1983) - p. 80-93.

Durand Y., 1983 : Développement d'un système d'analyse fine sur domaine limité. Internal Report available EERM/CRMD.

Juvanon du Vachat R. et al., 1983 : Fine-mesh numerical weather prediction over France. Proceedings of Sixth AMS Conference on Numerical Weather Prediction (OMAHA) p 57-61.

Phulpin T., Brard A., Derrien M., 1983 : Determination of clear HIRS-2 pixels and clear radiances retrieval by using AVHRR. Technical Proceedings of the First International TOVS Study Conference (Igls, September 1983) - p. 173-183.

APPENDIX 1 : Details of the analysis scheme

The statistical interpolation method is used for two main reasons :

- to construct a fully 3 dimensional analysis scheme which can directly produce analysed deviation fields on σ-levels of the forecast model.
- to make use of many different kinds of observations with differents characteristics (radiances...)

The interpolation is linear in terms of the deviation from a first guess

$$X_k^a = X_k^g + \sum_{i=1}^{n} \lambda_i \left(Y_i^o - Y_i^g \right)$$

(n observations are used)

The subscript : a means : analysed
g means : guess (denoted f = forecast in the text)
o means : observed

Quantities X may be T (temperature), U, V (wind components)

Each Y_i may be (with different i), Z (geopotential), T, U, V
DU, DV (thermal wind components)
R (radiances in 19 HIRS-2 channels)

By adding and substracting the true (and unknown) quantities X_k^t in analysis equation we obtain an equation in terms of error :

$$\varepsilon X_k^a = X_k^a - X_k^t$$

εX_k^a is the analysis error of the field X at point k.

We also have εX_k^g , εY_i^o , εY_i^g , such that

$$\varepsilon X_k^a = \varepsilon X_k^g + \sum_{i=1}^{n} \lambda_i \left(\varepsilon Y_i^o - \varepsilon Y_i^g \right)$$

The basic assumption is that εY^g and εX^g are realisations of random functions and we have to know some of their statistical characteristics (general law, bias, covariance). εY^c are random variable.

In our model we only assume an hypothesis of stationarity, homogeneity and isotropy for the geopotential correlation.

$$\mathrm{corr}\left(\varepsilon Z_i^g, \varepsilon Z_j^g\right)$$

i, j are two arbitrary points in space

we must also know $\overline{\varepsilon Z_i^{g\,2}}$ = variance of guess error in geopotential,

Optimal weights (λ_i) are found under the two conditions :

- $\overline{\varepsilon Z_k^a}$, bias of analysis error equals to zero
- $\overline{\varepsilon Z_k^{a\,2}}$, variance of analysis error minimum.

The second condition leads to solve a linear system which generic line is (with some assumptions about errors)

$$\sum_{i=1}^{n} \lambda_i \left(\overline{\varepsilon Y_i^g \varepsilon Y_j^g} + \overline{\varepsilon Y_i^c \varepsilon Y_j^c} \right) = \overline{\varepsilon X_k^g \varepsilon Y_j^g}$$

For j = 1... n

Linear equation as hydrostatic law or geostrophic law allows a simple estimation of covariances between εZg, εTg, εUg, εVg, εDUg, εDVg.

APPENDIX 2: The full covariance forecast error matrix.

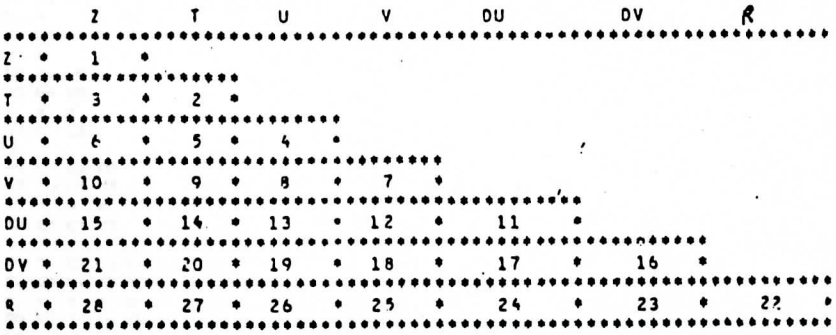

① $\overline{\varepsilon Z_1^a \varepsilon Z_3^a} = \sqrt{\overline{\varepsilon Z_1^{a2}}\ \overline{\varepsilon Z_3^{a2}}}\ c^h Z_1 Z_2\ c^v Z_2 Z_3$

② $\overline{\varepsilon T_1^a \varepsilon T_3^a} = \sqrt{\overline{\varepsilon T_1^{a2}}\ \overline{\varepsilon T_3^{a2}}}\ c^h Z_1 Z_2\ c^v T_2 T_3$

③ $\overline{\varepsilon T_1^a \varepsilon Z_3^a} = \sqrt{\overline{\varepsilon T_1^{a2}}\ \overline{\varepsilon Z_3^{a2}}}\ c^h Z_1 Z_2\ c^v T_2 Z_3$

④ $\overline{\varepsilon U_1^a \varepsilon U_3^a} = \sqrt{\overline{\varepsilon U_1^{a2}}\ \overline{\varepsilon U_3^{a2}}}\ c^h U_1 U_2\ c^v Z_2 Z_3$

⑤ $\overline{\varepsilon U_1^a \varepsilon T_3^a} = \sqrt{\overline{\varepsilon U_1^2}\ \overline{\varepsilon T_3^2}}\ c^h U_1 Z_2\ c^v Z_2 T_3$ α

⑥ $\overline{\varepsilon U_1^a \varepsilon Z_3^a} = \sqrt{\overline{\varepsilon U_1^2}\ \overline{\varepsilon Z_3^2}}\ c^h U_1 Z_2\ c^v Z_2 Z_3$ α

⑦ $\overline{\varepsilon V_1^a \varepsilon V_3^a} = \sqrt{\overline{\varepsilon V_1^{a2}}\ \overline{\varepsilon V_3^{a2}}}\ c^h V_1 V_2\ c^v Z_2 Z_3$

⑧ $\overline{\varepsilon V_1^a \varepsilon U_3^a} = \sqrt{\overline{\varepsilon V_1^{a2}}\ \overline{\varepsilon U_3^{a2}}}\ c^h V_1 U_2\ c^v Z_2 Z_3$ β

⑨ $\overline{\varepsilon V_1^a \varepsilon T_3^a} = \sqrt{\overline{\varepsilon V_1^{a2}}\ \overline{\varepsilon T_3^{a2}}}\ c^h V_1 Z_2\ c^v Z_2 T_3$ α

⑩ $\overline{\varepsilon V_1^a \varepsilon Z_3^a} = \sqrt{\overline{\varepsilon V_1^{a2}}\ \overline{\varepsilon Z_3^{a2}}}\ c^h V_1 Z_2\ c^v Z_2 Z_3$ α

⑪ $\overline{\varepsilon DU_1 \varepsilon DU_3} = \sqrt{\overline{\varepsilon DU_1^2}\ \overline{\varepsilon DU_3^2}}\ c^h U_1 U_2\ c^v T_2 T_3$

⑫ $\overline{\varepsilon DU_1 \varepsilon V_3} = \sqrt{\overline{\varepsilon DU_1^2}\ \overline{\varepsilon V_3^2}}\ c^h U_1 V_2\ c^v T_2 Z_3$ β

⑬ $\overline{\varepsilon DU_1 \varepsilon U_3} = \sqrt{\overline{\varepsilon DU_1^2}\ \overline{\varepsilon U_3^2}}\ c^h U_1 U_2\ c^v T_2 Z_3$

⑭ $\overline{\varepsilon DU_1 \varepsilon T_3} = \sqrt{\overline{\varepsilon DU_1^2}\ \overline{\varepsilon T_3^2}}\ c^h U_1 Z_2\ c^v T_2 T_3$ α

⑮ $\overline{\varepsilon DU_1 \varepsilon Z_3} = \sqrt{\overline{\varepsilon DU_1^2}\ \overline{\varepsilon Z_3^2}}\ c^h U_1 Z_2\ c^v T_2 Z_3$ α

⑯ $\overline{\varepsilon DV_1 \varepsilon DV_3} = \sqrt{\overline{\varepsilon DV_1^2}\ \overline{\varepsilon DV_3^2}}\ c^h V_1 V_2\ c^v T_2 T_3$

⑰ $\overline{\varepsilon DV_1 \varepsilon DU_3} = \sqrt{\overline{\varepsilon DV_1^2}\ \overline{\varepsilon DU_3^2}}\ c^h V_1 U_2\ c^v T_2 T_3$ β

⑱ $\overline{\varepsilon DV_1 \varepsilon V_3} = \sqrt{\overline{\varepsilon DV_1^2}\ \overline{\varepsilon V_3^2}}\ c^h V_1 V_2\ c^v T_2 Z_3$

⑲ $\overline{\varepsilon DV_1 \varepsilon U_3} = \sqrt{\overline{\varepsilon DV_1^2}\ \overline{\varepsilon U_3^2}}\ c^h V_1 U_2\ c^v T_2 Z_3$ β

⑳ $\overline{\varepsilon DV_1 \varepsilon T_3} = \sqrt{\overline{\varepsilon DV_1^2}\ \overline{\varepsilon T_3^2}}\ c^h V_1 Z_2\ c^v T_2 T_3$ α

㉑ $\overline{\varepsilon DV_1 \varepsilon Z_3} = \sqrt{\overline{\varepsilon DV_1^2}\ \overline{\varepsilon Z_3^2}}\ c^h V_1 Z_2\ c^v T_2 Z_3$ α

㉒ $\overline{\varepsilon R_1 \varepsilon R_2} = \sqrt{\overline{\varepsilon R_1^2}\ \overline{\varepsilon R_2^2}}\ c^h T_1 T_2\ (= c^h Z_1 Z_2)$

㉓ $\overline{\varepsilon R_1 \varepsilon DV_3} = \sqrt{\overline{\varepsilon R_1^2}\ \overline{\varepsilon DV_3^2}}\ \mathrm{con}(\varepsilon R_1 \varepsilon T_2)\ c^h Z_2 V_3$ α

㉔ $\overline{\varepsilon R_1 \varepsilon DU_3} = \sqrt{\overline{\varepsilon R_1^2}\ \overline{\varepsilon DU_3^2}}\ \ \ c^h Z_2 U_3$ α

㉕ $\overline{\varepsilon R_2 \varepsilon V_3} = \sqrt{\overline{\varepsilon R_2^2}\ \overline{\varepsilon V_3^2}}\ \mathrm{con}(\varepsilon R_1 \varepsilon Z_2)\ c^h Z_2 V_3$ α

㉖ $\overline{\varepsilon R_1 \varepsilon U_3} = \sqrt{\overline{\varepsilon R_1^2}\ \overline{\varepsilon U_3^2}}\ \ \ c^h Z_2 U_3$ α β

㉗ $\overline{\varepsilon R_1 \varepsilon T_3} = \sqrt{\overline{\varepsilon R_1^2}\ \overline{\varepsilon T_3^2}}\ \mathrm{con}(\varepsilon R_1 \varepsilon T_2)\ c^h Z_2 Z_3$

㉘ $\overline{\varepsilon R_1 \varepsilon Z_3} = \sqrt{\overline{\varepsilon R_1^2}\ \overline{\varepsilon Z_3^2}}\ \mathrm{con}(\varepsilon R_1 \varepsilon Z_2)\ c^h Z_2 Z_3$

α = Corr (εZi, εTi)
β = damping coefficient in low levels
C^h means horizontal correlation
C^v means vertical correlation
Subscripts 1,2 mean at the same isobaric level
Subscripts 2,3 mean at the same vertical axis

2.08																		
2.26	2.72																	
1.95	2.27	1.98																
0.87	0.90	0.86	0.56															
0.46	0.43	0.38	0.31	0.52														
0.16	0.09	0.00	0.13	0.86	1.89													
-0.09	-0.11	0.00	0.00	1.70	4.31	10.68												
-0.63	-0.57	0.00	0.00	3.89	10.64	27.57	75.63											
-0.02	-0.02	0.00	0.00	0.13	0.37	0.96	2.72	0.10										
-0.47	-0.32	0.00	0.00	3.06	8.27	20.94	56.29	2.03	42.75									
0.12	0.00	0.00	0.32	0.88	1.64	2.97	4.70	0.14	4.65	8.09								
-0.17	-0.33	0.00	0.47	0.68	1.09	1.81	2.06	0.06	2.59	9.79	15.65							
-0.38	-0.35	0.00	0.00	2.47	6.60	16.91	45.45	1.64	34.17	3.00	1.25	27.87						
-0.11	-0.22	0.00	0.00	1.39	3.45	8.36	22.25	0.79	16.90	1.80	0.83	13.79	6.96					
0.17	0.04	0.00	0.22	0.58	1.07	2.22	5.45	0.19	4.16	0.70	0.42	3.50	1.93	0.78				
1.02	0.95	0.98	0.68	0.34	0.09	-0.21	-0.73	-0.02	-0.55	0.08	0.18	-0.44	-0.10	0.26	0.87			
1.82	1.55	1.56	0.87	0.47	0.23	0.35	-0.53	-0.02	-0.30	0.26	-0.06	-0.32	0.04	0.33	1.16	2.30		
-0.67	0.15	0.00	0.00	4.04	11.03	28.66	77.09	2.80	57.96	4.25	1.85	48.77	23.63	5.77	-0.78	-0.57	87.06	
-0.66	0.15	0.00	0.00	4.01	10.89	26.28	75.25	2.74	56.57	4.66	2.16	47.60	23.31	5.71	-0.76	-0.55	80.73	82.95
1	2	3	4	5	6	7	8	9	10	11	12	13	14	15	16	17	18	19

Table 1: Covariance matrix of radiance forecast errors for the 19 HIRS-2 channels.

mbar	1	2	3	4	5	6	7	8	9	10	11	12	13	14	15	16	17	18	19
1000	0.1000	.1200	.1100	.040-	.100-	.280-	.320-	.320-	.310-	.320-	.150-	.070-	.320-	.320-	.2000	.0100	.020-	.310-	.310
850	0.0000	.0200	.0300	.0300	.2400	.4700	.5100	.5100	.5100	.5100	.2200	.1000	.5300	.5300	.3300	.020-	.0100	.5100	.510
700	0.0900	.0600	.0600	.0800	.2400	.2900	.1900	.0900	.0900	.1100	.1900	.1000	.1500	.2500	.3500	.0700	.2000	.1000	.090
500	0.1100	.0600	.0400	.0400	.1900	.2200	.1200	.0500	.0500	.0700	.1900	.1500	.1000	.1800	.2700	.0300	.2300	.0500	.050
400	0.0900	.0800	.0700	.2200	.4000	.3600	.1300	.0200	.0200	.0400	.2100	.1700	.0900	.2500	.5900	.1700	.0700	.0300	.020
300	0.0900	.0700	.0600	.1800	.2900	.2200	.0600	.0000	.0100	.0100	.0300	.0300	.0600	.1800	.4300	.1600	.0800	.0200	.010
250	0.1500	.0700	.0800	.2800	.3300	.2600	.1000	.0600	.0700	.0700	.0900	.1100	.1000	.2300	.4900	.3300	.3200	.0800	.070
200	0.050-	.0100	.0200	.2200	.2800	.2700	.1400	.1100	.1200	.1200	.1300	.1500	.1500	.2600	.4500	.2800	.2300	.1300	.120
150	0.1200	.0900	.1400	.3300	.3700	.3200	.1900	.1500	.1500	.1600	.1300	.1000	.1700	.2600	.4600	.3800	.2400	.1500	.150
100	-.240-	.290-	.230-	.0300	.0300	.1600	.1400	.1300	.1300	.1400	.1100	.1200	.1500	.2100	.2900	.0900	.1500	.1300	.130
50	0.5000	.4800	.5300	.6100	.5200	.2800	.0900	.0500	.0500	.050-	.020-	.0100	.0700	.1500	.4100	.6100	.5600	.0600	.050

(HIRS-2 Channel No.)

Table 2: Forecast error correlation between goepotential (at standard levels) and HIRS-2 radiance (in the 19 channels).

mbar	1	2	3	4	5	6	7	8	9	10	11	12	13	14	15	16	17	18	19
1000	-.020	-.040	-.0500	.0600	.3500	.5800	.8000	.8000	.2500	.7900	.1900	.0400	.6600	.7000	.4000	.0100	.0000	.8000	.800
850	0.0100	.000-	.0200	.1500	.4500	.8000	.6500	.2900	.2000	.3300	.100-	.0200	.5200	.6000	.6500	.1500	.0100	.3600	.310
700	0.2500	.0900	.1000	.3000	.6000	.6500	.4400	.1900	.1500	.2700	.2200	.0500	.3800	.5500	.8000	.3000	.3800	.2300	.200
500	0.0500	.0200	.2000	.6000	.8500	.4400	.2500	.0700	.0800	.1000	.1200	.0900	.2200	.4000	.6000	.5500	.0800	.1200	.080
400	0.1200	.0600	.3000	.8500	.7000	.3600	.1700	.0600	.0700	.0800	.0900	.1000	.1400	.3100	.4900	.8000	.1700	.0900	.070
300	0.2200	.1000	.4000	.7000	.4500	.1500	.0300	.0600	.0700	.0500	.0100	.0400	.0500	.1400	.2600	.6500	.3200	.0700	.060
250	0.1600	.0700	.5500	.6000	.3000	.0800	.0000	.0600	.0700	.0500	.0300	.0800	.0200	.0800	.1500	.4700	.2500	.0600	.060
200	0.1800	.1200	.6500	.3500	.200-	.010-	.060-	.020-	.020-	.030-	.0100	.020-	.070-	.0400	.0400	.4000	.250-	.030-	.020
150	0.3000	.3200	.8000	.2000	.1000	.060-	.040-	.070-	.080-	.060-	.0200	.000-	.080-	.0300	.0900	.3000	.320-	.080-	.070
100	0.7800	.7700	.7200	.1000	.0500	.160-	.010-	.110-	.130-	.090-	.020-	.010-	.090-	.0200	.1900	.2000	.760-	.120-	.120
50	0.8000	.8000	.5000	.0500	.0300	.2200	.080-	.010-	.0100	.0000	.0000	.0000	.0000	.0500	.2000	.1000	.590-	.010-	.010

(HIRS-2 Channel No.)

Table 3: Forecast error correlation between temperature (at standard levels) and HIRS-2 radiance (in the 19 channels).

0.30	0.15	0.07	0.01	0.00	-0.01	-0.01	0.09	-0.08	0.03	-0.09	0.01	0.05	0.00	0.00	0.05	0.27	0.87	0.99
0.15	0.40	0.22	-0.03	-0.06	-0.12	-0.13	-0.58	-2.86	-0.30	-0.19	-0.25	-0.50	-0.20	-0.06	0.06	0.16	-0.36	-0.24
0.07	0.22	0.20	0.05	0.03	0.06	0.02	-0.10	1.01	0.38	0.16	0.11	0.27	0.13	0.03	0.10	-0.02	0.10	0.14
0.01	-0.03	0.05	0.10	0.10	0.20	0.16	0.66	4.34	0.90	0.36	0.42	0.94	0.38	0.10	0.09	-0.10	0.62	0.49
0.00	-0.06	0.03	0.10	0.10	0.20	0.17	0.73	4.43	0.91	0.36	0.43	0.96	0.38	0.10	0.08	-0.10	0.64	0.48
-0.01	-0.12	0.06	0.20	0.20	0.40	0.34	1.46	8.85	1.84	0.74	0.87	1.92	0.77	0.20	0.16	-0.21	1.26	0.94
-0.01	-0.13	0.02	0.16	0.17	0.34	0.30	1.45	7.67	1.63	0.60	0.74	1.70	0.66	0.17	0.12	-0.15	1.11	0.78
0.09	-0.58	-0.10	0.66	0.73	1.46	1.45	10.00	35.78	8.80	2.29	3.35	8.70	2.98	0.74	0.47	-0.29	5.70	3.00
-0.08	-2.86	1.01	4.34	4.43	8.85	7.67	35.78	200.00	42.04	15.76	19.00	43.83	17.15	4.43	3.44	-4.50	29.96	21.91
0.03	-0.30	0.38	0.90	0.91	1.84	1.63	8.80	42.04	10.00	3.29	3.98	9.80	3.68	0.92	0.76	-0.85	6.30	4.10
-0.09	-0.19	0.16	0.36	0.36	0.74	0.60	2.29	15.76	3.29	1.50	1.61	3.41	1.41	0.36	0.29	-0.48	1.74	1.28
0.01	-0.25	0.11	0.42	0.43	0.87	0.74	3.35	19.00	3.98	1.61	2.00	4.16	1.66	0.43	0.34	-0.33	2.41	1.65
0.05	-0.50	0.27	0.94	0.96	1.92	1.70	8.70	43.83	9.80	3.41	4.16	10.00	3.80	0.97	0.77	-0.87	6.80	4.80
0.00	-0.20	0.13	0.38	0.38	0.77	0.66	2.98	17.15	3.68	1.41	1.66	3.80	1.50	0.38	0.31	-0.39	2.52	1.86
0.00	-0.06	0.03	0.10	0.10	0.20	0.17	0.74	4.43	0.92	0.36	0.43	0.97	0.38	0.10	0.08	-0.10	0.66	0.50
0.05	0.06	0.10	0.09	0.08	0.16	0.12	0.47	3.44	0.76	0.29	0.34	0.77	0.31	0.08	0.10	-0.04	0.58	0.50
0.27	0.16	-0.02	-0.10	-0.10	-0.21	-0.15	-0.29	-4.50	-0.85	-0.48	-0.33	-0.87	-0.39	-0.10	-0.04	0.50	-0.04	0.09
0.87	-0.36	0.10	0.62	0.64	1.26	1.11	5.70	29.96	6.30	1.74	2.41	6.80	2.52	0.66	0.58	-0.04	10.00	9.50
0.99	-0.24	0.14	0.49	0.48	0.94	0.78	3.00	21.91	4.10	1.28	1.65	4.80	1.86	0.50	0.50	0.09	9.50	10.00

Table 4: Covariance Matrix of radiance observation errors for the 19 HIRS-2 channels.

Altitude	Mean (°)	σ	Min	Max
18 880	0.2	0.3	-0.7	1.5
12 060	-0.3	0.3	-1.5	0.9
8 975	0.5	0.7	-0.7	3.7
6 900	0.2	0.6	-2.1	2.7
5 345	0.4	0.7	-1.7	3.0
4 133	0.2	0.6	-1.6	2.6
3 161	0.1	0.5	-2.0	1.6
2 372	0.1	0.4	-1.8	1.8
1 730	0.3	0.5	-1.4	2.3
1 211	0.2	0.4	-1.1.	2.3
798	0.2	0.4	-0.6	2.3
479	0.1	0.3	-0.9	2.3
246	0.1	0.3	-1.2	2.0
94	0.2	0.4	-1.3	3.1
18	0.2	0.4	-1.3	3.1

Table 5 : Vertical structure of the horizontally averaged field = T(B) - T(A)
T(A) = Analysed temperature without satellite data
T(B) = Analysed temperature with satellite data.
Statistics on 4 cases in June 1984.

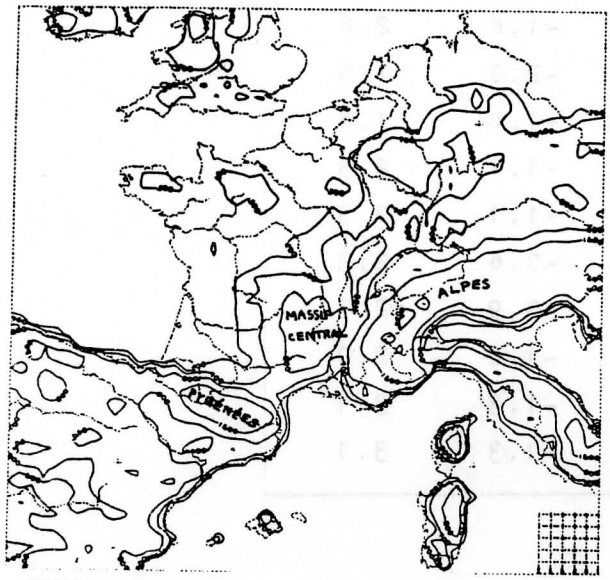

FIGURE 1 The domain and its topography with the grid-point ditribution (mesh-size 38 Kms)

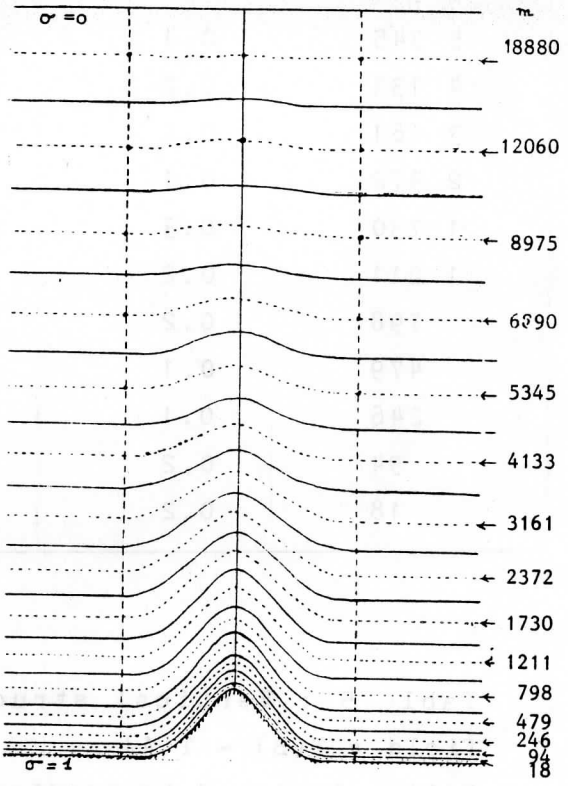

FTGURE 2 The vertical structure of the 15 layers,with the height of the middle σ-levels

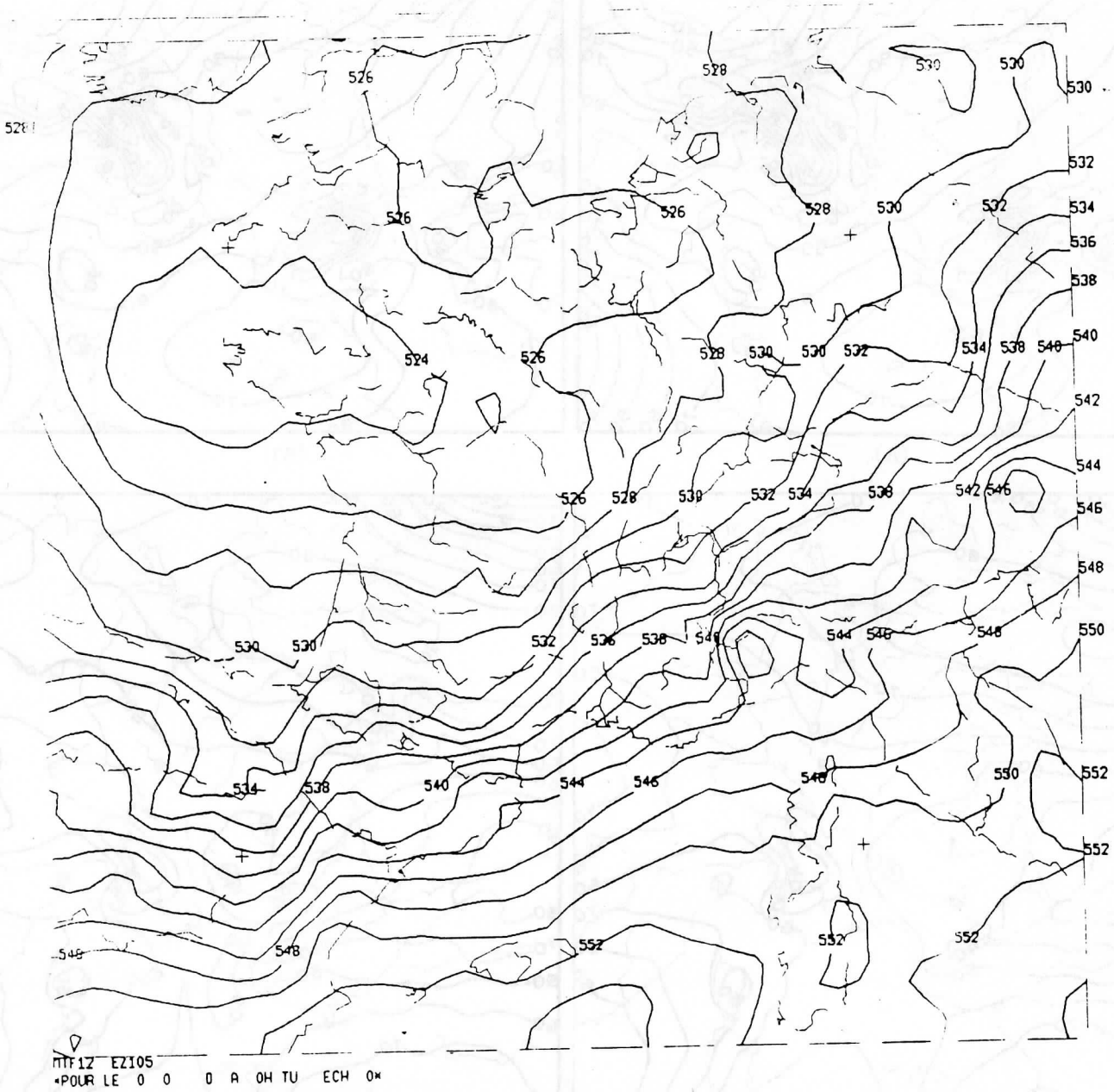

Figure 3: Thicknesses--↑000 - 500 mbar for the Alpex case (March 4, 1982, 12H).

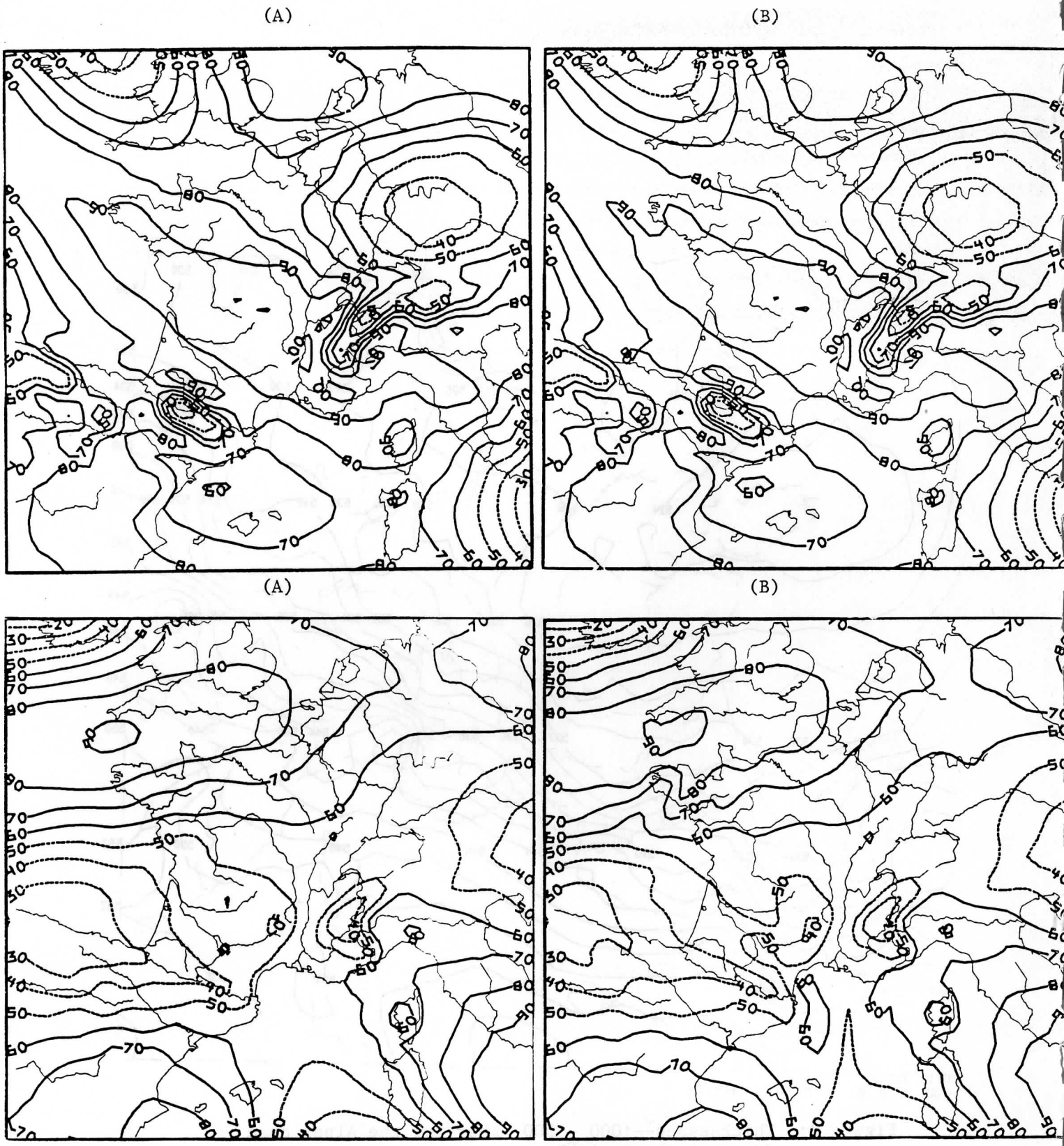

Figure 4: Humidity analysis at 850 mbar (above) and 500 mbar (below). Without satellite data (A); with satellite data (B).

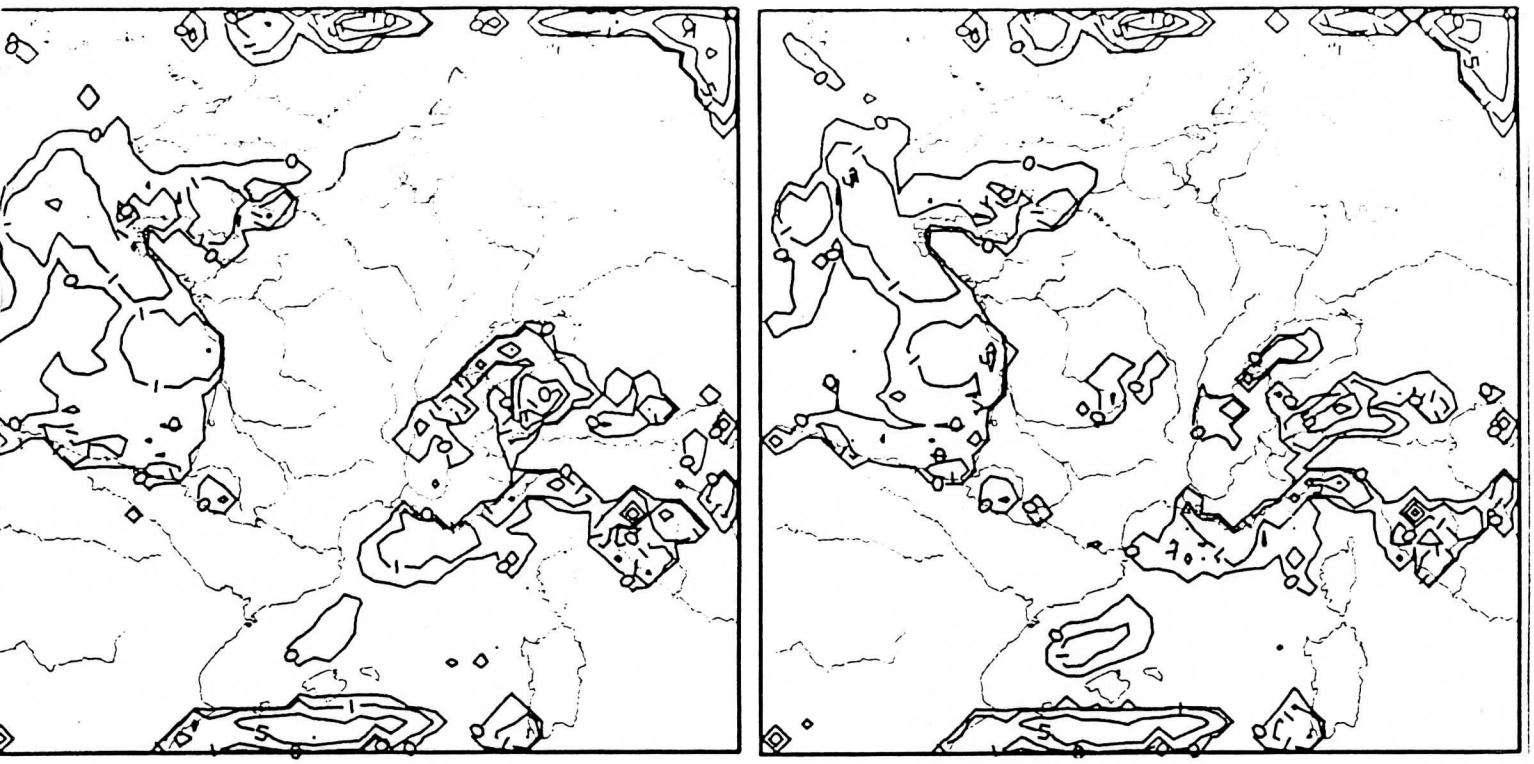

(A) (B)

Figure 5: Precipitation amount for six hours (from 5 June 1984, 18^h to 6 June, 1984, 0^h) predicted by the forecast model without satellite data (A), with satellite data (B) in the initial analysis (performed on 5 June, 1984, 0^h).

RESEARCH AND DEVELOPMENT ON TOVS RETRIEVALS IN THE U.K.

J R Eyre, P D Watts,

(Meteorological Office Unit, Hooke Institute,
Clarendon Laboratory, Oxford, U.K.)

J Turner and A C Lorenc

(Meteorological Office, London Road, Bracknell, U.K.)

1. INTRODUCTION

This paper describes research and development on TOVS retrievals at two centres in the UK: the Meteorological Office headquarters at Bracknell, and the new Robert Hooke Institute for Co-operative Atmospheric Research at Oxford. The Satellite Meteorology branch at Bracknell is responsible for running the operational system for real-time processing of TOVS data from the local reception area, for monitoring the performance of the system and for implementing improvements to it. Also at Bracknell, groups concerned with the development of the numerical forecasting system are engaged in work to assess and improve the use of TOVS retrievals in the current numerical forecast models and to develop techniques for improved assimilation of satellite sounding data in the future. Satellite meteorology research at Oxford involves the new Meteorological Office Unit and the Department of Atmospheric Physics of Oxford University, working closely together within a co-operative institute. One of the major activities of the joint group is the development of improved retrievals schemes for TOVS data. This work is being conducted in close collaboration with the groups at Bracknell, with the aim of providing improved retrieval schemes for operational implementation within the Meteorological Office.

At the time of the First International TOVS Study Conference (TOVS-I), the Meteorological Office was implementing a scheme to acquire and process real-time TOVS data for use in operational weather forecasting (Eyre, 1984b). The processing scheme is known as "LASS" (the local area sounding system). This paper outlines progress on this project since TOVS-I and discusses the lines of research and development currently being pursued or planned.

The TOVS case study of 7 June 1984, for which data were distributed to TOVS Conference participants in preparation for the Second International TOVS Study Conference, has been processed. The results obtained with the present operational retrieval scheme have been sent to the Australian Bureau of Meteorology for analysis. Some additional results are presented in section 4.

2. PROGRESS ON THE LOCAL-AREA SOUNDING SYSTEM (LASS) SINCE THE FIRST INTERNATIONAL TOVS STUDY CONFERENCE

2.1 Operational aspects

Following the delivery of the hardware for the HERMES (High-resolution Evaluation of Radiances from MEteorological Satellites) system in March 1983, the TOVS Export Package obtained from the NOAA/NESDIS Development Laboratory (Madison) was modified to run on the particular hardware configuration of the HERMES system. The TOVS data are received at Lasham in Hampshire and transmitted to Bracknell over telephone lines. Real-time processing was first achieved in August 1983 and was routine by September 1983. Following a period of product validation, the soundings were supplied to the Central Forecasting Office (CFO) at Bracknell from November 1983. The data were initially supplied as charts of 1000-500 mb thicknesses along with thermal winds derived from the local gradient of the thickness field. By January 1984 the software had been developed to handle NOAA-8 data in addition to that from NOAA-7, and the system was capable of processing data from the two satellites simultaneously.

Throughout 1984 the groups within the Meteorological Office concerned with the development of the operational numerical forecasting system conducted a number of experiments to investigate the impact of such large amounts of satellite sounding data on the numerical forecasts. Following evaluation of the results of these experiments, it was decided to include the LASS temperature data in the analyses of the "coarse-mesh" model (a global model with a horizontal resolution of 150 km) from 12 September 1984, with the data averaged to a horizontal resolution of 240 km. The data were only included in the 00Z and 12Z "update" global analyses (run over 11 hours after the analysis time and designed mainly to give a good starting field for the next assimilation) and the 6Z and 18Z intermediate global analyses. From mid-November 1984 the Meteorological Office began running a separate 3-hour assimilation cycle

specifically for the limited area "fine-mesh" model (of resolution 75 km), and the LASS data were included in these analyses at a resolution of 240 km. The data were included in all the assimilations except those from which the 36-hour forecasts were run. It was felt necessary to exclude the data from the main analyses prior to the forecasts until the impact of the data on the quality of the forecasts had been fully evaluated.

2.2 Retrieval scheme improvements

In most respects the retrieval scheme is unchanged from the version of the TOVS Export Package obtained from the NOAA/NESDIS Development Laboratory in 1980 (see Eyre, 1984b). However, minor improvements have been made since TOVS-I to overcome some of the problems identified during the development and early operational stages.

Some spurious thermal troughs were discovered over high terrain such as the Scandinavian massif, particularly in winter when the surface is very cold. These were caused by an error in the method used to compute thicknesses from the retrieved temperature profile (provided by the statistical regression inversion and extending down to 1000 mb) in high terrain areas where the surface pressure is much less than 1000 mb. A thickness correction scheme, which accounts approximately for the effects of an elevated surface on the retrieval, has been introduced (Eyre, 1984a). No retrieval products are generated in areas of very high terrain (where the mean surface elevation of a 1 deg-latitude x 1 deg-longitude box exceeds 1000 m).

Following concern that retrievals towards the edges of the TOVS scan contained biases with respect to the scan centre, an assessment was made of the mean MSU brightness temperatures at each scan position, averaged over many local area passes. Analysis of the results is complicated by the fact that the left side of the scan is always further south than the right side. For local area data, this introduces a "climatological" component into the variation of mean brightness temperature with scan angle. A scheme has been devised for removing this component to leave the "residual scan-dependent correction". Results from a preliminary assessment of these corrections is given in table 1. The data used in this analysis are MSU brightness temperatures corrected to nadir and corrected for antenna gain pattern and surface emissivity effects by the standard Export Package routines. They have also had applied the asymmetry correction calculated at Madison (values also given in

table 1), but they have not been mapped to HIRS sounding locations. The values obtained for the residual scan-dependent corrections are reasonably symmetric, indicating that they are probably compensating for biases in the mean nadir corrections rather than for an instrumental anomaly.

2.3 Validation activities and results

Since the start of routine production of LASS soundings there has been considerable effort devoted to validation of the derived profiles. This has mainly been through the generation of statistics from a data base of collocations of LASS soundings and radiosonde ascents from weather ships or land stations. Temperature, thickness and dew point bias and standard deviation (SD) statistics are produced each day for all collocations within the LASS area and monthly mean figures are also derived. Table 2 gives an example of the routine statistics produced on HERMES and shows the December 1984 bias and SD statistics for the temperatures, thicknesses and dew points for all standard levels up to 100 mb (the thickness figures being for layers from 1000 mb up to the level specified).

These monthly mean figures illustrate many of the known problems of the LASS soundings and, in particular, highlight the errors noted around the tropopause and at low levels. At these two levels the SDs for the temperatures are larger than at other levels and the biases give an indication of some of the problems that have been encountered in using the soundings. At the level of the tropopause, examination of individual collocations has indicated that the LASS soundings are unable to resolve fully the sharpness of the tropopause. Close to the ground the negative bias is thought to be due largely to the inability of the scheme always to detect cloud and provide correctly cloud-cleared radiances.

Subjective assessments of charts of the LASS 1000-500 mb thicknesses by the Central Forecast Office has highlighted a number of additional problems. In particular the forecasters suggested that the soundings at the edges of the swaths exhibit larger differences from radiosondes than those at the centre of the swath and that the differences are related to the synoptic pattern. The "residual scan-dependent corrections" described above have recently been introduced to remove some of the anomalies at the edges. However, further work has recently begun on examining the problems at the edges of the swaths and the

relationship to the synoptic type. This is mainly based on comparing the analysed LASS soundings with the routine numerical analyses interpolated to the time of the satellite overpass, and first results from these comparisons have confirmed many of the subjective views of the forecasters. Work is now in progress on explaining the differences observed and examining possible ways of correcting these errors.

3. CURRENT DEVELOPMENTS AND FUTURE PLANS

3.1 Locally generated regression coefficients

The LASS operational retrieval scheme currently performs a multiple linear regression inversion to obtain temperature and humidity profiles from cloud-cleared brightness temperatures using the operational regression coefficients generated weekly by NESDIS. While this approach maintains a large degree of compatibility between LASS retrievals and SATEMs, it has been thought for some time that improvements should be possible using coefficients which are:

- tuned to the area of local data reception, and
- generated by regression of a well-screened and climatologically balanced set of radiosonde profiles on the corresponding brightness temperatures calculated theoretically using a radiative transfer model.

An appropriate set of 9600 radiosonde profiles has been constructed (Pescod and Eyre, 1983) from which corresponding TOVS brightness temperatures can be calculated using a radiative transfer model (Eyre, 1984c). A scheme has been developed to generate regression coefficients from these (Watts, 1984b). The scheme will be implemented as soon as possible. In trial comparisons, the new coefficients have shown modest improvements over the NESDIS coefficients. Moreover they provide a basis for more sophisticated uses of climatological information (see section 3.4).

3.2 Improved cloud-clearing scheme

A new cloud-clearing scheme with the following characteristics is under development:

- it produces radiance fields in all channels which are more horizontally consistent than in the current operational scheme, and

- it assesses the estimated errors at each stage in the cloud-clearing process.

The principles behind the scheme are described by Eyre (1983). Briefly, it utilises the expected smoothness of the cloud-free radiance fields to provide a priori estimates of the clear radiances at each HIRS spot using estimates from adjacent spots.

If $x_{n,m}$ is the cloud-cleared brightness temperature estimate at HIRS spot, (line n, column m), with estimated error $\sigma_{n,m}$, then we can improve the estimate by combining it with information from a previously processed spot, ($\hat{x}_{n,m-1}$, $\hat{\sigma}_{n,m-1}$) using a sequential estimator of the form:

$$\hat{\sigma}^2_{n,m} = \left(\frac{1}{\sigma^2_{n,m}} + \frac{1}{\hat{\sigma}^2_{n,m-1} + \delta} \right)^{-1}, \qquad (3.1)$$

$$\hat{x}_{n,m} = \hat{\sigma}^2_{n,m} \left(\frac{x_{n,m}}{\sigma^2_{n,m}} + \frac{\hat{x}_{n,m-1}}{\hat{\sigma}^2_{n,m-1} + \delta} \right), \qquad (3.2)$$

where $\hat{x}_{n,m}$ and $\hat{\sigma}_{n,m}$ are the new estimate and its error, and δ is a term to take account of the expected spatial variation of x.

In practice the scheme is applied in 2 dimensions as illustrated in figure 1, and by running "forward" and "backward" filters information is "advected" uniformly from all directions. To date, the scheme has been developed for application to each channel in turn, but it could be extended to estimate all channels together.

The input data to the scheme can in principle be any independent estimates of the cloud-free radiance at each spot (together with an estimate of its error) derived by the best available method. At present we are using an extension of the current operational scheme; a HIRS cloud-free brightness temperature estimate is obtained from one of the following sources:

- The measured, pre-processed brightness temperature judged to be cloud-free through a comparison of measured MSU channel 2 with its value predicted from a linear combination of HIRS channels.

- An estimate obtained using the N* technique on adjacent

spots (Smith, 1968) with MSU channel 2 effectively acting as the "cloud-free" channel. Only colder adjacent spots are utilised to avoid overuse of the data.

- An estimate obtained from a regression on MSU data. It has been found necessary to identify and correct for the local bias between the measured HIRS cloud-free brightness temperature and the corresponding values predicted from MSU data. The local bias field is estimated in a similar manner to the cloud-free brightness temperature field itself.

The scheme has not yet undergone a thorough validation, but a preliminary example of its results is given in section 4.

3.3 Investigation of retrievals using a forecast first guess

Some consideration has been given to the idea of assimilating cloud-cleared brightness temperatures into the numerical forecast models, thus avoiding the need for an explicit "inversion". This may be the optimal approach in the longer term. However, it is planned to investigate a scheme which, whilst it does perform an explicit inversion, uses forecast information and is almost equivalent mathematically to direct assimilation of radiance data.

The proposed inversion takes the optimal linear form set out by several authors (e.g. Rodgers, 1976):

$$\hat{x} = x_o + (K.C)^T.(K.C.K^T + E)^{-1} . (y_m - y_c\{x_o\}) , \qquad (3.3)$$

where $\hat{x}$ is the retrieved profile vector (containing the humidity profile and surface radiative temperature, in addition to the temperature profile),
x_o is a first guess profile obtained from a forecast model,
C is the forecast error covariance (i.e. the covariance matrix of the expected error in x_o),
y_m is the measured, pre-processed, cloud-cleared brightness temperature vector,
E is the brightness temperature error covariance matrix,
$y_c\{x_o\}$ is the brightness temperature vector calculated from the first guess profile using a radiative transfer model,
and K is a matrix containing the derivatives of y with respect to x (ideally evaluated at $x = x_o$).

$y_c\{x_o\}$ will be calculated in real time from the first guess profile x_o using a modified form of the radiative transfer model TOVSRAD (Eyre, 1984c). This model will also be used off-line to compute the derivative matrix, K, since it is anticipated that a small number of constraint matrices, $D = (K.C)^T.(K.C.K^T+E)^{-1}$, will be adequate, and that a more precise specification of K is not justified given the uncertainties in C and E.

At the time of the forecast model assimilation it is possible to make an improvement to the retrieval, because we now have available an analysis x which should be more accurate than the forecast x . If we had possessed this at the time of the retrieval, it would have taken the form:

$$\hat{x}' = x_o' + (K.C)^T.(K.C.K^T + E)^{-1} . (y_m - y_c\{x_o'\}) . \quad (3.4)$$

Using the linear approximation:

$$y_c\{x_o\} - y_c\{x_o'\} = K . (x_o - x_o') , \quad (3.5)$$

and subtracting 3.3 from 3.4, we obtain the improved retrieval:

$$\hat{x}' = \hat{x} + [(K.C)^T.(K.C.K^T+E)^{-1}.K - I] . (x_o - x_o') , \quad (3.6)$$

where I is an identity matrix.

Again it is anticipated that $[(K.C)^T.(K.C.K^T+E)^{-1}.K - I]$ will be sufficiently stable to be pre-computed allowing a simple correction to $\hat{x}$.

In most areas, where the forecast is quite accurate, this approach is expected to give considerable improvement over the current operational method, which produces the largest retrieval errors in regions where the atmosphere is far from the climatological mean (which acts as the implicit "first guess"). Potential problems are expected with the new approach in areas where the forecast is seriously in error. However it may be possible using the radiances to identify such occasions, on which it may be better to use a "climatological" first guess and constraint (see section 3.4).

3.4 Investigation of stratified statistics

It has been demonstrated that retrievals which make use of a first guess and statistical constraint drawn from climatology can be improved by "stratifying" the statistical data base according to air mass type or profile shape, and then using the radiances with a discriminant function to select the most appropriate sub-set (Uddstrom and Wark, 1984).

Research is underway to explore this approach using either the "typical shape function" approach proposed by Uddstrom and Wark, or a simpler stratification as suggested by Kelly et al (1976). Given that an appropriate stratification is possible, the method could be applied either as a simple extension to the scheme described in section 3.1 or as an adjunct to the method outlined in section 3.3. If the measured radiances and those calculated from a forecast first guess have a high probability of belonging to the same sub-set, we have confirmed that the forecast is an appropriate first guess for the retrieval. Other probability conditions correspond to different situations which it would be useful to identify, including:

- the measured radiances have a low probability of belonging to any sub-set and so are probably in error, or

- the measured and forecast radiances have a high probability of belonging to different sub-sets, indicating perhaps that the forecast is seriously in error (in which case the mean and covariance of the sub-set corresponding to the measurements may be a better first guess and constraint for the inversion).

3.5 Investigation of use of AVHRR data with TOVS data

The usefulness of AVHRR data to improve HIRS cloud-clearing and as a diagnostic tool for testing TOVS-only cloud-clearing schemes is being explored (Lloyd et al., 1985).

3.6 Improved humidity retrieval

The present operational scheme retrieves humidity profiles through multiple linear regression of cloud-cleared HIRS brightness temperatures on water vapour mixing ratio profiles. A fundamental deficiency of this scheme lies in its attempt to represent a non-linear inversion problem by a

linear regression relation. An alternative approach proposed by Rosenkranz et al (1982) casts the humidity profile inversion in a linear form by attempting to retrieve the temperature profile at levels of constant water vapour over-burden. This approach has been applied to synthetic TOVS data (Watts, 1984a). The results show significant improvements over the current method in the mid-troposphere, particularly when the variance of the statistical data base is large, but no improvement close to the surface.

4. RESULTS OF CASE STUDY: 7 JUNE 1984

TOVS data for the NOAA-8 pass over the USA at 1350Z on 7 June 1984 have been processed by 3 methods. The pre-processing was the same in each case, using standard Export Package routines; HIRS calibrated brightness temperatures were converted to nadir and window channels corrected for water vapour, and MSU channels were corrected for off-nadir, surface emissivity and antenna gain pattern effects and then mapped to HIRS sounding locations. Three different methods have been applied to the cloud-clearing and inversion stages of the retrieval, and then common routines have been used to derive thicknesses, thermal winds, etc, from the retrieved temperature and humidity profiles. For each method the retrieved values of the 1000-500 mb thickness are presented for illustration.

The first method, illustrated in figure 2, is the standard operational method currently used at the Meteorological Office (Eyre, 1984b). The statistical inversion has used NESDIS regression coefficients for the appropriate week.

The second method, illustrated in figure 3, is the same as the first, except that the regression coefficients have been generated from a set of "historical" radiosondes and corresponding, theoretically calculated radiances for June for the European / N Atlantic area (see section 3.1). The coefficients are required both in the inversion and in the prediction of MSU channel 2 from HIRS brightness temperatures, which plays a vital role in the cloud-clearing. The application of the method to this particular case study is not entirely satisfactory for two reasons. Firstly, the regression coefficient data base was not designed to be used over continental USA and the Caribbean. Secondly, it is necessary in a physical-statistical method such as this to apply corrections for the biases between measured and

theoretically computed brightness temperatures, and these have not been thoroughly evaluated for NOAA-8. For these reasons the results may not merit too close a scrutiny and have not been analysed in detail. Nevertheless, they appear to be generally satisfactory. In particular, more retrievals have been obtained than with the first method (497 compared with 329), the increase coming mainly from a much greater number of N* retrievals. We have not made a detailed comparison of the retrieval types (clear, N* or MSU-only) with the corresponding AVHRR image in this case. However, in other cases for which such a comparison has been made, it has been found that the detection of low cloud is significantly better than with the NESDIS regression coefficients.

Figure 4 shows the results with the new cloud-clearing scheme outlined in section 3.2, also using the regression coefficients derived from the data base described in section 3.1. Validation of the new scheme is not yet complete, and so the results presented here are for illustration of the technique only. Qualitatively the results have the expected characteristics. The retrievals yield a denser and more continuous field, since a retrieval is attempted at each HIRS spot except over very high terrain. (To make the plotted fields legible, not all retrievals are shown in figure 4). Also the local noise in the retrievals is much lower than with the other two methods, in line with the objective of obtaining brightness temperature fields which are more horizontally consistent.

REFERENCES

Eyre J R, 1983: Towards an optimal approach to cloud-clearing for satellite temperature sounding. Internal report, Met.0.19 Branch Memorandum 72.

Eyre J R, 1984a: Calculation of thicknesses from satellite temperature retrievals over high ground. Internal report, Met.0.19 Branch Memorandum 73.

Eyre J R, 1984b: High-resolution temperature retrievals at the U.K. Meteorological Office. Technical proceedings of the First International TOVS Study Conference, 29 Aug - 2 Sept 1983, Igls, Austria; CIMSS Report, pp 94-100.

Eyre J R, 1984c: User guide to TOVSRAD. A program for

calculating synthetic HIRS-2 and MSU equivalent black body temperatures. Internal report, Met.0.19 Branch Memorandum 75.

Kelly G A, Powers P E, Gauntlett F J (1976): Temperature and water vapour retrievals from the NOAA 4 satellite in the Southern Hemisphere. Proc Symp on meteorological observations from space -- their contribution to FGGE; 8-10 June 1976; Philadelphia; pp 77-84.

Lloyd P E, Barnett J J, Eyre J R (1985): Investigations of AVHRR data to improve TOVS retrievals. Presented at 2nd International TOVS Study Conference, Igls, Austria February 1985.

Pescod R W, Eyre J R (1983): Accumulation of a set of radiosonde profiles for use with satellite sounding data from the European and North Atlantic areas. Internal report, Met.0.19 Branch Memorandum 71.

Rodgers C D (1976): Retrieval of atmospheric temperature and composition from remote measurements of thermal radiation. Rev Geophys Space Phys, 14, 609-624.

Rosenkranz P W, Komichak M J, Staelin D H (1982): A method for estimation of atmospheric water vapour profiles by microwave radiometry. J Appl Meteor, 21, 1364-1370.

Smith W L (1968): An improved method for calculating tropospheric temperature and moisture from satellite radiometer measurements. Mon Wea Rev, 96, 387-396.

Uddstrom M J, Wark D Q (1984): A classification scheme for satellite temperature retrievals. Submitted to J Clim Appl Meteor.

Watts P D, 1984a: Statistical retrieval of humidity profiles from TOVS data. Internal report, Met.0.19 Branch Memorandum 74.

Watts P D, 1984b: A study of local area synthetic coefficients for use in the "LASS" system. Internal report, Met.0.19 Branch Memorandum 76.

TABLE 1

MSU "asymmetry corrections" for NOAA-7 (in K)
(as provided by CIMSS, Madison)

	MSU scan position										
	1	2	3	4	5	6	7	8	9	10	11
channel											
MSU-2	1.36	0.90	0.57	0.29	0.11	0.00	0.08	0.21	0.42	0.73	1.09
MSU-3	1.19	0.65	0.36	0.17	0.07	0.00	0.00	0.04	0.11	0.32	0.71
MSU-4	0.04	0.11	0.08	0.02	0.02	0.00	0.04	0.05	0.13	0.17	0.15

MSU "residual scan-dependent corrections" for NOAA-7 (in K)
(correction = mean value in spot n - mean value in spot 6,
and is to be applied by subtracting it from the existing
corrections given above)

	MSU scan position										
	1	2	3	4	5	6	7	8	9	10	11
channel											
MSU-2	0.40	0.14	0.07	0.02	0.00	0.00	-0.01	0.03	0.08	0.22	0.44
MSU-3	-0.06	-0.08	-0.02	-0.01	-0.01	0.00	0.00	-0.01	-0.04	-0.03	-0.04
MSU-4	0.53	0.40	0.24	0.10	0.01	0.00	0.03	0.09	0.24	0.40	0.58

TABLE 2

December 1984 collocation statistics.
(Differences between retrievals and collocated radiosondes)

Pressure (mb)	Thickness (dam)		Temperature (K)		Dew Point (K)	
	Bias	SD	Bias	SD	Bias	SD
100	-0.41	5.02	-0.41	1.70	-	-
150	0.44	4.24	-0.91	1.82	-	-
200	0.74	4.00	0.71	2.57	-	-
250	-0.18	4.08	1.61	2.64	-	-
300	-0.92	4.07	0.53	2.56	-2.81	5.15
400	-1.44	3.61	-0.24	2.19	0.27	5.94
500	-1.31	3.08	-0.29	2.08	1.29	6.51
700	-0.85	2.12	-0.39	1.93	1.42	7.24
850	-0.59	1.31	-0.27	2.41	-0.91	5.20
1000	-	-	-2.06	3.58	-2.65	4.44

Figure 1: Illustrating a two-dimensional sequential estimation scheme for improving the cloud-cleared brightness temperature field.

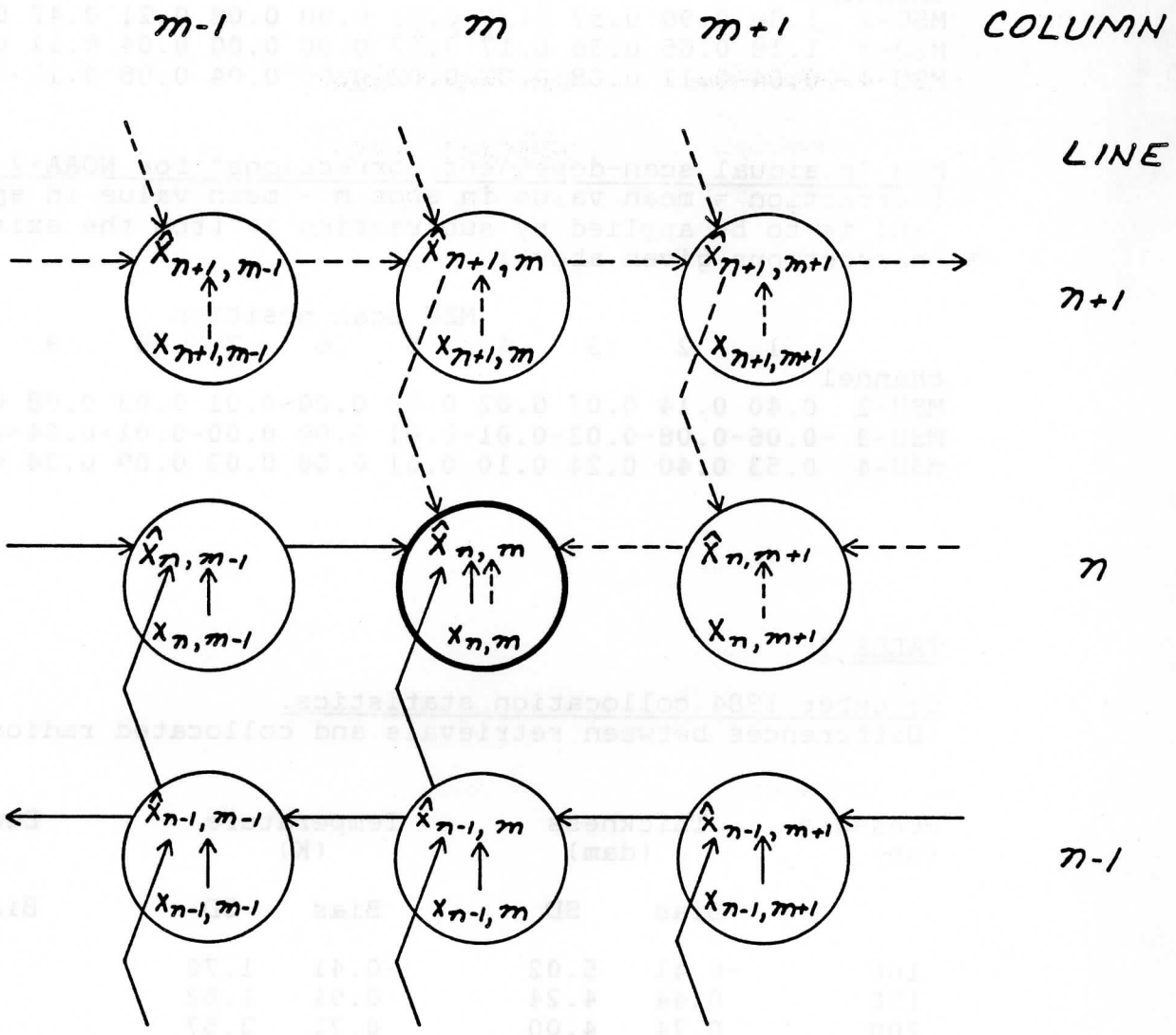

$X_{n,m}$ is the original estimate and $\hat{X}_{n,m}$ the new estimate at spot (n,m).

————, "forward filter" and - - - - - - - "backward filter" indicate the flow of information for improving the estimate at spot (n,m).

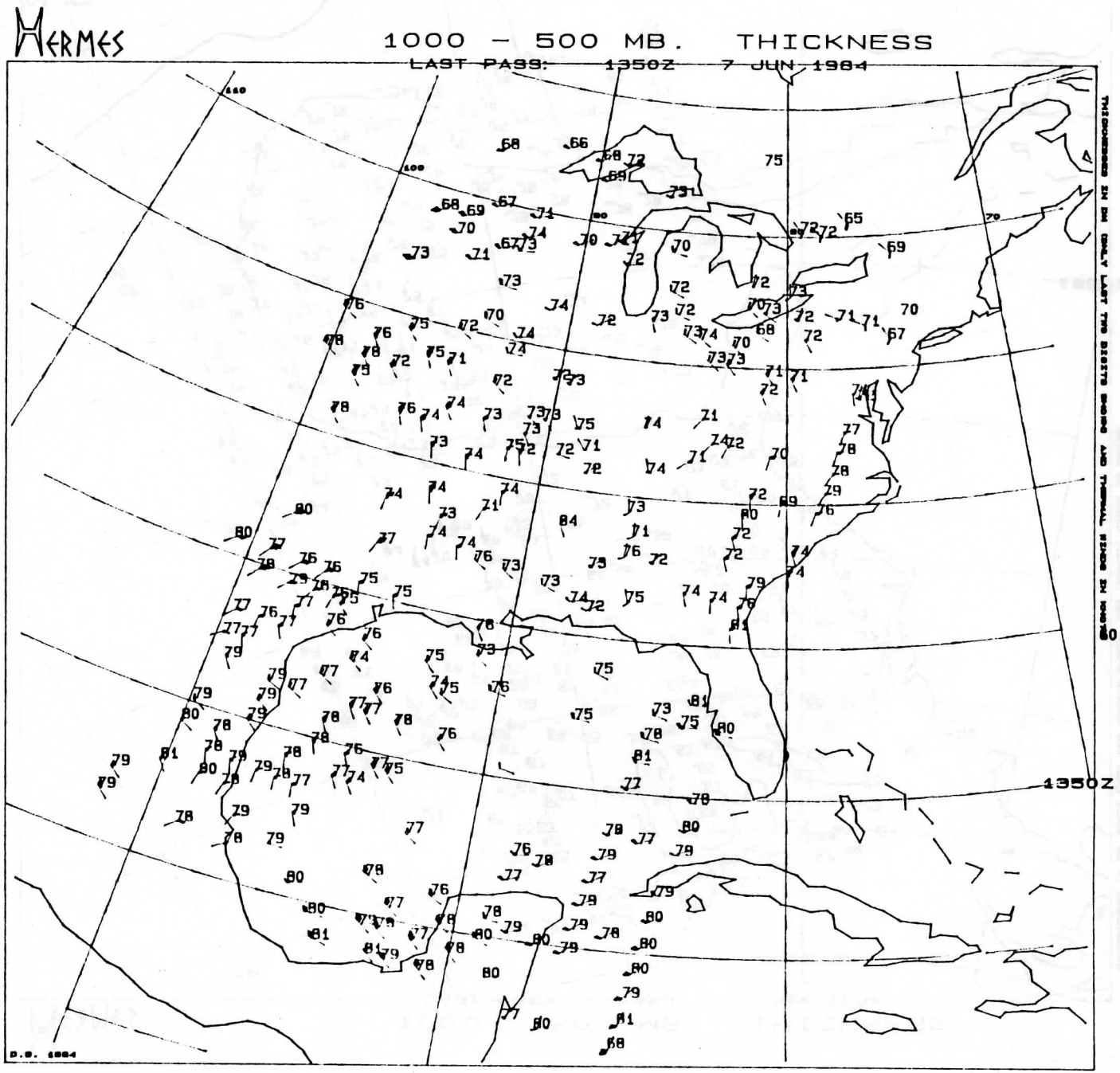

Figure 2

1000-500 mb thickness values from NOAA-8 TOVS data at 1350Z on 7 June, 1984. Operational retrieval scheme (using NESDIS regression coefficients).

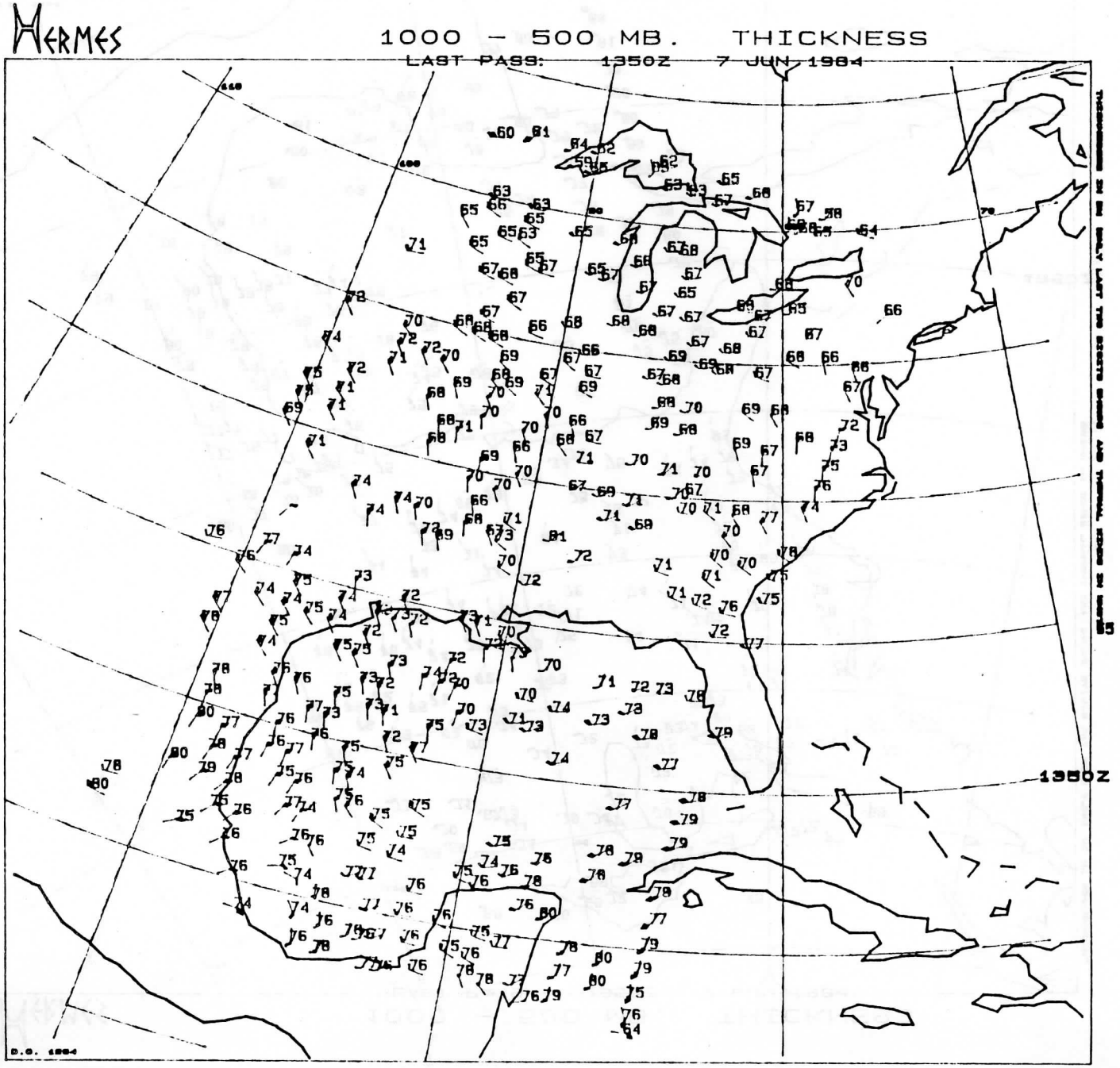

Figure 3

1000-500 mb thickness values from NOAA-8 TOVS data at 1350Z on 7 June, 1984. Retrieval scheme as for figure 2, except using locally generated regression coefficients.

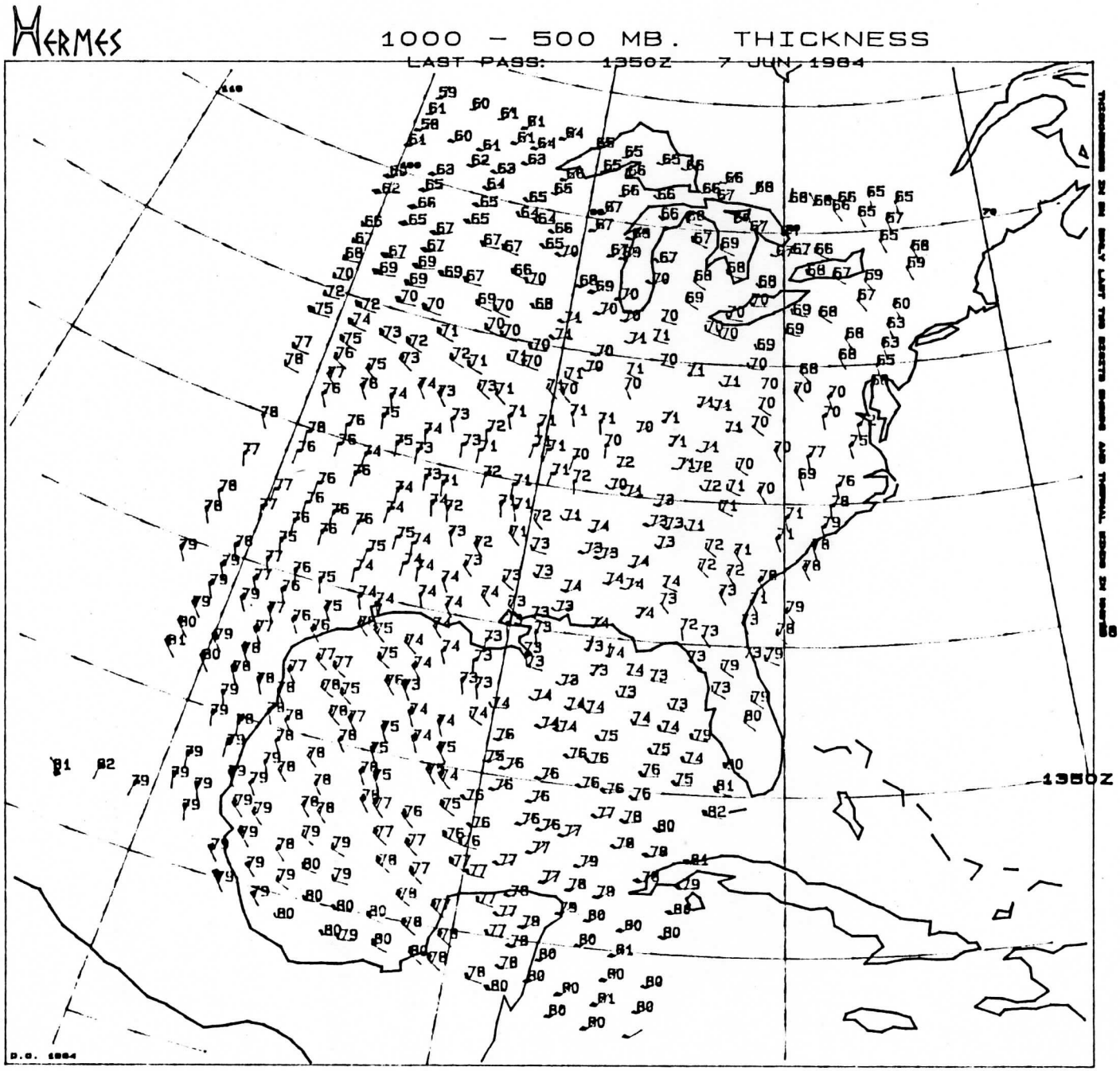

Figure 4

1000-500 mb thickness values from NOAA-8 TOVS data at 1350Z on 7 June, 1984. New cloud-clearing scheme and locally generated regression coefficients.

FUTURE U.S. POLAR-ORBITING METEOROLOGICAL SATELLITES EMPHASIS ON NOAA-K,L,M

Advanced Systems Concepts Group
Systems Planning and Development Staff
National Oceanic and Atmospheric Administration
National Environmental Satellite, Data, and Information Service
Washington, D.C. 20233, USA

presented by James Fischer

1. INTRODUCTION

Since the launch of the first meteorological satellite, TIROS I, on April 1, 1960, the U.S. has maintained in orbit an array of spacecraft in support of weather forecasting, and for monitoring of natural environmental hazards. Following the first TIROS (Television and Infrared Operational Satellite), the National Aeronautics and Space Administration supported the development of a series of "NIMBUS" experimental remote sensing spacecraft for weather observations, which served as test vehicles for ever-more-advanced sensors. As spacecraft advances and ground station processing reached a stage permitting quantitative analysis of remote sensing data, research satellites gave way to operational, "NOAA-series" platforms.

The current generation of U.S. polar meteorological satellites began with the launch of NOAA-8 (E) in 1983. (NOAA-series spacecraft have letter designations before launch, and are then numbered when operational in orbit.) The same family of platforms will continue through NOAA-J, slated for launch in March 1989. In a procurement of three more spacecraft, NOAA-K, -L, -M, small changes in the space platform are planned to support several significant changes in instrumentation. After NOAA-K, -L, -M (1990-92), a thorough redesign of the space platform is projected, accompanied by an increase in the number of sensors carried, to include modified versions of the present sensors, and also experimental sensors envisioned as replacements for the present operational sensors.

2. CURRENT NOAA-SERIES SPACECRAFT (NOAA-E THROUGH -J)

The present NOAA-Series polar orbiting spacecraft (See Table I) weighs more than 1000 Kg and carries an array of about eight sensors and data-relay systems, of which the most important are a high resolution surface imager (AVHRR), and an ensemble of three instruments lumped together as the TOVS (TIROS Operational Vertical Sounder). These instruments (HIRS, SSU, and MSU) provide sounding data, that is, values of emitted infrared and microwave brightness values from the Earth's surface and atmosphere, from which profiles of the atmospheric temperature, and moisture content aloft, may be calculated. While the calculation of soundings formerly required a major meteorological processing center, this can now be carried out by a tabletop computer. Soundings form the major satellite input to worldwide numerical weather prediction. Soundings are supplemented in prediction models by surface temperature values derived from AVHRR brightness values. (Winds calculated from apparent cloud motion as seen in sequential geostationary satellite images, are also of great value.)

Three of the four instruments providing imagery and soundings from the NOAA-series platform (AVHRR, HIRS, and SSU) operate in the infrared portion of the spectrum. (MSU is a four-channel Microwave Sounder Unit.) Since clouds are opaque to the passage of infrared energy, neither surface temperatures nor soundings are possible through cloud cover using infrared instruments. In winter, when much of the continental United States is cloud decked, this causes a serious data loss. While coarse soundings can be calculated from MSU data, the MSU's four channels (between 50 and 57 GHz) do not describe a detailed profile of temperature or moisture versus height.

3. NOAA-K, -L, -M

The major change planned for NOAA-K and subsequent satellites is the installation of an Advanced Microwave Sounding Unit (AMSU) (see Table III), a 20-channel sounder operating in frequencies between 23 and 183 GHz, including the 50 GHz channels used in the MSU. HIRS is retained; MSU and SSU are dropped. The resulting increase in sounding data is expected to reduce the error in soundings calculated from satellite data by about one-half. Other products to be calculated from AMSU microwave data include water vapor profiles, precipitation and global sea ice coverage. Table III lists the channel characteristics for the AMSU and Table IV provides a chart showing the weighting functions for the AMSU-A.

AVHRR will have changes made in several of its channels (see Table III). Channels 1 and 2 will be modified to make the visible and near-IR data more useful for the calculation of a "vegetation index," a data product indicating the "greenness" of the region imaged. Channel 3 will be timed shared with a near infrared channel, the present Channel 3 will be on during the night portion of the orbit and the new channel on during the day portion of the orbit. The present Channel 3 becomes Channel 3B and remains unchanged in spectral content. Channel 3A, the new channel, will enhance determination of cloud cover, versus surface snow and ice cover. For Channels 1 and 2 and 3A outputs will be changed from the present linear output to a "non-linear" output which will enhance the low energy portion of the data. (See Table III.)

The HIRS Channel 20 is to be broadened, to enhance its value as a data source for the Earth radiation budget. The change seeks to incorporate the Earth radiation budget data requirements into the HIRS whereas, in the present instruments this data is produced by the AVHRR. At present the HIRS Channel 20 covers only 0.6 to 0.7 um. Replacement of a visible radiation (silicon) detector by a thermal radiation (germanium) detector in the channel will widen the spectral response from 0.2 to approximately 2 um, without the necessity of an optical system redesign. (See Table III.)

An orbital change is scheduled for NOAA-H and subsequent spacecraft. The time for equatorial crossings is to be advanced from 1430 to 1330 local times. A sun-synchronous orbit is retained. The planned change required a thorough redesign of the spacecraft's thermal controls and instrument shades, since the spacecraft will observe the sun constantly at higher viewing angles, during all sunlit flight times. The change is planned to coordinate Eastern Pacific data collection with a change scheduled by the U.S. National Weather Service, to move forward the start-up time of its numerical prediction runs.

Installation of an Ocean Color Instrument (OCI), similar to the earlier Coastal Zone Color Scanner (CZCS), is also under consideration for the NOAA-K, -L, -M purchase. Flight of the OCI would increase data collection in support of near-shore marine interests including fisheries, and environmental monitoring of rivers, estuaries, and continental-shelf oceans.

Whether or not an Ocean Color Instrument is added to NOAA-K, -L, -M, the addition of the AMSU will force a change in the telemetry bands used by the spacecraft for direct to user broadcasts. One the beacon frequencies now used (136.77 MHz), falls into a band slated to be reallocated to use by commercial aviation, beginning in 1990. Various scenarios are now under consideration, in an effort to achieve sufficient data flows with a minimum impact on spacecraft and ground station telemetry hardware, and also to minimize the cost-impact on direct broadcast data users worldwide.

Tables V and VI show payloads carried on NOAA-D through -M, and details of NOAA-K, -L, -M changes.

4. FUTURE NOAA-SERIES SATELLITE SYSTEMS

With NOAA-K, -L, -M close to determined, extensive satellite improvements are now possible only aboard spacecraft to be purchased for launch in the decade of the 1990s and beyond.

Proposals are now under consideration within NOAA for a "block change", that is, for development of a new satellite bus, to replace the existing platform in the early 1990s. The major purpose of this change is to permit flight of experimental sensors, along with a required complement of operational imagers and sounders, as well as to optimize design for launch on the Space Transportation System (shuttle.) Candidates for development and experimental flight include active microwave instruments for measurement of winds and ocean surface parameters. (Active instruments send out pulses of microwave energy, comparable to radar units.) Two instruments, an active Synthetic Aperture Radar, and a multispectral Ocean Color Instrument (if not already operational), could provide data for marine interests including sub-surface contours in near-continent waters. An active Altimeter could determine ocean surface heights to accuracies sufficient to permit monitoring of the

strengths and directions of ocean currents. A major element of a new bus would be an enlarged solar-cell power supply, to permit operation of a larger suite of instruments. Also under consideration are plans for modular construction of the spacecraft, to facilitate shuttle repair or replacement of components.

TABLE I

"ADVANCED TIROS-N" (NOAA-E through -J) SUMMARY SHEET

Spacecraft: Total Weight - 1,030 Kg (2,270 lbs)
(Excludes expendables)

Payload: Weight, including tape recorders - 386 Kg (850 lbs)

Instrument Complement: Advanced Very High Resolution Radiometer (AVHRR/2)
High Resolution Infrared Radiation Sounder (HIRS/2)
Stratospheric Sounder Unit (SSU)
Microwave Sounder Unit (MSU)
ARGOS Data Collection System (DCS)
Space Environment Monitor (SEM)
Search and Rescue (SAR) Satellite Aided Tracking (SARSAT)
Solar Backscatter Ultra Violet Radiometer (SBUV/2)
- NOAA F and on PM satellites only
Earth Radiation Budget Experiment (ERBE)
- NOAA F and G only

Spacecraft Size: 3.71 meters in length (165 inches)
1.88 meters in diameter (74 inches)

Solar Array: 2.37 m x 4.91 m: 11.6 square meters
(7.8 ft. x 16.1 ft.: 125 square feet)

515 watts, end of life at worst solar angle
(high efficiency solar cells)

Power Requirement: Full operation - 475 watts
Reserved - 40 watts

Attitude Control System: 0.2 Degrees all axes
0.14 Degrees determination

Communications: Command Link - 148.56 MHz
Beacon - 136.77; 137.77 MHz
S-Band - 1698; 1702.5; 1707 MHz
APT - 137.50; 137.62 MHz
DCS (Uplink) - 401.65 Mhz
SAR - 1544.5 MHz
SAR (Uplink) - 121.5; 243.0; 406.0 MHz

Data Processing: All digital (APT translated to Analog)

Orbit: 833; 870 Km nominal, sun synchronous
0730 and 1330 local crossing times

TABLE II

POLAR IMAGERS AND SOUNDERS (NOAA-E through -J)

Sensors and Functions

o Advanced Very High Resolution Radiometer)AVHRR/2)
1.1 Km resolution; <2600 Km swath width

Channels	Wavelengths (um)	Primary Uses
1	0.58 - 0.68	Daytime cloud/surface mapping
2	0.725 - 1.10	Surface water delineation, ice and snow melt
3	3.55 - 3.93	Sea surface temperature, nightime cloud mapping
4	10.30 - 11.30	Sea surface temperature, day and night cloud mapping
5	11.50 - 12.50	Sea surface temperaturer, day and night cloud mapping

o TIROS Operational Vertical Sounder (TOVS)
(HIRS, MSU, and SSU make up TOVS)

1. High Resolution Infrared Radiation Sounder (HIRS/2)
Nadir Resolution -- 17.4 Km

Channels	Wavelengths (um)	Primary Uses
1-5	14.95 - 13.97	Temperature profiles, clouds
6-7	13.64 - 13.35	Carbon dioxide and water vapor bands
8	11.11	Surface temperature, clouds
9	9.71	Total ozone concentration
10-12	8.16 - 6.72	Humidity profiles, detection of thin cirrus clouds
13-17	4.57 - 4.24	Temperature profiles
18-20	4.00 - 0.69	Clouds, surface temperatures under partly cloudly skies

TABLE II (CON'T)

POLAR IMAGERS AND SOUNDERS (NOAA-E through -J)

2. Stratospheric Sounding Unit (SSU)
Nadir resolution 147.3 Km

Channels	Wavelengths (um)	Primary Uses
1-3	14.97	Temperature profiles

3. Microwave Sounding Unit (MSU)
Nadir resolution 105 Km

Channels	Frequencies	Primary Uses
1	50.31 GHz	
2	53.73 GHz	Temperature soundings through clouds
3	54.96 GHz	
4	57.95 GHz	

TABLE III

POLAR IMAGERS AND SOUNDERS (NOAA-K,L,M)

Sensors and Functions

o Advanced Very High Resolution Radiometer (AVHRR/3)
1.1 Km resolution; <2600 Km swath width

Channels	Wavelengths (um)	Primary Uses
1	0.58 - 0.68	Daytime cloud/surface mapping
2	0.84 - 0.87	Surface water delineation, ice and snow melt
3A	1.58 - 1.64	Daytime cloud/snow delineation, sea surface temperature
3B	3.55 - 3.93	Nighttime sea surface temperature and cloud mapping
4	10.30 - 11.30	Sea surface temperature, day and night cloud mapping
5	11.50 - 12.50	Sea surface temperature, day and night cloud mapping

o High Resolution Infrared Radiation Sounder (HIRS/3)
Nadir resolution 17.4 Km

Channels	Wavelengths (um)	Primary Uses
1-5	14.95 - 13.97	Temperature profiles, clouds
6-7	13.64 - 13.35	Carbon dioxide and water vapor bands
8	11.11	Surface temperature, clouds
9	9.71	Total ozone concentration
10-12	8.16 - 6.72	Humidity profiles,detection of thin cirrus clouds
13-17	4.57 - 4.24	Temperature profiles
18-19	4.00 - 3.76	Clouds, surface temperature
20	1.90 - 0.04	Radiation budget, clouds

TABLE III (CON'T)

POLAR IMAGERS AND SOUNDERS (NOAA-K,L,M)

3. Advanced Microwave Sounder Unit (AMSU-A)
Nadir resolution 47 Km

Channel	Center Frequency (GHz)	Bandwidth (MHz)	Use
1	23.800	270	Window
2	31.400	180	Window
3	50.300	200	Window
4	52.800	400	Temperature sounding
5	53.596	170	Temperature sounding
6	54.400	400	Temperature sounding
7	54.940	400	Temperature sounding
8	55.500	330	Temperature sounding
9	57.290344 =f(10)	330	Temperature sounding
10	f(10)+/-217 MHz	78	Temperature sounding
11	f(10)+/-322.2 MHz +/-48 MHz	36	Temperature sounding
12	f(10)+/-322.2 MHz +/-22 MHz	16	Temperature sounding
13	f(10)+/-322.2 MHz +/-10 MHz	8	Temperature sounding
14	f(10)+/-322.2 MHz +/-4.5 MHz	4	Temperature sounding
15	89.0	6000	Precipation, window

TABLE III (CON'T)

POLAR IMAGERS AND SOUNDERS (NOAA-K,L,M)

4. Advanced Microwave Sounder Unit (AMSU-B)
   Nadir resolution 15 Km

Channels	Center Frequency (GHz)	Bandwidth (MHz)	Use
16	89.0	6000	Precipation, ice, window
17	166.0	4000	Window
18	183.0 +/-1.0	1000	Water vapor profiling
19	183.0 +/-3.0	2000	Water vapor profiling
20	183.0 +/-7.0	4000	Water vapor profiling

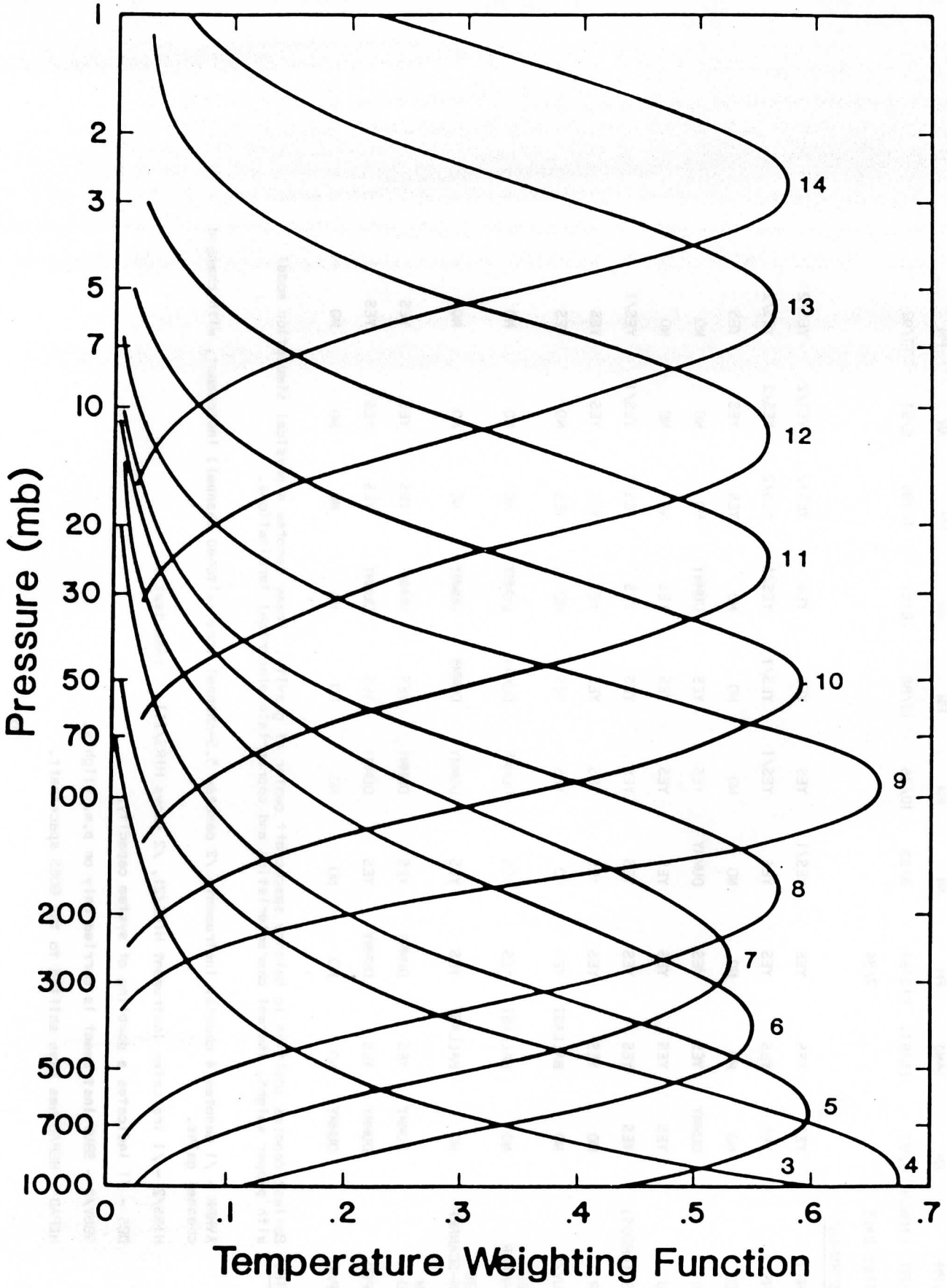

AMSU-A

TABLE IV

NOAA-K, L, M

TABLE V
PROJECTED PAYLOAD COMPLEMENT FOR NOAA C-M SATELLITES

SPACECRAFT	D	8	9	G	H	I	J	K	L	M
AM/PM	AM	(AM)	PM	AM	PM	PM	AM	PM	AM	PM
SCHED. LAUNCH	8/87	(3/83)	(12/84)	8/85	10/86	10/88	8/89	10/90	8/91	10/92
FAILED DATE			7/84							
INSTRUMENT										
AVHRR	YES	YES	YES	YES/1	YES	YES	YES	YES/2	YES/2	YES/2
HIRS/2	YES	YES	YES	YES	YES/1	YES/1	YES/1	YES/2	YES/2	YES/2
AMSU	NO	NO	NO	NO	NO	NO	NO	YES	YES	YES
SSU	DUMMY	YES	YES	DUMMY	YES	YES	DUMMY	NO	NO	NO
MSU	YES	YES	YES	YES	YES	YES	YES	NO	NO	NO
DCS (ARGOS)	YES	YES	YES	YES	YES	YES	YES	YES/1	YES/1	YES/1
SAR	NO	YES	YES	YES	YES	YES	YES	YES	YES	YES
SBUV/2	NO	BALLAST	YES	NO	YES	YES	NO	YES	NO	YES
ERBE SCANNER	NO	BALLAST	YES	YES	DUMMY	DUMMY	DUMMY	NO	NO	NO
ERBE NON-SCANNER	NO	BALLAST	YES	YES	DUMMY	DUMMY	DUMMY	NO	NO	NO
SEM TED	DUMMY	YES	DUMMY	YES	DUMMY	YES	DUMMY	YES	YES	YES
MEPED	DUMMY	YES	DUMMY	YES	DUMMY	YES	DUMMY	YES	YES	YES
HEPAD	DUMMY	NO	NO	NO	NO	NO	NO	NO	NO	NO

NOTE: Ballast denotes addition to balance spacecraft center of gravity. Dummy denotes a physical simulation model with proper weight, thermal characteristics and appropriate electrical terminations.

AVHRR - /1 denotes 4 channel instrument; /2 denotes 5.5-channel (one switched channel) instrument, with changed channel gains.

HIRS/2 - /1 indicates instrument HIRS/21, /2 shows HIRS/211. (See text.)

DCS - /1 indicates a doubling of system capacity.

SBUV/2 - SBUV instrument is carried only on p.m. flights.

HEPAD - HEPAD has been shifted to the GOES spacecraft.

TABLE VI

NOAA-K,L,M

Communications:

APT - 137.50; 137.62 MHz
S-Band - 1698.0; 1702.5; 1707.0 MHz
DCS (Uplink) - 401.65 MHz
SAR - 1544.5 MHz
SAR (Uplink) - 121.5; 243.0; 406.0 MHz
Command link - S-Band. Exact frequency not available

Space Environment Monitor

No change from present system.

Ozone Monitor

Solar Backscatter Ultra Violet (SBUV) instrument. No change from present instrument. SBUV is carried only on the PM satellite.

Data Colection System

Upgraded capacity with memory and greater sensitivity in the receivers.

Search and Rescue

Upgraded sensitivity and capacity.

AN APPLICATION OF AVHRR DATA TO TOVS RETRIEVALS

C. M. Hayden[1], W. L. Smith[2], H. M. Woolf[1]
and B. F. Taylor[3]

[1]NOAA/NESDIS Systems Design and Applications Branch
Madison, Wisconsin

[2]Cooperative Institute for Meteorological Satellite Studies
University of Wisconsin
Madison, Wisconsin

[3]Cooperative Institute for Meteorological Satellite Studies
University of Wisconsin and
New Zealand Meteorlogical Service, Wellington

1. INTRODUCTION

Since the inception of the improved TIROS series of polar orbiting satellites, beginning with TIROS-N launched in 1979, the Advanced Very High Resolution Radiometer (AVHRR) has been included. This instrument provides measurements at a special resolution of 1.1 km at Nadir in four or five (depending on the satellite) wave-length channels. The instrument has been used primarily to obtain sea surface temperatures (McClain and Strong, 1984) and for agricultural applications (Taylor, et al., 1985). There is also, however, an obvious opportunity for its application to the retrieval of temperature and moisture profiles. Precise definitions of surface temperature and cloud state are crucial to retrieval accuracy, and precision is difficult to achieve with the 35 km field-of-view of the high resolution infrared sounding instrument (HIRS) used with the NOAA satellites. The AVHRR, with its complement of visible and infrared window channels, offers promise in determining these factors. Only in Japan are the HIRS and AVHRR routinely integrated in the retrieval procedure (Aoki, 1980). The U.S. has not followed suit, primarily because of logistical problems in performing the task on global sounding sets. Also, in terms of large scale weather patterns, to which the TOVS data are primarily addressed, it is questionable that the AVHRR would have significant impact since the cloud problem is largely alleviated by microwave measurements. On the mesoscale, however, the situation is different, and as remote sounding development turns increasingly in this direction, it is appropriate to investigate further an AVHRR/HIRS amalgamation.

In this paper, a single case study is described. It is shown that the AVHRR data can be successfully merged with the HIRS to provide improved cloud identification and correction. The effect on final profiles of temperature and moisture is not dramatic, indicating that further tuning of the retrieval algorithm, which is currently highly biased to the microwave, is probably required. There is, however, strong evidence that the AVHRR has a positive impact, especially on the low level moisture field.

2. COLOCATION AND PROCESSING OF AVHRR

Colocation of the AVHRR with the HIRS field-of-view is a non-trivial problem since the instruments scan in opposite directions at different rates. This question has been treated by Aoki (1980) and we have used his technique as described in a companion paper (Taylor, et al.). As reported, statistical and imaged comparisons of "pseudo" HIRS averaged from the AVHRR have convinced us that the method works accurately, at least for the case investigated here.

For each HIRS field of view, three channels of AVHRR are processed: the visible, 11 micrometer, and 3.7 micrometer. As reported by Taylor, et al., a series of tests is performed to determine the "scene" within the HIRS, and as many as three radiance values may be returned for each channel, if the scene is determined to consist of two uniform targets (e.g. uniform cloud and surface or two uniform cloud decks). The three values correspond to the two uniform temperatures and the average of these. Failing a two scene scenario, a single uniform temperature, if it exists, and the average (which will be the same) are returned. Failing the single and the two scene tests, only the average is returned. In the last condition, no retrieval is attempted.

3. METHOD OF AMALGAMATION

The basic resolution element for a TOVS retrieval is 3x3 HIRS FOV. For each of the nine spots, given that the AVHRR and TOVS are accurately colocated and that the former has been processed to determine a one or two uniform scene within the TOVS FOV, the following procedures are followed:

- If the scene is uniform, the TOVS radiances are passed as measured.

- If the scene is two-fold, a cloud correction via the "adjacent pair" method (McMillan, 1978) is attempted. Since the processing of a retrieval involves a 3x3 array of FOV, there are as many as 35 independent "adjacent pair" comparisons. It should be recalled that in the "adjacent pair" method, there are two fundamental assumptions: that the same type of cloud exists in both fields; and that the clouds are at a single level. The role of the AVHRR is to determine that the assumptions are upheld. Violation of either invalidates the method as demonstrated by McMillan (loc cit.).

In our processing, it is required that both cold and warm uniform scene radiances in the two FOV be similar (within five degrees of brightness temperature in the 11 micrometer channel). If so, an "N*" is determined and the "adjacent pair" correction is made as follows:

$$N = (\hat{I} - I_H) / (I_L - I_H) \quad (1)$$

$$N^* = N_1/N_2 \quad (2)$$

$$I_{cl} = (I_1 + N^* I_2) / (1 - N^*) \quad (3)$$

where N is cloud amount, I_{cl} is the corrected clear column radiance, $\hat{I}$ is the TOVS measurement and I_H and I_L are "HIRS equivalent" measurements for the two uniform scenes determined from the AVHRR. The subscripts (admittedly confusing) represent "higher" or "lower" in brightness temperature corresponding to clear and cloudy scenes; or two uniform cloud levels. Subscripts 1 and 2 refer to the two HIRS FOV. "HIRS equivalence" is accomplished by a local regression analysis which relates HIRS measurements to the averaged AVHRR measurements for the 3x3 HIRS FOV. In these regressions, we usually find correlations to be .95 or higher.

Cloud amount N can be determined from the visible or infrared window channels (3.7 and 11 micrometer) of the AVHRR. There is no guarantee that similar amounts will result from different frequencies, and in fact, they often don't. The shortwave infrared in the presence of reflected sunlight is especially troublesome. As in so many other decisions made in retrieval processing, there is no clear cut way of sorting out the confusion of computed N*. We have chosen to put highest reliance on the 11 micrometer determination, ordering the FOV such that N* lies between zero and 0.75 for this frequency. N* for the 3.7 micrometer channel is then constrained to be within 0.2 of the 11 micrometer estimate (but again limited to less than 0.75) or the shortwave HIRS measurements for the pair are not used in the retrieval.

Any pair which survives the adjacent pair testing is subjected to an extrapolation constraint. By this, the corrected brightness temperature for either window channel is not permitted to exceed the averaged warm uniform value by more than two degrees.

Finally, all survivors from the 3x3 array, whether uniform or N*, are averaged, weighted by their clearness (1-N). The final radiance estimates are accepted if the sum $(\Sigma_j(1-N_j))$ exceeds 0.5. The final estimates are examined to determine whether the retrieval will take the "clear" or "cloudy" path. This decision is determined from the TOVS measurements of bi-directional reflectance and a variety of comparisons between the three (11, 3.7 and 4 micrometer) windows and the surface air temperature. The latter is obtained from the surface network of reporting stations.

4. CASE STUDY

The data treated in this study is a four minute swath of AVHRR over the central U.S. near 1345 GMT on 7 June 1984. The synoptic situation was characterized by a large low pressure system centered over southern Canada with a weak stationary front extending eastward along the Canada/U.S. border and a second stationary front with waves

stretching from Lake Superior across Wisconsin and Iowa and dropping down through South Dakota and Nebraska to a low pressure system forming over Kansas and Oklahoma. To the east of this front, a large pool of warm, moist air contained considerable cloudiness of several types as can be seen in Figures 1 and 2. Figure 1 is an image of the water vapor sensed by the VISSR Atmospheric Sounder (VAS) 6.7 micrometer channel carried on GOES-5. The surface pressure and 500 mb geopotential contours from the National Weather Service analyses at 1200 GMT are superimposed. Strong southwesterly flow aloft contributed to the development of a wave over Kansas and convection along and ahead of the front to the northeast later in the day.

The area covered by the TOVS data is indicated by the plotted values in Figure 2 which also shows an image of the VAS 11 micrometer window. The considerable and varied cloudiness of the situation offers a challange to the AVHRR/HIRS amalgamation although the loose gradients of temperature and moisture make verification of mesoscale detail very difficult.

5. RESULTS

The TOVS data for 7 June 1984 was processed with and without the AVHRR. The yield was very similar in both cases as can be seen by contrasting Figures 3 and 4. The former represents the run using AVHRR. It has slightly fewer retrievals because of the decision to skip scenes where no uniform temperature is available from the AVHRR. In the "No-AVHRR" version, a retrieval is always attempted (an expression of confidence in the microwave measurements) although it may fail internal consistency checks.

Our primary objective in this exercise was to obtain more clear and cloud corrected soundings using the AVHRR. In this we were successful. The brighter numbers of Figure 3 and 4 represent the clear or partly cloudy, while the fainter entries represent overcast determinations. Judging by the cloud imagery, the algorithm has performed as expected.

Several parameters in the AVHRR amalgamation were varied to test sensitivity. One of these was the uniformity constraint imposed on the warm and cold scenes of paired FOV. The total yield of soundings turned out to be rather insensitive. The constraint was varied from three to five to seven degrees with the result shown in Table 1. Note, however, that the number of partly cloudy retrievals increases systematically as the gate is widened. The increase is at the expense of previously uniform retrievals (both clear and overcast) when additional N* samples are added in the averaging over the 3x3 array.

Table 1. Uniformity constraint variation and retrieval yield. Limit is in degrees of brightness temperature for 11 and 3.7 micrometers.

Limit	Total Soundings	Total N*
3	164	15
5	164	22
7	167	27

We find that failure in the adjacent field of view testing is usually caused by the colder scene comparison. The AVHRR processing has been tuned to provide two scene estimates a majority of the time (see Taylor, et al.), but the spacial variation of the cold scene is marked. This can be seen in the image shown in Figure 5. In the figure, each square represents a TOVS field-of-view. The black squares show where no second scene was obtained. Otherwise, the shading depicts the change in the scene temperature, with lightest being coldest. "Uniform" 3x3 arrays are rather rare.

The change from uniform to partly cloudy retrievals as shown in Table 1 has rather little effect on retrieval quality. This is unquestionably because of the extrapolation constraint imposed on all N* estimates such that they cannot vary from the warm uniform estimate by more than two degrees. When this constraint was loosened, the soundings became noisy showing that the N* estimates certainly need this or an equivalent filter.

The goal in introducing AVHRR data into the TOVS retrieval processing is to provide better profiles of temperatures and moisture, particularly in partly cloudy situations. Achievement of this goal has proven to be elusive. There is the usual paucity of ground truth to verify the subtle modifications caused by the AVHRR, and the modifications introduced are indeed small. The types of change introduced by the AVHRR seem correct in principal. The retrieval process (the "simultaneous" algorithm described by Smith, et al. in a companion paper) is basically a two pass procedure where the first pass is primarily a microwave retrieval with the transparent HIRS channels suppressed. The second pass adjusts the first retrieval, to a greater or lesser extent according to cloud determination. We find that with AVHRR included, the second pass retrieval produces significantly larger changes to the first pass in the lower layers of the atmosphere. However, the changes are rarely greater than a degree, which put them below the sensitivity of available verification.

Figure 6 shows analyses of the 850 mb dewpoint derived from the processing with and without AVHRR. The fields are quite amorphous as should be anticipated in this weather situation. There are three areas where there are marked differences in the analyses. In the Mississippi Valley south of Illinois, the field with AVHRR shows a distinct moisture minimum which is not present in the other analysis. Also, over the Georgia/Alabama border the No-AVHRR field shows a moisture maximum which is absent in the AVHRR version. Finally, over Michigan and Lake Huron, the AVHRR analysis is drier. In all instances, the differences are caused by the change from "overcast" to "partly-cloudy" retrievals, as can be seen in Figures 3 and 4; and in all instances the AVHRR versions appear to be more correct, as deduced from the water vapor imagery of Figure 1. There is, in fact, good coherence between the AVHRR analysis and the dry/moist areas visible in the VAS image; much better than for the No-AVHRR analysis. Thus, at least qualitatively we can show improvement in the retrievals when the AVHRR is used.

5. SUMMARY

This paper reports the early findings of a research project which is far from complete. Both the techniques for extracting AVHRR information at HIRS FOV and the methods of incorporating this in the retrieval algorithm need further development. Also, more than a single case study must be addressed. Nevertheless, progress to date is highly encouraging. There is little doubt that the high resolution data are having their anticipated effect in resolving the infrared cloud problem, and that they are improving, albeit marginally, the final products of temperature and moisture generated from the TOVS retrievals.

5.1 References

Aoki, T., 1980: A method for matching the HIRS/2 and AVHRR pictures of TIROS-N satellites. Tech. Note No. 2, Met. Sat. Center, Japan, 15-26.

McClain, E. P., and A. E. Strong, 1984: Improved ocean surface temperatures from space--comparisons with drifting buoys. Bull. Am. Meteorol. Soc., 65, 138-142.

McMillan, L. M., 1978: An improved technique for obtaining clear radiances from cloud contaminated radiances. Mon. Wea. Rev., 11, 1590-1597.

Smith, W. L., H. M. Woolf, C. M. Hayden and A. J. Schreiner: The simultaneous retrieval export package (companion paper).

Taylor, B. F., P. W. Dmi, and J. W. Kidson, 1984: Vegetation index of New Zealand pasture from NOAA-7: seasonal and interannual variation. Submitted to Remote Sensing of the Environment.

Taylor, B. F., C. M. Hayden, and W. L. Smith: The determination of HIRS scene temperatures from AVHRR data (companion paper).

Figure 1. The VISSR Atmospheric Sounder image of the 6.7 micrometer (water vapor) channel for 7 June 1984 1400 GMT. Analyses of 500 mb geopotential (solid) and surface pressure (dashed) for 1200 GMT, obtained from the National Meteorological Service, are overlaid.

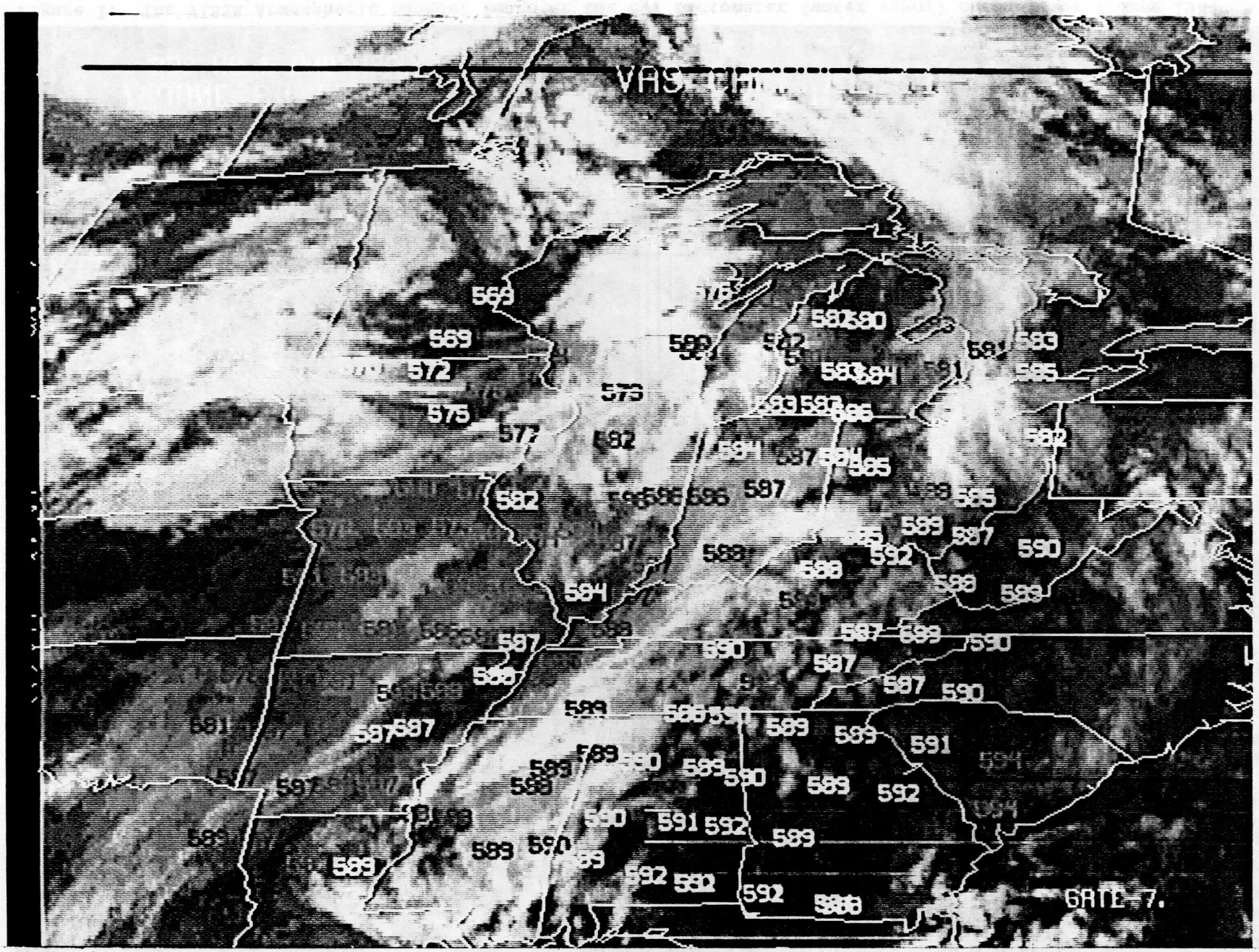

Figure 2. TOVS retrievals of 500 mb geopotential displayed over the VISSR 11 micrometer image. Dark (faint) numerals indicate "overcast" whereas brighter and brightest numerals indicate "clear" and "partly-cloudy" as determined by the AVHRR processing algorithm.

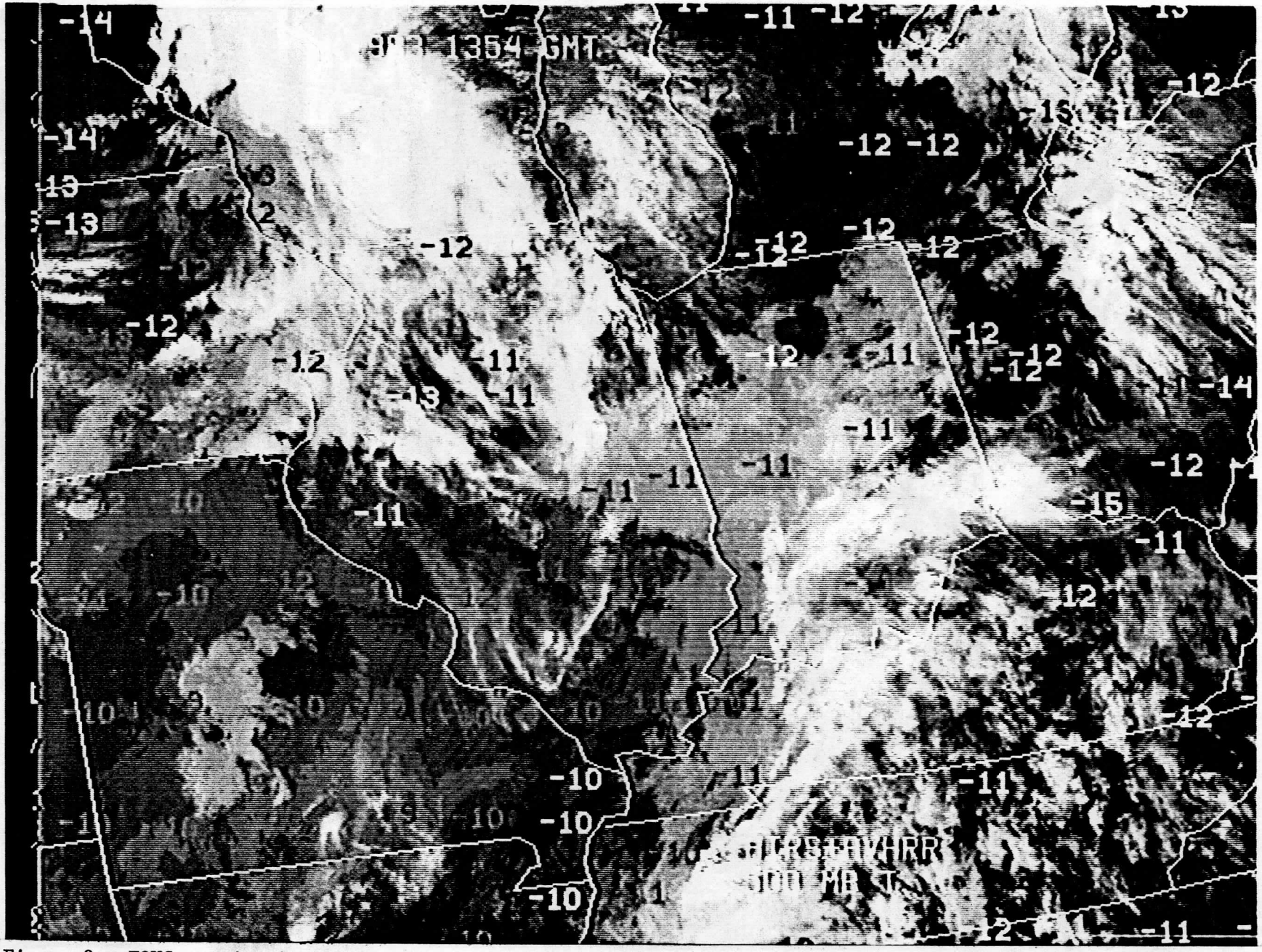

Figure 3. TOVS retrievals of 500 mb temperature displayed over the AVHRR 11 micrometer image. Retrievals were processed without AVHRR. Brightness of digits represents perceived cloud conditions as in Figure 2.

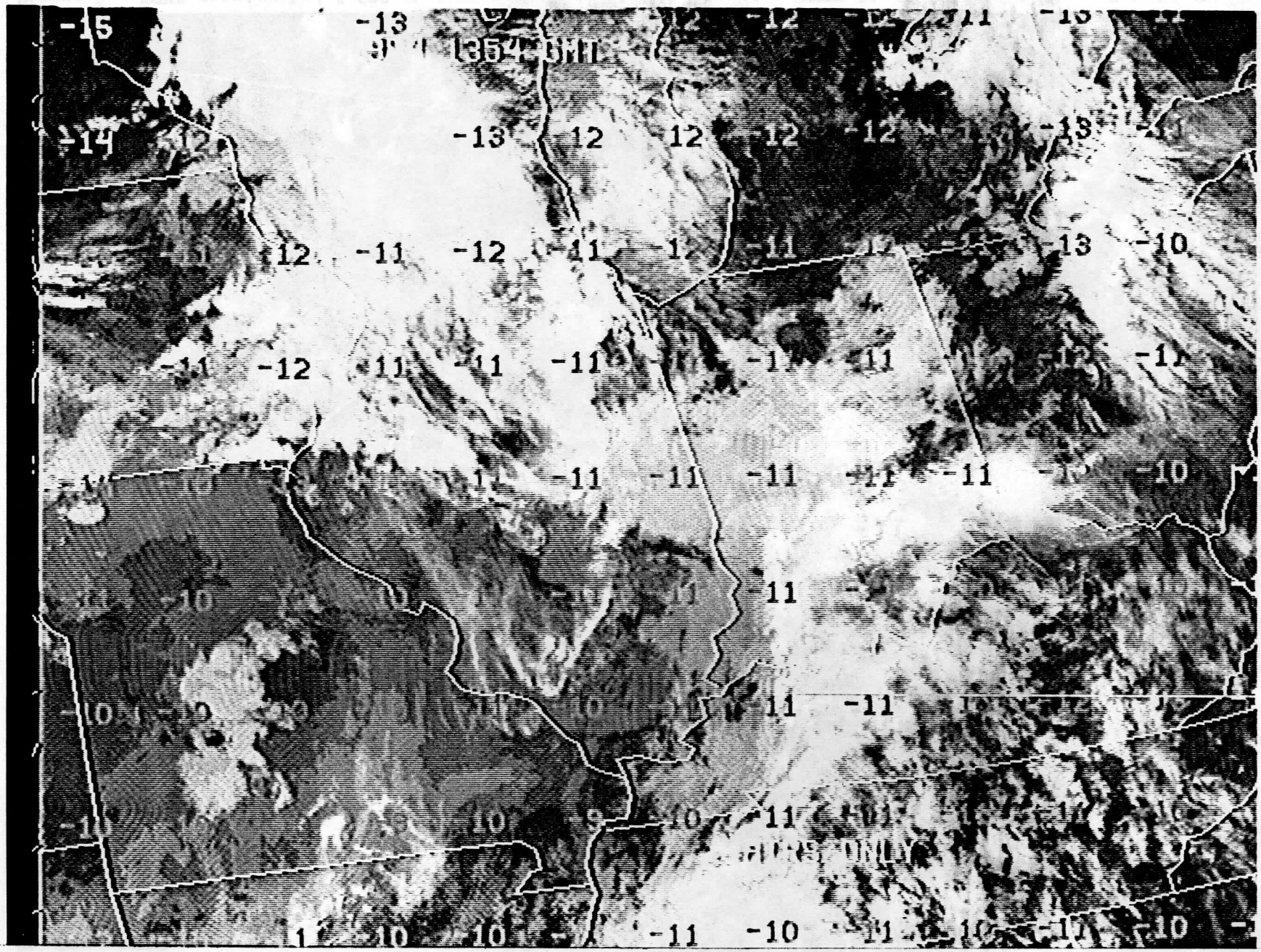

Figure 4. Same as Figure 3, except that retrievals were processed with AVHRR data.

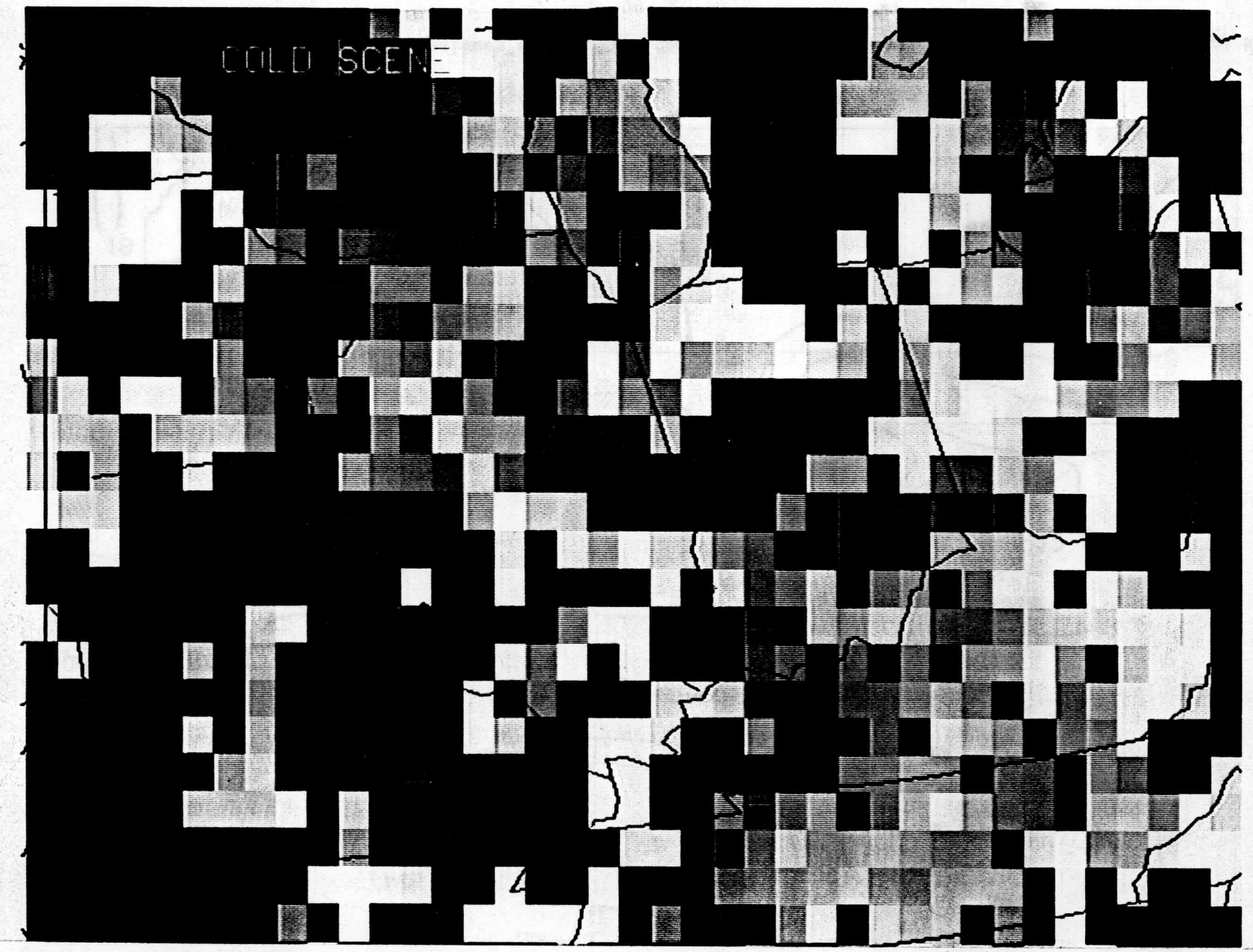

Figure 5. AVHRR estimates of "cold scene" temperatures at HIRS FOV resolution (represented by squares). Black indicates that two scene identification could not be made. Shading indicates temperature of scene (white coldest).

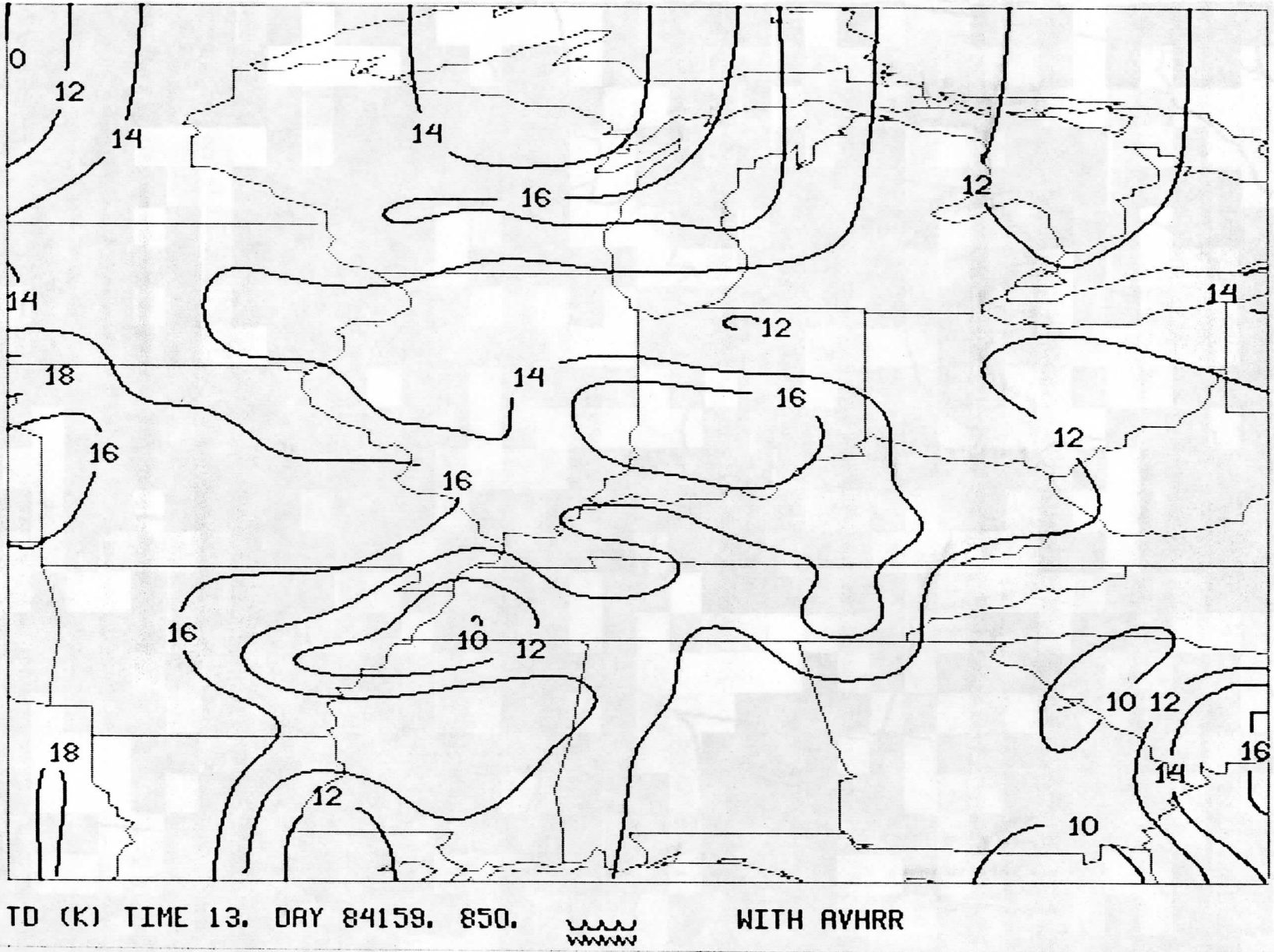

Figure 6. (With AVHRR) 850 mb analyses of dewpoint derived from TOVS retrievals with AVHRR. Units are K.

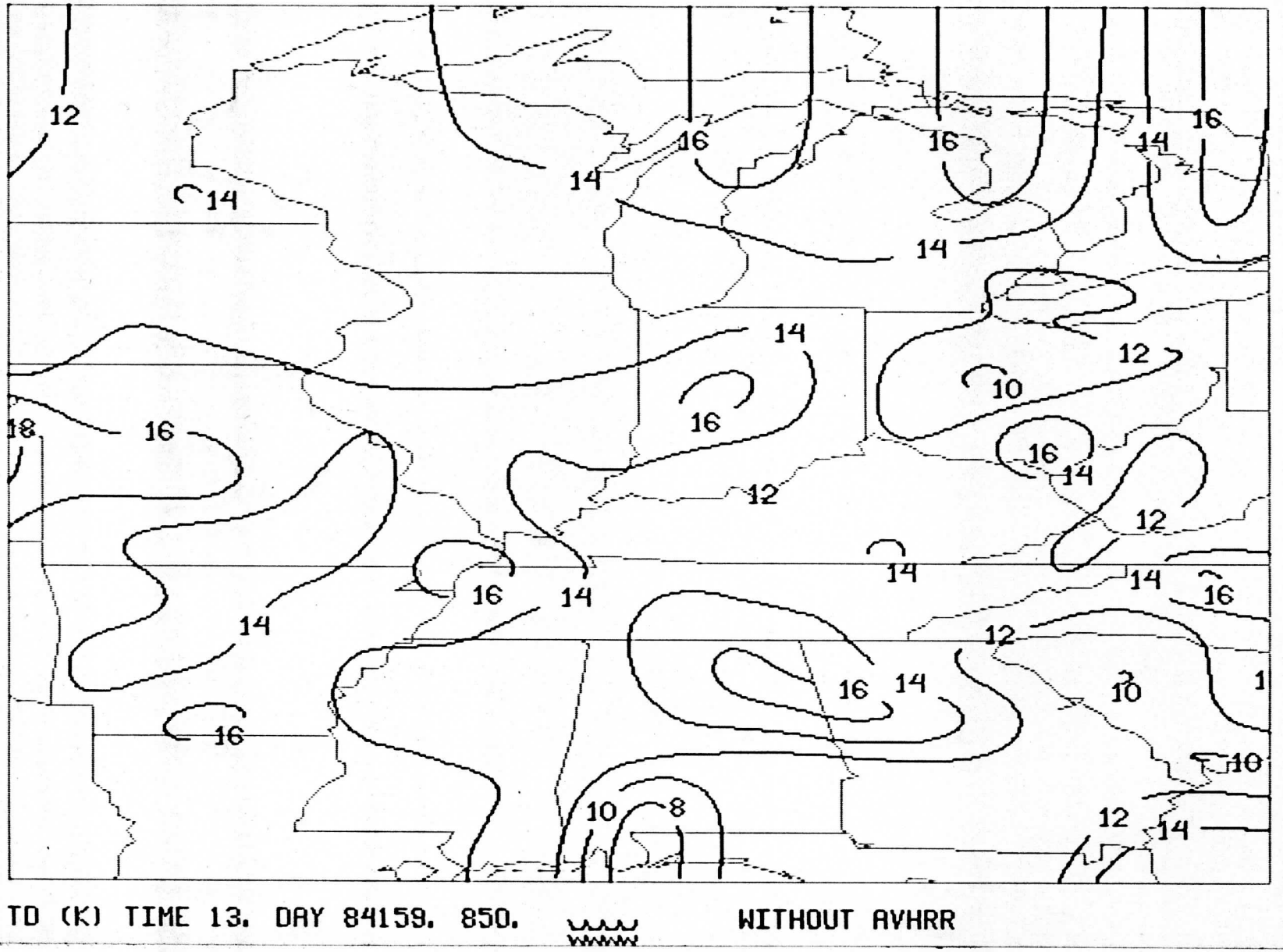

Figure 6. (Without AVHRR) 850 mb analyses of dewpoint derived from TOVS retrievals without AVHRR. Units are K.

ECMWF PROCESSING SCHEME

Graeme A. Kelly

European Centre for Medium Range Weather Forecasts
Berkshire, UNITED KINGDOM

1. INTRODUCTION

The main objective of the data assimilation scheme that has been developed at ECMWF is to provide initial states for the Centre's operational forecast model. The scheme produces global analyses in numerical form using all appropriate types of available observations on the GTS. It is designed to run efficiently, with minimal human intervention, on a large, fast, vector processing computer.

2. DATA ASSIMILATION

An analysis, if it is to be as accurate as possible, must supplement information from the currently available observations by two means:

1) Information from earlier observations.

2) Knowledge of the likely structure and scales of atmospheric motion, and of the balance which is usually observed between the various fields (mass, wind, humidity) of the atmosphere.

In a data assimilation scheme, both of these are provided with the help of a numerical model of the atmosphere, which can update information from past observations to the current analysis time, and assimilate all the data into a consistent multivariate three-dimensional analysis which represents the atmospheric motion in a realistic way. When, as at ECMWF, the main use of the analysis is to provide initial conditions for a numerical forecast, the advantage of using a numerical model outweighs the main disadvantage, which is that biases and inaccuracies in the model's formulation and limitations to its resolution mean that the final analysis does not always accurately represent all the detail available in the observations.

Ideally, observations should be inserted into the assimilating model at the valid model time. However, this is difficult to organize, particularly if sophisticated analysis methods are used to help ensure that the information is inserted into realistic scales of motion, with approximate balance between the various fields. At ECMWF a compromise 6 hourly intermittent data-assimilation is used, illustrated in Figure 1.

Observations from a 6 hour period spanning the nominal analysis time are used to correct a 6 hour forecast made from the previous analysis. Deviations of the observations from the forecast are analyzed to give increment fields which are then added to the forecast fields.

Since the analysis methods cannot represent the atmosphere's balance as accurately as the model can, we use the model equations

subsequently in a non-linear normal mode initialization. The balance achieved by this is sufficiently realistic that even fields sensitive to the balance, such as the vertical velocity, are meteorologically realistic. For this reason, we usually consider the initialized fields to be the analysis, despite the fact that the uninitialized fields usually fit the individual observations somewhat better.

The initialized analysis is then used as initial conditions for a 6 hour forecast, using a version of ECMWF's prediction model. Since we use the forecast field in the next analysis, we also estimate its statistical uncertainty, so it can be given appropriate weight.

3. ANALYZED VARIABLES AND COORDINATE SYSTEMS

While accepting the need for a numerical forecast model in the data assimilation scheme,we wished the scheme to be readily adaptable to use any forecast model, and not too closely tied to that of the model currently in use. Thus we chose, for the analysis, vertical coordinates and variables appropriate for the majority of the observations and for the simple multivariate relationships used. The analyzed variables are geopotential height and northward and eastward components of wind. These are normally analyzed at 15 standard pressure levels: 1000, 850, 700, 500, 400, 300, 250, 200, 150, 100, 70, 50, 20, 20 and 10 mbs, on a regular latitude/longitude grid (Arakawa A) with a resolution of 1.875°. In addition to geopotential height and wind a humidity analysis is performed for the 5 layers associated with the above standard pressure levels up to 300 mb. The variable analyzed is the precipitable water content of the layer. Figures 2 and 3 show schematically the horizontal and vertical coordinate system for the analysis and forecast system.

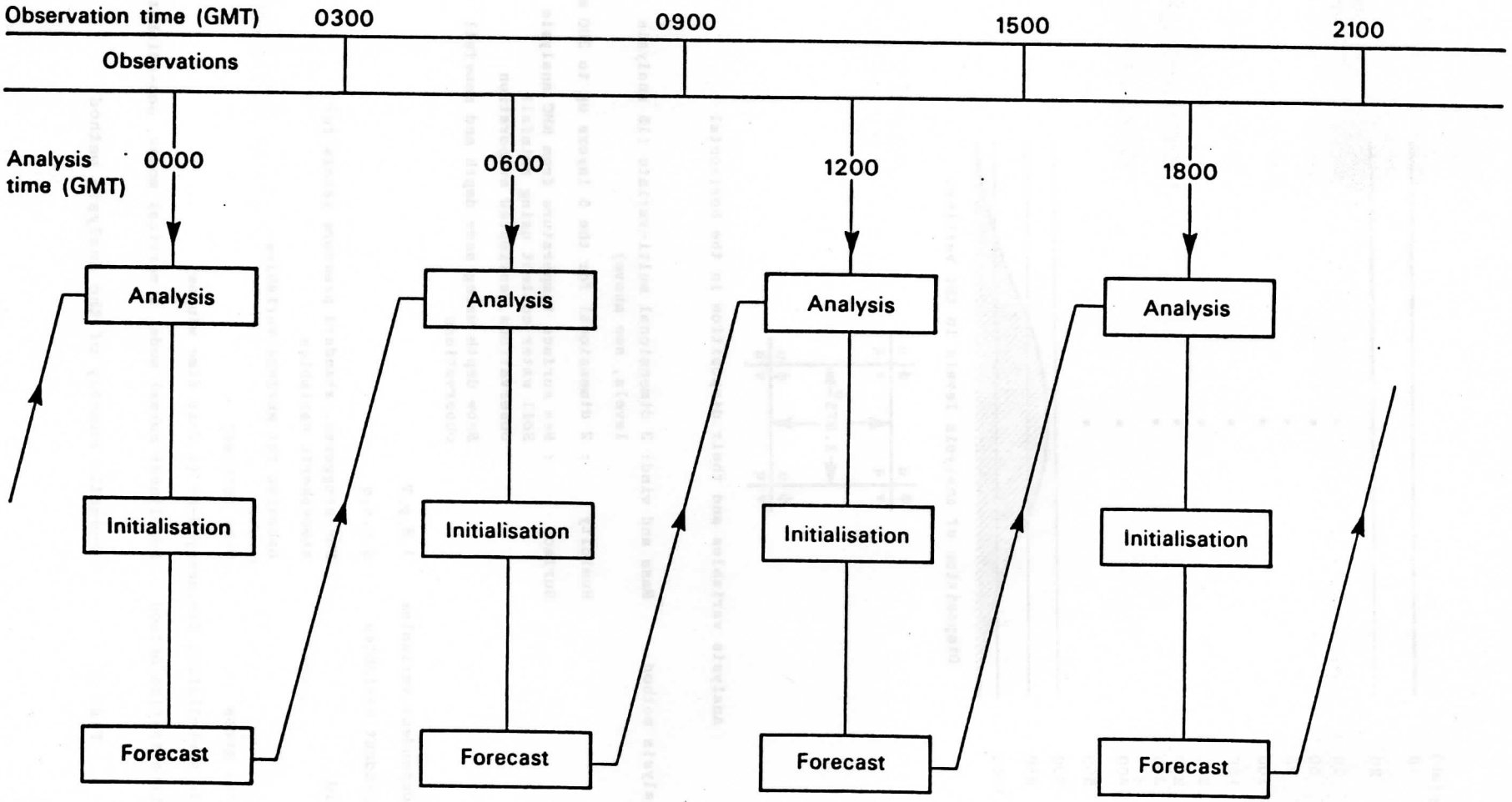

Fig. 1 The 6 hourly intermittent data assimilation

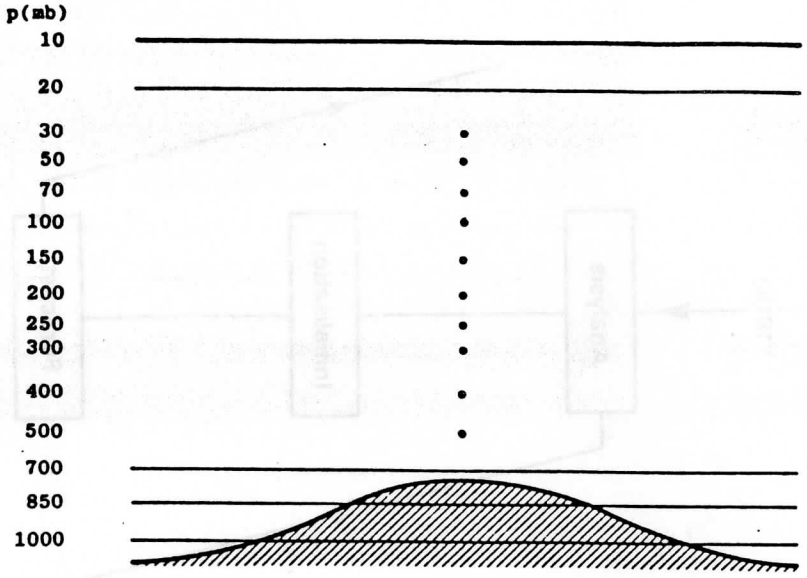

Disposition of analysis levels in the vertical

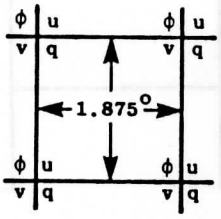

Analysis variables and their disposition in the horizontal

Analysis method	Mass and wind:	3 dimensional multi-variate (15 analysis levels, see above)
	Humidity	: 2 dimensional for the 5 layers up to 300 mb
	Surface	: Sea surface temperature from NMC analysis Soil water content using rainfall observations, estimated evaporation Snow depth using snow depth and snowfall observations
Independent variables	λ,θ,p,T	
Dependent variables	ϕ,u,v,q	
Grid	Non staggered, standard pressure levels for atmospheric variables Gaussian for surface variables	
First guess	6-hr forecast	
Data assimilation frequency	6-hr ($\pm$ 3-hr time window)	
Initialisation method	Non-linear normal mode, 5 vertical modes, non-adiabatic	

Fig. 2 Schematic summary of the analysis method

$A_{k+\frac{1}{2}}$ (mb)	$B_{k+\frac{1}{2}}$
0	0
50	0
99	0.002
142	0.013
173	0.042
191	0.094
194	0.170
182	0.268
157	0.384
125	0.511
89	0.638
54	0.756
26	0.856
8	0.929
0	0.973
0	0.992
0	1

Vertical Coordinate Table (NL=16)

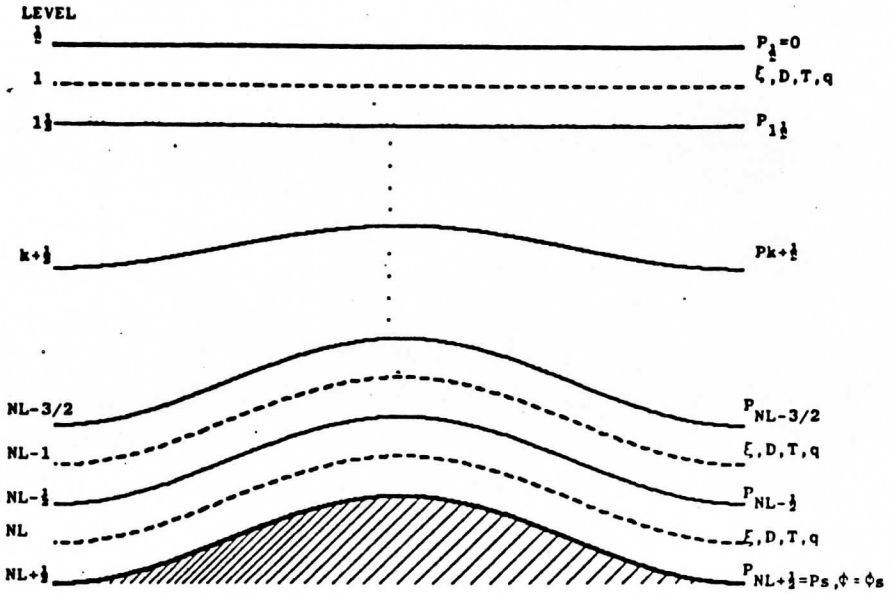

Disposition of variables in the vertical

Dependent variables	ξ,D,T,q,ln(ps)
Vertical coordinate	Hybrid, $P_{k+\frac{1}{2}}=A_{k+\frac{1}{2}}+B_{k+\frac{1}{2}}Ps$, details as above.
Vertical representation	Finite-difference, energy and angular-momentum conserving.
Horizontal representation	Spectral, with triangular truncation at wavenumber 63.
Horizontal grid	96x192 points on a quasi-regular ($\approx 1.875^{o}$) "Gaussian"grid.
Time integration	Leapfrog, semi-implicit (Δt=20,in.), time filter (V=0.06).
Horizontal diffusion	Linear, fourth-order ($K=2\times10^{15}\,m^{4}s^{-1}$).
Orography	Grid-scale average from high resolution data set, enhanced by $\sqrt{2}\times$(standard deviation of sub grid-scale orography), spectrally-fitted.
Vertical boundary conditions	Kinematic.
Physical parameterisation	(i) Boundary eddy fluxes dependent on local roughness length and stability (Monin Obukov).
	(ii) Free-atmosphere turbulent fluxes dependent on mixing length and Richardson number.
	(iii) Kuo convection scheme.
	(iv) Interaction between radiation and model-generated clouds. Albedo dependent on model snow cover.
	(v) Large-scale condensation when grid-square saturated. Evaporation of precipitation.
	(vi) Computed land temperature, no diurnal cycle.
	(vii) Computed soil moisture and snow cover.
	(viii) Fixed, analysed sea-surface temperature.

Fig. 3 Schematic summary of the forecast method

AN INTERCOMPARISON OF TEMPERATURE AND MOISTURE FIELDS RETRIEVED FROM TIROS OPERATIONAL VERTICAL SOUNDER DATA

J. F. LeMarshall
Bureau of Meteorology Research Centre
Melbourne, Australia

ABSTRACT

Fields of temperature, thickness and precipitable water, derived from common sets of Tiros Operational Vertical Sounder (TOVS) radiance data have been intercompared. These fields were produced by a variety of institutions using different retrieval techniques. The fields have been derived over three regions. The region associated with the Alpine Experiment (ALPEX) in 1982, the Tasman Sea and the United States of America (US). Basic statistics have been produced for these derived fields by comparing them to analyses produced by the European Centre for Medium Range Forecasting (ECMWF) and with co-located radiosonde (RAOB) data.

In most cases, it appeared for both physical and statistical retrieval techniques, that in the mid-troposphere (700 to 400 millibars (mb)) the satellite temperature soundings generally exhibited root mean square (RMS) temperature differences of near two degrees Kelvin (2K) when compared to ECMWF analysis or colocated radiosonde data. These figures include contributions due to radiosonde error, colocation differences, analysis error and other factors. Larger differences, which were contributed to by different vertical resolutions amongst the compared fields were evident near the tropopause and the surface. Near the surface they appeared more a function of the use of ancillary data or constraints rather than the retrieval scheme. Basic statistics for thickness and moisture fields have also been presented in this study.

1. INTRODUCTION

The First International TIROS Operational Vertical Sounder (TOVS) Study Conference (ITSC-1) was held in Igls, Austria from 29 August to 2 September 1983. It was attended by scientists from fourteen different countries.

Most of these countries were already producing soundings with high horizontal resolution from the direct readout of TOVS data, for research and operational applications. It appeared that a high level of skill in retrieving satellite soundings had been achieved on an international scale. This widespread use of TOVS data in forecasting and research at all scales has led to a common goal among satellite sounding producers, namely to optimize and standardise TOVS processing procedures so that accurate and uniformly consistent satellite temperature and moisture soundings can be made available to the international meteorological community. To this end one of the key activities of this conference was an evaluation of TOVS processing techniques and data analysis. The ITSC-1 conference made a significant start on this, with initial assessments being made on retrievals from the ALPEX and Tasman sea regions (Menzel and Lynch, 1983). It was concluded however, that a quantitative comparison of temperature and moisture soundings derived by the participants in this study was a vital part of the intercomparison which still remained to be addressed. As a first step in addressing this problem, basic statistics have been derived for temperatures, layer mean temperatures, geopotential thickness and precipitable water observations derived from satellite radiances. The statistics have been derived by comparing these fields to the corresponding ECMWF fields (which over land have not used the NESDIS operational soundings) and to colocated radiosonde data. A representative subset of this intercomparison data, which includes fields nominated for intercomparison at ITSC-1 are presented here.

A description of the synoptic situations associated with the cases studied are found in Menzel and Lynch, 1983.

2. THE CONTRIBUTIONS TO THE INTERCOMPARISON

Eighteen sets of atmospheric soundings derived from common sets of radiance data were provided by the eleven institutions involved in the intercomparison study. The sounding sets were generally a mix of clear and cloudy cases. The participants and a summary of the data sets they have provided are given in Table 1. The entries in the Table are grouped according to the cases studied i.e. the Alpex, Tasman Sea or US Case. A description of, or reference to, the retrieval techniques used in the production of the soundings provided for this study can generally be found in the technical proceedings from the ITSC-1 and ITSC-2 (Menzel, 1983 and Menzel, 1985 respectively). A cryptic summary of the salient features of the retrieval schemes is presented in the table along with the approximate number of soundings received for intercomparison.

3. THE INTERCOMPARISON

This paper both illustrates and discusses the basic statistics generated from the atmospheric sounding sets. Temperature at the fifteen standard levels as well as other fields nominated for intercomparison at the ITSC-1, namely the geopotential thickness of the layers 1000 to 700 mb, 700 to 500 mb, 500 to 300 mb, 300 to 100 mb and 1000 to 500 mb and the precipitable water in the layers 1000 to 400 mb, 850 to 400 mb, 700 to 400 mb and 500 to 400 mb have been compared to their respective ECMWF analysis fields interpolated to the sounding position in time and space. These satellite data have also been compared to colocated within (150 km) RAOB data. In the ALPEX and US cases the RAOB data used was subjected to a gross error checking procedure using the ECMWF analyses The operational validation procedure at the Australian Bureau of Meteorology was used to check the RAOBS in the TASMAN sea case.

Standard differences, biases and RMS differences between the satellite observations and the related ECMWF and RAOB data have been computed and displayed. The standard deviation of standard level temperatures both from satellite measurements and from ECMWF analyses or RAOB measurements about their respective means has been calculated from data located at the satellite sounding points. These standard deviations along with correlation coefficients between temperatures derived from satellite observations and the corresponding ECMWF or RAOB data have also been displayed. The basic statistics are seen in Figures 1 to 43.

4. THE BASIC STATISTICS

4.1 ALPEX Case

Comparison of the satellite soundings for the ALPEX case with ECMWF data (Figures 1 to 22) indicated both the physical and statistical retrieval schemes generally have standard differences just below 2K between 850 and 400 mb, while a comparison with RAOB data indicates standard differences close to 2K. (It should be noted comparison of this radiosonde data set with ECMWF data has indicated a standard difference near 1.5K between 850 and 300 mb (Smith el al., 1983), reflecting both the lack of small horizontal scale detail in the ECMWF archived analyses, which have a grid resolution near 200 km and also the errors and systematic differences among the radiosondes themselves.) The standard differences above 850 mb generally appeared larger in comparison to RAOB data rather than ECMWF data as a result of the inherent smoothing in the TOVS and ECMWF profiles relative to the radiosonde profiles. This was quite noticeable near the tropopause where the larger standard differences compared to RAOB data were around 4K, while compared to ECMWF data they were closer to 3K.

Near 850 mb and below, the standard difference for both physical and statistical schemes was generally significantly larger

than in the 850 to 300 mb layer and was strongly influenced by the use of ancillary data or other constraints. This can be seen by examining the basic statistics for, the ALIT1 and ALIT2 cases which differ in that the ALIT2 case used surface data as a constraint when solving for the temperature and moisture profiles, Smith et al., 1983 and the ALFR case which used ECMWF forecast data as part of an ancillary data set.

An examination of the biases for these ALPEX soundings indicated the soundings have been mostly too cold near the surface, have smaller biases in the mid troposphere and then often exhibited a negative bias (too cold near 300 mb) positive bias (too warm near 200 mb), then negative bias (too cold near 100 mb) with increasing altitude near the tropopause. This variation in bias near the tropopause was contributed to by the inherent vertical smoothing of the TOVS profile which was quite detrimental in this region of sharp vertical temperature variation. A similar variation in bias was seen when comparing the ALPEX radiosonde data with ECMWF data around the tropopause region (see e.g. Smith et al., 1983). Again near 850 mb and below the biases showed the strong influence of ancillary data or other constraints on the soundings. The basic statistics for the ALIT1 and ALIT2 cases, Smith et al., 1983 and the ALFR case again illustrated this.

Root mean square difference statistics reflected the net effect of bias and standard difference. As a result they were generally larger near the tropopause and near and below 850 mb where they were strongly influenced by ancillary data or other constraints. Near the tropopause RMS differences compared to ECMWF data were generally a little larger than 3K while compared to RAOB data they were generally just over 4K. Comparison with ECMWF data also indicated RMS differences in the 850 to 400 mb layer, just below 2K while comparison with RAOB data indicated RMS differences close to 2K.

The thickness data illustrated in Figures 1(c) and (d) to 22(c) and (d) show for those fields nominated for intercomparison at ITSC-1, the standard differences, biases and RMS differences compared to ECMWF analysis and RAOB data. The thickness data result from the vertical integration of the temperature data already described. The statistics generally showed a cold bias in the lowest level, 1000 to 700 mb. The RMS differences for the 700 to 500 mb layer were near 20 metres (m), and for the 500 to 300 mb layer between 30 and 40m. It should be noted the mean 1000 to 500 mb thickness RMS difference compared to the ECMWF analyses was only 32 m.

The correlation coefficients relating coincident satellite and ECMWF standard level temperatures have also been illustrated. Generally the coefficients exceeded 0.9, except near the surface and tropopause and above 100 mb. Again the impact of surface constraints can be seen by examining the data for ALIT1 and ALIT2. The correlation coefficients relating colocated satellite and RAOB temperatures showed a similar variation with height. They were

reduced in magnitude compared to the satellite/ECMWF comparison data, particularly near the tropopause; where the difference in resolution of the two data forms is expected to have an influence.

The standard deviation (SD) of both the satellite standard level temperatures and the related colocated RAOB or coincident ECMWF temperatures is illustrated in Fig 1(e) to 22(e). Although the vertical variation of satellite and related comparison fields with height were similar, some differences were seen, particularly in relation to the TOVS/RAOB comparison. In comparison to radiosondes, the TOVS data almost always appeared to have a similar SD near 700 mb, a larger SD below about 700 mb and a lesser SD above about 700 mb. A significant reduction in SD for the satellite data compared to the RAOB data was seen near the tropopause as expected, while the effect of surface constraints could also be seen in the SD's (see e.g. ALIT1 and ALIT2). Explanation of the relative size of the SD's near the surface awaits amongst other things, on the completion of an examination of the horizontal distribution and correlation of differences at those levels. In comparison to ECMWF analyses the TOVS data, in the majority of cases, showed a larger standard deviation near the surface and usually had a smaller SD in the mid and upper troposphere. A significant reduction in SD was again evident near the tropopause (around 200mb).

The basis statistics for the retrieved precipitable water are illustrated in Figures 37 to 39. They show only small differences between the regression and statistical schemes in an RMS sense; the regression schemes appeared to have slightly larger biases and smaller standard differences. The one step simultaneous solution scheme however appeared quite skillful in estimating the moisture in the lowest levels, a result consistent with previous simulation studies. In the ALPEX case, RMS differences for precipitable water often represented just over forty percent of the moisture in the 1000 to 400 mb and 850 to 400 mb column. It should be borne in mind however moisture varies rapidly in time and space. This combined with the errors associated with the measurement of moisture by radiosonde, the resolution of the ECMWF analyses and the colocation criteria employed, may result in the basic statistics not truly reflecting the skill of the various schemes in depicting the mesoscale structure of these moisture fields. As a result further detailed intercomparisons of these moisture fields are presently underway.

4.2 TASMAN SEA Case

The four data sets examined for the TASMAN SEA case exhibited basic statistics similar in many ways to those seen in the ALPEX study. A difficulty besetting the TASMAN SEA study however was a lack of non-satellite data for the intercomparison. As a result the comparisons with RAOB data often represent only ten to twenty colocations and the ECMWF analyses used in the study which are predominantly over the sea have been influenced by NESDIS sounding

data. Interpretation of the intercomparison may be further complicated by the use of NESDIS retrieval coefficients in the New Zealand retrieval scheme. Despite the very limited amount of RAOB data available for the intercomparison and the influence of NESDIS sounding data in the ECMWF analyses the basic statistics have been presented (albeit very reluctantly in the case of RAOB comparisons) in Figures 23 to 30 chiefly because they provide some broadening of the intercomparison study.

The comparison of the satellite measured standard level temperatures with ECMWF analyses again showed RMS differences near 2K in between 850 and 300 mb, while comparison with the very limited number of radiosondes resulted in a wider scatter of results. The characteristics of the standard differences and RMS differences near the surface and tropopause appeared similar to those for the ALPEX case. An examination of the biases for these TASMAN SEA soundings indicated they appear a little cold relative to the ECMWF analyses and RAOBS between 800 and 400 mb and too warm near 200 mb. The variation in bias near the tropopause has again reflected the inherent vertical smoothing of the TOVS data in that region.

The basic statistics for the thickness data, which as noted results from vertical integration of the temperature data are also shown in Figures 23(c) and (d) to 30(c) and (d). Generally the RMS differences compared to either ECMWF or RAOB data for the 1000 to 700 mb layer were around 20m, for the 700 to 500 mb layer they were near 20m and for the 500 to 300 mb layer were around 25m. The mean RMS difference for the 1000 to 500 mb layer compared to ECMWF analyses was 29 m.

The correlation coefficients related to coincident satellite and ECMWF or RAOB standard level temperatures are illustrated, they show a similar variation with height to the ALPEX case. The standard deviations of the standard level temperatures are also shown and although the sample in the RAOB comparison is very small (and possibly not representative) it appears the standard deviation of the satellite standard level temperatures below 100 mb is generally smaller than those of the RAOBS or the ECMWF analyses.

The precipitable water plots are seen in Figures 40 and 41. The standard difference of these fields generated by different retrieval techniques, compared to the ECMWF data, were very similar while in comparison to the very small radiosonde sample there was a wider scatter of results. Differences in RMS differences compared to ECMWF data reflected a difference in bias amongst the sets of sounding data. The RMS differences compared to the ECMWF moisture data represent over thirty percent of the moisture for the 1000 to 400 mb column and well over forty percent of the moisture in the 850 to 400 mb column.

4.3 US Case

Three data sets have been examined for the US case and the basic statistics are seen in Figures 32 to 36. For the standard level temperatures, the standard difference and RMS difference distributions derived by comparison with ECMWF or RAOB data are of the same general shape as those for the ALPEX study. The standard differences and RMS differences were mostly near or below 2K between 850 and 300 mb and are larger near the surface and tropopause. The general reduction in the magnitude of these differences compared to the ALPEX study was probably contributed to by the small gradients in the temperature fields, which mitigated differences caused by the colocation criteria, interpolation and the different resolution of the data being compared.

Basic Statistics for thickness are shown for two data sets. The RMS differences compared to ECMWF fields or RAOB data for the 1000 to 700 mb and 700 to 500 mb layers were generally near or less than 20 m. The mean RMS difference for the 1000 to 500 mb thickness compared to ECMWF was 28 m.

The correlation coefficients relating coincident satellite and ECMWF or RAOB standard level temperatures are illustrated. They had a similar variation with height to the ALPEX data, but a reduced magnitude. This was contributed to by the lack of variation in the temperature field. This lack of variance in the temperature field is seen in reduced values of standard deviations which are apparent at most levels.

The precipitable water intercomparisons are seen in Figures 42 and 43. The RMS difference compared to the ECMWF analyses represented over thirty percent of the moisture in the 1000 to 400 column and just over forty percent of the water in the 850 to 400 mb column. The differences compared to RAOB data represented over thirty percent of the moisture in both the 1000 to 400 mb and in the 850 to 400 mb column.

SUMMARY AND CONCLUSIONS

Eighteen sets of soundings from internationally distributed institutions, which were derived using a variety of statistical and physical retrieval techniques have been intercompared. No attempt has been made, nor is there any intention to rank the retrieval schemes relative to one another. Although no doubt, some readers will attempt this. It should be borne in mind however that the basic statistics presented here are not simply a function of the basic retrieval scheme but related in a complex way to:

(i) the number of retrievals ie. they are very susceptible to change as a result of editing procedures and as a result of which particular radiances are processed.

(ii) the characteristics of the first guess fields.

(iii) the use of ancillary date eg. the use of surface observations, AVHRR data, etc.

(iv) The scheme used to remove the effect of clouds from the observed radiances.

(v) the resolution of the retrieval scheme ie. the number of radiance observations used to generate each retrieval and in some cases whether the same radiances have been used in the generation of different soundings.

(vi) the relative contributions of clear, cloudy and overcast soundings; and

... a variety of other influences.

As a result all attempts at comparison should keep these points in mind as well as the size of the samples being compared.

With these sentiments in mind however valuable general comments about the salient features of the various retrieval schemes can be made:

(i) Notwithstanding the recognised advantages of the physical retrieval schemes, the general accuracy and consistency of the retrieved soundings at the scale examined, were to a significant degree independent of the retrieval scheme used. This was illustrated by comparison of satellite significant level temperatures, thickness and precipitable water values to both ECMWF and RAOB data.

(ii) Both operational and research processing of TOVS radiances data has indicated the TOVS instrument is capable of providing soundings with RMS differences near 2K compared to ECMWF analyses and RAOB data from 850 mb to the tropopause region.

The size of these differences illustrate the utility of the data especially when one considers the differences in scale associated with the RAOB and ECMWF data, differences generated as a result of the colocation criteria and the errors in the RAOB and ECMWF temperature values themselves.

The TOVS versus RAOB statistics can be analysed further using the figures provided by Bruce et al., 1977 to estimate radiosonde errors and to estimate the temperature variability over small horizontal distances. A typical calculation for the mid-troposphere shows the contribution to the RMS

difference from radiosonde error and the contribution resulting from comparison of an area averaged temperature and a point temperature is near 1K for typical separation distances in this study. At 700mb for example, removal of these effects reduces a typical RMS difference of 2.1K to 1.8K. This figure (1.8K) however still contains differences due to the systematic errors arising from the use of different radiosonde types and correction procedures for radiation effects (factors not included in the Bruce et al. 1977 study). It also contains differences due to the time differences between the compared soundings, the effects of RAOB translation during flight and other factors.

(iii) There was an increase in the magnitude of the differences near the tropopause and surface. This was contributed to by the inherent vertical smoothing of the TOVS profile in these regions of sharp vertical temperature profile. These differences were changed considerably by ancillary data (eg. surface data) or constraints.

(iv) The magnitude of geopotential thickness differences displayed in this study attests to the utility of the data, particularly those thicknesses over significant layers where a cancellation of biases tends to occur. The 1000 to 500 mb thickness for example, a field of considerable meteorological significance, shows RMS differences of around only three to four decameters. It is interesting to note in the southern hemisphere the alternative to using this data over most of the hemisphere is cloud picture interpretation (Guymer, 1978) where the resulting RMS errors are considerably higher away from conventional data areas.

(v) The basic statistics associated with the retrieval of moisture show a useful degree of skill, particularly when one is mindful of the effects of comparing a field of such high spatial and temporal variability with ECWMF fields and RAOB data and of the errors associated with the measurement of moisture by radiosonde. The degree of skill shown suggests a utility for both NWP and nowcasting applications where a detailed horizontal distribution as well as the vertical distribution of moisture is required for forecasting purposes. The utility of the sounding data for nowcasting applications has already been demonstrated by Keller and Smith, 1983 in a study of severe weather occurrence over the US. They found in that study the objective forecasting of the location of severe weather events had more skill when based on satellite data rather than RAOB data, largely because of its dependence on the horizontal moisture distribution which could only be determined by measurements at the resolution of the TOVS data.

In summary eighteen sets of sounding data, derived using different retrieval techniques have been examined. The basic statistics for the derived temperature, geopotential thickness and moisture have been calculated, illustrated and summarized. They indicate an almost uniformly high standard of retrieval skill has been established on an international level. Two major problems still hinder further refinement of the intercomparison study. One is use of radiosondes which as yet have not been reliably intercalibrated. Although this task is being addressed by recent WMO intercomparison studies and several data analysis centres, there is still no way of removing systematic differences, reliably from data derived from different radiosondes. The establishment of a Baseline Upper-Air Network may be significant step in solving this problem. The second problem is the estimation and removal of differences generated by comparing quantities observed at different resolutions. This problem, particularly as it related to the moisture field is presently being examined. A study of the effects of measurement scale on the intercomparison, additional statistics and further contrasting of the differences between the physical and statistical techniques will appear in a companion paper.

Acknowledgements

I would like to thank Graeme Kelly who provided the ECMWF tapes used for this intercomparison study and Tony Schreiner and Geary Callan who provided the RAOB data for the ALPEX and US cases. Many thanks are also due to Jenny Guarino and Paul Hambleton for their part in the data processing and to Bob Seaman for helpful comments.

References

Bruce, R.E., L.D. Duncan and J.H. Pierluissi, 1977: Experimental Study of the Relationship Between Radiosonde Temperatures and Satellite-Derived Temperatures. Mon Wea. Rev. 105, 493-496.

Guymer, L.B. (1978): Operational Application of Satellite Imagery to Synoptic Analyses in the Southern Hemisphere. Tech. Rep. 29, Bur. Met. Australia.

Keller, D.L. and W.L. Smith, 1983: A Statistical Technique for Forecasting Severe Weather from Vertical Soundings by Satellite and Radiosonde. NOAA Technical Report, NESDIS 5. NOAA, US Dept. of Commerce, Washington DC, June 1983. 35pp.

Menzel, W.P., 1983: Tech. Proc. First International TOVS Study Conference, Igls, Austria. A report from the Cooperative Institute for Meteorological Satellite Studies, Space Science and Engineering Centre, University of Wisconsin-Madison. 352pp.
Menzel, W.P. and M.J. Lynch, 1983: A report on the first International TOVS Study Conference, Igls, Austria. A report from the Cooperative Institute for Meteorological Satellite Studies, Space Science and Engineering Center, University of Wisconsin-Madison 32pp.

Smith, W.L., H.M. Woolf, C.M. Hayden, A.J. Schreiner and J.F. Le Marshall, 1983: The physical retrieval TOVS export package. Tech. Proc. First International TOVS Study Conference, Igls, Austria. A report from the Cooperative Institute for Meteorological Satellite Studies, Space Science and Engineering Center, University of Wisconsin-Madison.

TABLE 1

Summary of contributions to the intercomparison study. (Note T represents temperature data, Z represents thickness data, P represents moisture data, WEI, WEII and WEIII represent the Wisconsin TOVS Export Package I, II and III respectively, RFG represents regression first guess field, CFG represents climatology first guess field, MFG represents first guess fields derived from a forecast model, SD indicates use of surface data in the retrieval scheme, AVHRR represents the use of AVHRR in the data processing algorithms, LRC represents the use of locally generated regression coefficients and NRC indicates the use of NESDIS regression coefficients.)

DATA ORIGIN	CASE		ABBREV.	CONTENT	NOBS	RET. SCHEME
ALPEX						
British Met. Office	1	ALPEX	ALUK	T, Z, P	~ 695	Statistical (modified WEI) (NRC)
CIMSS/NOAA-NESDIS Wisconsin	2	ALPEX	ALWI1	T, Z, P	~1717	Physical (Iterative) (WEII, RFG, SD)
	3	ALPEX	ALWI2	T, Z, P	~1818	Physical (One step) (WEIII, CFG, SD)
	4	ALPEX	ALWI3	T, Z, P	~1828	Physical (One step) (WEIII, RFG, SD)
DFVLR West Germany	5	ALPEX	ALDF	T, Z, P	~1376	Physical (Iterative) (modified WEII, RFG, SD)
Laboratoire de Meteorology Dynamique France	6	ALPEX	ALFR	T, Z	~4080	Physical/ Statistical
NASA/GLAS United States	7	ALPEX	ALNA	T, Z, P	~ 903	Physical (relaxation) (MFG)
NOAA-NESDIS Washington	8	ALPEX	ALNE	T, Z	~213	Statistical (Operational Algorithm)

DATA ORIGIN	CASE	ABBREV.	CONTENT	NOBS	RET. SCHEME
University of Bologna Italy	9	ALPEX ALIT1	T, Z, P	~1514	Physical (Iterative) (modified WEII)
	10	ALPEX ALIT2	T, Z, P	~1757	Physical (Iterative) (modified WEII, SD)
Western Australia Institute of Technology	11	ALPEX ALWA	T, Z, P	~2807	Statistical (Modified WEI) (NRC)
TASMAN					
Bureau of Meteorology Australia	12	TASMAN TAAU	T, Z, P	~2755	Statistical (Modified WEI) (discriminant anal, LRC, operational algorithm with SD)
CIMSS/NOAA NESDIS Wisconsin	13	TASMAN TAWI	T, Z, P	~1625	Statistical (WEII, RFG, SD)
New Zealand Meteorological Service	14	TASMAN TANZ	T, Z, P	~2009	Statistical (Modified WEI) (NRC)
NOAA-NESDIS Washington	15	TASMAN TANE	T, Z	~217	Statistical (Operational Algorithm)
US CASE					
Atmospheric Environment Service (AES) Canada	16	US USCA	T, P	~254	Statistical (Modified WEI) (NRC)
British Met. Office	17	US USUK	T, Z, P	~163	Statistical (Modified WEI) (NRC)
CIMSS/NOAA-NESDIS	18	US USWI	T, Z, P	~132	Physical (Iterative, AVHRR)

ALUK

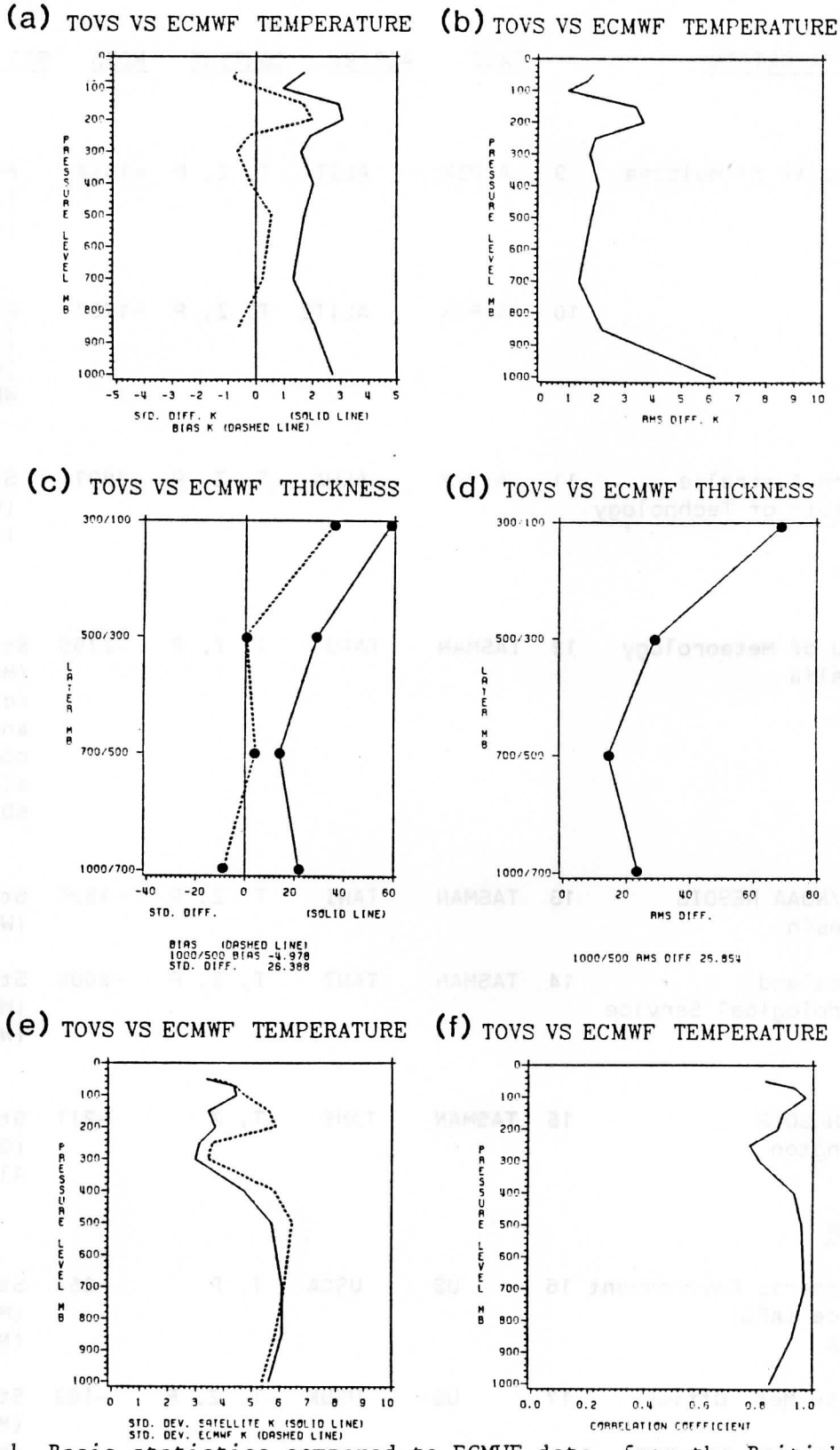

Fig. 1 Basic statistics compared to ECMWF data, from the British Met. Office retrievals for the ALPEX case (a) Standard difference and bias of temperature observations compared to ECMWF analyses (b) the associated root mean square (RMS) difference (c) Standard difference and bias (m) of the layer thicknesses nominated for intercomparison at ITSC-1 compared to ECMWF (d) the associated RMS difference (e) Standard deviation of coincident standard level temperatures from satellite observations and ECMWF analyses (f) the correlation between coincident standard level temperatures from satellite observations and ECMWF analyses. (see ALUK in Table 1).

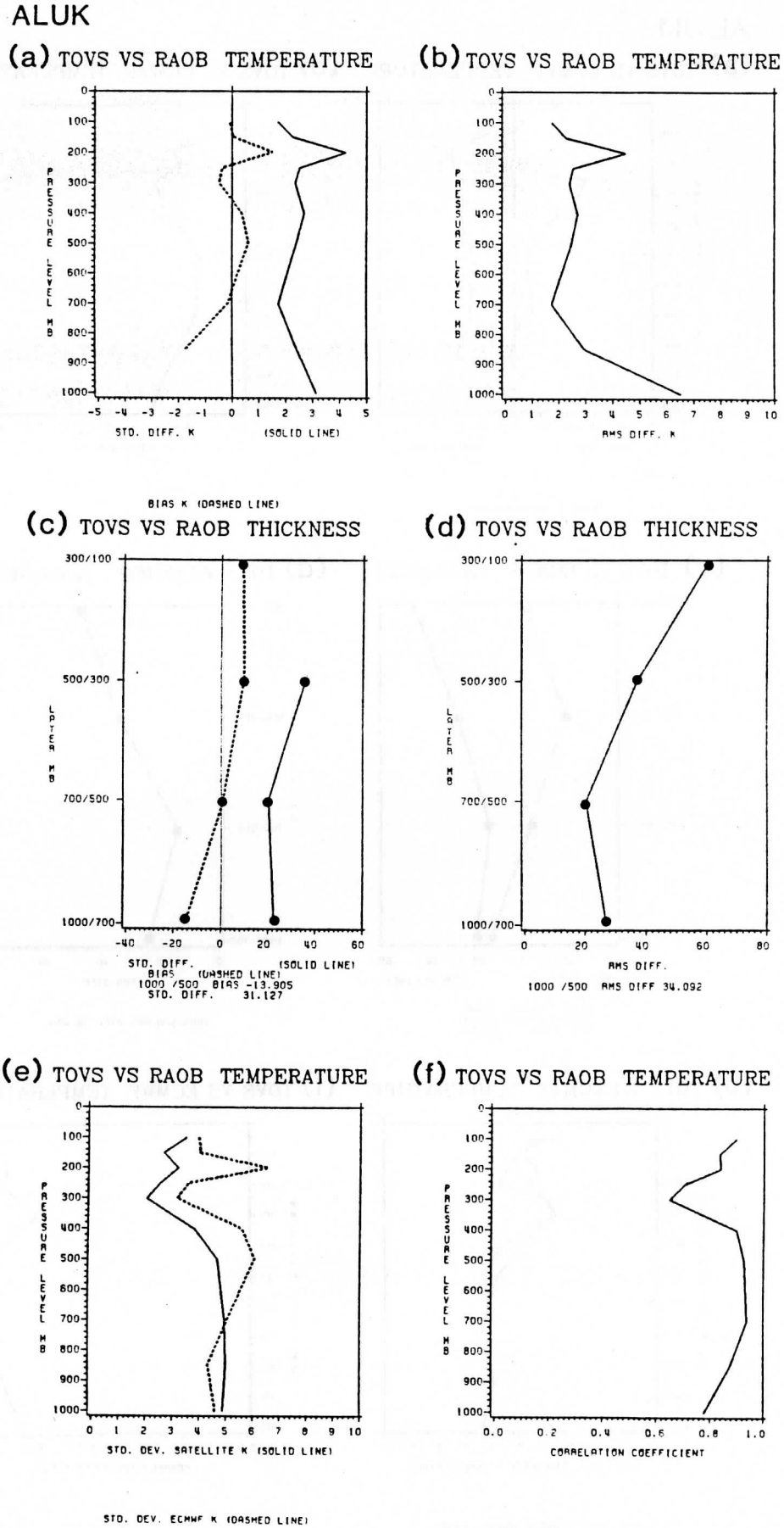

Fig. 2 As in Figure 1 but with the comparisons done with colocated radiosondes (see ALUK in Table 1).

ALWI1

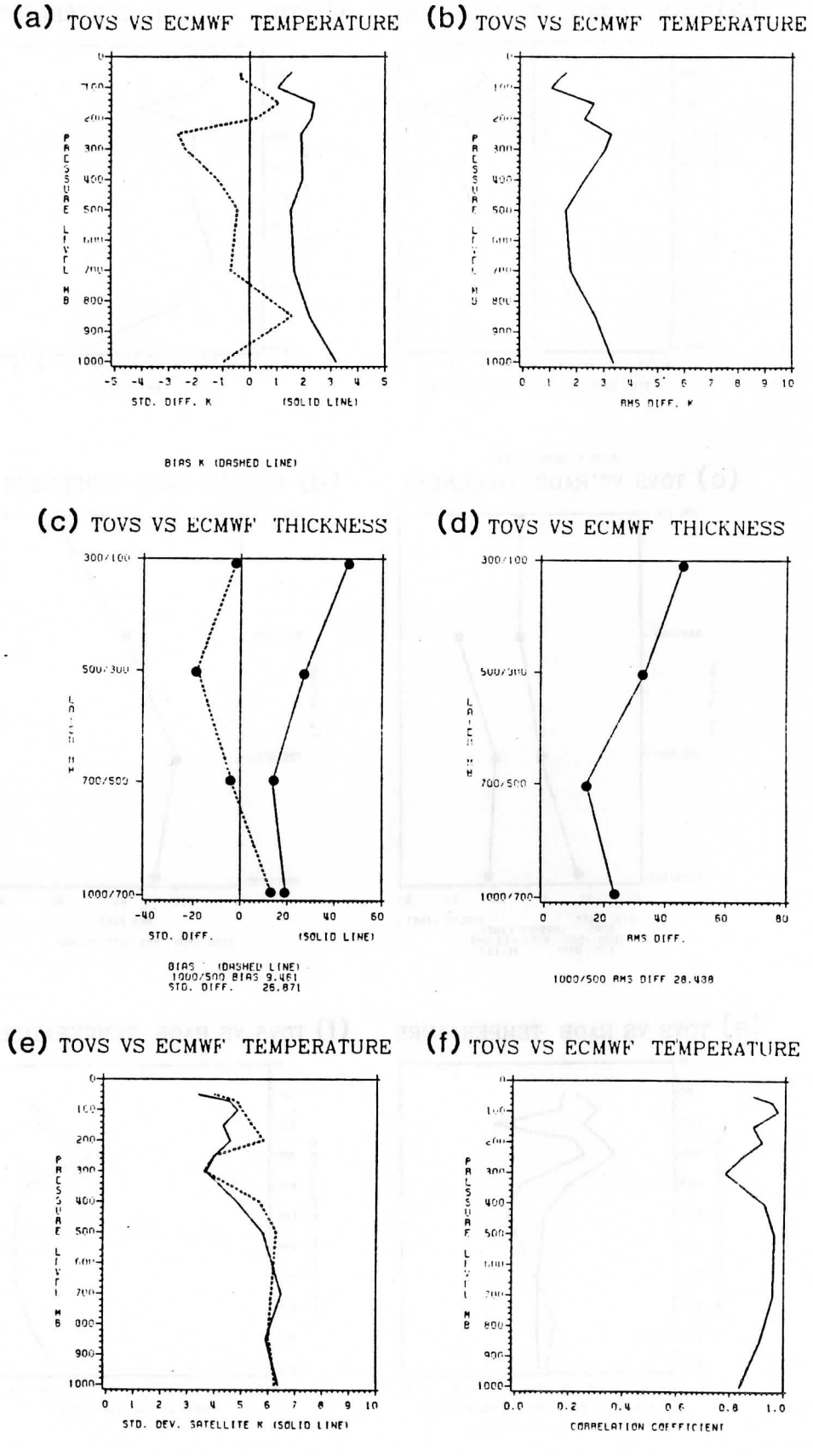

Fig. 3 As in Figure 1 but data from CIMSS, Wisconsin (see ALWI1 in Table 1).

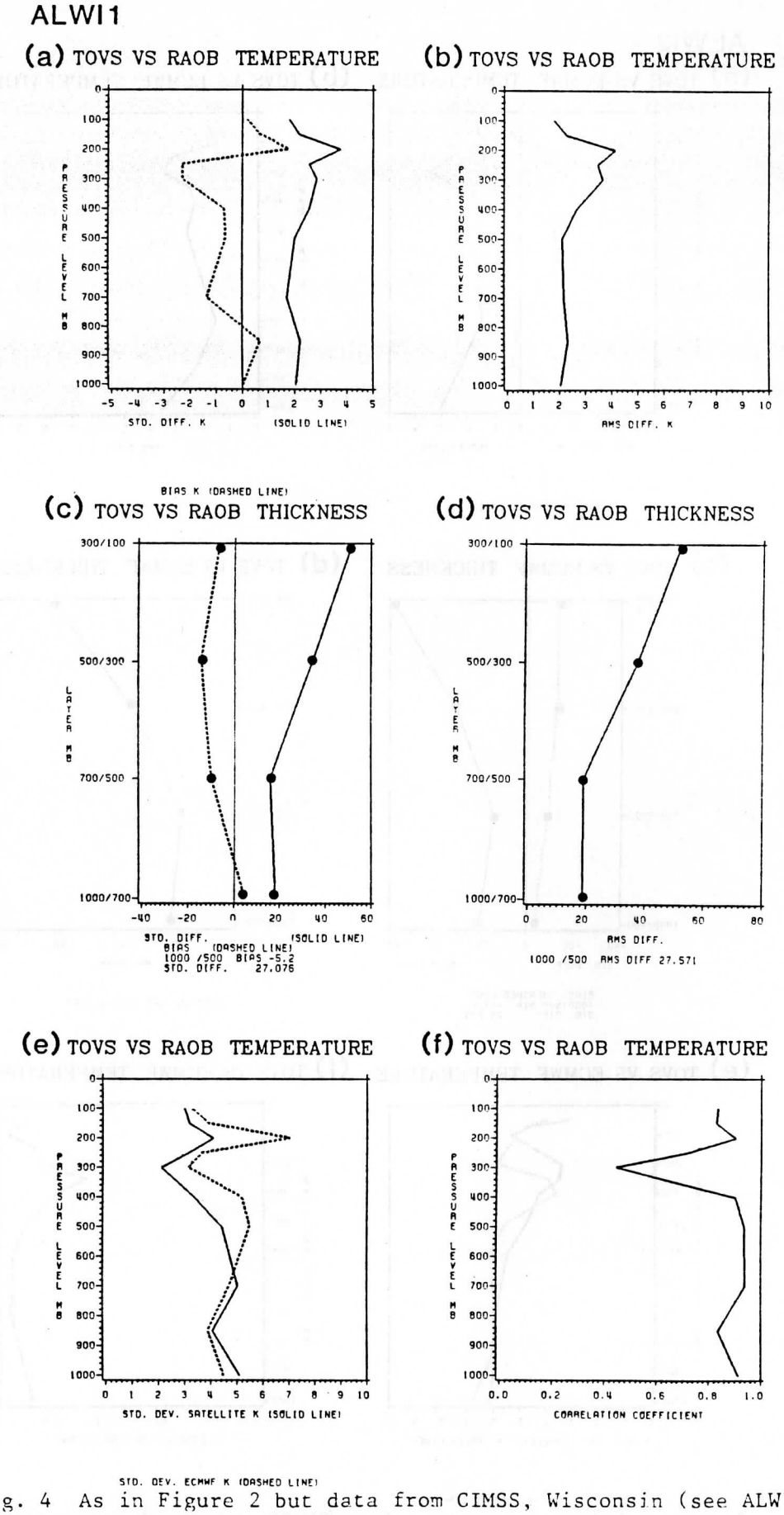

Fig. 4 As in Figure 2 but data from CIMSS, Wisconsin (see ALWI1 in Table 1).

ALWI2

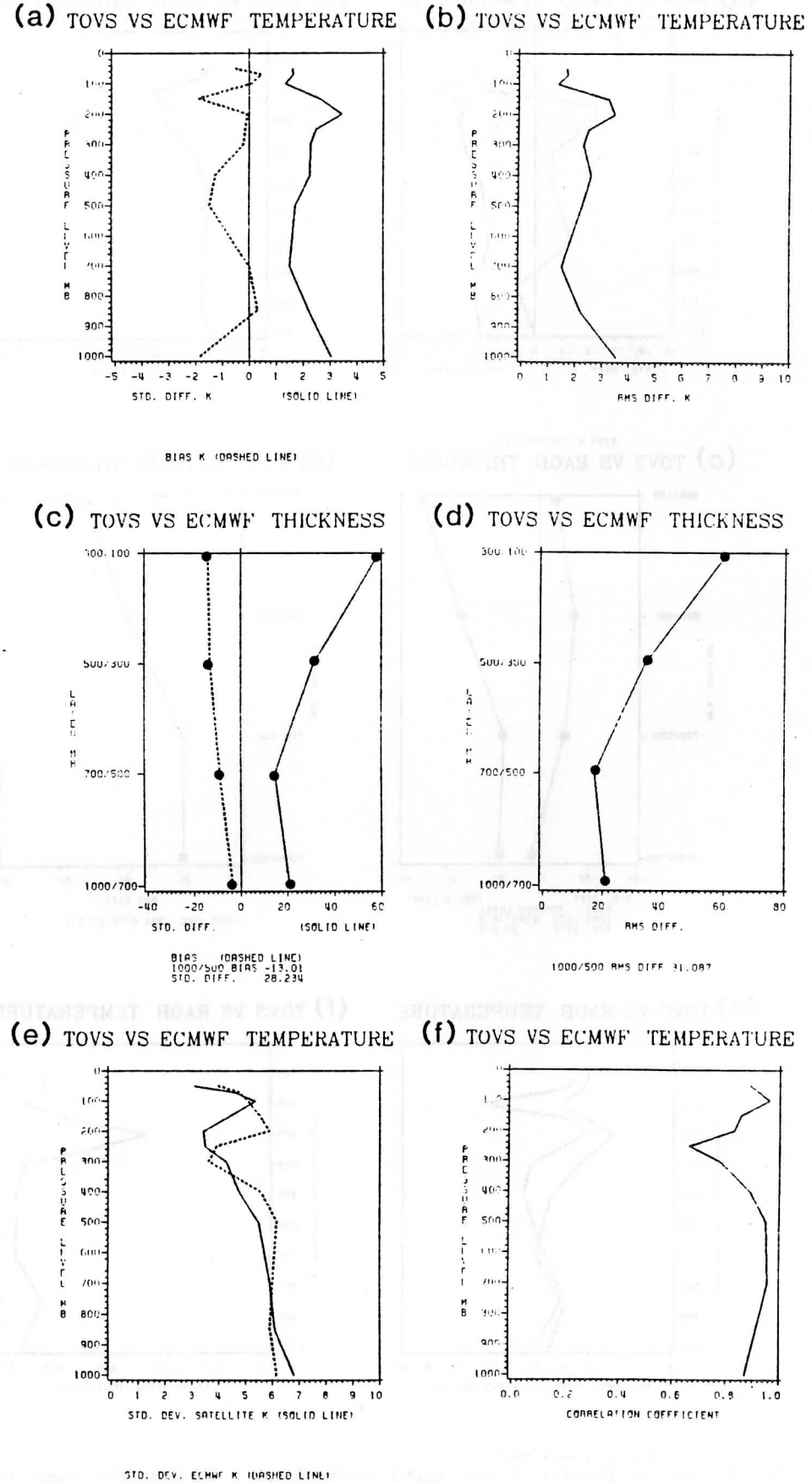

Fig. 5 As in Figure 1 but data from CIMSS, Wisconsin (see ALWI2 in Table 1).

ALWI2

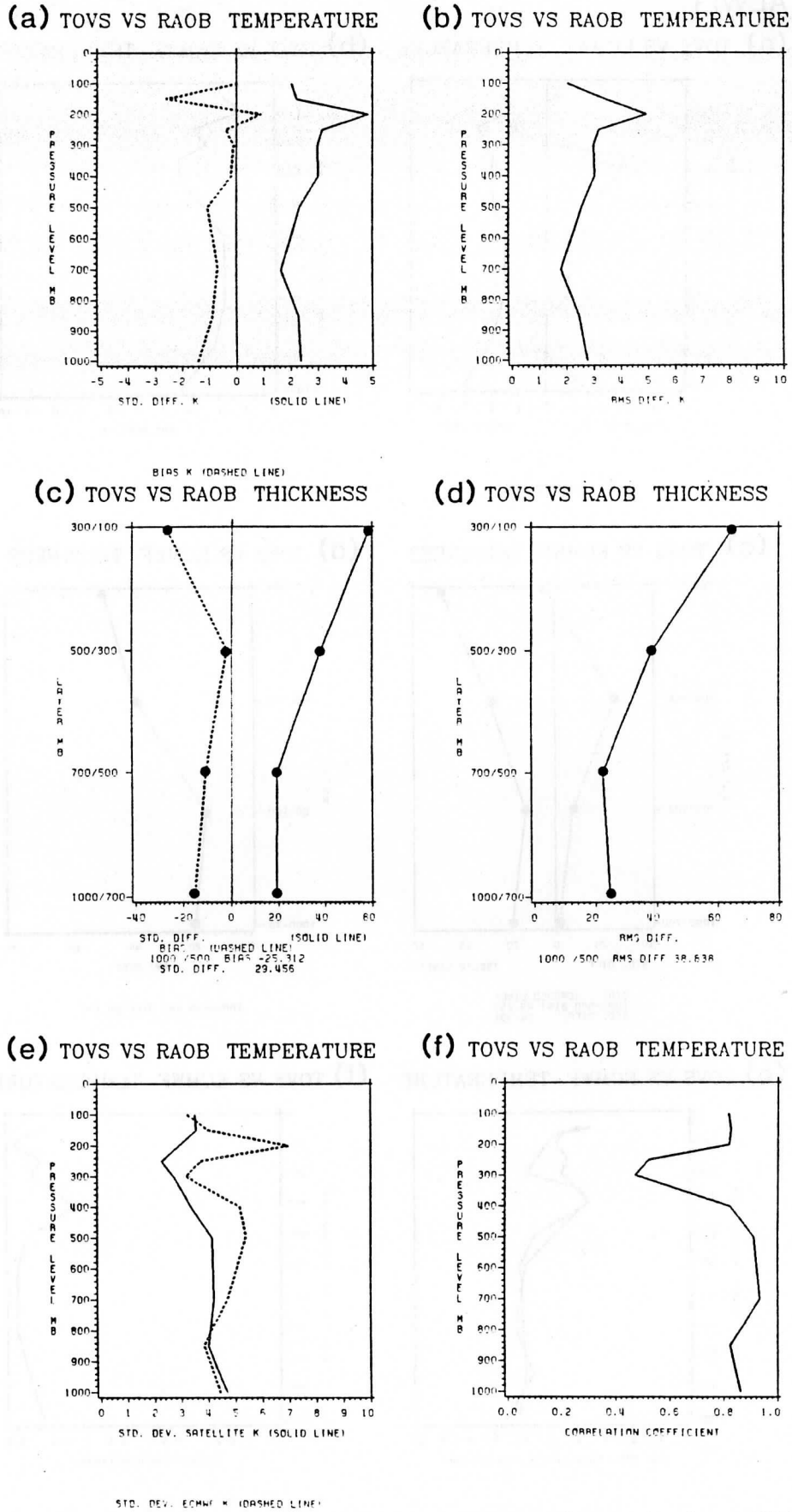

Fig. 6 As in Figure 2 but data from CIMSS, Wisconsin (see ALWI2 in Table 1).

ALWI3

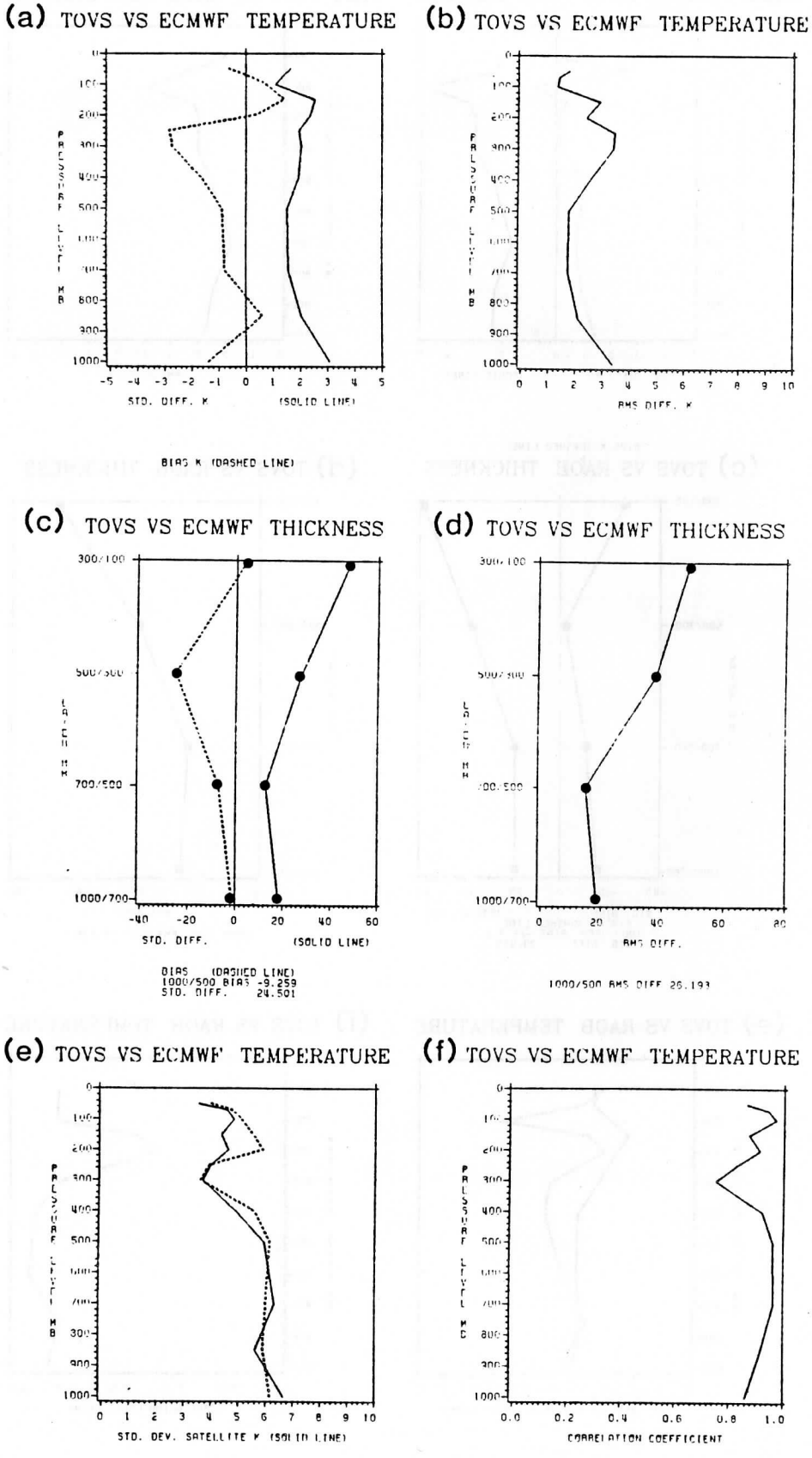

Fig. 7 As in Figure 1 but data from CIMSS, Wisconsin (see ALWI3 in Table 1).

ALWI3

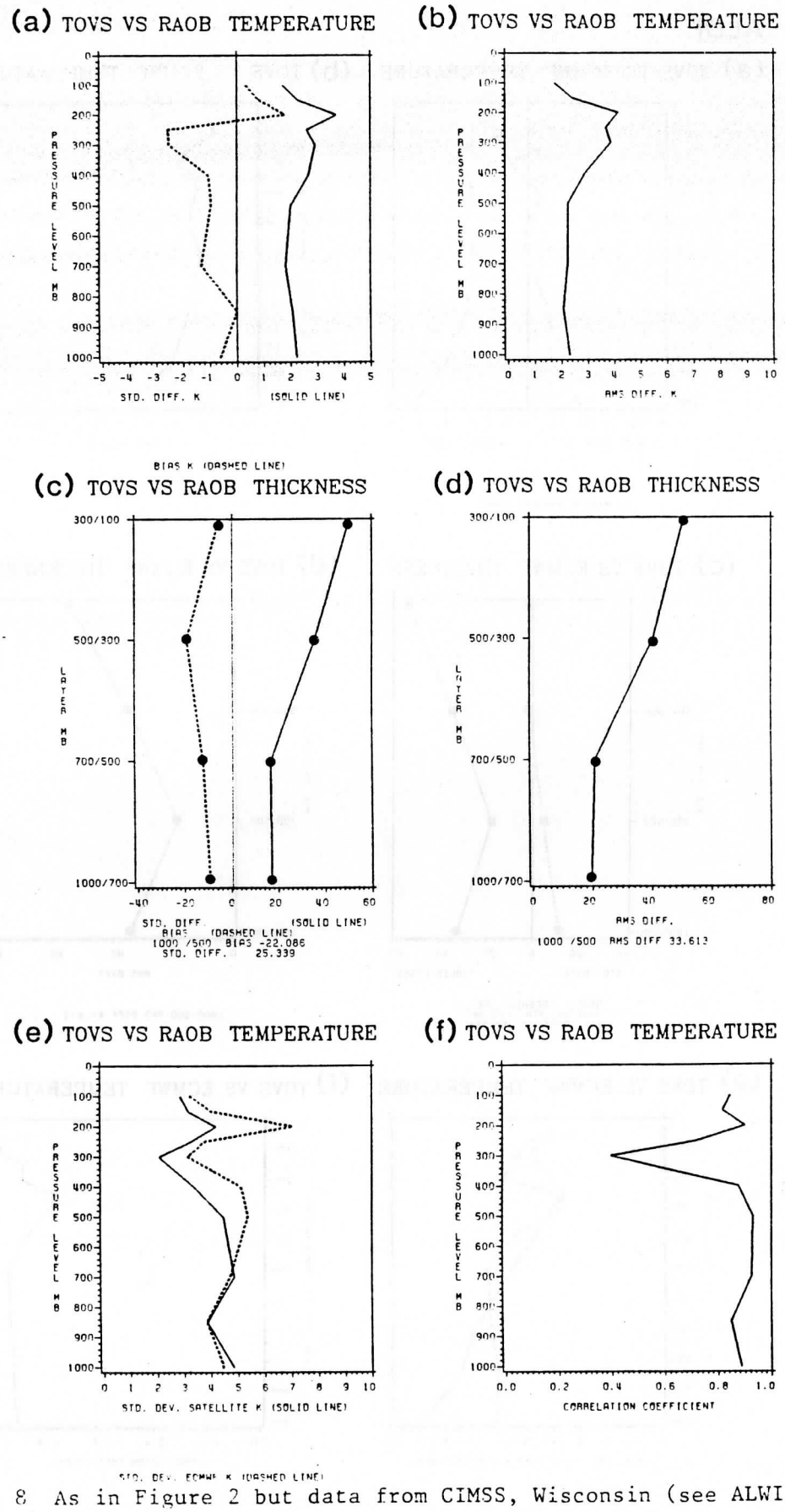

Fig. 8 As in Figure 2 but data from CIMSS, Wisconsin (see ALWI3 in Table 1).

ALDF

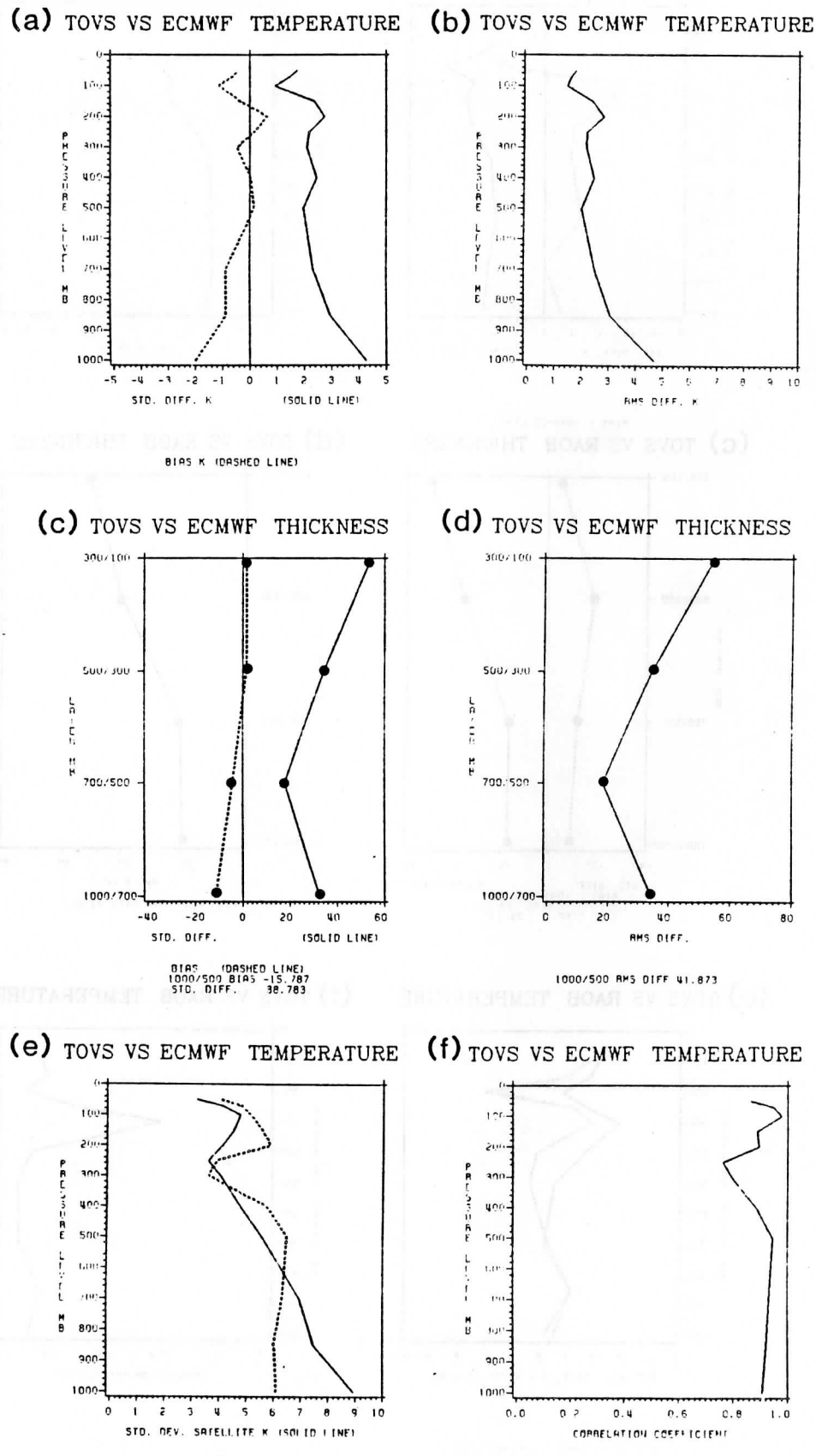

Fig. 9 As in Figure 1 but data from DFVLR, West Germany (see ALDF in Table 1).

ALDF

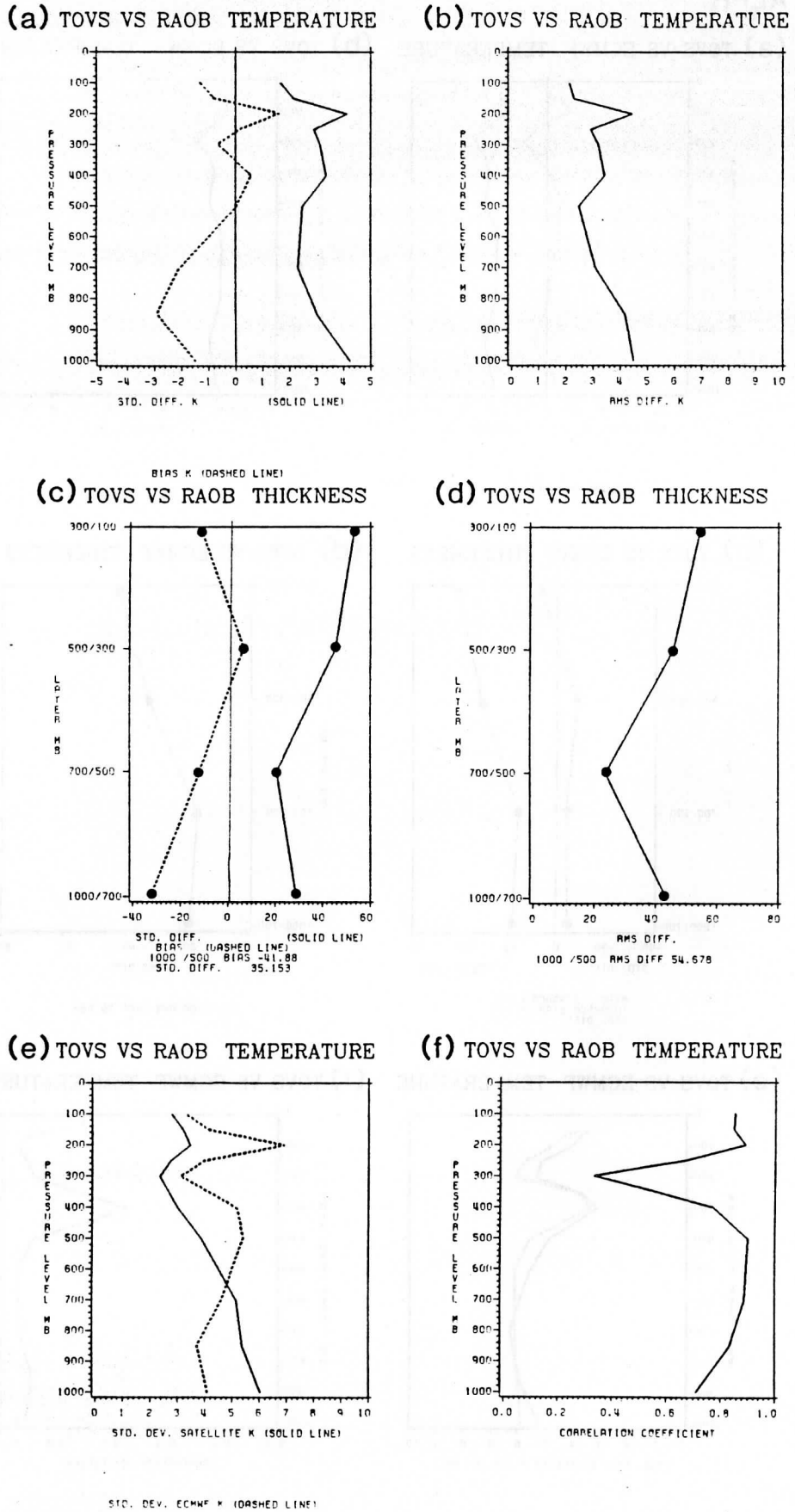

Fig. 10 As in Figure 2 but data from DFVLR, West Germany (see ALDF in Table 1).

ALFR

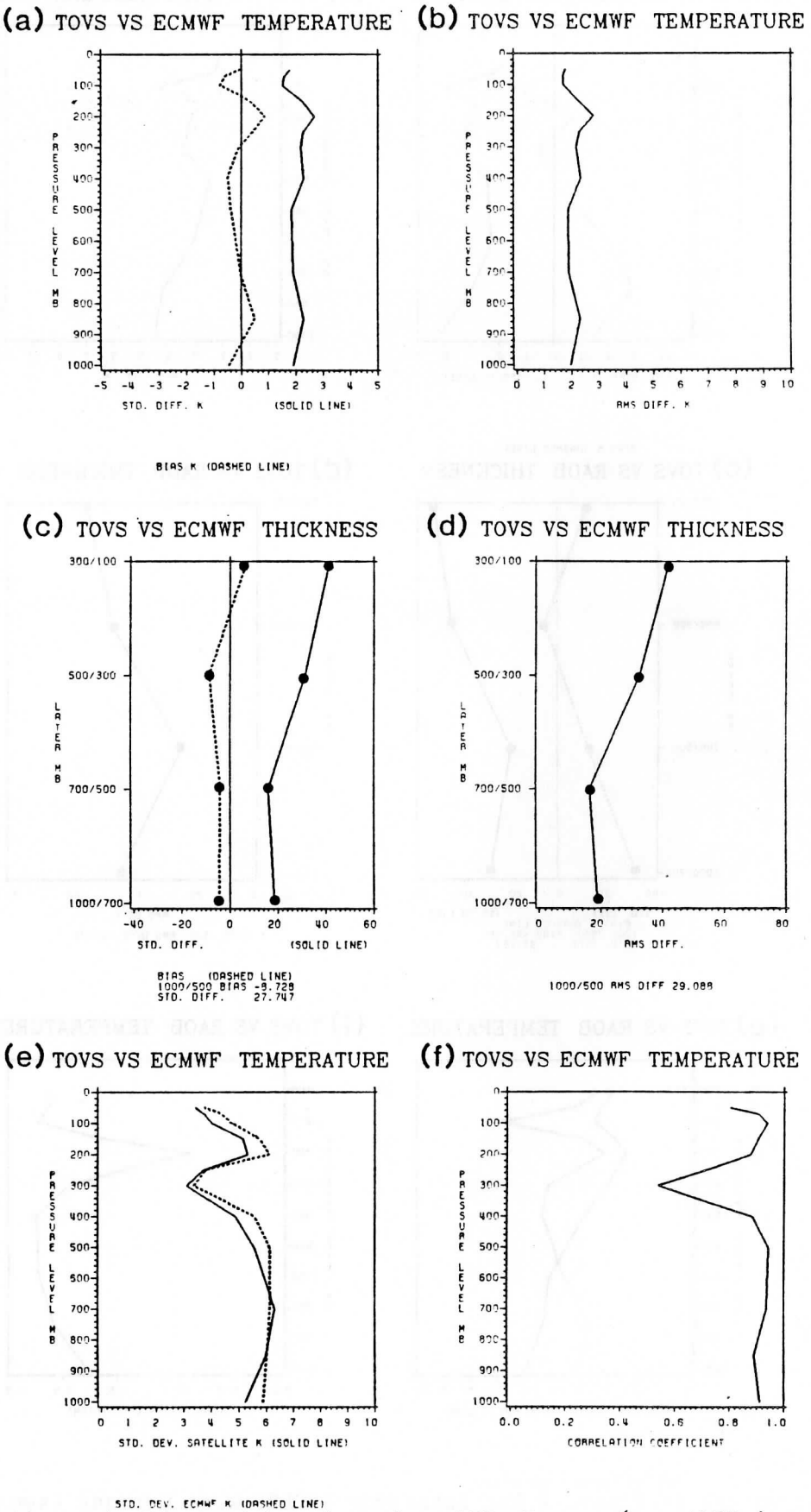

Fig. 11 As in Figure 1 but data from LMD, France (see ALFR in Table 1).

ALFR

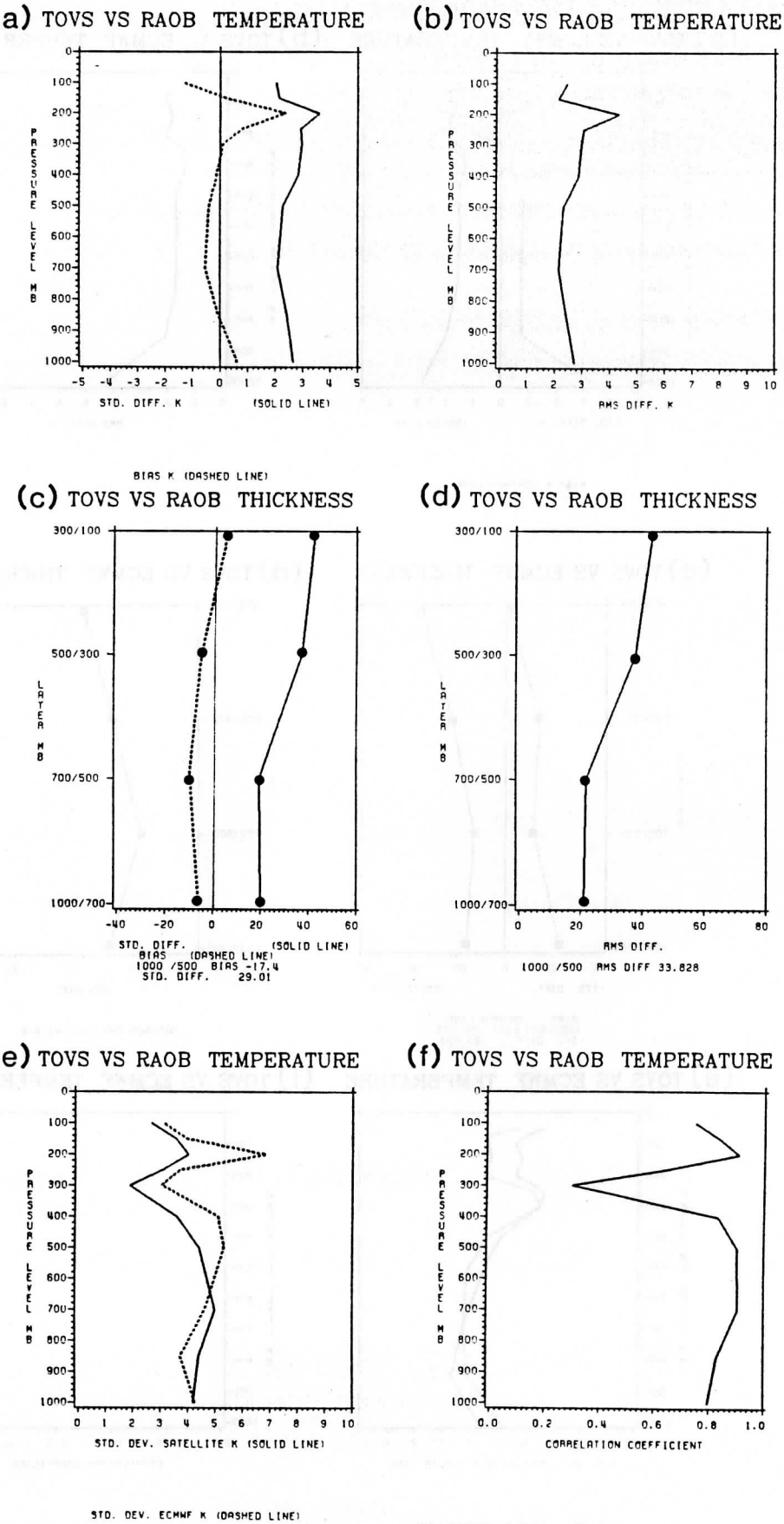

Fig. 12 As in Figure 2 but data from LMD, France (see ALFR in Table 1).

ALNA

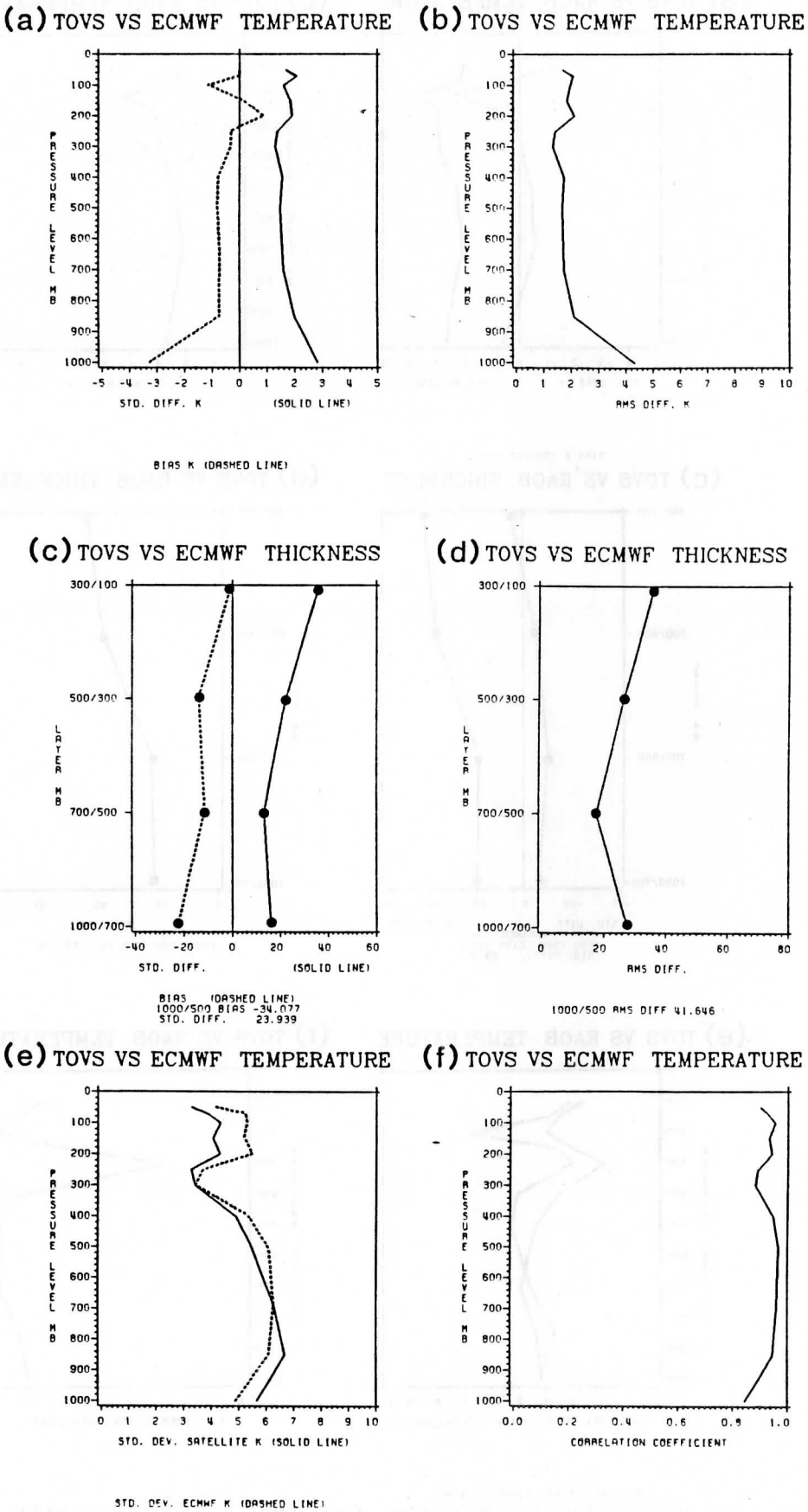

Fig. 13 As in Figure 1 but data from NASA/GLAS, USA (see ALNA in Table 1).

ALNA

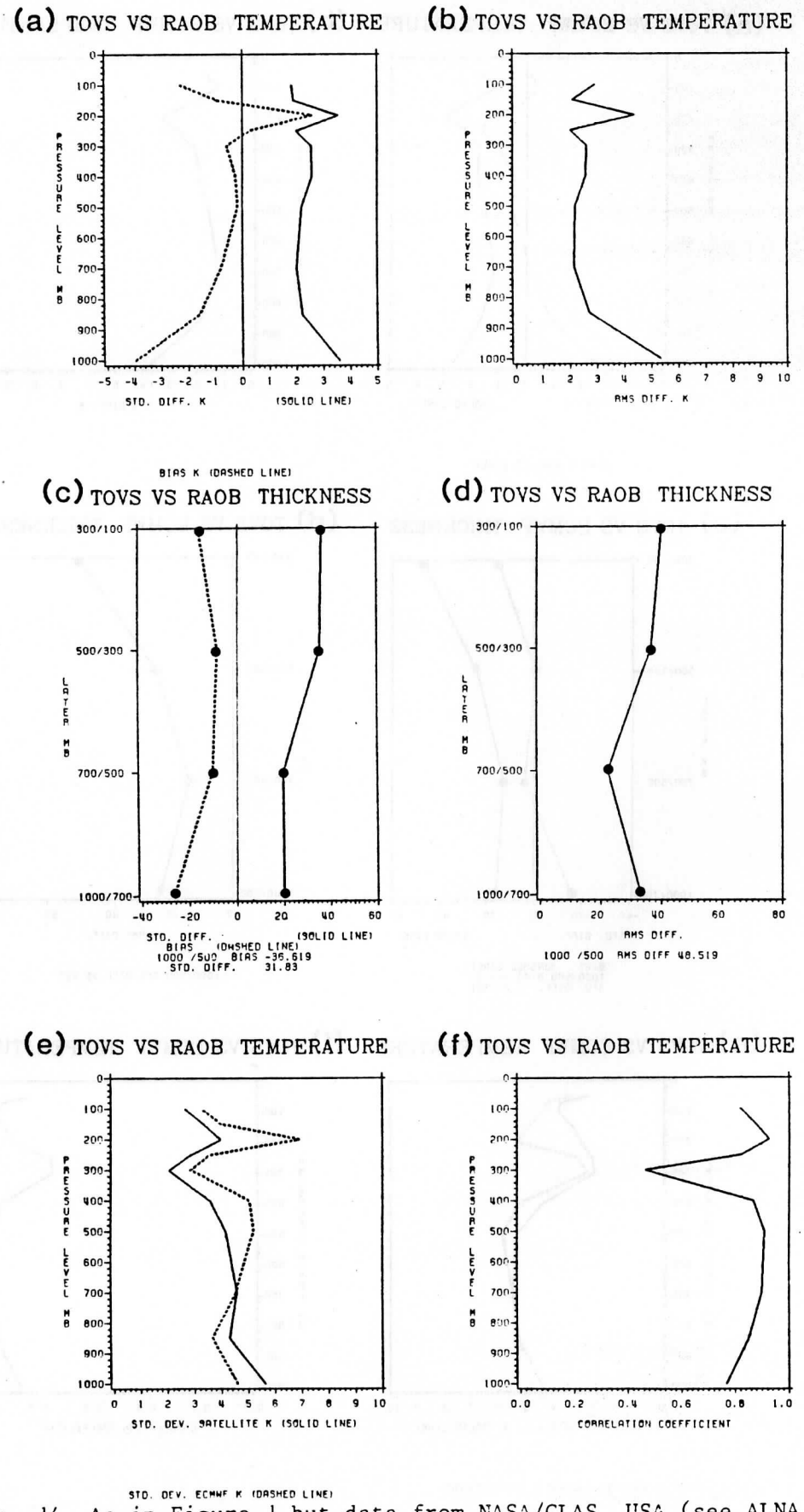

Fig. 14 As in Figure 1 but data from NASA/GLAS, USA (see ALNA in Table 1).

ALNE

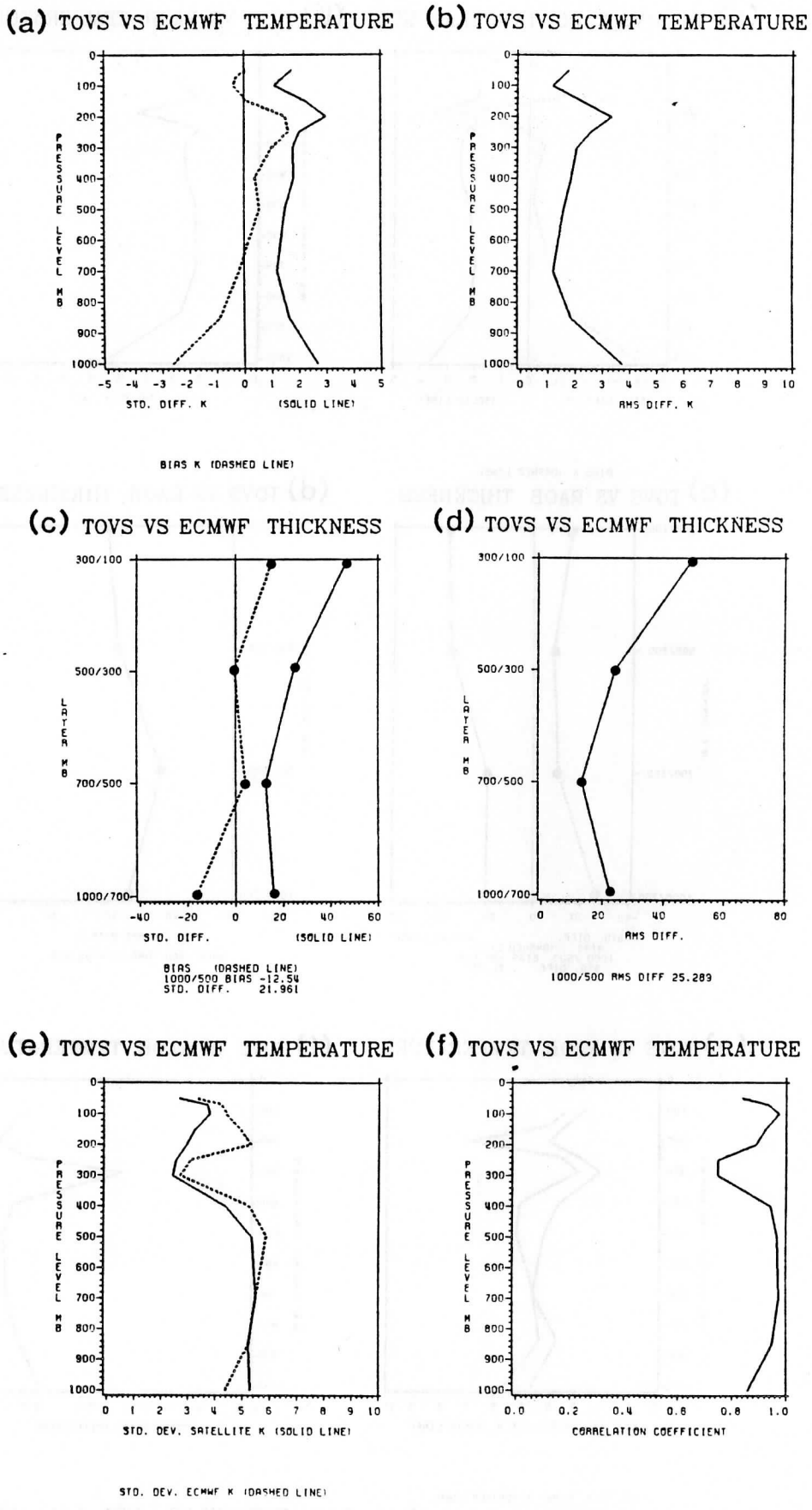

Fig. 15 As in Figure 1 but data from NOAA/NESDIS, Washington (see ALNE in Table 1).

ALNE

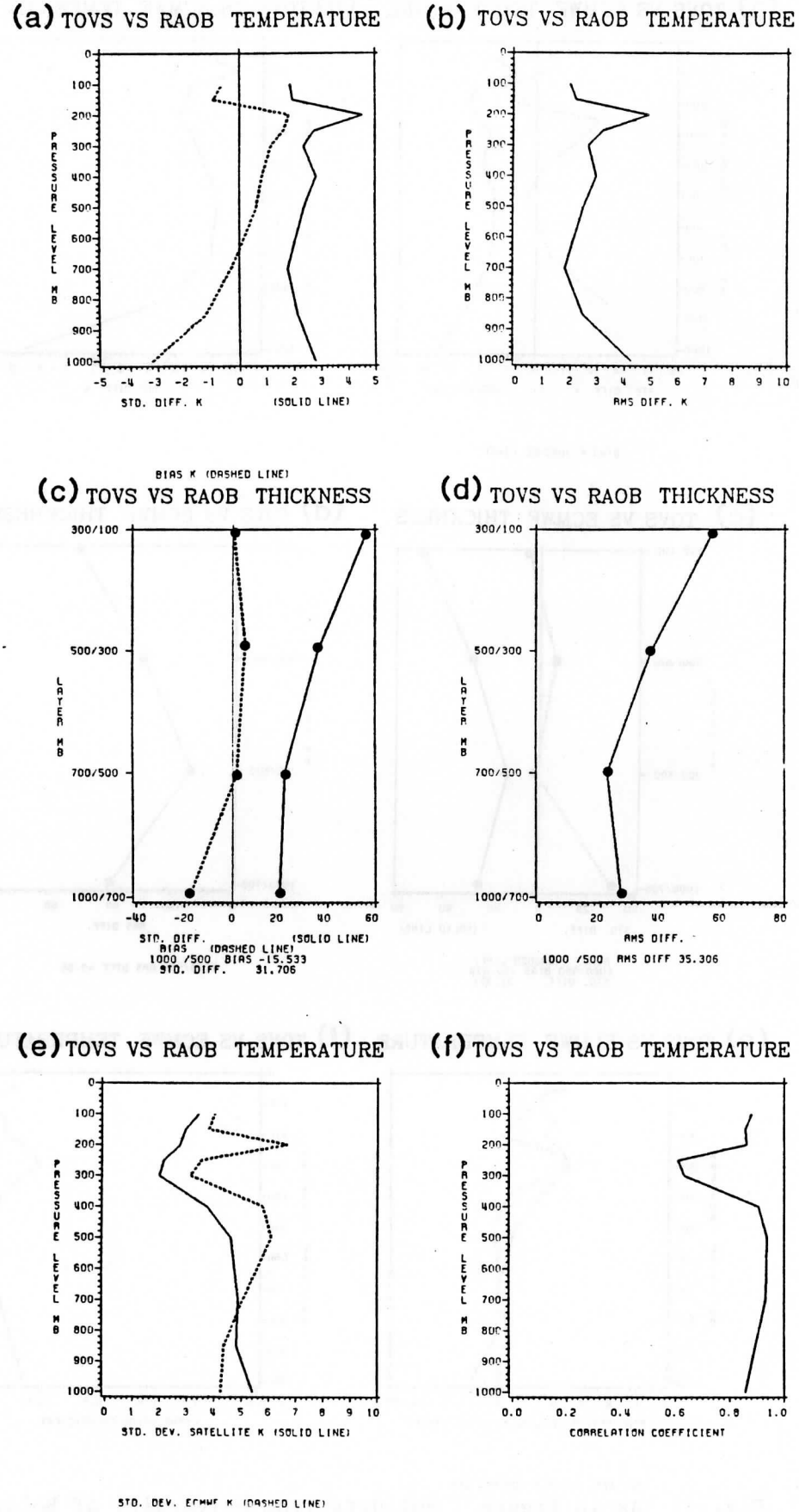

Fig. 16 As in Figure 2 but data from NOAA/NESDIS, Washington (see ALNE in Table 1).

ALIT 1

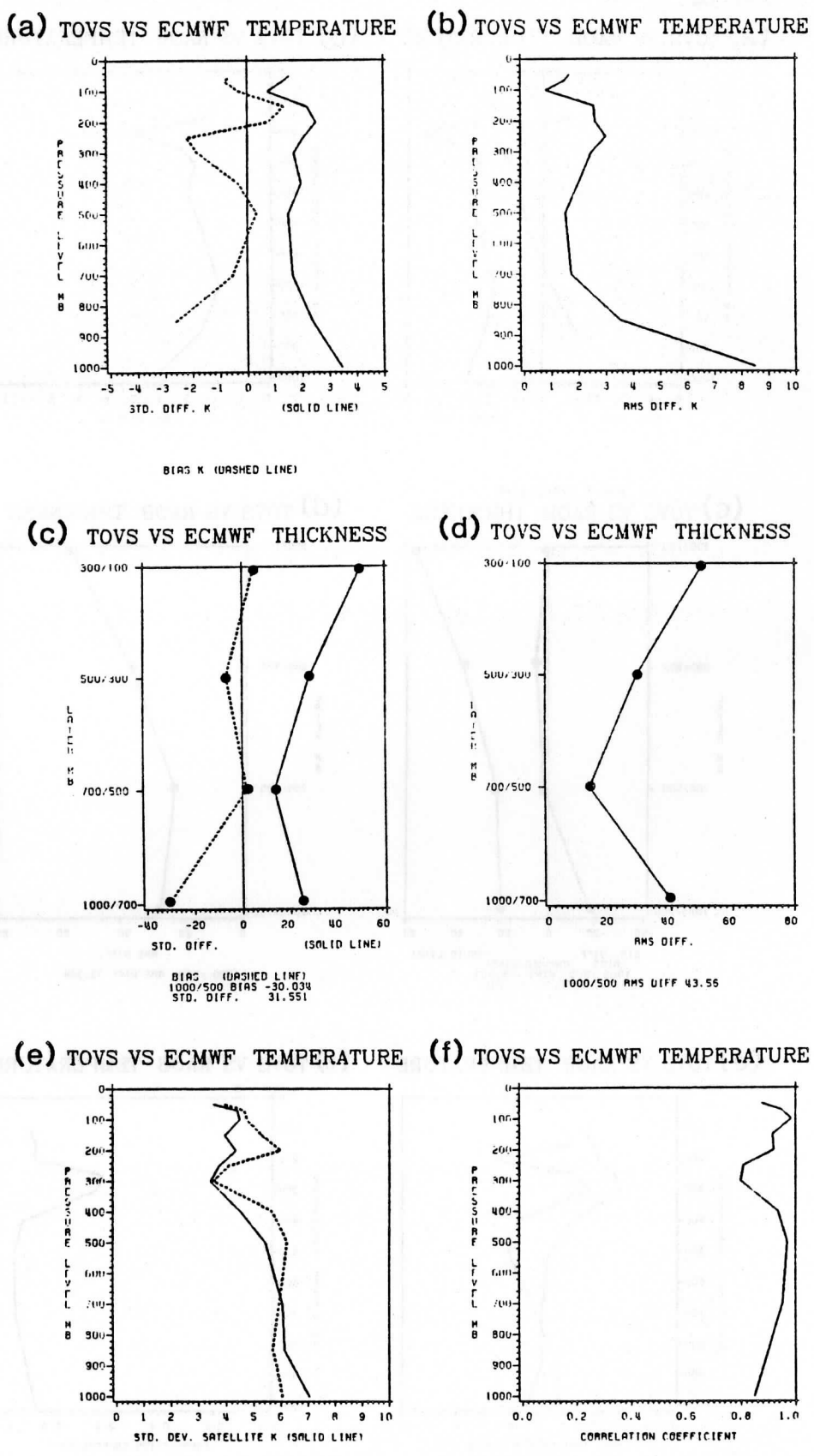

Fig. 17 As in Figure 1 but data from University of Bologna, Italy (see ALIT1 in Table 1).

ALIT 1

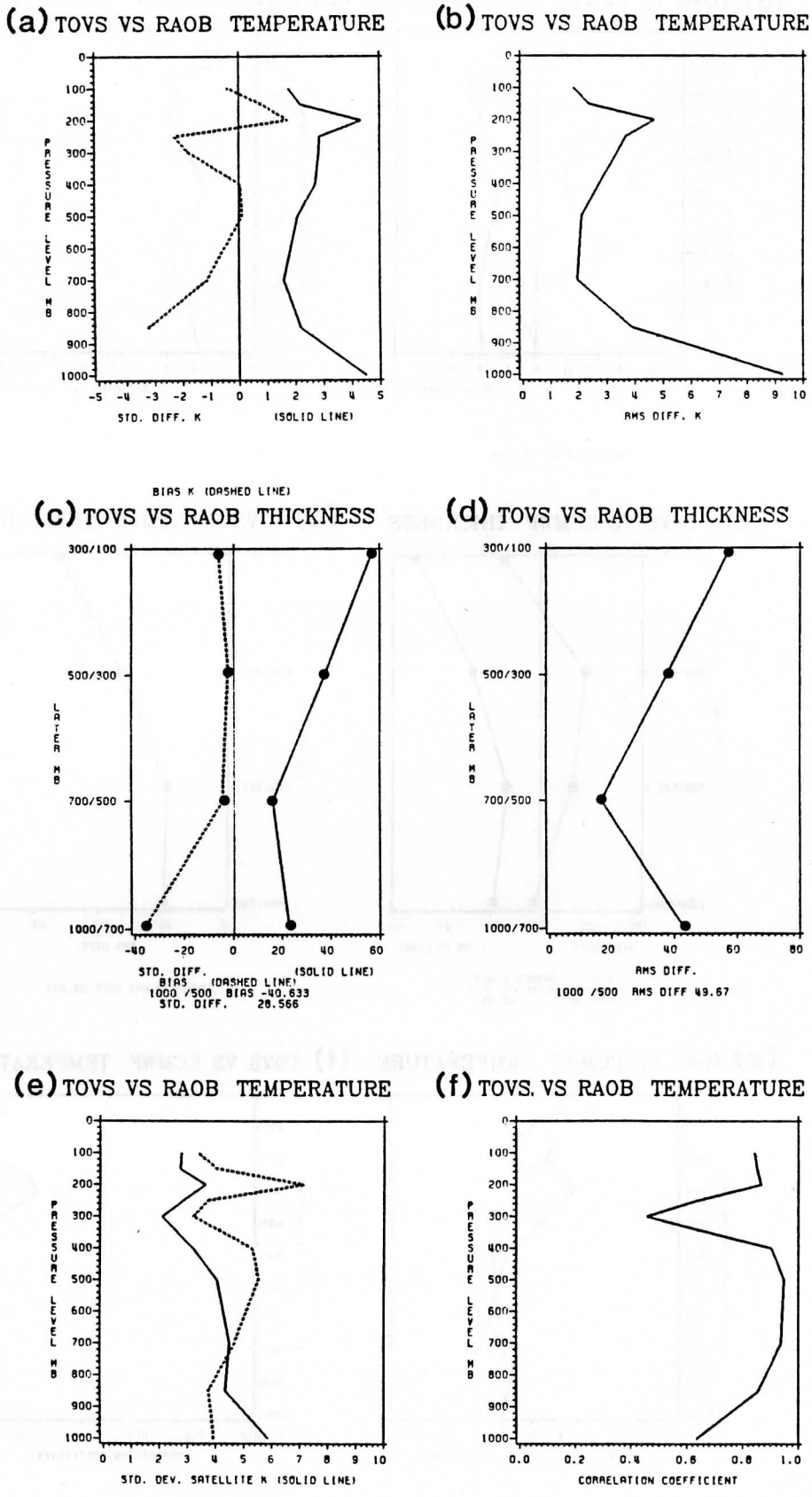

Fig. 18 As in Figure 2 but data from University of Bologna, Italy (see ALIT1 in Table 1).

ALIT2

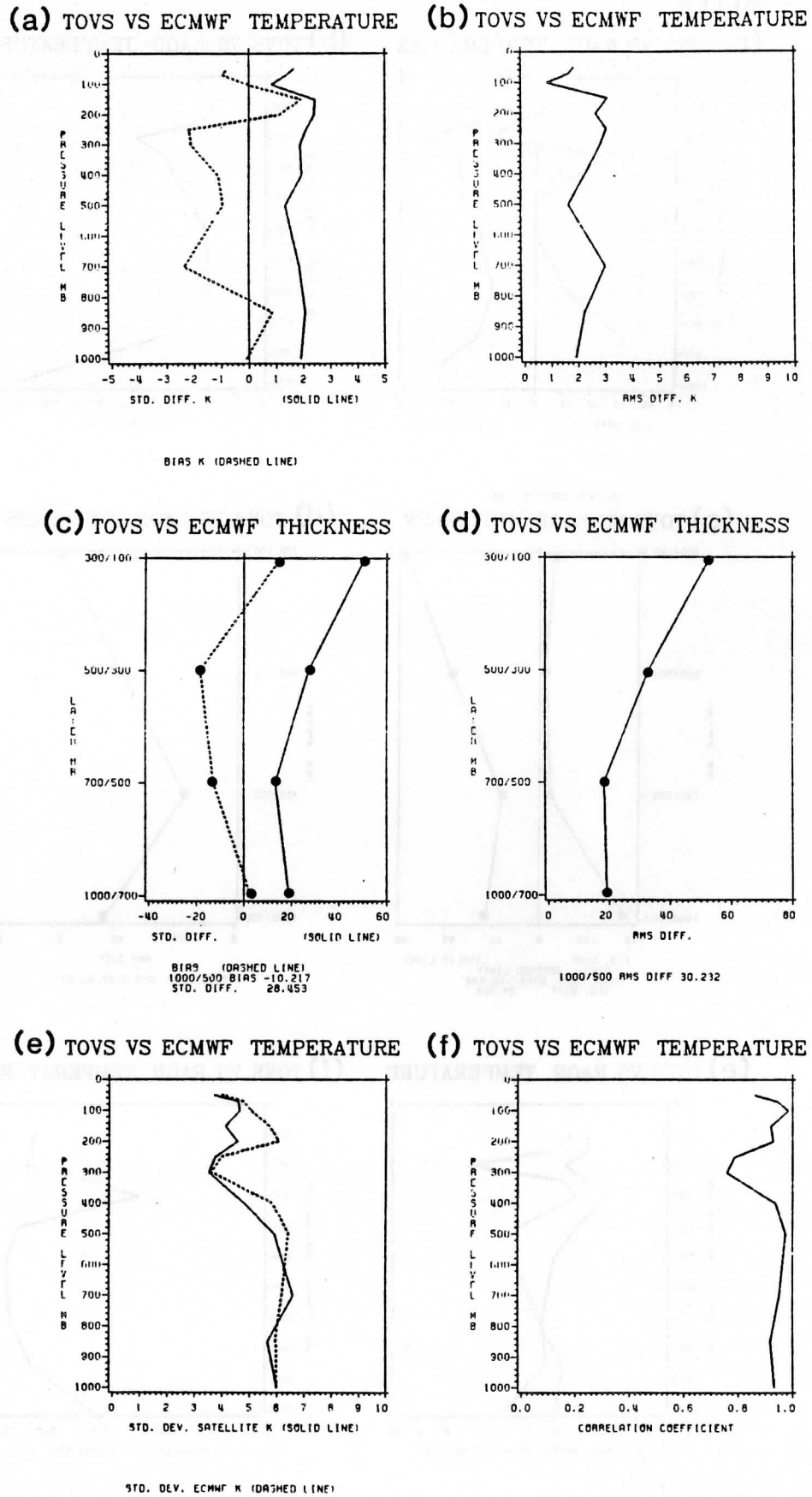

Fig. 19 As in Figure 1 but data from the University of Bologna, Italy (see ALIT2 in Table 1).

ALIT2

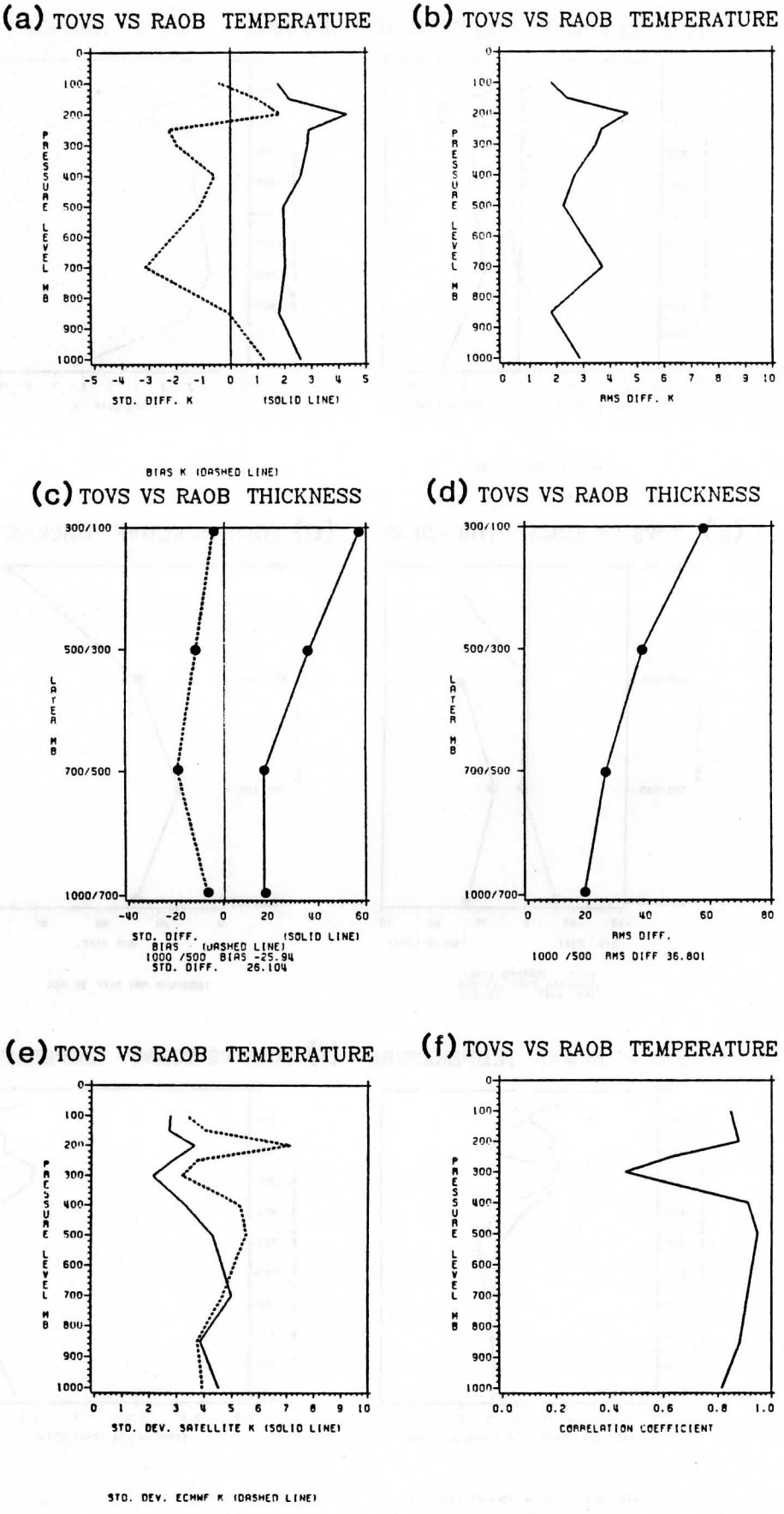

Fig. 20 As in Figure 2 but data from the University of Bologna, Italy (see ALIT2 in Table 1).

ALWA

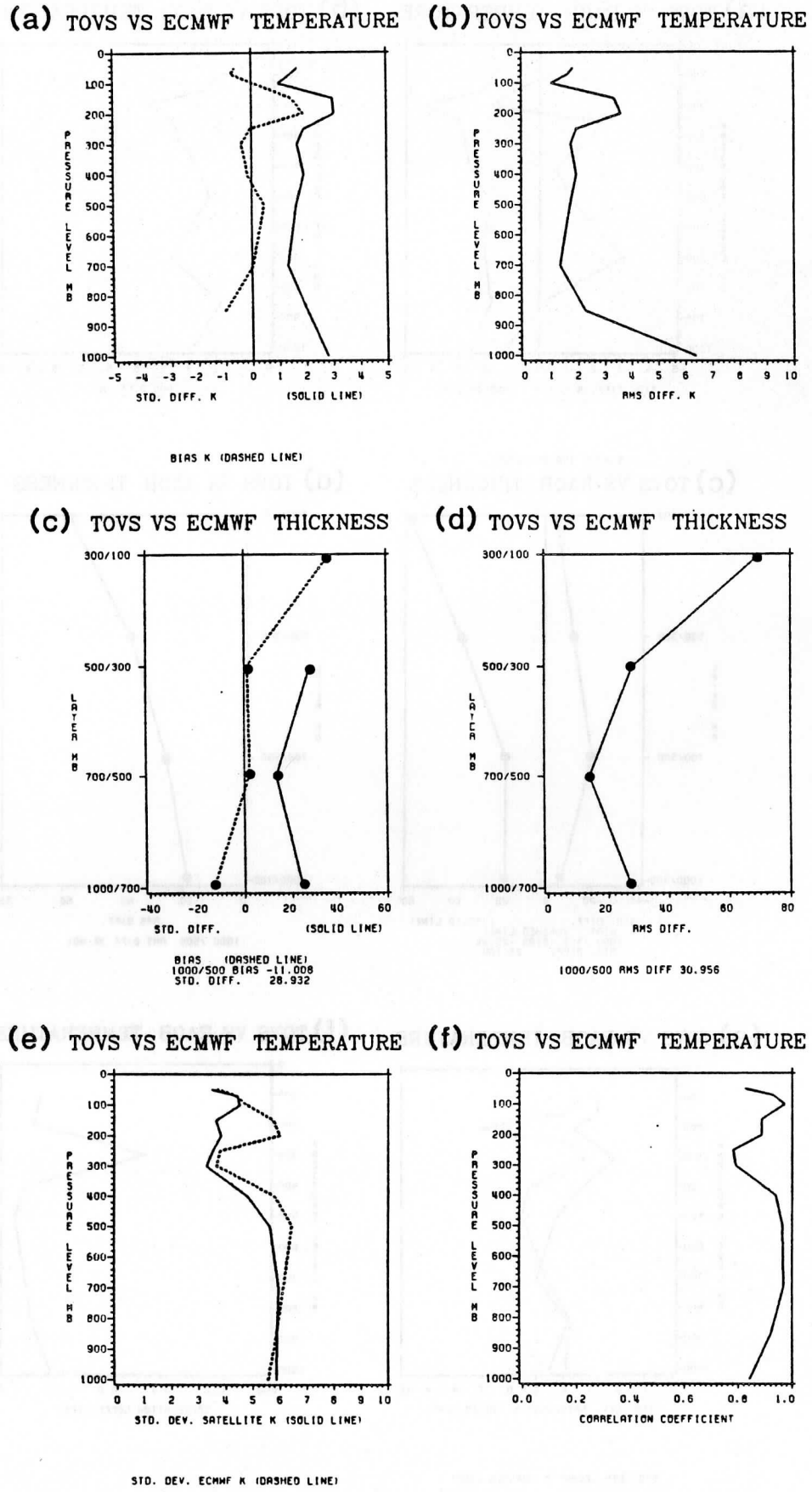

Fig. 21 As in Figure 1 but data from WAIT, Western Australia (see ALWA in Table 1).

ALWA

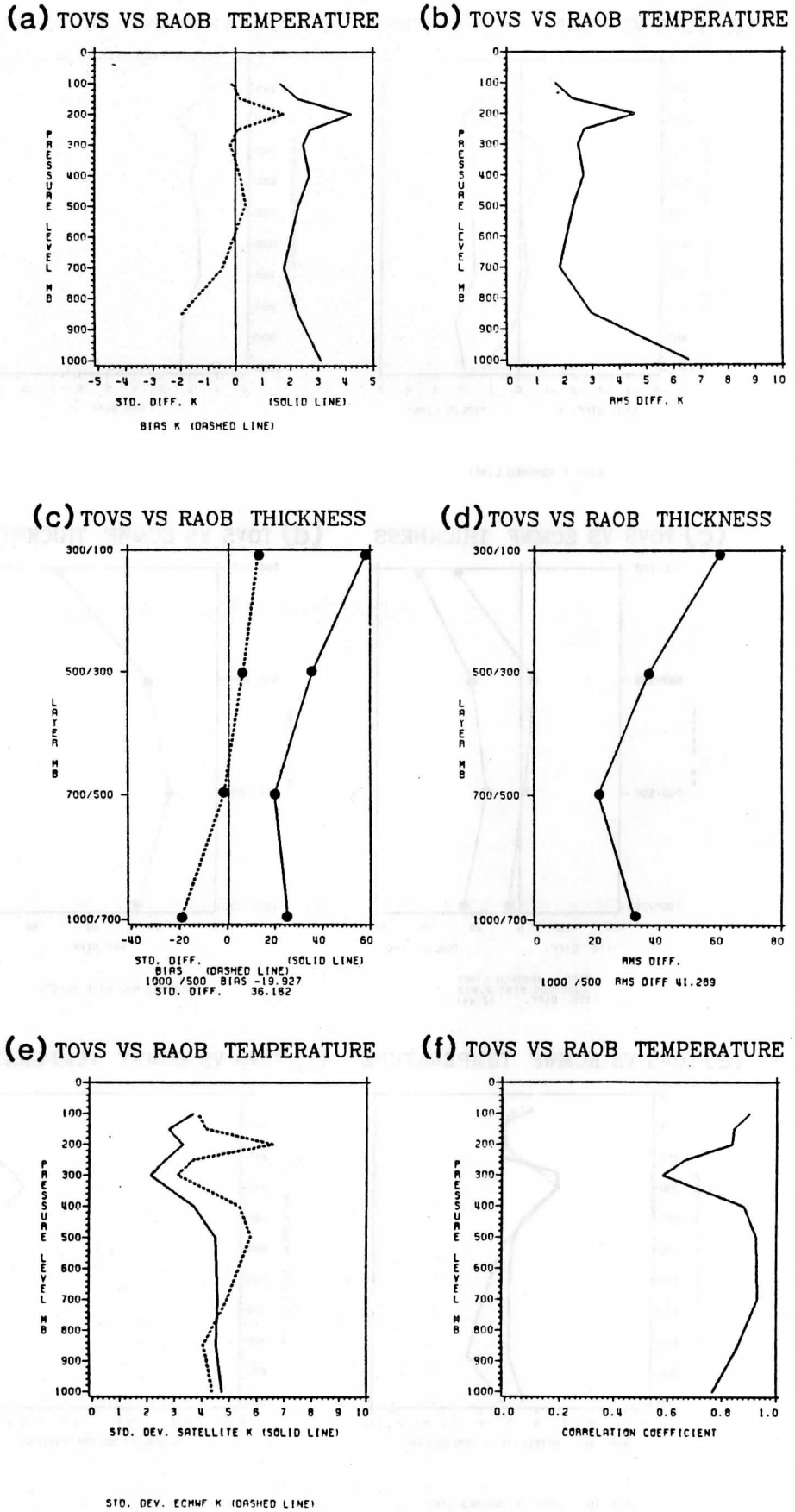

Fig. 22 As in Figure 2 but data from WAIT, Western Australia (see ALWA in Table 1).

TAAU

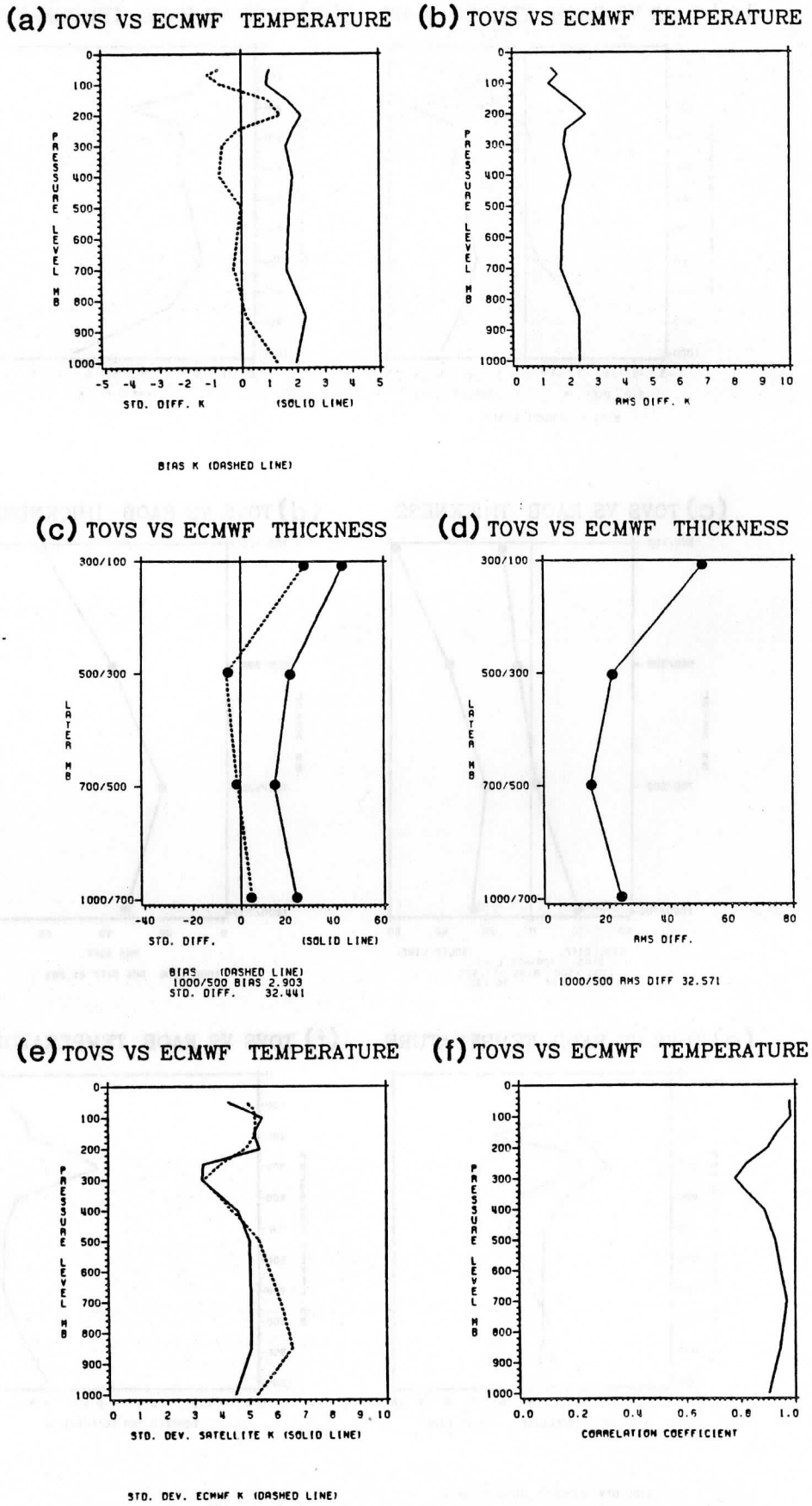

Fig. 23 As in Figure 1 but with data from the Bureau of Meteorology, Australia and for the Tasman Sea Case (see TAAU in Table 1).

TAAU

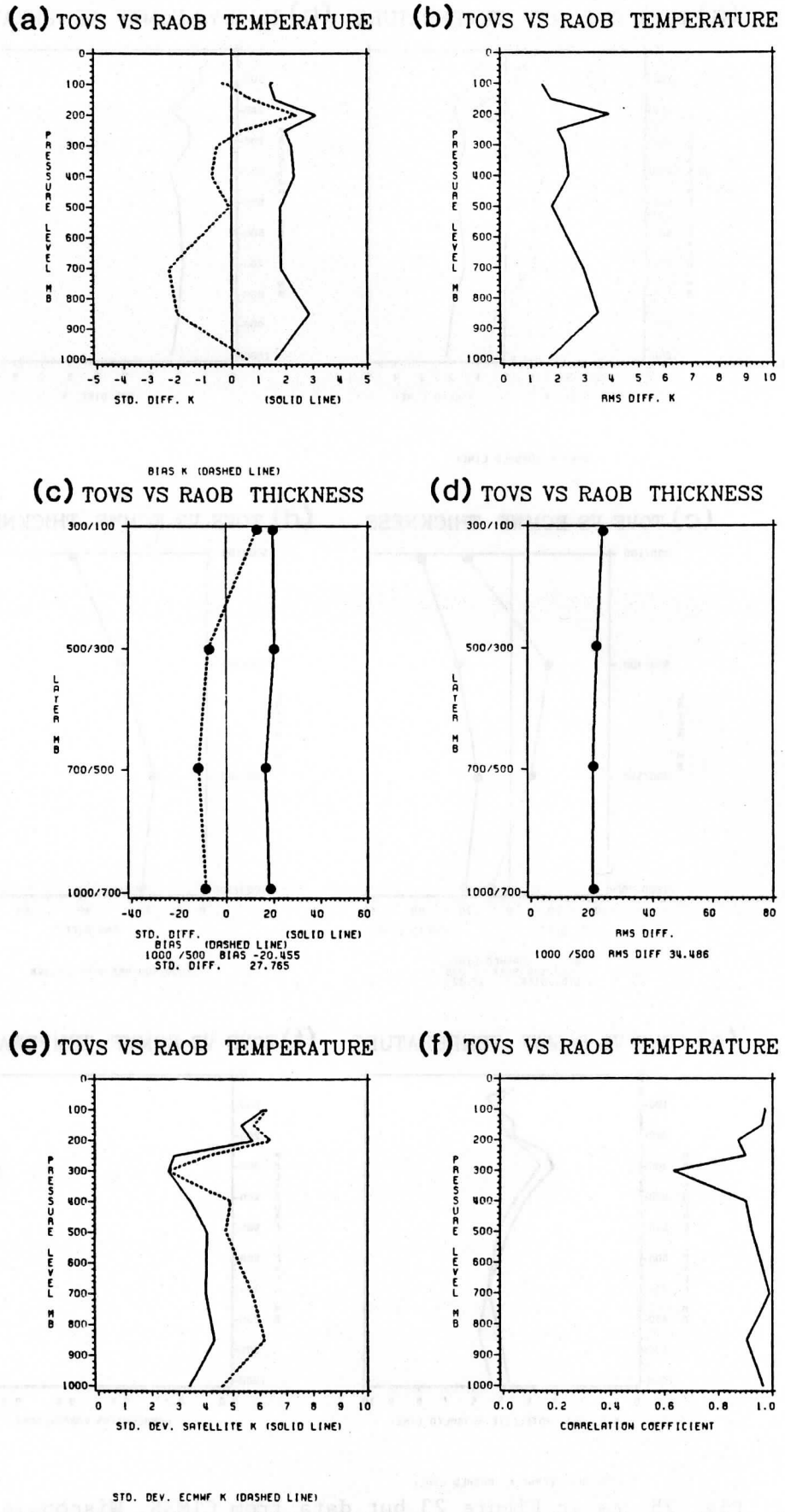

Fig. 24 As in Figure 23 but with the comparison done with colocated radiosonde data (see TAAU in Table 1).

TAWI

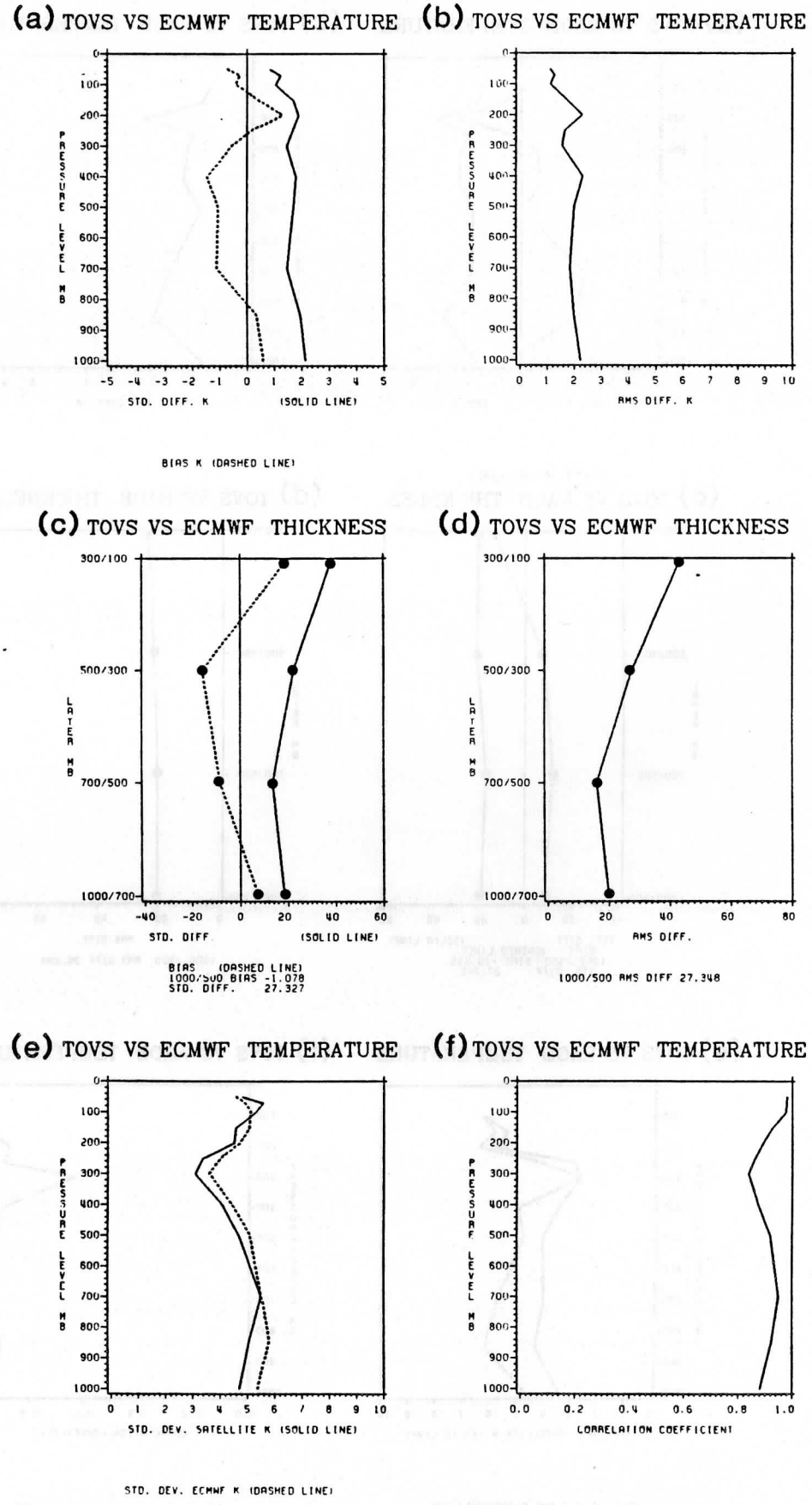

Fig. 25 As in Figure 23 but data from CIMSS, Wisconsin (see TAWI in Table 1).

TAWI

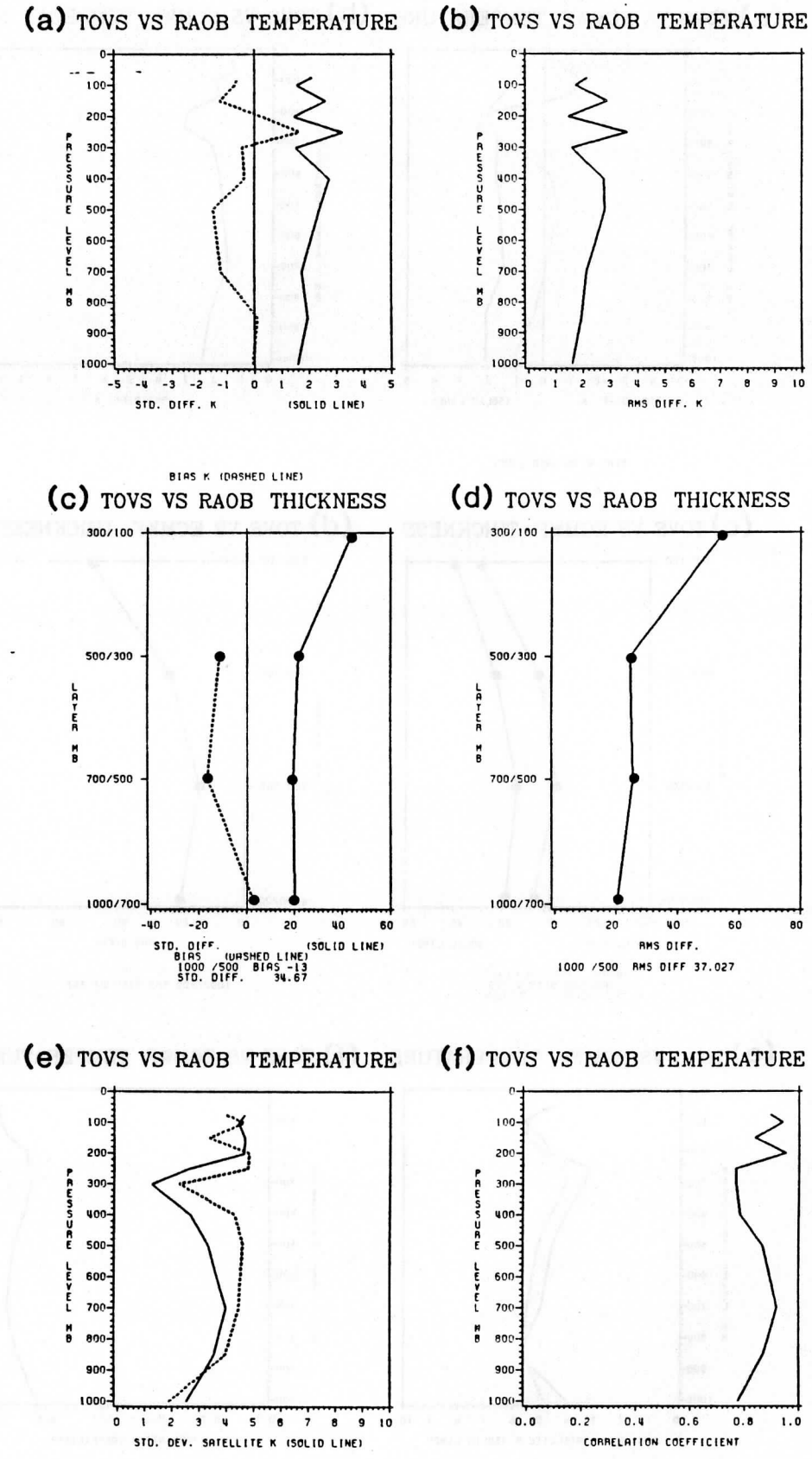

Fig. 26 As in Figure 24 but data from CIMSS, Wisconsin (see TAWI in Table 1).

TANZ

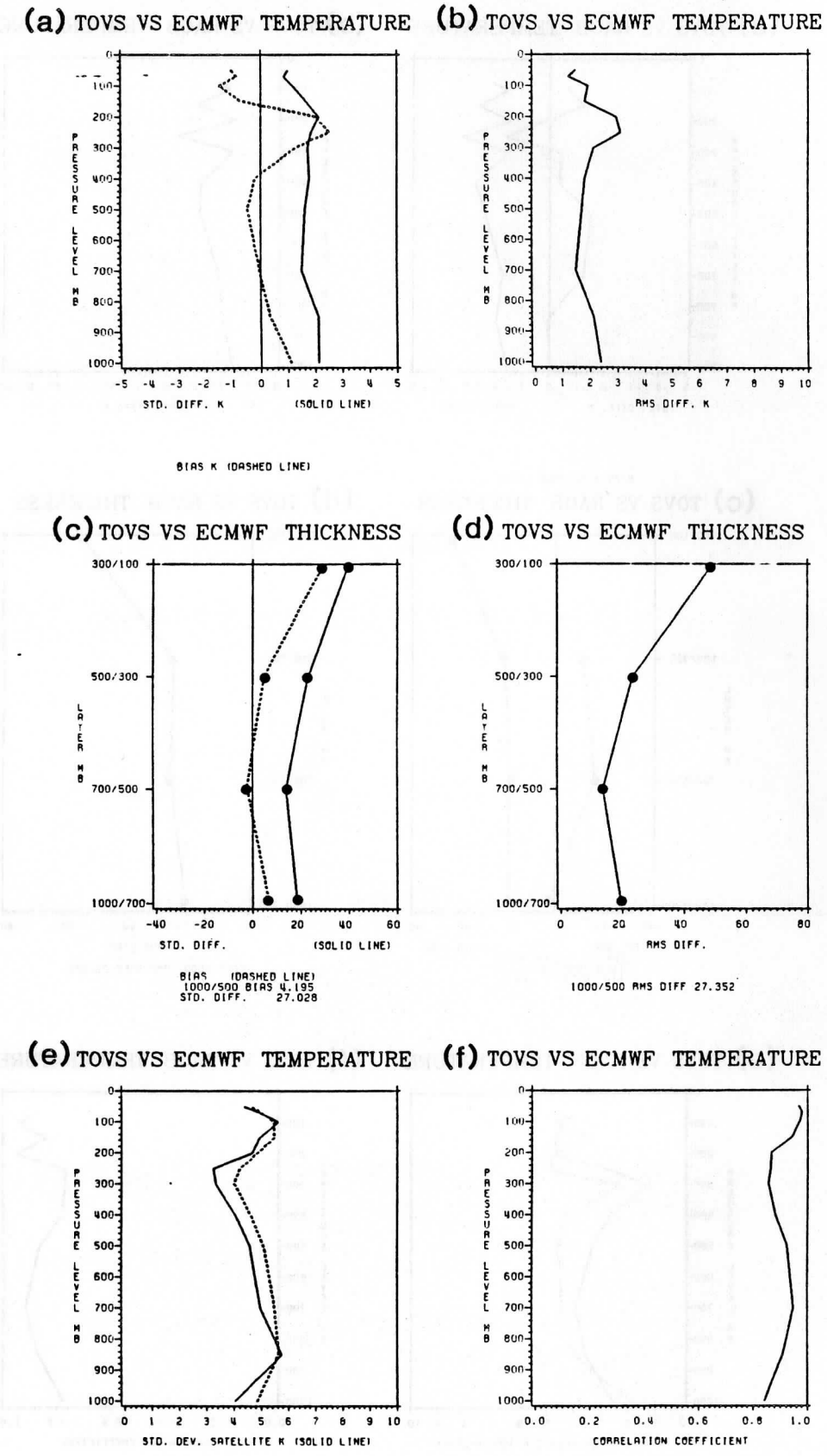

Fig. 27 As in Figure 23 but data from New Zealand Met. Service (see TANZ in Table 1).

TANZ

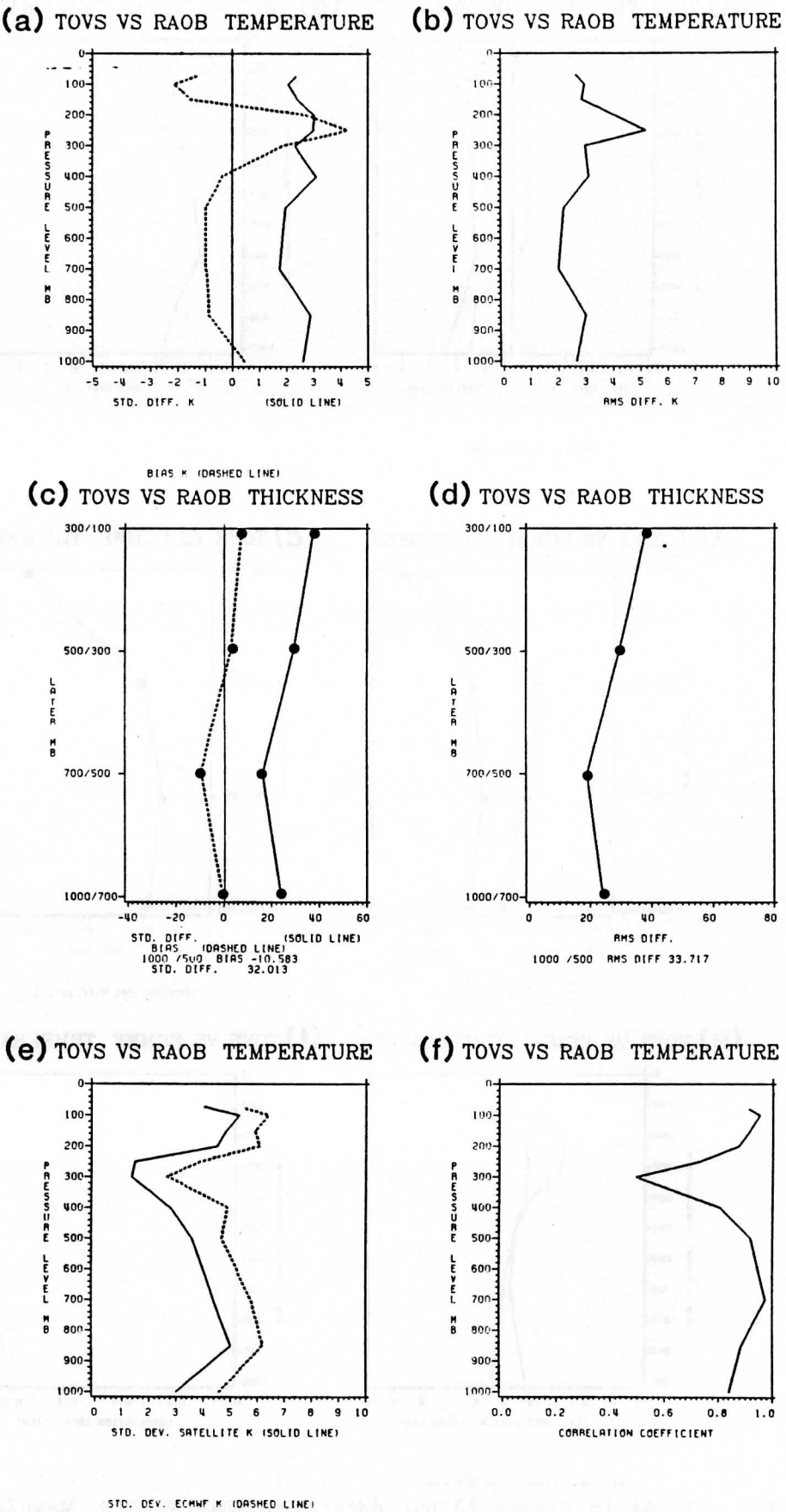

Fig. 28 As in Figure 24 but data from New Zealand Met. Service (see TANZ in Table 1).

TANE

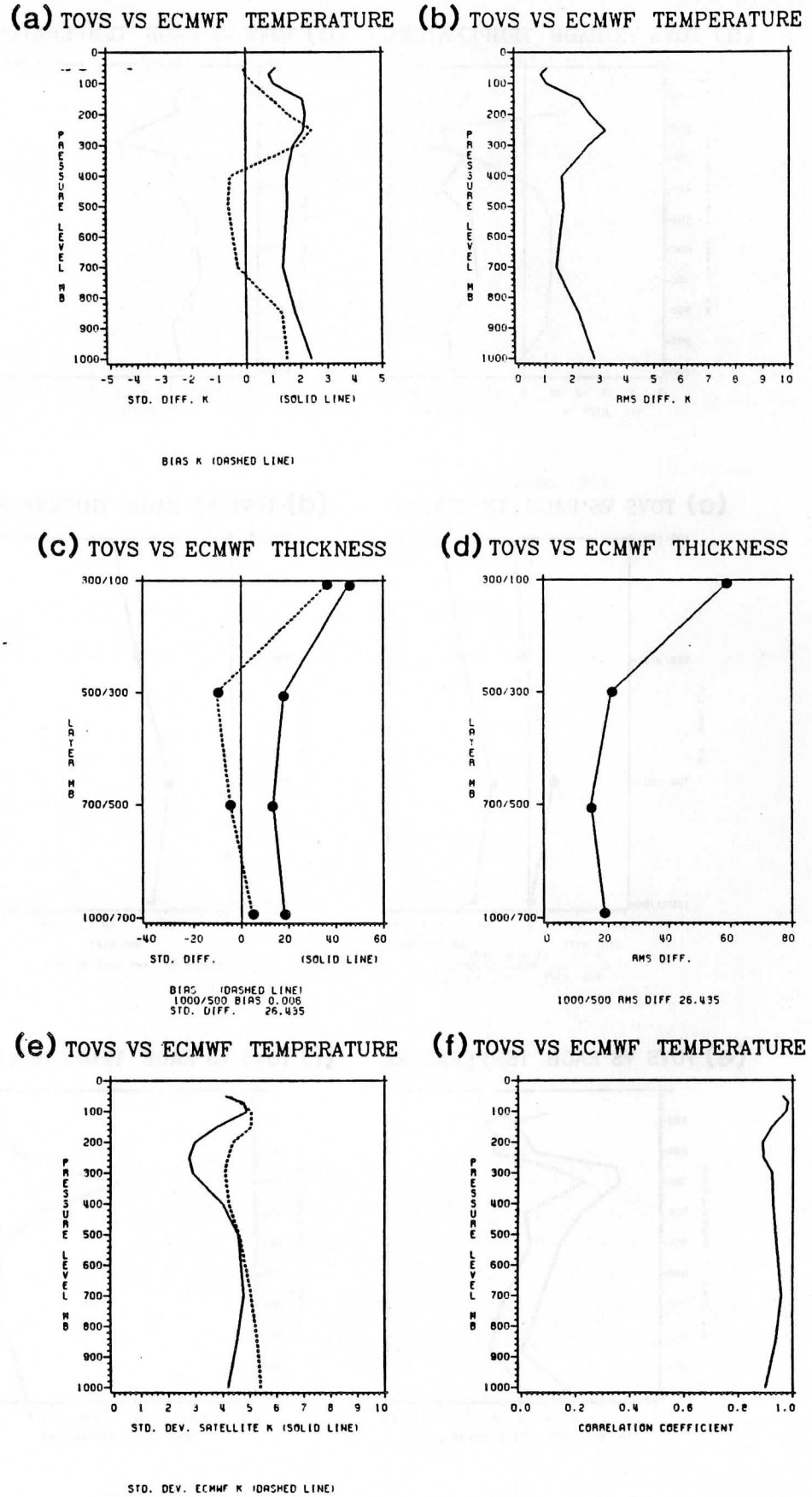

Fig. 29 As in Figure 23 but data from NOAA/NESDIS, Washington (see TANE in Table 1).

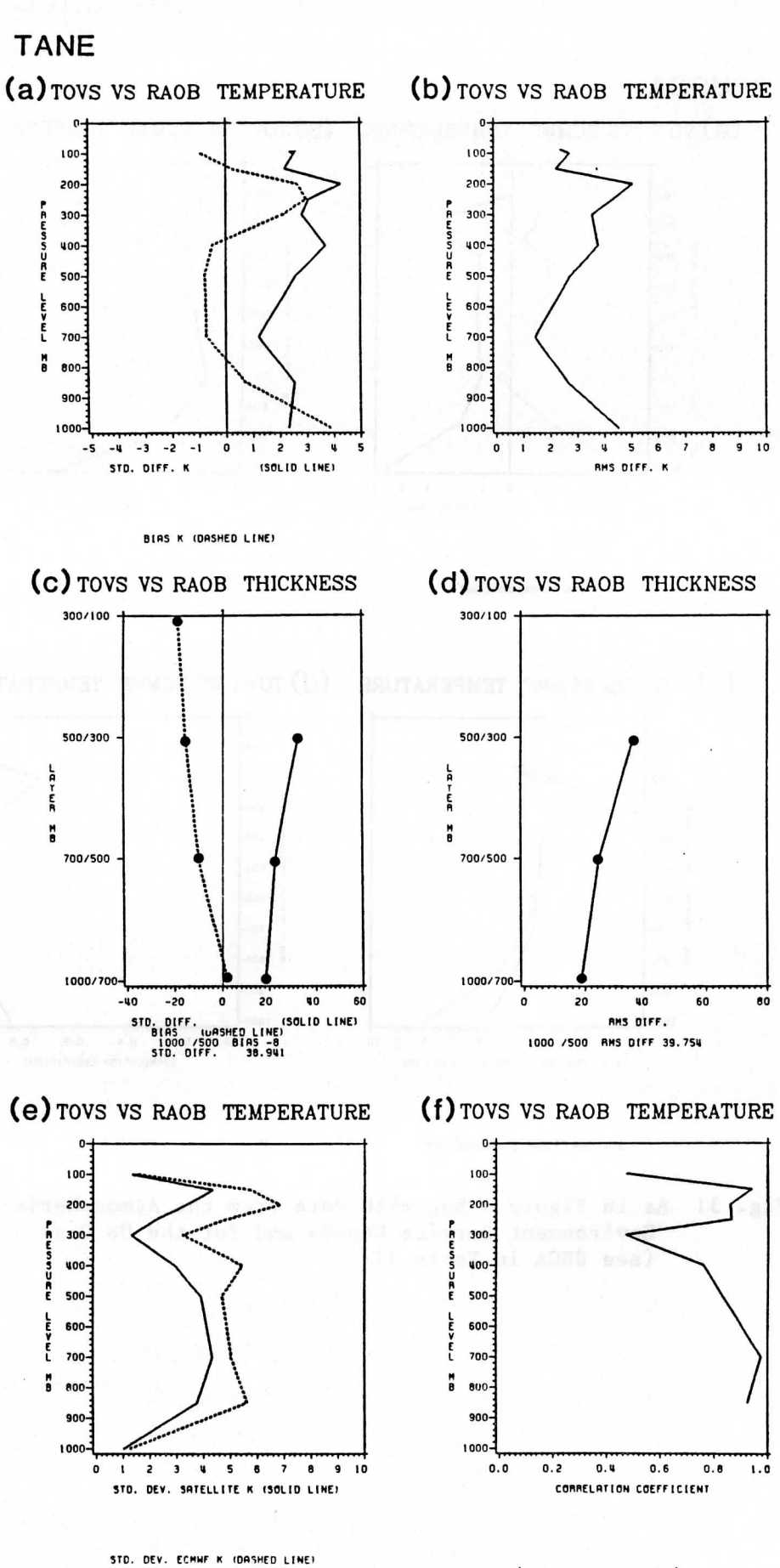

Fig. 30 As in Figure 24 but data from NOAA/NESDIS Washington (see TANE in Table 1).

USCA

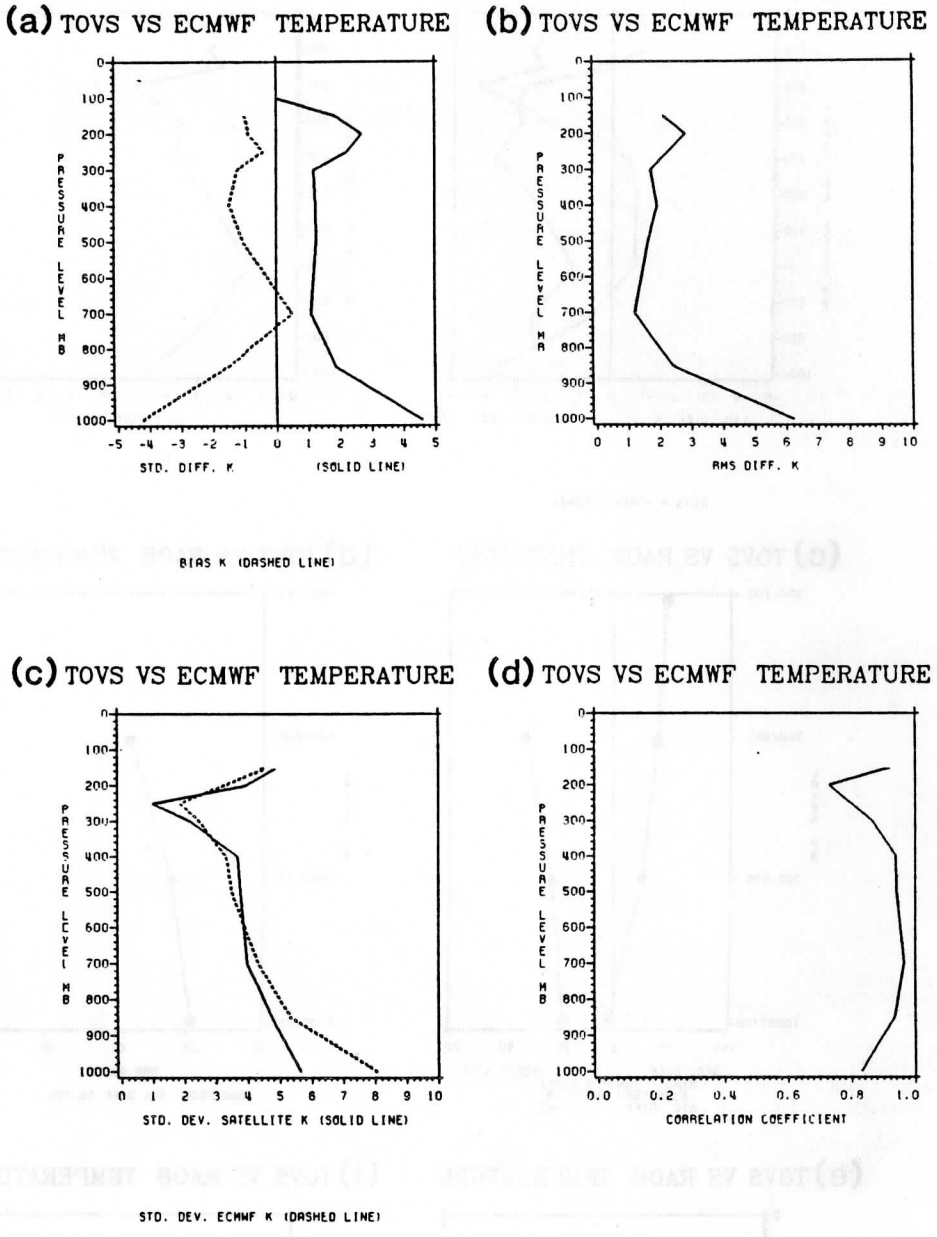

Fig. 31 As in Figure 1 but with data from the Atmospheric Environment Service Canada and for the US Case (see USCA in Table 1).

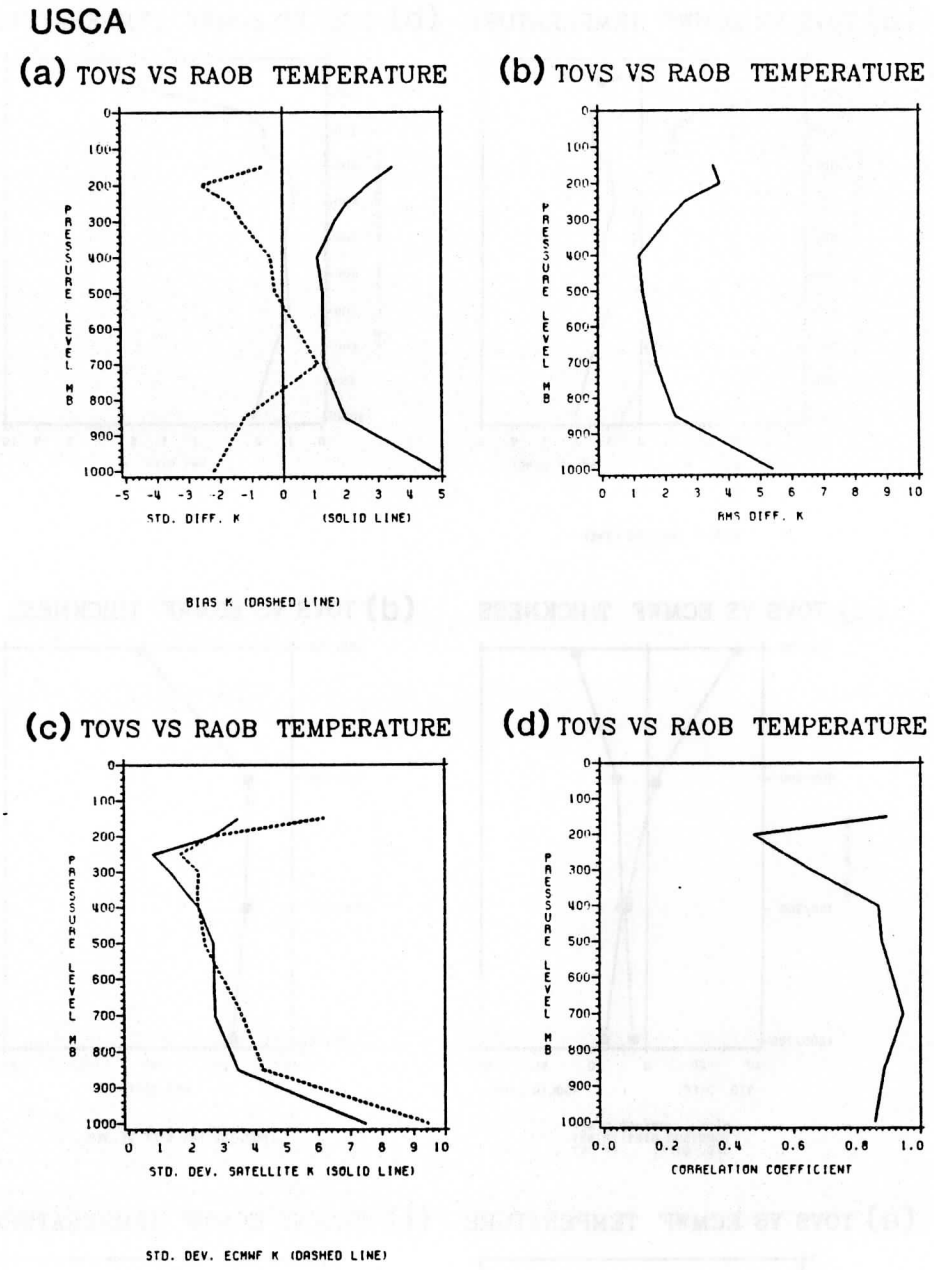

Fig. 32 As in Figure 31 but comparison with colocated radiosondes (see USCA in Table 1).

USUK

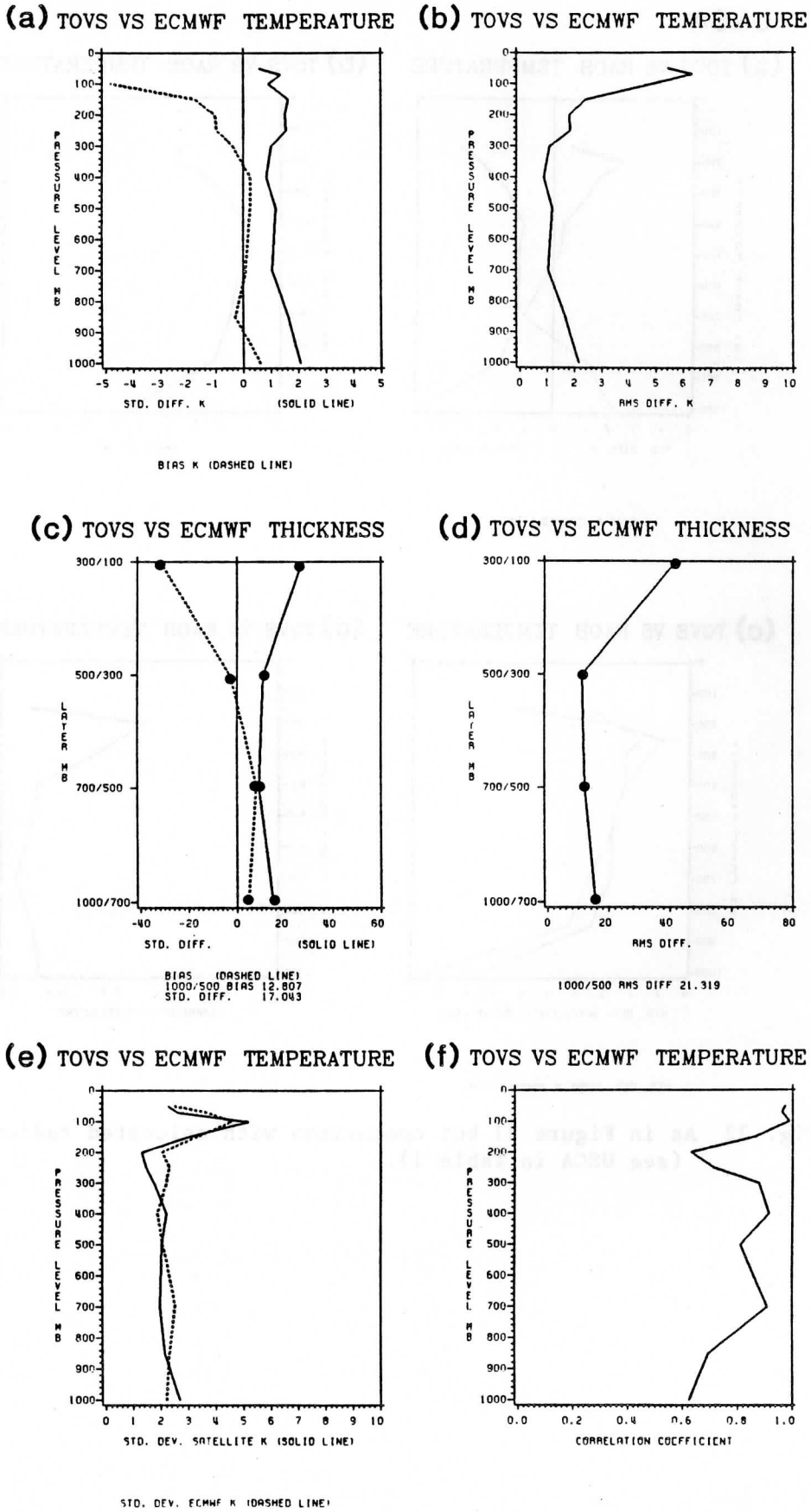

Fig. 33 As in Figure 31 but with data from the British Met. Office (see USUK in Table 1).

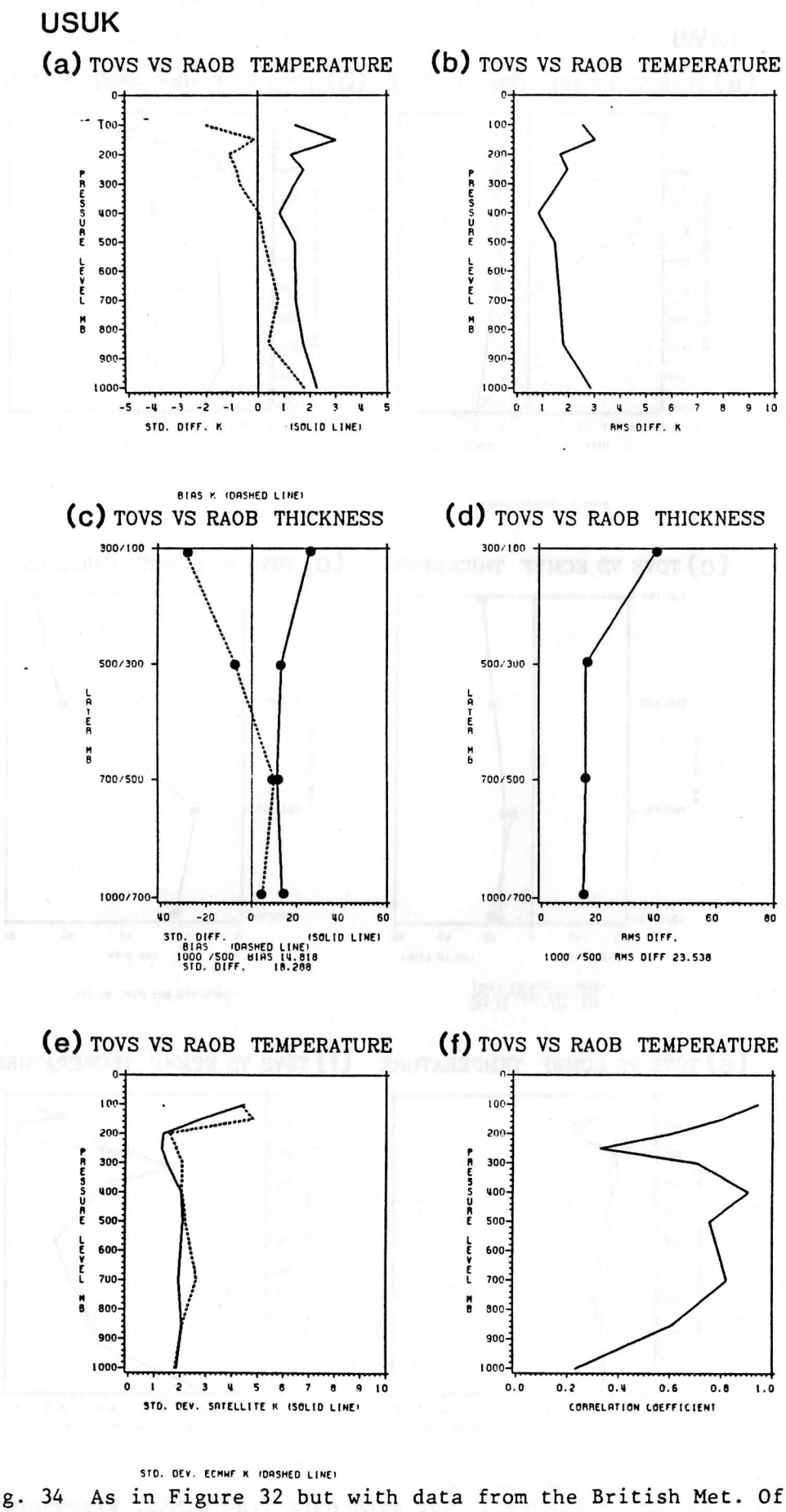

Fig. 34 As in Figure 32 but with data from the British Met. Office (see USUK in Table 1).

USWI

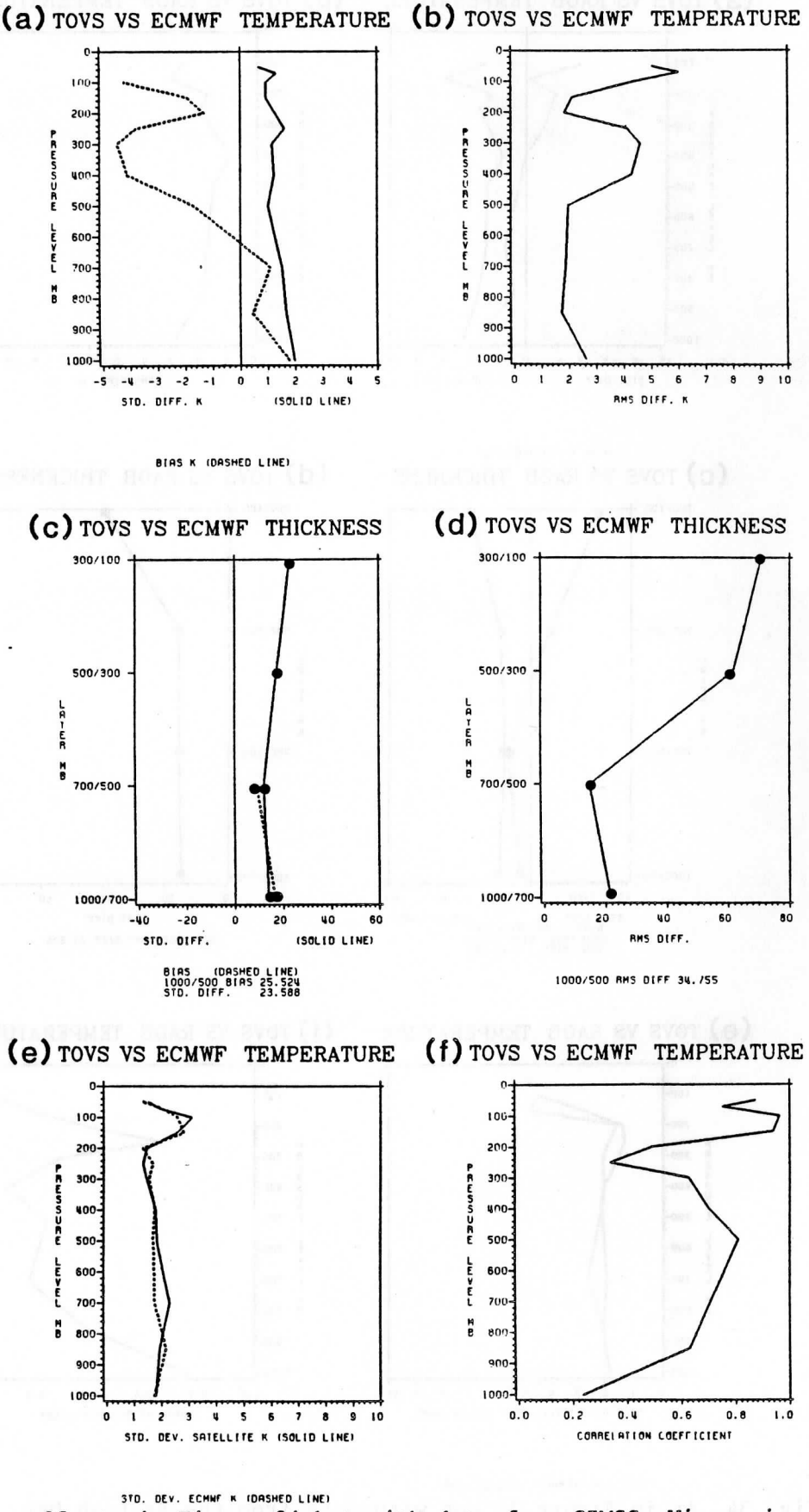

Fig. 35 As in Figure 31 but with data from CIMSS, Wisconsin (see USWI in Table 1).

USWI

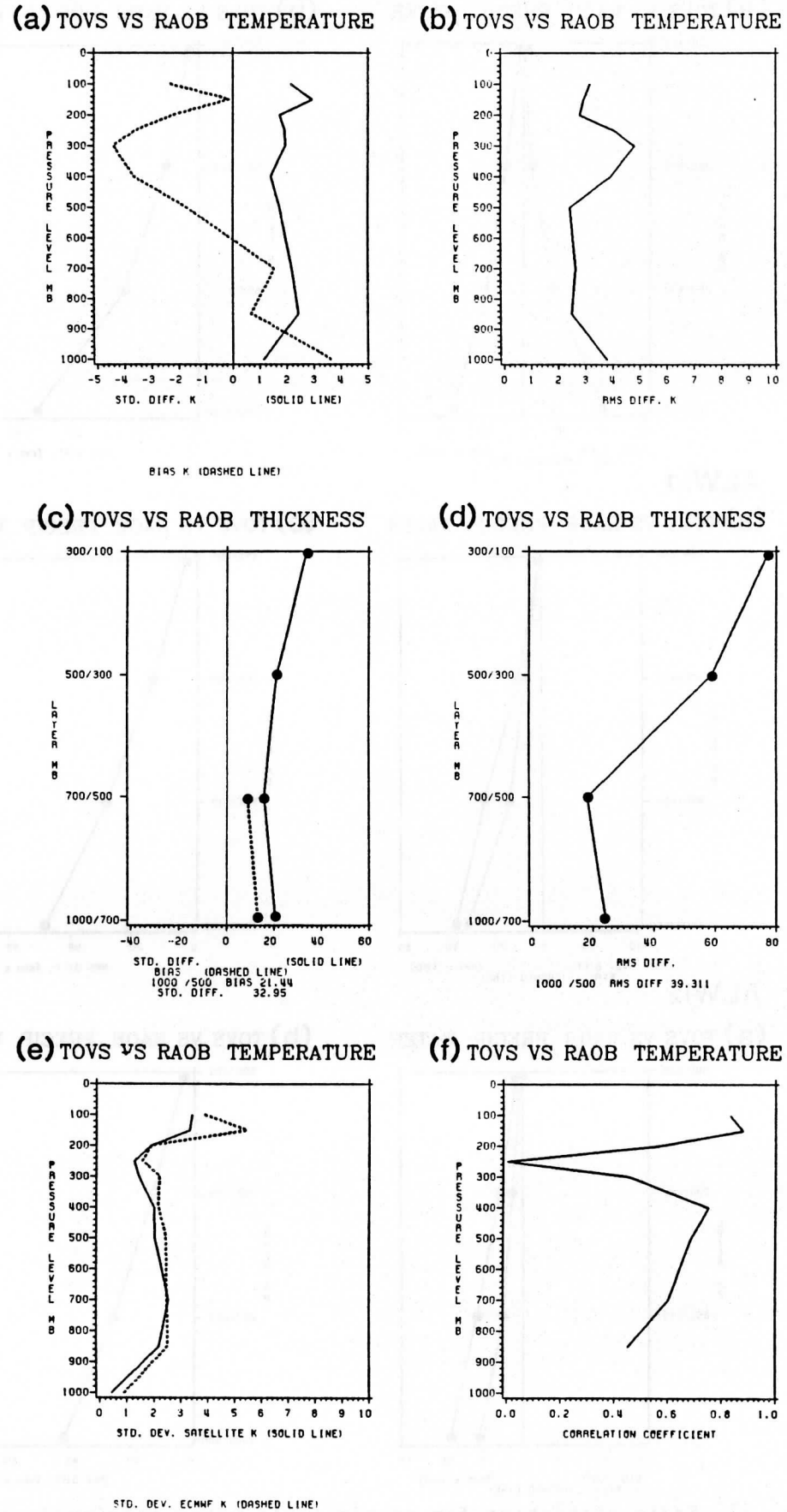

Fig. 36 As in Figure 32 but data from CIMSS, Wisconsin (see USWI in Table 1).

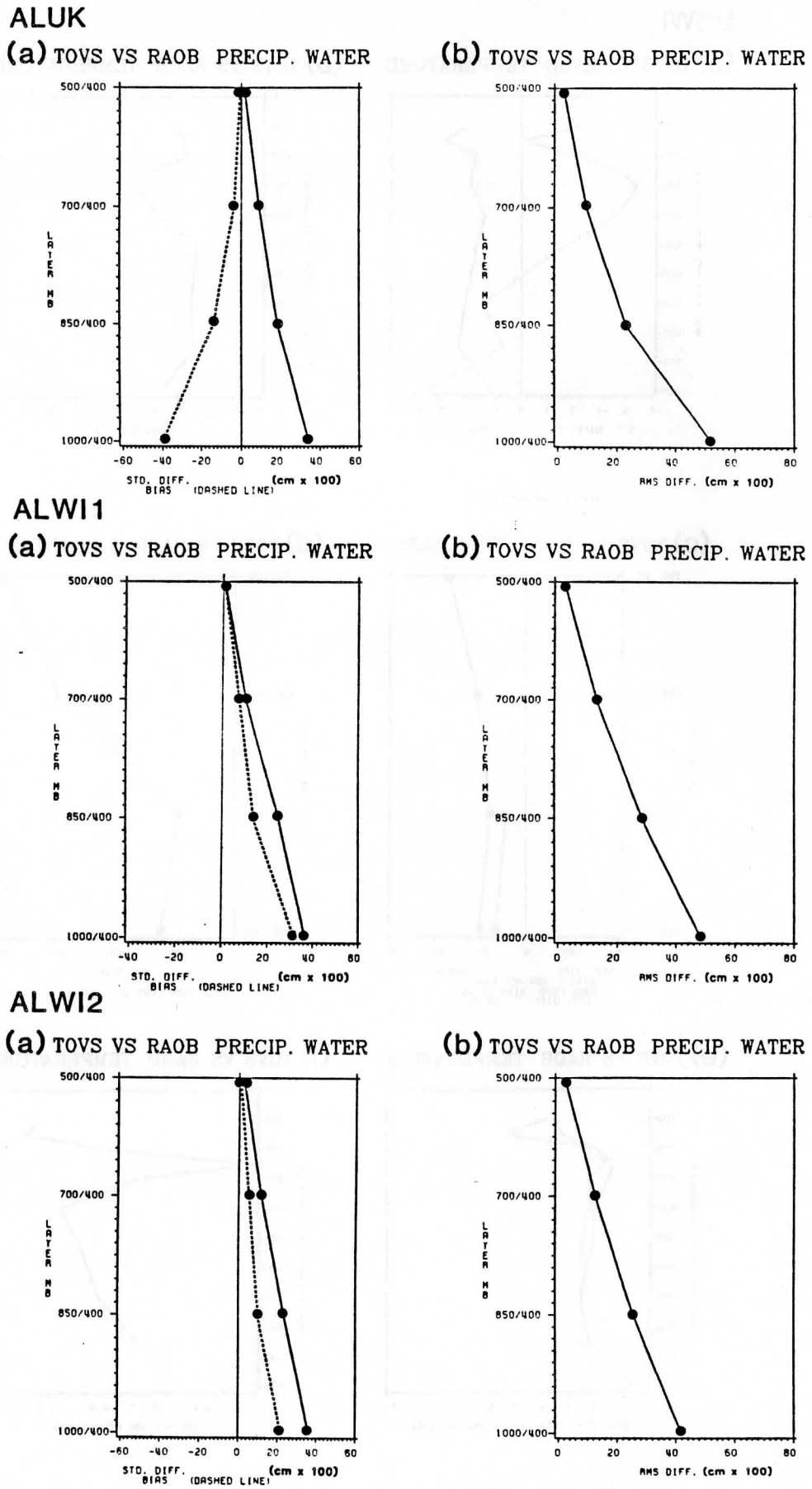

Fig. 37 Basic statistics for precipitable water retrievals compared to colocated radiosondes (see ALUK, ALWI1 and ALWI2 in Table 1). (a) Standard difference and bias of layer precipitable water from satellite observations (b) the associated root mean square difference.

ALWI3

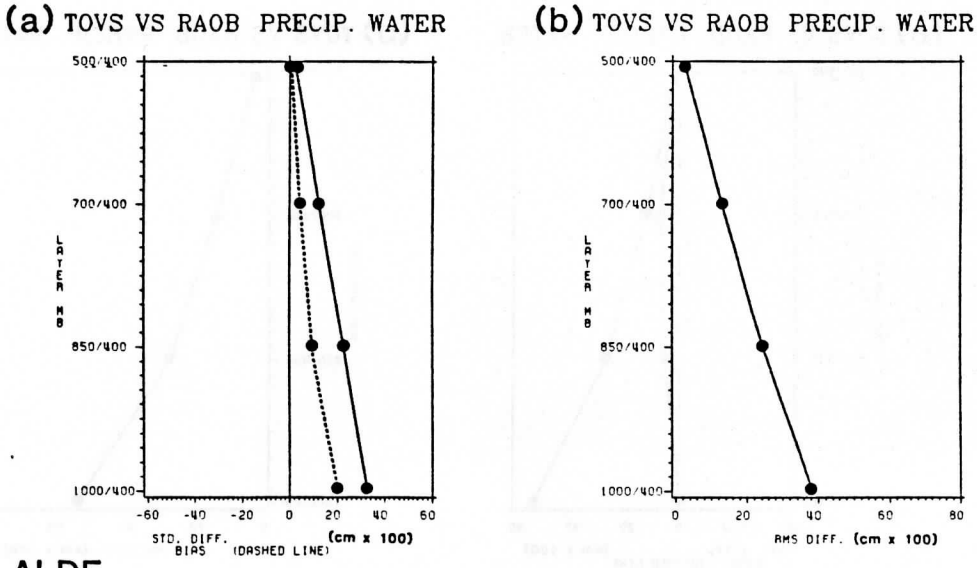

ALDF

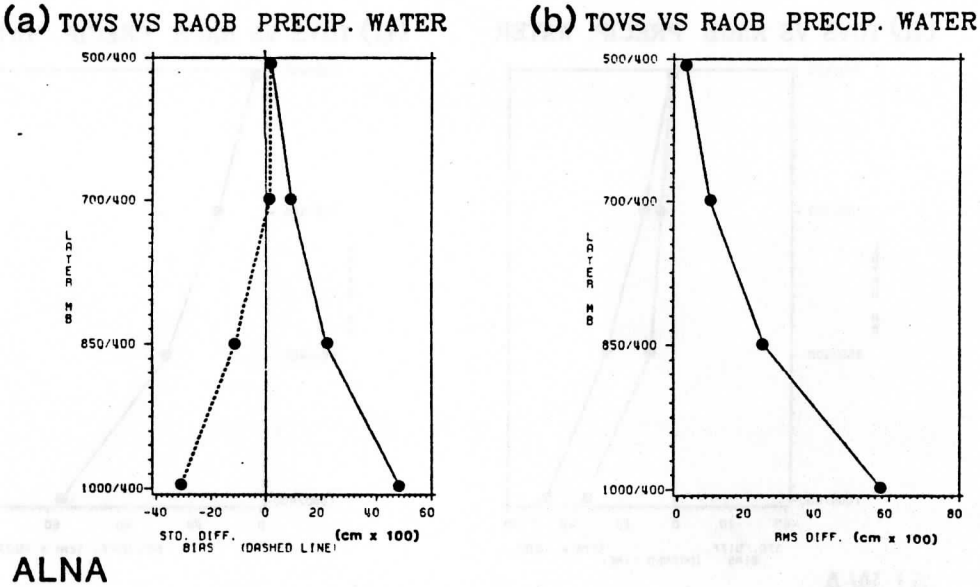

ALNA

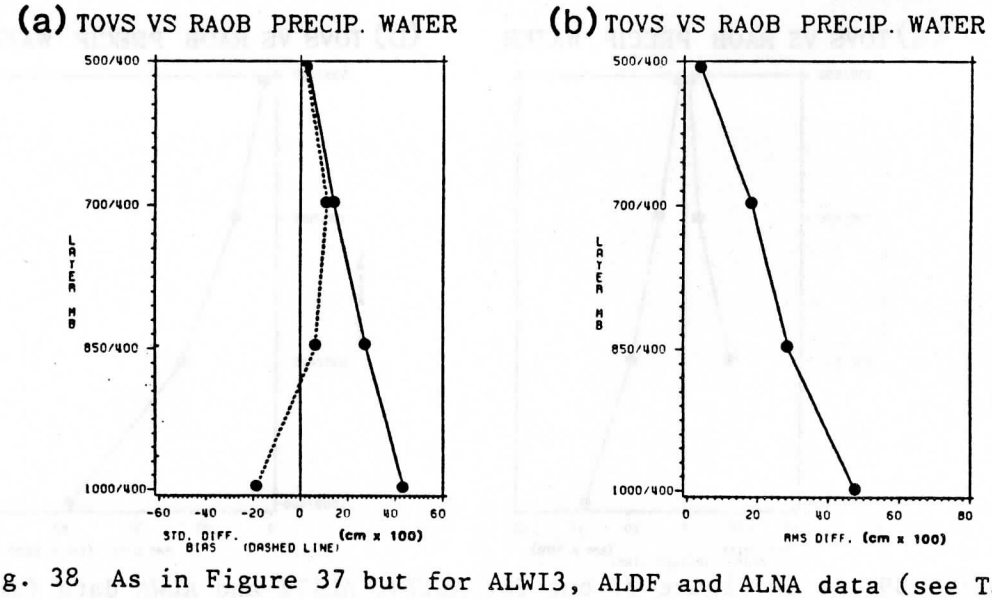

Fig. 38 As in Figure 37 but for ALWI3, ALDF and ALNA data (see Table 1).

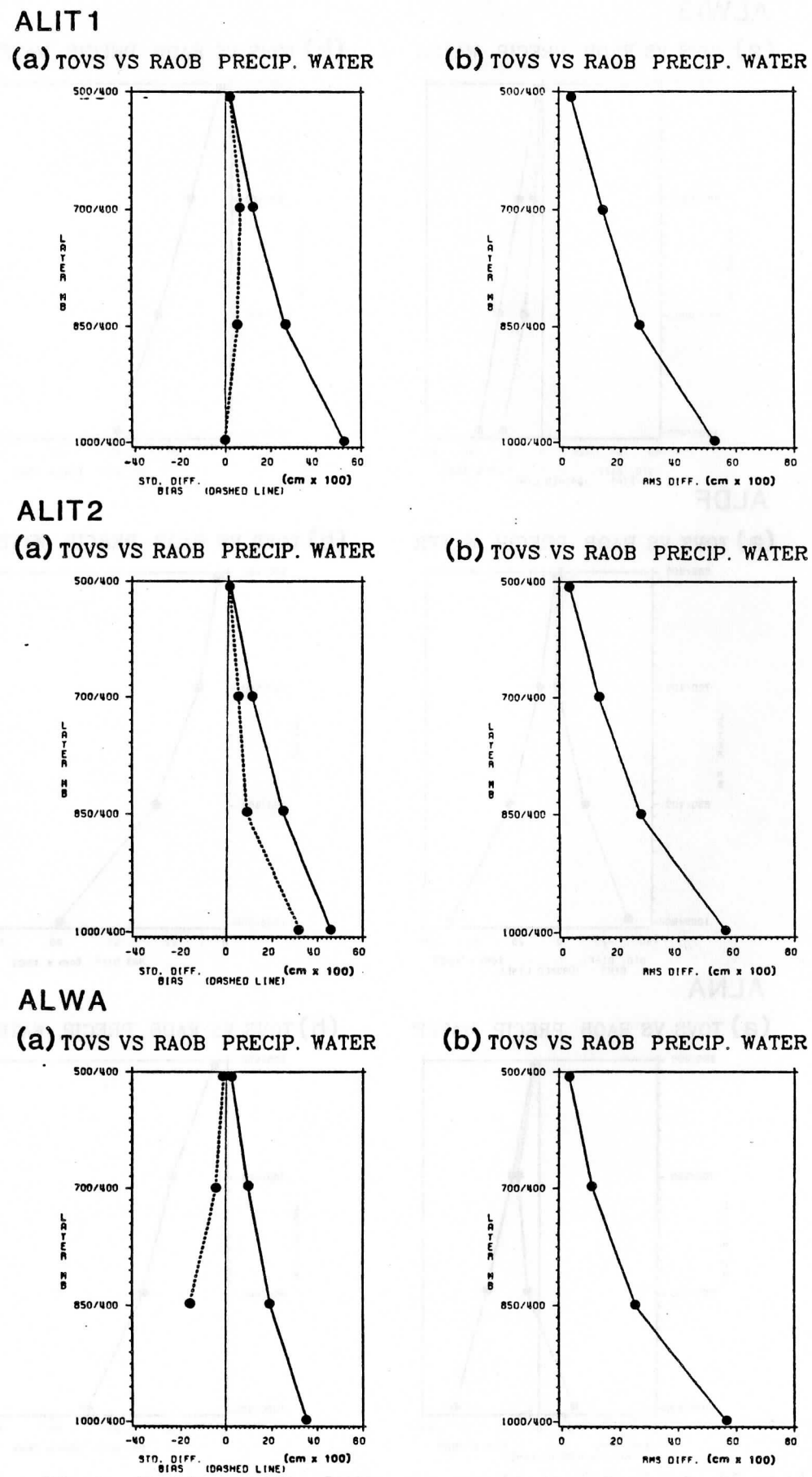

Fig. 39 As in Figure 37 but for ALIT1, ALIT2 and ALWA data (see Table 1).

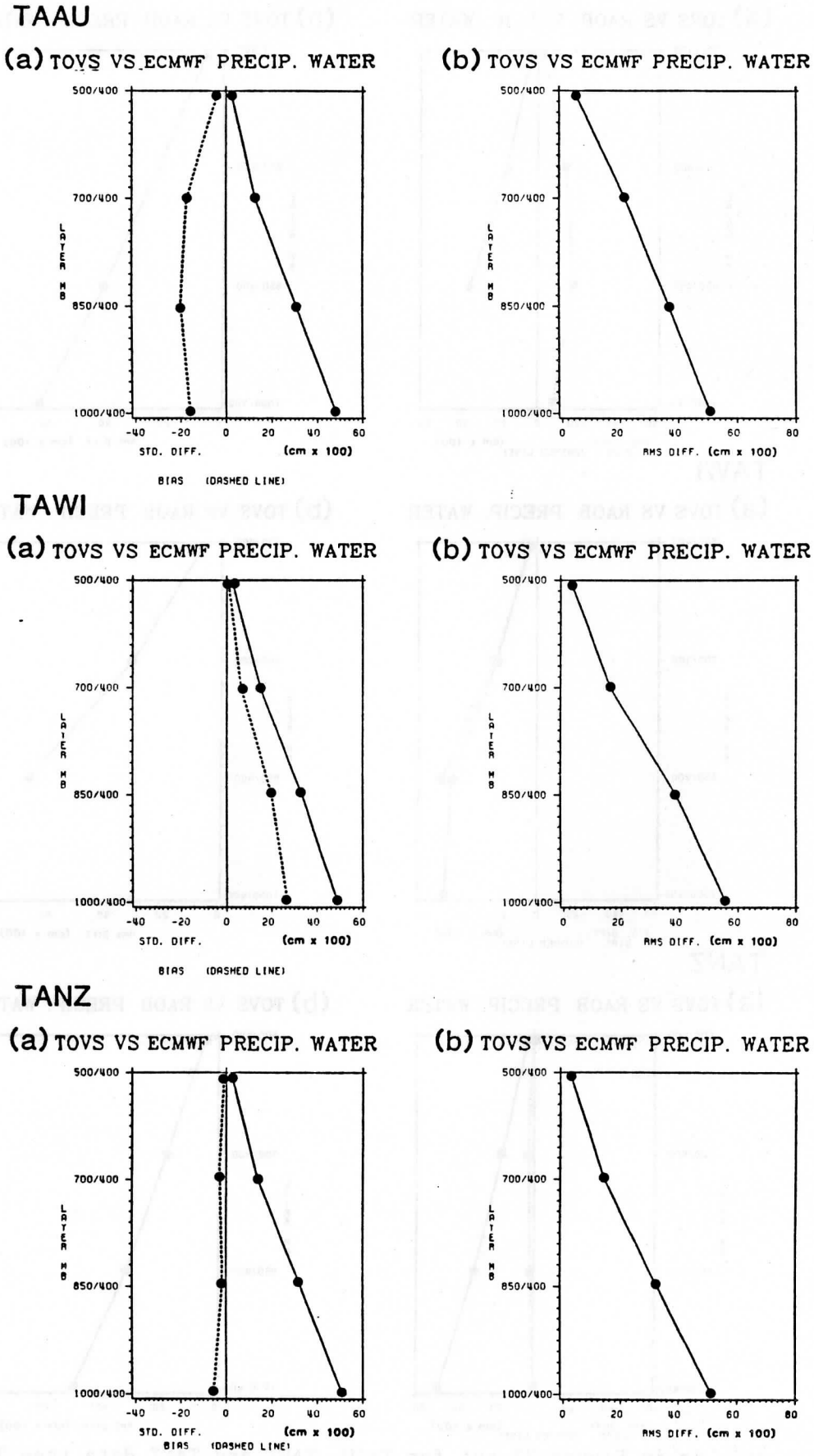

Fig. 40 As in Figure 37 but comparisons done with ECMWF analysis fields for TAAU, TAWI and TANZ data (see Table 1).

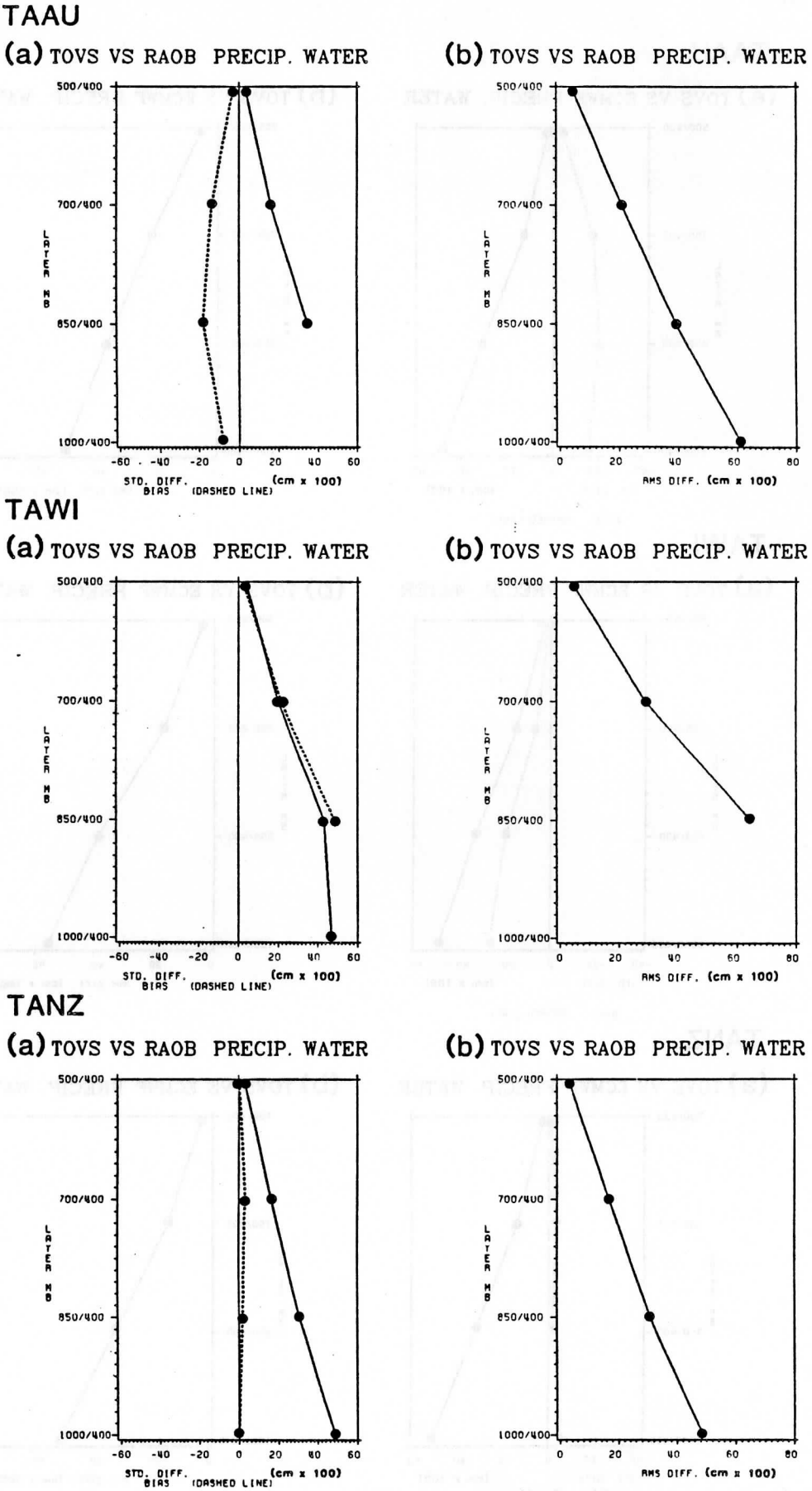

Fig. 41 As in Figure 37 but for TAAU, TAWI and TANZ data (see Table 1).

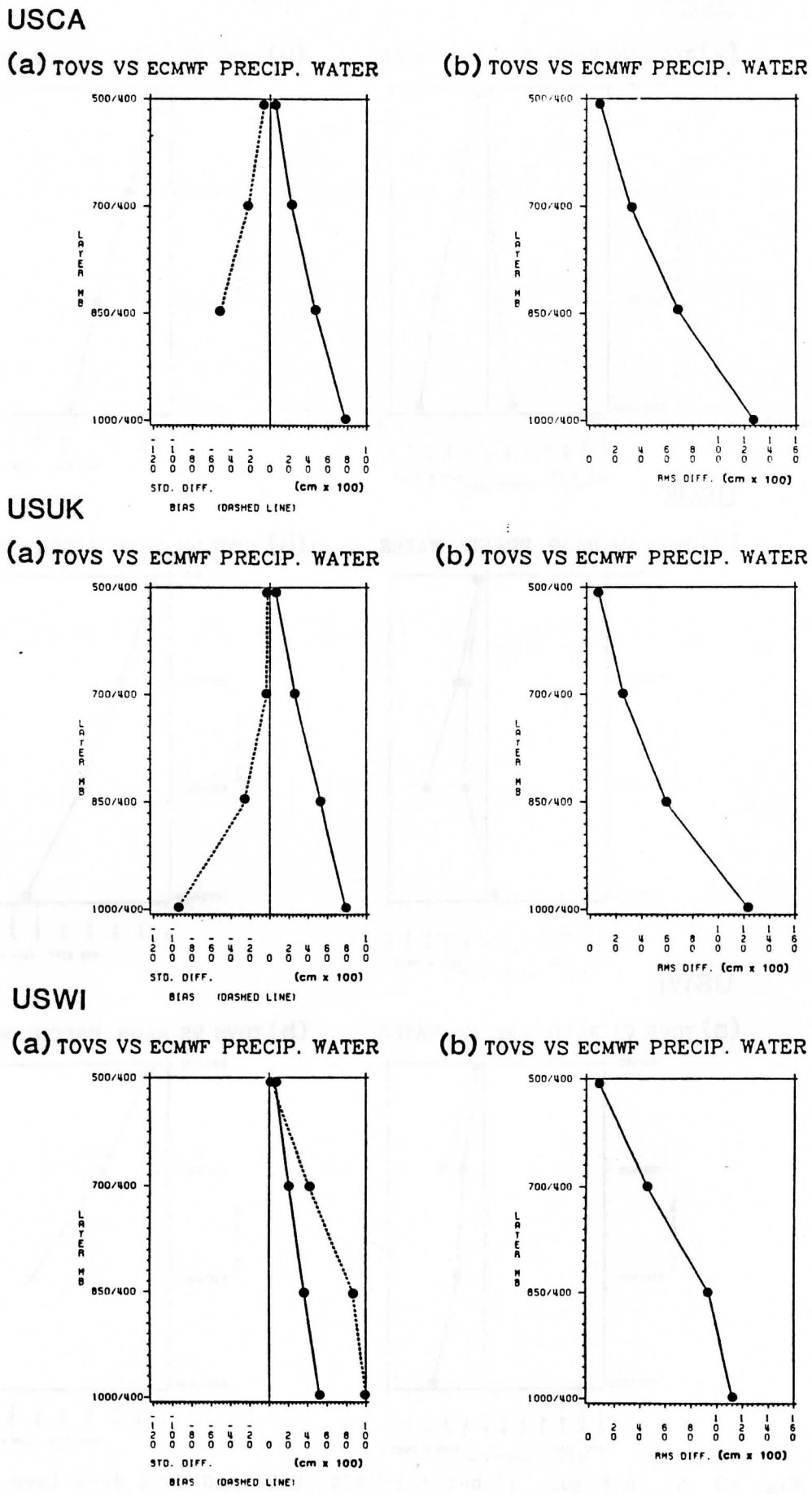

Fig. 42 As in Figure 37 but comparisons done with ECMWF analysis fields for USCA, USUK and USWI data (see Table 1).

USCA

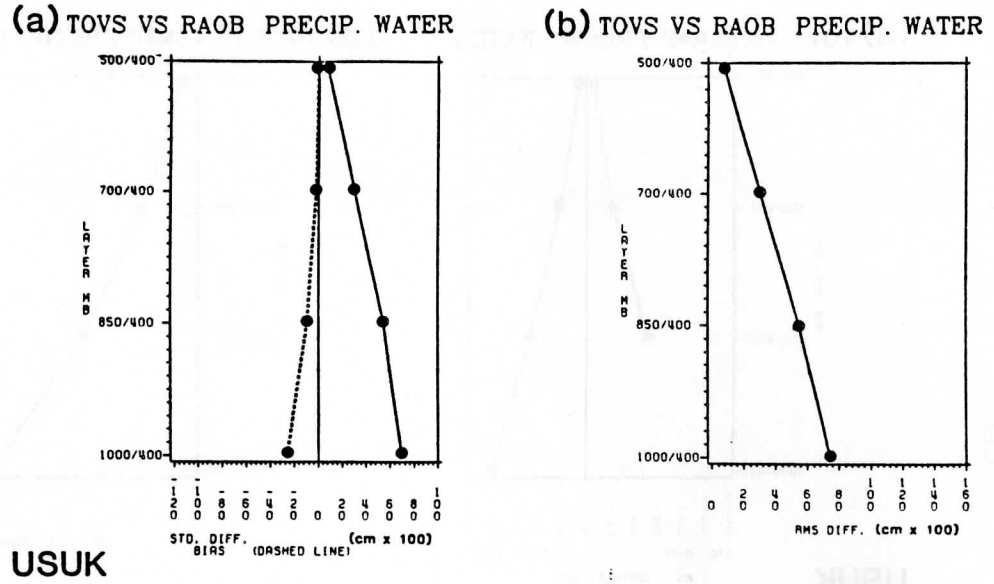

USUK

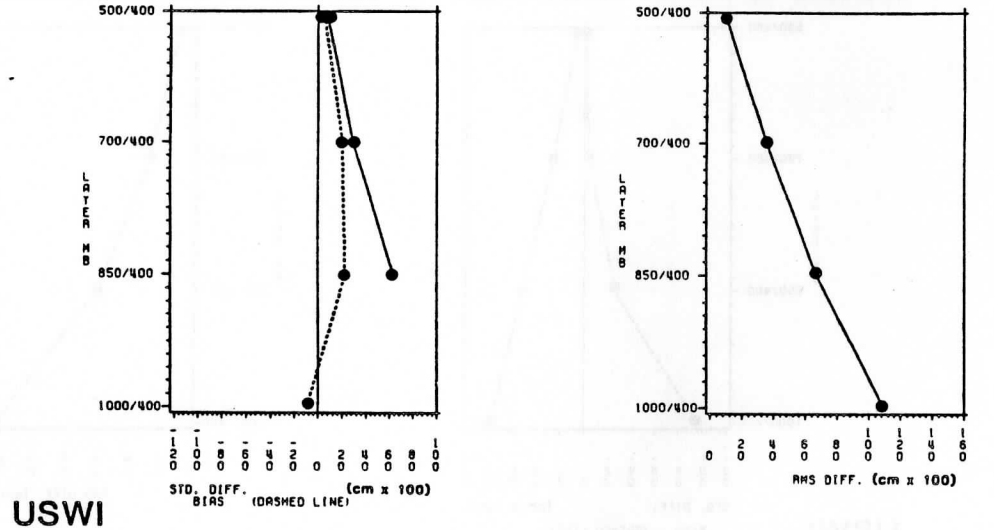

USWI

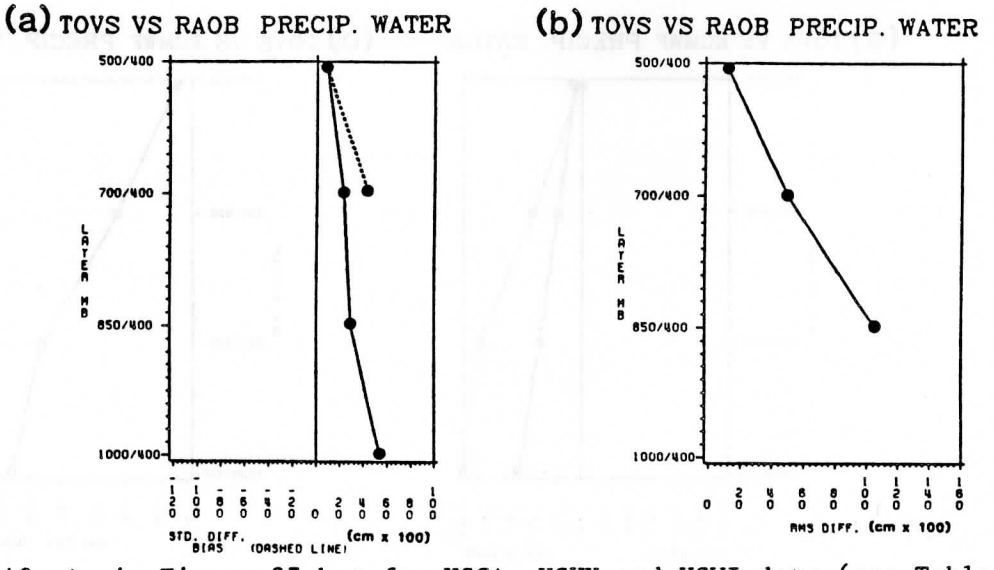

Fig. 43 As in Figure 37 but for USCA, USUK and USWI data (see Table 1).

INVESTIGATION OF AVHRR DATA TO IMPROVE TOVS RETRIEVALS

P E Lloyd, J J Barnett,

(Department of Atmospheric Physics,
Clarendon Laboratory, Oxford, U.K.)

J R Eyre

(Meteorological Office Unit, Hooke Institute,
Clarendon Laboratory, Oxford, U.K.)

1. INTRODUCTION

In this paper, some ideas of how AVHRR (the Advanced Very High Resolution Radiometer) data can be used to improve TOVS (the TIROS Operational Vertical Sounder) are put forward and preliminary investigations made. The relative calibration and location of the HIRS (High Resolution Infra-red Sounder) and AVHRR instruments are studied and ideas concerning the utilisation of AVHRR data in HIRS cloud-clearing are outlined and some results given.

The aim of this work is to develop techniques for extracting parameters from AVHRR data which may in the future have application within the operational satellite sounding data processing schemes of the U.K. Meteorological Office.

2. RELATIVE CALIBRATION OF THE HIRS AND AVHRR INSTRUMENTS

The raw HIRS and AVHRR data are in the form of digital counts and must be converted into physical units. This is done using the calibration procedure described by Lauritson et al (1979). The latitude and longitude of each sounding are calculated from knowledge of the satellite's orbital elements using the standard algorithm in the TOVS Export package obtained from the NOAA/NESDIS Development Laboratory at Madison.

HIRS and AVHRR data from 5 March 1982 have been processed and analysed. Channels 4 and 5 of the AVHRR were compared with the HIRS channel 8 (these channels being all in the 11μm window), and AVHRR channel 3 was compared with HIRS channel 19 (both in the 3.7μm window). The filter

profiles for these channels are shown in Figs 1 and 2.

The AVHRR data were averaged over a HIRS field of view with allowance being made for the relative elongation of the HIRS field of view towards the edges of the scan line. The HIRS field of view was treated as an ellipse with respect to both AVHRR line-pixel co-ordinates and scan angle co-ordinates. This procedure is described below. Plots of the appropriate AVHRR data against the HIRS data were produced as shown in Fig. 3. The "error bars" indicate the standard deviation of the AVHRR data over a HIRS spot. AVHRR channel 4 and HIRS channel 8 showed the best agreement as would be expected from looking at their respective filter profiles. No anomalies were detected in this intercomparison other than differences expected from the different response functions of the channels.

3. RELATIVE REGISTRATION OF THE HIRS AND AVHRR INSTRUMENTS

To make best use of the AVHRR data in conjunction with the HIRS data, it is necessary to know the relative positions of the HIRS and AVHRR fields of view accurately. With the relative positions of the two instruments known to an accuracy of a few kilometres, the AVHRR data could be used to yield more information on cloud top temperature and surface temperature. Also, it could enable one to detect mixed cloud height and give greater knowledge of the cloud amount present in the general vicinity of a HIRS sounding.

If the two instruments are collocated very accurately, say to 1 km, then the AVHRR data can be used to give:

- direct measurement of cloud cover within a HIRS field of view, and

- the proportion of multi-layer cloud, the temperature of each layer and hence the cloud height.

However, to derive this extra information correctly it would also be necessary to know the relative response across the HIRS field of view to the same accuracy.

Using the information given by Lauritson et al (1979) concerning the AVHRR and HIRS instruments, it can be seen that a circular HIRS spot corresponds to about 23 AVHRR pixels across by 16 AVHRR lines (at nadir). Towards the edges of the scan the HIRS spot cover more AVHRR lines but

retains the same width. To reduce the computation time necessary to derive the correlation coefficients between the two radiometers at a large number of relative offsets, this field of view has been approximated by a rectangle, 21 pixels by 15 lines (area A). HIRS view centres are spaced by about 33 AVHRR pixels and 38 lines; for the purposes of this collocation exercise a rectangle of 41 pixels by 35 lines (area B) surrounding each HIRS spot was extracted using the scan geometry of the two instruments and the time code.

Calculations were accordingly performed to work out the correlations between the HIRS and AVHRR data for the same areas to determine the spatial offsets between them. For this particular problem we considered the rectangular box, A inside the box, B, for every possible offset. The AVHRR data were averaged over A and correlated with the HIRS value. Correlation coefficients were accumulated over five portions of the HIRS scan of 1-56 spots; 1-14, 15-28, 29-42, 43-56 and 1-56 (the whole scan). This procedure was carried out for different AVHRR channels to ensure that the offsets did not vary for different radiometer channels. Contours of the correlation coefficients are shown in Fig. 4.

From the correlation coefficients calculated at integer values of pixel and line offset, we wished to determine the position of the maximum within the continuous field of correlation coefficients. This was done by deriving the following quantities:

$$G(\Delta J) = \sum_{y=-\Delta y}^{\Delta y} \sum_{y=-\Delta x}^{\Delta x} [C(x + \Delta J, y) - C(-x + \Delta J, y)]^2$$

$$H(\Delta I) = \sum_{y=-\Delta y}^{\Delta y} \sum_{x=-\Delta x}^{\Delta x} [C(x, y + \Delta I) - C(x, -y + \Delta I)]^2$$

where C(x,y) is the correlation coefficient for pixel offset, x, and line offset, y, of AVHRR relative to HIRS, ΔJ, ΔI are respective offsets within the correlation coefficient fields, and have units of AVHRR line/pixel increment. Δx, Δy define the limits of the search within the correlation coefficient field and, in this case, were

empirically chosen to be $\Delta x=6$, $\Delta y=6$. The non-integer pixel and line offsets for which $G(\Delta J)$ and $H(\Delta I)$ are zero were then determined using linear interpolation. They are marked by a cross in Fig 4. These have been compared with those of Aoki (1980) for both NOAA-7 and NOAA-8. The results are shown in Table 1. The sign convention is: y positive along the satellite's velocity vector and x positive to the right when facing along the velocity vector.

Aoki

Satellite	ΔJ	ΔI
NOAA-7	0.25	- 0.90
NOAA-8	4.87	1.14

This Work

Satellite	ΔJ	ΔI
NOAA-7	0.02	-1.61
NOAA-8	4.95	2.15

Table 1.

4. USE OF AVHRR DATA IN HIRS CLOUD-CLEARING

4.1 Introduction

Current methods for observing the temperature of the atmosphere from satellites are based on measurements of upwelling radiation in the infra-red and microwave spectral regions. These radiances are affected by the presence of cloud. At infra-red wavelengths, most clouds are almost opaque; in the microwave region clouds usually have a negligible effect on the radiances although problems occur in areas of heavy precipitation. Hence, the data processing routines must be able to detect clouds and, if possible, make allowances for their effects. For infra-red soundings, this is usually done by correcting the measured radiances to 'clear-column' values, i.e. to the radiances which would be measured from the same temperature and humidity profiles in

the absence of cloud. Cloud-clearing therefore plays a major role in current retrieval schemes.

The operational scheme in use at the U.K. Meteorological Office utilises a cloud-clearing algorithm similar to that described by McMillin and Dean (1982). The algorithm is based on the N* method (Smith, 1968) and takes some care to allow for the fact that the assumption of equal cloud height in adjacent scan spots is often invalid.

An attractive idea for improving the cloud-clearing is to use the simultaneously measured AVHRR data in conjunction with the HIRS data. Such high resolution imagery enables more details to be obtained about the cloud field characteristics and gives an opportunity to see through holes in the cloud field which are of the same order or smaller than the resolution of the sounding instrument. The following sections discuss some ideas for AVHRR processing to extract useful products. These ideas have so far undergone preliminary investigations only, with tests on nighttime data from 5 March 1982.

4.2 Potential products from AVHRR data

It is possible to envisage a processing scheme in which AVHRR pixels collocated with HIRS spots are processed to produce a few parameters which can then assist the HIRS analysis. For an operational scheme the processing should, if possible , be simple in the interest of speed. This section describes a number of simple statistical parameters which could be derived from AVHRR data.

The simplest condition to recognise is a homogeneous HIRS spot - one within which the variance of AVHRR radiances in one channel is below some threshold, e.g.

$$\sigma_{R4} < \sigma_1$$

where σ_{R4} is the standard deviation of the AVHRR channel 4 radiances within a HIRS spot, and σ_1 is some empirical threshold. A similar check could be made for channel 3, but it is likely to be complicated by variable cloud emissivity and, during the day, by solar reflection.

A homogeneous spot can be either cloud-free or uniformly cloudy, and this can be determined in a number of ways:

- by looking at the mean value of the channel 4 brightness temperature as a gross check,

- during the day, by looking at the shortwave channel radiances (i.e. AVHRR channel 1 or 2)

- during the night, by looking at the difference between the mean brightness temperatures in channels 3 and 4, which is a very sensitive indicator of fog or low cloud (see Eyre et al, 1984).

If the HIRS spot is not homogeneous ($\sigma_{R_4} \geq \sigma_i$), then we can derive a statistical parameter to determine whether the conditions required for the N* method hold within the spot and between adjacent spots. These are:

- that the atmospheric profiles and surface characteristics in the adjacent spots are the same,

- that only one layer of cloud is present, and

- that the cloud top has the same height (and temperature) in both spots.

If the second condition applies within one HIRS spot, then we can expect the following relation between radiances in channels 3 and 4:

$$R_{3i} = a + b R_{4i} + E_i$$

where R_{3i}, R_{4i} are the radiances in channels 3 and 4 for AVHRR pixel i, a and b are constants, and E_i is small for all pixels, representing the radiometric noise.

If we calculate for AVHRR pixels within a HIRS spot the residual variance from the straight line fit represented by equation 2, then:

- if the residual variance is below some empirically determined threshold we have identified that only two homogeneous "surfaces" are present within the HIRS spot: either land/sea plus one cloud layer (N* conditions) or two cloud layers (and no land/sea);

- otherwise we have identified "mixed cloud" conditions (either land/sea plus two or more cloud layers, or three or more cloud layers and no land/sea), under which the N* method is expected to fail.

Having detected spots which individually satisfy N* conditions, we can check that they hold between adjacent spots by comparing the coefficients of the straight line fit, a and b, between adjacent spots.

Once we have established that N* conditions apply, this information can be fed to the HIRS cloud-clearing algorithm together with an estimate of a cloud-free window channel radiance obtained from analysis of a histogram of AVHRR radiances within the HIRS spot.

The algorithm outlined above would be directly applicable to nighttime data. However, in the daytime the use of channel 3 radiances in this way is complicated by reflected solar radiation and a more sophisticated algorithm may be required, utilising channel 1 or 2 in addition to channels 3 and 4.

4.3 Some preliminary results

At present the above ideas have not been fully implemented and considerable development is still required to prove the usefulness of this approach. However, the following results, obtained using an AVHRR image at 0339Z (nighttime) on 5 March 1982, serve to illustrate the approach. In Figs 5,6 and 7, channel 3 radiances are plotted against channel 4 radiances for AVHRR data within a HIRS field of view for three particular spots. Fig 5 is an example of a warm homogeneous spot since there is a small variance in each channel. Figure 6 shows an area in which, from subjective examination of the image, one might expect N* conditions to apply. Most of the radiances lie close to a straight line. The outlying points are few in number and will not affect the residual variances too greatly. Nevertheless, it is expected that other cloud conditions, not evident in this image, will be better examples of ideal N* conditions. Figure 7 is a plot for an area of multi-layer cloud, and as expected the pixels lie close to a curve rather than a straight line. This shows that at least three different types of cloud top or surface are present in this area.

REFERENCES

Aoki T, 1983: Clear radiance retrieval of HIRS channels with the use of AVHRR data. Technical Proceedings of the First International TOVS Study Conference, 29 Aug-2 Sept 1983, Igls, Austria; CIMSS Report, pp 1-9.

Eyre J R, Brownscombe J L, Allam R J 1984: Detection of fog at night using Advanced Very High Resolution Radiometer (AVHRR) imagery. Met Mag, 113, 266-271.

Eyre J R, Watts P D, Turner J, Lorenc A C 1985: Research and development on TOVS retrievals in the U.K. Presented at 2nd International TOVS Study Conference, Igls, Austria; February 1985.

Lauritson L, Nelson G J, Porto F W, 1979: Data extraction and calibration of TIROS-N/NOAA radiometers. NOAA Tech Mem NESS 107.

McMillin L M, Dean C 1982: Evaluation of a new operational technique for producing clear radiances. J.Appl.Met., 12, 1005-1014.

Smith W L 1968: An improved method for calculating tropospheric temperature and moisture from satellite radiometer measurements. Mon Wea Rev, 96, 387-396.

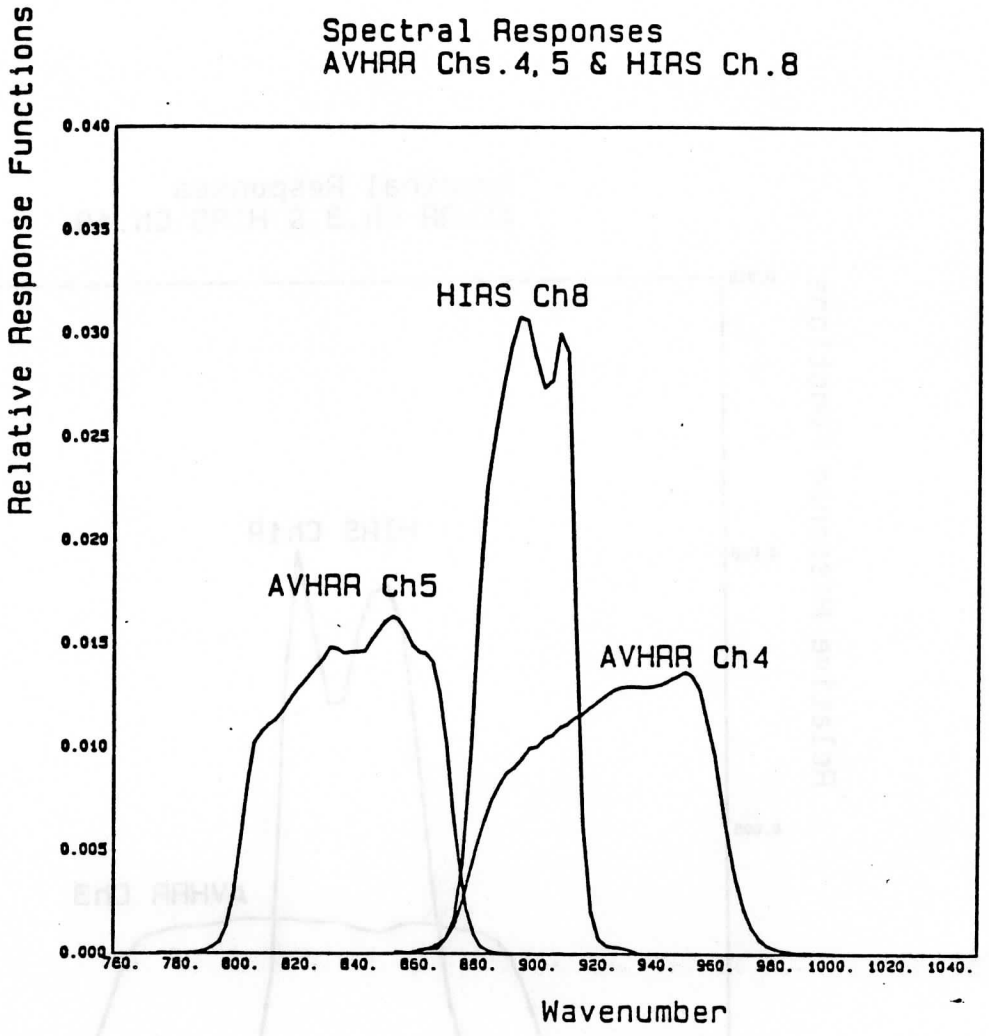

Fig. 1 Filter profiles for HIRS channel 8 and AVHRR channels 4 and 5 on NOAA-7.

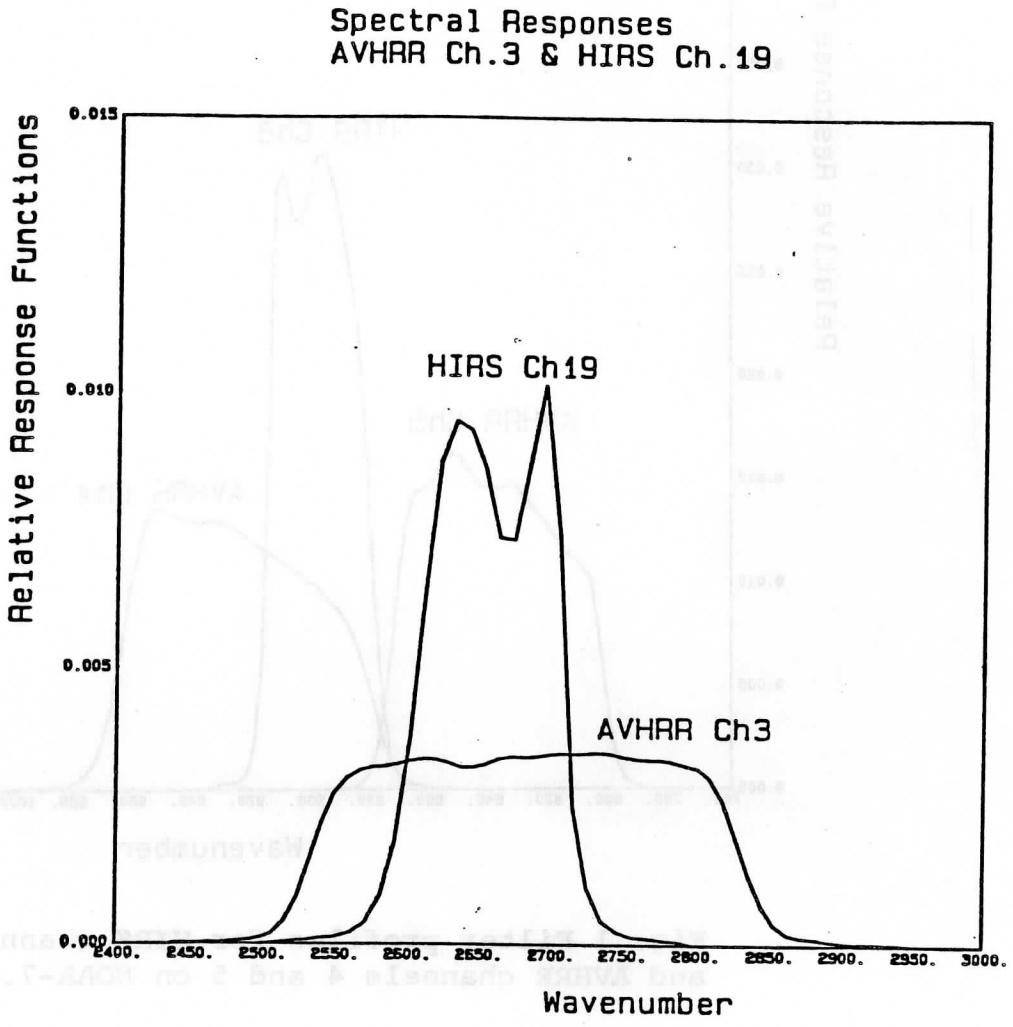

Fig. 2 Filter profiles for HIRS Channel 19 and AVHRR channel 3 on NOAA-7.

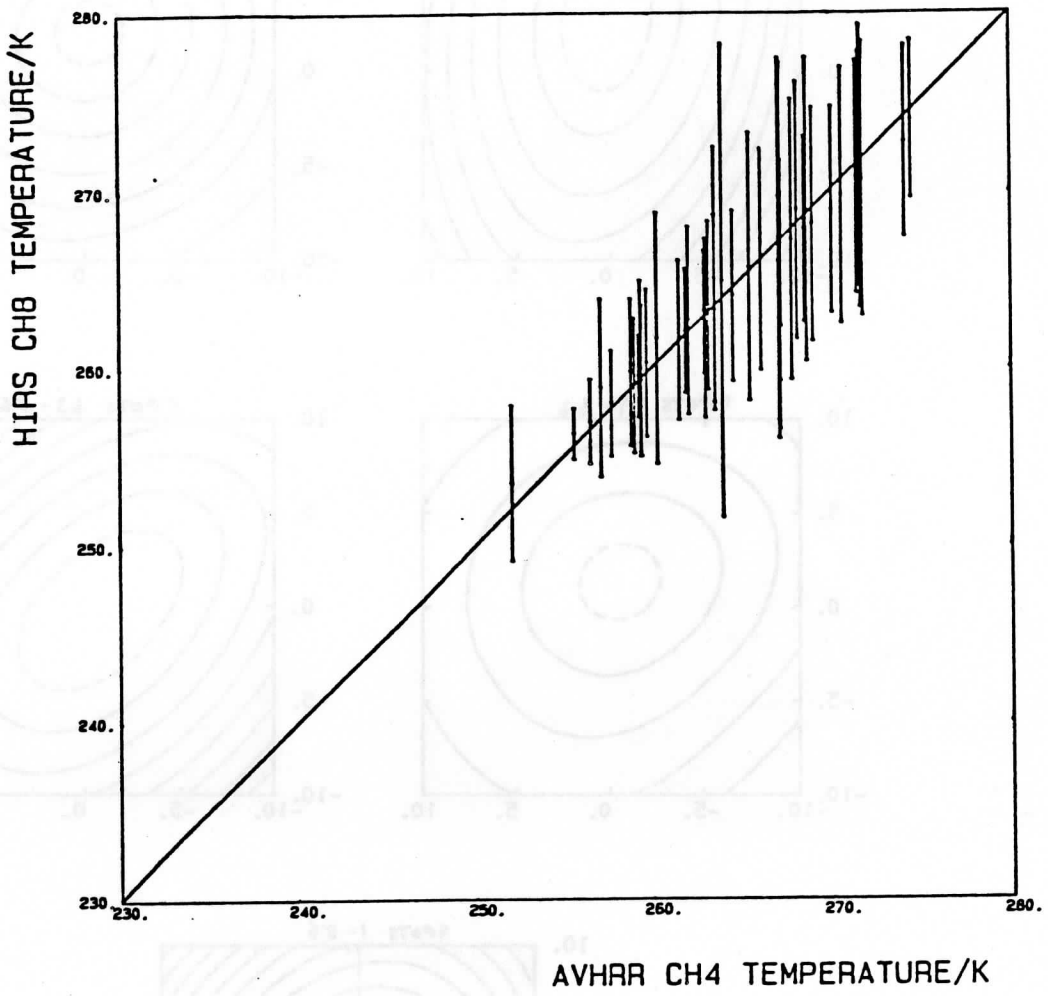

Fig. 3 Plot of HIRS Channel 8 brightness temperatures against AVHRR Channel 4 temperatures with each point representing the mean of the AVHRR data and the standard deviation shown an error bar, over an area of 5 by 10 HIRS spots.

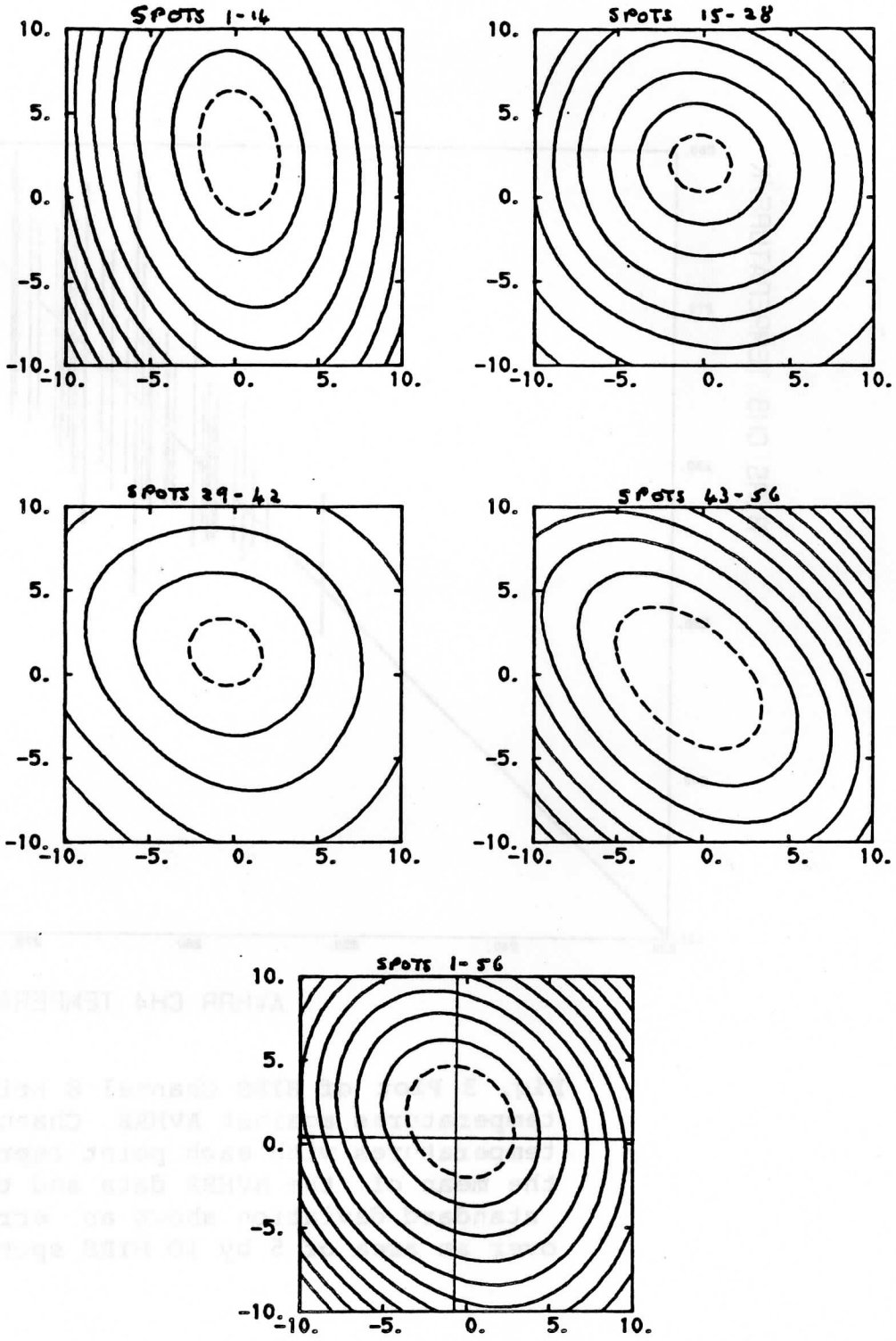

Fig. 4 Contours of the correlation coefficients for different ranges of HIRS scan position. 0.99 contour is shown dashed. Solid contour values chosen arbitrarily to suit individual plots (for NOAA-7).

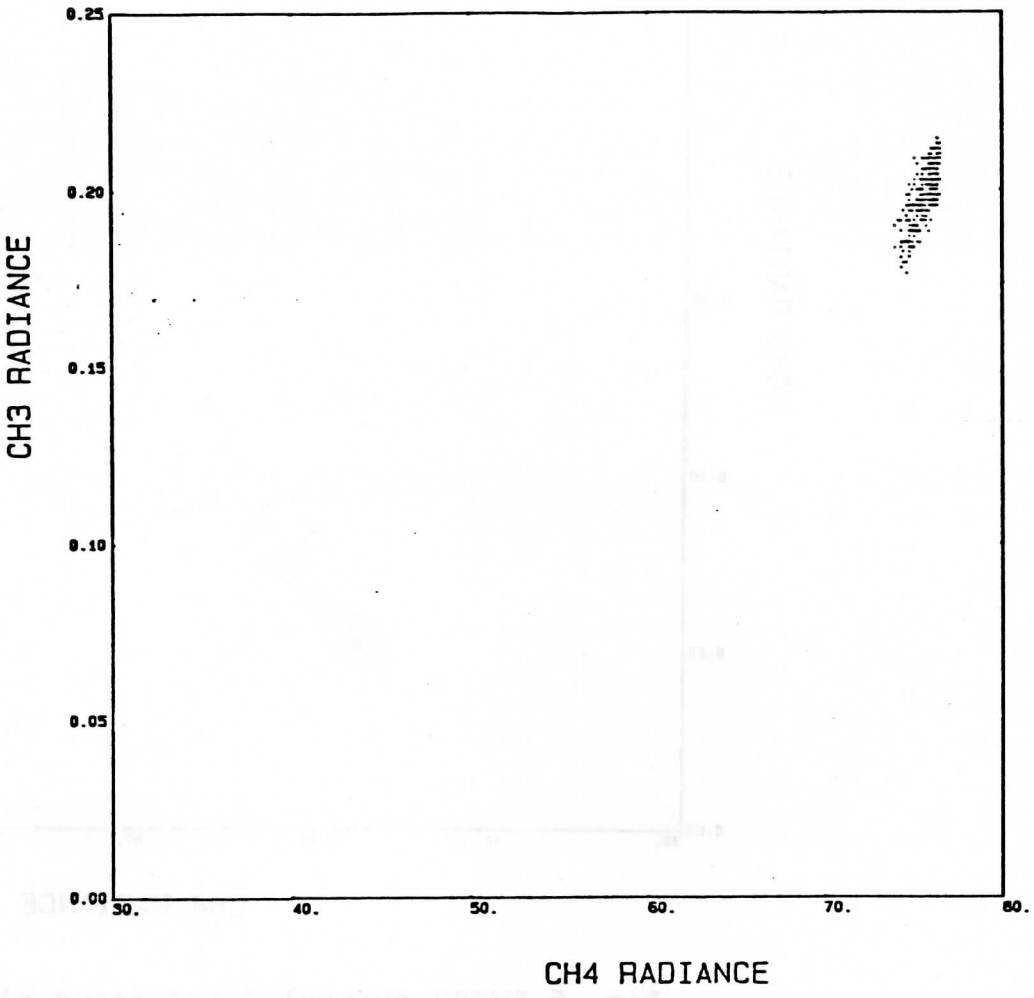

Fig. 5 AVHRR channel 3 radiances plotted against channel 4 radiances within a HIRS spot in units of mW/cm-1.Str.m^2.

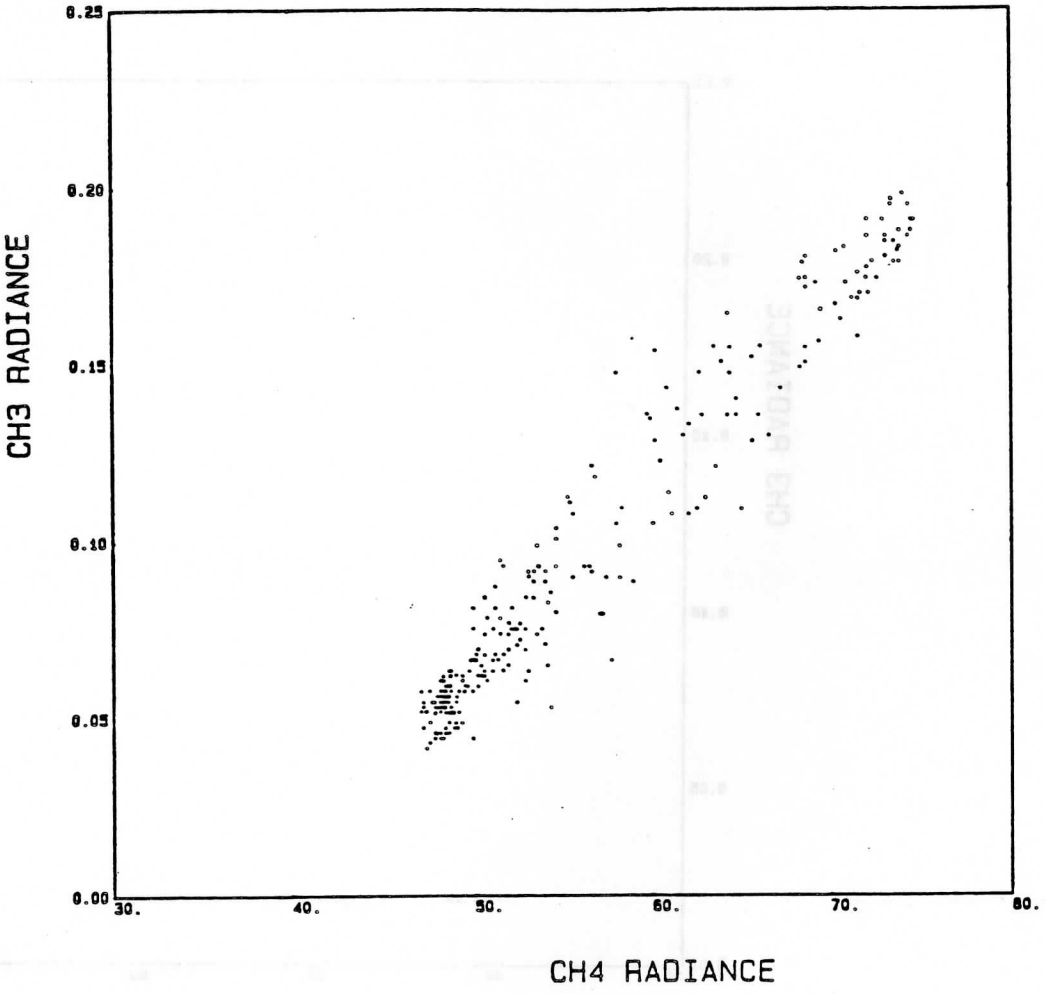

Fig. 6 AVHRR channel 3 radiances plotted against channel 4 radiances within a HIRS spot in units of mW/cm-1.Str.m^2

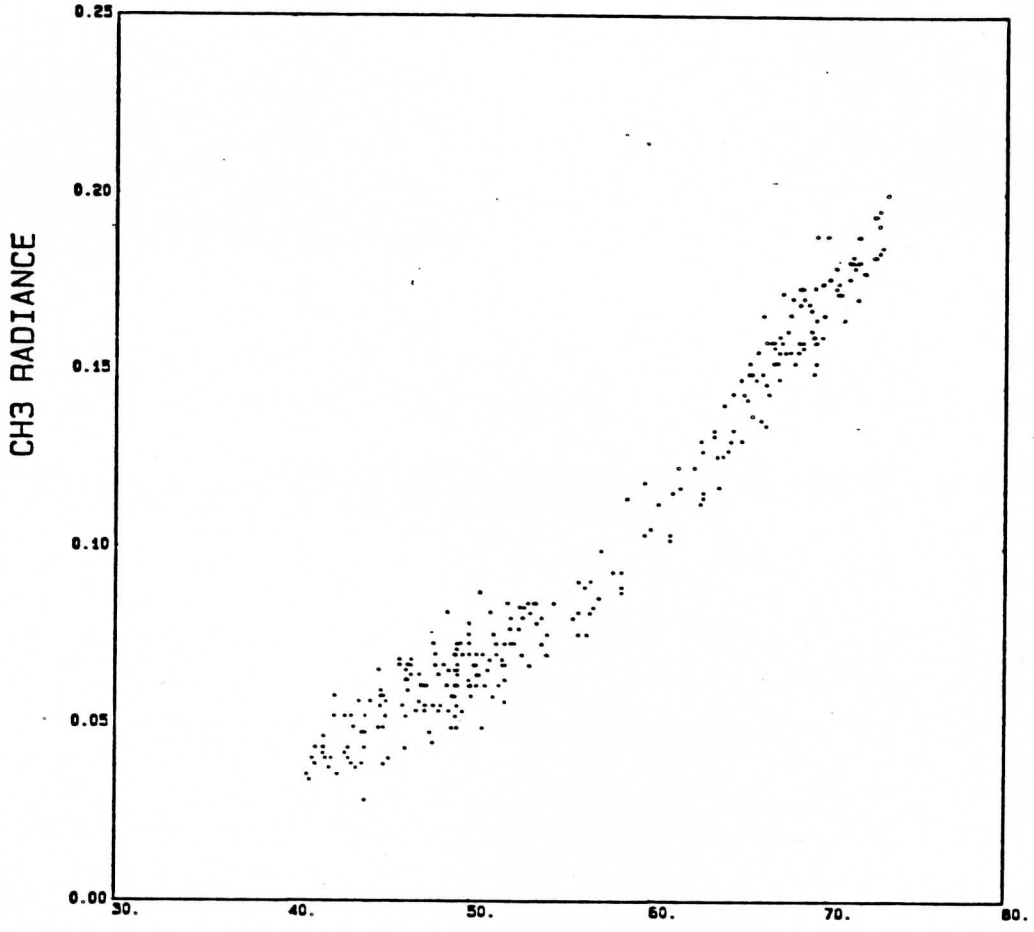

Fig. 7 AVHRR channel 3 radiance plotted against channel 4 radiances within a HIRS spot in units of mW/cm-1.Str.m.^{2}

STATUS OF SURFACE TEMPERATURE MEASUREMENT AND IMPACT UPON ATMOSPHERIC SOUNDING

M.J. Lynch, A.J. Prata and J.D. Penrose

School of Physics and Geosciences
Western Australian Institute of Technology
Perth, Australia

1. INTRODUCTION

At the previous TOVS Conference (Menzel and Lynch, 1983) the effective utilisation of ancillary data emerged as an area for increased attention. In particular, the use of the higher resolution AVHRR data for improving the accuracy of TOVS products via the radiative transfer equation (RTE) was identified as a task where gains might be made.

This paper aims to

(i) function primarily as a status report, reviewing what has been achieved in sea surface and land surface temperature determinations from satellite platforms;

(ii) draw attention to specific problems which exist in accurately extracting these measurements from observations; and

(iii) provide recommendations on the utilisation of AVHRR to support TOVS products, including a discussion of benefits and overheads.

Rather than being a definitive document we intend this paper to provide a basis for discussion out of which areas for further research will be stimulated.

2. BACKGROUND

The radiance reaching a satellite sensor is given by

$$I(\nu,T,\theta) = B(\nu_s,T_s)\tau_s(\nu,\theta) + \int_{\tau_s(\nu,\theta)}^{1} B(\nu,T_p)\,d\tau(\nu,p,\theta) \qquad \ldots(1)$$

where ν = the wavenumber
T = the brightness temperature
θ = the zenith angle
τ = atmospheric transmittance

The subscripts s and p reference parameters to the surface and pressure level p respectively. Changes in received radiance due to variations in surface temperature enter through the Planck function $B(\nu,T_s)$ in equation (1).

If we assume, by way of example, that we use a 12μm window to sense the surface, which typically is at 300K, then the Planck term (using λ in place of ν).

$$B(\lambda,T_s) = \frac{c_1}{\lambda^5(e^{c_2/\lambda T} - 1)} \qquad ...(2)$$

approximates to

$$B(\lambda,T_s) = \frac{c_1}{\lambda^5} \cdot e^{-c_2/\lambda T}$$

and

$$dB = -\left[\frac{c_1 c_2}{\lambda^6} e^{-c_2/\lambda T_s}\right] \ln T_s \, dT_s \qquad ...(3)$$

We have the well known result that the outgoing spectral radiance in this region is relatively insensitive to changes in surface temperature. This is to our disadvantage if we wish to measure surface temperature but, of course, is a bonus if we are trying to profile the atmosphere and wish surface variations to be minimised.

The Joint Organising Committee of GARP recommended 0.25K as a desired accuracy goal for surface temperature measurements. While the accuracy required is very much a function of what one wishes to do with the data, it is clear for example from climate research that specification of boundary conditions in atmospheric models requires surface temperatures to an accuracy of < 0.5K.

If we examine briefly equation (3) at a temperature T_s = 300K with λ = 12 μm, a ΔT_s = 0.25K produces a change in ln T_s of only 0.015% and a corresponding change ΔB in the outgoing spectral radiance at the surface of 0.33%. With the noise equivalent temperature diffeence (NE ΔT) of the order 0.1K, radiance changes of this magnitude are measureable. However, if we examine the depression of say the 12 μm brightness temperature betwen moist and dry atmospheres, we see this can be the order of 5-10K. Clearly precise corrections for atmospheric moisture are required if we wish to achieve our target accuracy in surface temperature measurement.

If we examine the 3.7 μm window region for T_s = 300K and a ΔT = 0.25K the radiance change ΔB is some 1.1%; just over threefold that in the 12 μm region. Additionally, the water vapour correction to brightness temperature at 3.7 μm is typically half that in the 12 μm window region.

While the bulk of work in sea surface temperatures (SST) is undertaken in the 11-12 μm region, persuasive arguments can be made to support more emphasis being given to the 3.7 μm window region.

To date the majority of SST work on AVHRR data has proceeded either by

(i) transmission simulations and statistical regression often with some adjustment of coefficients to remove small biases (McClain, 1983), or

(ii) generating coefficients by direct regression of satellite measured radiances against in-situ measurements (Bernstein, 1982).

An analysis of the literature suggests that extreme caution should be exercised in applying coeffients derived for one geographic area to another region. A measure of seasonal tuning of coefficients also seems appropriate.

A recent review of theoretical aspects of multiple window SST approaches has been provided by McMillin and Crosby (1984). They demonstrate that the form

$$I_s = I_1 + (I_1 - I_2')\gamma \qquad \ldots(4)$$

where I_s = radiance due to the sea surface
I_1 = radiance at wavelength 1
I_2' = radiance at the wavelength 1 which would have the same brightness temperature as the radiance measured at wavelength 2.
and γ = constant is derivable from radiative transfer arguments. The parameter γ, when calculated from transmittance models, varies by about 5%.

Providing absorption is small, so that a linear approximation is valid, the value of γ is independent of temperature and moisture profiles. This assumption is invalid for large viewing angles and moist atmospheres.

A further approximation requires that the average equivalent radiative temperature of the atmosphere be relatively insensitive to wavelength. This requires that absorption should be due to the same atmospheric constituents and suggests that λ_1 and λ_2 should be closely spaced (i.e. a split-window).

An alternate algorithm (McMillin and Crosby, 1984) which is frequently used

$$T_s = T_1 + (T_1 - T_2)\gamma \qquad \ldots(5)$$

may be less accurate in certain circumstances. The differences in using equation (4) and (5) can be very significant particularly in moist atmospheres.

Comparison of ship and buoy-derived data with satellite measured SST's has its own difficulties with respect to spatial and temporal

considerations, accuracy, and bulk versus skin sampling. In view of these difficulties and for the benefit of users of the data, a case has been made for the development of reliability indicators for SST measurements.

A survey of the literature suggests that typically SST measurement uncertainties lie in the vicinity of $\pm$1K and in some cases closer to $\pm$2K. The application of statistical procedures and rejection criteria for bad or contaminated data may bring uncertainties down to closer to 0.5K, but in general the procedure would be site specific and employ a fine tuned algorithm.

Deschamps and Phulpin (1980), using climatological temperature and moisture profiles, claim that SST's may be measured to a high degree of accuracy (0.14 to 0.39K) given acceptable noise levels on the radiometers. A clear disadvantage of the dual channel technique lies in the measurement error amplification in differencing the brightness temperature. For example, an error of 0.1K in T_B in the two channels can lead to an uncertainty of ~0.6K in the SST. Barton (1983a) has recommended the use of scan angle-dependent regression coefficients in two-channel SST derivations.

Instead of using radiances at different wavelengths the angular dependence of transmittance may be used (McMillin (1975), Barton (1983b), Chedin et al (1982)). In particular Barton (1983b) claims that the dual angle technique applied at 3.7 μm is the most accurate of a variety of schemes investigated. McMillin and Crosby (1984) point to particular situations in which either the angle or wavelength approaches have specific advantages.

Further comment is necessary on transmission models. Imbault et al (1981) have investigated the effect of atmospheric absorption on brightness temperature for the 2-channel, split window situation. Their seperate analysis for line and continuum absorption reveals that considerable care is required in channel selection for accurate SST determinations. The regression equations for the 11 and 12 μm split window for a high humidity tropical model atmosphere showed significant departure from the other atmospheres studied.

Chahine (1981), in a discussion of direct inversion methods, has presented arguments for using 'super-windows' (3.723, 3.822 and 3.992 μm) in the 3.7 μm window region where the water vapour continuum correction is significantly lower than for correspondingly narrow windows in the 9 and 11 μm regions.

It is important that well tested cloud filtering schemes be applied to satellite data if accurate SST's are to be produced. McClain (1983) provides extensive detail on the cloud tests applied in operational multichannel SST processing. Llewellyn-Jones et al (1983) claim that cloud filtering remains a serious problem and recommend investigation of new procedures.

Finally, while the water vapour absorption (particularly the continuum component) is a major effect, the role of the other constitutents (HNO_3, CO_2, O_3, H_2O dimer and aerosols) which affect SST accuracy should not be neglected. Grassl and Koepke (1981) have provided an analysis of minor constituent effects and argue that spectrally narrow channels which avoid the absorption lines still have to contend with the continuum-like absorption of the H_2O dimer and aerosols.

3. TASKS REQUIRING FURTHER INVESTIGATION IN SST MEASUREMENTS

1. Improve knowledge of the water vapour continuum absorption in atmospheric windows.

2. Continue research into the refinement of transmission models in the infrared region.

3. Investigate further the performance and refinement of SST algorithms in high humidity atmospheres.

4. Investigate how the variation of ocean surface emissivity in the infrared as a function of surface roughness may be incorporated as a correction to SST's.

5. On the basis of research findings, make recommendations on cloud filtering procedures.

6. Investigate the impact of other minor atmospheric constituents including nitric acid, carbon dioxide and ozone. In particular the residual quasi-continuum absorption of the H_2O dimer and aerosols requires investigation.

4. LAND SURFACE TEMPERATURE MEASUREMENT

While extensive comment has been made in the literature on the problems associated with poor consistency among various means for measuring sea surface temperature, it is clear that the situation is somewhat worse for land surface temperature (LST). Although the techniques are well established (Marlatt, 1967) using thermistors and radiometers it is the logistics that limit satellite and in situ LST comparisons. Little work would appear to have been undertaken using aircraft mounted infrared scanners in the 10-12 μm region for regional mapping of LST for comparison with satellite-derived fields. A strong case exists for acquiring accurate data from satellites for frost forecasting, forestry studies, crop/soil mositure studies (Carlson et al. 1981) and thermal inertia-based geological studies (Watson, 1975).

The standard 2 meter height air temperature recorded during daytime can differ from the LST by 10-15K or more depending on the nature of the surface (moist, vegetated, bare soil, rock). As such comparisons of satellite LST's with these data are not particularly meaningful. Further, the optical variability of LST and the

development of rejection criteria for bad retrievals (as frequently used for SST's) are difficulties.

If we follow the analysis of Deschamps and Phulpin (1980) beginning with

$$\frac{dI_\lambda}{dz} = - k_\lambda U \, (I_\lambda + B_\lambda(T(z))) \qquad \ldots(6)$$

where I_λ is the intensity of radiation passing through an absorber of density U with an absorption co-efficient k_λ and B_λ is the Planck function.

If k_λ and B_λ can be expressed in a form

$$k_\lambda = C(\lambda)f(U, T, P) \qquad \ldots(7)$$

where $C(\lambda)$ is a scaling factor and f a function of atmospheric parameters, then a split-window formulation gives

$$T_s = T_{11} + \frac{1}{(C_{11}/C_{12} - 1)} (T_{11} - T_{12}) \qquad \ldots(8)$$

Price (1984) has investigated the value of the ratio $R = C_{11}/C_{12}$.

Using observational data and radiative transfer theory Price (1984) has determined a value of $R = 1.36 \pm 0.03$. Expressing T_s in the form of equation (5) yields γ values in the range 2.78 ± 0.23 which compare to the daytime value $\gamma = 3.046$ derived by McClain (1983).

The investigations by Price (1983, 1984) have been hampered by lack of direct measures of surface temperature and out of necessity it has been assumed that T_s exceed the 2m air temperature by 10K.

Surface emissivity ε is approximately unity for the land surface in the 10-12 μm region. It is not just the variability in emissivity with surface type that is a difficulty but the variation in emissivity between the 11 and 12 μm channels for the same field of view.

For example (Vincent et al. 1975; Taylor, 1979, and Slater, 1980) indicate that agricultural areas have $\varepsilon \sim 0.97$ and vegetation $\varepsilon \sim 0.96$ in the 10-12 μm region. A relation of the form

$$I_\lambda \sim \varepsilon_\lambda T^{n_\lambda} \qquad \ldots(9)$$

seems appropriate with $n_{11} \sim 4.5$ and $n_{12} \sim 4.3$.

Incorporation of the emissivity correction (Price, 1984) gives

$$T_s = \left[T_{11} + 3.33(T_{11} - T_{12}) \right] \left[\frac{3.5 + \varepsilon_{11}}{4.5} \right] + 0.75 T_{12} \left[\varepsilon_{11} - \varepsilon_{12} \right] \quad \ldots(10)$$

For a surface of $\varepsilon \sim 1$ at 300K, a difference between ε_{11} and ε_{12} of 0.01 affects the T_s determination by 2K.

While the AVHRR may be able to determine land surface temperatures to within a few degrees K ($\sim$ 3 or 4) the instrument was not designed for this purpose. Channel saturation at 320K remains an obstacle to universal coverage.

Susskind et al. (1984) have reported on ground temperature measurement using the HIRS 3.98 and 3.74 μm channels. T_s is solved for interatively using fixed values for emissivity (ε_{LAND} = 0.85, ε_{OCEAN} = 0.96) and the assumption that the surface effective reflectivity is the same for both channels. The ground temperature is used to estimate the clear column radiances. This approach has not been subjected to independent validation.

5. TASKS REQUIRING FURTHER INVESTIGATION IN LAND SURFACE TEMPERATURE (LST) MEASUREMENT

1. Clearly, if the 10-12 μm or 3.7 μm windows are used in LST measurement using multiple channel and split-window techniques, a number of problems (water vapour, cloud etc.) exist in common with the determination of SST's, as discussed in Section 3.

2. A knowledge of the emissivity of land surfaces and, in particular, the variation of emissivity with wavelength appears to be a significant factor limiting accuracy.

3. Available measurements (Slater, 1980) indicate that the power law relating brightness temperature to radiance (equation (9)) shows a strong dependence on wavelength. The scarcity of such information and a knowledge of the variation with the nature of the surface (soil, vegetated) is a matter of concern if split-window approaches are to be employed.

4. Perhaps the major difficulty with LST measurements from space platforms is that there is little to compare them with to enable an assessment of accuracy of the retrievals. A survey of what is available suggests that definitive experiments remain to be done. Such investigations should include aircraft measurements with dual channel radiometers set at the same wavelength as those channels used on the satellite.

5. McMillin et al. (1984) have advised caution in using brightness temperatures in SST regression relations in situations where warm air of continental origin overlays the cooler ocean. Susskind et al. (1984) have expressed particular concern over the use of regression approaches over land regions because the differences between skin and near surface air temperature are even greater.

6. SUMMARY

1. SST retrievals using AVHRR data have achieved an accuracy which when coupled with spatial resolution has proved to be very valuable in the analysis of oceanographic processes. Clearly, improvements in retrieval accuracy are possible particularly once water vapour absorption processes are better understood. It appears unlikely that one universal algorithm will emerge in that adaption to region and season may remain essential.

2. While limited research has been conducted on the accuracy of LST retrievals, it seems that, in the absence of more details of the surface (geology, vegetation and associated emissivities), the accuracy will remain inferior to SST measurements. Existing accuracy nevertheless is adequate for a range of other applications in agriculture and forestry.

3. No matter which atmospheric temperature retrieval scheme is used (regression, iterative physical retrieval etc.) an independent knowledge of a relevant parameter in the RTE improves the retrieval. This has been demonstrated to be effective for example in the case of knowledge of the tropopause height (Westwater, 1982). Experience shows that inaccurate surface temperatures (from say, climatology or a forecast model), if held fixed in the retrieval, can seriously degrade the retrieved profile in the lower levels. Unfortunately, the converse is not true. Determination of low level inversions or lapse rate in the near surface layer remains a difficulty with current instruments. Climatology and synoptics used in a two - step retrieval scheme may improve this situation.

4. The use of AVHRR to estimate cloud amount can make a positive impact on TOVS retrievals (Aoki, 1983; Aoki, 1985). The question of whether AVHRR has a further role in improving TOVS retrievals can be answered in the affirmative in that AVHRR SST's have claimed accuracies of ~ 1.0K whereas surface temperatures from TOVS (e.g. Susskind et al. 1984) using the 3.7 and 4.0 μm channels are claimed to be small but more like 2K. In broken cloud conditions where TOVS retrievals fail, AVHRR will frequently permit a surface temperature to be retrieved and the clear column radiance estimated. The tropical region falls into this category but unfortunately AVHRR products in the tropics are degraded by humidity

effects. Convergence zones generally pose a probelm for AVHRR and in some regions it may not be possible to retrieve SST's for a month or more.

5. From a practical standpoint the overheads in processing AVHRR data are considerable, with respect to the receiving facility, computer system and processing time. Additionally, earth location of AVHRR over the oceans is a continuing problem. The appeal of doing retrievals with TOVS data only is strong given the limited scientific gains and the significant practical problems associated with acquiring and utilising AVHRR data. The absence of the split-window channels on alternate NOAA satellites probably will discourage the merging of AVHRR and TOVS data bases.

6. The contribution of the AVHRR to oceanography is impressive despite a number of problems outlined earlier. The AVHRR brightness temperature difference field $T_{11}-T_{12}$ reveals the horizontal scale of moisture spatial variability to be typically the order of tens of kilometers or greater. It is more likely that the moisture soundings from TOVS will impact upon AVHRR SST retrievals by guiding the selection of regression co-efficients in the SST algorithm. This is a task worthy of further investigation.

7. In looking to the future there is little doubt that a more judicious choice of channels for a TOVS like instrument will produce improved surface temperature measurements. The same argument applies to the AVHRR instrument.

8. In this review the performance of the microwave retrieved SST's has not been discussed, the emphasis being on current instruments and associated problems. As has been pointed out by others (JPL, 1984) instruments like the first generation SMMR flown on NIMBUS-7 have a number of problems, many of which can be overcome. There is not doubt that new microwave instruments such as the Advanced Microwave Sounding Unit (AMSU) will improve significantly surface temperature retrievals.

7. REFERENCES

Aoki, T., 1983: Clear radiance retrievals of HIRS channels with the use of AVHRR data. The technical proceedings of the first TOVS study conference, Igls, Austria, W.P. Menzel, ed. August 29 - September 2, 1983, CIMSS Report, Space Science and Engineering Centre, University of Wisconsin, Madison.

Aoki, T., 1985: Companion paper this conference.

Barton, I.J., 1983a: Atmospheric windows are always dirty. 53rd ANZAAS Congress, Perth, May.

Barton, I.J., 1983b: Satellite measurements of sea surface temperature. Q.J.R. Meteorol. Soc., 109, 365-378.

Bernstein, R.L., 1982: Sea surface temperature estimation using NOAA-6 satellite advanced very high resolution radiometer. J. Geophys. Res., 87, 9455-9465.

Carlson, T.N., J.K. Dodd, S.G. Benjamin, and J.N. Cooper, 1981: Satellite estimation of surface energy balance, moisture availability and thermal inertia. J. Appl. Meteorol., 20, 60-87.

Chahine, M.T., 1981: Remote sensing of sea surface temperature in the 3.7 μm Co_2 band, in Oceanography from Space, J.F.R. Gower, ed., Plenum Press (New York).

Chedin, A., N.A. Scott, and A. Berrior, 1982: A single-channel, double viewing angle method for sea surface temperature determination from coincident METEOSAT and TIROS-N radiometric measurements. J. Appl. Meteorol., 21, 613-618.

Deschamps, P.Y. and T. Phulpin, 1980: Atmospheric correction of infrared measurements of sea surface temperature using channels 3.7, 11 and 12 μm. Bound. Layer Met., 18, 131-143.

Grassl, H. and P. Koepke, 1981: Corrections for atmospheric attenuation and surface reflectivity in satellite-borne SST measurements, in Oceanography from Space, J.F.R. Gower, ed., Plenum Press (New York).

Imbault, D., A. Chedin, A. and N.A. Scott, 1981: Multichannel sea surface temperature retrievals, in Oceanography from Space, J.F.R. Gower, ed., Plenum Press (New York).

Llewellyn-Jones, D.T., P.J. Minnett and A.M. Zavody, 1984: Infrared measurements of SST: ship-satellite comparisons in the North Atlantic, and future developments. Satellite-derived sea surface temperature workshop II, June 22-24, Pasadena, JPL Publication 84-85.

Marlatt, W.E., 1967: Remote and in-situ temperature measurements of land and water surfaces. J. of App. Meteorol., 6, 272-279.

McClain, E.P., 1983: Multi-channel sea surface temperatures from AVHRR and NOAA-7, in satellite-derived surface temperature workshop II, June 22-24, Pasadena, JPL Publication 84-85.

McMillin, L.M. and D.S. Crosby, 1984: Theory and validation of the multiple window sea surface temperature technique. J. Geophy. Res., 89, 3655-3661.

McMillin, L.M., 1975: Estimation of sea surface temperatures from two infrared window measurements with different absorption. J. Geophy. Res., 80, 5113-5117.

Menzel, W.P. and M.J. Lynch, 1983: A report on the first international TOVS study conference, Igls, Austria, August 29 - September 2, CMISS Report, Space Science and Engineering Centre, University of Wisconsin, Madison.

Price, J.C., 1983: Estimating Surface temperatures from satellite thermal infrared data - a simple formulation for atmospheric effects. Remote Sensing Environ., 13, 353-361.

Price, J.C., 1984: Land surface temperature measurements from the split window channels of the NOAA-7 advanced very high resolution radiometer. J. Geophy. Res., 89, 7231-7237.

Slater, P.N., 1980: Remote sensing, optics and optical systems (Addison-Wesley, Mass.) 246-247.

Susskind, J., J. Rosenfield, D. Reuter and M.T. Chahine, 1984: Remote sensing of weather and climate parameters from HIRS2/MSU on TIROS-N. J. Geophys. Res., 89, 4677-4697.

Taylor, S.E., 1979: Emissivity of soils in the Southeast United States. Remote Sensing Environ., 8, 359-364.

Vincent, R.K., L.C. Rowan, R.E. Gillespie and C. Knapp, 1975: Thermal infrared spectra and chemical analysis of twenty-six igneous rock samples, Remote Sensing Environ., 4, 199-209.

Watson, K., 1975: Geologic applications of thermal infrared imagery. Proc. IEEE, 63, 128-137.

Westwater, E. 1982: private communication.

PLANS FOR NESDIS OPERATIONAL WATER VAPOR RETRIEVALS

Larry M. McMillin

National Oceanic and Atmospheric Administration
National Environmental Satellite, Data, and Information Service
Washington, D.C. 20233, USA

1. INTRODUCTION

The results provided by NESDIS for this study are the values obtained from the routine processing and are not reprocessed. Although there are several reasons for this, a significant one is that the operation uses fields that are continually updated. Unless these fields are captured at the right instant and stored, reprocessed data do not exactly match the operational ones. The other reason is that the operational program has not been designed to reprocess historical data. One of the impacts of this that is particularly significant for this comparison is that NESDIS has an improved water vapor model that will soon become operational. It is not being used now only because the operational programs are being switched to a new computer and no changes are allowed during the changeover. The tape prepared for this intercomparison does not reflect the improvement. It should also be mentioned that the format in which water vapor is stored does not allow much precision.

The current water vapor retrieval, and the one used for this intercomparison, is a multiple linear regression in which the mixing ratio q is predicted from satellite measurements of brightness temperatures BT using the relationship

$$q = C_o + \sum_{i=1}^{21} C_i BT_i \qquad (1)$$

where C's are the regression coefficients and the subscript i denotes channel. The channels used are HIRS 1-16, 18, 19 and MSU 2-4. Water vapor values are produced for the clear (A) and N* (B) retrievals because clear column HIRS radiances are not available for the microwave (C) retrievals.

The new method will produce water vapor from the relation

$$T_d = C'_o + \sum_{i=1}^{21} C'_i ABT_i \qquad (2)$$

where T_d is the dewpoint temperature and the values of ABT_i are atmospheric brightness temperatures obtained from the radiative transfer equation

$$I = B_s \tau_s + \int_{\tau_s}^{1} B d\tau \qquad (3)$$

where I is the observed radiance, B_s is the Planck surface radiance, τ_s is the surface transmittance, and B and $d\tau$ are the Planck radiance and change in transmittance for a given layer. The integral is the atmospheric term which, from the mean value theorem, may be written as

$$\bar{B}_a(1-\tau_s) = \int_{\tau_s}^{1} B d\tau \qquad (4)$$

where $\bar{B}_a$ is the average atmospheric radiance used to obtain values of ABT_i. Values of τ_s are obtained by a separate regression and constrained to be between the maximum and minimum values for the particular channel. It should be noted that the new method is an adaptation of one described by Hayden et al. (1981).

A comparison study of several water vapor methods was recently conducted at NESDIS. Besides these methods, one other alternative is of interest. It is given by

$$q = k_o + \sum_{j=1}^{nl} k_j T_j \qquad (5)$$

where k's are coefficients, T_j are retrieved atmospheric temperatures, and the subscript j denotes level. This method contains no direct information about water vapor but represents a minimum that should be achievable. It gives surprisingly accurate results when compared to the other methods.

2. RESULTS

In the process of evaluating an operational change, several successive tests are typically made, each of which is increasingly more expensive and closer to the operation. In this case, three successive comparisons are shown in Tables 1, 2 and 3. Tables 1 and 2 are based on a simulation.

The data used in this test consisted of 1000 sets of TOVS radiances matched with corresponding radiosondes. In the matches, the distance varies slightly with latitude even within a 30 degree latitude zone so the exact upper limit is difficult to define. However, all matches had locations that agreed to within $\pm$ 1 degree of latitude or better. In addition, two radiosondes 12 hours apart were interpolated to the radiosonde time. These data were collected during the period of 11/23-12/30, 1983, and were between 20 to 50 N latitude. Every third sounding was selected as an independent observation and grouped together to form the independent data set which was used to determine the statistics given in this paper. The other two thirds were grouped to form a dependent data set which was used to determine the coefficients.

It should be noted that this division of dependent and independent data differs from the operation which produces new coefficients every week from data collected over the previous two to four weeks. Because

of this difference, method 2, which is the operational method, does not produce results which exactly duplicate the actual operation. However, for this comparison it was important for all methods to be identical except for the changes being evaluated. The relative performances of the various methods should be independent of the selection procedure for the dependent sample, provided that all methods are treated equally.

Results of the comparison are shown in Table 1. The units used in the table require some explanation. The computer runs provided results in terms of mixing ratios for individual levels. Because of the number of levels and a tendency for the relative accuracies to oscillate with height, it was difficult to get a clear picture from these numbers. Since water vapor is output in terms of precipitable water in three layers, it was decided that an evaluation based on the three layers would be less confusing than one based on the 15 levels. To accurately determine the errors for the layers, it would have been necessary to rerun all the results. Actually, the final case and a couple of comparisons were rerun. However, the results shown in Table 1 were obtained from the level values. They were obtained by summing the rms errors of the individual levels, then dividing the total by the average precipitable water for the layer as given by the radiosonde to obtain a percent. Although this method provides a slight overestimate of the retrieval error, the relative performances of the various methods are still valid. The magnitude of the approximation can be determined from a comparison of Tables 1 and 2.

Although the other methods are generally better, method 1, which uses only the correlation between temperature and water vapor, produces a surprisingly good retrieval, especially when compared to the other methods. Three factors limit the improvements of the other methods over method 1. One is that since radiosondes are subject to measurement errors, they are not a true measurement of water vapor. Because of this, even a perfect satellite instrument would produce differences from radiosondes that are significantly greater than zero. A second is that the atmospheric temperature is highly correlated with water vapor and thus is a good predictor. Finally, when inversions are present, there are layers for which the incoming radiation is matched by the emitted radiation, making the outgoing radiation insensitive to water vapor.

Comparison of the three methods shown in Table 1 shows that the current operation is better than the results from temperatures only and the proposed method is better still. In the important 1000-850 mb layer, the errors, expressed as percentages of the average, are 54.6%, 44.6%, and 41.0%, respectively. Table 2 gives a more accurate calculation of the errors for the operational and proposed methods. Again there is significant improvement, especially in the 1000-850 mb layer, which contains most of the water vapor.

Table 3 contains the results of a limited operational test. Results are shown as percentages at the TOVS levels between 300 and 1000 mb. A plus denotes improvement and a simple average is given at the bottom. It is clear from the table that while there are selected

zones and levels for which current operational results are better, the dominant pattern favors the new method.

Recently, Smith & Woolf (1984) proposed a simultaneous solution for water vapor which retrieves water vapor and temperature together. NESDIS at Suitland has plans to evaluate the new method. It is likely that some form of a simultaneous solution will be adopted, but until results are obtained, conjecture is premature.

3. RESULTS OF THE CURRENT MODEL

Figures 1-6 show the results of the current operational retrieval model for the two European cases. Lines of longitude are 3E, 13E, etc., and the latitudes are 30, 40, 50 and 60N. The values shown are precipitable water over the layer bounded on the high side by the given pressure. Values shown on the figures are plotted by the computer and analyzed by hand. Comparisons at the conference will establish the validity of the patterns shown. Currently, water vapor is being output, but it is unclear if anyone is using it as extensively as the temperature soundings. However, it is clear from Figs. 3 and 6 that the formats for at least the 300-500 mb layer need to be modified to allow more resolution.

4. SUMMARY

In summary, it should be noted that the results for water vapor are from a model that has remained essentially unchanged from the initial implementation. Recently, a rather extensive evaluation of alternative methods was made. As a result of that evaluation, a new water vapor retrieval system has been developed and will soon be implemented.

5. REFERENCES

Hayden, C.M., W.L. Smith and H.M. Woolf, 1981: Determination of Moisture from NOAA Polar Orbiting Satellite Sounder Radiances. J. Appl. Meteor., 20, 450-466.

Smith, W.L., and H.M. Woolf, 1984: Improved Vertical Soundings from an Amalgamation of Polar and Geostationary Radiance Observations. Conf. on Satellite/Remote Sensing and Applications, American Meteorological Society, 45-48.

Table 1. Accuracies of Water Vapor Retrieval Methods

Method	1000-850 (% of avg)	850-500 (% of avg)	500-300 (% of avg)	total (% of avg)
1	54.6	49.8	34.6	40.3
2	44.6	43.6	35.1	38.2
3	41.6	40.7	29.7	34.4

Table 2. RMS errors for true layer averages

Layer (mb.)	Method 2 (% of avg)	Method 3 (% of avg)
1000-850	37.6	32.3
850-500	34.0	30.5
500-300	29.6	27.4

Table 3. Improvements of method 3 over the current operation in units of percent of operational error for the week of July 1, 1984

level	pressure (mb.)	60-90N (%)	30-60N (%)	30S-30N (%)	60-30S (%)	90-60S (%)
26	300	9.3	1.5	14.6	26.7	12.5
27	350	16.7	10.1	23.0	24.0	-7.7
28	400	17.3	12.6	14.2	21.1	9.5
29	430	15.8	13.6	14.8	18.3	22.2
30	475	14.2	7.9	14.1	9.0	35.0
31	500	11.9	5.2	12.3	4.9	39.6
32	570	-2.0	7.2	1.9	2.1	29.0
31	620	-1.8	8.5	-1.0	1.1	14.3
34	670	-3.6	5.8	-4.8	2.7	21.2
35	700	-3.7	2.3	-6.2	3.9	20.4
36	780	1.7	-0.3	-11.0	3.7	18.7
37	850	2.6	1.1	-9.2	2.5	22.7
38	920	-0.2	23.7	25.0	8.4	23.8
39	950	6.4	41.1	27.4	6.9	14.8
40	1000	44.4	54.4	33.5	28.4	16.7
AVG.		8.8	21.6	11.9	10.1	20.1

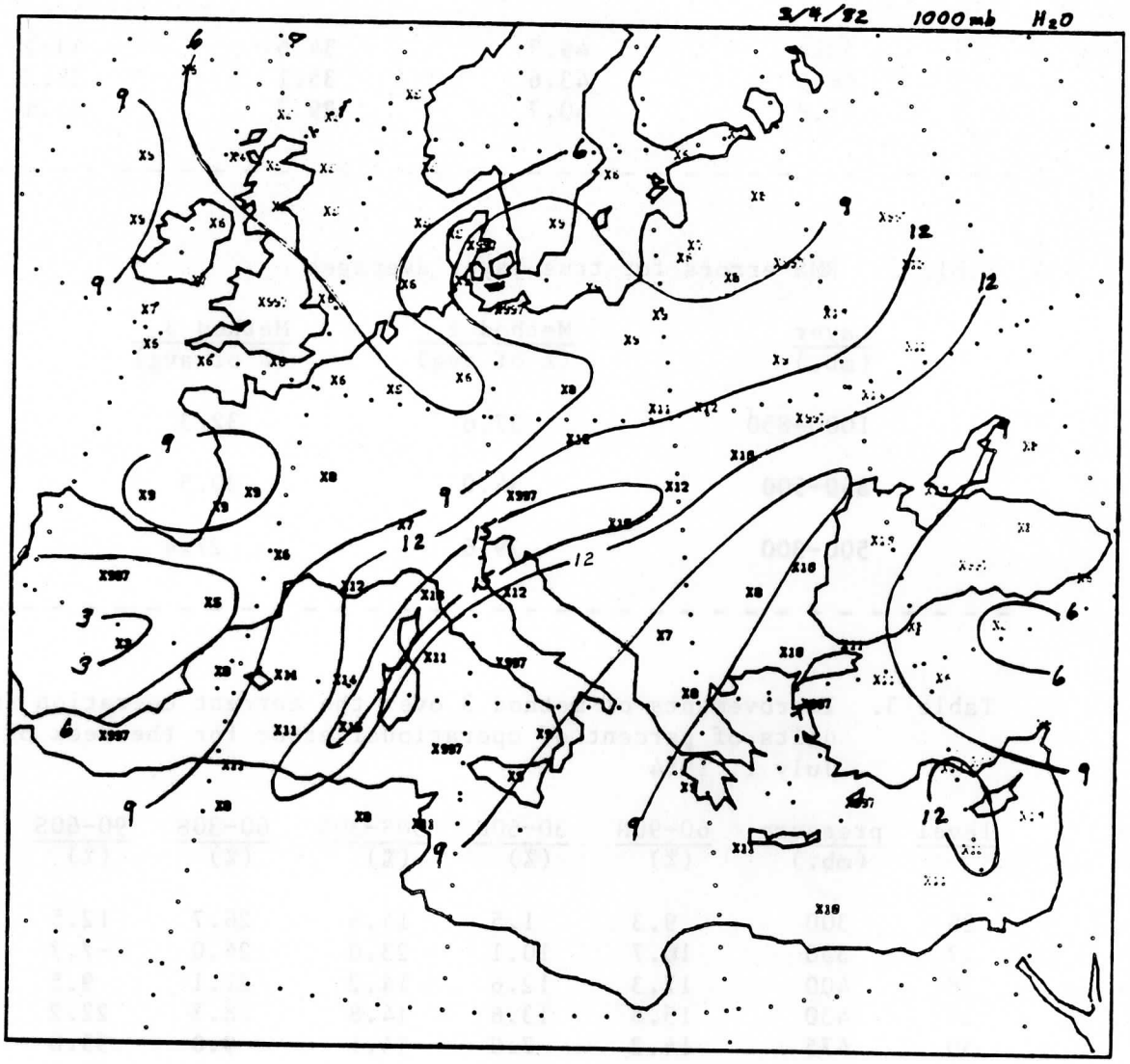

Figure 1. Precipitable water vapor for the 1000-700 mb layer for March 4, 1982.

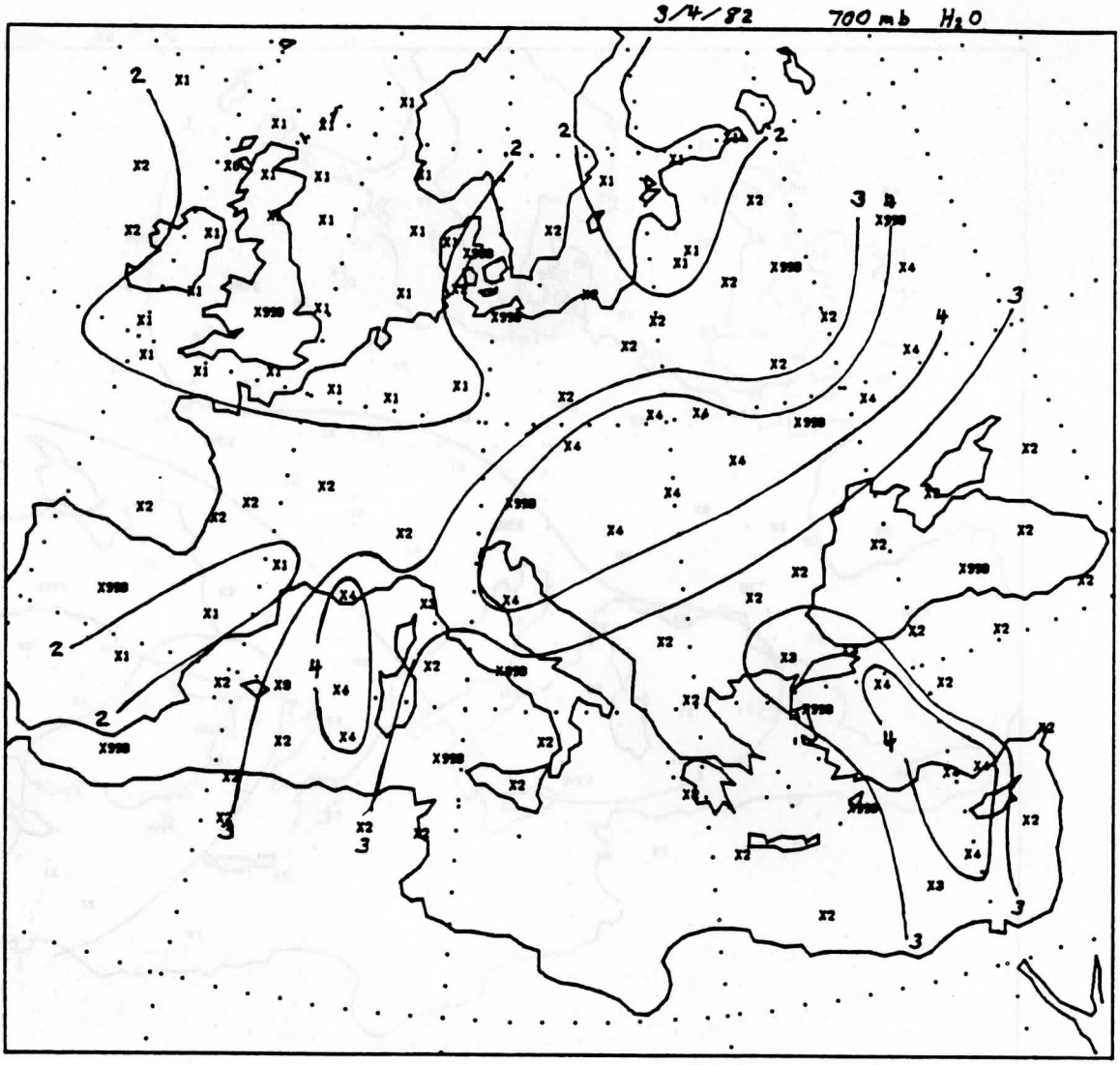

Figure 2. Precipitable water vapor for the 700-500 mb layer for March 4, 1982.

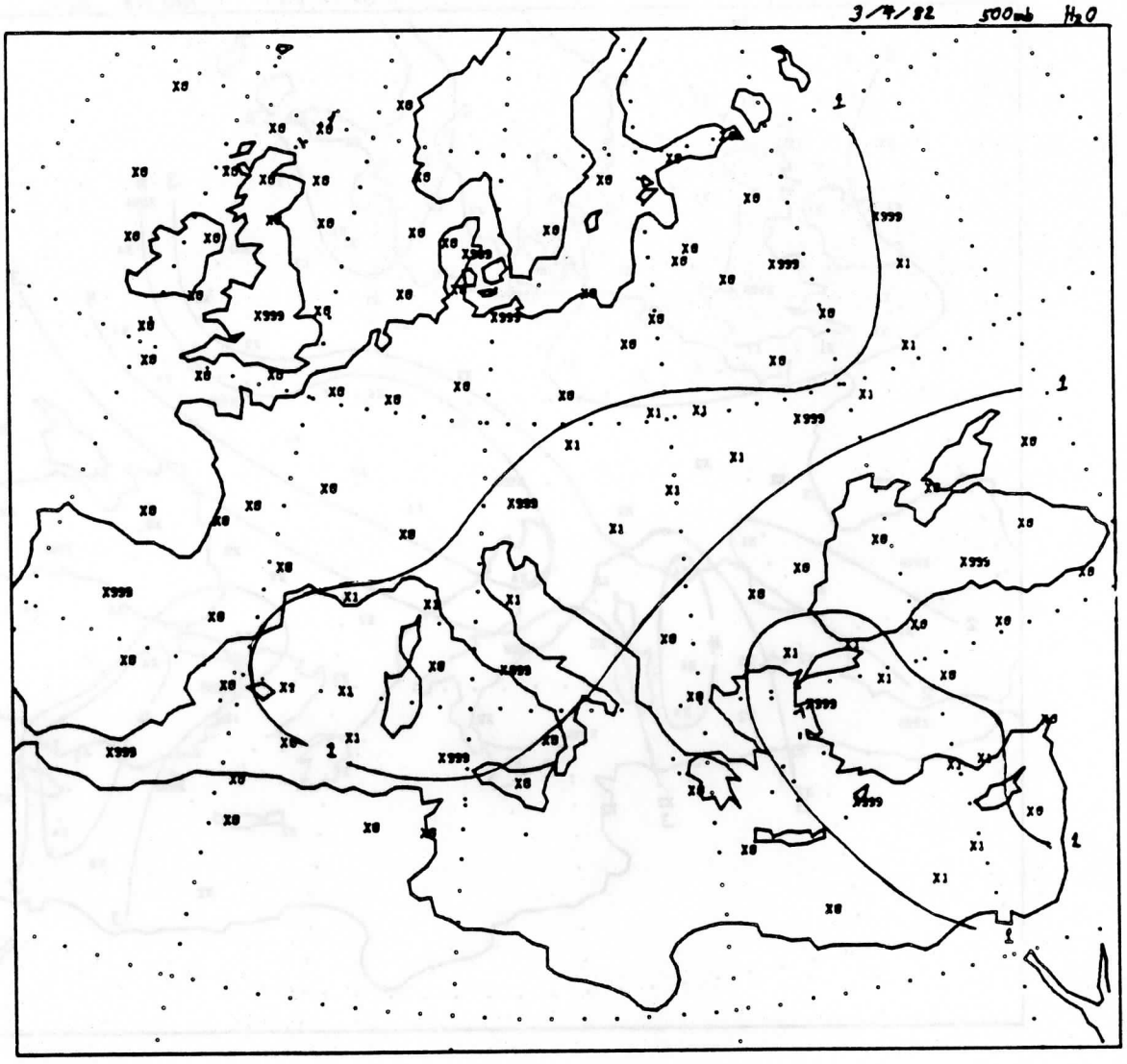

Figure 3. Precipitable water vapor for the 500-300 mb layer for March 4, 1982.

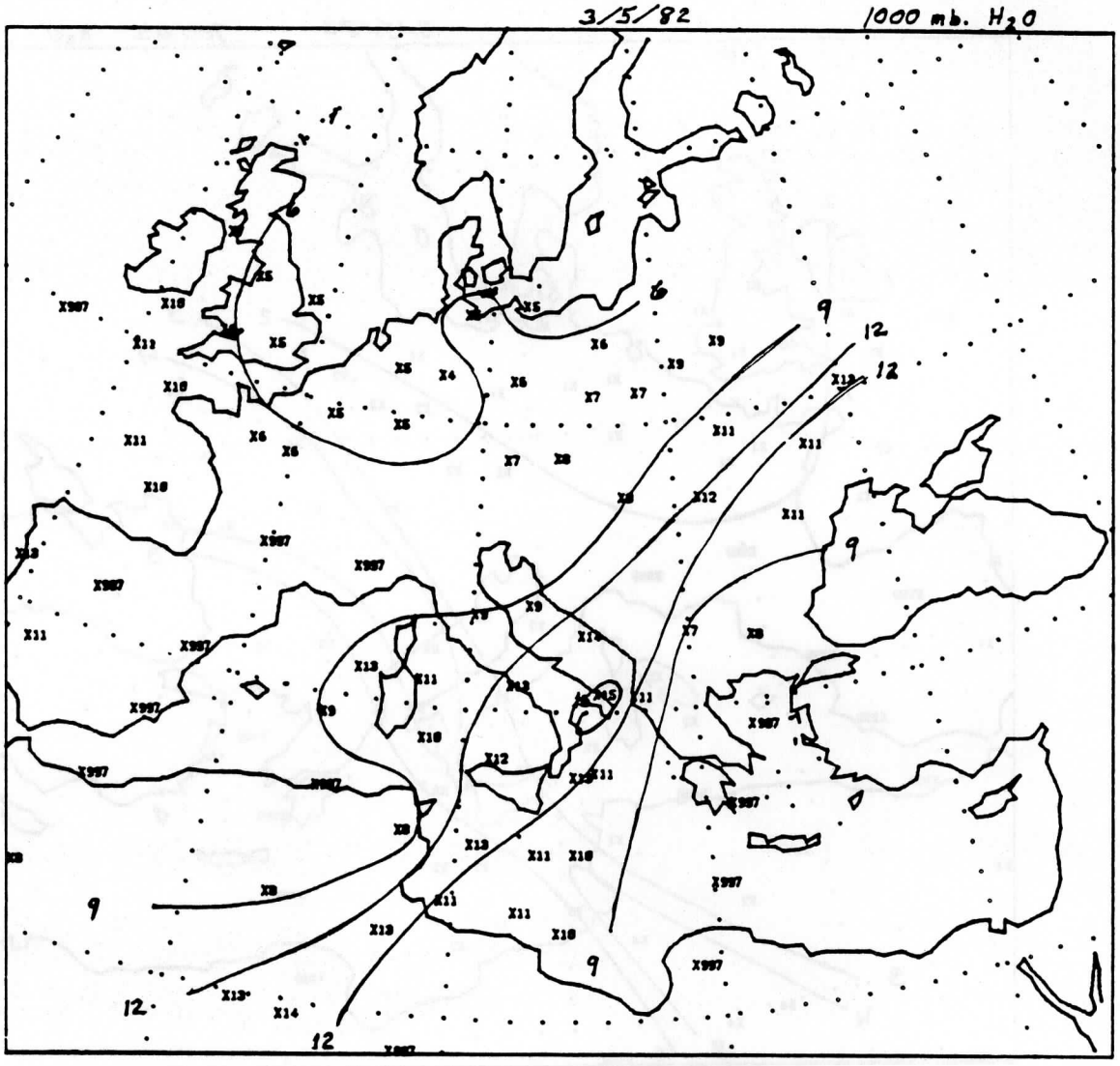

Figure 4. Precipitable water vapor for the 1000-700 mb layer for March 5, 1982.

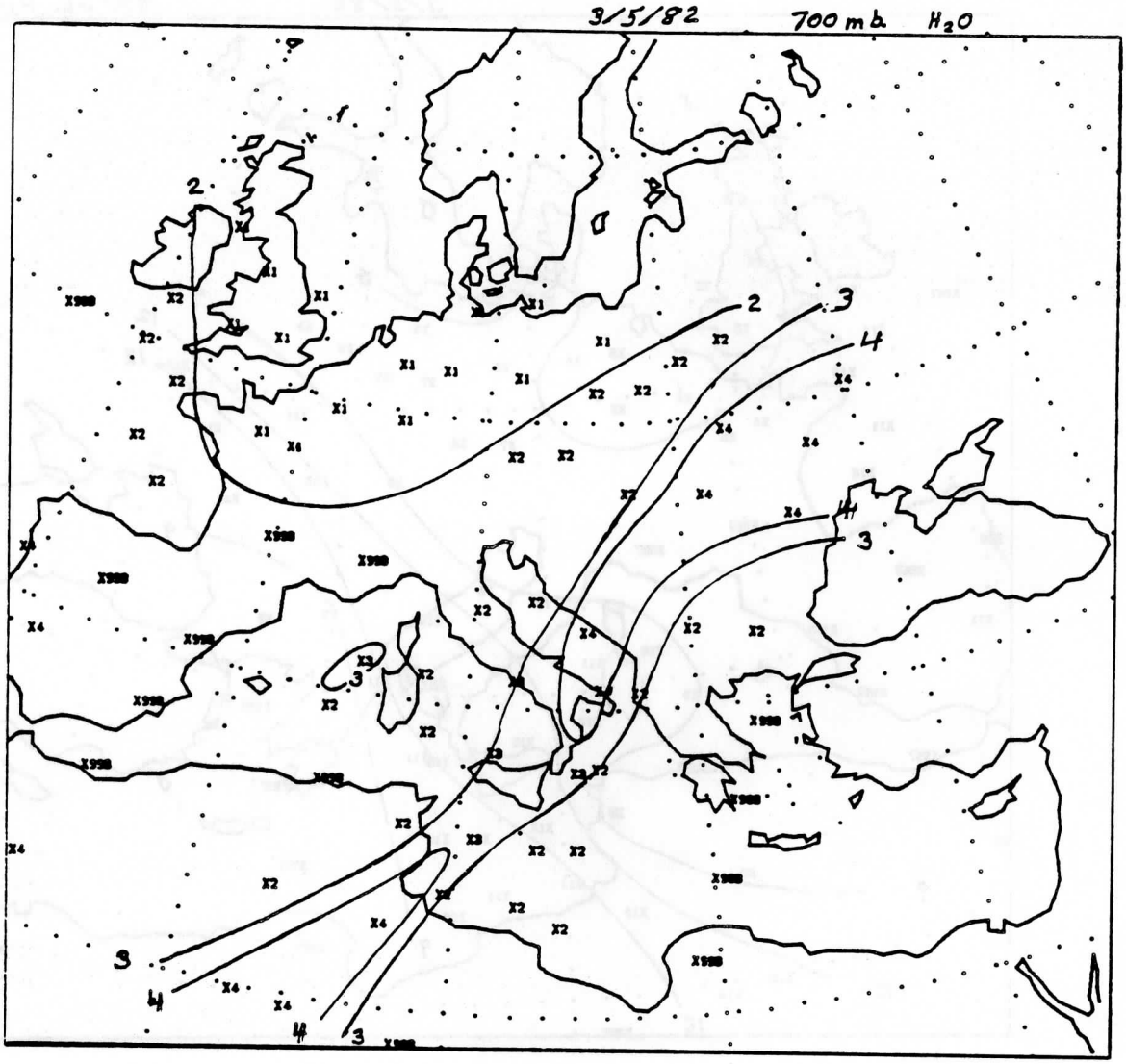

Figure 5. Precipitable water vapor for the 700-500 mb layer for March 5, 1982.

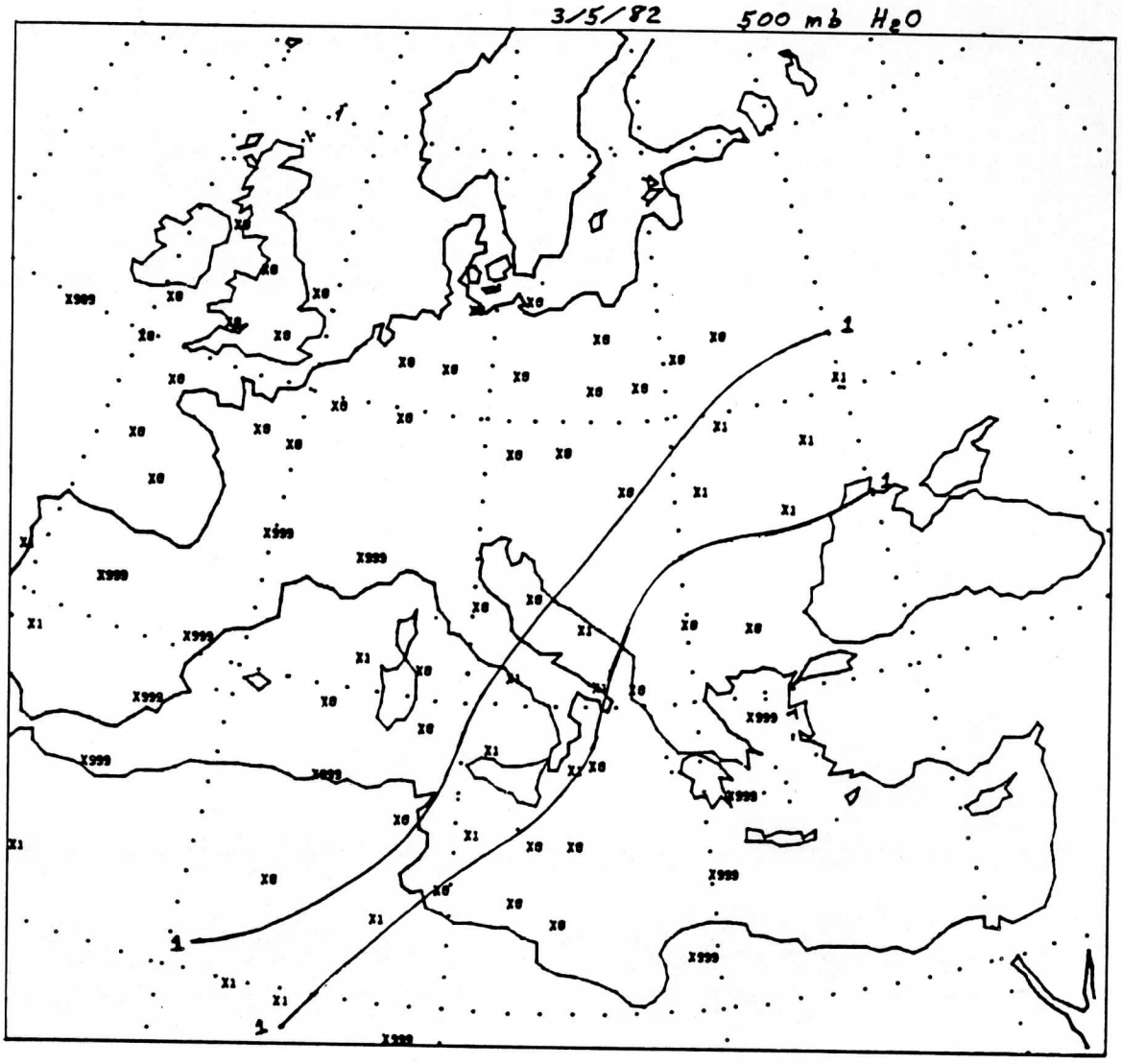

Figure 6. Precipitable water vapor for the 500-300 mb layer for March 5, 1982.

A LOW COST METEOROLOGICAL WORKSTATION

W. Paul Menzel[1], H. Ben Howell[1], Harold Woolf[1], Ralph Dedecker[2] and William L. Smith[2]

[1]NOAA/NESDIS Satellite Applications Laboratory
Advanced Satellite Products Project
Madison, Wisconsin 53706

[2]Cooperative Institute for Meteorological Satellite Studies
University of Wisconsin
Madison, Wisconsin 53706

1. INTRODUCTION

Over the past two years, considerable progress has been made in packaging a low cost interactive workstation with image and graphic displays for meteorological research and forecast applications (see references). Standard off the shelf hardware from the IBM personal computer family was used to minimize costs and to facilitate easy international implementation (a parts list can be found in Dedecker, et al.). CIMSS (Cooperative Institute for Meteorological Satellite Studies) is developing software to provide the following capabilities:

(a) accessing the satellite data;
(b) display of satellite images and loops of images;
(c) derivation and display of meteorological products;
(d) amalgamation with conventional weather data.

2. CAPABILITIES FOR POLAR ORBITING SOUNDERS

For the NOAA polar orbiting satellite sounding data, the workstation will be capable of interfacing with a direct readout receiving antenna and processing the TIP (TIROS Information Processor) or HRPT (High Resolution Picture Transmission) bit streams into displays of meteorological parameters such as vertical temperature and moisture profiles, surface temperature, geopotential heights, and total ozone. This software, known as the Export Package, has been installed on the IBM-PC-XT by Woolf et al.; the processing of a typical eight to ten minute orbital pass, from TIP formatting through statistical profile retrieval, takes approximately one hour. More efficient operation will be possible on the IBM-PC-AT; a factor of two improvement was realized and more optimization is planned.

3. CAPABILITIES FOR GEOSTATIONARY SOUNDERS

For the geostationary satellite sounding data, the workstation is capable of remote access to a satellite data base via automatic communications and subsequent display of derived information. A menu driven software system was developed by Dedecker, et al. on the IBM-PC-XT to enable general data base communications, retrieval analysis, and satellite image acquisition and analysis. Portions of this software are on display during TOVS-II.

4. CONCLUSION

While more work remains, it is clear that an inexpensive display of meteorological data is evolving. This will make the TOVS data processing capability affordable to many more users (a workstation for roughly $7000 US, the tracking antenna for roughly $15,000 US). This technology development needs the support and guidance of the international TOVS user community so that an organized transfer to new users in developing countries can be brought about.

5. REFERENCES

Dedecker, R. G., R. N. Green, H. B. Howell, January, 1985: VAS (VISSR Atmospheric Sounder) data acquisition and processing system for a personal computer. AMS Conference on Interactive Information and Processing Systems for Meteorology, Oceanography, and Hydrology held in Los Angeles, California.

Menzel, W. P., September, 1983: A study of several different numerical iteration solutions of the radiative transfer equation. Technical Proceedings of the First International TOVS Study Conference.

Woolf, H. M., H. B. Howell, W. L. Smith, W. P. Menzel, June, 1984: A low cost interactive system for processing and displaying direct-readout satellite soundings. Presentation at XXV COSPAR Meeting in Graz, Austria.

CLEAR COLUMN RADIANCES BY OPTIMAL ESTIMATION

A.J. Prata

Western Australian Institute of Technology
Perth, WA, Australia

1. INTRODUCTION

A method for estimating the clear column radiance for the measurements of the HIRS instrument is described. The basic method assumes the form of an optimal estimation problem, in which HIRS radiances and a priori values of the clear column radiance are used sequentially to derive the clear column radiance. The method is optimal in the sense that radiances from all of the fields of view (FOV) of a single HIRS channel are used to estimate the clear radiance in each FOV and the mean square estimation error is minimised. Some of the difficulties and advantages of the method are described and results using HIRS channel 6 are shown.

2. OPTIMAL ESTIMATION

Optimal estimation or optimal filtering in this context, has been used in previous studies involving satellite radiances (e.g. Rodgers, 1977, Ledsham and Staelin, 1978). For linear systems a commonly used estimator is the Kalman filter (Kalman, 1960, Schweppe, 1970, Gelb, 1974). The algorithm is characterised by the observed system and its error structure, the measurement and its error structure and the filter plus any a priori information necessary. To apply the algorithm in the case of estimating clear radiances we begin by describing the measurement model.

Consider the HIRS scan pattern for a single HIRS channel as a two dimensional array of measurements. For simplicity the co-ordinate system is chosen with axes of time and scan angle. A transformation exists to convert these co-ordinates to earth latitude and longitude or to a scan spot-line system. Figure 1 illustrates a typical pattern.

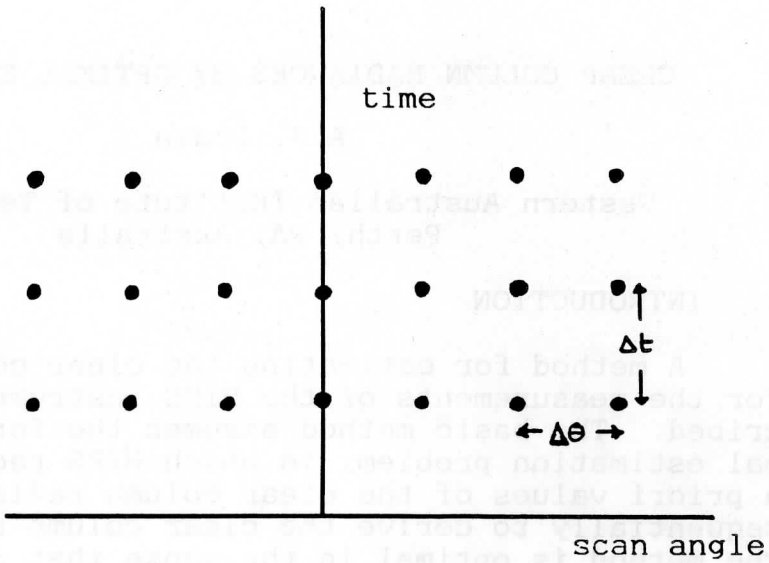

Figure 1. HIRS scan pattern

The radiance at any spot is written

$$R(t,\theta) = \bar{R}(t) + \sum_{i=1}^{N} a_i(t)\sin(i\theta) + b_i(t)\cos(i\theta) \pm e \qquad (1)$$

where $R(t,\theta)$ is the radiance
t is time
θ is scan angle
a, b are coefficients to be estimated, and
e is a random measurement error.

In matrix notation (1) may be written

$$R = \underline{K}^T \underline{x} \pm e \qquad (2)$$

with $\underline{K}^T = [1, \cos\theta, \sin\theta, \cos 2\theta, \sin 2\theta, \ldots, \cos N\theta, \sin N\theta]$

$$\underline{x} = \begin{bmatrix} \bar{R} \\ b_1 \\ a_1 \\ . \\ b_N \\ a_N \end{bmatrix}$$

Equation (2) constitutes the measurement model. We now define the system model to be the Markov process given by (3).

$$\underline{x}^{\circ}_{t} = \underset{\sim}{A}_{t-1}\,\hat{\underline{x}}_{t-1} + \underline{w}_{t-1} \qquad (3)$$

where $\hat{\underline{x}}_{t-1}$ is the best estimate available at t-1
$\underset{\sim}{A}$ is the state transition matrix, and
$\underline{w}_{t-1}$ is a Gaussian process with zero mean.

The covariance of the system model is propagated forward in time by

$$\underset{\sim}{S}^{\circ}_{t} = \underset{\sim}{A}_{t-1}\,\hat{\underset{\sim}{S}}_{t-1}\,\underset{\sim}{A}_{t-1} + \underset{\sim}{Q}_{t-1} \qquad (4)$$

where $\underset{\sim}{S}$ is the covariance matrix and $\underset{\sim}{Q}$ is a diagonal matrix of variances representing system noise.

The maximum liklihood estimate of the measurement R_t and the a priori value $(\underline{K}^{T}\underline{x}^{\circ})_t$ at time t leads to the Kalman filtering equations

$$\hat{\underline{x}}_{t} = \underline{x}^{\circ}_{t} + \underset{\sim}{S}^{\circ}_{t}\,\underset{\sim}{A}_{t}\,(\underset{\sim}{A}^{T}_{t}\underset{\sim}{S}^{\circ}_{t}\,\underset{\sim}{A}_{t} + \sigma_R^2)\,(R - \underset{\sim}{A}^{T}_{t}\underline{x}^{\circ}_{t}) \qquad (5)$$

$$\hat{\underset{\sim}{S}}_{t} = \underset{\sim}{S}^{\circ}_{t} - \underset{\sim}{S}^{\circ}_{t}\,\underset{\sim}{A}_{t}\,(\underset{\sim}{A}^{T}_{t}\underset{\sim}{S}^{\circ}_{t}\,\underset{\sim}{A}_{t} + \sigma_R^2)\,\underset{\sim}{A}^{T}_{t}\underset{\sim}{S}^{\circ}_{t} \qquad (6)$$

where σ_R^2 is the variance of the measurement assumed to be independent of time. The derivation of these equations may be found in any of the texts cited earlier. The sequential nature of the algorithm is evident from the form of (5) and (6).

3. IMPLEMENTATION

For simplicity we choose a state transition matrix ßI where I is the identity matrix and ß is a constant of the form $\exp(-\Delta t/2\tau)$. Here Δt is the time interval between scan lines and τ is a time constant which is adjustable. The value of τ determines the degree of correlation between successive values of the parameter to be estimated.

At the start of the processing, a covariance matrix has to be specified. This is usually difficult to determine accurately, however provided that there are enough good measurements, the precise choice of $\underset{\sim}{S}_{t=0}$ is not too critical. The measurement error and a truncation point N must also be specified.

As an added refinement, we can include estimation of the cross-track and along-track gradients of the radiance field into the problem. This is easily done by differentiating (1) with respect to scan-angle (cross-track gradient) and with respect to time (along-track gradient). We assume that the measurements made across the track are simultaneous. In fact as long as the radiance across the track does not vary significantly with time the approximation is good. The time to complete one scan for the HIRS instrument is 6.4 seconds.

4. RESULTS

The Kalman filter has been used to estimate the radiance field in HIRS channel 6 (13.7μm) on the NOAA-7 satellite. This channel has a weighting function peak at 800mb and the radiance is generally expected to be cloud contaminated whenever cloud is present in the FOV. The radiances were limb corrected using the standard TOVS procedures, although this is not a requirement for the operation of the filter. A mean

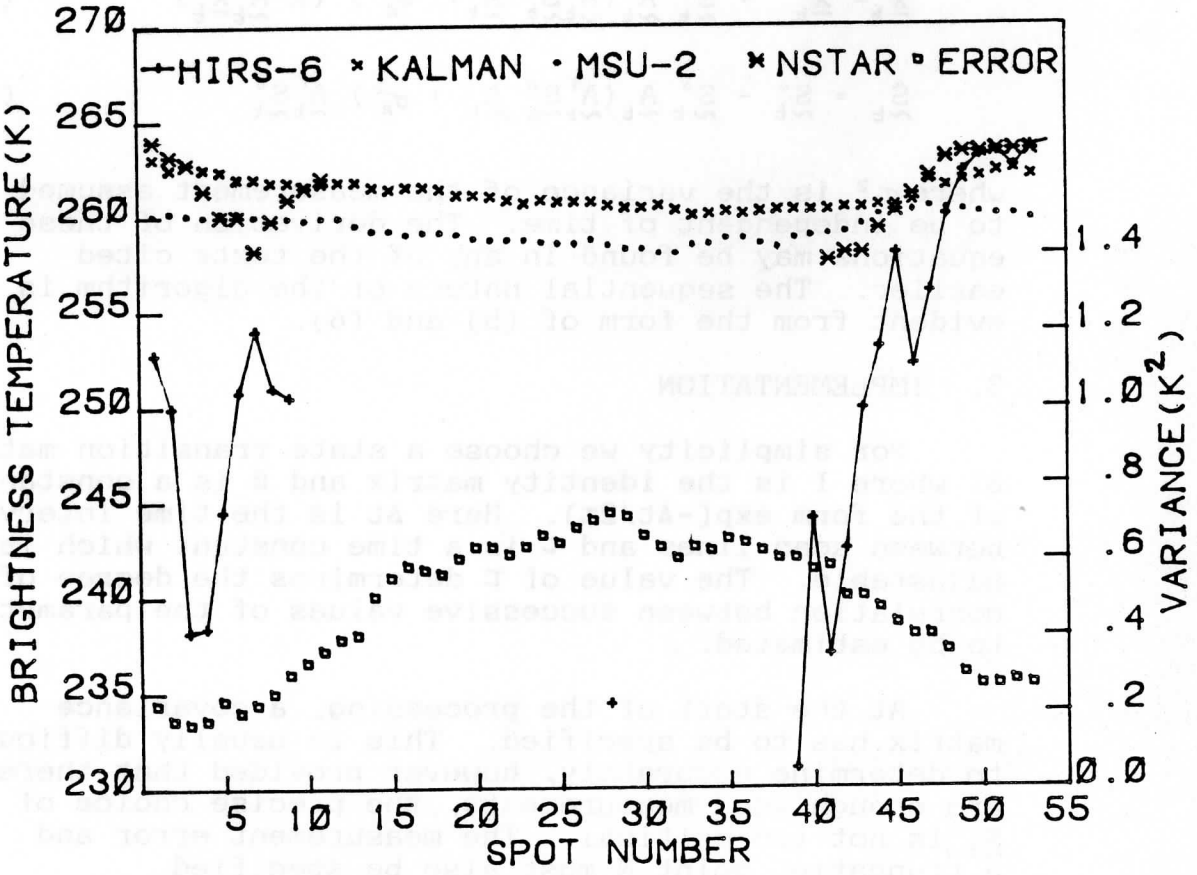

Figure 2. Brightness temperature versus spot number for part of a single HIRS scan line (NOAA-7 13 February 1984, 0730Z).

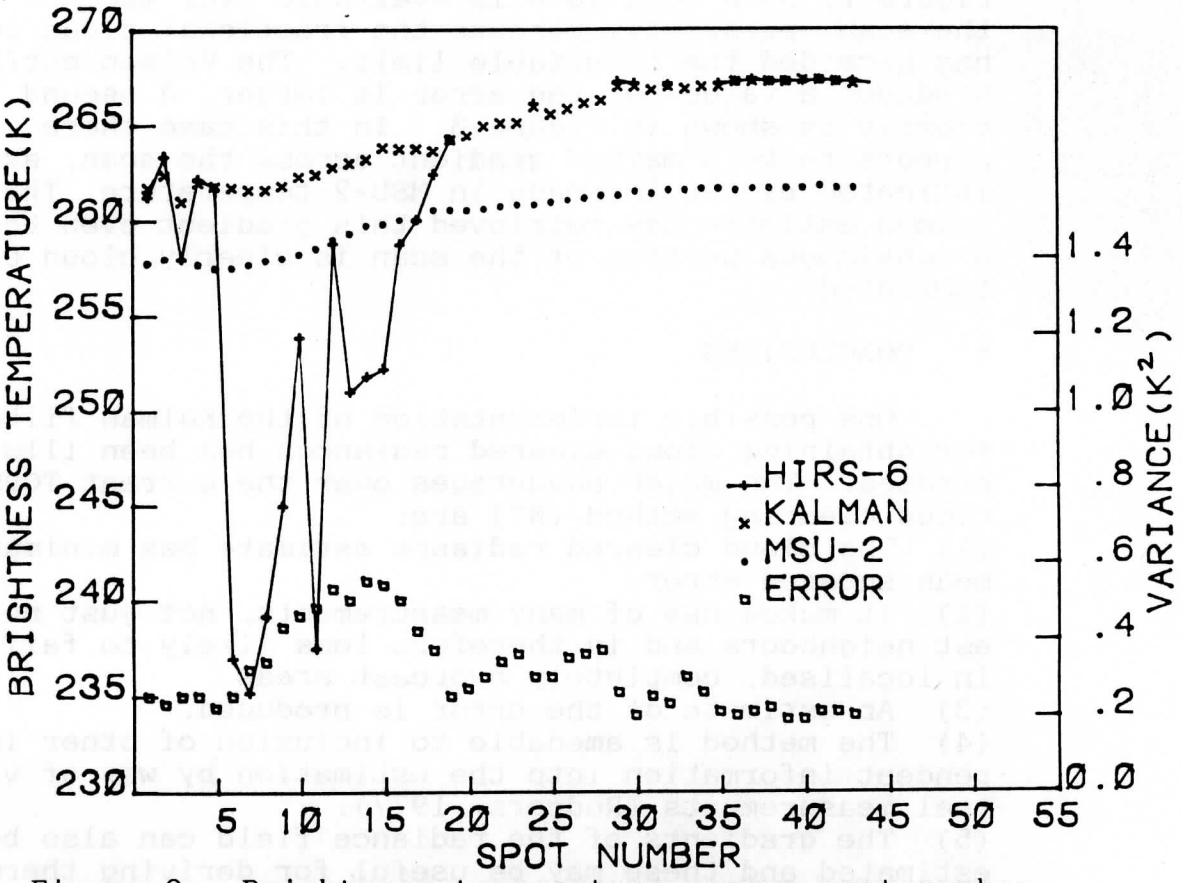

Figure 3. Brightness temperature versus spot number for part of a single HIRS scan line (NOAA-7 29 February 1984, 0744Z).

value for the radiance (R) was assumed as 85 $mWm^{-2}str^{-1}(cm^{-1})^{-1}$ and a measurement error, estimated from calibration data to be 0.1 $mWm^{-2}str^{-1}(cm^{-1})^{-1}$. The truncation was set at N=12 and ß=0.994. The initial covariance matrix $\underset{\sim}{S}^{\circ}_{t=0}$ was diagonal with elements equal to 50 $(mWm^{-2}str^{-1}(cm^{-1})^{-1})^2$. The filter is run forwards and backwards over the radiance field, and the two estimates combined by weighting with the inverse of their respective variances, to produce the final estimate and its error.

The results for one line of a single pass of local area data are shown in Figure 2. The N* estimate (Smith, 1968) and the MSU-2 temperature are also shown. All values have been converted to brightness temperature using the inverse Planck function, for the purpose of the comparison. MSU-2 peaks at around 700mb and essentially senses radiation from the same layer of atmosphere as HIRS-6, however MSU-2 is much less affected by cloud. In the extreme case shown in

Figure 2, no N* estimate is available over much of the scan, presumably because the fractional cloud cover has exceeded the acceptable limit. The Kalman estimate produces a value but the error is larger. A second example is shown in Figure 3. In this case there appears to be a marked gradient across the scan, as indicated by the increase in MSU-2 temperature. The Kalman estimate has retrieved this gradient even though a continuous portion of the scan is clearly cloud contaminated.

5. CONCLUSIONS

One possible implementation of the Kalman filter for obtaining cloud cleared radiances has been illustrated. The major advantages over the current TOVS cloud clearing method (N*) are:

(1) The cloud cleared radiance estimate has minimum mean squared error.

(2) It makes use of many measurements, not just nearest neighbours and is therefore less likely to fail in localised, completely overcast areas.

(3) An estimate of the error is produced.

(4) The method is amenable to inclusion of other independent information into the estimation by way of virtual measurements (Rodgers, 1977).

(5) The gradients of the radiance field can also be estimated and these may be useful for deriving thermal winds at a later stage.

(6) The filter also smooths the data. The amount of smoothing can be controlled by adjusting ß. In addition the filter does not discriminate between radiances that are too warm (e.g. spikes) and those that are too cold (cloudy). The N* method will produce erroneous results in the presence of a warm spike in the data.

(7) Calibration lines for which there is no earth view data are included as bad data in the processing and estimates for these lines are obtained.

Some of the disadvantages of the method are:

(1) The filter passes over the data for each channel twice and will consume computer time. For TOVS implementations operating on mini-computers with no vectorisation this may be a serious problem. Storage requirements for the matrices may also be an added restriction. Note however there are no matrix inversions to perform.

(2) Specification of some of the parameters is a little ad hoc. Further experimentation is necessary in order to obtain better understanding of the effects of varying some of these parameters (e.g. ß, N, $\underset{\sim}{S}$, $\underset{\sim}{A}$).

(3) In extremely cloudy cases, in which perhaps more than 30% of the data is cloud contaminated, the filter is likely to be unreliable. An implicit assumption of the method is that the corruption of the measurements is of a random nature and is a small perturbation to the measurement signal. If the noise swamps the signal the assumption is violated.

There are a number of refinements which could be made to the filter. For example, the covariance matrices could be stored and used as initial guesses for a subsequent pass. A multi-channel filter could be developed, in which several channels are used simultaneously at each time step. Finally, incorporation of other data, such as AVHRR or numerical forecasts would improve the estimator.

6. REFERENCES

Gelb, A., Ed., 1974: Applied Optimal Estimation. The MIT Press, 347 pp.

Kalman, R.E., 1960: A new approach to linear filtering and prediction problems. Trans. ASME, 880, 35-70.

Ledsham, W.H. and D.H. Staelin, 1978: An extended Kalman-Bucy filter for atmospheric temperature profile retrieval with a passive microwave sounder. J. Appl. Meteor., 17, 1023-1033.

Rodgers, C.D., 1977: Statistical principles of inversion theory. Inversion Methods in Atmospheric Remote Sounding. Ed. A. Deepak, Academic Press, 622 pp.

Schweppe, F.C., 1973: Uncertain Dynamic Systems, Prentice Hall, 363 pp.

Smith, W.L., 1968: An improved method for calculating tropospheric temperature and moisture from satellite radiometer measurements. Mon. Wea. Rev., 387-396.

RETRIEVAL OF ATMOSPHERIC TEMPERATURE IN HUNGARY

M. Putsay

Central Institute for Weather Forecasting,
Remote Sensing Department,
H-1675 Budapest, P.O.B.32

1. INTRODUCTION

At the beginning of 1986 Hungary will have a direct read-out station which will be able to receive the high resolution digital data and TOVS data too.

This gives us the possibility to retrieve regularly the temperature and water vapour profiles from the measured spectral radiances. From the temperature and moisture data several other parameter fields can be determined which are also necessary for the weather forecasting, e.g. level thicknesses, geostrophical winds, stability parameters etc. All the parameters retrieved from satellite measurements are available in much higher resolution than the conventional measurements.

In Hungary in the Institute for Atmospheric Physics G.Major, F. Miskolczi and Gy. Molnár dealt with this subject during some years. They investigated several methods for retrieval of the temperature profile and for accurate calculation of the transmission function. They had difficulties to get satellite data to test their methods with. Unfortunately their research was interrupted because they left for working abroad. Our department has decided to continue their work considering that we will continuously receive the TOVS data by the direct read-out station.

In the following sections Major's, Miskolczi's and Molnár's calculations and results are presented.

2. THE RADIATION TRANSFER

The purpose was to find a simple /from the point of view of computer techniques/ method for determining the atmospheric temperature profile from infrared spectral radiance data obtained by meteorological satellites in the 15 μm absorption band of CO_2.

The intensity of thermal radiance measured by a satellite radiometer in its k^{th} channel at the top of a clear atmosphere can be written:

$$I_{\nu_k} = B(\nu_k, T_0)\,\tau(\nu_k, p_0) - \int_0^{p_0} B(\nu_k, T(p))\,\frac{\partial \tau(\nu_k, p)}{\partial p}\,dp \qquad (1)$$

where

$B(\nu_k, T)$ is the Plank-function at central wavenumber ν_k of the satellite infrared filters and at temperature T.

$\tau(\nu_k, p)$ is the transmission function at pressure level p, appropriate to the spectral response, of the k^{th} channel.

T_0, p_0 are the temperature and pressure at the surface.

Introducing a numerical integration, Eq. /1/ can be expressed as a matrix equation. There are two essential problems: how to determine the transmission function, and how to solve this matrix equation.

3. THE TRANSMISSION FUNCTION

The first step was to look for simple and fast methods in order to obtain correct enough transmission values. It was found that the approximate methods did not reach the necessary precision, so Miskolczi decided to compute the transmission function by the direct method, line by line. As the computer facilities were not good at that time and the calculations using the direct method required too much time, a so-called "semi-direct method" was developed which was found quite accurate (see for details Major et al. /1978/ and Miskolczi /1974/).

The values of the transmission function were calculated by this method for the U.S. Standard Atmosphere. For every other case when the temperature profile differs from that of the U.S. Standard Atmosphere, the transmission function will be different since absorption coefficients depend on the air temperature too. They determined some formulae for the temperature correction using the approximate methods for the calculations of the transmission functions (see for details Major et al. /1978/ and Molnár /1979/).

They had in this way an iterative procedure. The transmission function must be determined at first for a "first guess" temperature profile using that for the U.S. Standard Atmosphere and the temperature correction. Then a temperature profile will be computed from the radiances using this transmission function. Next another correction

will be made for the transmission function according to the just obtained temperature profile, and using it a new temperature profile will be determined from the Eq. /1/ etc.

4. THE STATISTICAL INVERSION METHOD

A few methods were tried to solve Eq. /1/: physical, statistical and combined methods. The statistical inversion method elaborated by Rodgers /1970/ and Westwater and Stand /1963/ was also chosen for determining the temperature profile from the radiances. This method requires the covariance matrices of the temperature profile. These statistical parameters have been determined for the four seasons from the data of the radiosonde ascents made at Budapest /Molnár et al, 1974/. The "First guess" for the temperature profile was the climatological average profile for the given season.

The final matrix equation of this method:

$$T(p)=\overline{T}(p)+\overline{\overline{S}}\overline{A}^{*}(A\overline{\overline{S}}\overline{A}^{*}+\overline{N})^{-1}(I-\overline{I}) \qquad (2)$$

$\overline{T}(p)$ being the climatological average profile,
$\overline{I}$ I the radiance vector measured by the satellite
the calculated radiance vector valid at the top of the climatological average atmosphere
$\overline{\overline{S}}$ the autocovariance matrix of the temperature profile
$\overline{N}$ the variance-covariance matrix of the errors
A matirx containing the weigting functions.

5. RESULTS

They received data from the satellite NIMBUS-5 measured by the SCR instrument for the Middle-Europe region. Numerous temperature profiles were determined for every season with the above described procedure. The atmosphere was divided into 18 layers. They found that one iteration step was enough. The results of one retrieval for each season can be seen in Fig. 1.

Comparing with the radiosonde observations /interpolated linearly in time/ the average RMS error was about 3K including the cloudy cases /Molnár, 1979/. The largest errors occurred in the tropopause. It was found that the autocovariance matrix of the radiosonde observations in Budapest could be used to about 700 km distance, since the average RMS errors of the retrievals only slightly increased with the distance, less then 1K to 700 km.

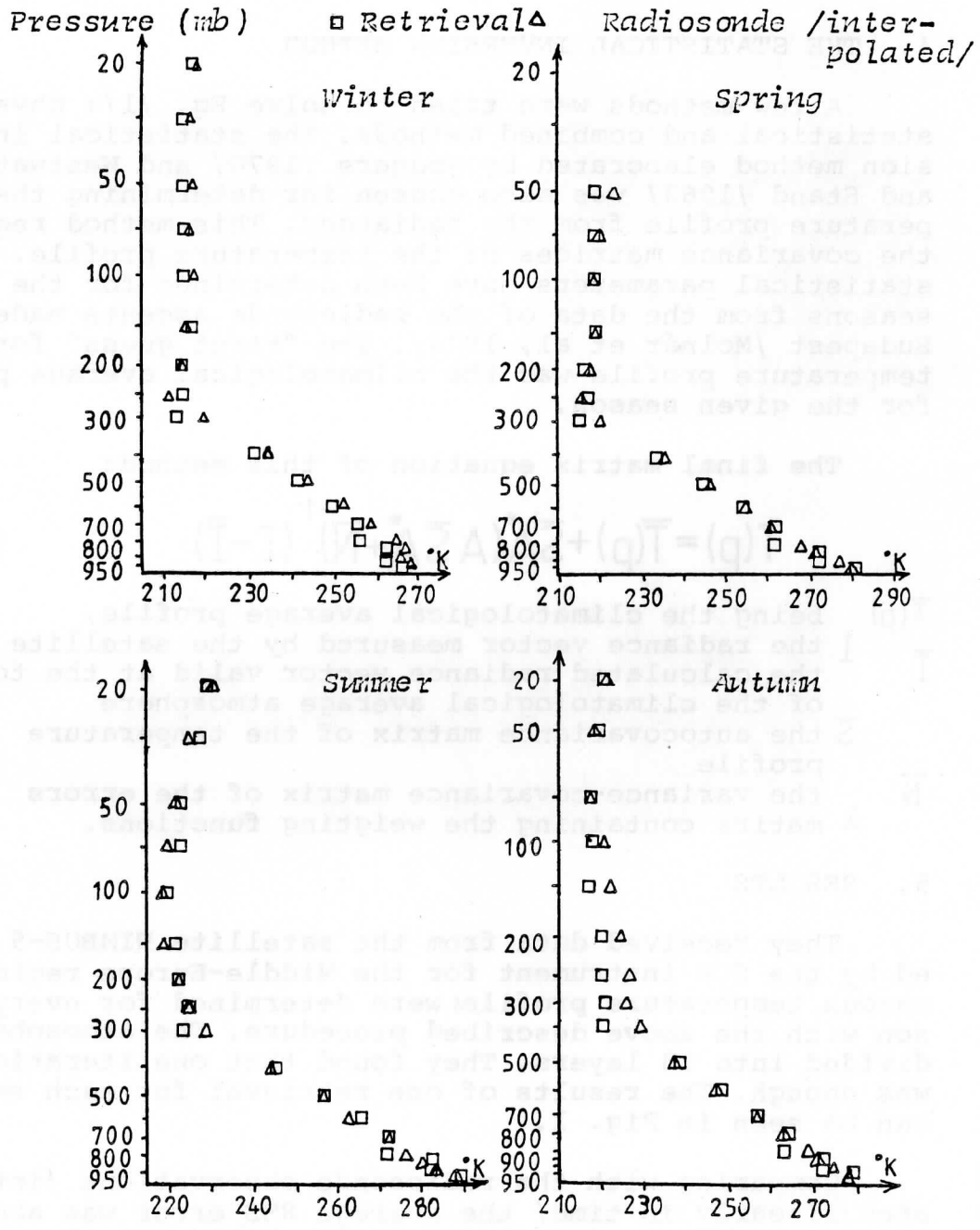

Fig. 1. Budapest radiosonde profiles and the retrieved ones using NIMBUS-5 SCR's data for different seasons

REFERENCES

Major, G., Miskolczi, F., Molnár, G., 1978: Studies carried out in Hungary on remote sounding of the atmospheric temperature. Proceedings of the Met.Ser. of Hungary, 44, Budapest

Miskolczi, F., 1974: Investigations concerning the atmospheric CO_2 transmittance, in the problem of satellite temperature sounding /in Hungarian/. D.Phil Thesis, Institute for Atmospheric Physics, Budapest

Molnár, G. and Varga, M., 1974: Autocorrelation matrices of the vertical temperature profiles measured at Budapest /in Hungarian/. Report on Scientific Researches carried out in 1974, Met. Ser. of Hungary

Molnár, G., 1979: Interpretation of NIMBUS-5 SCR data for obtaining vertical temperature profiles. Quart. J.R. Met. Soc., 105, 461-467

Rodgers, C.D., 1970: Remote Sounding of the atmospheric temperature profile in the presence of cloud. Quart. J. R. Met. Soc., 96, 654-666

Westwater, E.R. and Stand, N.O., 1968: Statistical information content of radiation measurements used in indirect sensing, J.Atmos.Sci., 25, 750.

COMPARISON BETWEEN SATELLITE DATA AND ALPEX DATA USING AN HIGH RESOLUTION OBJECTIVE ANALYSIS

Rolando Rizzi, Ennio Tosi
Dipartimento di Fisica, Bologna Italia

I. INTRODUCTION

In the latest years much work has been done in developing physical solutions of the radiative transfer equations in order to account explicitly for the influence of surface variables (such as skin temperature, terrain elevation and emissivity) in order to increase the skill of the techniques over the prior purely statistical regression methods. However the operationally available upper air conventional data can hardly be used to verify any proposed solution since these are too sparse for this purpose and the analyses produced from observations filter out mesoscale informations eventually present in individual upper air observations. Moreover at least four satellite overpasses per day are available in any region of the globe against the twelve hours interval between conventional upper air observations. To this it must be added the inherent difference between the high vertical resolution and horizontally fairly well localized RAOBs and the radiometric measurements over field of views (FOV), whose major axis ranges from about 9 to 30 kilometers for nadir respectively laterally viewing FOVs.

The Alpine Experiment (ALPEX 1982a, 1982b, 1982c) experimental phase has produced conventional data which, during some Intensive Observing Periods (IOP), possess the desired horizontal as well as temporal resolution to enable a cross verification with the high resolution satellite data.

This paper presents an intercomparison between satellite and conventional products using an high resolution objective analysis. The period covered by the present study coincides with the first phases of the 4-5 march IOP and the area coverage includes but is not limited to the ALPEX Inner Area.

II. THE RETRIEVAL SCHEME

The software used to process the data presented in this paper is based on a package provided by CIMMS (Cooperative Institute for Mesoscale Meteorological Studies) , Madison. A description of most aspects of temperature and humidity retrieval techniques can be found in Smith et al. (1983) which contains also an extensive bibliography.

1. First guess solution. The retrieval algorithm computes the difference between the "true" temperature and humidity profiles and a first guess solution as a function of the difference between the observed radiances and those computed using the first guess profile. Since no cloud clearing method is adopted, the multiple linear regression is applied only to HIRS/2 channels which are little sensitive to the low tropospheric state (channels 1, 2 and 3) and to MSU channels 2, 3 and 4. The statistical coefficients used for the study are produced every week and used operationally by NOAA/NESDIS, Washington D.C.. The technique is therefore expected to introduce into the first guess solution informations, such as the average tropopause height for the time and latitude belt under exam, which are not retrievable with sufficient accuracy from the satellite informations alone.

3. Surface data. Analyses of 1000 mb temperature,relative humidity and geopotential height, produced by ECMWF are only used to compute hidrostatically the pressure at surface whose elevation is a weighted average of the single FOV values, the weights being proportional to the inverse of the roughness. The first guess profiles are not adjusted to match the ECMWF operational analyses close to the lower boundary.

4. The algorithm developed to compute skin temperature is described in Rizzi (1984).

III. THE OBJECTIVE ANALYSIS SCHEME.

The ALPEX level IIb dataset provides conventional surface and upper air reports, and in addition, data from the ECMWF operational analysis are used for the definition of the lateral boundary condition. Surface data are used to obtain pressure p, virtual potential temperature θ , and humidity values. The upper air soundings are processed to obtain the virtual potential temperature and humidity at any reported level. Values of $p(\theta_i)$ are obtained by linear interpolation in p^k

(where k=R/cp=.256) to the reference isentropic levels ϑ_i. We have chosen 42 ϑ-levels, 2K apart from 270 to 336 K and 6k apart from 342 to 384 K. For each sounding the values of the inverse of static stability $\partial p/\partial \vartheta$ in the layer of 40 mb immediately above the ground are computed for use in the analysis near the ground. The domain chosen is comprised between 33 and 57 degrees north and 14.25 west to 27 degrees east. The grid size is 0.5 degrees in latitude and 0.75 in longitude. (about 55 Km at 45N).

The method used is based on the concept of variational analysis and can be applied by using a variable degree of smoothing of the interpolated values and, when required, also of the original data. The solution r(x,y) is obtained by minimizing a finite difference form of the functional

$$J[r(x,y)] = \alpha \int_D \left[\left(\frac{\partial r}{\partial x} \right)^2 + \left(\frac{\partial r}{\partial y} \right)^2 \right] dxdy + \beta \int \left[\left(\frac{\partial^2 r}{\partial x^2} \right) + 2 \left(\frac{\partial^2 r}{\partial x \partial y} \right) + \right.$$

$$\left. + \left(\frac{\partial^2 r}{\partial y^2} \right) \right]^2 dxdy + \sum_{n=1}^{N} W_n \left[r_n \left(X_n, Y_n \right) - \tilde{r}_n \left(X_n, Y_n \right) \right]^2$$

where w_n is the weight to be attributed to the particular data value $\tilde{r}_n(x_n, y_n)$ and α and β are numerical coefficients regulating the filter response. For semplicity cartesian coordinates x,y are introduced, but in the analysis geographical coordinated are actually used. The first term is a measure of the area of the surface and minimizes oscillations in sparse data areas; the second, which is a measure of curvature, assures the smoothness of r. At lateral boundaries r and its normal derivatives are prescribed using the ECMWF analysis data.

For the analysis of pressure on isentropic surfaces, a definition of the boundary conditions at the intersections with the ground is required. These can be obtained once analyses of pressure, virtual potential temperature and inverse stability at the ground are available.

Once the thermal field $p(x,y,\vartheta)$ is known, the Montgomery streamfunction M is obtained by vertically integrating the hydrostatic equation starting from the values of M computed at the ground. Fields on pressure surfaces are obtained by interpolation of the quantities defined on isentropic surfaces. The high vertical resolution of the latter assures the final interpolation to be sufficiently accurate.

Extensive details on the analysis scheme can be found in Buzzi et al. (1984).

When applied to satellite data some modifications were introduced in the analysis to assure consistency between ground and upper air values. In particular satellite derived surface data were used to produce the analysis of temperature, pressure and static stability at the ground.

IV. RESULTS AND DISCUSSION.

North-south cross sections along the 0.75 degrees meridian are shown in fig. 1a and 1b. The cross sections clearly identify the major differences among conventional and satellite data. Since the retrieval scheme is not constrained to match the conventional data at low levels, the region of relatively cold air related to the developing trough is colder than in the conventional analysis. The poor vertical resolution of the satellite profiles forces the solution at low levels to be strongly influenced by the cold dome which is clearly evident in the conventional analysis in mid-troposphere. Two frontal regions are localized in the conventional analysis south of the Pyrenees, one at the ground and the other in mid-troposphere. The same two regions can be found also in the satellite analysis although with less structure.

Fields of virtual potential temperature on pressure surfaces are shown in fig. 2 to 6 (parts a and b). The satellite products show clearly the cold bias already mentioned up to 700 mb. Lateral boundaries from ECMWF analysis are common to both the analyses and the inconsistency between the satellite derived low level temperatures and the boundaries gives rise to the stange features observed in fig 2a. Best agreement is found in mid troposphere. Absolute values and temperature gradients are consistent. Localized gradients in the conventional analysis found over Sicily at 700 mb and northwestern Spain at 500 mb are probably due to lack of data in those areas. At 300 mb the tropopause structure, as defined by the statistical first guess, is to a large extent retained by the final retrieved profiles, and therefore temperature gradients are weaker than in the conventional data. The position of the trough over Spain as seen in the satellite analysis is different from the one observed in the conventional data. The displacement can be attributed to the difference between synoptic time and the satellite pass for the western orbit which is about two hours and 15 minutes.

Geopotential fields are shown in fig. 2 to 6 (parts c and d). The analyses at the ground for conventional and satellite data are different. The analysis scheme discussed previously in section III is applied to the conventional data while, for the satellite analysis, the pressure at the ground is taken from ECMWF and the temperature is computed after the retrievals. Therefore the two sets of geopotential heights show sistematic differences due to the lower boundary conditions. For this reason it is not possible to make a detailed comparison of the two sets of data although the general structure of the geopotential field is quite similar. In particular the time difference effect already mentioned is observed.

V. FUTURE WORK

These results are good enough to justify a continuation of the effort. Next steps will be: 1) to constraint the first guess of the retrieval scheme to be in accordance with conventional analyses at the ground; 2) to make a detailed comparison of the fields thus obtained with the high resolution analysis of the final IIb ALPEX data set.

VI. REFERENCES

ALPEX 1982a, ALPEX Experiment Design. Geneva GARP-ALPEX n.1.

ALPEX 1982b, ALPEX Field Phase Report. Geneva GARP-ALPEX n.6a.

ALPEX 1982c, ALPEX Preliminary Scientific Results. Geneva GARP-ALPEX n.7.

Buzzi A., A. Trevisan and E. Tosi, 1984 "Isentropic analysis of a case of alpine cyclogenesis" in print Beit. Phys. Atmos.

Rizzi R., 1984 "High resolution satellite soundings over the ALPEX area. The 4-5 march case study" Il Nuovo Cimento, 7C,3, 317-337.

Smith W.L., H.M. Woolf, C.M. Hayden, A.J. Schreiner and J.M. LeMarshall, 1983 "The Physical Retrieval TOVS Export Package" First International Study Conference, Igls sept. 1983.

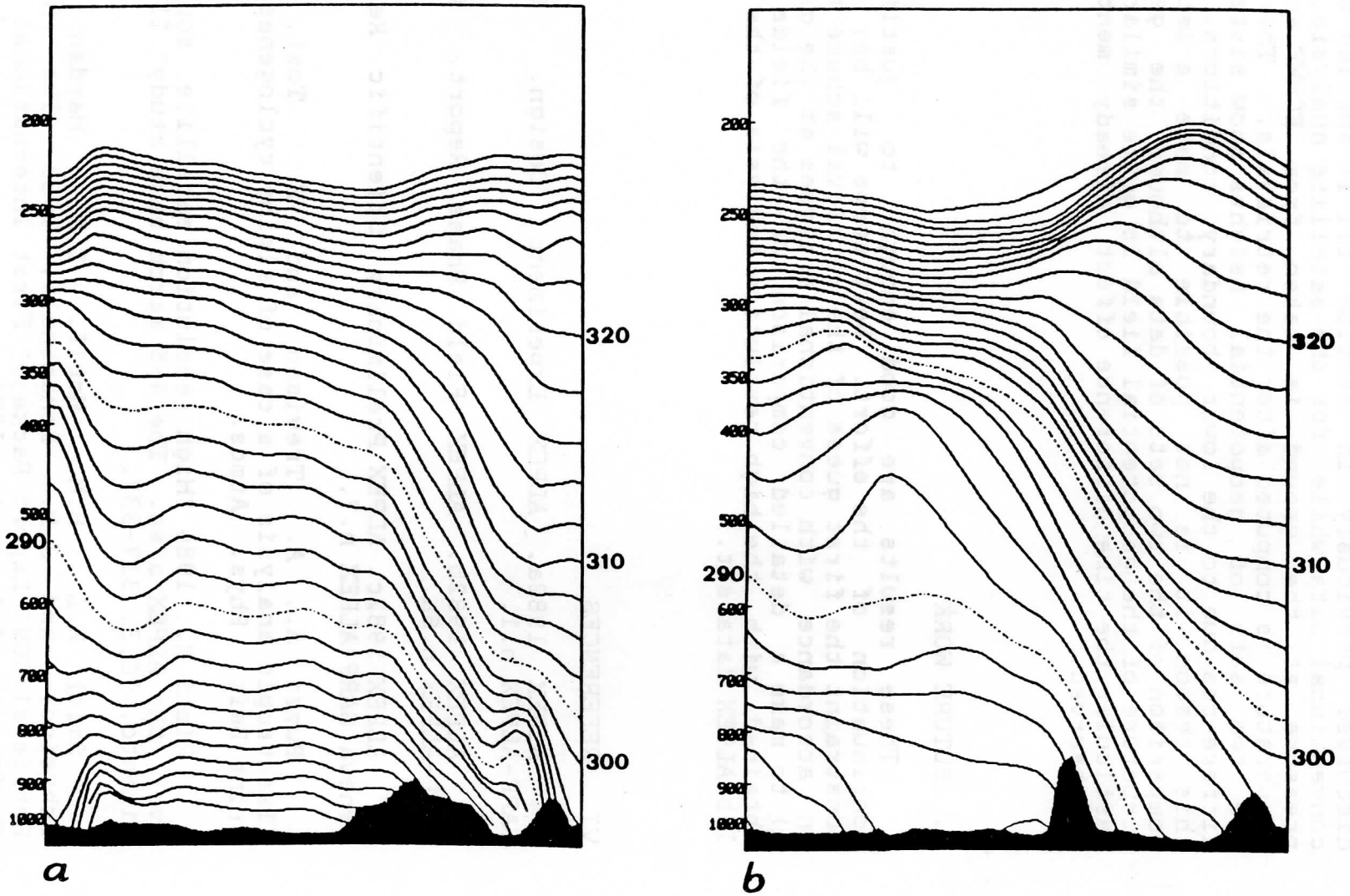

Fig. 1. North-south isentropic cross sections along meridian 0.15 degrees obtained from satellite (a) and conventional (b) data .

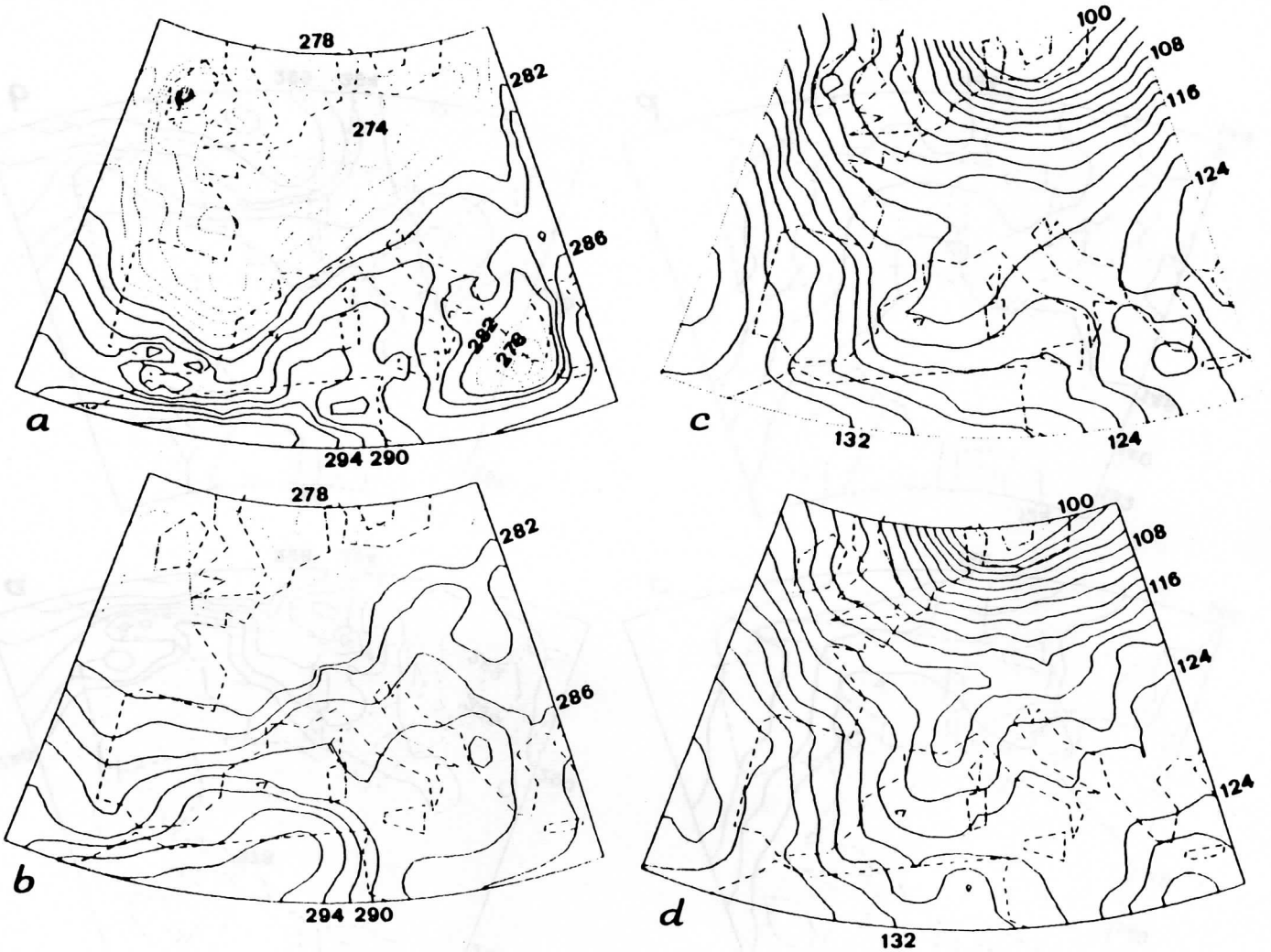

Fig. 2. Analysed temperature and geopotential heigh field at 900 mb obtained from satellite (respectively a and c) and conventional (b and d) for March 4, 1982, 12GMT. Two consecutive NOAA-7 orbits are displayed (12.06 and 13.48 mean pass time)

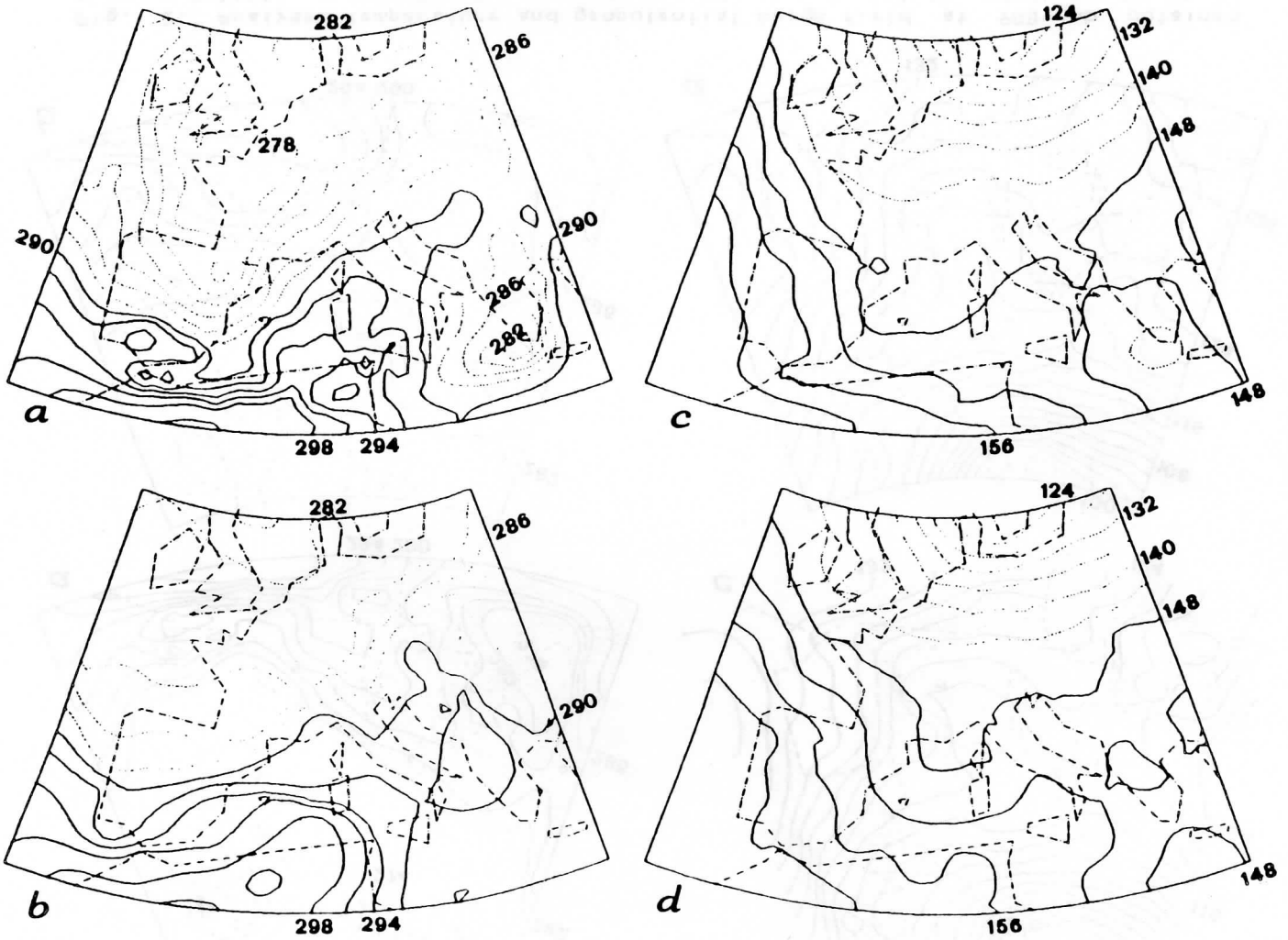

Fig. 3. Same as in fig.2 for the surface 850 mb.

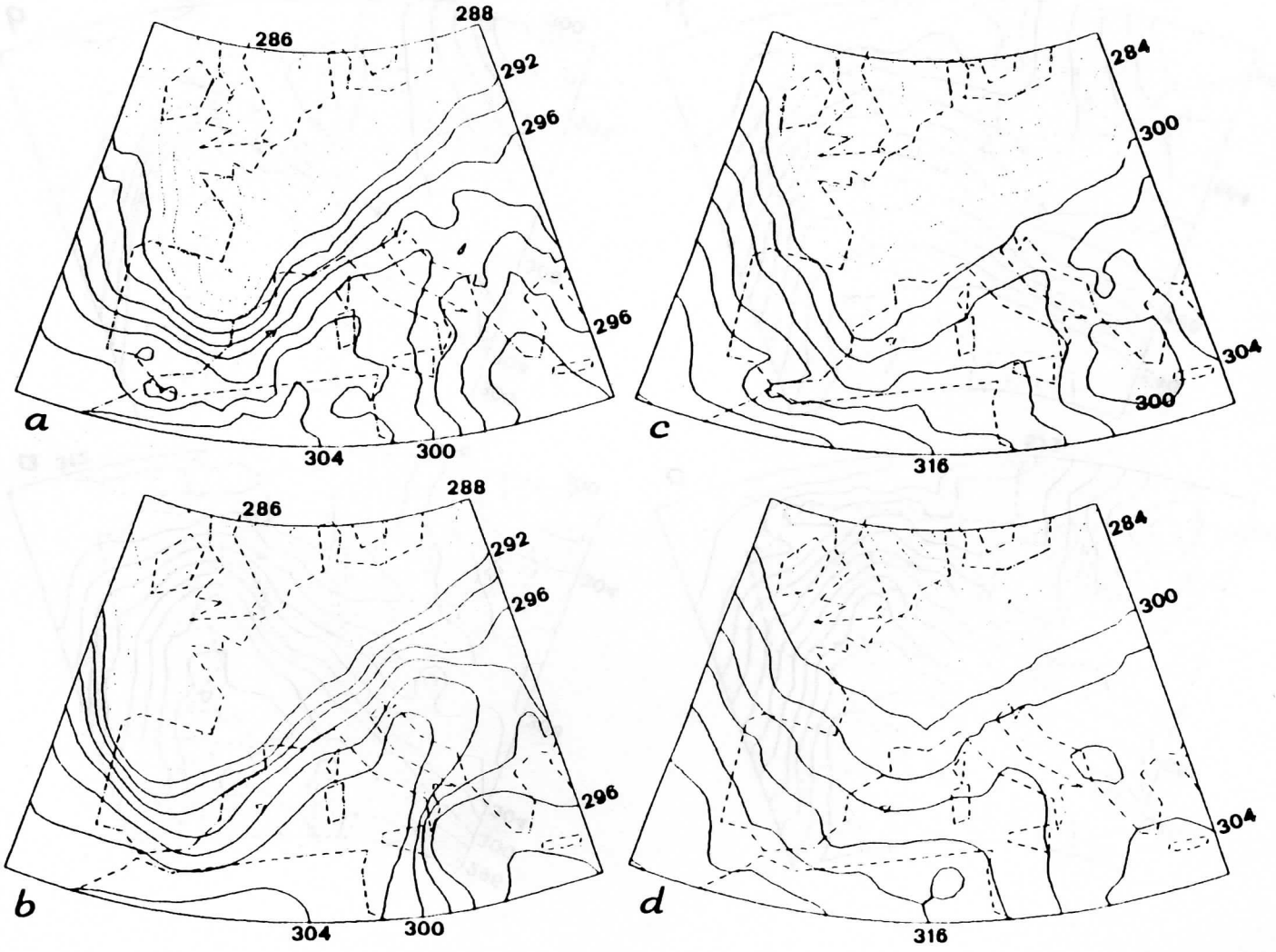

Fig. 4. Same as in fig.2 for the surface 700 mb.

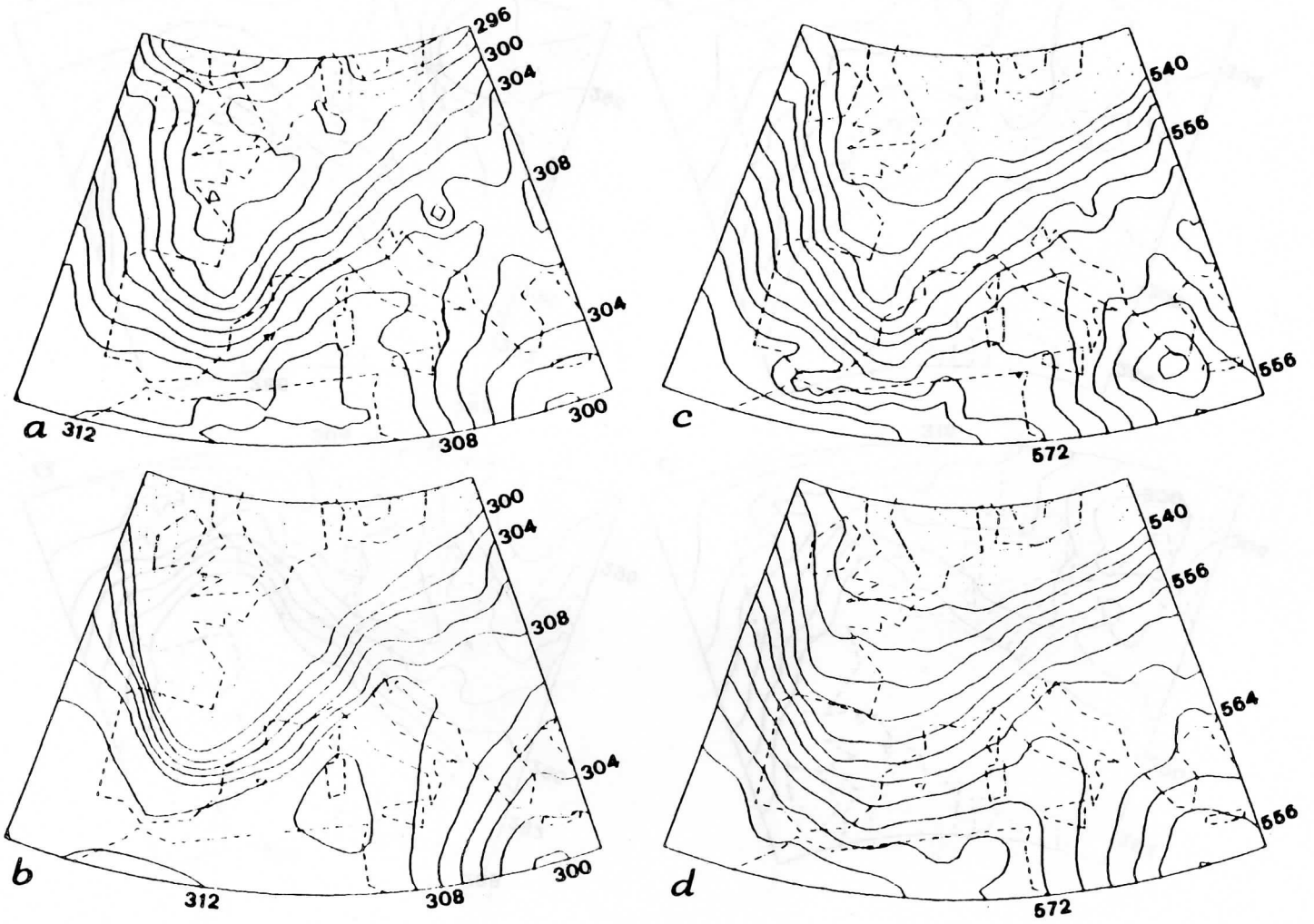

Fig. 5. Same as in fig.2 for the surface 500 mb.

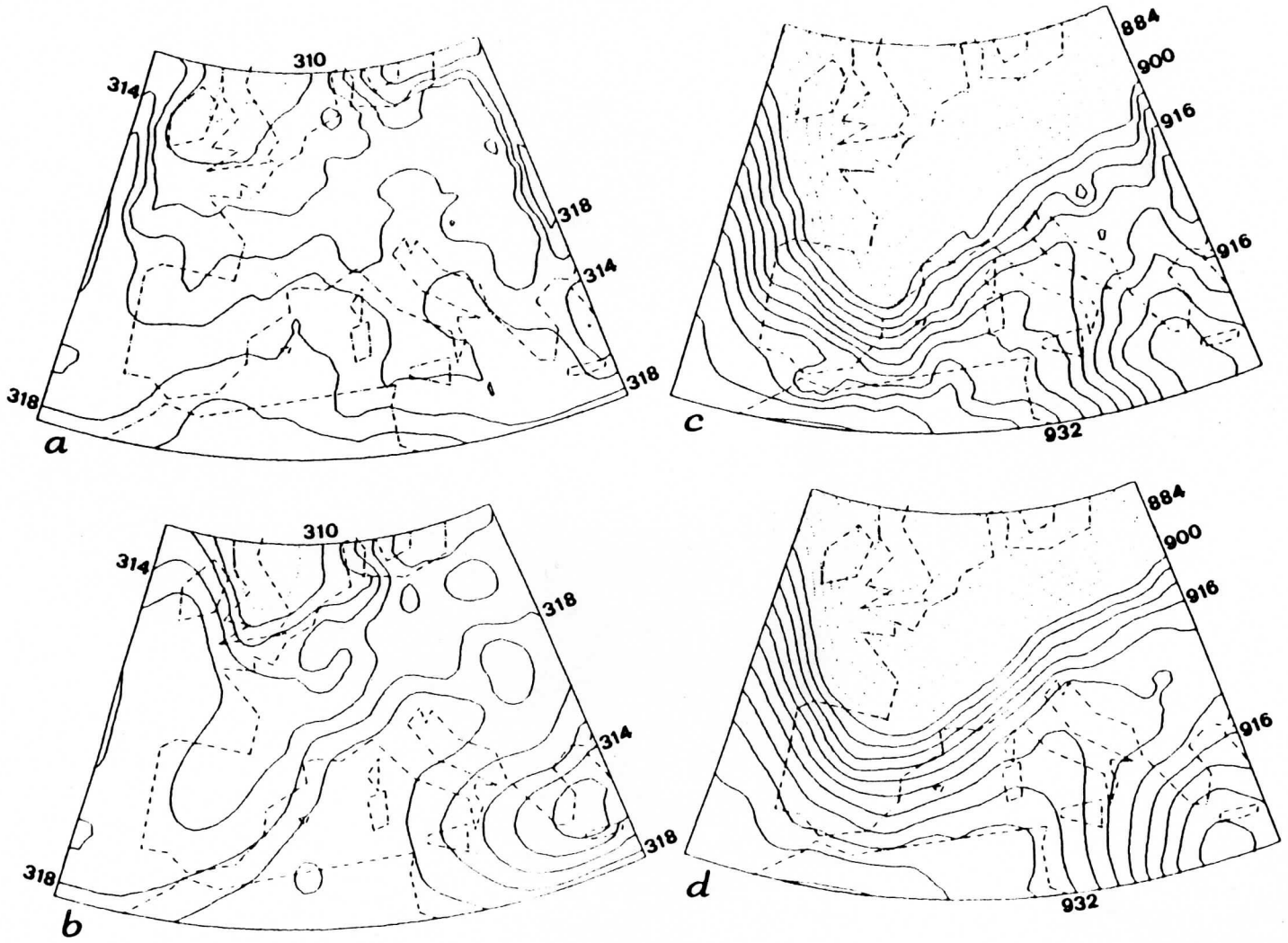

Fig. 6. Same as in fig.2 for the surface 300 mb.

THE SIMULTANEOUS RETRIEVAL EXPORT PACKAGE

W. L. Smith[1], H. M. Woolf[2], C. M. Hayden[2], A. J. Schreiner[1]
Cooperative Institute for Meteorological Satellite Studies
University of Wisconsin
Madison, Wisconsin 53706, USA

[1] Space Science and Engineering Center
[2] NOAA/NESDIS

1. INTRODUCTION

As part of the "First International TOVS Study Conference", a description of a physical algorithm for retrieving temperature and moisture soundings from TOVS radiance data was described (Smith et al., 1983). This algorithm was incorporated into the "TOVS Export Package" made available by CIMSS to direct readout users of TOVS data. The physical algorithm consisted of the application of the Smith-Iterative Solution (Smith, 1970) for temperature and moisture profiles. In that approach, (1) an initial profile for temperature and water vapor is specified from climatology, statistical regression, or from an NWP model, (2) radiances are calculated from the initial profiles, (3) the temperature profile is adjusted in an iterative manner until there is agreement between the observed and calculated radiances in the cloud insensitive microwave O_2 channels, (4) the infrared window channels are used to define either the surface skin temperature or the temperature of cloud within the instrument's field of view and the cloud level is defined using the microwave specified temperature profile, (5) the guess moisture profile is adjusted to reflect the existence of cloud by assuming 100% relative humidity at the cloud level and then further adjusted in an iterative manner in order to achieve convergence between observed and calculated radiance for the water vapor channels, and (6) the temperature profile is then further adjusted in an iterative manner in order to achieve convergence between the radiances observed and calculated in the infrared CO_2 channels.

Since the first Igls conference, a new retrieval algorithm has been developed which permits the simultaneous retrieval of surface-skin (or cloud) temperature, and the temperature and moisture profiles. The advantage of the "simultaneous solution" is two-fold: (1) the radiances observed in all channels are used to solve for all parameters simultaneously, thus alleviating the problem of the interdependence of the radiance observation upon the three parameters, and (2) since a direct analytical solution is employed, the process is computationally efficient.

In this paper the new algorithm now incorporated in the "TOVS export package" is described. As with the prior "iterative" algorithm, the physical nature of the solution permits the influence of surface variables (i.e., terrain elevation, emissivity, and temperature) and cloudiness to be accounted for in the profile determinations. The cloud handling algorithm

is modified to enable the infrared data to be utilized in partly cloudy as well as cloud overcast sky conditions. The low sensitivity of the simultaneous solution to the initial guess profile and the improved performance of the simultaneous retrieval method compared to the previously established iterative technique (Smith et al., 1983; Susskind, 1984) are demonstrated from TOVS orbits over Europe obtained during the ALPine EXperiment (ALPEX) as selected by the International Radiation Commission's TOVS Working Group for the intercomparison of retrieval methods. The physics for treating surface emissivity, terrain elevation, and reflected sunlight are not described here since these aspects have been provided in the previous report (Smith et al., 1983).

2. DIRECT PHYSICAL SOLUTION

An important advance in the profile retrieval methodology is the simultaneous temperature and water vapor solution (Smith and Woolf, 1984). In order to achieve the simultaneous solution, the integral form of the radiative transfer equation is integrated by parts and treated in the perturbation form:

$$\delta T^* = \int_0^{P_s} \delta U \frac{\partial T}{\partial p}\frac{\partial \tau}{\partial U}\frac{(\partial B/\partial T)}{(\partial B/\partial T^*)}\,dp - \int_0^{P_s} \delta T \frac{\partial \tau}{\partial p}\frac{(\partial B/\partial T)}{(\partial B/\partial T^*)}\,dp + \delta T_s \frac{(\partial B_s/\partial T_s)}{(\partial B/\partial T^*)} \qquad (1)$$

where T^* is brightness temperature, U is precipitable water vapor, B is Planck radiance, T is temperature, T_s is surface-skin temperature, τ is transmittance, and p is pressure. The perturbation, δ, is with respect to an a-priori estimated or mean condition. The pressure dependence of all integrand variables is to be understood. In order to solve (1) for δU, δT, and δT_s from a set of spectrally independent radiance observations, the perturbation profiles are represented in terms of arbitrary pressure functions, $\phi(p)$:

$$\delta q(p) = g \sum_{i=1}^{N} \alpha_i q_o(p)\phi_i(p) \qquad (2a)$$

$$\delta T(p) = -\sum_{i=N+1}^{N} \alpha_i \phi_i(p) \qquad (2b)$$

where q(p) is the water vapor mixing ratio and g is gravity. The zero subscript indicates the a priori condition. Equation 2a implies from the gas law and hydrostatic equation that

$$\delta U(p) = \sum_{i=1}^{N} \alpha_i \int_0^P q_o(p)\phi_i(p)\,dp \,. \qquad (2c)$$

Substituting representations (2b) and (2c) into (1) and letting $\alpha_0=\delta T_s$ yields for each spectral radiance observation, δT_j^*, for a set of K spectral channels:

$$\delta T_j^* = \sum_{i=0}^{M} \alpha_i \Phi_{ij} \qquad j=1,2,\ldots,K \tag{3}$$

where

$$\Phi_{0,j} = \frac{\partial B_j/\partial T_s}{\partial B_j/\partial T_j^*}\, \tau_{s,j}$$

$$\Phi_{i,j} = \int_0^{P_s} \left[\int_0^{P} q_0 \phi_i dp\right] \left[\frac{\partial T}{\partial p} \frac{\partial \tau_j}{\partial U} \frac{\partial B_j/\partial T}{\partial B_j/\partial T_j^*}\right] dp \qquad i \leq N \tag{4}$$

$$\Phi_{i,j} = \int_0^{P_s} \phi_i \left[\frac{\partial \tau_j}{\partial p} \frac{\partial B_j/\partial T}{\partial B_j/\partial T_j^*}\right] dp \qquad N < i \leq M .$$

The $\Phi_{i,j}$ quantities are calculated from the a- priori estimated or mean profile conditions. Written in matrix form

$$t^* = \Phi\alpha \tag{5}$$

where t^* is a row vector of K radiance observations, α is a row vector of M+1 coefficients, and Φ is a matrix having dimensions (K×M+1). Assuming that K≥M+1, then the least squares solution of (5) is employed to give

$$\alpha = (\Phi^T\Phi)^{-1}\, \Phi^T t^* \approx (\Phi^T\Phi + \gamma I)^{-1}\, \Phi^T t^* \tag{6}$$

where $(\ )^T$ indicates matrix transposition and $(\ )^{-1}$ indicates matrix inverse. The γI term, where γ (nominally 0.1) is a scalar and I is the identity matrix, is incorporated to stabilize the matrix inverse. Once the α_i's are determined, δT_s, δq, and δT are specified from (2) and added to the a-priori estimates to yield the final solutions for surface-skin temperature and the water vapor mixing ratio and temperature profiles.

The choice of pressure basis functions $\phi(p)$ is arbitrary. For example, empirical orthogonal functions (i.e., eigenvectors of the water vapor and temperature profile covariance matrices) can be used in order to include statistical information in the solution. However, here for its application to the TIROS Operational Vertical Sounder (TOVS) data, physical functions, the profile weighting functions ($d\tau/d\ln p$) of the radiative transfer equation, are used as the basis functions.

Ancillary information such as surface observations can be easily incorporated into the profile solutions. For example, for surface observations it follows from (2) that

$$q(p_s) - q_o(p_s) = g \sum_{i=1}^{N} \alpha_i q_0(p_s)\phi_i(p_s) \tag{7}$$

and

$$T(p_s) - T_o(p_s) = - \sum_{i=N+1}^{M} \alpha_i \phi_i(p_s) \tag{8}$$

have the same form as (3) and therefore can be added to the set to yield K+2 equations to solve for M+1 unknowns (α).

The main advantage of the "simultaneous" retrieval method is that it enables the temperature and water vapor profiles and the surface skin temperature to be determined simultaneously using all the radiance information available. The simultaneity directly addresses the problems associated with water vapor radiance dependence upon temperature and the dependence of several of the carbon dioxide channel radiance observations used for temperature profiling, on the water vapor concentration. The dependence of the radiance observations on surface emissions is accounted for in the simultaneous solution by the inclusion of surface temperature as an unknown. Also, since only a single matrix inversion is required for the specification of all parameters, the solution is more computationally efficient than the iterative technique. Finally, but significantly, ancillary observations of temperature and/or moisture from surface sensors or aircraft, for example, can be readily incorporated in the solution.

Logistics

The processing of the TOVS data begins with the specification of an initial profile including surface observations, if available. The initial profile can be specified either from climatology or through the use of regression coefficients, based either on synthetic radiances or on real radiances matched to radiosonde observations. The climatological and regression generated initial profile algorithms are internal to the Export Package. A third option exists whereby an analysis or forecast generated grid field of temperature and water vapor profiles can be used to create initial profiles. In this case the grid fields are external to the Export Package as are the surface data grid fields.

MSU and HIRS radiances are obtained for a 3 x 3 array (75 km resolution) of HIRS FOV's, as described in the earlier report (Smith et al., 1983); the MSU data having been interpolated to each HIRS FOV. These are used in a two step procedure to generate an initial solution, to estimate cloud contamination, and to produce final estimates of temperature and moisture as follows:

Step 1: The stratospheric HIRS brightness temperatures (channels 1-3), the MSU brightness temperatures (MSU 1-4), and the middle and upper tropospheric HIRS water vapor channels (HIRS 11 and 12) are used to derive a first estimate of the temperature and moisture profile for the sounding location. With this channel selection, the estimate should be relatively free of error due to cloud attenuation. The weighting functions for HIRS-1 and MSU 2-4 are utilized as the basis functions for temperature and the HIRS

7 and 12 weighting functions are used as the basis functions for water vapor in the initial retrieval. Once the first estimate of the temperature and water vapor profile is achieved, the height and amount of any cloud affecting the infrared observations are determined by the method described in the next section. After this is accomplished all channels (except HIRS channels 13-19 in the cloudy case) are used to calculate the final surface temperature and the temperature and water vapor profiles.

Step 2: For the achievement of the final profile estimates the weighting functions for HIRS 1, 3, 7 and MSU 2-4 are used as the temperature profile basis functions, and those for HIRS 7, 11, and 12 are used as the water vapor profile basis functions. Since as many as nineteen different spectral radiance observations are used for the surface temperature and profile retrievals, the system of equations to be inverted is heavily overdetermined, thereby stabilizing the solution. (It should be noted that ozone and geopotential height are determined in the same manner as described for the iterative solution Export Package.)

Handling the Influence of Clouds

In the TOVS data processing, soundings are derived from a 3 x 3 matrix of HIRS fields of view (FOV), the Microwave Sounding Unit (MSU) data being spatially interpolated to the location of the HIRS spots. From the array, the observations for the "clearest" FOV's, defined as those whose 11μm radiance values are within 2°K of the local maximum, are averaged for the sounding determination. The magnitude of the visible channel reflectance and the 3.7μm, 4.0μm, and 11μm window channel brightness temperatures are used in conjunction with surface temperature observations, if available, to specify whether the "clearest" radiances are contaminated by clouds. If the radiances are determined to be affected by clouds, their pressure height and fractional coverage are specified on the basis of certain CO_2 channel infrared radiances and the microwave radiance specified temperature profile. The cloud height is calculated using the CO_2 slicing technique (Smith and Platt, 1977, Menzel et al., 1983) from the relation

$$\frac{I(\nu_1) - \hat{I}_c(\nu_1)}{I(\nu_2) - \hat{I}_c(\nu_2)} = \frac{\int_{P_c}^{P_o} \tau(\nu_1,p) \frac{\partial B(\nu_1,\hat{T})}{\partial p} dp}{\int_{P_c}^{P_o} \tau(\nu_2,p) \frac{\partial B(\nu_2,\hat{T})}{\partial p} dp} \qquad (9)$$

where $\hat{I}_c(2)$ is the clear-column radiance calculated from the microwave specified temperature profile, T, and ν_1 and ν_2 refer to HIRS channels 5 and 7 respectively. The cloud pressure P_c is obtained by trial and error. The cloud fraction, N, is then obtained from the relation

$$N = \frac{I(\nu_1) - \hat{I}_c(\nu_1)}{I(\nu_2) - \hat{I}_c(\nu_2)} \qquad (10)$$

where $\hat{I}_{cd}(\nu_1)$ is the radiance calculated for an opaque cloud overcast condition.

Given P_c and N, the guess mixing ratio profile is adjusted by assuming that the mixing ratio at the cloud level is given by

$$W(p_c) = NW_{sat}\,[\hat{T}(p_c)] + (1 - N)\hat{W}(p_c) \qquad (11)$$

where W_{sat} is the saturation mixing ratio corresponding to the microwave specified temperature at the cloud pressure P_c and W is the original guess value of mixing ratio. Below the cloud a new guess mixing profile is achieved by interpolation using the original surface mixing ratio value.

Once the cloud parameters and the guess mixing ratio profile are established the brightness temperature discrepancies from the guess conditions, δT^*, can be calculated, including the effects of cloud within the field of view of the HIRS instrument. For the infrared channels the effects of cloud in the solution of (4) can be properly included by assuming that

$$\tau = (1 - N)\,\tau^{orig} \qquad (12)$$

for pressures greater than the cloud pressure. This transmittance function modification reduces the influence of the infrared observations on the solution below the cloud in proportion to the cloud obscuration. After this adjustment, the simultaneous solution proceeds exactly as in the clear sky condition.

3. RESULTS

Retrieval Analyses

In this section, objective analyses of the TOVS retrievals achieved using two independent initial guess profile procedures: (a) statistical regression using MSU brightness temperatures as predictors; and (b) climatology based on the U.S. Standard Supplemental Atmospheres, are compared for the March 4, 5 ALPEX data sets. The first guess profile specification procedures have been described in the previous ITOVS-I conference report. The analyses of the 75 Km resolution TOVS soundings were produced using the BARNES method (Barnes, 1973). These analyses are compared to each other and to the operational analyses of radiosonde data for this area by the European Center for Medium Range Weather Forecasting (ECMWF).

Figures 1-4 show the temperature analysis comparisons for the mandatory pressure levels from 850 mb to 300 mb, respectively. There is little difference between the analyses achieved from the two different first guess-based TOVS retrievals, indicating weak dependence of the simultaneous retrieval method on the first guess profile. Both sets of retrievals capture the rapid intensification of the trough over western Europe between 12 GMT of 4 March and 00 GMT of 5 March, 1982. The magnitude of the differences from the ECMWF analyses are generally less than 3°C. Curiously, the differences appear to be slightly smaller for the climatological first guess retrievals, particularly at the 300 mb level. It is also noteworthy that

the largest differences of the TOVS analyses from those of the ECMWF are generally over radiosonde data-void areas (e.g.. the eastern North Atlantic and the Mediterranean). The largest differences between the two TOVS analyses are about 3°C at the 300 mb level over southeastern Europe.

Figure 5-8 show analyses of the TOVS dewpoint temperatures for the mandatory levels from 850 to 300 mb levels, respectively. Superimposed are the radiosonde values shown for verification. As with the temperature analyses, the analyses of the dewpoint temperatures reveal very close agreement between the "regression" and "climatology" first guess based retrievals. There is also very good qualitative agreement between the volume-sampled satellite dewpoints and the point sampled radiosonde observations. Most striking is the qualitative agreement between the highly structured 500 mb dewpoint temperatures and the radiosonde observations (Fig. 7). It is interesting to note that the gradiants in the TOVS retrievals are as large, if not larger, than the values displayed by the radiosondes. Also, the radiosonde data appear somewhat "noisy" relative to the coherent analyses of the TOVS retrievals. Because of the gaps in the radiosonde, particularly over the Mediterranean region, it would be impossible to achieve analyses with the same degree of horizontal and temporal consistency as displayed in the TOVS analyses. The horizontal sampling limitation of the radiosonde data is even more striking at the 300 mb level where many of the latter are missing due to "motorboating."

Finally, Figure 9 shows a comparison of 500 mb dewpoint analyses achieved using the prior iterative retrieval method ("Export II"). The significant improvement achieved with the simultaneous method is striking. Similar improvements are obtained at the other pressure levels (not shown). We have found, in general, that the largest improvements gained by the simultaneous retrieval system ("Export III") over those achieved by the iterative retrieval method ("Export II") are in the moisture results.

Statistics

Statistical comparisons between the TOVS retrievals and the ECMWF analyses are restricted here to the root mean square deviation (RMSD) after the mean difference has been removed. Curves of the mean difference are not given because they are generally less than 2°C and very similar for the "regression" and "climatology" cases, except for the 300 mb level where there exists a 2°C mean difference between the two retrieval types.

For all the TOVS statistics, the ECMWF analyses serve as a standard of "truth" although this is an approximation as shown in Figure 10 where the RMSD of radiosonde data and the ECMWF analyses is shown. It is noted that the RMSD values range between 1.2 and 3.0°C which puts bounds on the validity of the "truth." As shown in Figures 10-14, the RMSD values for the TOVS retrievals are not significantly larger than the RMSD values for the radiosonde. Since radiosonde data believed to have an accuracy better than 0.5°C, the explanation for their large RMSD values can be attributed to the synoptic scale smoothing displayed by the ECMWF analyses and the volume sampled TOVS soundings.

Figure 11 compares RMSD values achieved from the simultaneous retrieval algorithm "Export III" with those achieved with the prior iterative retrieval method "Export II." As may be seen, there is consistent improvement of the "Export III" soundings over those achieved with "Export II," being as large as 0.5°C at individual levels. In fact, the RMSD values shown for the simultaneous retrieval method are not significantly larger than the radiosonde RMSD values (compare Figs. 10 and 11).

Figure 12 shows a comparison between the RMSD values for "Export III" for the "regression" and "climatology" first guess conditions. The differences are insignificant, except in the upper troposphere where the regression statistics apparently aid in the initialization of the tropopause structure. Because of the limited vertical resolution of the TOVS radiance observations, the initial guess tropopause structure is reflected in the retrieval.

Figure 13 shows the impact that surface data has on the TOVS simultaneous retrievals. As expected, the influence is largely confined to the atmosphere below the 700 mb level. As may be seen, however, it is important to use surface analyses in the retrieval process; otherwise the expected error in the results will almost double near the earth's surface.

4. CONCLUSIONS

A new and improved retrieval algorithm has been developed and included in the "Export III" software system for TOVS temperature and moisture sounding retrieval. Small, but significant improvements are shown for temperature profiling with very large improvements demonstrated in the moisture sounding capabilities of the TOVS. As with the prior "Export" software packages, Export III is available to interested users who should contact the CIMSS of the University of Wisconsin.

5. REFERENCES

Barnes, S. L., 1973: Mesoscale objective analysis using weighted time-series observations. NOAA Tech. Memo. ERL NESSL-62, National Severe Storms Laboratory, 1313 Halley Circle, Norman, OK 73069, 60 pp.

Greaves, J. R., H. E. Montgomery, L. W. Uccellini, and D. L. Endres, 1982: AVE/VAS Field Experiment NASA/GSFC Technical Report X-903-82-17, September 1982.

Smith, W. L., 1983: The retrieval of atmospheric profiles from VAS geostationary radiance observations. J. Atmos. Sci., 40, 2025-2035.

Smith, W. L., H. M. Woolf, C. M. Hayden, A. J. Schreiner, and J. M. Le Marshall, 1983: The physical retrieval TOVS export package. Presented at the First International TOVS Study Conference, Igls, Austria, 29 August - 2 September 1983.

Smith, W. L., and H. M. Woolf, 1984: Improved vertical soundings from an amalgamation of polar and geostationary radiance observations. Preprint volume: Conference on Satellite Meteorology/Remote Sensing and Applications, June 25-29, 1984, Clearwater Beach, Florida. Published by American Meteorological Society, Boston, Massachusetts.

Susskind, J., J. Rosenfield, D. Reuter, and M. T. Chahine: Remote Sensing of Weather and Climate Parameters from HIRS 2/MSU on TIROS-N, Journal of Geophysical Research, Vol. 89, No. C6, June 20, 1984.

4/WLS18/02

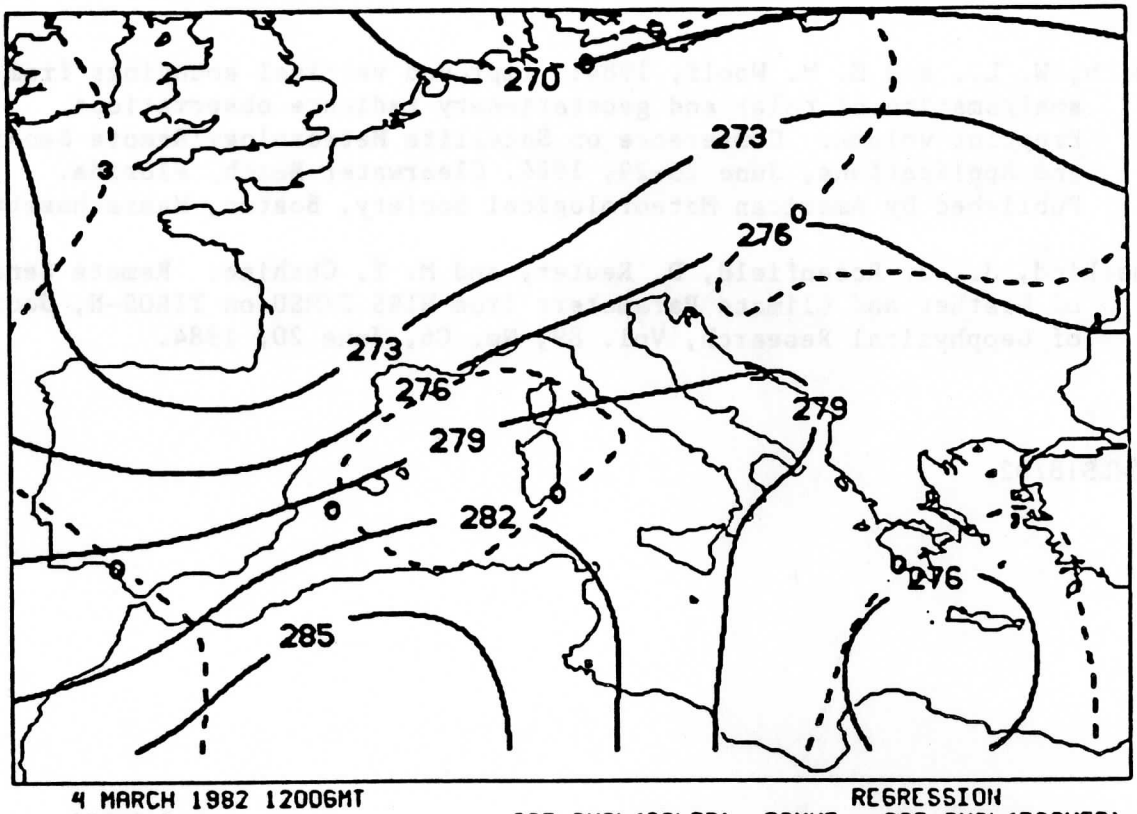

(a) 4 MARCH 1982 12006MT
850MB T(K)
REGRESSION
SAT ANAL(SOLID) ECMWF - SAT ANAL(DASHED)

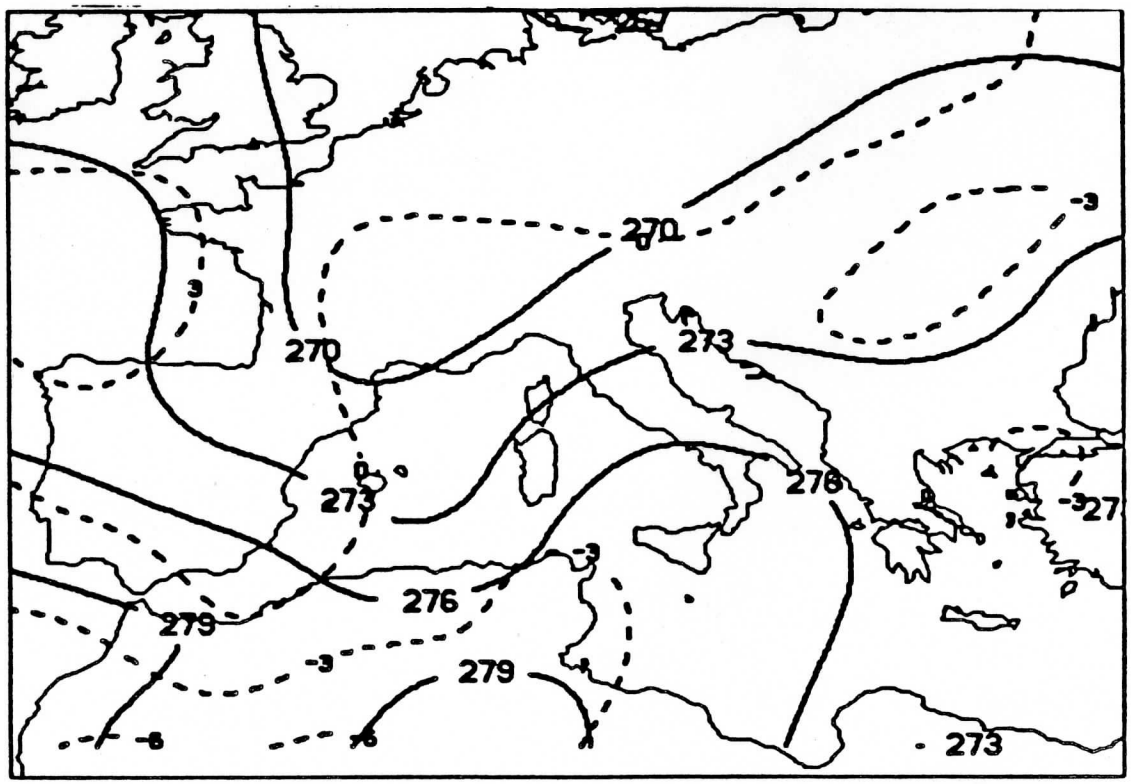

(c) 5 MARCH 1982 00006MT
850MB T(K)
REGRESSION
SAT ANAL(SOLID) ECMWF - SAT ANAL(DASHED)

Figure 1: Analyses of TOVS retrievals (solid contours) and differences between the operational analyses of the ECMWF and the TOVS analyses (dashed contours).

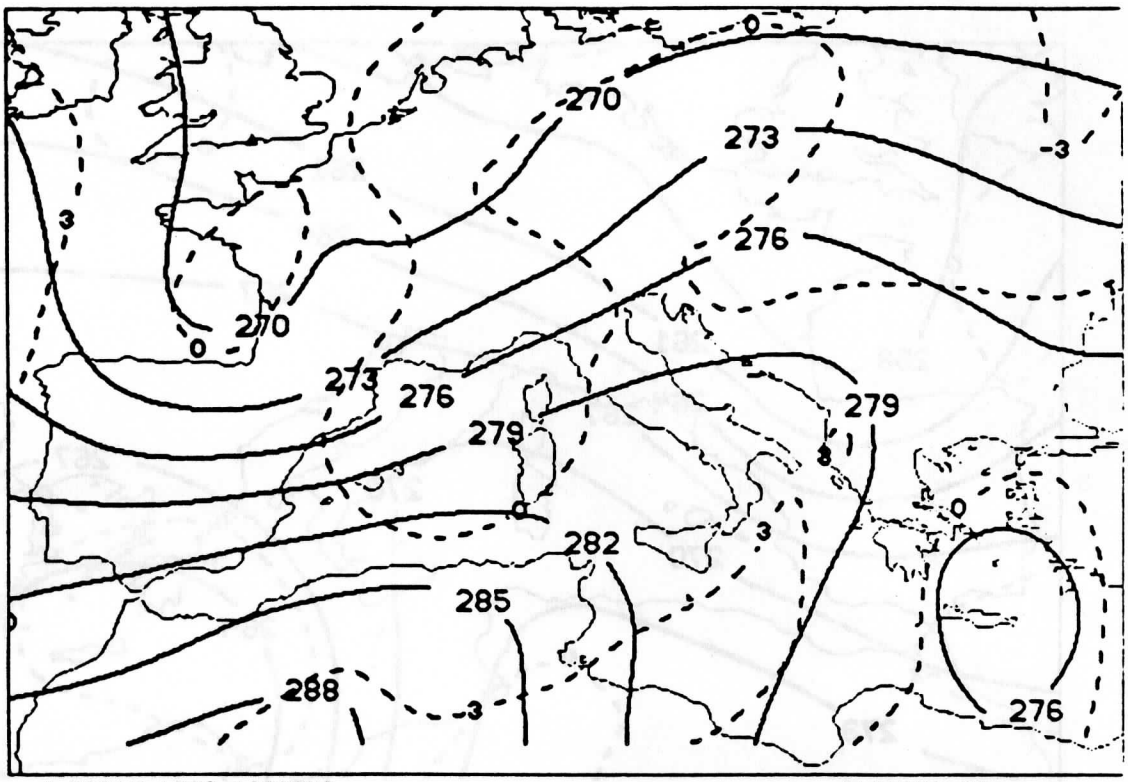

(b)

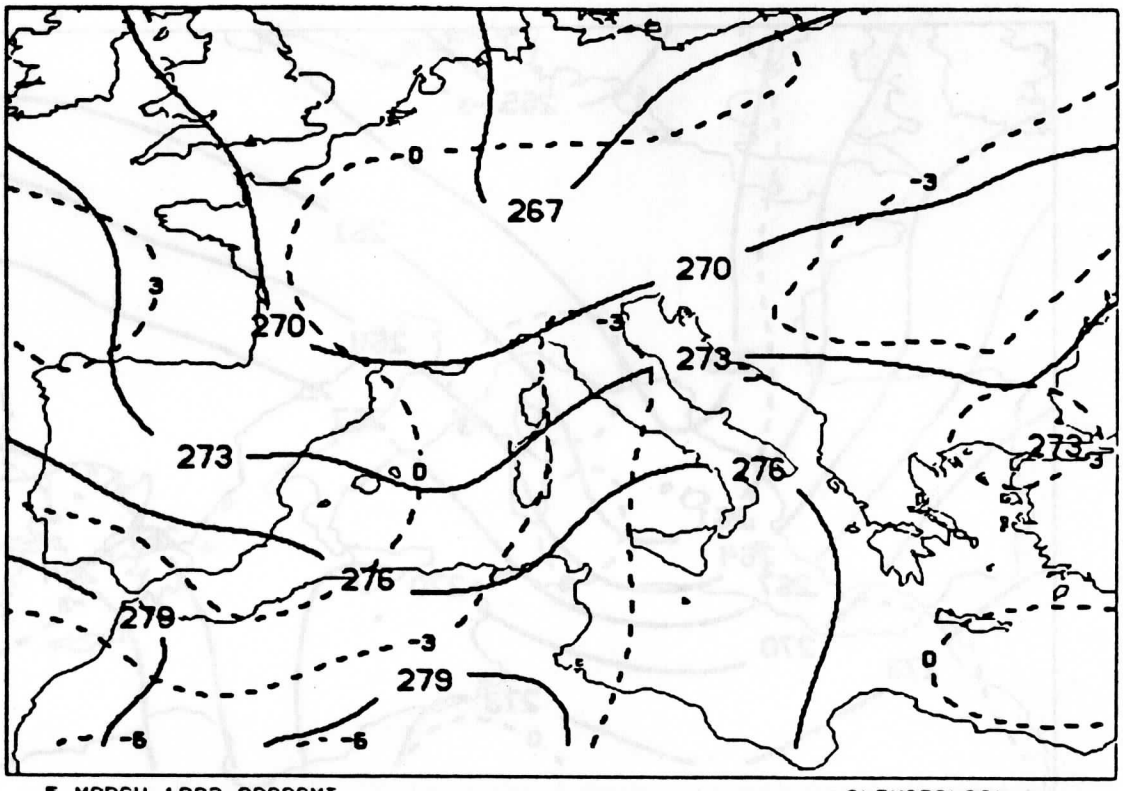

(d)

Figure 1: Analyses of TOVS retrievals (solid contours) and differences between the operational analyses of the ECMWF and the TOVS analyses (dashed contours).

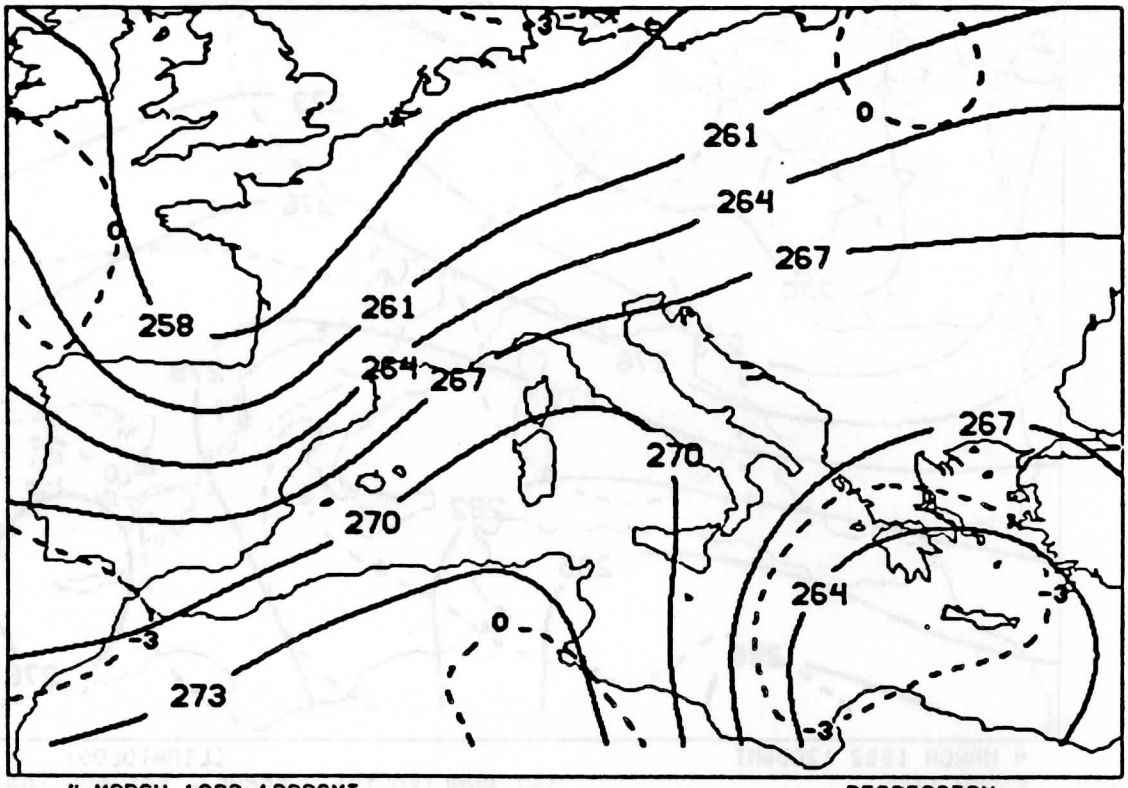

(a)

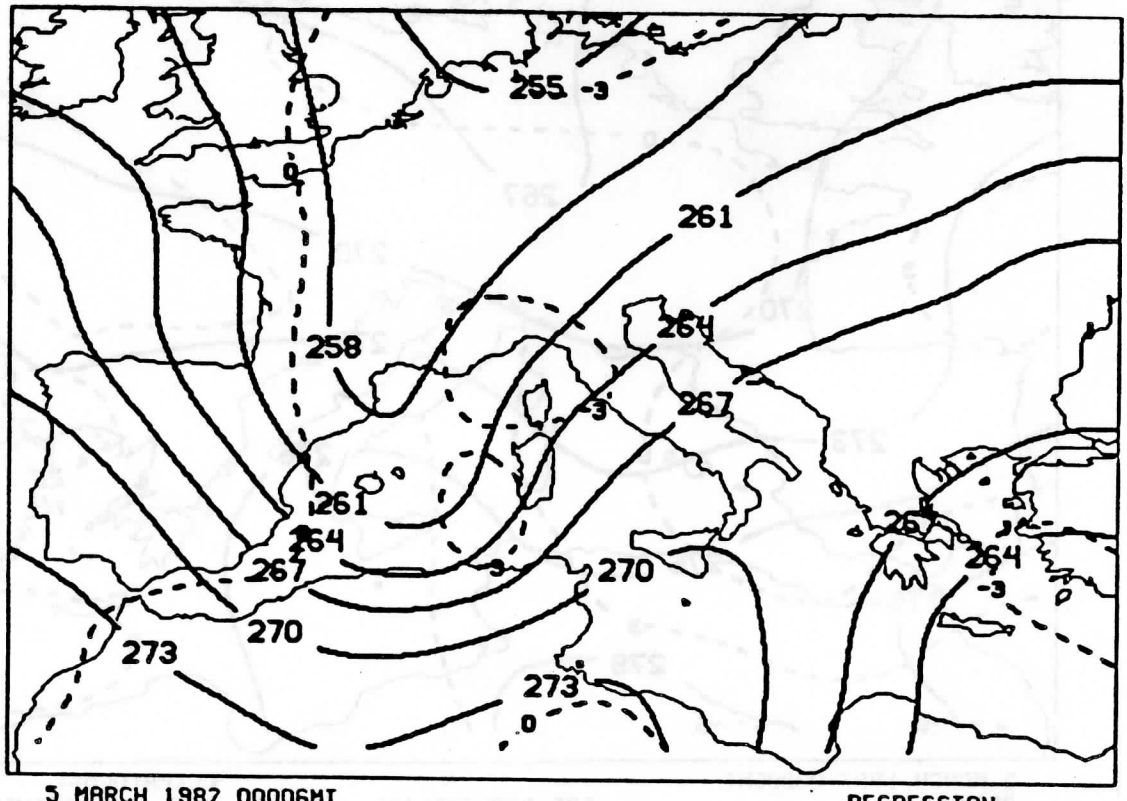

(c)

Figure 2: Analyses of TOVS retrievals (solid contours) and differences between the operational analyses of the ECMWF and the TOVS analyses (dashed contours).

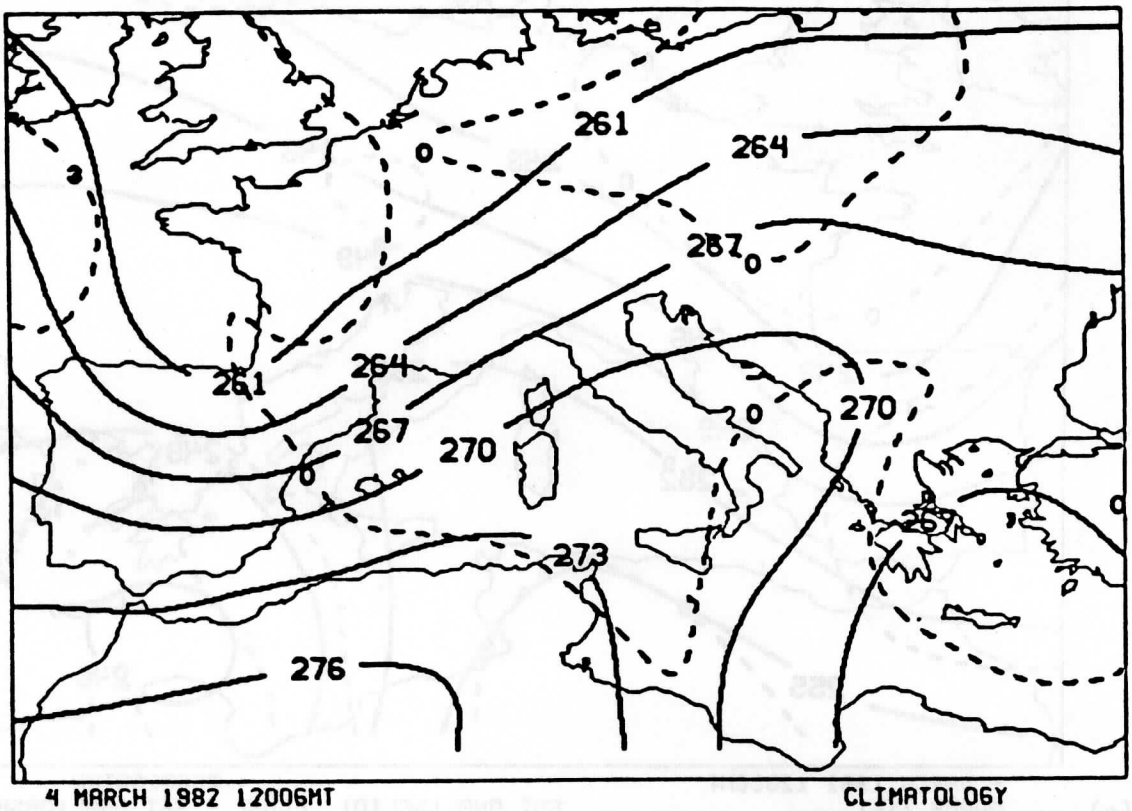

(b)

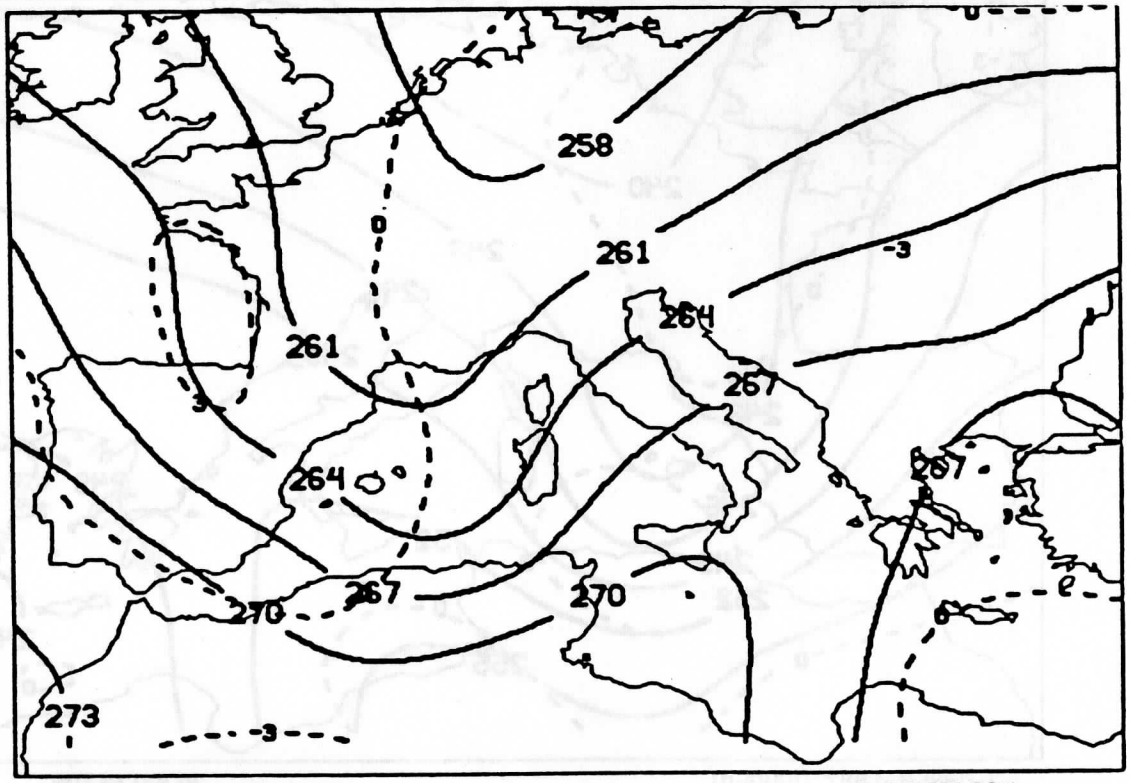

(d)

Figure 2: Analyses of TOVS retrievals (solid contours) and differences between the operational analyses of the ECMWF and the TOVS analyses (dashed contours).

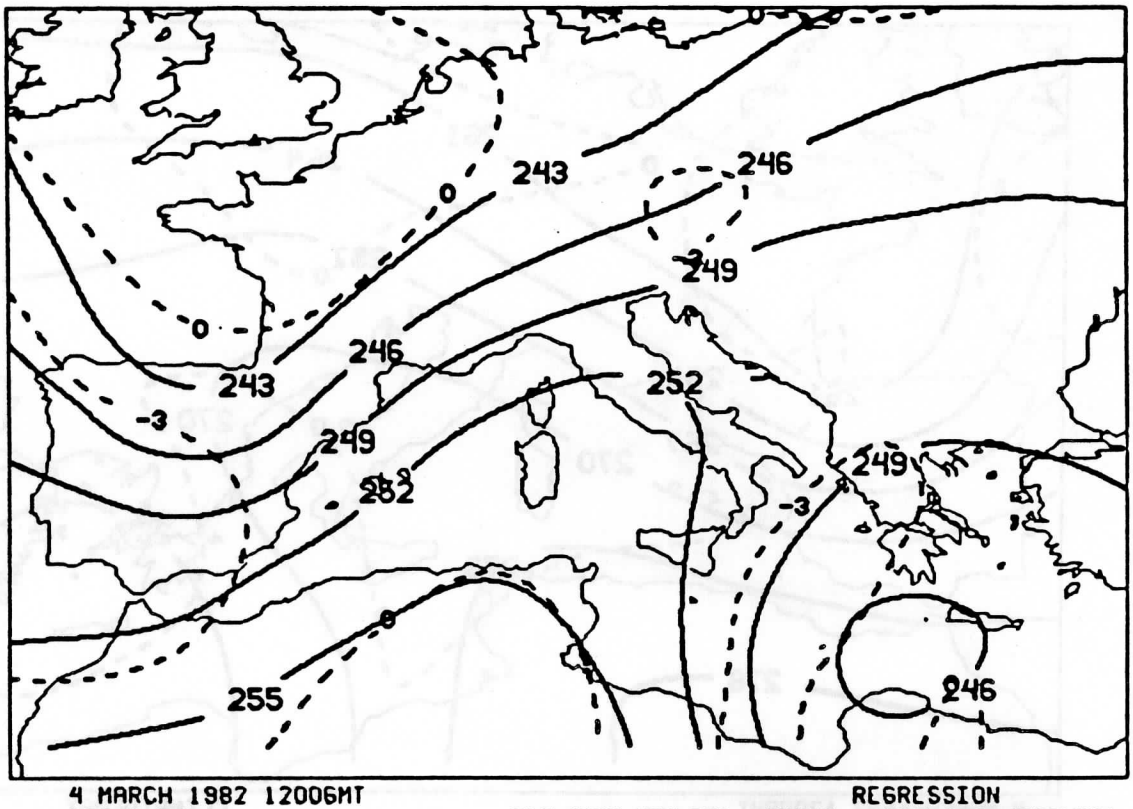

(a) 4 MARCH 1982 12006MT
500MB T(K)
REGRESSION
SAT ANAL(SOLID) ECMWF - SAT ANAL(DASHED)

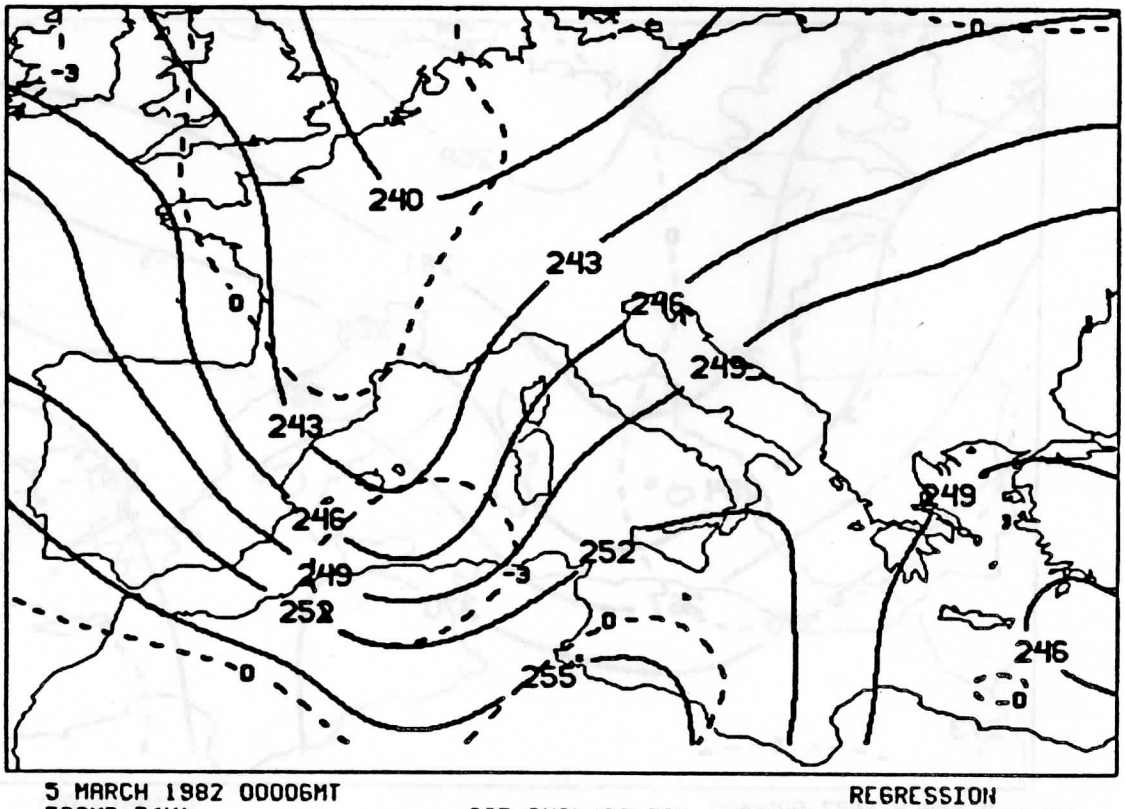

(c) 5 MARCH 1982 00006MT
500MB T(K)
REGRESSION
SAT ANAL(SOLID) ECMWF - SAT ANAL(DASHED)

Figure 3: Analyses of TOVS retrievals (solid contours) and differences between the operational analyses of the ECMWF and the TOVS analyses (dashed contours).

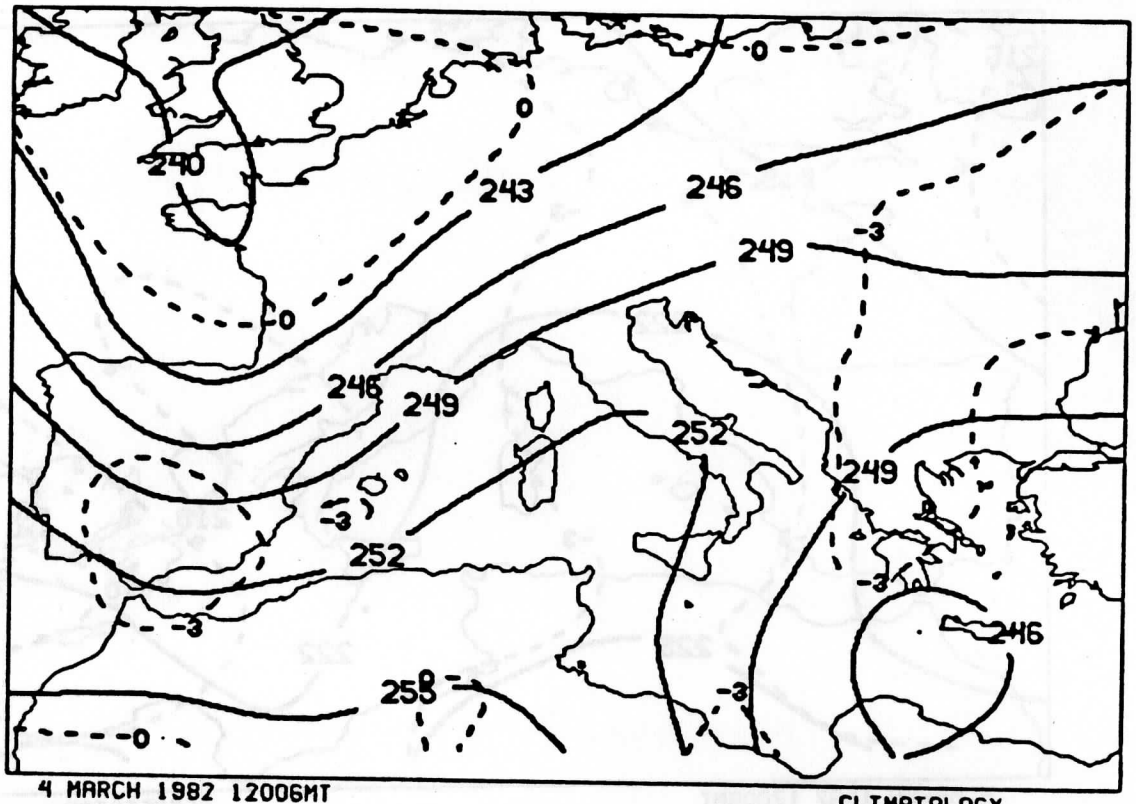

(b)

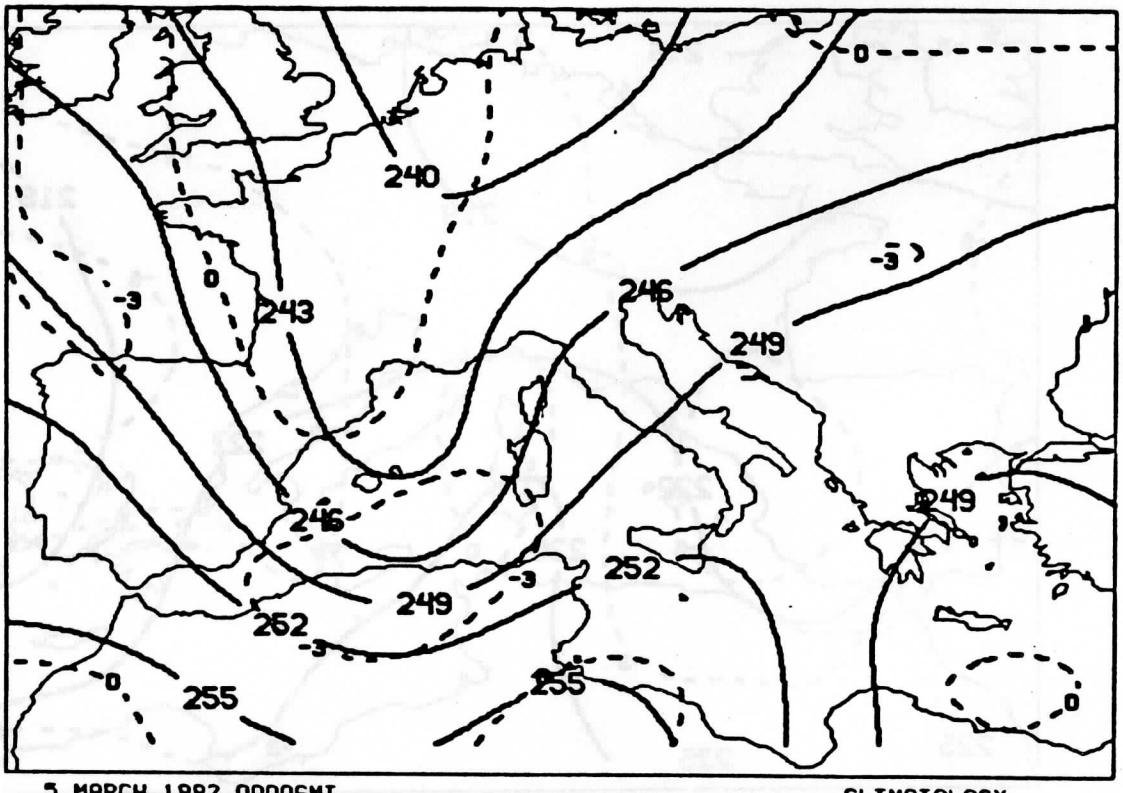

(d)

Figure 3: Analyses of TOVS retrievals (solid contours) and differences between the operational analyses of the ECMWF and the TOVS analyses (dashed contours).

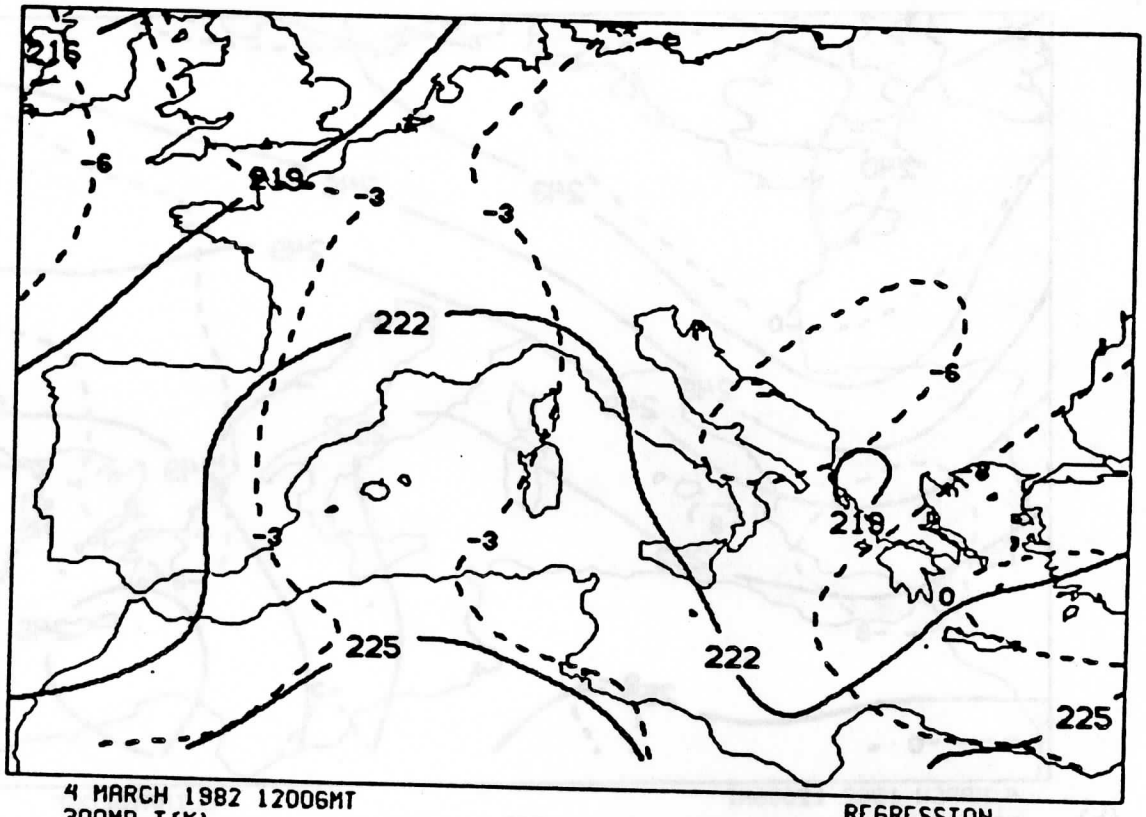

(a)

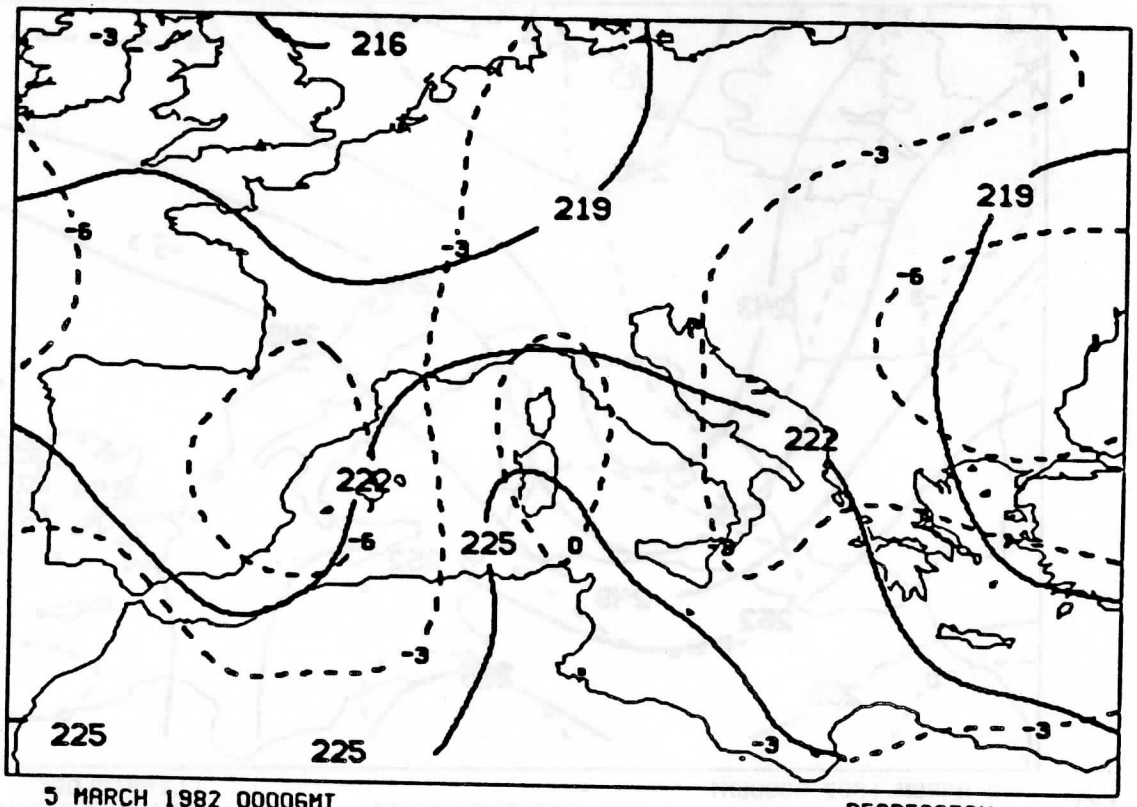

(c)

Figure 4: Analyses of TOVS retrievals (solid contours) and differences between the operational analyses of the ECMWF and the TOVS analyses (dashed contours).

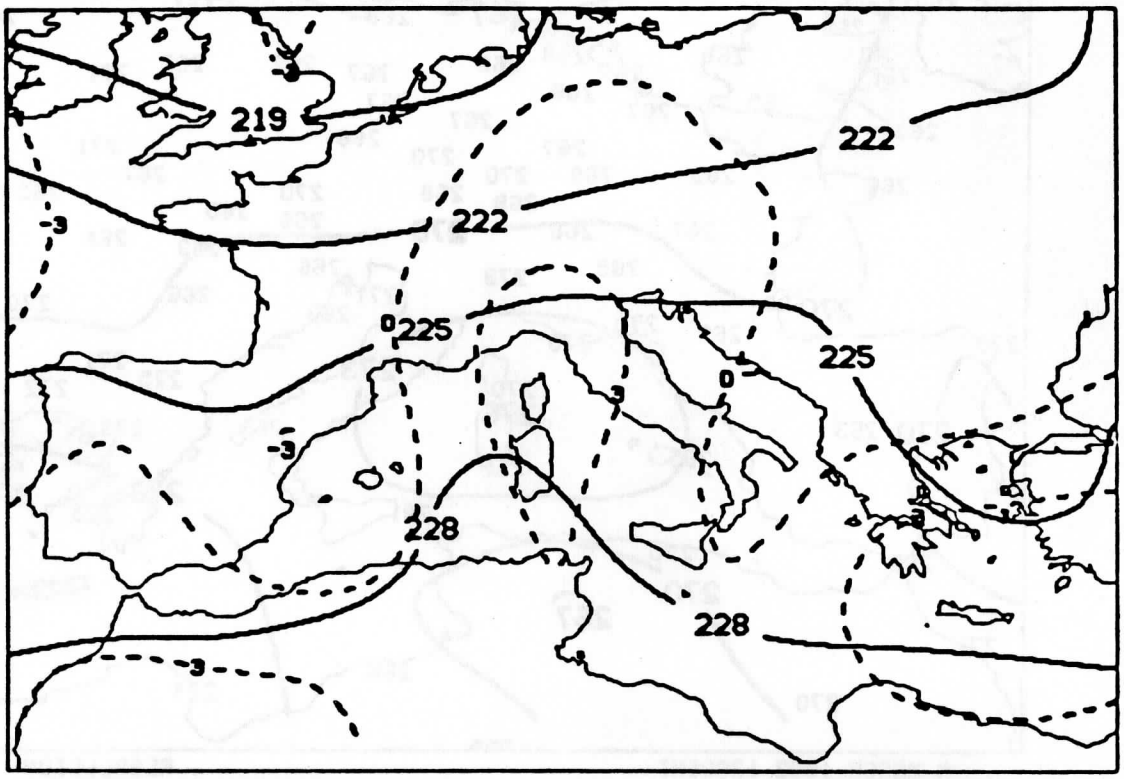

(b) 5 MARCH 1982 00006MT
300MB T(K)
SAT ANAL(SOLID) CLIMATOLOGY ECMWF - SAT ANAL(DASHED)

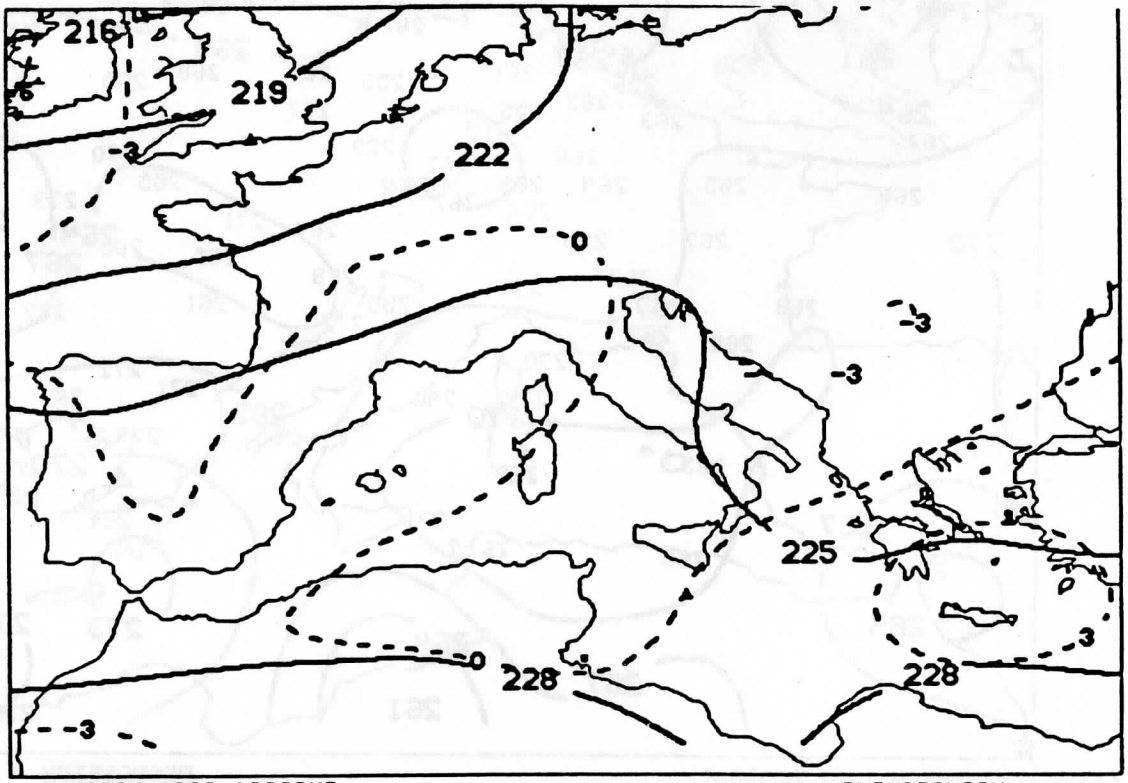

(d) 4 MARCH 1982 12006MT
300MB T(K)
SAT ANAL(SOLID) CLIMATOLOGY ECMWF - SAT ANAL(DASHED)

Figure 4: Analyses of TOVS retrievals (solid contours) and differences between the operational analyses of the ECMWF and the TOVS analyses (dashed contours).

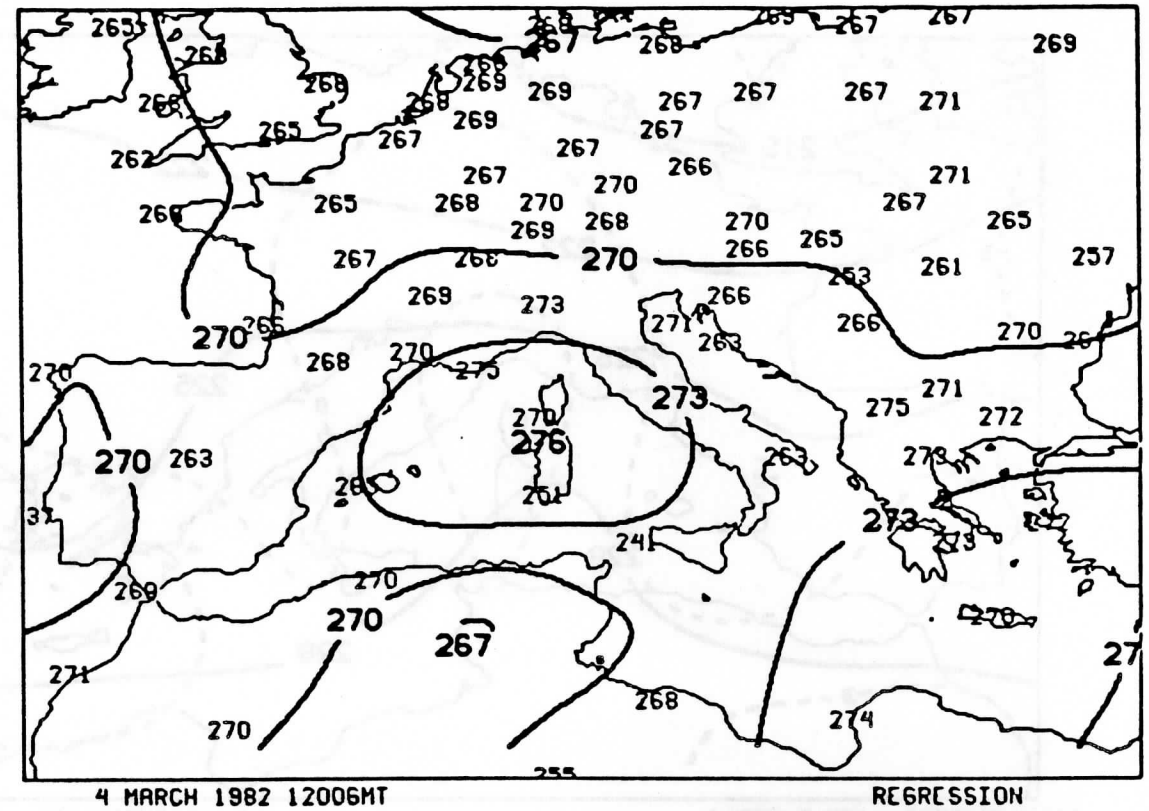

(a)

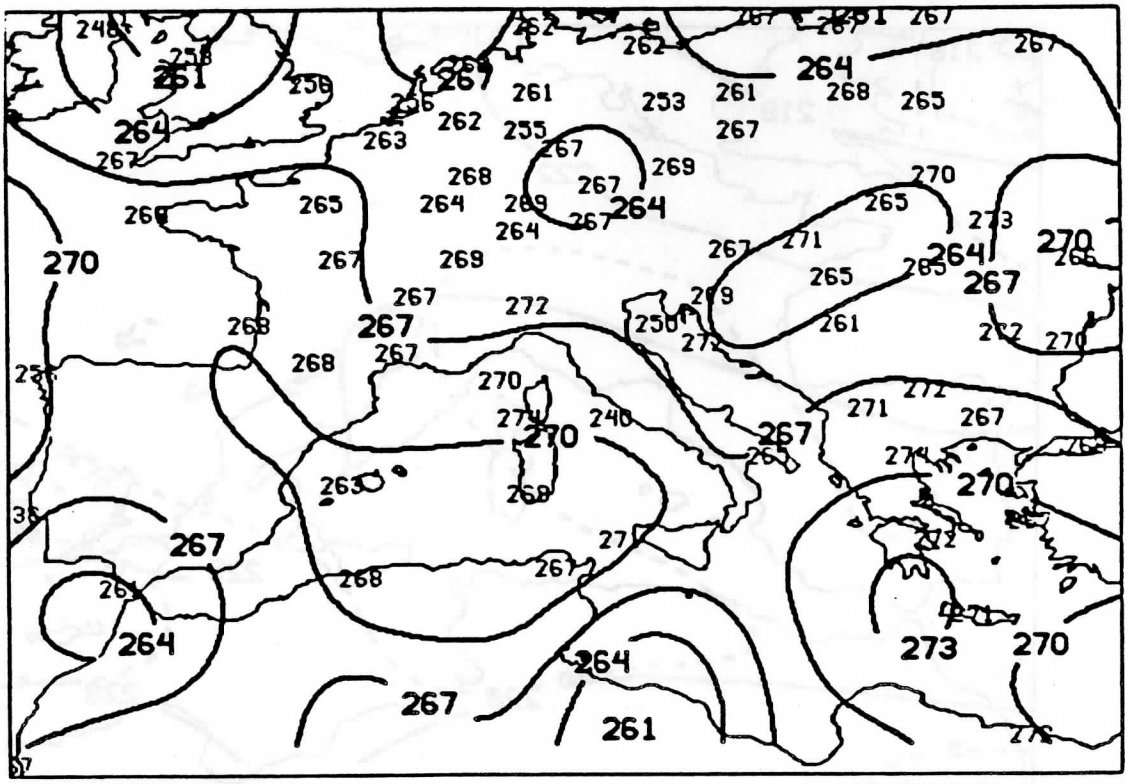

(c)

Figure 5: Analyses of TOVS retrievals (solid contours).

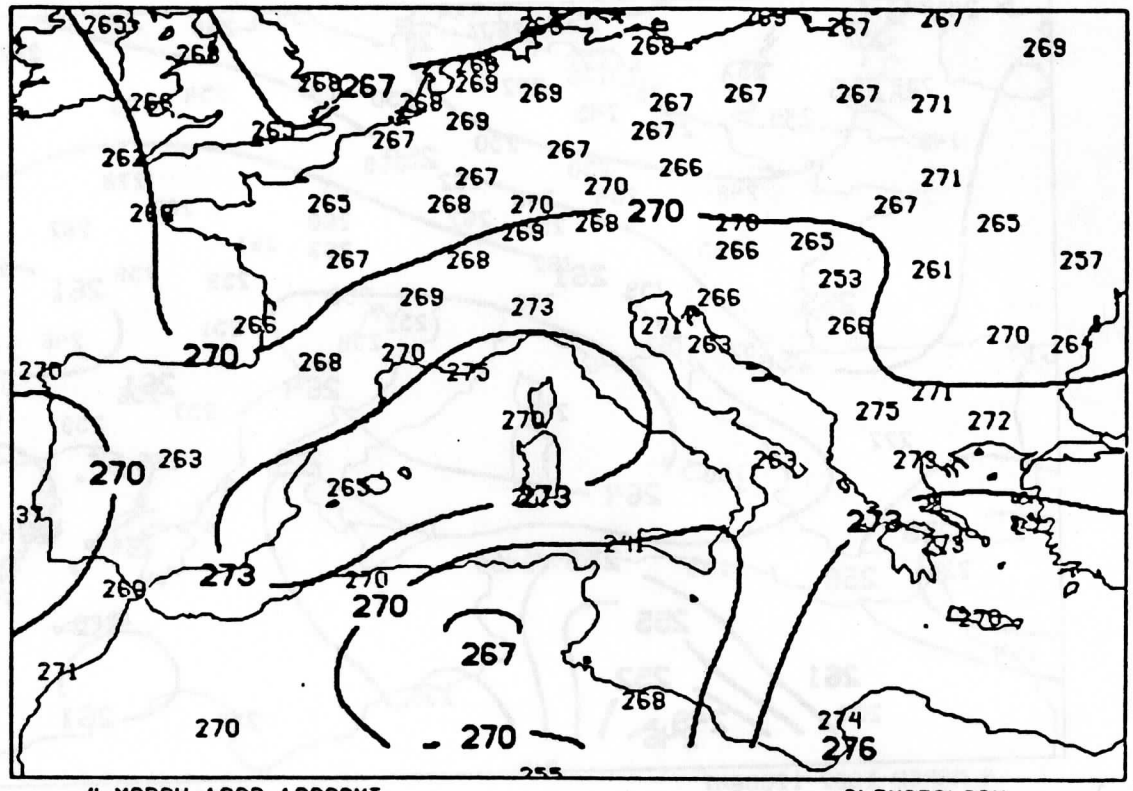

(b)

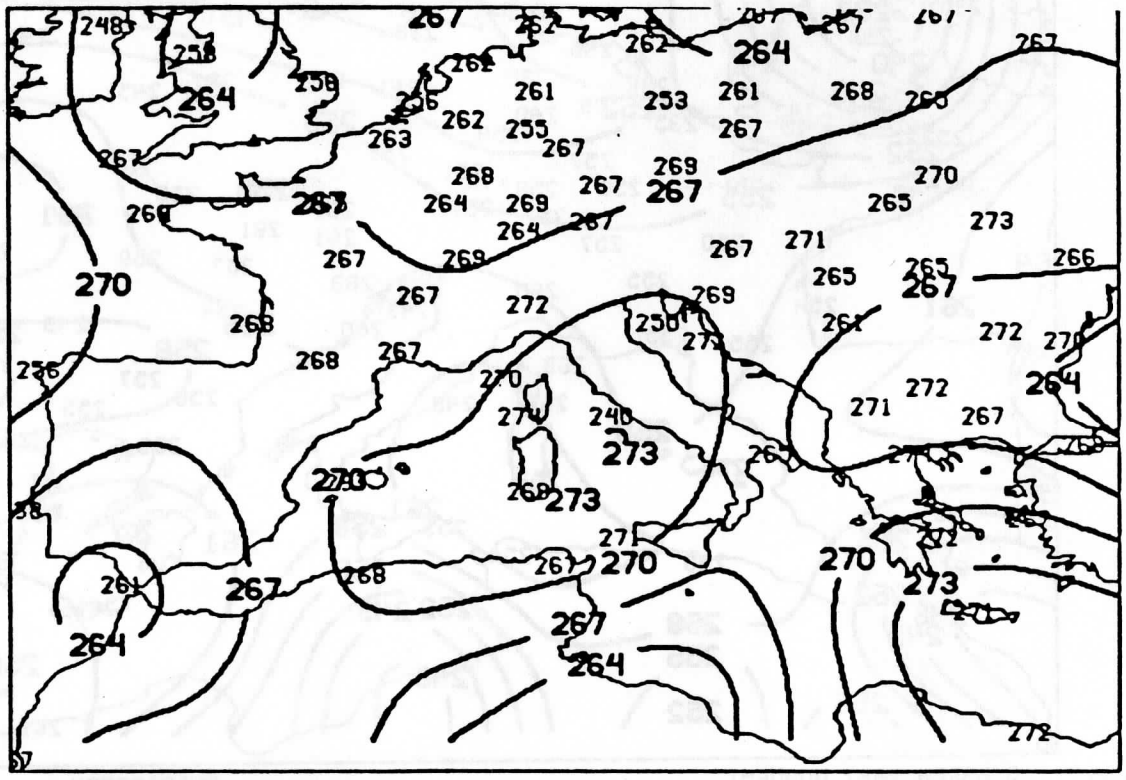

(d)

Figure 5: Analyses of TOVS retrievals (solid contours).

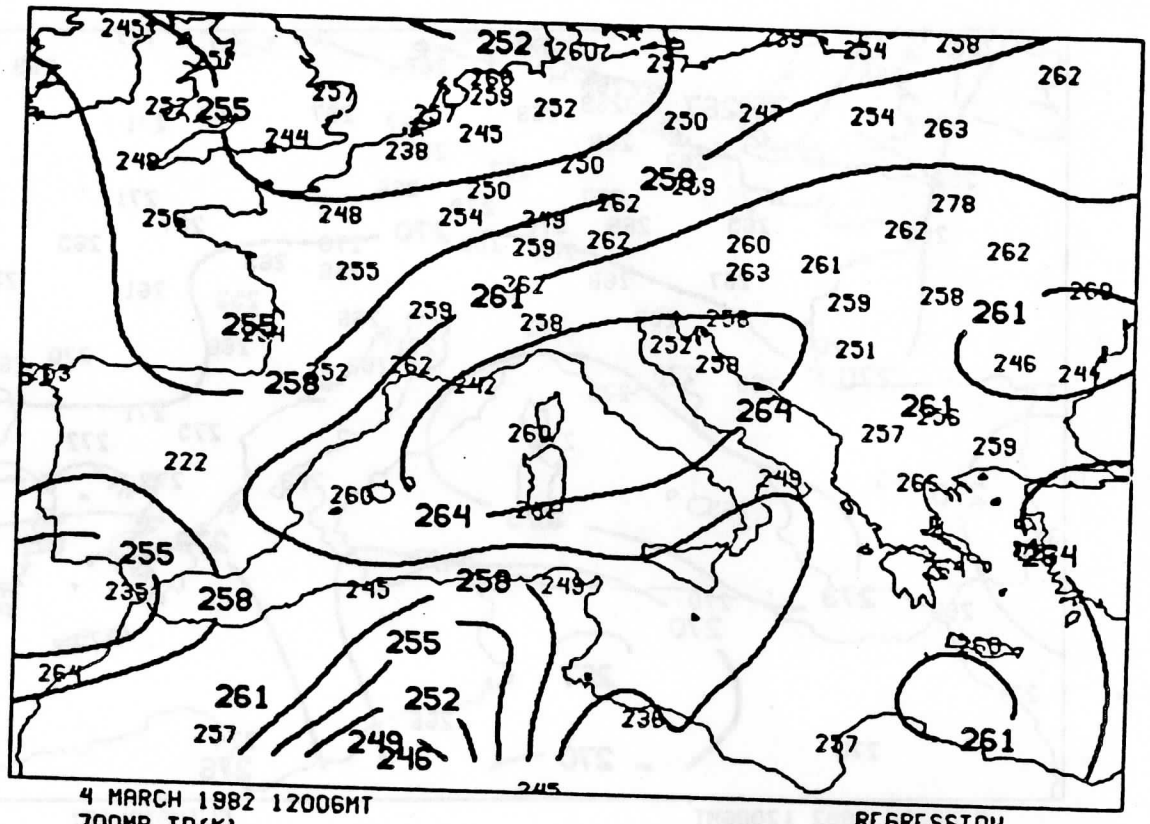

(a)

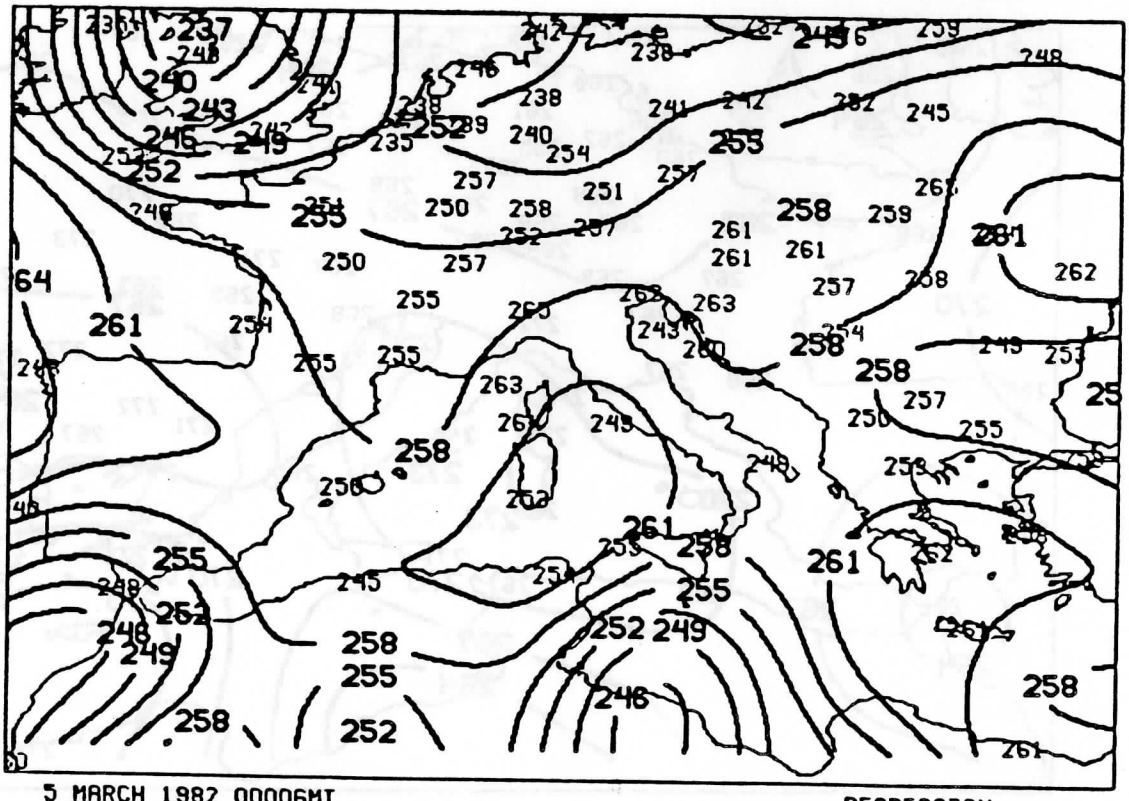

(c)

Figure 6: Analyses of TOVS retrievals (solid contours).

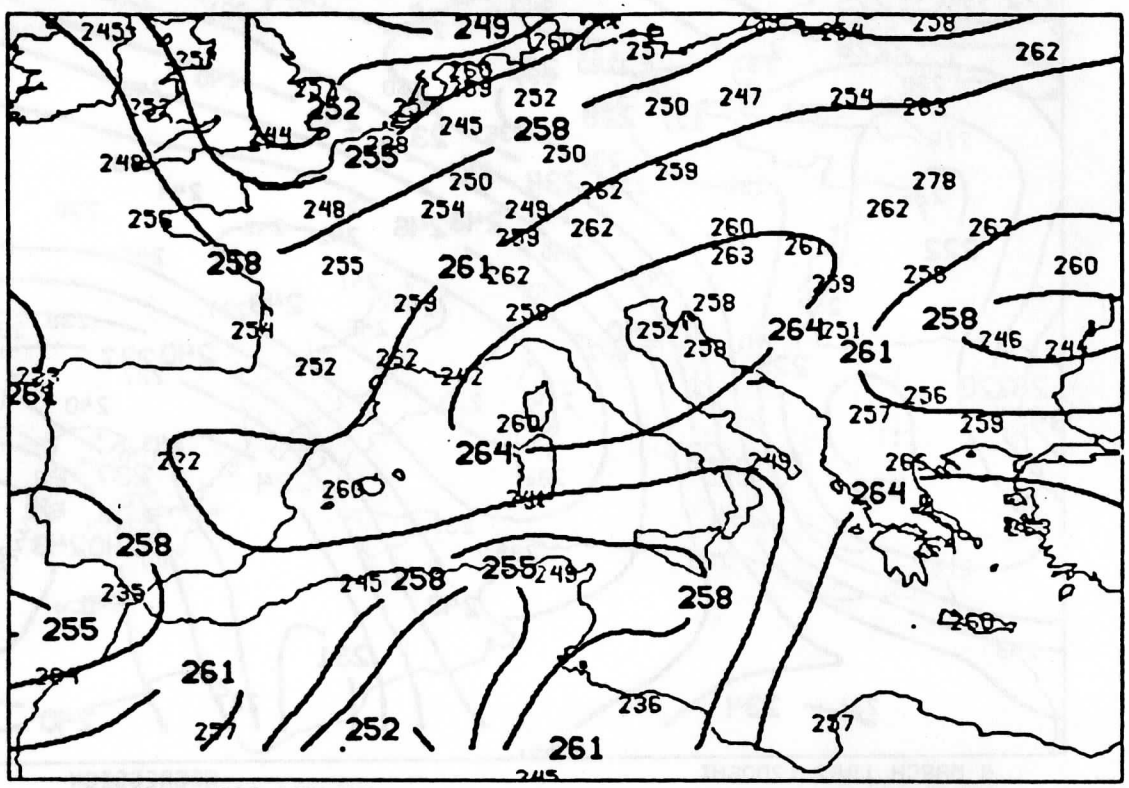

(b)

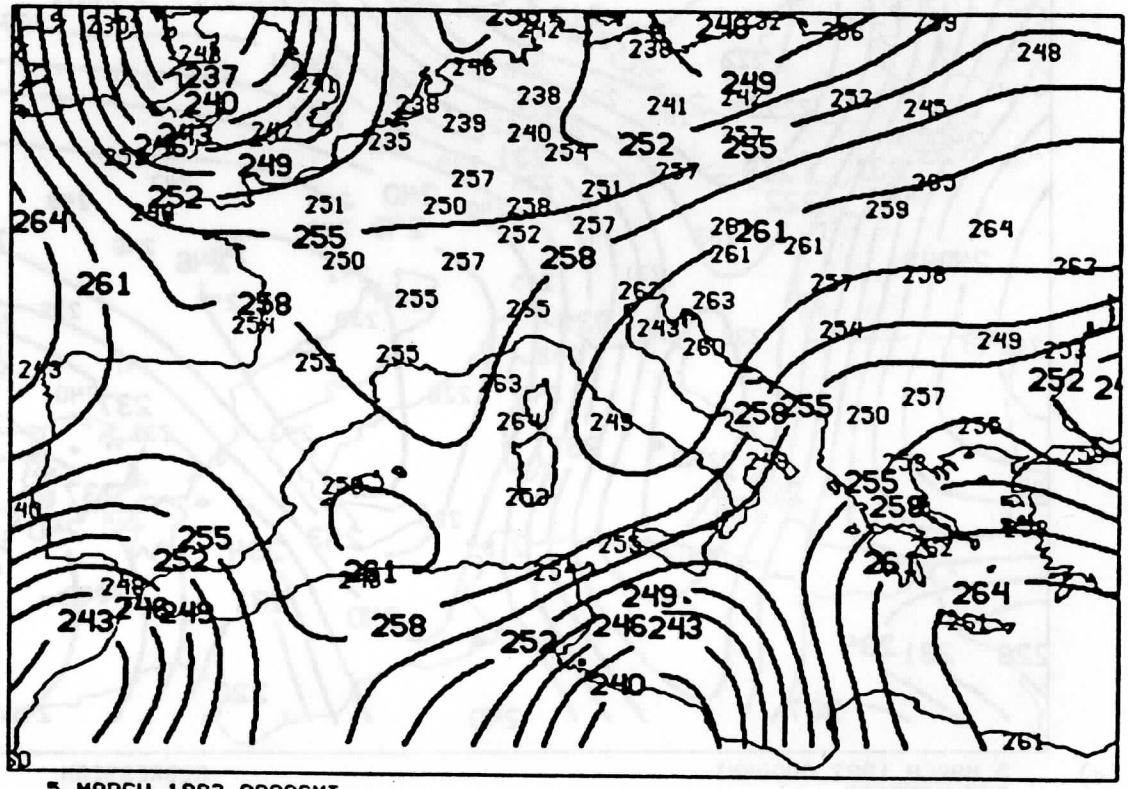

(d)

Figure 6: Analyses of TOVS retrievals (solid contours).

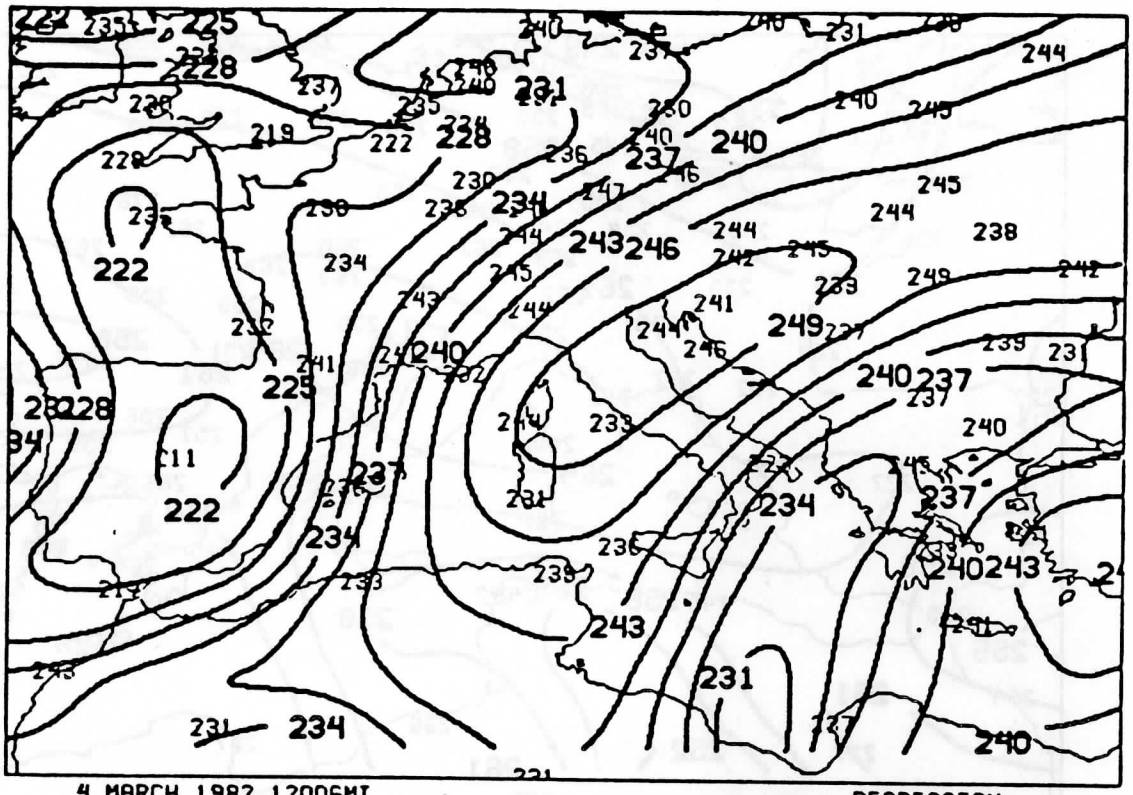

(a)

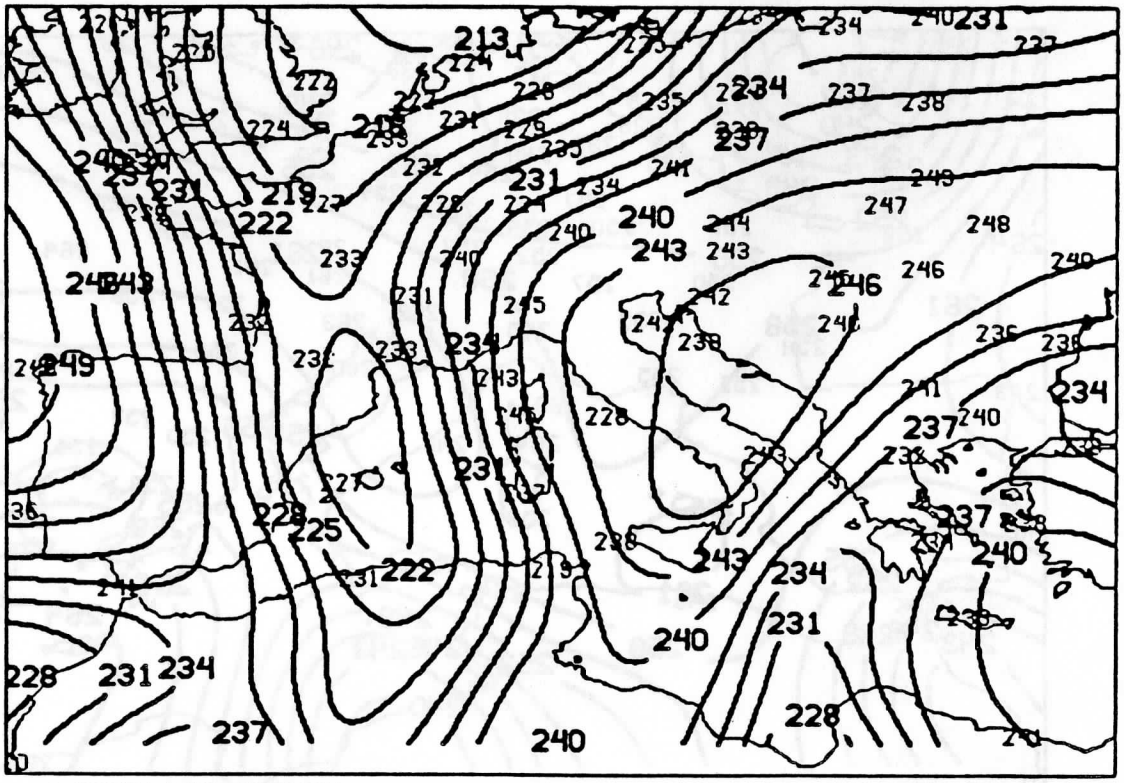

(c)

Figure 7: Analyses of TOVS retrievals (solid contours).

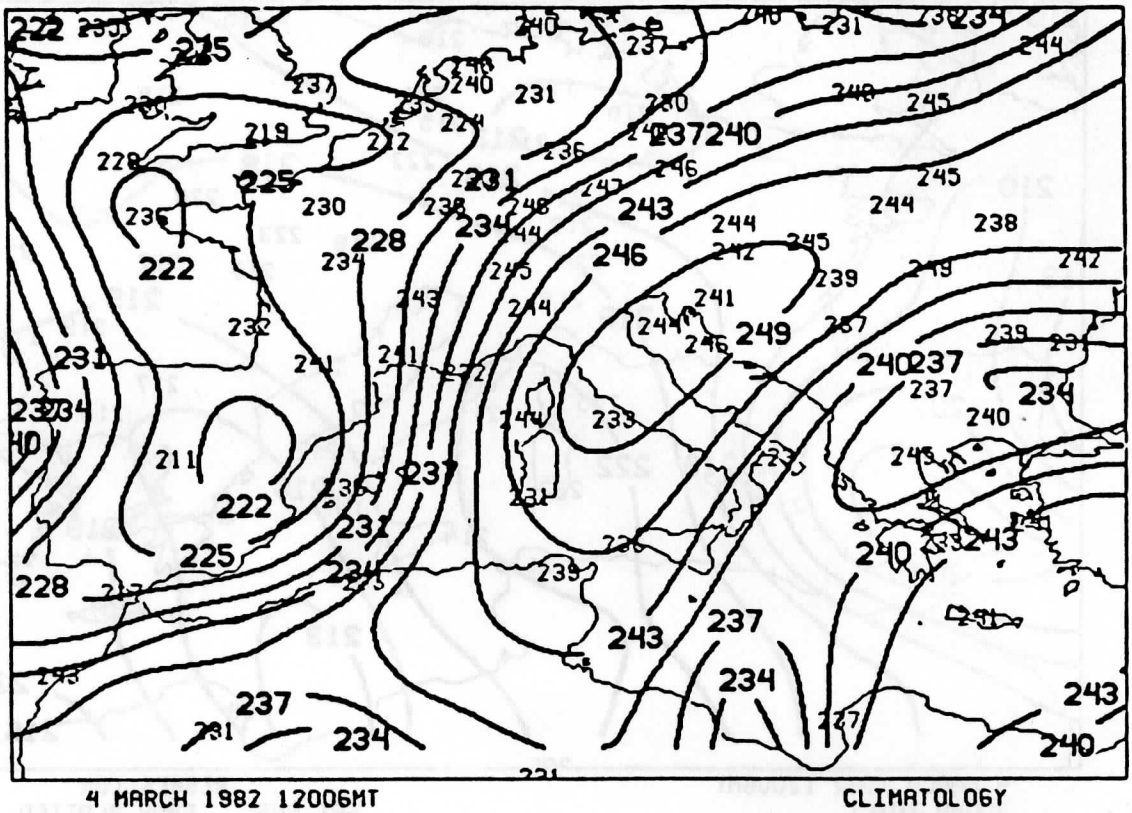

(b)

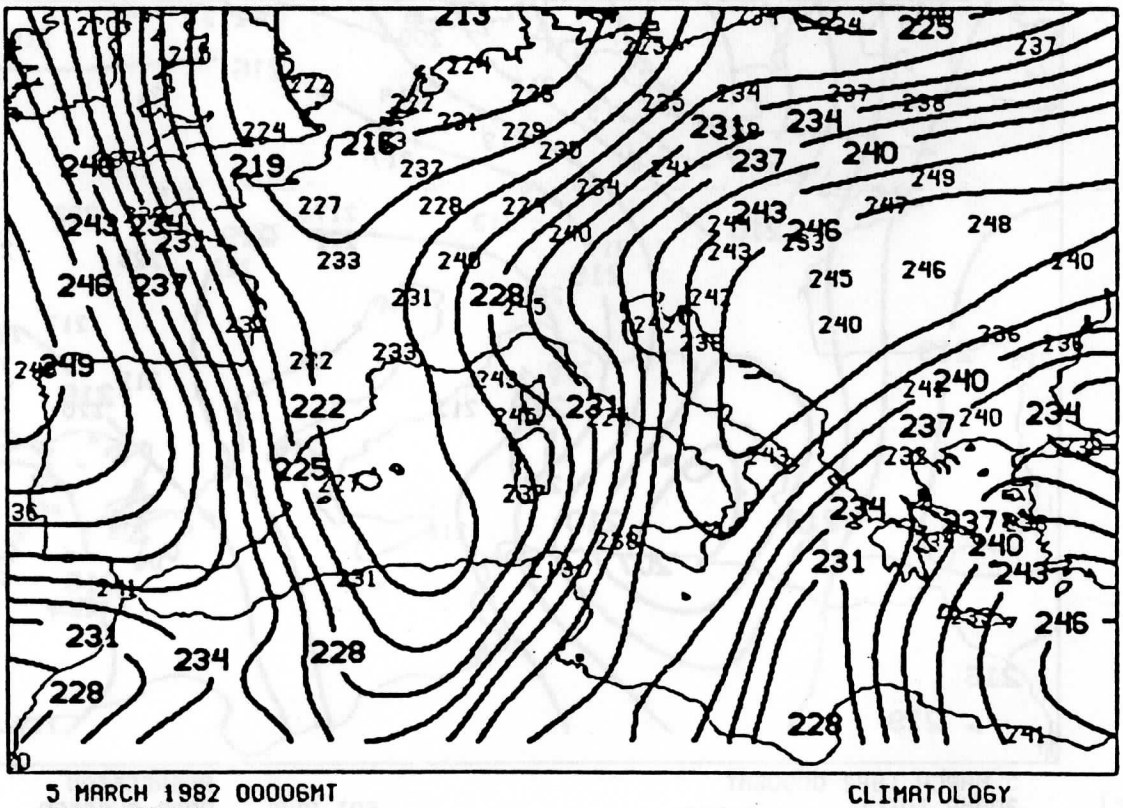

(d)

Figure 7: Analyses of TOVS retrievals (solid contours).

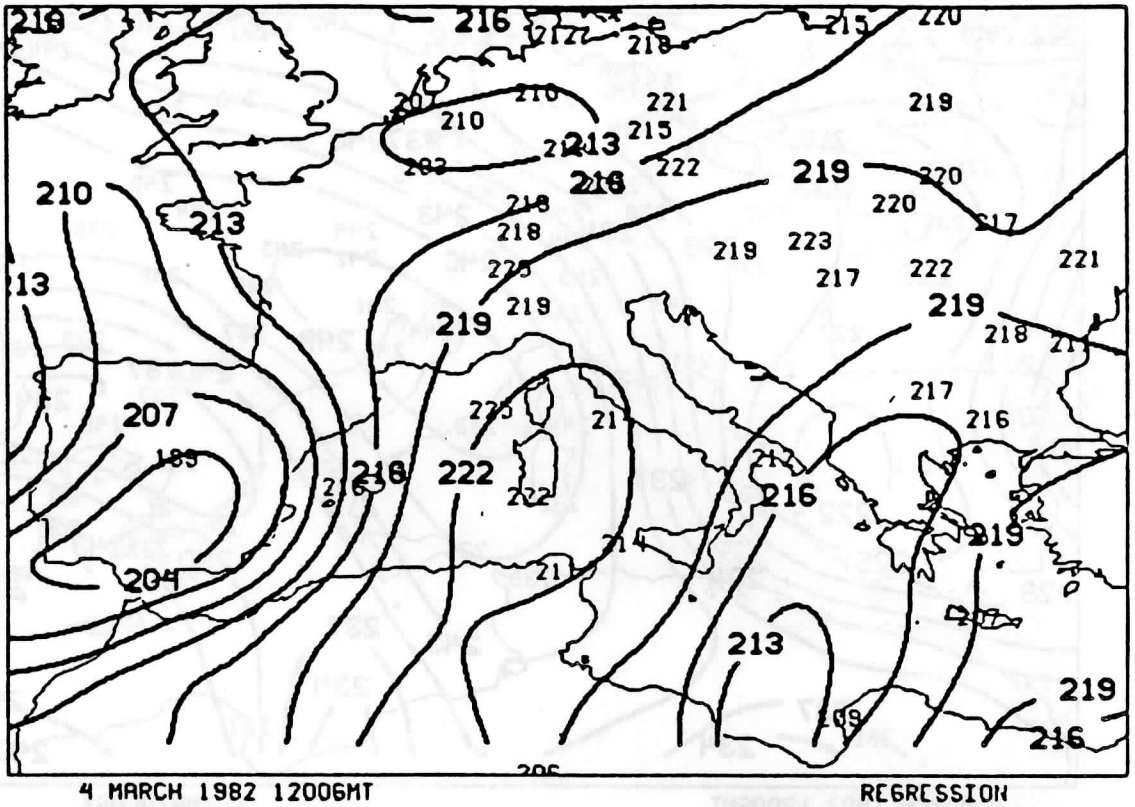

(a)

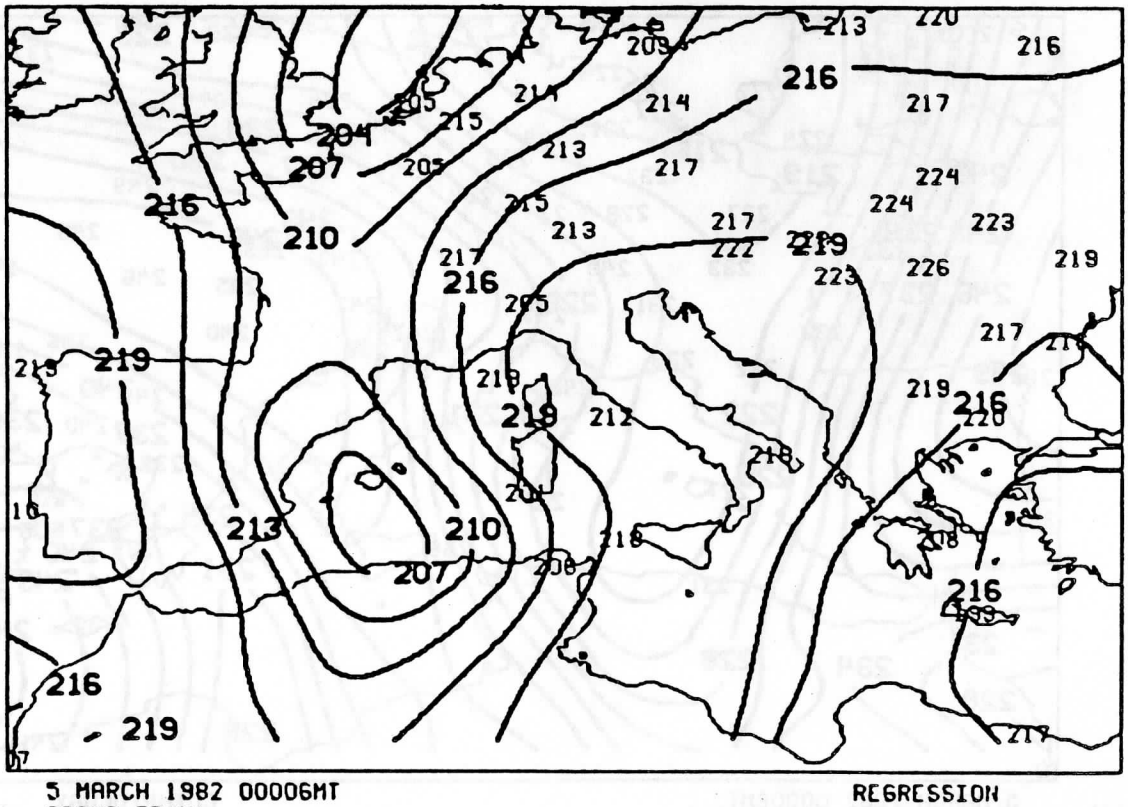

(c)

Figure 8: Analyses of TOVS retrievals (solid contours).

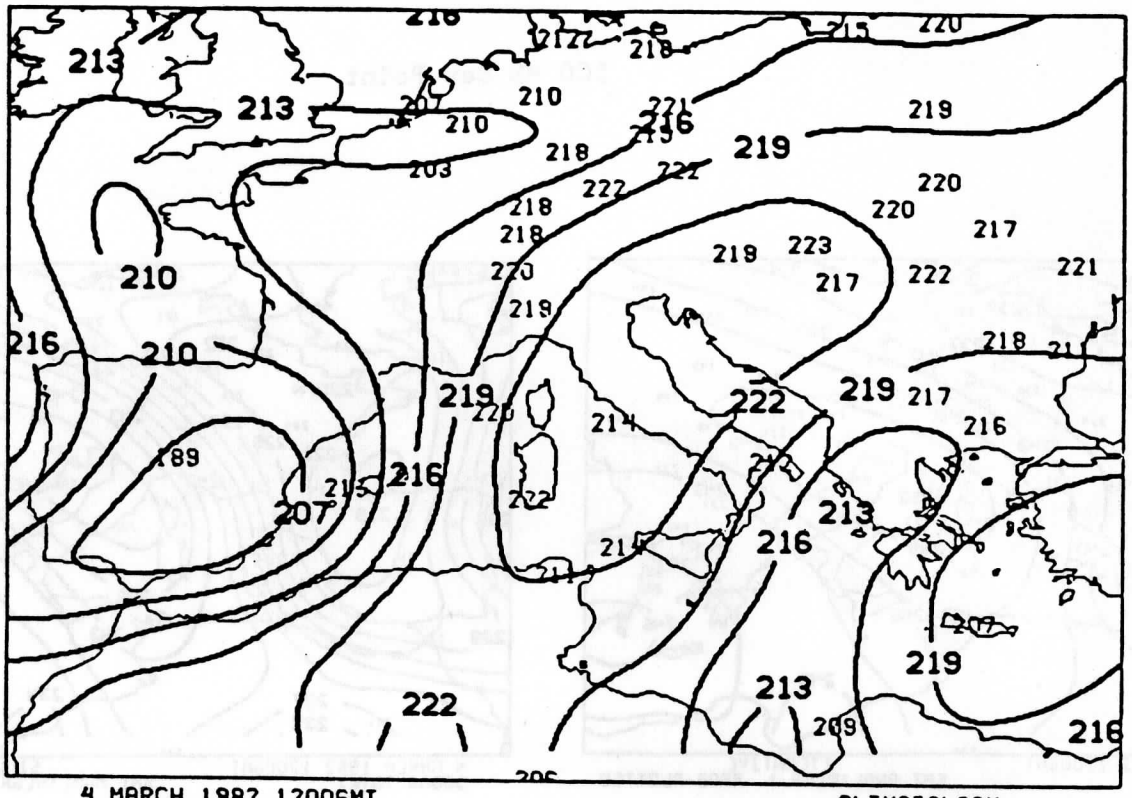

(b)

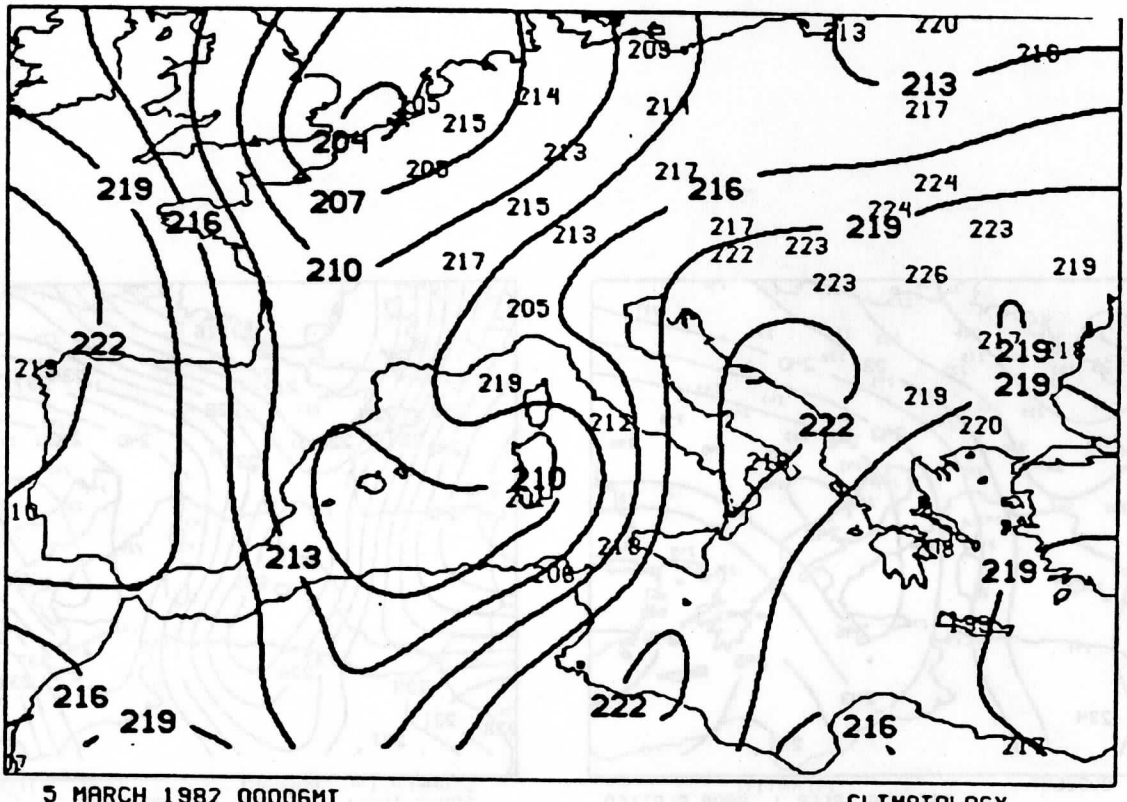

(d)

Figure 8: Analyses of TOVS retrievals (solid contours).

500 MB Dew Point

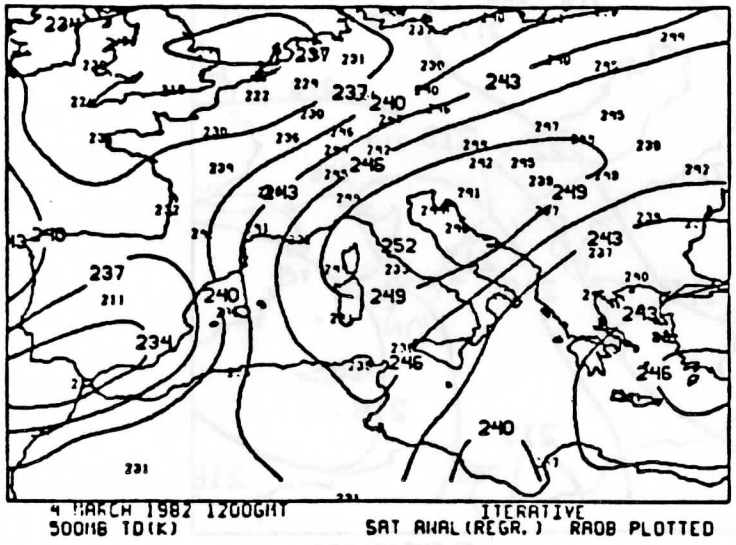

Simultaneous Mar 4

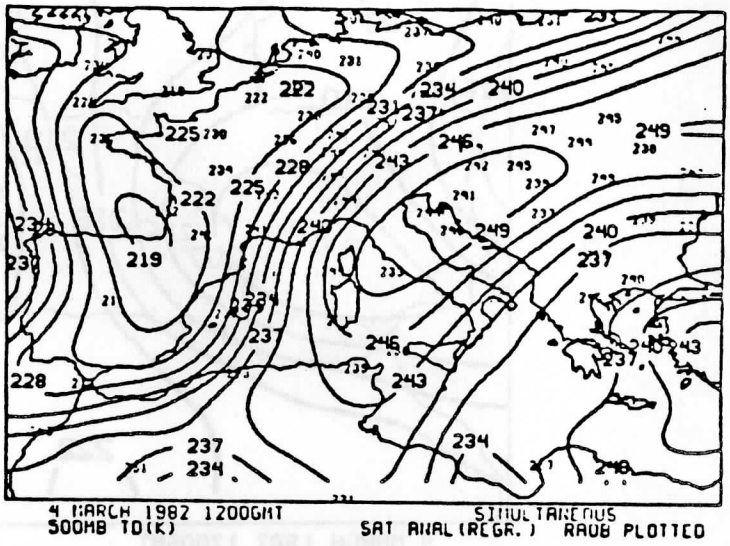

Iterative Mar 4

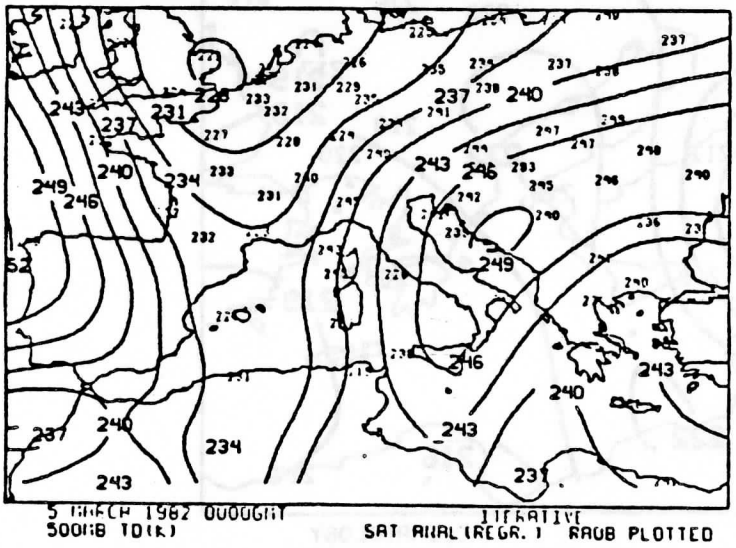

Simultaneous Mar 5

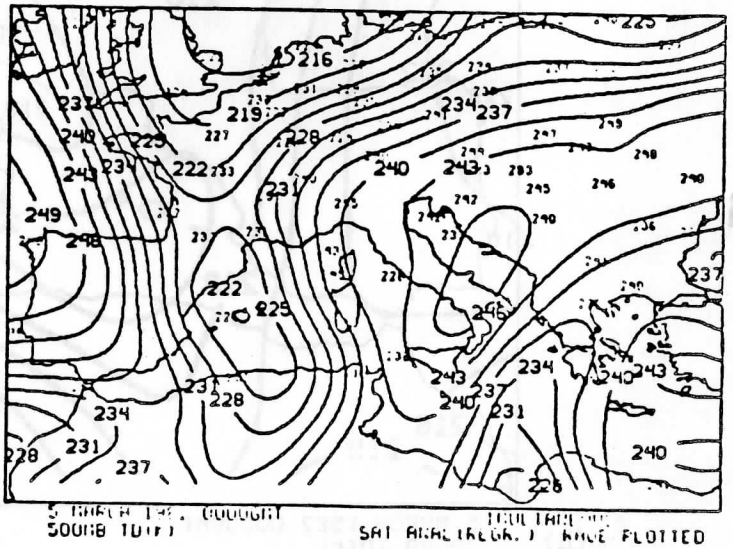

Iterative Mar 5

Figure 9

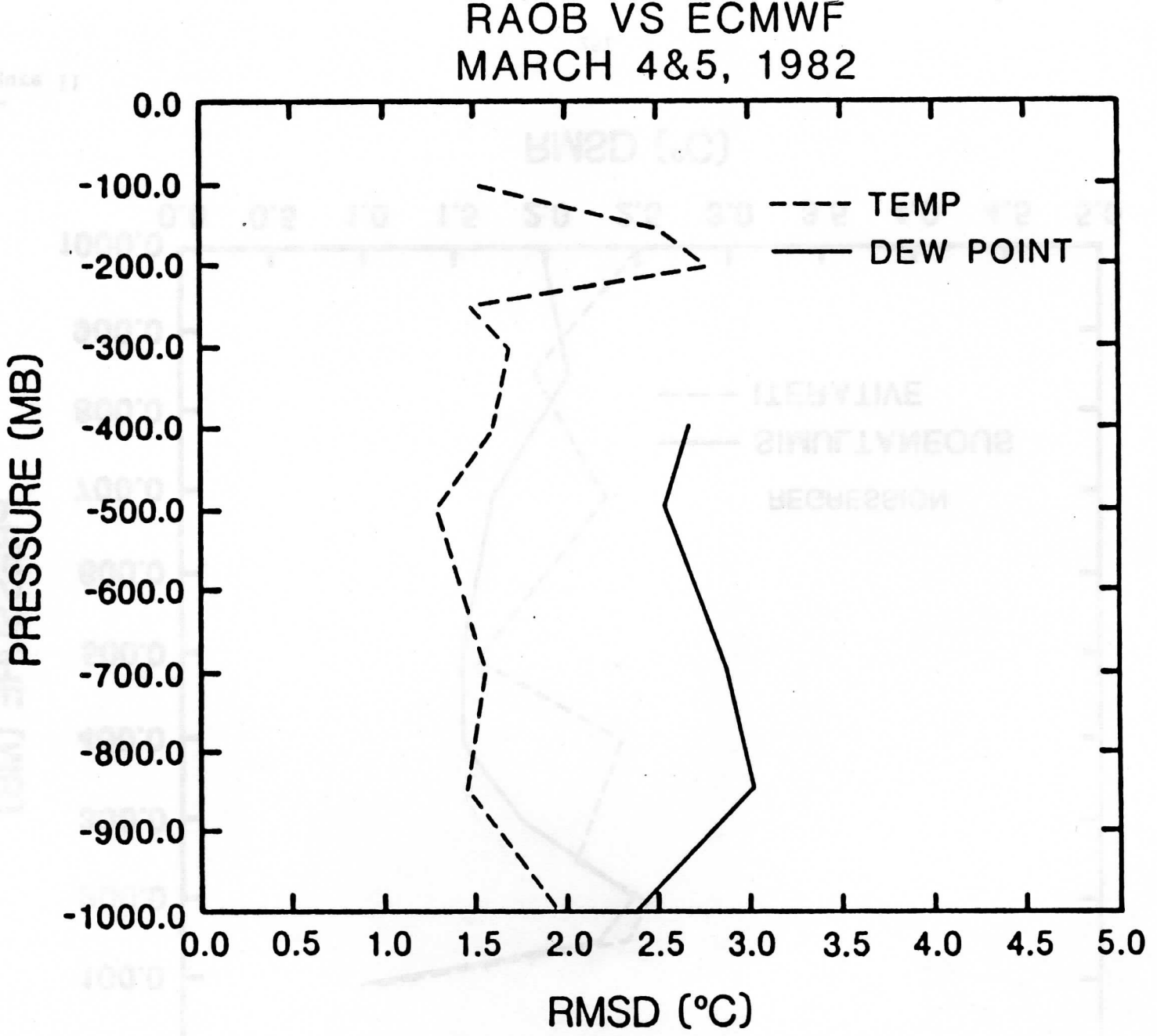
RAOB VS ECMWF
MARCH 4&5, 1982
0.0
-100.0
-200.0
-300.0
-400.0
-500.0
-600.0
-700.0
-800.0
-900.0
-1000.0
PRESSURE (MB)
TEMP
DEW POINT
0.0
0.5
1.0
1.5
2.0
2.5
3.0
3.5
4.0
4.5
5.0
RMSD (°C)

Figure 10

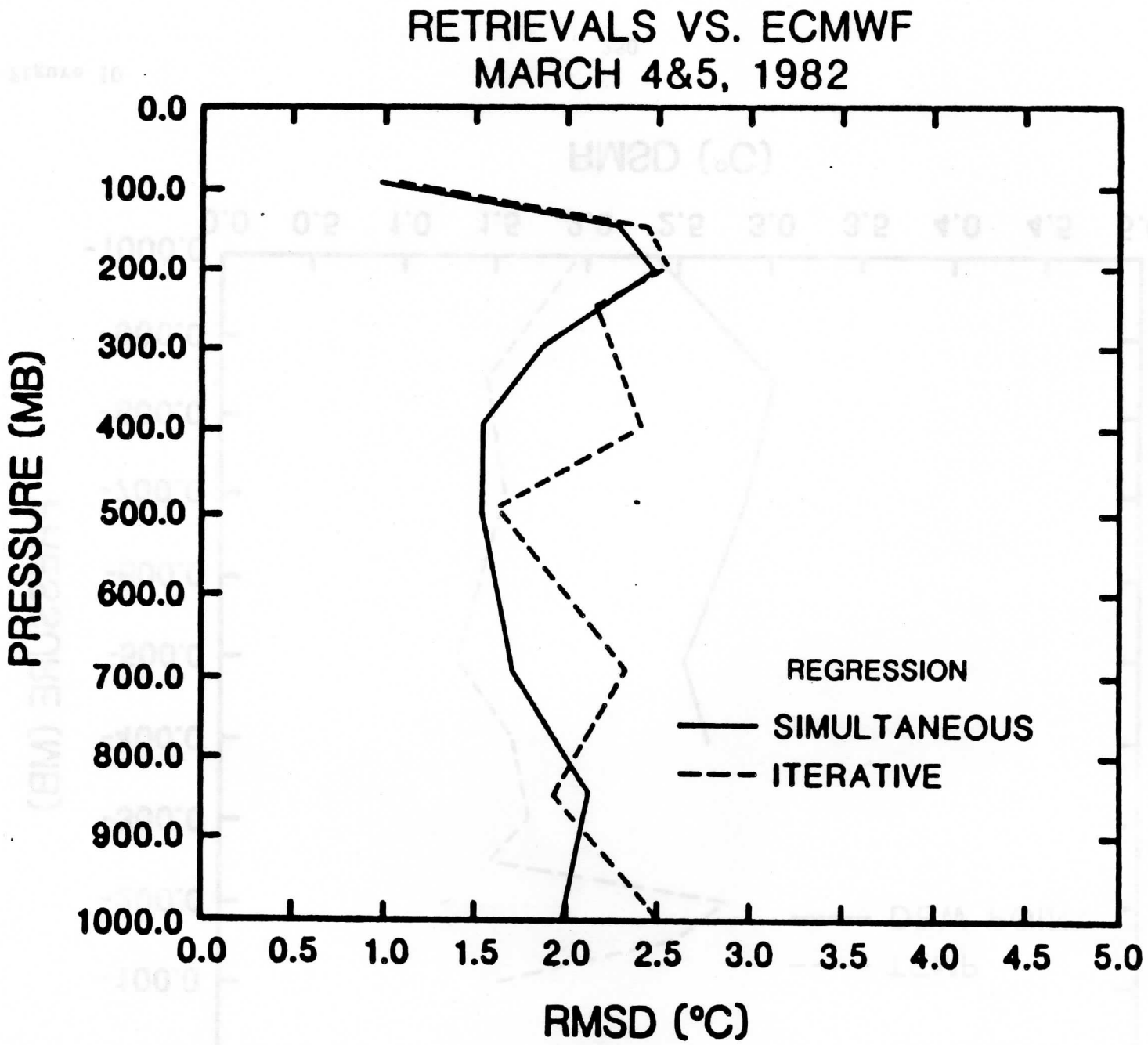
RETRIEVALS VS. ECMWF
MARCH 4&5, 1982
PRESSURE (MB)
0.0
100.0
200.0
300.0
400.0
500.0
600.0
700.0
800.0
900.0
1000.0
0.0
0.5
1.0
1.5
2.0
2.5
3.0
3.5
4.0
4.5
5.0
RMSD (°C)
REGRESSION
SIMULTANEOUS
ITERATIVE

Figure 11

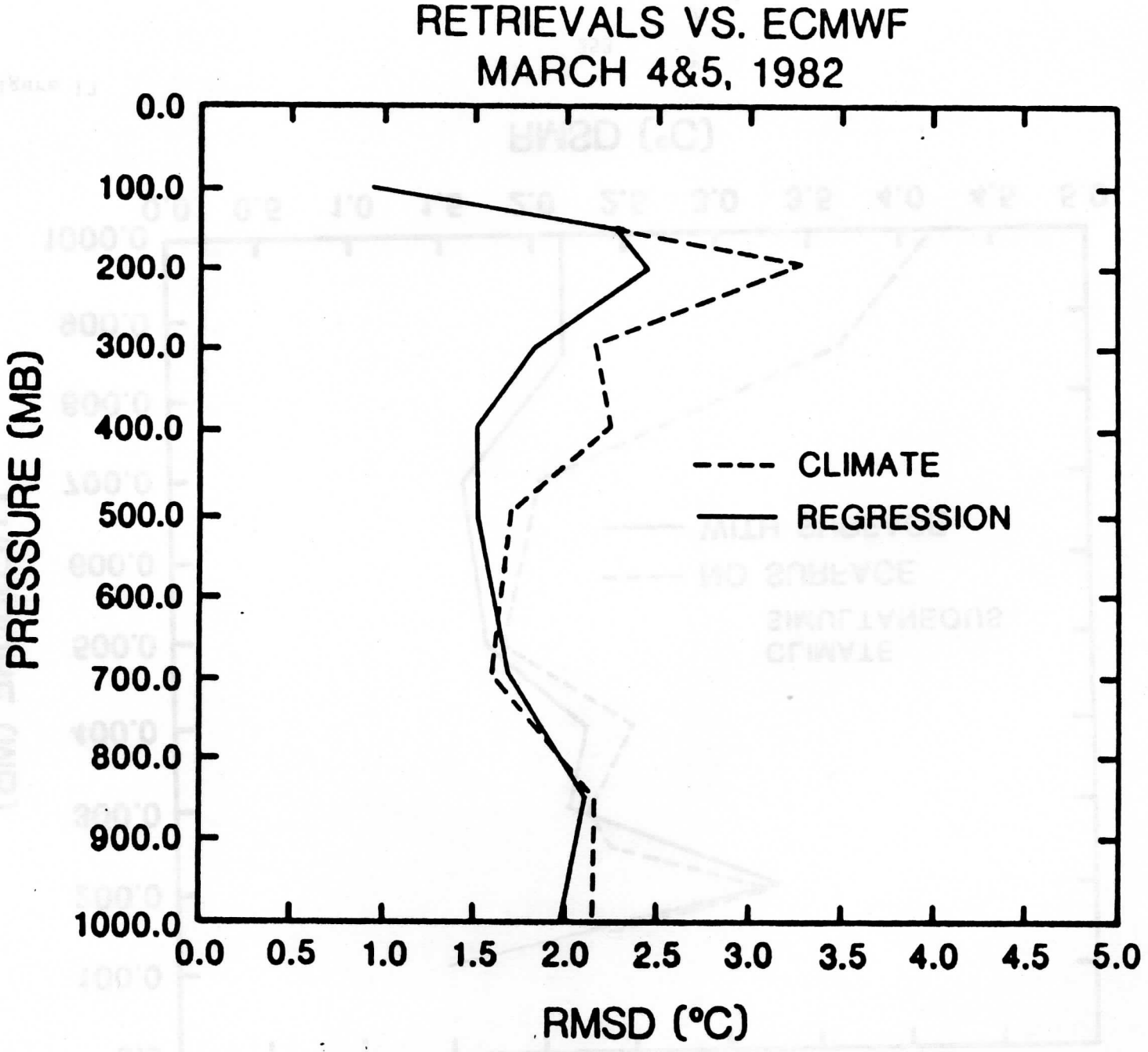
RETRIEVALS VS. ECMWF
MARCH 4&5, 1982
PRESSURE (MB)
0.0
100.0
200.0
300.0
400.0
500.0
600.0
700.0
800.0
900.0
1000.0
CLIMATE
REGRESSION
0.0
0.5
1.0
1.5
2.0
2.5
3.0
3.5
4.0
4.5
5.0
RMSD (°C)

Figure 12

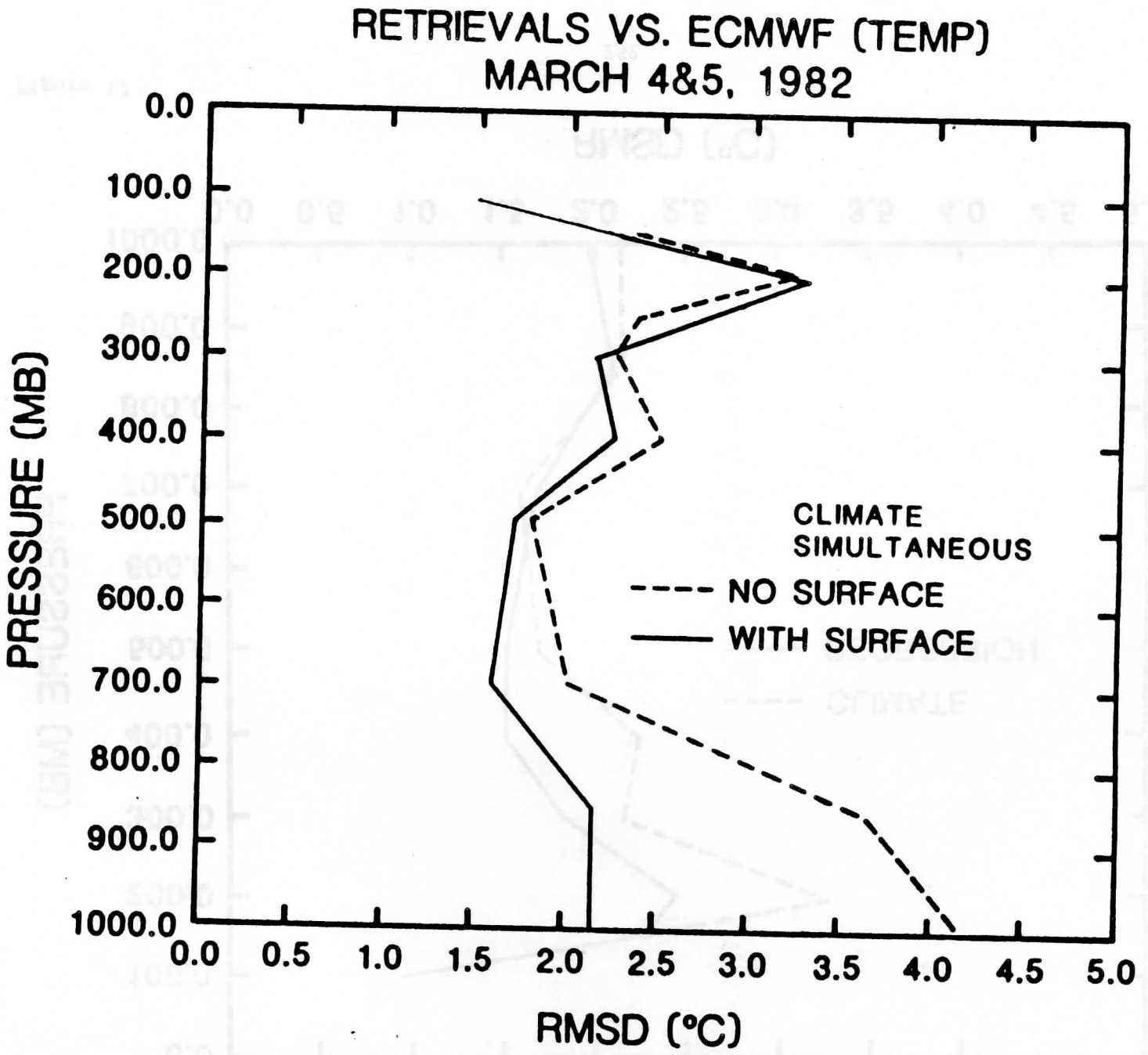
RETRIEVALS VS. ECMWF (TEMP)
MARCH 4&5, 1982
PRESSURE (MB)
0.0
100.0
200.0
300.0
400.0
500.0
600.0
700.0
800.0
900.0
1000.0
0.0
0.5
1.0
1.5
2.0
2.5
3.0
3.5
4.0
4.5
5.0
RMSD (°C)
CLIMATE
SIMULTANEOUS
NO SURFACE
WITH SURFACE

Figure 13

TOVS TRANSMITTANCES: IS THERE AN OPTIMUM SPECTROSCOPIC DATA SET?

D. Spänkuch and W. Döhler

Meteorological Service of the GDR
Potsdam, German Democratic Republic

1. INTRODUCTION

Physical retrieval methods require in contrast to simple regression methods explicitly the knowledge of atmospheric transmittances. Inaccuracies in these transmittances enhance retrieval errors. This fact is demonstrated in Figure 1 taken from Spänkuch et al. (1981 a,b) where the bias in temperature retrieval is shown for some reference cases. The full line represents the bias using the most appropriate atmospheric transmittances calculated line-by-line on the basis of in situ measurements. The dashed line represents the bias caused by not taking into account the effect of trace gases. Figure 1 is the result of comparisons of retrievals of interferometric data in the the 15 µm region (Spänkuch 1980) with colocated radiosonde measurements for cloudless cases in midlatitudes. The use of the most appropriate transmittance reduces the retrieval error in altitude regions with weighting function peaks (troposphere with the exception of the tropopause region, lower stratosphere).

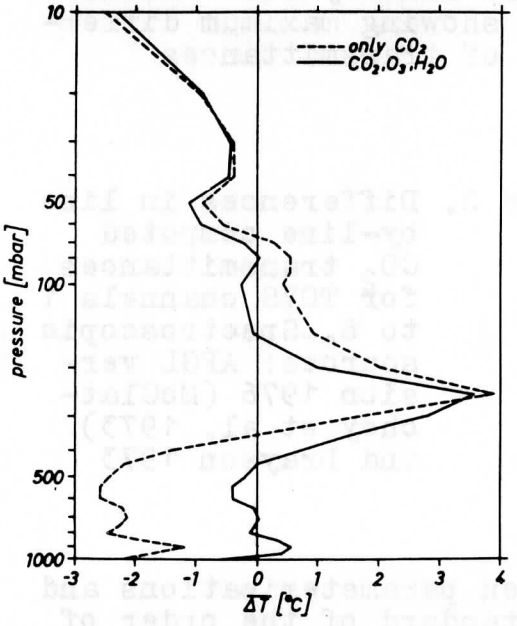

Figure 1. Bias in temperature retrievals using transmittances without (– – –) and(———) trace gases. For the retrievals only the 15 µm channels were used. Meteorological input data for transmittance calculations are from quasisimultaneous radiosonde ascents.

Errors in atmospheric transmittances are of systematic and random nature and cause, therefore, systematic and random retrieval errors. The transmittance error sources are twofold (Kondratyev and Timofeyev 1978). One source is an incorrect radiative transfer model due to incorrect spectroscopic line parameters (line intensity, line shape, half width, temperature dependence and so on) as well as numerical deficiencies (use of approximations, handling of line wings and far lines, and others). The second error source is the incorrect knowledge of that physical parameters responsible for atmospheric emission (concentration of atmospheric gases and aerosols, temperature, clouds). Errors caused by the first source are mainly systematic errors and can be minimized by special experimental and theoretical investigations. The second source produces mainly random errors and is the limiting factor for the accuracy of atmospheric transmittances.

This paper is a contribution to the first source of errors in atmospheric transmittances.

2. TOVS TRANSMITTANCES

The operational use of TOVS data requires a computationally fast and accurate transmittance model (McMillin and Fleming 1976, Weinreb et al. 1981). Such a model can not rely on line-by-line calculations but has to be highly parameterized. The accuracy of this and other parameterizations was checked against line-by-line calculations showing maximum differences of transmittances

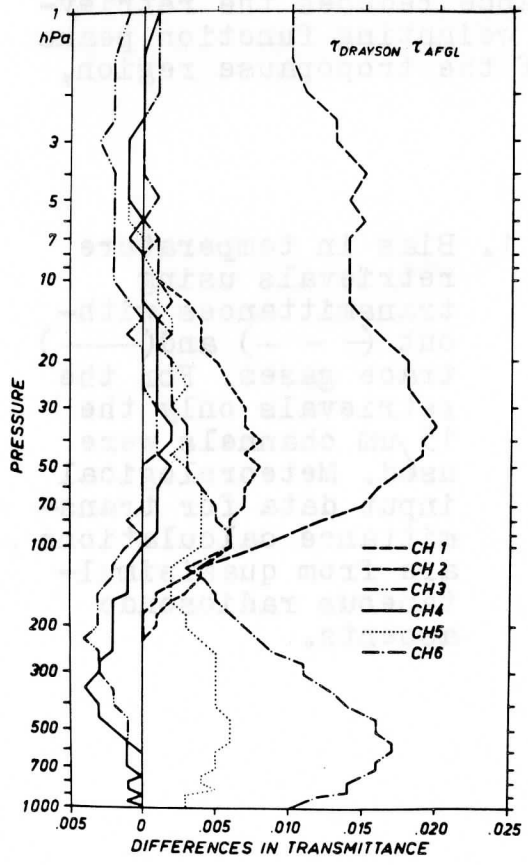

Figure 2. Differences in line by-line computed CO_2 transmittances for TOVS channels 1 to 6. Spectroscopic sources: AFGL version 1976 (McClatchey et al. 1973) and Drayson 1973

between parameterizations and the standard of the order of .001 (McMillin et al. 1980). $\Delta\tau$ of line-by-line calcula-

tions using two different spectroscopic data sources are shown in Figure 2 for the 15 µm temperature retrieval channels. Maximum $\Delta\tau$ are considerably larger between the two -standards' than between the parameterization and one 'standard' and are especially large for TOVS channels 1 (668.5 cm^{-1}) and 6 (733.2 cm^{-1}). That is to say, the uncertainty of the 'standard' is significantly higher than the capability of parameterizations to approximate the standard! Details of the line-by-line calculations based on line data of Drayson (1973) and McClatchey et al. (1973) are given by Spänkuch et al. (1984) and do not consider trace gases. We emphasize once again, that the differences are only caused by the first error source as the same atmospheric input data (midlatitude summer standard atmosphere with zero nadir angle) were used. There is no significant change of $\Delta\tau$ with nadir angle. Central wavenumber ν_o and half-width $\Delta\nu$ of the TOVS channels assumed are given in Table 1 and are only added for completeness.

Table 1: Assumed ν_o and $\Delta\nu$ for TOVS channels

CH	ν_o (cm^{-1})	$\Delta\nu$ (cm^{-1})
1	668.50	4.0
2	680.00	14.0
3	691.56	12.0
4	703.00	20.0
5	716.00	20.0
6	733.20	16.0

3. COMPARISON OF MEASURED AND COMPUTED TRANSMITTANCES FOR HOMOGENEOUS CONDITIONS

To improve the accuracy of the 'standard' means to solve the problem of the most appropriate line data. Spectroscopic line data are not accurate in the proper sense of the word due to the semiempiric character of line absorption theory and the necessary tuning to experimental data. Hence, this problem can only be solved by comparing computed transmittances with measured ones at wellknown conditions. The comparison for homogeneous conditions is the first necessary step. Without going into detail we present in Figure 3 the averaged systematic differences between measured (τ^{exp}) and calculated CO_2 transmittances (τ^{calc})

$$\overline{\Delta\tau} = \frac{1}{N}\sum_{i=1}^{N}\left(\tau^{exp} - \tau^{calc}\right)$$

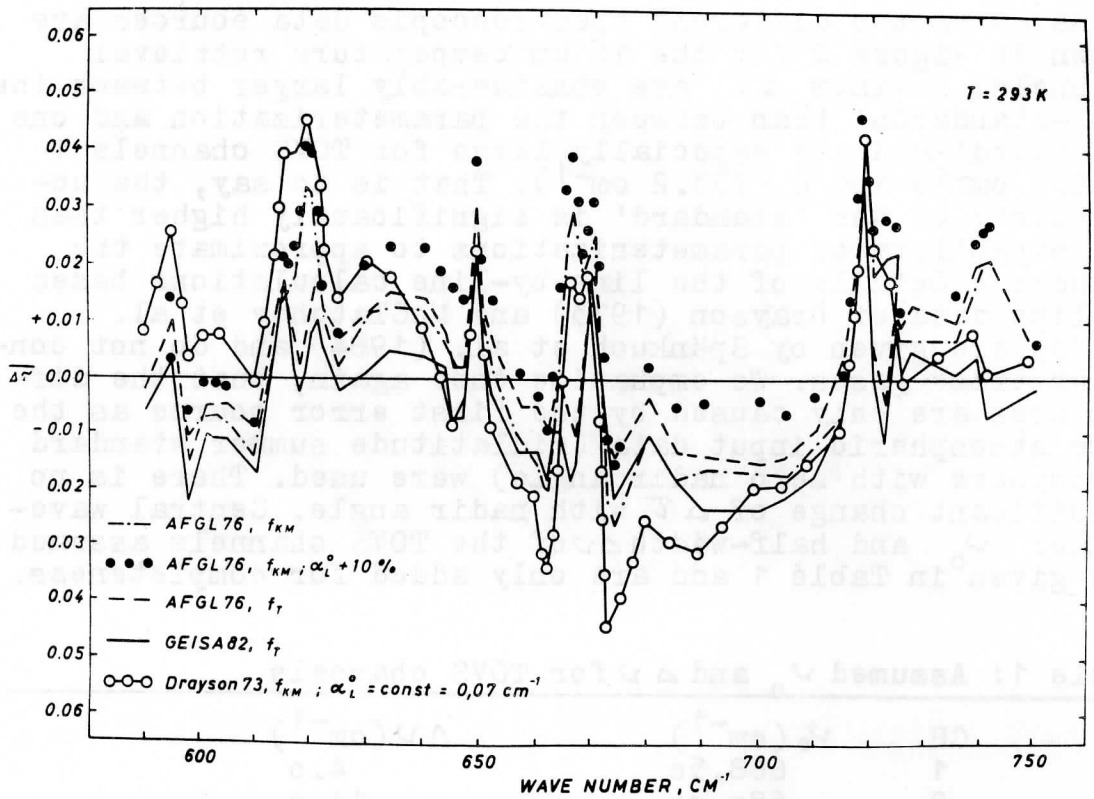

Figure 3. Averaged differences between line-by-line computed (τ^{calc}) and experimental (τ^{exp}) CO_2 transmittances for homogeneous conditions (see Döhler and Spänkuch 1985). T = 293 K
Spectroscopic sources: AFGL version 1976 (McClatchey et al. 1973), GEISA 1982 (Chedin et al. 1982) and Drayson 1973. f_{KM} and f_T = line shape after Kunde and Maguire (1974) and Dokuchaev et al. (1982), the latter one includes the effect of line interference; α_L^o - Lorentzian half-width.

versus wavenumber from 590 cm^{-1} to 750 cm^{-1} with N = 8 number of experimental homogeneous conditions for T = 293 K. Theoretical transmittances were calculated for a variety of input data including different line sources (AFGL 1976, GEISA 1982, Drayson 1973), line shapes f and half-widths α_L^o. Details are given in Döhler and Spänkuch (1985). Comparisons made for stratospheric temperatures (T = 213 K), too, give similar results and demonstrate that the temperature dependence of spectroscopic data is well reflected. TOVS channel 1 to 6 lie on the right half of Figure 3. Note that the differences of Figure 2 are reflected by the differences between the curves of Figure 3 (different spectroscopic sources) but not by the difference against the measured values. Figure 3 demonstrates that empirical adjustments (e.g. the enhancement of half-width by 10% for

AFGL version 1976) can considerably reduce the discrepancy of theoretical against experimental transmittances in some spectral intervals (670 - 715 cm^{-1}). There are, on the other hand, spectral intervals (e.g. around the band center 668 cm^{-1}) where only the inclusion of additional physical effects (line interference, considered in f_T) is able to reduce this discrepancy to an acceptable degree. For other regions the spectroscopic data have to be corrected. This is the case for the 10001 - 01101 band intensity which is too large by about 10% (Clough 1984).

4. CONCLUSIONS

(i) Differences in line-by-line computed atmospheric transmittances using different spectroscopic input data are considerably larger as differences between modern parameterizations of transmittances and line-by-line computations.
(ii) Improvements in spectroscopic line parameters can be done on the basis of comparisons between calculated and measured atmospheric transmittances for well-defined conditions.
(iii) Those improvements include corrections in line data by empirical adjustment as well as the consideration of additional physical processes.
(iv) The question for an optimum spectroscopic data set of the presently available sets can at present not definitely be answered. The most appropriate spectroscopic data source for one spectral interval is not necessarily the most appropriate one for another interval (see Figure 3).

5. REFERENCES

Chedin, A., Husson, N., Scott, N.A., Jobard, I., Cohen-Hallaleh, I. and A. Berroir, 1982: La banque de données GEISA. Description et logiciel d'utilisation. LMD du C.N.R.S., Note Interne.

Clough, S.A., 1984: Private communication

Döhler, W. and D. Spänkuch, 1985: New comparison between measured and calculated CO_2 transmittances in the 15 /um region for homogeneous conditions. In G. Fiocco (ed.): Proc. International Radiation Symposium, Perugia, Italy, August 1984

Dokuchaev, A.B., Filippov, N.N. and Tonkov, M.V., 1982: Line interference in ν_3 rotational-vibrational band of N_2O in the strong interaction approximation. Physica scripta 25, 378 - 380

Drayson, S.R., 1973: A listing of wavenumbers and intensities of carbon dioxide absorption lines between 12 and 20 /um . Techn. Rep. 036350 - 4 - T, Univ. of Michigan, Ann Arbor

Kondratyev, K. Ya. and Yu. M. Timofeyev, 1978: Meteorologicheskoe zondirovanie atmosfery iz kosmosa. Gidrometeoizdat Leningrad, pp. 118

Kunde, V.G. and W.C. Maguire, 1974: Direct integration transmittance model. J. Quant. Spectrosc. Radiat. Transfer, 14, 803 - 817

Mc Clatchey, R.A., Benedict, W.S., Clough, S.A., Burch, D. E., Calfee, R.F., Fox, K., Rothman, L.S. and J.S. Garing, 1973: AFCRL atmospheric absorption line parameters compilation. Environm. Res. Rep. 434, AFCRL - TR-73 - 0096, Bedford, Mass.

Mc Millin, L.M. and H.E. Fleming, 1976: Atmospheric transmittance of an absorbing gas: a computationally fast and accurate transmittance model for absorbing gases with constant mixing ratios in inhomogeneous atmospheres. Appl. Opt. 15, 358 - 363

Mc Millin, L.M., H.E. Fleming, A. Arking and D. Chesters, 1980: Accuracies of three computationally efficient algorithms for computing atmospheric transmittances. Appl. Opt. 19, 2267 - 2269

Spänkuch, D., 1980: Arbeiten des Meteorologischen Dienstes der DDR auf dem Gebiet der indirekten Sondierung. Z.f. Meteorologie 30, 205 - 214

Spänkuch, D., W. Döhler and J. Güldner, 1981a: Some aspects of temperature sounding of the atmosphere. Adv. Space Res., 1, No. 4, 239 - 243

Spänkuch, D., W. Döhler and J. Güldner, 1981b: Einige Aspekte der thermischen Sondierung der Atmosphäre für den Bereich von 15 /um . Z.f. Meteorologie 31, 3 - 13

Spänkuch, D., W. Döhler, and J. Güldner, 1984: Comments on TOVS transmittances. The Technical Proceedings of the First International TOVS Study Conference, Igls, Austria, 29 August - 2 September 1983 (ed. W.P. Menzel), 279 - 284

Weinreb, M.P., Fleming, H.E., McMillin, L.M. and A.C. Neuendorffer,1981: Transmittances for the TIROS Operational Vertical Sounder, NOAA Techn. Rep. NESS 85, Washington, D.C.

FIRST GUESS DEPENDENCE OF PHYSICALLY BASED TEMPERATURE-HUMIDITY RETRIEVALS FROM HIRS2/MSU DATA

J. Susskind and D. Reuter
Goddard Laboratory for Atmospheres
Code 611
NASA/Goddard Space Flight Center
Greenbelt MD 20771

and

Andrew Pursch
Sigma Data Services Corp.

1. INTRODUCTION

Physical retrievals of temperature and humidity profiles from atmospheric sounders such as HIRS2/MSU have a number of advantages over purely statistical approaches. Most significantly they allow directly for the incorporation of factors affecting the radiances, other than atmospheric temperature humidity profiles, such as surface properties, zenith angle of observation, and most important of all, clouds. As shown in Susskind et al., 1984, the GLA (formerly called GLAS) physical retrieval scheme produces temperature fields which do not degrade appreciably with increasing cloudiness. In addition, the analysis method allows for determination of surface properties and cloud fields from the data.

Another advantage of physical retrievals is the ability to incorporate first guess information into the retrieval process. This is potentially helpful information if the first guess is good and potentially harmful information if the first guess is poor. A good retrieval scheme should have the property that significant changes can be made to improve a very poor first guess but only minor changes should be made to an excellent first guess. Indeed, a question often asked about physical retrievals utilizing a first guess is how much of the result comes from data and how much from the guess.

In this study, temperature humidity retrievals over the ALPEX region were done for two successive overpasses of NOAA 7 on roughly March 4 12Z and March 5 0Z 1982. This period was characterized by a rapidly changing synoptic situation with a sharp trough moving to the east. Three sets of retrievals were done for each synoptic period using different initial guess fields. The first initial guess field was a 24 hour lagged NMC analysis, which is an extremely poor representation of the actual synoptic situation. The second initial guess field was the NMC analysis at the closest synoptic time to the flight overpass, which might be taken as "almost truth", the almost arising both because the analysis is not perfect and because of a time difference between the satellite overpasses and the analysis time. The third guess was a forecast for the region made from an analysis guess 6 hours

hours earlier using the GLA forecast analysis system (Baker et al.,1984). This guess is the same as that used routinely in the GLA processing of global fields from HIRS2/MSU data.

Ideally, the three sets of results should look very much like each other and like the concurrent NMC analysis, while representing a significant improvement over the lagged analysis first guess and perhaps a minor improvement over the six hour forecast. One does not expect the three sets of retrievals to be identical, for that would mean that the retrievals are totally independent of the guess.

The temperature retrievals are done in a manner very similar to that described in Susskind et al. (1984). Modifications to the system as well as results comparing the thickness fields, will be described in the next section. The humidity retrieval algorithm, which has been recently developed, together with the results comparing the humidity fields, will be shown in the third section.

The humidity retrievals at this point are done subsequent to the temperature retrievals, that is, the retrieved temperature profiles influence the results of the humidity retrievals, but the retrieved humidity profiles do not influence the retrieved temperature profiles. The first guess relative humidity profile is held constant during the temperature analysis. This does not have a major effect on the retrieved temperature profiles but does introduce a subtle first guess dependence which might be reduced (or amplified) if the modified relative humidities are allowed to affect the temperature retrievals. Research on this will be done in the future.

2.1 Determination of atmospheric temperature profiles

The retrievals of atmospheric and surface temperatures were done almost exactly as in Susskind et al. (1984) with three exceptions, retrieval density, cloud filtering algorithm, and rejection criterion. Retrievals for this study were run one retrieval per 4 x 4 array of HIRS2 spots. This array was broken into four 2 x 2 spot sub-arrays each divided into two "fields of view" constructed by averaging the radiances for each channel for the two spots with the largest 11 μm window radiances, called field of view 1, and with the smallest 11 μm window radiances, called field of view 2. This is the finest resolution with which we feel HIRS2 retrievals can be done. One retrieval can be done in each of the four sub-arrays. In this study, only one retrieval was done in a 4 x 4 array of spots, located in the 2 x 2 sub-array containing the highest 11 μm window field of view radiance in the array. The closest MSU spot to the center of the sub-array was taken to be representative of the measurement for the sub-array. No interpolation of MSU radiances was done because of the large zenith angle dependence of the MSU observations.

Given radiances for fields of view 1 and 2 in a sub-array, $R_{i,1}$ and $R_{i,2}$, clear column radiances for channel i, $\tilde{R}_i$ are reconstructed, much as in Susskind et al. (1984), according to

$$\tilde{R}_i = R_{i,1} + \eta(R_{i,1} - R_{i,2}) \quad (1)$$

where $R_{i,1}$ is the observed radiance for channel i in the field of view having the larger 11 μm radiance, and $R_{i,2}$ is the observation of channel i in the second field of view. If $R_{i,CLR}$ is known for a given channel, then η can be solved for according to

$$\eta = \frac{R_{i,CLR} - R_{i,1}}{R_{i,1} - R_{i,2}} \quad (2)$$

Since $\eta = \alpha_1/(\alpha_1 - \alpha_2)$, it should not be dependent on the channel used. In Susskind et al. (1984), η was determined by combined use of HIRS2 channel 13 and MSU channel 2. $R^N_{13,CLR}$ is computed in each iteration (N) using the Nth iterative temperature profile and ground temperature. If the N^{th} guess is too warm (or cold), $R^{(N)}_{i,CLR}$ would be too large (or small). The effect on the computed brightness temperature of channel 13 of a bias in the temperature profile in the troposphere is accounted for, to first order, by modifying the brightness temperature according to

$$\theta'_{13} = \theta^N_{13,CLR} + \theta_{M2} - \theta^N_{M2} \quad (3)$$

where $\theta^N_{13,CLR}$ is the equivalent brightness temperature to $R^N_{13,CLR}$, θ_{M2} is the observed brightness temperature in MSU channel 2, which is sensitive to the average tropospheric temperature, and θ^N_{M2} is the computed computed brightness temperature in MSU channel 2. This procedure works reasonably well even though channel 13 is sensitive primarily to radiation mcuh closer to the surface than that of MSU channel 2. η_{13} is then computed according to

$$\eta_{13} = \frac{B_{13}[\theta'_{13}] - R_{13,1}}{R_{13,1} - R_{13,2}} \quad (4)$$

where $B(\theta')$, the black body function of the corrected equivalent brightness temperature, is the corrected estimate of the clear column radiance. While results using equations (1-4) are quite good, it has been found that in cases where the initial guess has a lapse rate error, improved results are obtained by defining η_{14} in an analogous manner to η_{13} in equations (3) and (4) and setting η equal to the average of η_{13} and η_{14} weighted by the square of the difference in radiances for each channel in each field of view:

$$\eta = \frac{\eta_{13}(R_{13,1}-R_{13,2})^2 + \eta_{14}(R_{14,1}-R_{14,2})^2}{(R_{13,1}-R_{13,2})^2 + (R_{14,1}-R_{14,2})^2} \quad (5)$$

Including channel 14 radiances in the determination of η has the effect of utilizing a single infra-red channel with a broader weighting function, more in line with that of the microwave channel, to correct for

cloud effects. Combined use of channels 13 and 14 was especially necessary for NOAA 7 data because the weighting functions for both channels 13 and 14 were shifted lower in the atmosphere relative to TIROS-N and channel 13 provided an even poorer match with MSU channel 2. The procedure gives improved results with TIROS-N data as well.

In Susskind et al. (1984), retrievals were rejected as non-convergent if either 1) R, the root mean square difference between the reconstructed brightness temperatures for the seven temperature sounding channels (HIRS2 channels 2, 4, 13, 14, and 15, and MSU channels 3 and 4) and the brightness temperatures computed for these channels using the solution, is greater than 1°C or 2) D, the absolute difference between the observed and computed brightness temperature for MSU channel 2, is greater than 1°C. In the region of this study, it was found that many differences for MSU channel 2 were greater than 1°C but the retrievals still looked reasonable when R was small. Therefore, a new more flexible criterion was used, involving the sum of the two quantities R and D. The retrieval was accepted and called good quality if R + D was less than 1.8°C, was called fair quality if R + D was between 1.8°C and 2.3°C, and poor quality if R + D was between 2.2°C and 2.8°C. Retrievals were rejected if R + D was greater than 2.8°C. These quality indicators were written on the tapes sent to the workshop. In constructing the fields shown in the next section, all accepted retrievals were weighted equally. Retrievals rejected because of the above criterion or others such as the scene being too cloudy to perform an infrared retrieval ($\eta > 4$) were not included in the analyses. No "microwave only retrievals" are performed.

2.2 First guess dependence of atmospheric thicknesses

Figures 1-10 show local analyzed fields for a number of thicknesses at times corresponding roughly to March 4, 1982 12Z and March 5, 1982 0Z. Each figure contains three analyses based only on quantities derived from satellite retrievals using as a first guess the concurrent NMC analysis, the 24 hour lagged analysis and a 6 hour forecast based on the GLAS GCM. The analyses based on the retrievals are shown in panels (A), (C) and (E). The analyses based on the first guess fields themselves are shown in panels (B), (D), and (F). In the case of satellite retrievals, data is included in the analysis only in locations where acceptable retrievals were performed. The first guess fields include data at all grid points (4° x 5°) in the area. The only information used in generating the retrievals, aside from topography and climatological sea surface temperatures, was the observed radiances, which are identical in all three sets of retrievals, and the first guess temperature-humidity profiles and surface pressure, which is different. No surface analysis or other concurrent measurements are used which are not shown in the guess field.

Figures 1-5 show the 700-1000 mb thickness, the 500-1000 mb thickness, the 500 - 700 mb thickness, the 300 - 500 mb thickness, and the 100 - 300 mb thickness for the March 4 12Z time period. The satellite retrievals are based on two orbits crossing at about 1330Z in the center and west and 1200Z in the east. No attempt was made to account for the time difference in computing the satellite analysis. For the

purpose of this comparison, we may consider panel (B), the concurrent NMC analysis, as the truth. It is clear by comparing figures 1-5(B) with 1-5(D) that the 24 hour lagged analysis guess was grossly different at all levels. The 6 hour forecast guess shown in figures 1-5(F) is in general much closer to the analysis, as might be expected, but significant differences exist.

Figures 6-10 show the same fields for the time period March 5 00Z. In this case, the satellite overpasses were at 0200Z in Eastern Europe and about 0345Z in the west and central portions of the field . Here, differences between retrievals and analysis fields may be real, due to the 2-4 hour time difference and the rapidly moving field. As in figures 1-5, the 24 hour lagged analysis guess is grossly different from the true field while the 6 hour forecast is similar, but not identical, to the analysis.

It is of interest to compare the three sets of retrievals with each other for consistency and with the analysis for accuracy. The three sets of retrievals are in general much closer to each other than the guesses are to each other, and also show good agreement compared to the analyis. In figure 2, showing 500 - 1000 mb thickness, for example, the analysis shows a moderate trough with north-south orientation centered at about 2°W longitude, and a ridge with north-east, south-west orientation running roughly through 10°W, 30°N and 20°E, 42°N. These main features are found with slightly varying degrees of intensity in all the fields shown, with the exception of the 24 hour lagged analysis, which is almost 180° out of phase. It is apparent then that in this thick layer, the retreivals are relatively first guess independent and can significantly improve a poor guess while not degrading a good guess. The same basic result holds for the 700-1000 mb thickness field and the 500-700 mb thickness field as well. In the latter field, the gradient in the trough in the retrieved field using the lagged analysis guess is somewhat weaker than in the other retrieved fields or in the analysis. It is also interesting to note that in this field, the retreival from the forecast guess gives a better depiction of the intensity and shape of the trough, as compared to the analysis, than does the forecast guess. This indicates some guess dependence but also the ability to improve on a 6 hour forecast which is already fairly accurate. The upper level thicknesses, 300-500mb and 100-300 mb, also show similar findings. Again, all retrievals fields show the same patterns as each other and the analysis, but the gradients are somewhat weaker, expecially in the 100-300 mb thickness field when an extremely poor first guess is used.

By March 5 0Z, the center of the trough at 500 mb has moved about 5° further east and deepened. The 6 hour forecast has the trough centered about 7° too far west. The 24 hour lagged analysis, as in the earlier period, shows a totally different synoptic situation. The findings with regard to guess dependence as a function of layer are basically the same as in the previous period. The differences between the retrievals at the lower atmospheric levels, 700 - 1000 mb and 500 - 1000 mb, are very small. At the higher levels, the retrieved features all are again very similar to each other and the concurrent analysis, but the gradients are weakened somewhat with the poorer first guesses.

It is extemely interesting to note in figure 7, the 500 - 1000 mb thickness for March 5 0Z, that all retreival fields have the trough centered at about 5°E, while the concurrent analysis has the trough centered at 2°E, the forecast at 2°W, and the lagged analysis at about 10°W. The location of the satellite retreived trough 3° east of the analysis trough may well be a real effect due to movement in time. The same result is found in the 700-1000 mb and 500-700 mb thickness fields. Perhaps the most striking result is in the 100-300 mb thickness field for March 5 0Z. Here figures 10(C) and 10(D) both show highly structured fields with large gradients that are totally different from one another. All retreivals show a closed high centered at about 44°N, 5°E and a closed low at about 44°N, 22°E, in good agreement with the analysis. The sharp gradients around the high are not found in the forecast guess and the lagged analysis contains a low in this area. This figure clearly shows the degree to which satellite data can improve upper air analysis, though the gradients are weaker than reality in the case of a very bad guess.

3.1 Humidity Retrieval Algorithm

The method used for retrieving atmospheric water vapor profiles is similar to that used for the temperature retrievals, in that heavy reliance is placed on the ability to accurately model the response of a given channel to changes in atmospheric water vapor, as opposed to using statistical relationships between brightness temperature and water vapor content. It should be noted that the effect of changes of water vapor on those channels most sensitive to water vapor content, channels 8, 10, 11, and 12 on the HIRS instrument, is somewhat different than the effect of temperature changes on the temperature sounding channels. In the latter case, the change in observed radiance is due primarily to changes in the Planck function in the radiative transfer equation, while the former case the radiance change is due mainly to changes in the transmittance function. In other words, for the temperature sounding channels the weighting functions are relatively insensitive to moderate changes in temperature, while for a humidity sounding channel the major effect of a change in water vapor profile is to alter the region of the atmosphere which is probed by the channel. Because of this, accurate water vapor distributions may only be obtained if the atmospheric temperature profile is well determined. Therefore, in the method to be described below, the humidity retrieval is performed after the temperature retrieval.

The iterative relaxation method for determination of atmospheric water vapor proceeds in the following steps:

1) Given the retrieved atmospheric and surface temperatures and a first guess water vapor distribution, q^o (P), the brightness temperature, θ_i^c, which would be expected to be observed in a given channel may be calculated from the radiative transfer equation. The first guess will be modified according to the difference between θ_i^c and $\tilde{\theta}_i$, the reconstructed (observed) brightness temperature and the sensitivity of θ_i^c to changes in humidity.

2) In order to estimate the sensitivity of brightness temperatures to humidity changes, the entire guess water vapor profile is alternately increased and decreased by a fixed fraction δ and estimates of the brightness temperature are obtained for each case, for each channel to be used in the retrieval. The change in brightness temperature in channel i for a fractional change in water vapor of $\pm\ \delta$ is approximated as

$$\Delta\Theta^{c}_{i\pm} = \Theta^{c}_{i}[q^{N}(P)] - \Theta^{c}_{i}[q^{N}(P)\cdot(1\pm\delta)] \qquad (6)$$

3) Each channel i then provides an estimate of the fractional change to be made in humidity, f_i, computed according to

$$f_i = \left(\frac{\Theta_i - \Theta^{c}_{i}}{\Delta\Theta^{c}_{i\pm}}\right)\delta \qquad (7)$$

where $\Delta\Theta^{c}_{i+}$, the estimate of sensitivity to increasing humidity, is used if the computed brightness temperature is too high, in which case f is taken as positive, and $\Delta\Theta^{c}_{i-}$ is used otherwise, resulting in a negative f_i. Because the problem is nonlinear, $|f_i|$ is never allowed to be greater than 0.7 in any iteration.

4) Since each channel senses a different region of the atmosphere, the 4 estimates of f_i will not be the same in general. A fractional change, $\varepsilon(P_j)$ must be found at each of the n discrete pressure levels used in modeling the radiative transfer equation. This is done by weighting the values of f_i according to

$$\varepsilon(P_j) = \sum_i W_i(P_j) f_i \Big/ \sum_i W_i(P_j) \qquad (8)$$

where $W_i(P_j)$ represents the relative sensitivity of channel i to humidity changes at P_j. In these calculations, $W_i(P_j)$ was approximated by the analog of the temperature sounding weighting function

$$W_i(P_j) = \left(\frac{d\tau_i}{d\ell n p}\right)_{P_j} / (1 - \tau(P_s)) \qquad (9)$$

which is easier to compute than the actual sensitivity function relating changes in brightness temperatures to changes in humidity at specific levels, and provides essentially identical soudings. Equation 8 is evaluated discretly at mid-mandatory levels and the values of $\varepsilon(P_j)$ are linearly interpolated in P at intermediate values.

5) Using the values of ε (P) determined in step 4, a new estimate of the water vapor profile at the n discrete pressure levels is found as

$$q^{N+1}(P) = q^{N}(P)(1+ \varepsilon (P)) \quad . \tag{10}$$

If, for any level, $q^{N+1}(P)$ is found to correspond to a relative humidity of greater than 100%, then for that level $q^{N+1}(P)$ is set to the value of the specific humidity which corresponds to 100% relative humidity. Furthermore, because of the limited sensitivity of the infrared brightness temperatures to changes in water vapor near the surface, the values of ε (P) beneath the mandatory level pressure closest to the surface are set to the value of ε (P) at that mandatory level. This profile is used to obtain new values for the atmospheric transmittances for the 4 channels which are then used to calculate new estimates of the brightness temperatures $\Theta_i{}^c\,[q^{N+1}(P)]$. If the residuals between $\Theta_i{}^c[q^{N+1}(P)]$ and Θ_i are sufficiently small, or if there is little change in the residuals, the process is considered to have converged and q^{N+1} (P) is taken to be the retrieved water vapor profile. If this is not the case, steps 2 through 5 are repeated. Currently the process is limited to at most seven iterations.

There are some exceptions to this procedure in actual practice. For example, if a temperature retrieval is not performed for any reason, or, if the temperature retrieval is flagged as nonconvergent, then no water vapor retrieval is performed. Furthermore if the sensitivity of a given channel to changes in water vapor content, as defined in step 2 above, is too small, then that channel is not used in the retrieval process. This is accomplished by setting $W_i(P) = 0$ for the channel. This situation arises occasionally for channels 8 and 10 which sense near the surface where there is sometimes little thermal contrast. Indeed, for an isothermal atmosphere and a surface with unit emissivity, a passive sounding has no information about water vapor content.

After a full iterative cycle has been performed, the residual differences between the observed and calculated brightness temperatures may be used to reject a retrieved profile. At the present time only a very gross check is done and a water vapor retrieval is rejected if the rms of the residuals of channels 11 and 12 is more than 2° or if the absolute value of the residual of either channels 8 or 10 is more than 5°. A looser criterion is used for these channels because they are affected by uncertainties in ground temperature and surface emissivity. If, as described above, either channel 8 or 10 is not used in the retrieval process, the residual is allowed to be 10° before the profile is rejected. As with the thickness fields shown previously, the retrieved fields shown in the next section contain only accepted retrievals while the first guess fields contain first guess humidities at all locations.

3.2 First guess dependence of humidity retrievals

Figures 11-16 A-F show the precipitable water above 1000 mb (actually above the surface), 700 mb and 500 mb and dewpoints at 850 mb, 700 mb and 500 mb for the retrieval and first guess fields for March 4 12Z. Analogous fields for March 5 0Z are shown in figures 17-22 A-F.

In the case of thickness retrievals, it was found that all retrievals produced very similar fields to each other and to the concurrent analysis, with the largest first guess sensitivity coming at the higher levels of the atmosphere, for which the vertical resolution of HIRS/MSU is poorest. A very different result is obtained for the humidity retrievals, in which retrieved fields are more different from each other, and especially from the analysis. Furthermore, the guess dependence for humidity retrievals is greatest closer to the surface. The larger guess dependence for humidity retrievals occurs because the HIRS2 observations are not as sensitive to changes in humidity, especially close to the surface, as they are to changes in temperature, and the vertical resolution of the humidity sounding channels is poor. The poorer agreement of retreivals with the NMC humidity analysis is partially due to this decreased sensitivity in the retrievals. Another factor is that the analysis is itself of poorer quality than the thickness analysis and therefore cannot necessarily be taken as truth. While verification is difficult and sensitivity is relatively poor, there is no question that useful information is present, especially at 500 mb.

Figure 13 A-F shows the precipitable water above 500 mb at March 4 12Z constructed from the three first guesses and the three sets of retrievals. The NMC analysis shows a moist tongue running northeast diagonally through the scene with the northeast containing the most moisture. The twenty-four hour lagged analysis is considerably more moist, with the moist line having the same orientation but shifted toward the northwest. The six hour forecast from the GLA GCM looks quite different from the NMC analysis, as it will in all cases. In this case, the forecast field is characterized by two moist centers in its northeast and southeast corners. It is pleasing to see that all retrievals are generally similar in structure to each other and to the NMC analysis, though they all tend to have more precipitable water above 500 mb than the analysis. This bias may be a real error or it may be due to an underestimate of precipitable water above 500 mb by the analysis, in which humidity information above 500 mb is sparse. All retrievals also tend to show an increase in humidity at the southeast corner of the field though less so than in the forecast guess.

The general features in the precipitable water above 700 mb and above 1000 mb field in figures 11 and 12 are similar to those in the upper level humidity field, though the first guess dependence, and the difference between the fields, increases with increasing reference pressure. Note for example that the precipitable water above 1000 mb fields in figures 11 C and D show an extremely moist first guess field in the northwest quadrant which was corrected somewhat in the retrieval, but is still moist compared to the other retrievals. Likewise, the central area of the field is considerably more moist in figure 10E, reflecting the moist guess in figure 10F, than in other fields. The results are more clearly depicted in the retrieved dewpoint fields (figures 14-16) which do not show major dif-

ferences at 500 mb but show significant differences at 850 mb in the northwest corner, where a very dry forecast first guess (figure 14F) was left virtually unchanged in the retrieval (figure 14E).

At March 5 0Z, the precipitable water above 500 mb (figure 19) is characterized by a dry area centered about 4° E with increasing moisture on either side, particularly over central Italy and to the northeast. The first guess fields are all rather different while the retrievals generally share the same characteristics. The six hour forecast field appears to be the biggest outlier and it was corrected appreciably by the retrieval if the analysis is taken as truth. The retrieved precipitable water above 700 mb fields (figure 18) are again similar to each other but contain a moist area centered about 42 N, 6W, which is not evident in any guess field. The largest differences between retrieval fields again occurs in the precipitable water above 1000 mb fields (figure 17), where the forecast field is particularly dry in the southwest corner and this dry area is again reflected in the retrieval. Likewise, the 24 hour lagged analysis guess is too dry over Italy and little was done to correct this in the retrieval field. The differences are more apparent in the dew point fields in which the retrieved results are basically similar at 500 mb but show major differences at 850 mb.

4. CONCLUSIONS

It has been demonstrated that the method described in Susskind et al. (1984) for atmospheric temperature retrievals, results in a very low first guess dependence for retrieved thickness fields, which is smallest close to the surface, and increases at higher levels, where the weighting functions of HIRS2/MSU are not as sharp. A poor first guess is changed and improved considerably whereas an accurate first guess is not degraded. No surface informaton was used in the retrieval process.

The situation for humidity retrievals, as performed in this paper, is somewhat less ideal. A larger first guess dependence is observed, especially close to the surface, where the radiances are less sensitive to changes in humidity. On the other hand, there is evidence that a poor first guess can be improved upon, especially in the mid-troposphere, though there is a question as to what constitutes "truth".

References

Baker, W. E., R. Atlas, M. Halem, and J. Susskind, 1984: A Case Study of Forecast Sensitivity to Data and Data Analysis Techniques. Mon. Wea. Rev., 112, 1544-1561.

Susskind, J., J. Rosenfield, D. Reuter, and M. T. Chahine, 1984: Remote Sensing of Weather and Climate Parameters from HIRS2/MSU on TIROS-N. J. Geophys. Res., 89, 4677-4697.

700–1000 MB THICKNESS MARCH 4, 1982

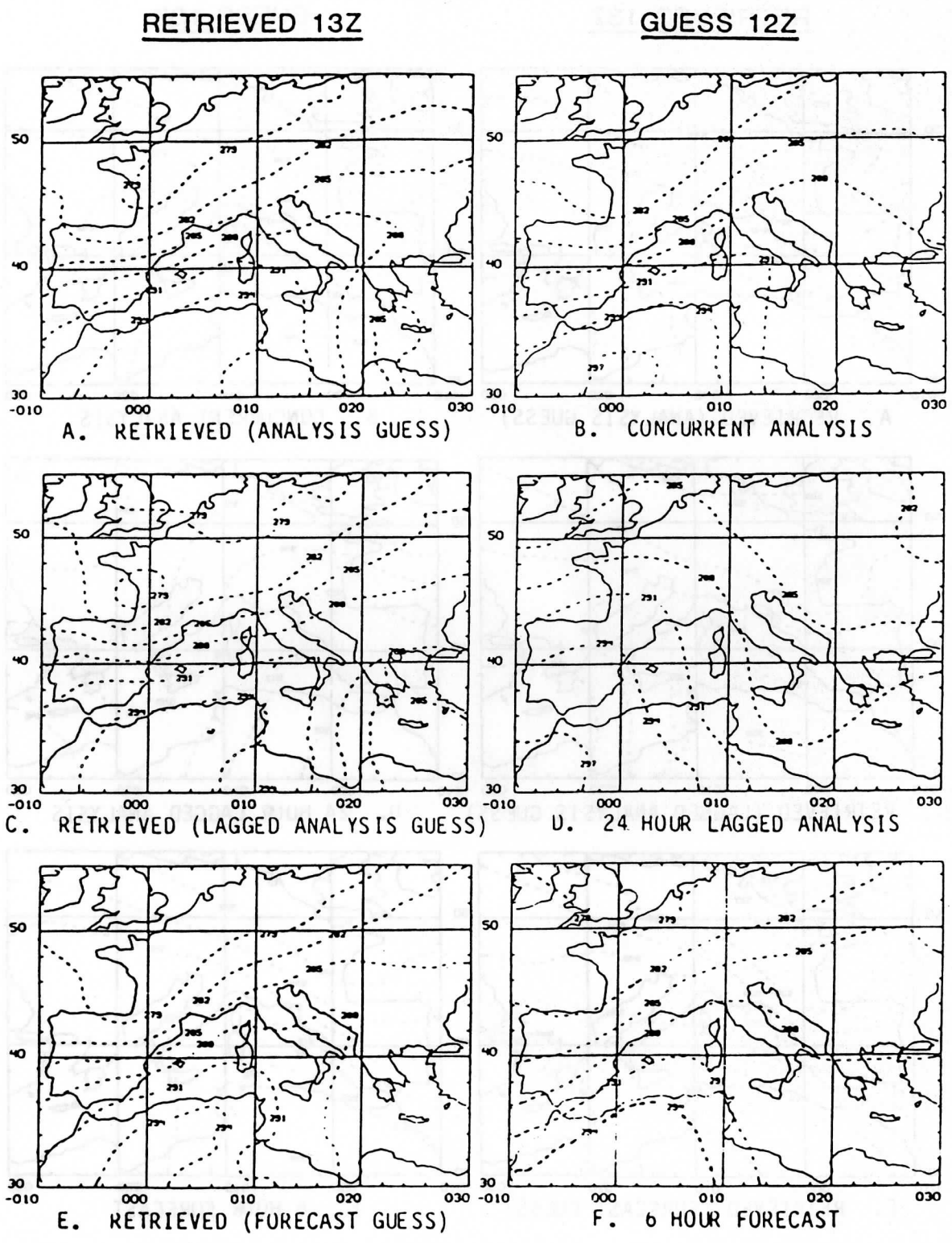

Figure 1

500-1000 MB THICKNESS MARCH 4, 1982

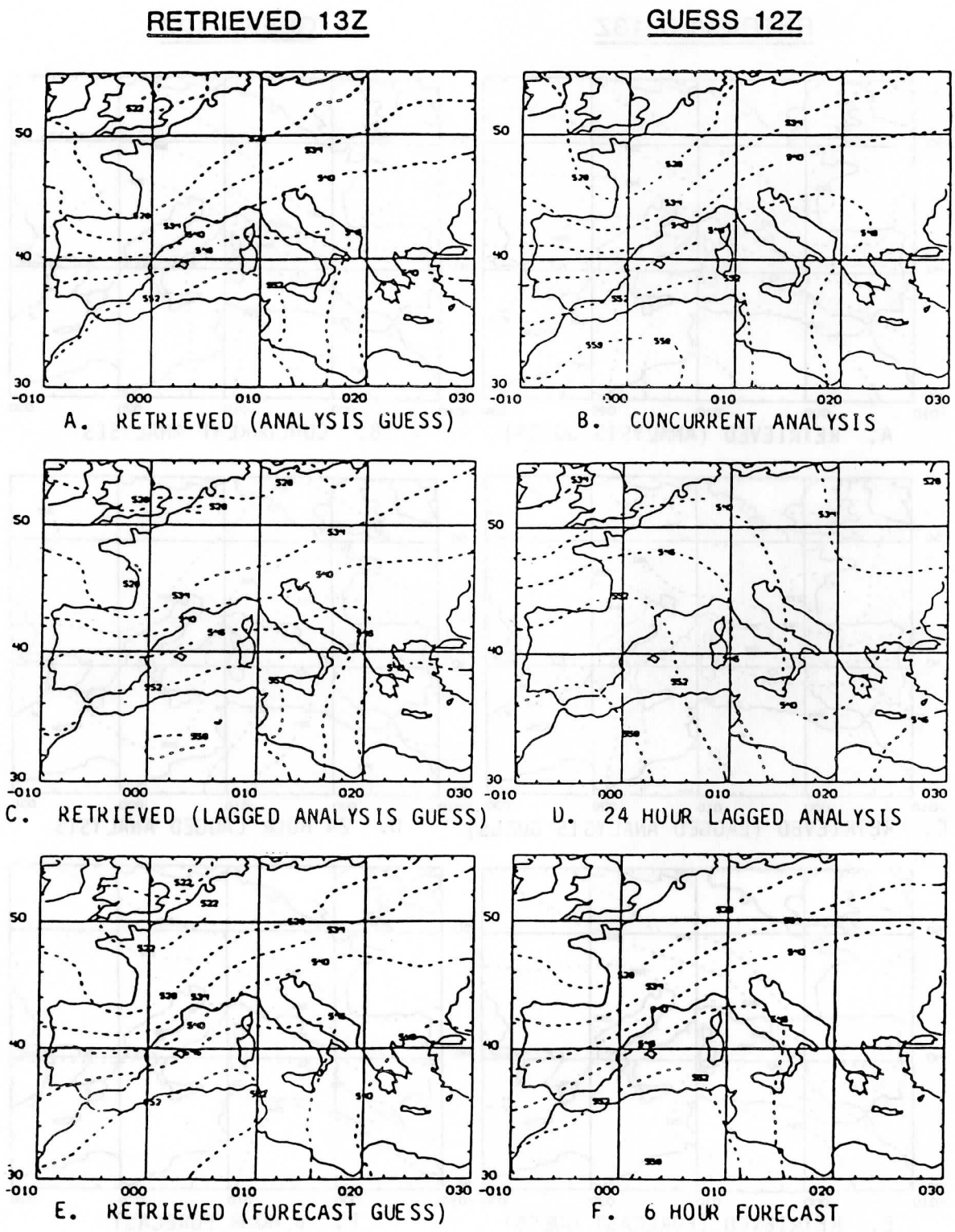

Figure 2

500-700 MB THICKNESS MARCH 4, 1982

RETRIEVED 13Z

GUESS 12Z

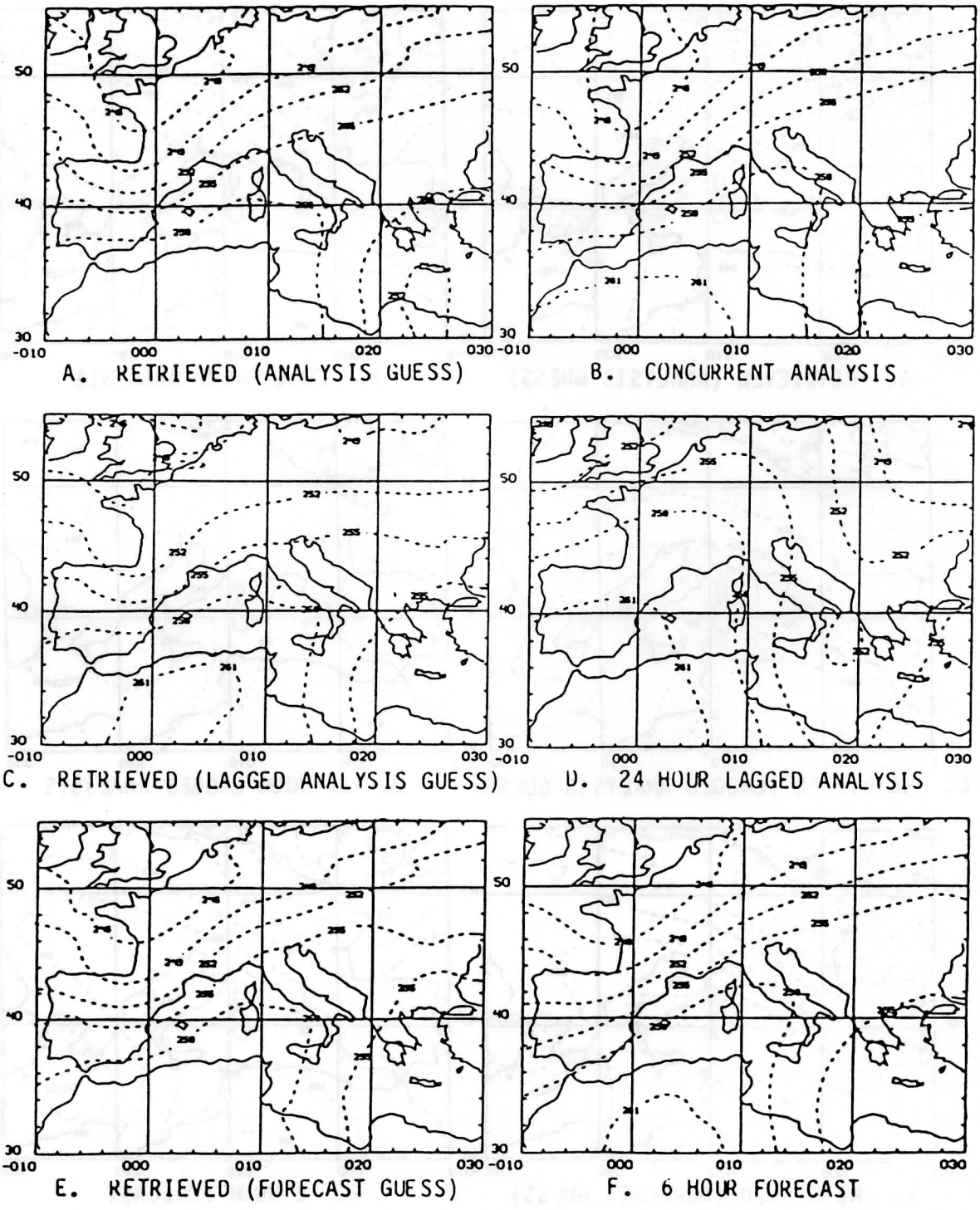

Figure 3

300-500 MB THICKNESS MARCH 4, 1982

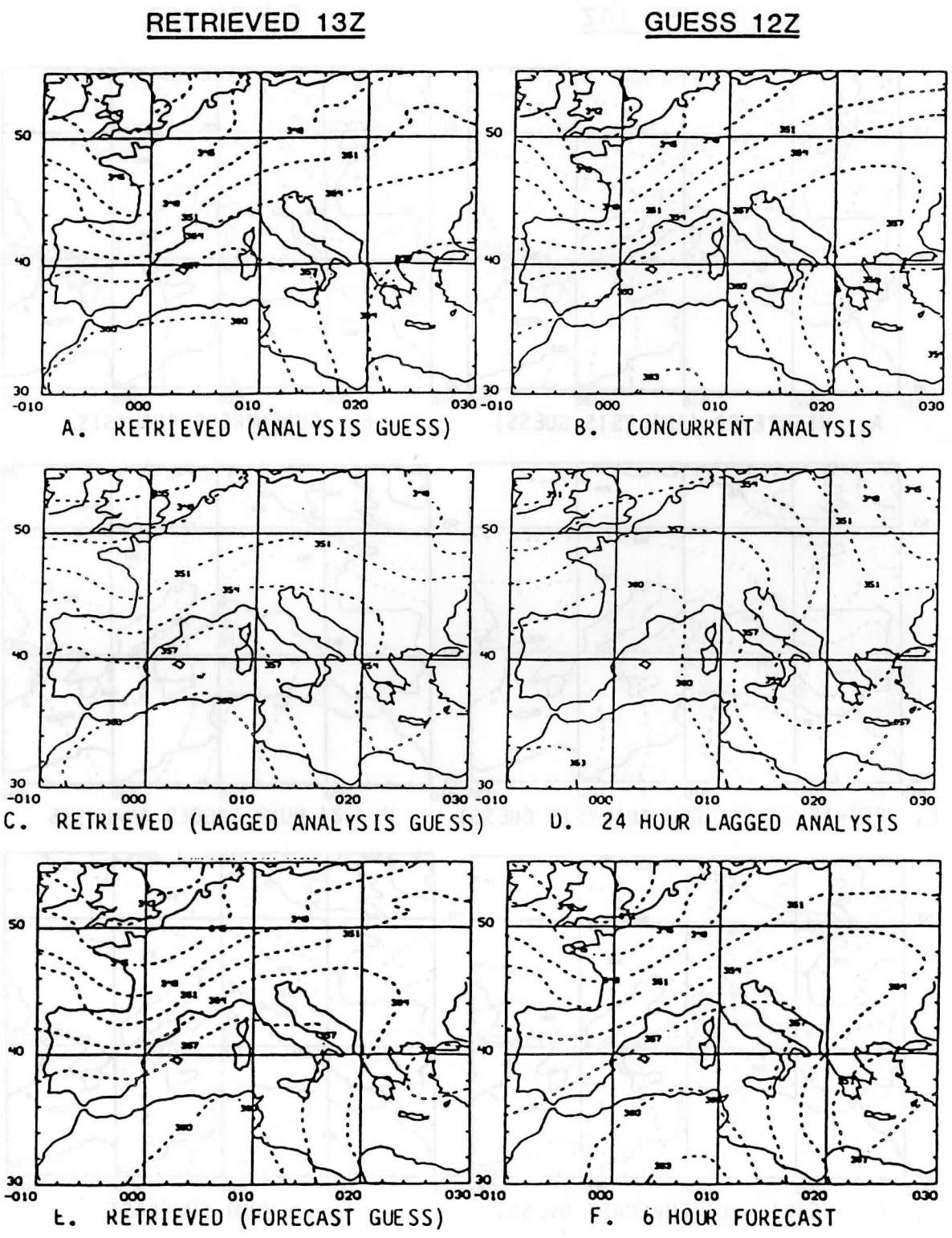

Figure 4

100-300 MB THICKNESS MARCH 4, 1982

RETRIEVED 13Z

GUESS 12Z

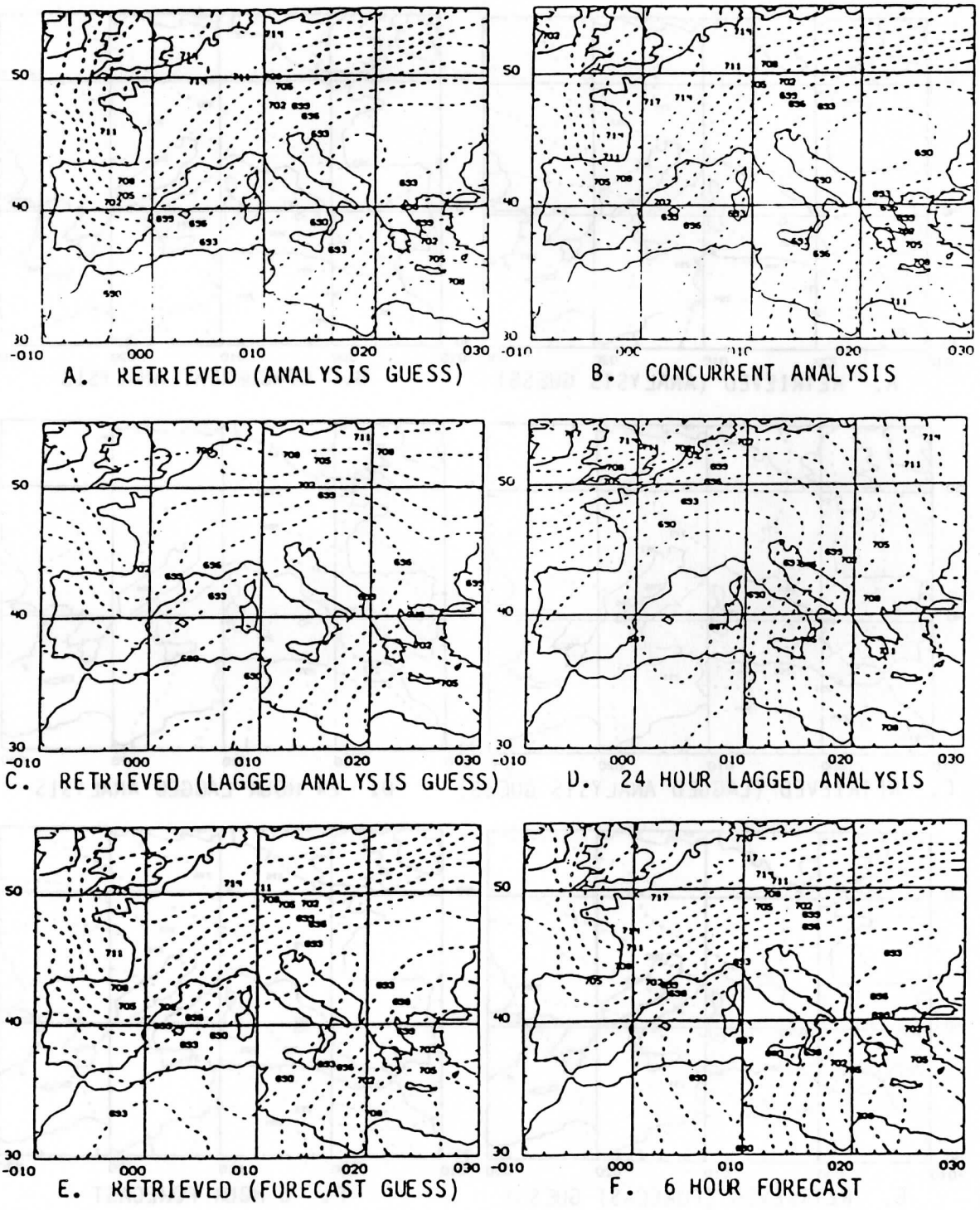

A. RETRIEVED (ANALYSIS GUESS)

B. CONCURRENT ANALYSIS

C. RETRIEVED (LAGGED ANALYSIS GUESS)

D. 24 HOUR LAGGED ANALYSIS

E. RETRIEVED (FORECAST GUESS)

F. 6 HOUR FORECAST

Figure 5

700-1000 MB THICKNESS MARCH 5, 1982

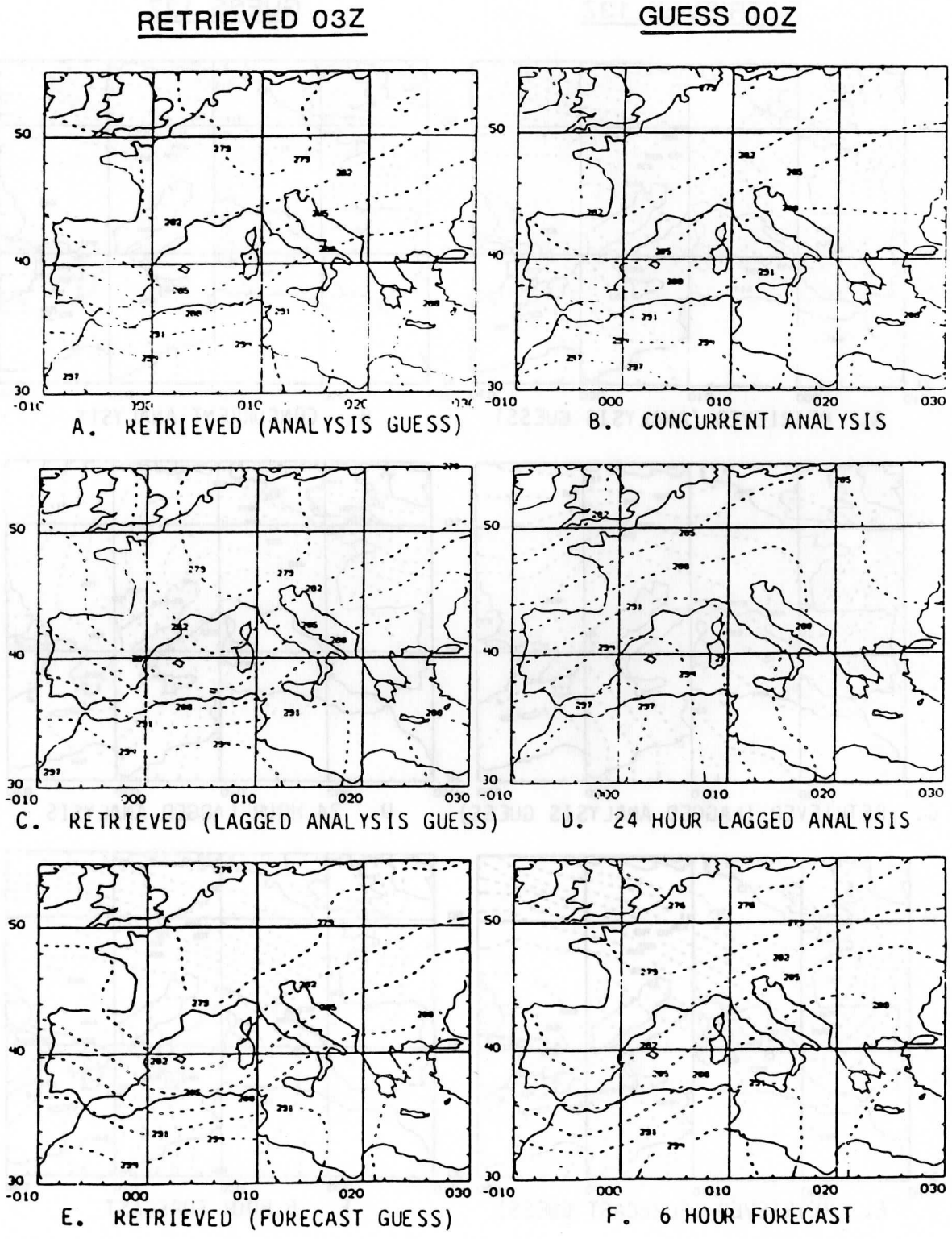

Figure 6

500-1000 MB THICKNESS MARCH 5, 1982

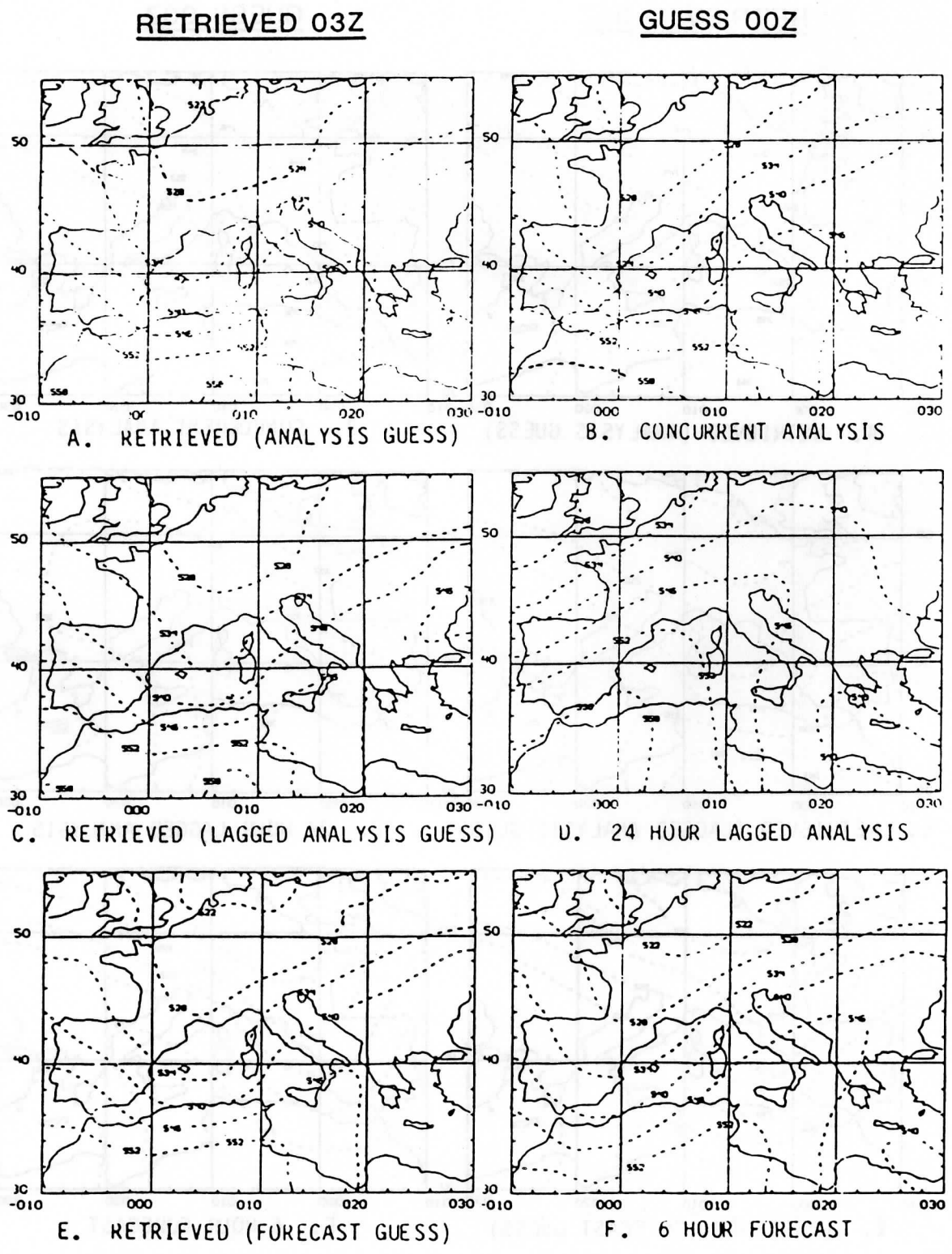

Figure 7

500-700 MB THICKNESS MARCH 5, 1982

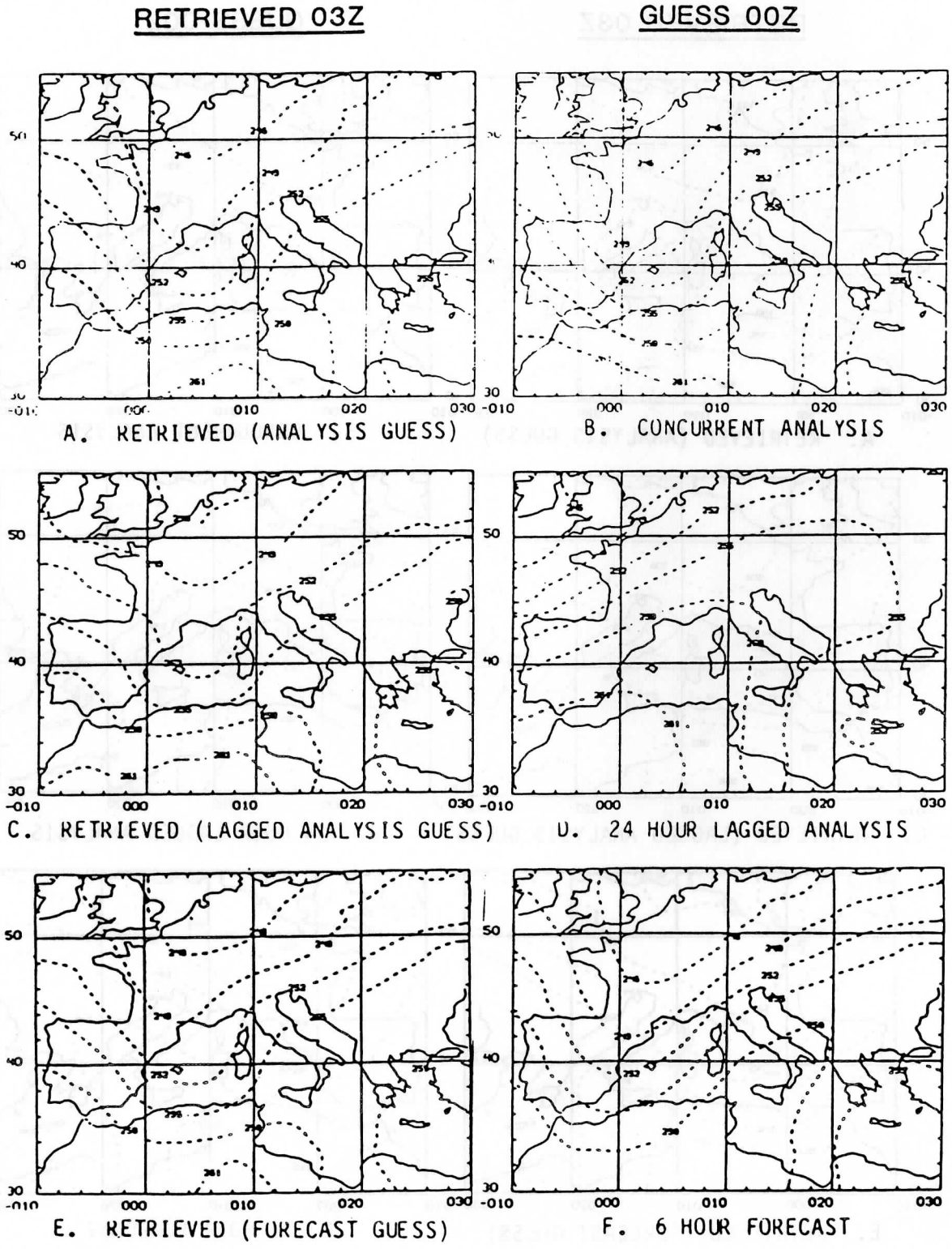

Figure 8

300-500 MB THICKNESS MARCH 5, 1982

RETRIEVED 03Z

GUESS 00Z

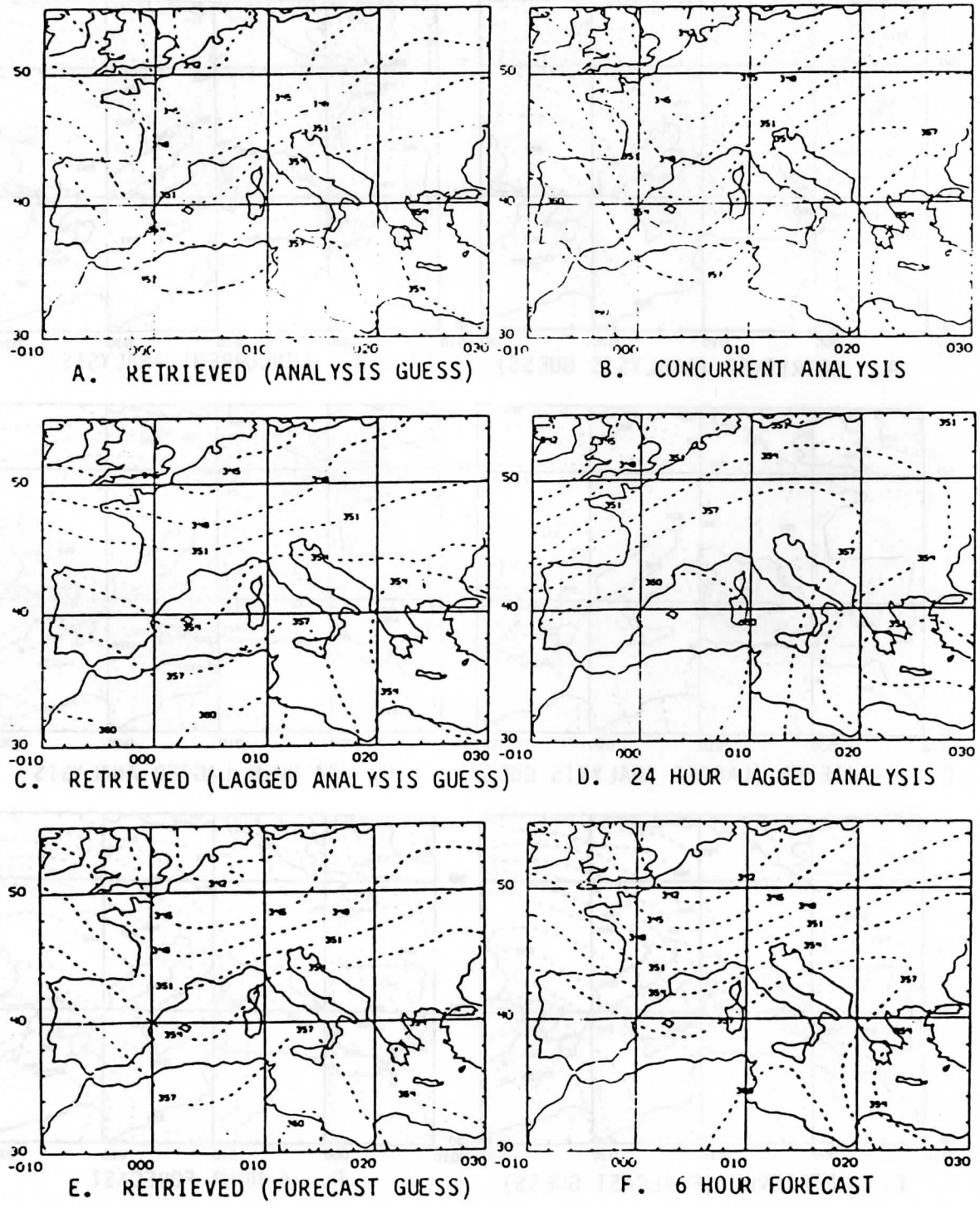

A. RETRIEVED (ANALYSIS GUESS)

B. CONCURRENT ANALYSIS

C. RETRIEVED (LAGGED ANALYSIS GUESS)

D. 24 HOUR LAGGED ANALYSIS

E. RETRIEVED (FORECAST GUESS)

F. 6 HOUR FORECAST

Figure 9

100-300 MB THICKNESS MARCH 5, 1982

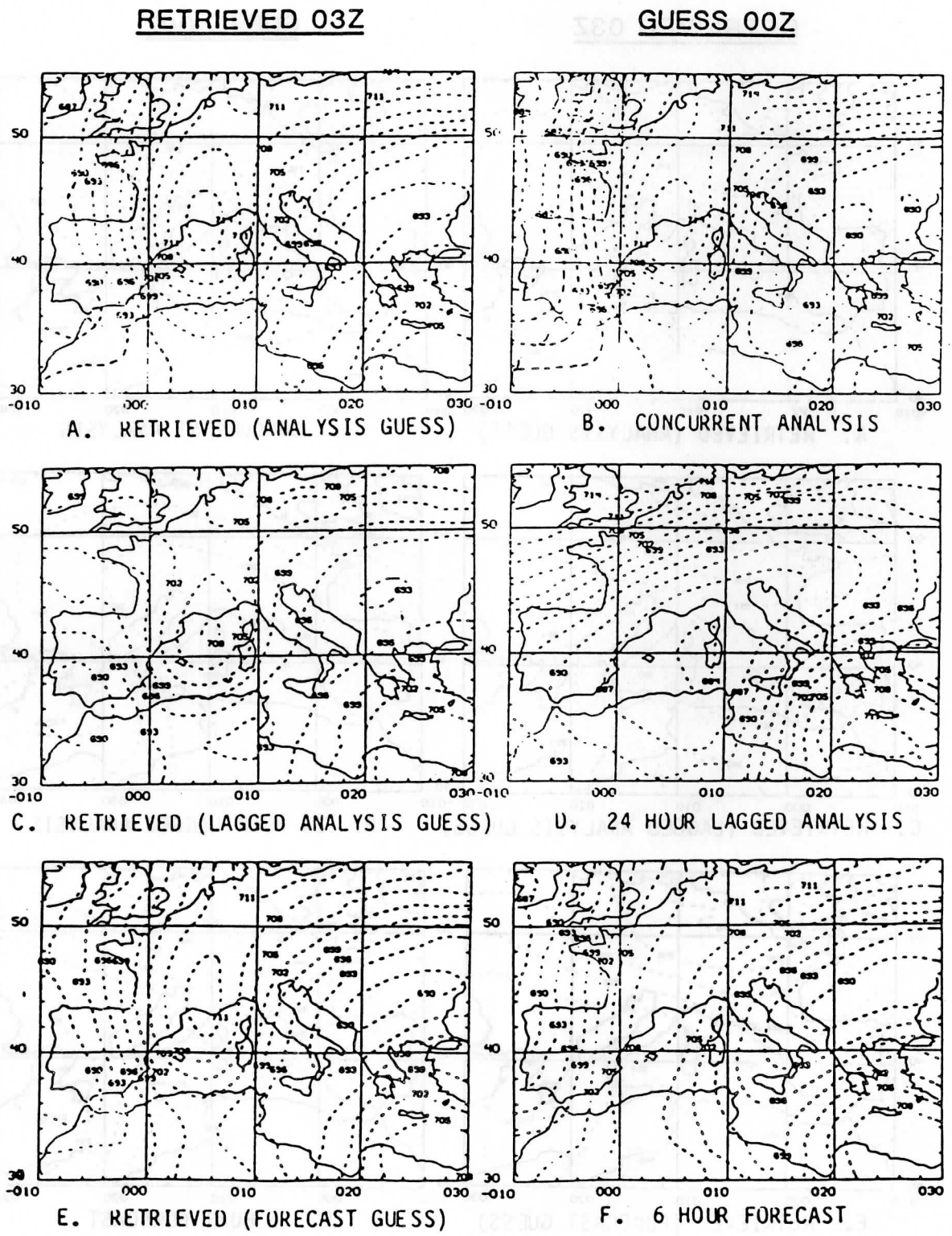

Figure 10

PRECIPITABLE WATER 1000 MB-TOP MARCH 4, 1982 (G/CM^2)

RETRIEVED 13Z

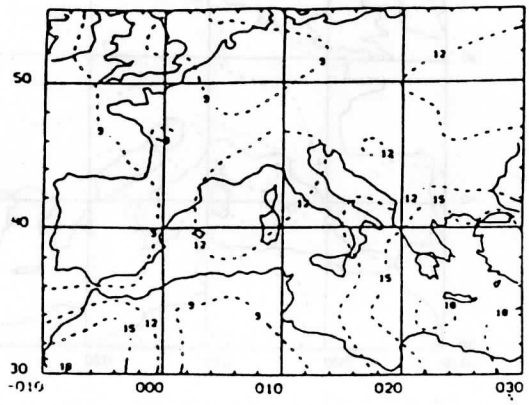

A. RETRIEVED (ANALYSIS GUESS)

GUESS 12Z

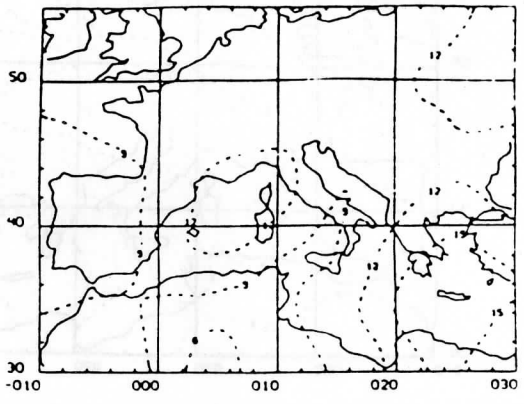

B. CONCURRENT ANALYSIS

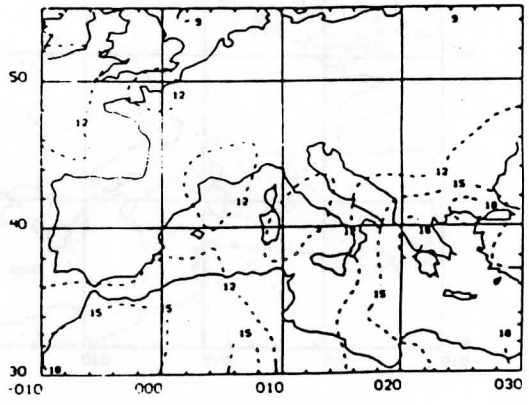

C. RETRIEVED (LAGGED ANALYSIS GUESS)

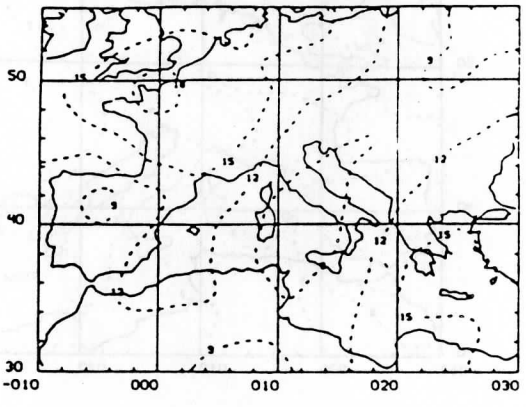

D. 24 HOUR LAGGED ANALYSIS

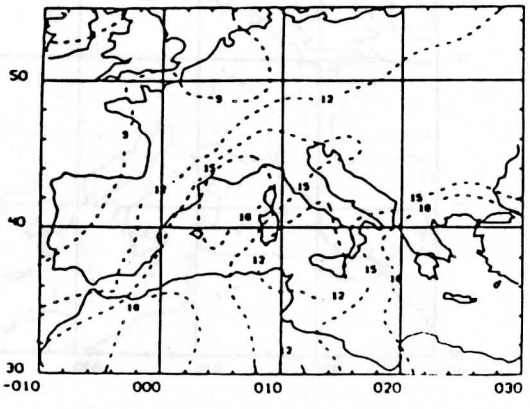

E. RETRIEVED (FORECAST GUESS)

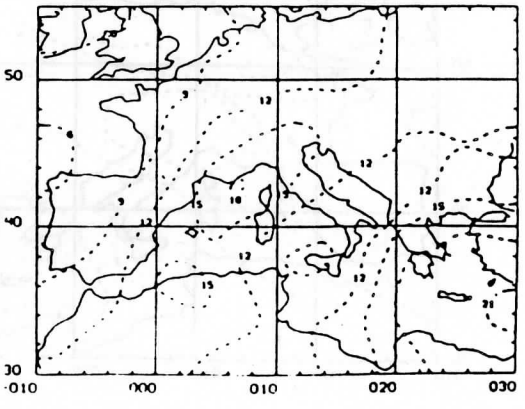

F. 6 HOUR FORECAST

Figure 11

PRECIPITABLE WATER 700 MB-TOP MARCH 4, 1982 (G/CM^2 x 10)

RETRIEVED 13Z

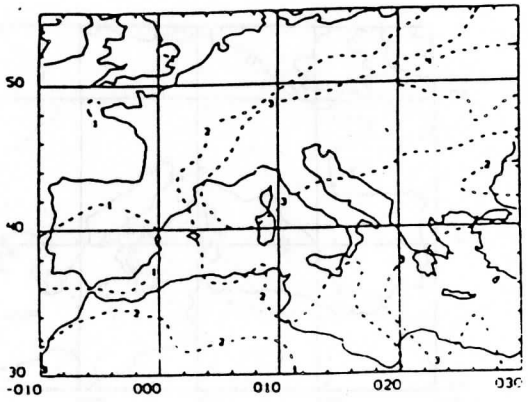

A. RETRIEVED (ANALYSIS GUESS)

GUESS 12Z

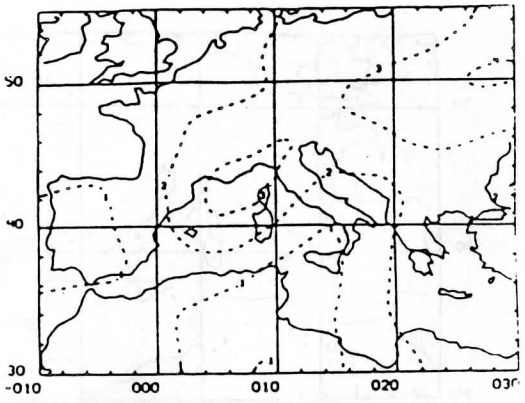

B. CONCURRENT ANALYSIS

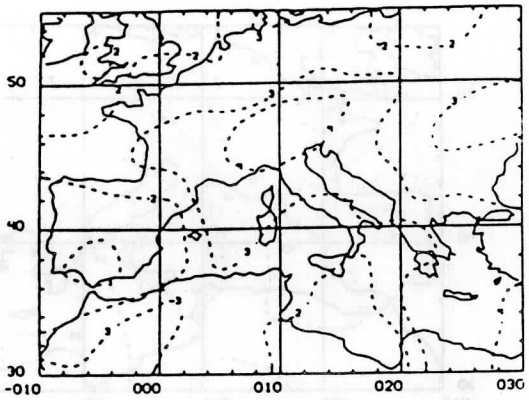

C. RETRIEVED (LAGGED ANALYSIS GUESS)

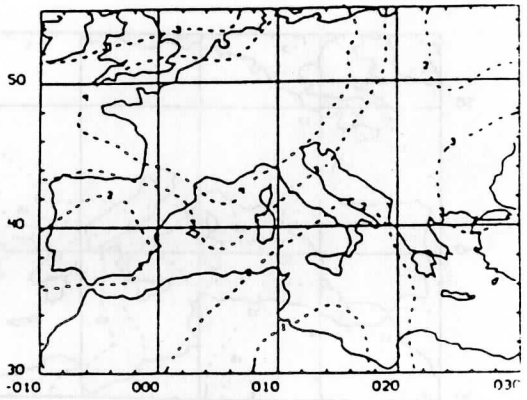

D. 24 HOUR LAGGED ANALYSIS

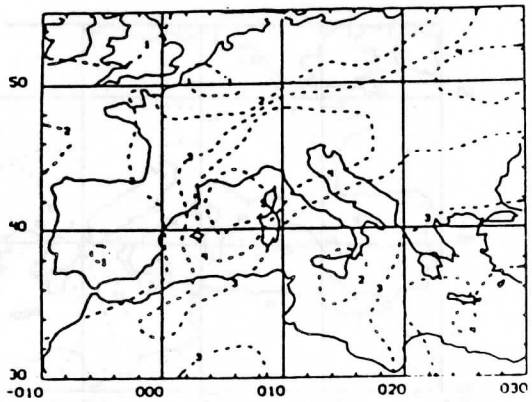

E. RETRIEVED (FORECAST GUESS)

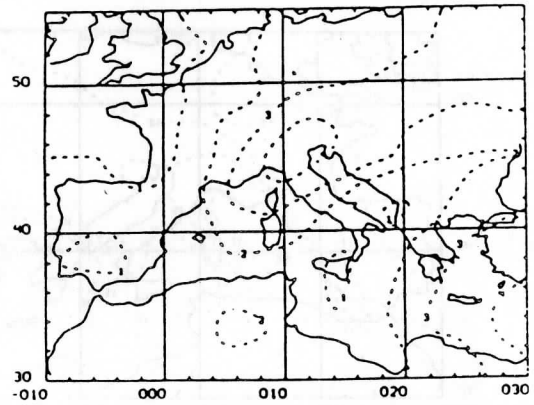

F. 6 HOUR FORECAST

Figure 12

PRECIPITABLE WATER 500 MB-TOP MARCH 4, 1982 (G/CM^2 x 100)

RETRIEVED 13Z

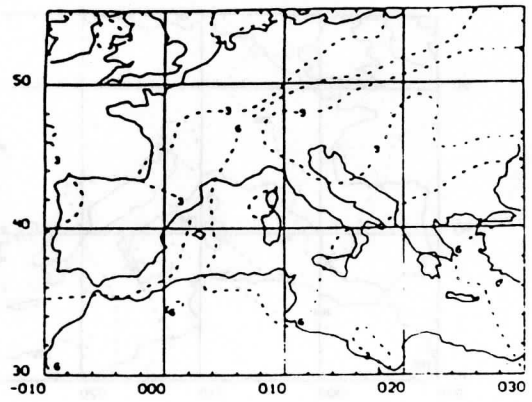

A. RETRIEVED (ANALYSIS GUESS)

GUESS 12Z

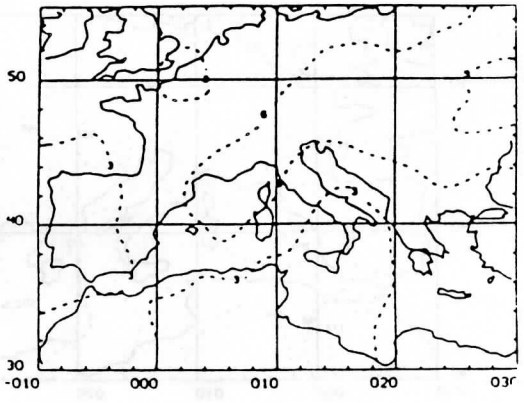

B. CONCURRENT ANALYSIS

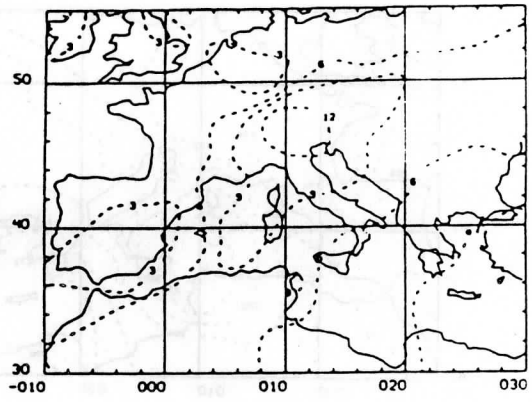

C. RETRIEVED (LAGGED ANALYSIS GUESS)

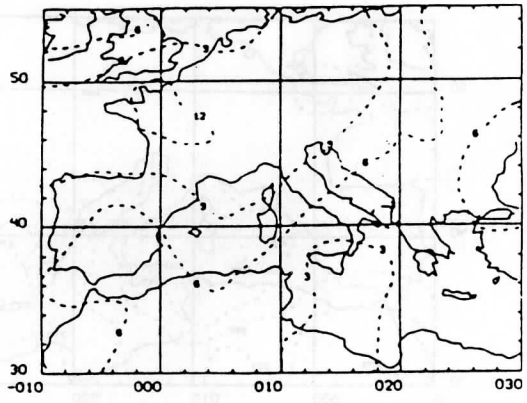

D. 24 HOUR LAGGED ANALYSIS

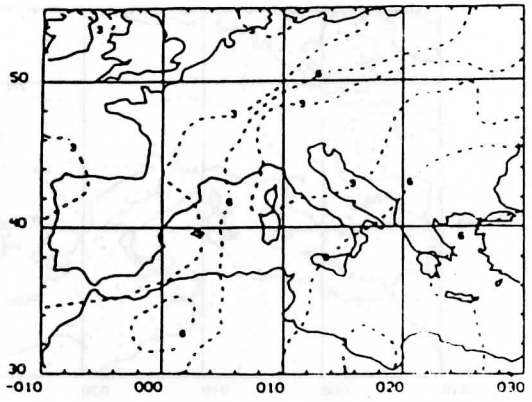

E. RETRIEVED (FORECAST GUESS)

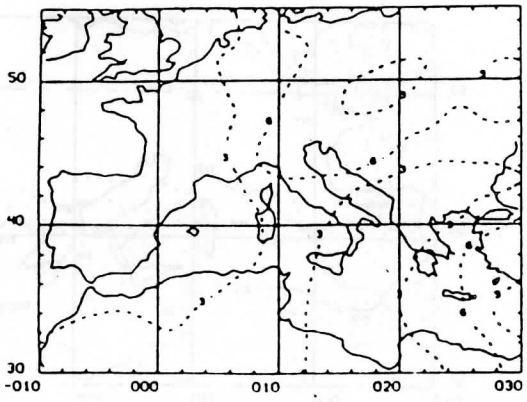

F. 6 HOUR FORECAST

Figure 13

DEW POINT 850 MB MARCH 4, 1982

RETRIEVED 13Z

GUESS 12Z

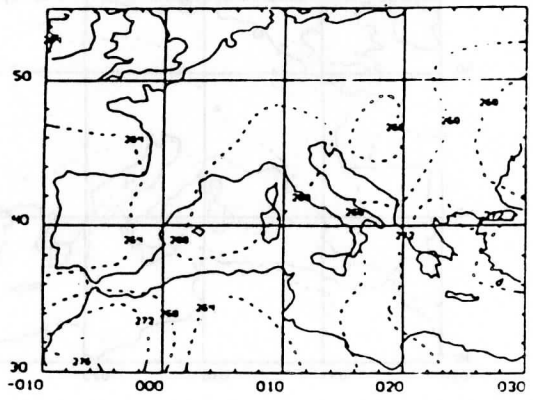

A. RETRIEVED (ANALYSIS GUESS)

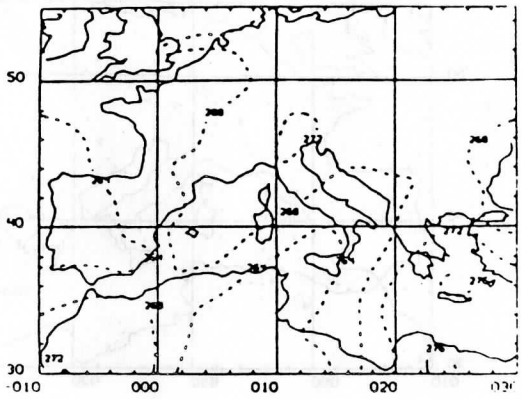

B. CONCURRENT ANALYSIS

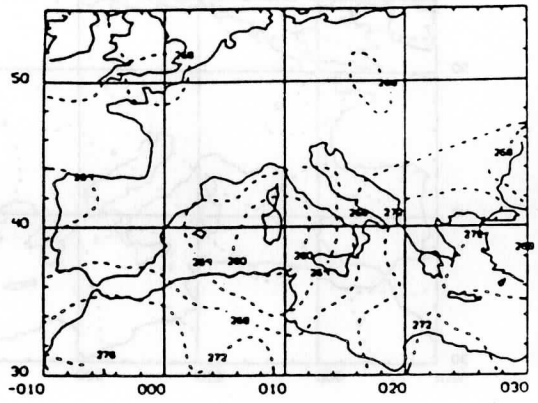

C. RETRIEVED (LAGGED ANALYSIS GUESS)

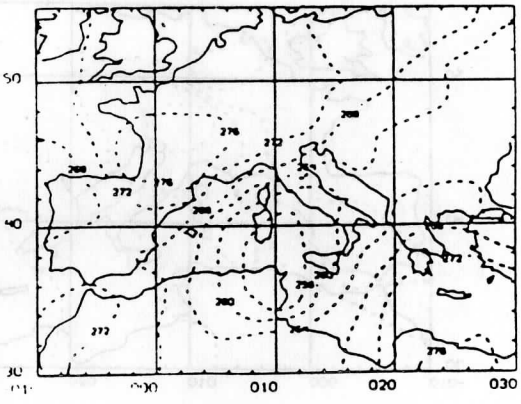

D. 24 HOUR LAGGED ANALYSIS

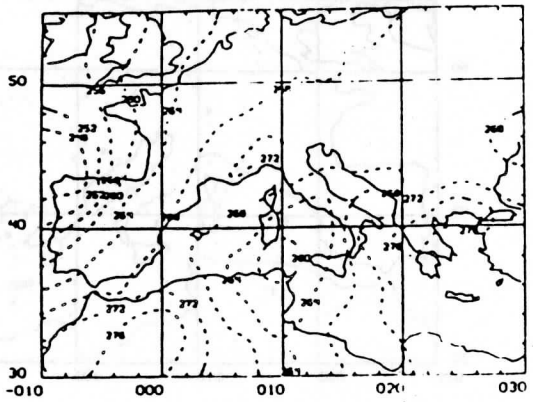

E. RETRIEVED (FORECAST GUESS)

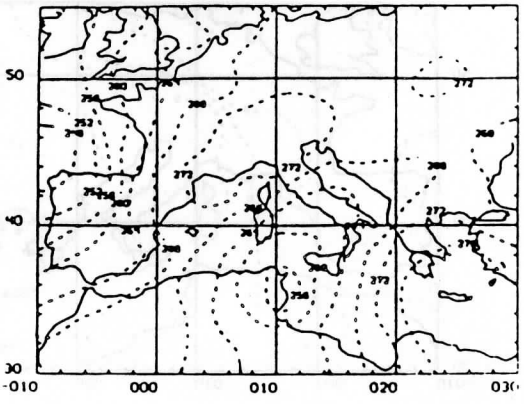

F. 6 HOUR FORECAST

Figure 14

DEW POINT 700 MB MARCH 4, 1982

RETRIEVED 13Z

GUESS 12Z

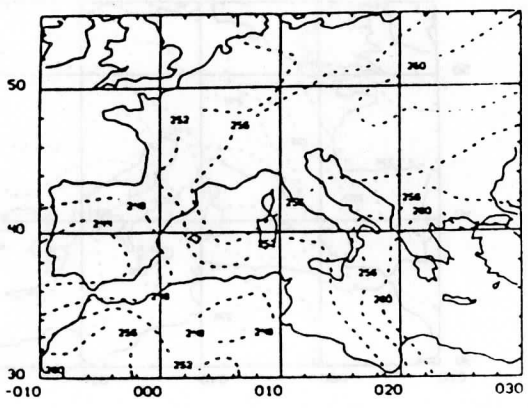

A. RETRIEVED (ANALYSIS GUESS)

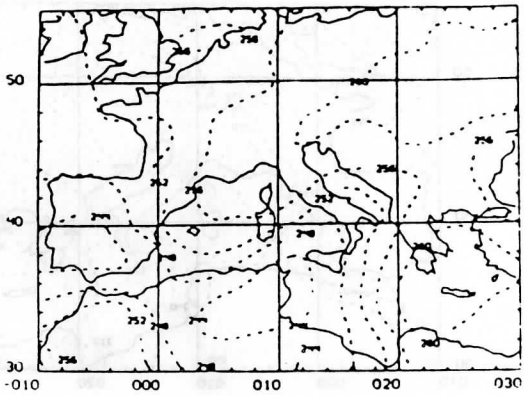

B. CONCURRENT ANALYSIS

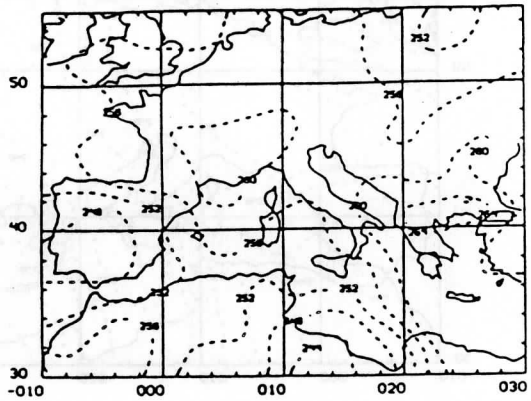

C. RETRIEVED (LAGGED ANALYSIS GUESS)

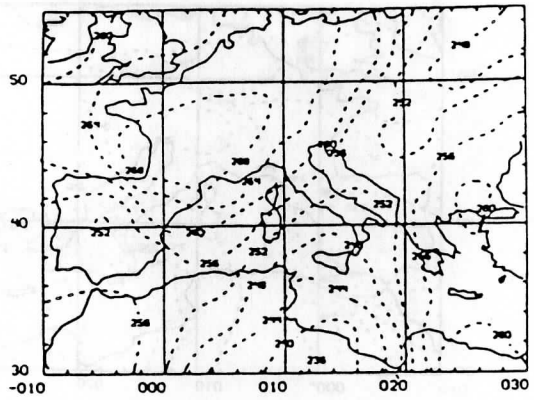

D. 24 HOUR LAGGED ANALYSIS

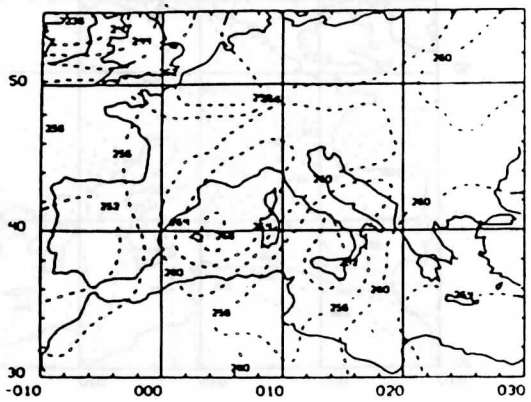

E. RETRIEVED (FORECAST GUESS)

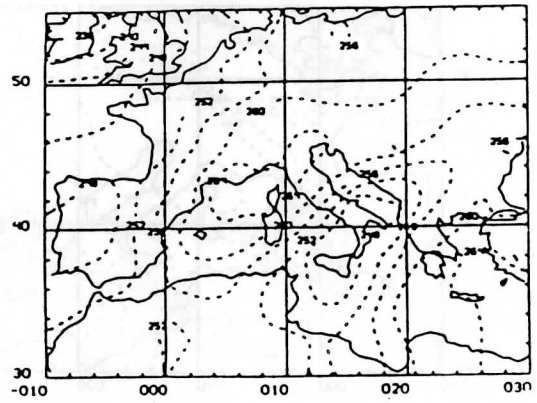

F. 6 HOUR FORECAST

Figure 15

DEW POINT 500 MB MARCH 4, 1982

RETRIEVED 13Z

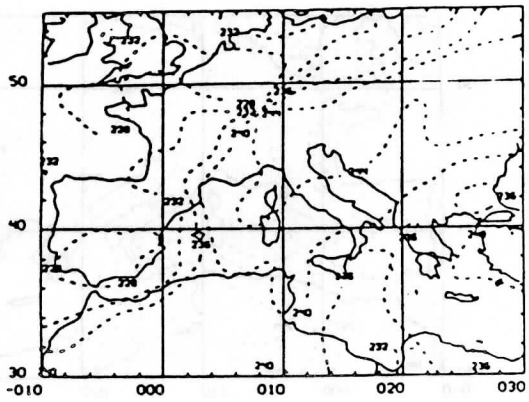

A. RETRIEVED (ANALYSIS GUESS)

GUESS 12Z

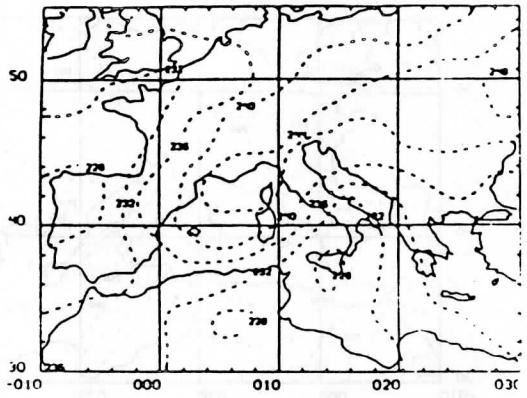

B. CONCURRENT ANALYSIS

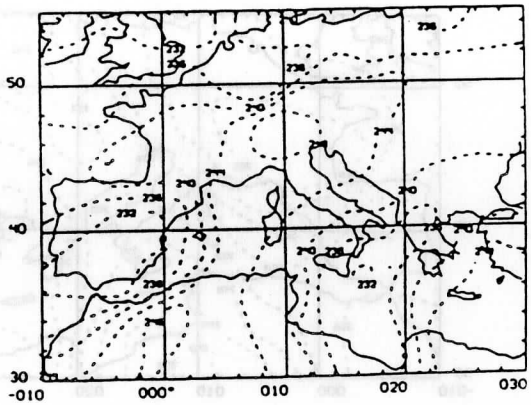

C. RETRIEVED (LAGGED ANALYSIS GUESS)

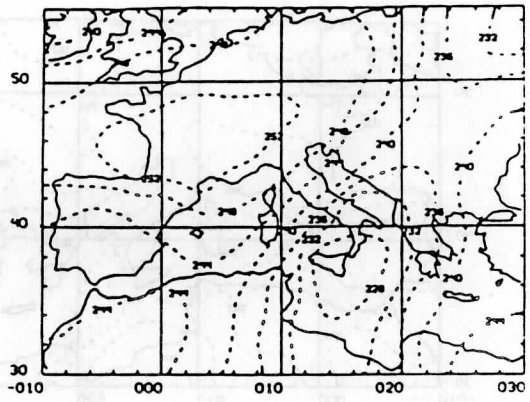

D. 24 HOUR LAGGED ANALYSIS

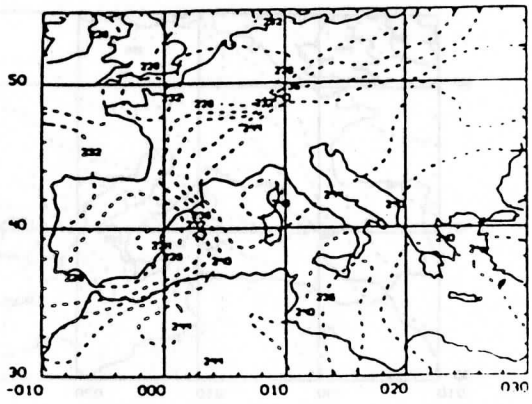

E. RETRIEVED (FORECAST GUESS)

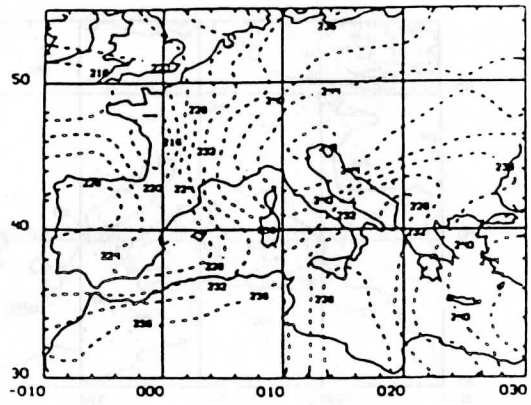

F. 6 HOUR FORECAST

Figure 16

PRECIPITABLE WATER 1000 MB-TOP MARCH 5, 1982 (G/CM^2)

RETRIEVED 03Z

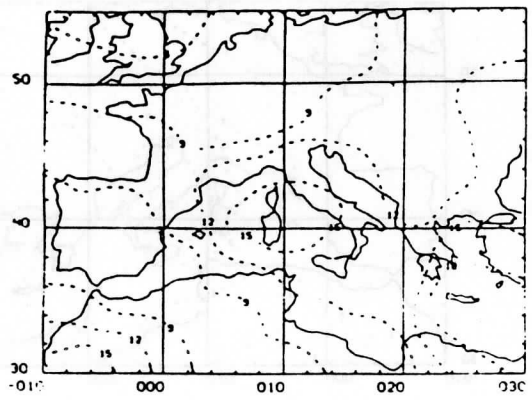

A. RETRIEVED (ANALYSIS GUESS)

GUESS 00Z

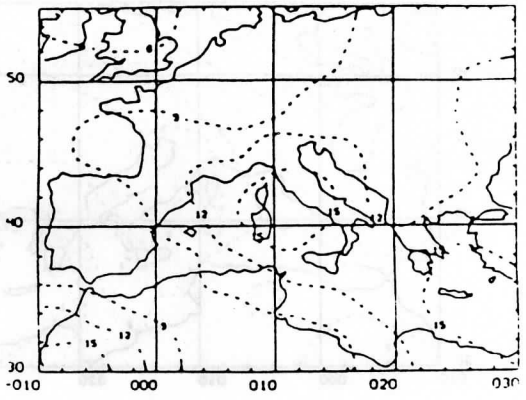

B. CONCURRENT ANALYSIS

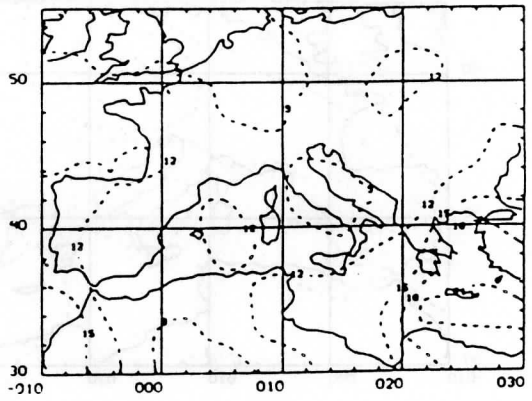

C. RETRIEVED (LAGGED ANALYSIS GUESS)

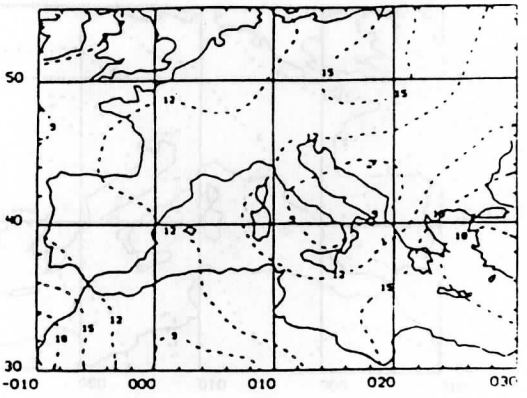

D. 24 HOUR LAGGED ANALYSIS

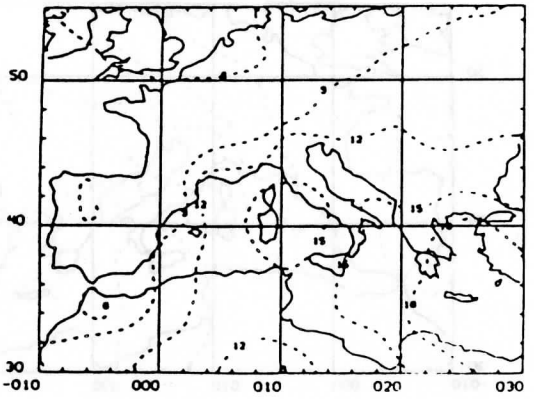

E. RETRIEVED (FORECAST GUESS)

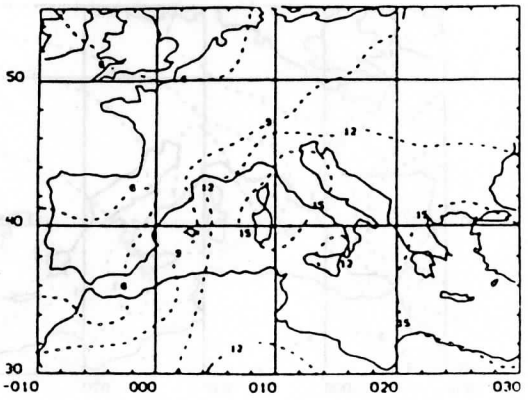

F. 6 HOUR FORECAST

Figure 17

PRECIPITABLE WATER 700 MB-TOP MARCH 5, 1982 (G/CM^2 x 10)

RETRIEVED 03Z

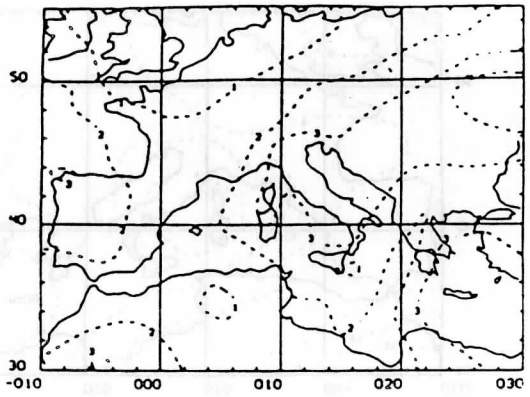

A. RETRIEVED (ANALYSIS GUESS)

GUESS 00Z

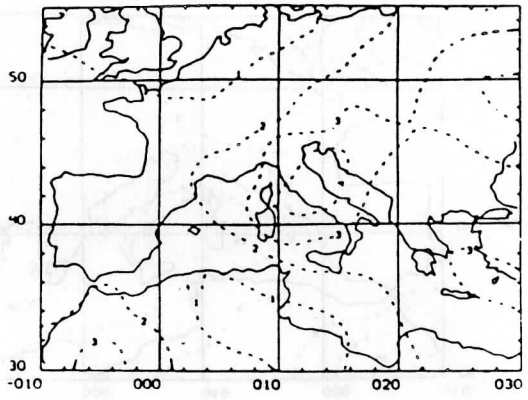

B. CONCURRENT ANALYSIS

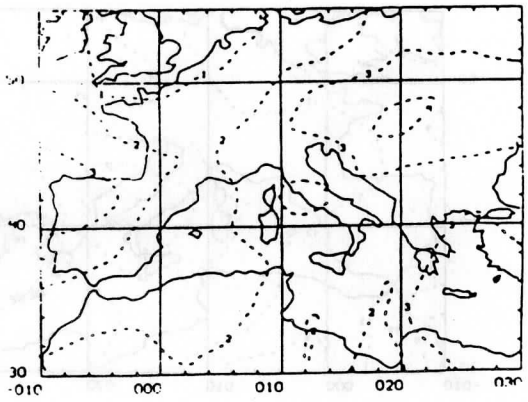

C. RETRIEVED (LAGGED ANALYSIS GUESS)

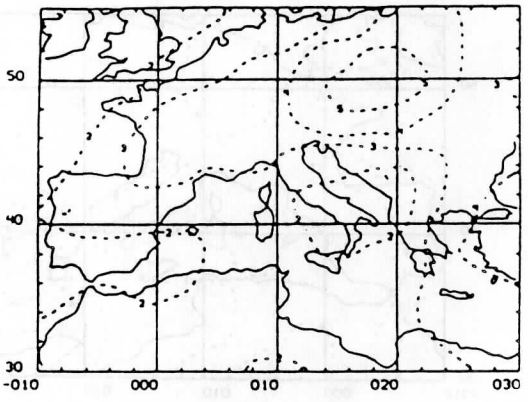

D. 24 HOUR LAGGED ANALYSIS

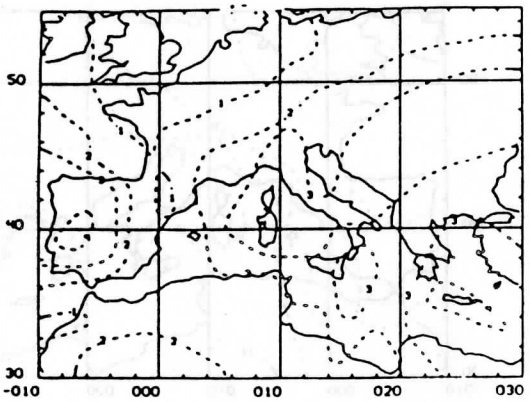

E. RETRIEVED (FORECAST GUESS)

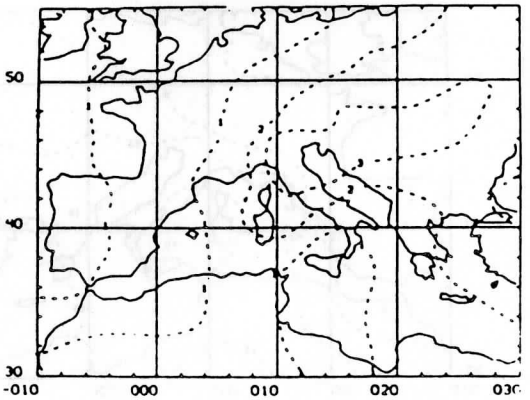

F. 6 HOUR FORECAST

Figure 18

PRECIPITABLE WATER 500 MB-TOP MARCH 5, 1982 (G/CM^2 x 100)

RETRIEVED 03Z

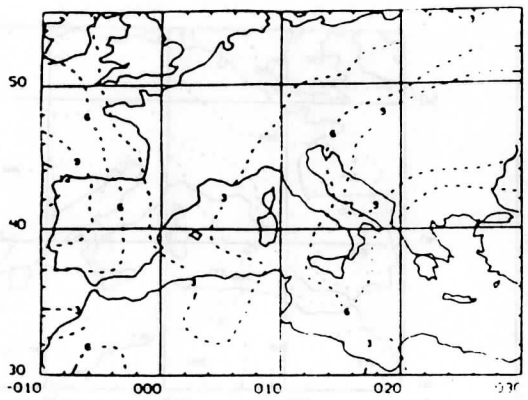

A. RETRIEVED (ANALYSIS GUESS)

GUESS 00Z

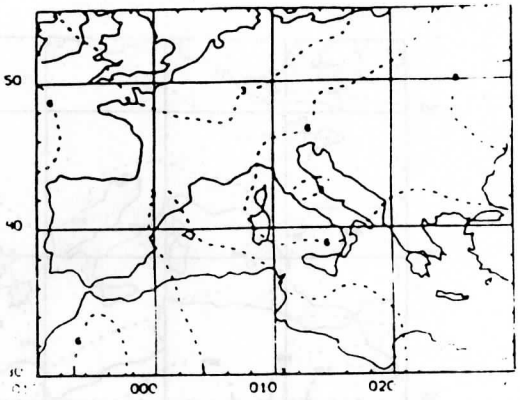

B. CONCURRENT ANALYSIS

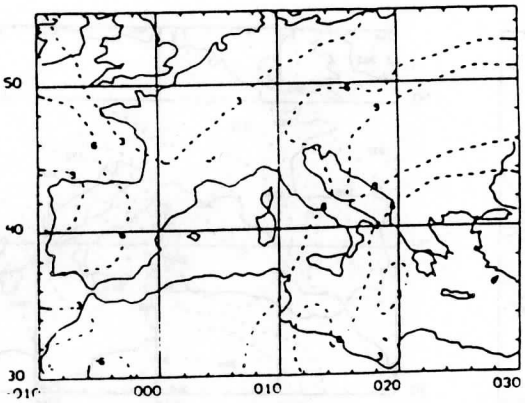

C. RETRIEVED (LAGGED ANALYSIS GUESS)

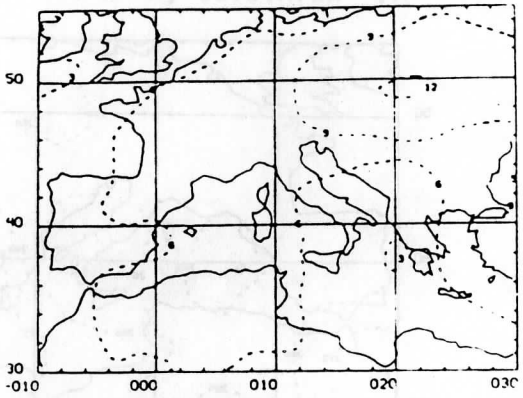

D. 24 HOUR LAGGED ANALYSIS

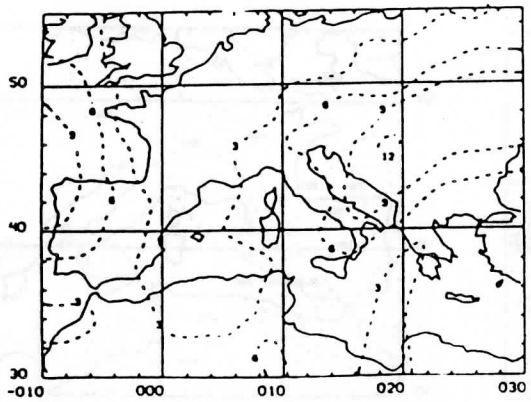

E. RETRIEVED (FORECAST GUESS)

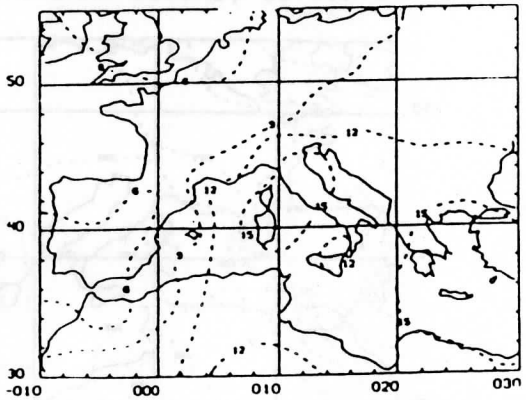

F. 6 HOUR FORECAST

Figure 19

DEW POINT 850 MB MARCH 5, 1982

RETRIEVED 03Z

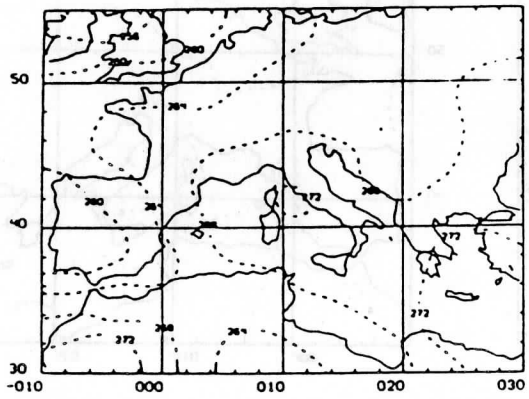

A. RETRIEVED (ANALYSIS GUESS)

GUESS 00Z

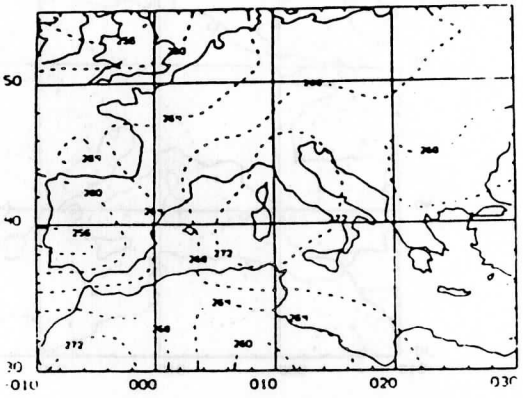

B. CONCURRENT ANALYSIS

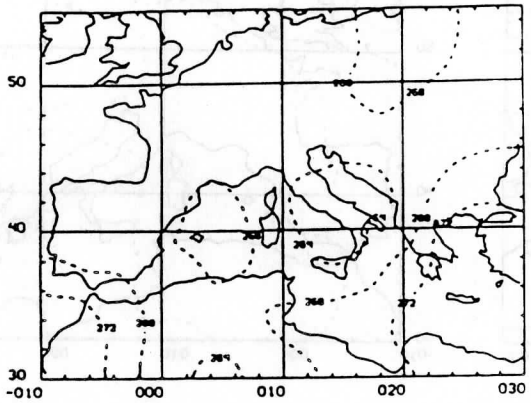

C. RETRIEVED (LAGGED ANALYSIS GUESS)

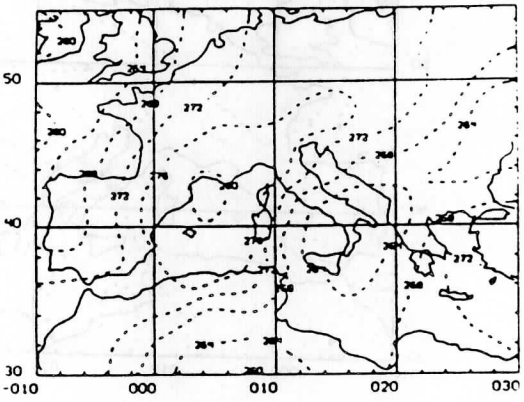

D. 24 HOUR LAGGED ANALYSIS

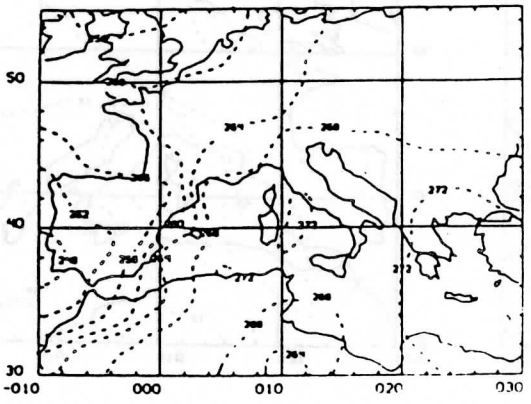

E. RETRIEVED (FORECAST GUESS)

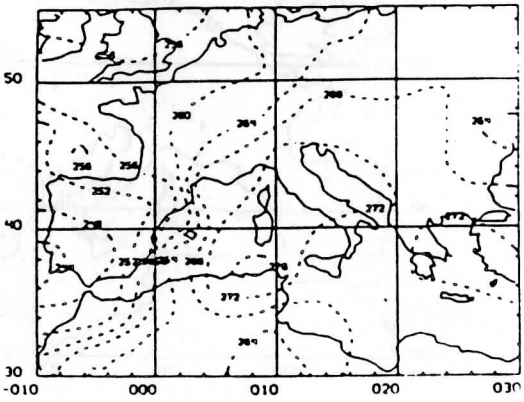

F. 6 HOUR FORECAST

Figure 20

DEW POINT 700 MB MARCH 5, 1982

RETRIEVED 03Z

GUESS 00Z

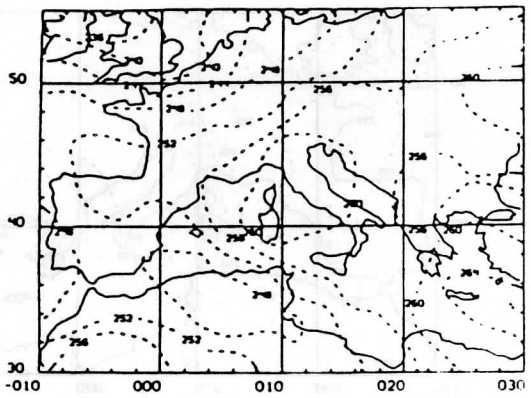

A. RETRIEVED (ANALYSIS GUESS)

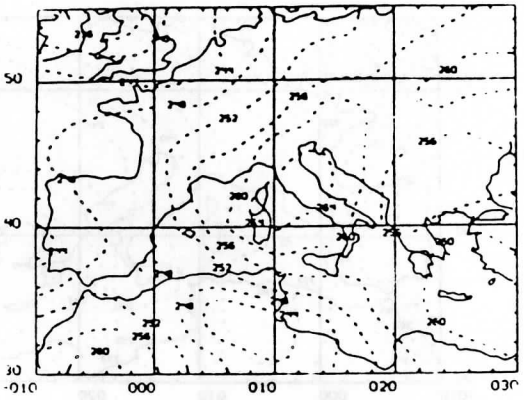

B. CONCURRENT ANALYSIS

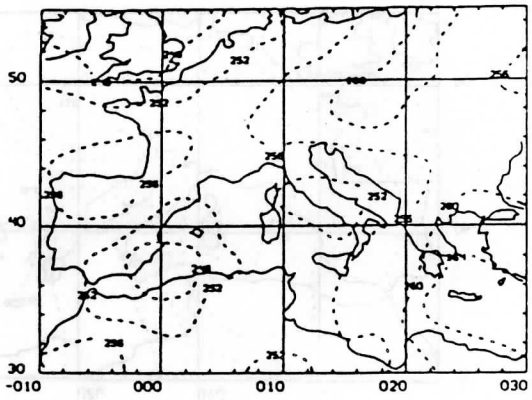

C. RETRIEVED (LAGGED ANALYSIS GUESS)

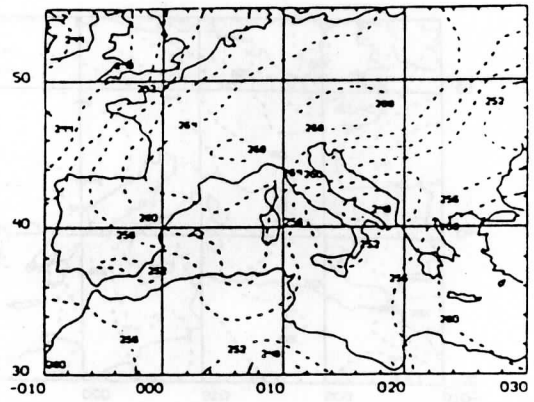

D. 24 HOUR LAGGED ANALYSIS

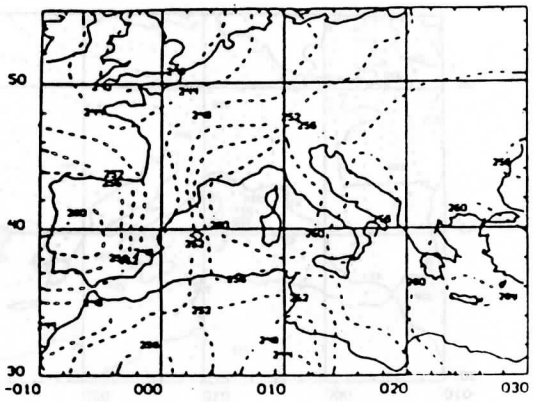

E. RETRIEVED (FORECAST GUESS)

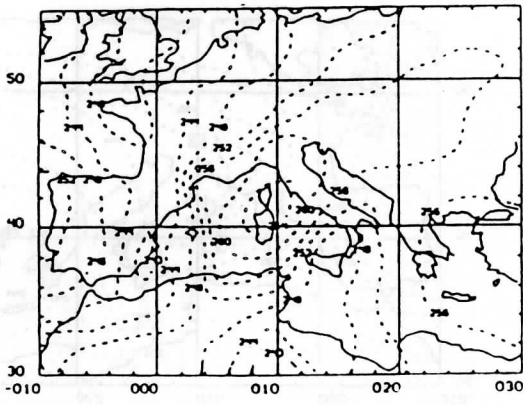

F. 6 HOUR FORECAST

Figure 21

DEW POINT 500MB MARCH 5, 1982

RETRIEVED 03Z

GUESS 00Z

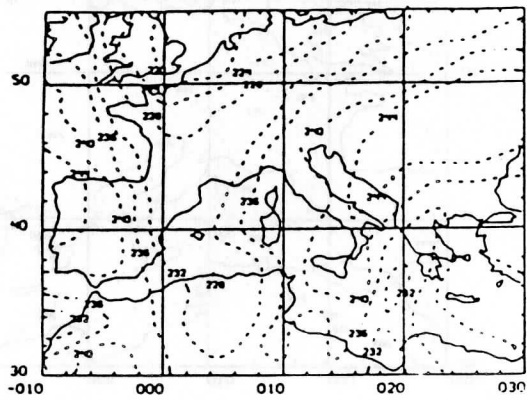

A. RETRIEVED (ANALYSIS GUESS)

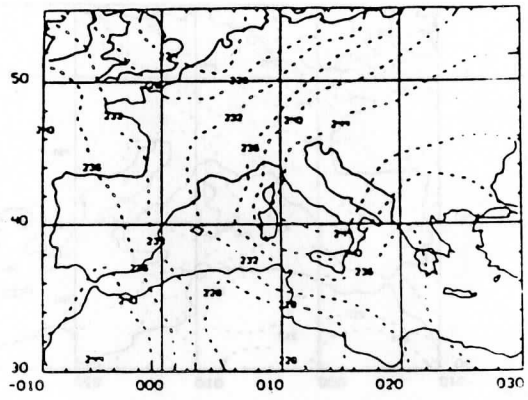

B. CONCURRENT ANALYSIS

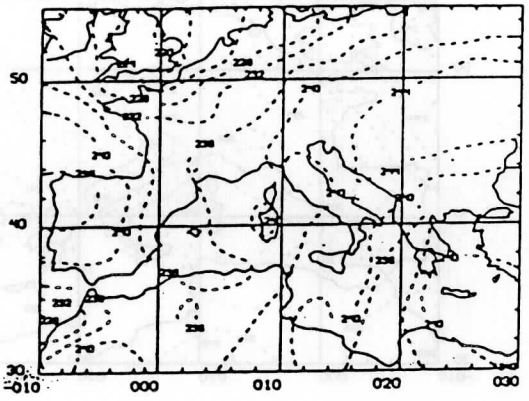

C. RETRIEVED (LAGGED ANALYSIS GUESS)

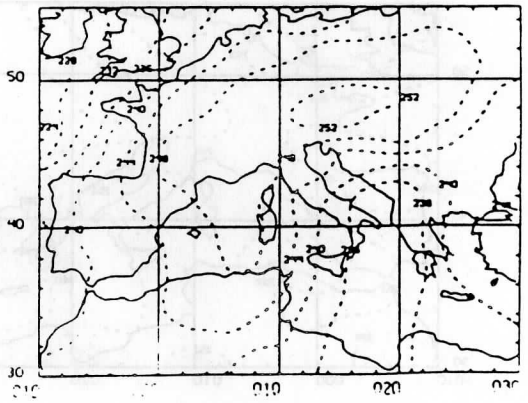

D. 24 HOUR LAGGED ANALYSIS

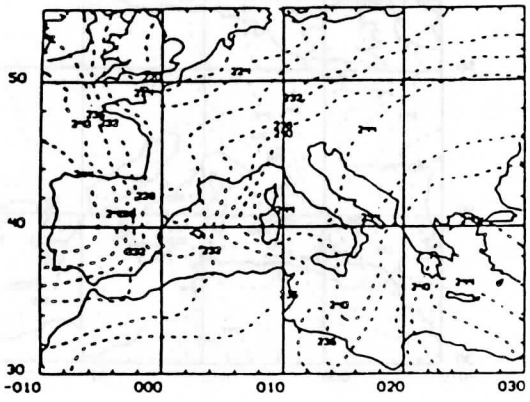

E. RETRIEVED (FORECAST GUESS)

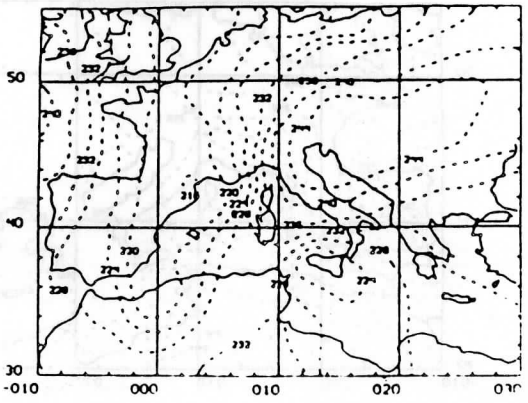

F. 6 HOUR FORECAST

Figure 22

A NONLINEAR INVERSION METHOD FOR DERIVATION OF TEMPERATURE PROFILES FROM TOVS-DATA

J. Svensson

The Swedish Meteorological and Hydrological Institute (SMHI)
Norrköping, Sweden

1. INTRODUCTION

The Physical Retrieval TOVS Export Package, developed by the Cooperative Institute for Meteorological Satellite Studies (CIMSS), Madison, Wisconsin, has been implemented on the computer system at SMHI. The ONSAM-experiment gave an opportunity to test the software package. The ONSAM-experiment took place at Onsala Space Observatory (57°24'N, 11°55'E), May 2-26, 1983. The primary objective of this project was to test the performance and profiling capability of ground-based temperature and water vapour microwave radiometers developed at Chalmers University of Technology (Askne, 1984).

During the ONSAM-experiment TIP-data were received from the Danish Meteorological Institute, Observatory for Space Research, Rude Skov, Birkeröd, Denmark, where a read-out station is situated. The implementation of the TOVS Export Package and test results are described by Svensson (1984). The results from the TOVS Export Package are compared to those from a new physical, nonlinear inversion method developed at SMHI. In the development of the new inversion method the approach was

1) efficient and publically available numerical software should be used,
2) the method should be easy to analyse,
3) new ancillary data should be easy to incorporate.

Those readers who are not already familiar with the characteristics of the TIROS Operational Vertical Sounder (TOVS) are referred to Lauritsen et al (1979), Werbowetski (1981) or Smith and Woolf (1976).

2. INVERSION METHOD

The basis of the inversion method is the radiative transfer equation (RTE). Surface observations of temperature, humidity and pressure are also incorporated in the inversion method. Basis splines (B-splines) have been used to represent the temperature and humidity profiles. Some physical constraints, represented as linear inequality constraints are also included. This leads to a linear least-squares problem with linear inequality constraints to solve. Because of the nonlinear properties of the radiative transfer equation, we may have to repeat this process once or twice.

This chapter describes all the parts of the inversion method, which is called THAP (Temperature and Humidity Atmospheric Profiler). More details about the algorithms and computations are found in Svensson (1985).

2.1 Radiative transfer equation

The radiative transfer equation for satellite based radiance measurements is

$$\gamma_\nu = \varepsilon_\nu \cdot B_\nu(T_S) \cdot \tau_\nu(P_S) - \int_0^{P_S} B_\nu(T) \cdot \frac{\partial \tau_\nu(P)}{\partial P} \cdot dP,$$

where the following notation is used:

γ_ν	radiance measured at channel 'ν',
ν	channel number (20 infrared and 4 microwave channels are available),
P	pressure (P_S is surface pressure),
$T(P)$	temperature (T_S is surface skin temperature),
ε_ν	emissivity,
$\tau_\nu(P)$	transmittance,
$B_\nu(T)$	Planck function.

The dependency of zenith angle is to be understood. Calculation of transmittance is described in Weinreb et al (1981). These calculations are made available through a NOAA software package for 40 different levels, between 0.1 and 1000 mb. For simplicity we assume that P_S is 1000 mb. Transmittance depends not only on frequency, angle and pressure level, but also on temperature, water content and ozone content between the pressure level of interest and the satellite. We also define

$W(P)$	water vapour mixing ratio (g/kg),
$V(P)$	ln (W).

Throughout this paper, we will indicate matrices with a double wavy underline and vectors with one wavy underline. The element in row 'i' and column 'j' for a matrix $\underset{\approx}{A}$ is denoted a_{ij} and the element 'i' in a vector $\underset{\sim}{A}$ is denoted a_i. Especially we note that P, T and V are vectorized into $\underset{\sim}{P}$, $\underset{\sim}{T}$ and $\underset{\sim}{V}$ for the 40 pressure levels.

2.2 Taylor expansion

Suppose we have an initial guess of temperature, surface skin temperature and humidity ($T^{(0)}$, $T_S^{(0)}$ and $V^{(0)}$). We make a first-order Taylor expansion about $T^{(0)}$, $T_S^{(0)}$ and $V^{(0)}$ and get

$$y_\nu = \gamma_\nu - \varepsilon_\nu \cdot B_\nu(T_S^{(0)}) \cdot \tau_\nu(P_S) + \int_0^{P_S} B_\nu(T^{(0)}) \cdot \frac{\partial \tau_\nu(P)}{\partial P} \cdot dP$$

$$\approx \frac{\partial \gamma_\nu}{\partial \underset{\sim}{T}} \cdot \Delta \underset{\sim}{T} + \frac{\partial \gamma_\nu}{\partial T_S} \cdot \Delta T_S + \frac{\partial \gamma_\nu}{\partial \underset{\sim}{V}} \cdot \Delta \underset{\sim}{V}. \qquad (1)$$

In the calculation of the partial derivatives we use standard software for numerical differentiation and numerical quadrature. Equation (1) may in a shorter form be written

$$\underset{\sim}{Y} = \underset{\approx}{R}_T \cdot \Delta\underset{\sim}{T} + \underset{\sim}{R}_S \cdot \Delta T_S + \underset{\approx}{R}_V \cdot \Delta\underset{\sim}{V} ,$$

where $\underset{\approx}{R}_T$ and $\underset{\approx}{R}_V$ are mxn-dimensional matrices, $\underset{\sim}{R}_S$ is a m-dimensional vector, m is the number of frequencies and n is the number of pressure levels (=40). With $\underset{\sim}{T}^{(0)} + \Delta\underset{\sim}{T}$, $T_S^{(0)} + \Delta T_S$ and $\underset{\sim}{V}^{(0)} + \Delta\underset{\sim}{V}$, we receive better approximation of $\underset{\sim}{T}$, T_S and $\underset{\sim}{V}$.

In order to scale the equations properly, each equation, corresponding to channel ν should be multiplied by $1/\frac{\partial B_\nu(B^{-1}(\gamma_\nu))}{\partial T}$. The term $B^{-1}(\gamma_\nu)$ is called brightness temperature. The weights, of each equation, are based upon the estimated errors in the brightness temperature for each frequency.

2.3 Ancillary data

Ancillary data are given by surface observations of temperature (T_{OBS}) and humidity ($V_{OBS} = \ln(W_{OBS})$). This will give two equations

$$\Delta t_{40} = T_{OBS} - t_{40}^{(0)} \tag{2}$$

and

$$\Delta v_{40} = V_{OBS} - v_{40}^{(0)} . \tag{3}$$

The initial temperature profile is given for 40 levels. However we only allow ΔT to be non-zero for pressure levels up to 10 mb (which corresponds to level 11). Besides we require that Δt_{11} should not be too large. This will give the equation

$$\Delta t_{11} = 0 . \tag{4}$$

The difference between the variables t_{40} and T_S is assumed to be small. The equation

$$\Delta t_{40} - \Delta T_S = T_S^{(0)} - t_{40}^{(0)} \tag{5}$$

will express this relation.

The equations (2)-(5) are weighted, based upon the estimated errors in the variables involved.

2.4 B-splines

We use a set of basis functions, for the variables T and V, instead of discretizing the variables in 40 levels. This will increase the accuracy of the solution and decrease the number of arithmetic operations. We choose cubic B-splines, with ln(P) as independent variable, to form the basis functions. Some very attractive features of B-splines are

1) well-developed theory,
2) excellent approximation properties;
   the function, its integral and derivatives are calculated easy and accurate,
3) publically available numerical software exists.

B-splines are described by de Boor (1978).

We have already mentioned, that we do not allow the temperature to be changed above the 10 mb-level. Besides we do not allow the water vapour to be changed over the 300 mb-level (level 26). This can be expressed in the choice of the knots, which define the B-splines. The knots for the B-splines representing T are the logarithms of Ψ_T = {4*10, 100,200,300,400,500,600,700,850,4*1000}.

Thus we may express the initial guess temperature profile up to 10 mb as

$$T^{(0)}(P) = \sum_{i=1}^{12} c_i \cdot B_i(\Psi_T, P) \quad ,$$

where c_i are spline coefficients for temperature profile and $B_i(\Psi_T,P)$ is the B-spline 'i' for the given set of knots, Ψ_T, at pressure P.

In the same way we will have

$$V^{(0)}(P) = \sum_{i=1}^{9} d_i \cdot B_i(\Psi_V, P)$$

where d_i are spline coefficients for V and $B_i(\Psi_V,P)$ is the B-spline 'i' for the given set of knots, Ψ_V, at pressure P.

The knots for the B-splines representing V up to 300 mb are the logarithms of Ψ_V = {4*300,400,500,600,700,850,4*1000}.

We may represent ΔT and ΔV with B-splines in the same way, with the spline coefficients $\underset{\sim}{\Delta C}$ and $\underset{\sim}{\Delta D}$ respectively. Then (1)-(5) together with the new basis functions will give the linear system

$$\underset{\approx}{R}_T \cdot \underset{\approx}{S} \cdot \underset{\sim}{\Delta C} + \underset{\sim}{R}_S \cdot \Delta T_S + \underset{\approx}{R}_V \cdot \underset{\approx}{U} \cdot \underset{\sim}{\Delta D} = \underset{\sim}{Y} \qquad (6)$$

$$\underset{\approx}{A}_T \cdot \underset{\sim}{\Delta C} + \underset{\sim}{A}_S \cdot \Delta T_S + \underset{\approx}{A}_V \cdot \underset{\sim}{\Delta D} = \underset{\sim}{Z} \qquad (7)$$

where the new elements in (6) are

$$s_{ij} = \begin{cases} 0 & , \quad i = 1,2,....10, \quad j = 1,....12, \\ B_j(\Psi_T, P_i) & , \quad i = 11,12,...40, \quad j = 1,....12, \end{cases}$$

$$u_{ij} = \begin{cases} 0 & , \quad i = 1,2,....25, \quad j = 1,....9, \\ B_j(\Psi_V, P_i) & , \quad i = 26,27,....40, j = 1,....9. \end{cases}$$

Equation (7) is formed by (2)-(5) where

$$\underset{\approx}{A}_T = \begin{pmatrix} 000000000001 \\ 000000000000 \\ 100000000000 \\ 000000000001 \end{pmatrix} ,$$

$$\underset{\sim}{A}_S = (0,0,0-1)^T ,$$

$$\underset{\approx}{A}_V = \begin{pmatrix} 000000000 \\ 000000001 \\ 000000000 \\ 000000000 \end{pmatrix} ,$$

$$\underset{\sim}{Z} = (T_{OBS} - t_{40}^{(0)}, V_{OBS} - v_{40}^{(0)}, 0, T_S^{(0)} - t_{40}^{(0)})^T .$$

We have a linear least-squares problem with 22 unknown and m+4 equations. Optimization problems, including least-squares problems, are described in Gill et al (1981). The weighted (6) and (7) can in short form be written

$$\min_{\underset{\sim}{F}} \{||\underset{\approx}{K} \cdot \underset{\sim}{F} - \underset{\sim}{G}||_2\} \qquad (8)$$

where

$$\underset{\approx}{K} = \underset{\approx}{E} \cdot \begin{pmatrix} \underset{\approx}{R}_T \cdot \underset{\approx}{S} & \underset{\sim}{R}_S & \underset{\approx}{R}_V \cdot \underset{\approx}{U} \\ \underset{\approx}{A}_T & \underset{\sim}{A}_S & \underset{\approx}{A}_V \end{pmatrix} ,$$

$$\underset{\sim}{F} = (\Delta\underset{\sim}{C}^T, \Delta T_S, \Delta\underset{\sim}{D}^T)^T ,$$

$$\underset{\sim}{G} = \underset{\approx}{E} \cdot (\underset{\sim}{Y}^T, \underset{\sim}{Z}^T)^T ,$$

$\underset{\approx}{E}$ is a (m+4) x (m+4)-diagonal matrix, where element e_{ii} is the weight for equation 'i'.

This problem is ill-posed. That is, taking the least-squares solution

$$\underset{\sim}{F} = (\underset{\approx}{K}^T\underset{\approx}{K})^{-1}\cdot\underset{\approx}{K}^T\cdot\underset{\sim}{G} ,$$

we will have a physically unacceptable solution, because of the influence of measurement error in the RTE. A survey of inversion problems in remote sensing is found in Twomey (1977). In order to have a physically acceptable and mathematically accurate solution, we may add physical constraints and penalty terms.

2.5 Physical constraints

Physical constraints added to an inverse problem will often, as a complement to other methods, improve the solution. Here we will use two physical constraints, which are transformed to linear inequality constraints.

The dry adiabatic lapse rate, defined in Holton (1979), is constraining the temperature variations by $\frac{dT}{d\ln(P)} \leq R/C_p \cdot T$ where R and C_p are constants. With a representation of T in B-splines we will have in terms of the unknown $\underset{\sim}{\Delta C}$,

$$\sum_{i=1}^{12} (B_i'(\Psi_T,P) - R/C_p\cdot B_i(\Psi_T,P))\cdot\Delta c_i \leq$$

$$\sum_{i=1}^{12} (-B_i'(\Psi_T,P) + R/C_p\cdot B_i(\Psi_T,P))\cdot c_i .$$

We check these constraints for the pressure levels 26, 27 ,,,, 40.

The relative humidity has to be in the interval 0 to 100%. The lower limit is automatically fulfilled because we use the variable V = ln(W). From the basic laws of thermodynamics we derive $V \leq \alpha + \beta(1/273 - 1/T)$, where α and β are constants (α depends on the pressure).

This is a nonlinear constraint. We may linearize it by doing a Taylor expansion about $T^{(0)}$ and $V^{(0)}$. In terms of the unknown $\underset{\sim}{\Delta C}$ and $\underset{\sim}{\Delta D}$ we then have

$$\sum_{i=1}^{9} B_i(\Psi_V,P)\cdot\Delta d_i - \beta/(T^{(0)}\cdot T^{(0)})\cdot\sum_{i=1}^{12} B_i(\Psi_T,P)\cdot\Delta c_i \leq$$

$$\alpha + \beta(1/273-1/T^{(0)}) - V^{(0)} .$$

We check these constraints for the pressure levels 26, 27, ..., 40.

2.6 Penalty terms

We will add penalty terms, or regularization functionals, which reflects the supposed behaviour of the solution to the inverse problem. We will require that the variables T and V will be smooth. We then change (8) to

$$\min_{\underset{\sim}{F}} \{||\underset{\approx}{K}\cdot\underset{\sim}{F} - \underset{\sim}{G}||_2 + \lambda_T \cdot I_T + \lambda_V \cdot I_V\} \qquad (9)$$

where

$$I_T = \int_{\ln(10)}^{\ln(1000)} (T"(P))^2 d\ln(P) ,$$

$$I_V = \int_{\ln(300)}^{\ln(1000)} (V"(P))^2 d\ln(P)$$

and λ_T, λ_V are positive, regularization parameters to be decided (T" and V" are short for $\frac{d^2T}{d\ln(P)^2}$ and $\frac{d^2V}{d\ln(P)^2}$. A similar penalty term for temperature profiles, where $(\Delta T)"$ is used instead of T", have been proposed by O'Sullivan and Wahba (1984).

If we use spline representation we will have $I_T = (\underset{\sim}{C} + \underset{\sim}{\Delta C})^T \underset{\approx}{Q} (\underset{\sim}{C} + \underset{\sim}{\Delta C})$ and $I_V = (\underset{\sim}{D} + \underset{\sim}{\Delta D})^T \underset{\approx}{H} (\underset{\sim}{D} + \underset{\sim}{\Delta D})$,

where

$$q_{ij} = \int_{\ln(10)}^{\ln(1000)} B_i"(\Psi_T,P)\cdot B_j"(\Psi_T,P)\cdot d\ln(P) , \qquad i, j \leq 12,$$

and

$$h_{ij} = \int_{\ln(300)}^{\ln(1000)} B_i"(\Psi_V,P)\cdot B_j"(\Psi_V,P)\cdot d\ln(P) , \qquad i, j \leq 9.$$

The matrices $\underset{\approx}{Q}$ and $\underset{\approx}{H}$ can be calculated analytically with few arithmetic operations. Both matrices are symmetric and positive definite. We make a Cholesky factorization, which gives $\underset{\approx}{Q} = \underset{\approx}{L}_T^T \cdot \underset{\approx}{L}_T$ and $\underset{\approx}{H} = \underset{\approx}{L}_V^T \cdot \underset{\approx}{L}_V$ ($\underset{\approx}{L}_T$ and $\underset{\approx}{L}_V$ are triangular matrices).

Now (9) may be rewritten

$$\min_{\underset{\sim}{F}} (||\underset{\approx}{K}\cdot\underset{\sim}{F} - \underset{\sim}{G}||_2 + \lambda_T ||\underset{\approx}{L}_T \cdot \underset{\sim}{\Delta C} + \underset{\approx}{L}_T \cdot \underset{\sim}{C}||_2 + \lambda_V ||\underset{\approx}{L}_V \cdot \underset{\sim}{\Delta D} + \underset{\approx}{L}_V \cdot \underset{\sim}{D}||_2), \qquad (10)$$

which is an ordinary least-squares problem in the unknown $\Delta\underset{\sim}{C}$, ΔT_S and $\Delta\underset{\sim}{D}$. The regularization parameters λ_T and λ_V have to be estimated. We will do a subjective estimation of the parameters. Several different values of these parameters have been tested and those two, which seemed to give the best result were chosen. The regularization parameters may be automatically computed by the method of generalized cross-validation, see Craven and Wahba (1979) or Golub et al (1979). The algorithms are developed for non-constrained linear, least-squares problems with one regularization parameter. Generalized cross-validation has recently been extended to be used for nonlinear problems by O'Sullivan and Wahba (1984).

2.7 Solving the linear least-squares problems subject to linear inequality constraints

We will now solve the linear least-squares problem (10) subject to the linear inequality constraints described in Section 2.5. We use the algorithm developed by Stoer (1971). This algorithm also solves least-squares problems with equality constraints. If none of the constraints is active, the computational work in solving the problem, is comparable with methods used for linear least-squares problems without constraints.

We have now received a better approximation of $\underset{\sim}{T}$, T_S and $\underset{\sim}{V}$, with $\underset{\sim}{T}^{(1)} = \underset{\sim}{T}^{(0)} + \Delta\underset{\sim}{T}$, $T_S^{(1)} = T_S^{(0)} + \Delta T_S$ and $\underset{\sim}{V}^{(1)} = \underset{\sim}{V}^{(0)} + \Delta\underset{\sim}{V}$. With few modifications of the algorithms, we may use $\underset{\sim}{T}^{(1)}$, $T_S^{(1)}$ and $\underset{\sim}{V}^{(1)}$ as a new initial guess, and repeat the procedure. This will account for the non-linear properties of the radiative transfer equation. Two or three iterations seem to be enough.

3. DATA PROCESSING

The Physical TOVS Export Package, dated 24 September, 1983 and described by Smith et al (1984), was used. The ordinary retrieval program (FXTIRO) was replaced by our method (THAP). The retrieval programs, both FXTIRO and THAP, offer a lot of alternatives. The programs were executed with the following options:

1) Analysed values of surface temperature, surface dewpoint temperature and surface pressure are included.
2) Climate was used as first guess profile.
   In THAP we use another first guess for the water vapour. We use the formula $W(P) = W_{OBS} * (P/P_S)^3$, which is suggested by Smith (1966).
3) Profiles are produced from 3 x 3 arrays of HIRS spots. This will give an approximate horizontal resolution of 75 km.
4) The high-resolution topography with a horizontal resolution of ten nautical miles was used.

In THAP we use the HIRS-channels 3,4,5,6,7,8,10,11,12,13,14,15 and 16 and the MSU-channels 3 and 4. This will give a total of 15 equations derived from the radiative transfer equation. Surface emissivities for

the HIRS-channels are given in Table 1, which is taken from Chedin and Scott (1984). Surface emissivity for the MSU-channels is 0.7.

Channel number		7	8	9	10	13	14	18	19
Emissivity	Land	0.98	0.96	0.96	0.93	0.91	0.93	0.88	0.88
	Sea	1.0	0.98	0.98	0.98	0.97	0.98	0.96	0.96

TABLE 1. Surface emissivities for the HIRS channels. An emissivity of 1 is given to the remaining channels.

The weights for the different equations are given in Table 2.

Equation	Weight
Derived from RTE for channel 'ν', eq (6)	$1/\frac{\partial B_\nu(B^{-1}(\gamma_\nu))}{\partial T}$ *
Surface observation of temperature, eq (2)	0.5
Surface observation of humidity, eq (3)	10
Temperature at 10 mb, eq (4)	0.5
Difference between surface temperature and surface skin temperature, eq (5)	0.33

* This weight should be divided with the assumed measurement error in the brightness temperature. According to Susskind and Chahine (1984) this error is estimated to 0.7°K for clear retrievals and 1°K for partly cloudy retrievals. We assume an error of 1°K.

TABLE 2. Weights for each equation used in the inversion method THAP

The regularization parameters were; $\lambda_T = 0.03$ and $\lambda_V = 0.06$. Three iterations were done for each sounding.

4. TESTS

Test data are taken from the Meso-scale Analysis Area for PROMIS 600 at SMHI, see Gustafsson and Törnevik (1984), during the period May 3-26, 1983. Fifteen satellite passages were processed. This area, with the radiosonde stations marked off, is shown in Fig. 1. Temperature retrievals from these radiosondes were compared with satellite soundings in the following way.

1) Radiosonde observations at 00Z and 12Z were used. The nearest time to the satellite passage was used. The radiosonde data have passed certain gross quality checks.
2) The nearest satellite sounding to each radiosonde was chosen. Distance should be less than 150 km.
3) Layer mean temperatures for eight levels were calculated and compared. Root-mean-square difference (RMS), standard deviation (STD) and mean difference (MEAN) were calculated.

Only clear retrievals were analyzed, because the cloud correction algorithms in this version of TOVS Export Package, was not well adapted for our kind of inversion method. Later versions of TOVS Export Package use more suitable cloud correction algorithms. The results from FXTIRO are shown in Fig. 2, while the results from THAP are shown in Fig. 3.

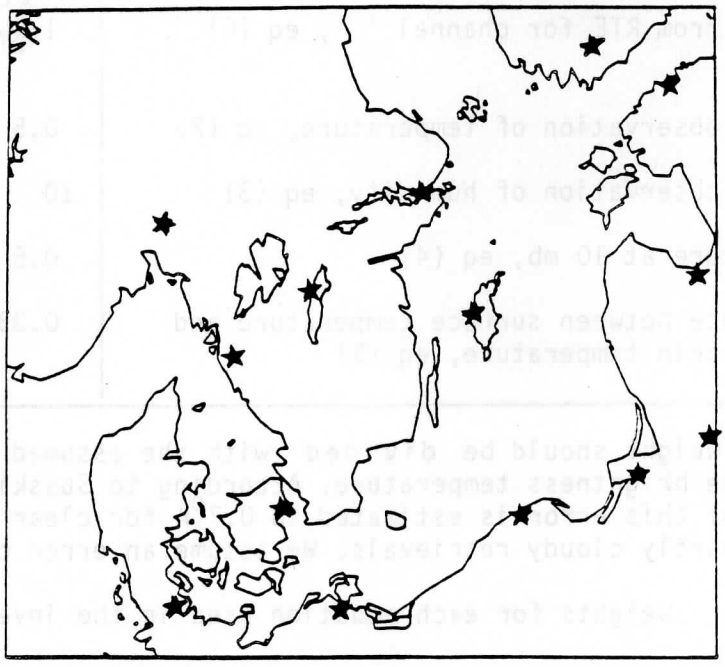

Figure 1. Radiosonde stations in the Meso-scale Analysis Area (appr. 54-61°N, 6-28°E)

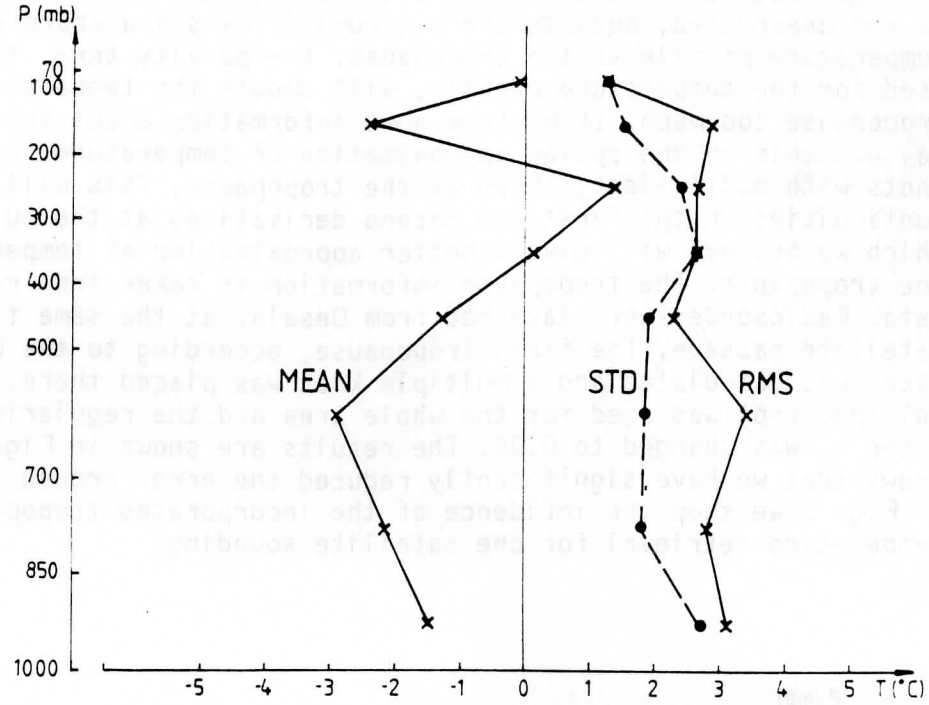

Figure 2. Differences in layer mean temperature between satellite soundings from FXTIRO and radiosondes, launched in the Meso-scale Analysis Area. 104 clear retrievals are included.

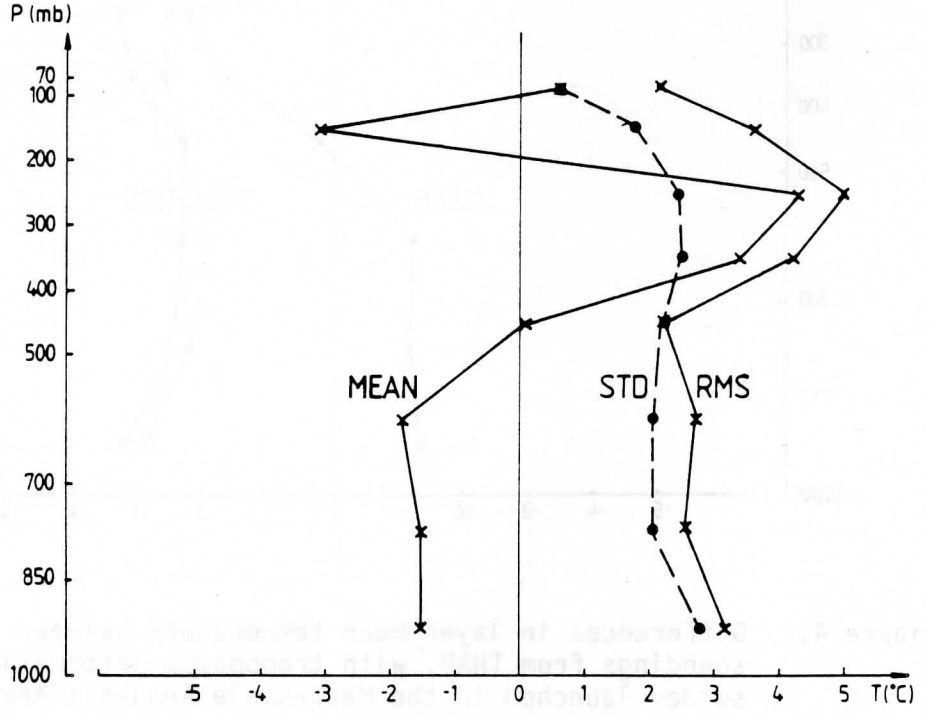

Figure 3. Differences in layer mean temperature between satellite soundings from THAP, without tropopause information, and radiosondes launched in the Meso-scale Analysis Area. 118 clear retrievals are included.

Our method shows a large RMS-difference around the tropopause. This is not unexpected, because there generally exists a sharp edge in the temperature profile at the tropopause. The penalty term, that we have used for the temperature profile, will smooth the temperature around the tropopause too much. If we have some information about the tropopause we may use this in the spline approximation of temperature, by placing knots with multiplicity three at the tropopause. This will give discontinuities in the first and second derivatives at the multiple knot, which we believe will give a better approximation of temperature around the tropopause. The tropopause information is taken from radiosonde data. Radiosondes were launched from Onsala, at the same time as the satellite passage. The first tropopause, according to the WMO definition, was calculated and a multiple knot was placed there. The same multiple knot was used for the whole area and the regularization parameter λ_T was changed to 0.05. The results are shown in Fig. 4. This shows that we have significantly reduced the error around the tropopause. In Fig. 5 we show the influence of the incorporated tropopause on the temperature retrieval for one satellite sounding.

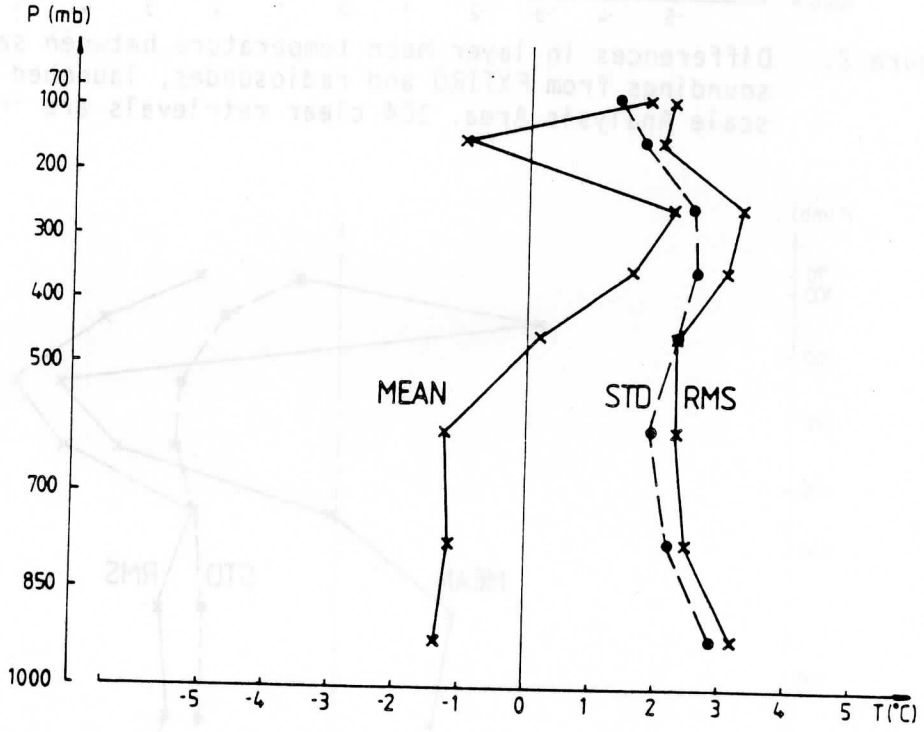

Figure 4. Differences in layer mean temperature between satellite soundings from THAP, with tropopause information, and radiosondes launched in the Meso-scale Analysis Area. 118 clear retrievals are included.

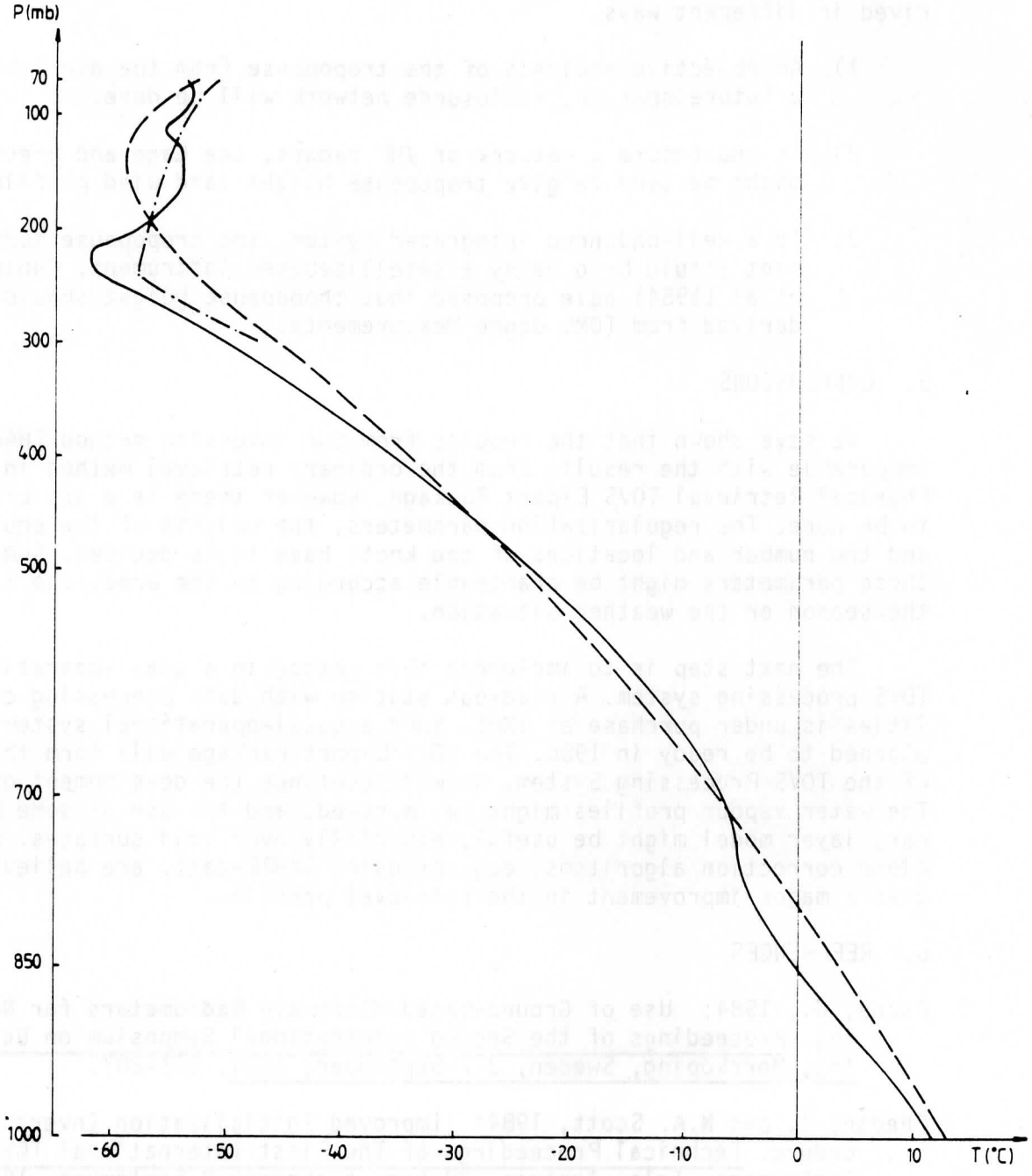

Figure 5. Temperature retrieval from one satellite sounding (1983-05-06 1345, 57°N, 12°E)

——— = radiosonde
------ = THAP, without tropopause
— . — = THAP, with tropopause
(temperature below 300 mb will coincide with the retrieval, without tropopause information)

In an operational system, the tropopause information might be derived in different ways.

1) An objective analysis of the tropopause from the available, or a future sparser, radiosonde network will be done.

2) In the future a network of VHF radars, see Gage and Green (1982) might be used to give tropopause height (and wind profiles).

3) In a well-balanced integrated system, the tropopause measurement should be done by a satellitebased instrument. Munteanu et al (1984) have proposed that tropopause height should be derived from TOMS Ozone Measurements.

5. CONCLUSIONS

We have shown that the results from our inversion method THAP are comparable with the results from the ordinary retrieval method in the Physical Retrieval TOVS Export Package. However there is a lot of tuning to be done. The regularization parameters, the weights of the equations and the number and locations of the knots have to be decided. Some of these parameters might be changeable according to the area, the time of the season or the weather situation.

The next step is to implement this method in a quasi-operational TOVS processing system. A read-out station with data processing capabilities is under purchase at SMHI. Such a quasi-operational system is planned to be ready in 1986. The TOVS Export Package will form the base of the TOVS Processing System. We will continue the development of THAP. The water vapour profiles might be improved, and the use of some boundary layer model might be useful, especially over cold surfaces. Better cloud correction algorithms, e.g. by using AVHRR-data, are believed to give a major improvement in the retrieval profiles.

6. REFERENCES

Askne, J., 1984: Use of Ground-Based Microwave Radiometers for Nowcasting. Proceedings of the Second International Symposium on Nowcasting, Norrköping, Sweden, 3-7 September, 1984, 201-207.

Chedin, A. and N.A. Scott, 1984: Improved Initialization Inversion Procedure. Technical Proceedings of The First International TOVS Study Conference, Igls, Austria, 29 August through 2 September, 1983, 14-79.

Craven, P. and C. Wahba, 1979: Smoothing noisy data with spline functions: estimating the correct degree of smoothing by the method of generalized cross-validation. Numerische Mathematik, 31, 377-403.

de Boor, C., 1978: A Practical Guide to Splines. Springer Verlag, New York.

Gage, K.S. and J.L. Green, 1982: An Objective Method for the Determination of Tropopause Height from VHF Radar Observations. Journal of Applied Meteorology, 21, 1150-1154.

Gill, P.E., W. Murray and M.H. Wright, 1981: Practical Optimization, Academic Press, London.

Golub, G., M. Heath and G. Wahba, 1979: Generalized cross validation as a method for choosing a good ridge parameter. Technometrics, 21, 215-223.

Gustafsson, N. and H. Törnevik, 1984: Development of an Operational System for Very-Short-Range Forecasting (VSRF) at SMHI. Proceedings of the Second International Symposium on Nowcasting, Norrköping, Sweden, 3-7 September, 1984, 473-477.

Holton, J.R., 1979: An Introduction to Dynamic Meteorology, Academic Press, New York.

Lauritsen, L., G.J. Nelson and F.W. Porto, 1979: Data extraction and calibration of TIROS-N/NOAA radiometers. NOAA Technical Memorandum NESS 107. U.S. Department of Commerce, National Oceanic and Atmospheric Administration, National Earth Satellite Service, Washington D.C., 73 pp.

Munteanu, M.J., E.R. Westwater and N.C. Grody, 1984: Improvement of MSU Temperature Retrievals by Use of Tropopause Heights Derived from TOMS Ozone Measurements. Technical Proceedings of The First International TOVS Study Conference, Igls, Austria, 29 August through 2 September, 1983, 165-172.

O'Sullivan, F. and G. Wahba, 1984: A cross validated bayesian retrieval algorithm for non-linear remote sensing experiments. Technical Report No 747, Dept of statistics, University of Wisconsin, Madison, Wisconsin, 20 pp.

Smith, W.L., 1966: Note on the Relationship between Total Precipitation Water and Surface Dew Point, Journal of Applied Meteorology, 5, 726-727.

Smith, W.L. and H.M. Woolf, 1976: The use of eigenvectors of statistical covariance matrices for interpreting satellite sounding radiometer observations. Journal of Atmospheric Science, 35, 1127-1140.

Smith, W.L., H.M. Woolf, C.M. Hayden, A.J. Schreiner and J.F. Le Marshall, 1984: The Physical Retrieval TOVS Export Package. Technical Proceedings of The First International TOVS Study Conference, Igls, Austria, 29 August through 2 September, 1983, 227-278.

Stoer, J., 1971: On the numerical solution of constrained least-squares problems. SIAM Journal of Numerical Analysis, 8, 382-411.

Susskind, J. and M.T. Chahine, 1984: The GLAS Physical Numerical Algorithm for Analysis of HIRS 2/MSU Data. Technical Proceedings of The First International TOVS Study Conference, Igls, Austria, 29 August through 2 September, 1983, 285-299.

Svensson, J., 1984: Temperature profile retrievals from TIROS Operational Vertical Sounder during the ONSAM-experiment. R & D notes 33, SMHI, Norrköping, Sweden, 13 pp.

Svensson, J., 1985: Remote sensing of atmospheric temperature profiles by TIROS Operational Vertical Sounder, RMK 45, SMHI, Norrköping, Sweden, (to appear).

Twomey, S., 1977: An introduction to the mathematics of inversion in remote sensing and indirect measurements. Elsevier, New York.

Weinreb, M.P., H.E. Fleming, L.M. McMillin and A.C. Neundorffer, 1981: Transmittances for the TIROS Operational Vertical Sounder, NOAA Technical Report NESS 85, U.S. Department of Commerce, National Oceanic and Atmospheric Administration, National Earth Satellite Service, Washington D.C., 65 pp.

Werbowetski, A. (Ed.), 1981: Atmospheric Sounding User's Guide. NOAA Technical Report NESS 83, U.S. Department of Commerce, National Oceanic and Atmospheric Administration, National Earth Satellite Service, Washington D.C., 82 pp.

THE DETERMINATION OF HIRS SCENE TEMPERATURES FROM AVHRR DATA

B. F. Taylor

Cooperative Institute for Meteorological Satellite Studies
University of Wisconsin and
New Zealand Meteorological Service, Wellington

C. M. Hayden

NOAA/NESDIS Systems Design and Applications Branch
Madison, Wisconsin

W. L. Smith

Cooperative Institute for Meteorological Satellite Studies
University of Wisconsin
Madison, Wisconsin

1. INTRODUCTION

This paper introduces a technique for providing AVHRR estimates of the cloud-free and cloud overcast visible and window infrared radiance contributions within the field of view of the High Resolution Infrared Sounding (HIRS) instrument. The purpose is to identify uniform scenes within the HIRS field of view to facilitate cloud identification and provide surface/cloud temperatures for temperature and moisture profile processing.

2. COLOCATION OF AVHRR WITH HIRS

Colocation of the AVHRR and HIRS is complicated by two factors. First, the instruments scan in opposite directions. Second, the scan time for the AVHRR is 1/6 s and for the HIRS 6.4 s (including retrace). Thus, there are 38.4 AVHRR lines per HIRS line and the lines are tilted with respect to each other such that the 38.4 AVHRR lines actually overlap parts of three HIRS lines. Aoki (1980) has analyzed the geometry of this situation and provided a look-up table such that the pixel numbers of 39 AVHRR lines are identified as to where they fall within the HIRS FOV (56 spots per line; three lines). We have used Aoki's method for our colocation, without any adjustment for sensor misalignment (such as described by Aoki). To account for the timing problem, AVHRR data are processed in a repeating cycle of 38, 39, 38, 39, 38 (mean 38.4) lines. A complete cycle accommodates three complete HIRS lines and parts of another four. The geometry associated with this procedure is shown in Figure 1. Note that the first 38 lines of the next full cycle will complete HIRS line 4 which is numbered in parentheses. The entire swath is processed to output AVHRR/HIRS lines for AVHRR ch-1 (0.58-0.68 μm), ch-3 (3.55-3.93 μm) and ch-4 (10.3-11.3 μm).

2.2 Detection of Uniform or Multiple-Temperature Scenes

For retrieving temperature and moisture profiles, it is important that the scene be uniform, i.e. not containing multiple levels of cloud or even rugged topography. It is permissible that the FOV contain targets at two uniform temperatures since these FOVs may be reduced to a single scene by the adjacent-field-of-view correction method described in a companion paper (Hayden, et al.). The large samples (approximately 300-600) of AVHRR spots within the HIRS FOV are used to determine the uniformity by some simple statistical tests applied to channel 4. The data are then reduced to three radiances per channel per HIRS FOV to give:

- cold target;
- average;
- warm target.

All three values are filled for dual-temperature scenes, while uniform scenes have the same value in both average and warm target positions. If the warm target radiance is missing the HIRS retrieval algorithm will skip the scene.

Initially, the scatter of the data determines whether the FOV contains a single or multiple temperature scene. A standard deviation of 4 mW m^{-2} SR^{-1} cm is used as the threshold (corresponding to 2K at a temperature of 300K). For FOVs which pass this test, average scene and warm uniform scene radiances are provided (in each channel).

FOVs failing the uniformity test are examined by the spatial coherence technique of Coakley and Bretherton (1982). Considering the AVHRR pixels to be divided into 3x3 sub-arrays, the mean radiance and standard deviation of each sub-array is found. If standard deviation is plotted against mean, the resulting scatter diagram has a characteristic form when targets at two or more temperatures are present (see for example Fig. 6). Points at the "feet" correspond to data from a single target (i.e., cloud-free or cloud overcast) while points in the "arches" represent sub-arrays containing multiple targets (i.e., partly cloudy field of views).

A rather simple algorithm (as contrasted to the method used by Coakley and Bretherton) is currently used to define the "feet." A histogram with class interval of two radiance units is assembled from the sample of subarrays. Each contribution to a class interval is weighted according to its standard deviation

$$W_i = 0 \text{ for } SD_i > 4 \quad (1)$$

$$W_i = 0.25\ (4. - SD_i) \quad (2)$$

Where SD is the standard deviation (trapped at 4.) and i refers to the subarray. A running mean filter of two intervals is passed over the final histogram. Cold and warm "peaks" are then located by moving in from the extremes until a class interval containing a maximum with a value of 1. or greater is located. A final cold or warm value is determined by averaging over two class intervals on either side of

each peak. If this procedure finds two "feet" which are not the same, three scene radiances are passed to subsequent processing.

For this case study, FOVs successfully processed are assumed to consist of targets at two temperatures only, corresponding to the warmest and coldest feet. A further test to eliminate scenes with more than two targets is available; regression of channel 3 against channel 4 may reject FOVs on the basis of excessive standard error of regression. However, this proved severe and was suspended to maximize the number of FOVs available for downstream processing by the retrieval algorithm.

3. DATA

Data for 7 June 1984 were obtained for a case study. TOVS data are available from 13:56:03 GMT to 14:04:16 GMT. The AVHRR data are available from 13:54:10 GMT to 14:01:15 GMT, but the infrared channels are missing or excessively noisy until 13:56:48 GMT. Hence, the period when AVHRR data may be used to assist the TOVS retrieval processing is from 13:56:48 GMT to 14:01:15 GMT. This period contains the 37 HIRS lines between the first and second HIRS calibration gaps.

4. RESULTS

4.1 Colocation

Figures 2 and 3 show, respectively, an image of the HIRS channel-8 (11.1 micrometer) and the corresponding average value from the colocated AVHRR channel-4. Each square represents a HIRS FOV. Over the full sample, the brightness temperatures from each source produced a correlation of 0.994. Visually, it is apparent that the colocation is quite successful.

4.2 Scene Discrimination

With the present algorithms and quality-control thresholds, 90% of the FOVs yielded uniform or dual radiances (approximately half of each).

Figure 4 shows, for part of the scene, the positions and types of classifiable FOVs superimposed over the AVHRR image. Note that despite the ragged nature of the clouds, most of the HIRS FOVs are deemed adequate for further processing. It is not obvious at this resolution why an FOV has been selected as uniform or dual-temperature, but at higher magnification the eye can usually verify the decision of the algorithm. For example, in Figure 5, three scenes are shown from the left central portion of Figure 4. Only spot (18'11) was successfully processed as a uniform scene. The other two were correctly identified as multiple scene.

Figure 6 shows a graphic of the AVHRR distribution as processed by the Coakley-Bretherton algorithm. The ordinate is a standard deviation and the abscissa is mean radiance. In the diagram, a cold and warm "foot" are clearly evident and there is even a hint of an

intermediate foot although the last is not sufficiently distinct to cause a multiple scene categorization. These features are consistent with the imagery (Figure 4) which shows in FOV (line 17' spot 9) a nearly even division between clear air and high cloud, the latter showing a cellular structure, affording a view of lower cloud (the intermediate foot).

Figure 7 shows superimposed points for three adjacent FOVs which cross the edge of the main cumulonimbus anvil at the top centre of Figure 4. The FOV (11'16) has a well-defined low radiance from the anvil while 11'14 has a well-defined higher radiance from the surrounding lower layer. FOV (11'15) spans the two layers and produces the expected arch structure with feet located precisely at the two layer radiances.

5. SUMMARY

Preliminary results are encouraging in that sensor colocation accuracy is acceptable and scene discrimination/temperature determination algorithms yield results which generally agree with subjective interpretation of the data. This work is not yet complete, however; and additional effort is required to adjust the various quality control checks for optimum performance on this and other cases. The example of the use of these AVHRR uniform scene radiances in the processing of TOVS data is given in a companion paper by Hayden, et al. (1985).

6. REFERENCES

Aoki, T., 1980: A method for matching the HIRS/2 and AVHRR pictures of TIROS-N satellites. Tech. Note No. 2, Met. Sat. Center, Japan, 15-26.

Coakley, J. A. Jr. and Bretherton, F. P., 1982: Cloud cover from high resolution scanner data: detecting and allowing for partially-filled fields of view. J. Geophys. Res., 87, 4917-4932.

Hayden, C. M., W. L. Smith, H. M. Woolf, B. F. Taylor, 1985: An application of AVHRR data to TOVS retrievals. Submitted to TOVS-II Conference.

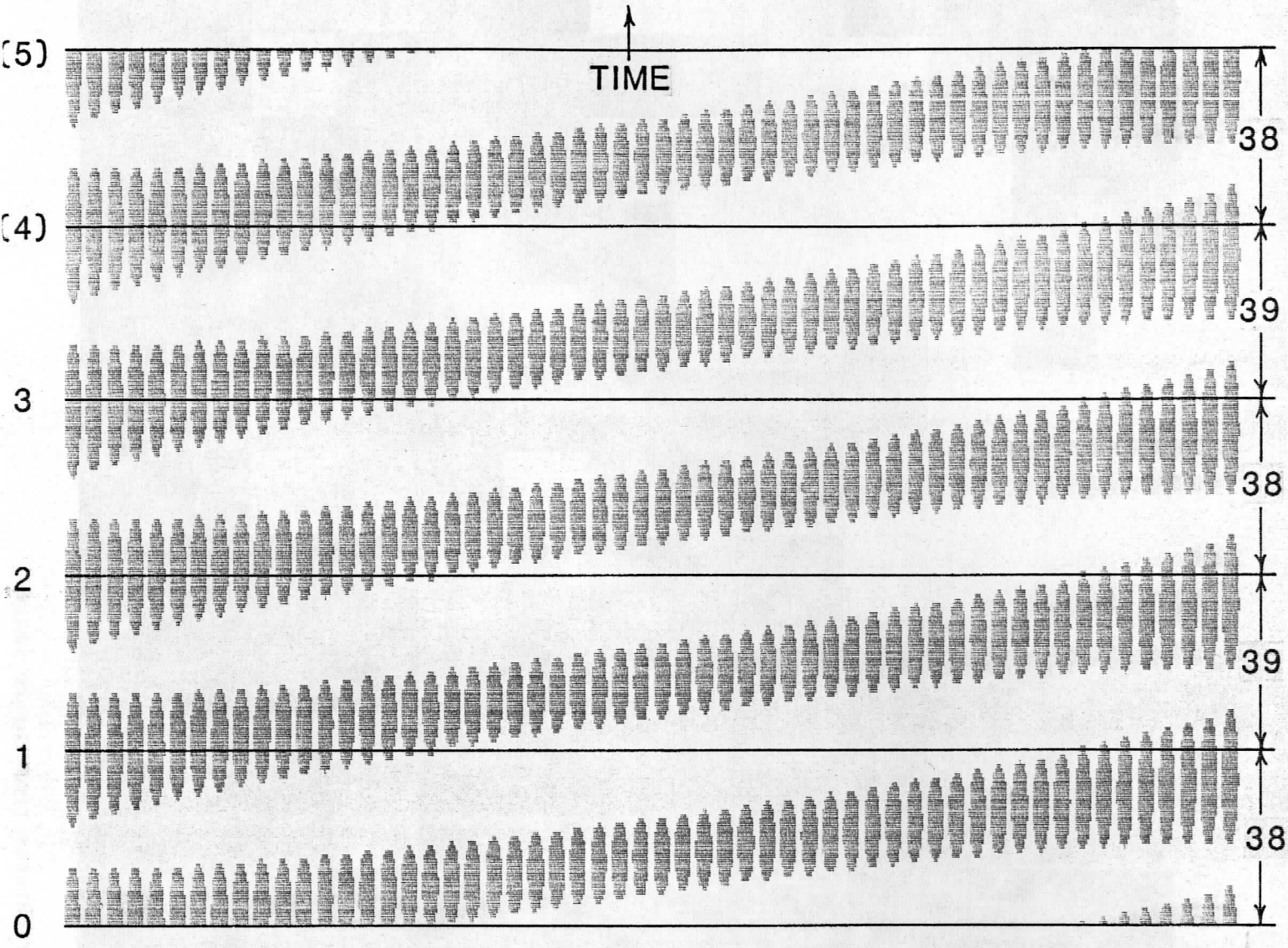

Figure 1. A schematic of the Aoki colocation of AVHRR and HIRS FOV (ovals). HIRS FOV are distorted for convenience of figure. A cycle of five batches of AVHRR lines is shown (numbered at right) corresponding to three complete lines of HIRS (numbered at left). HIRS lines numbered parenthetically will be filled in the next cycle.

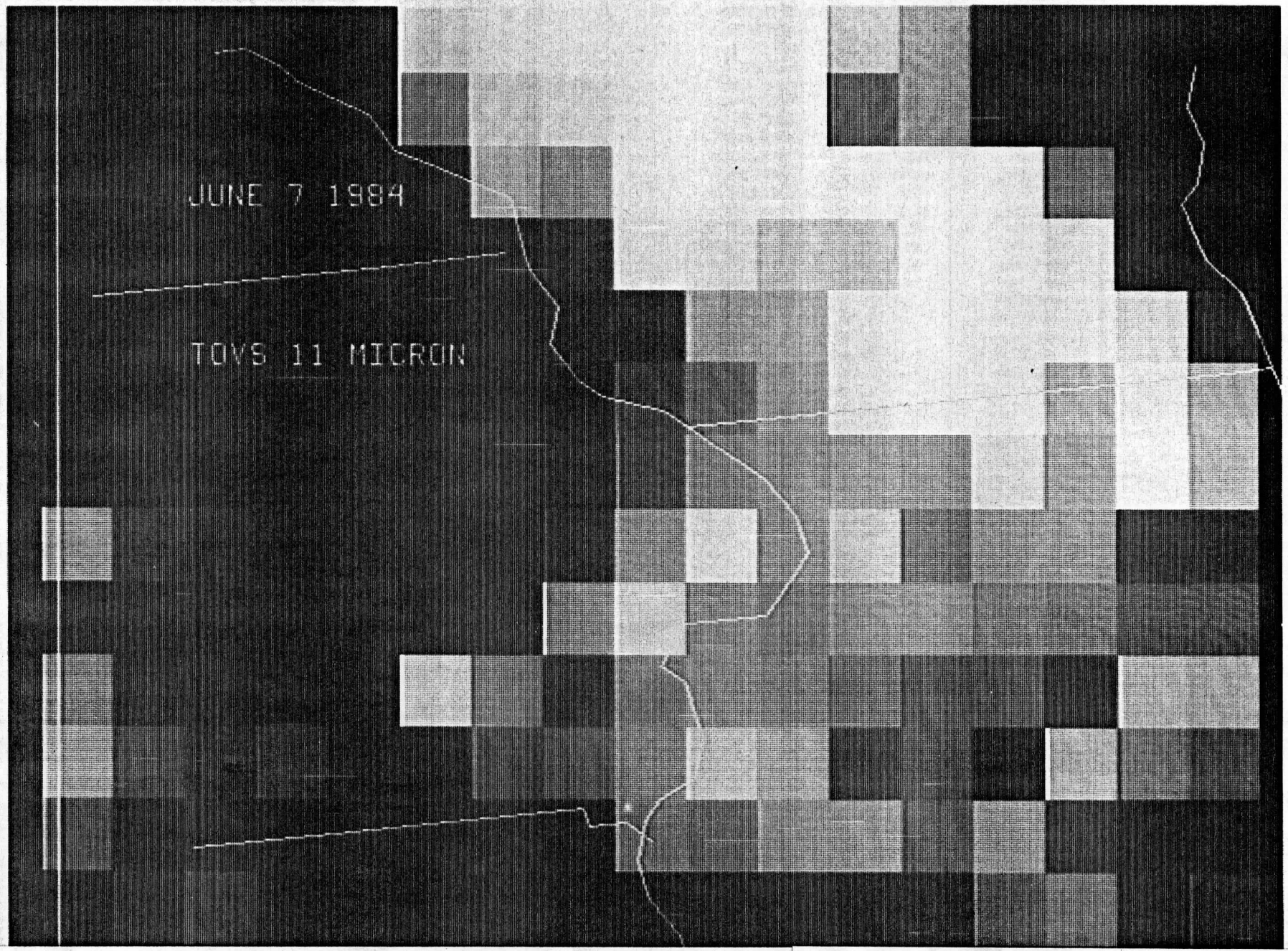

Figure 2. HIRS channel-8 brightness temperature image.

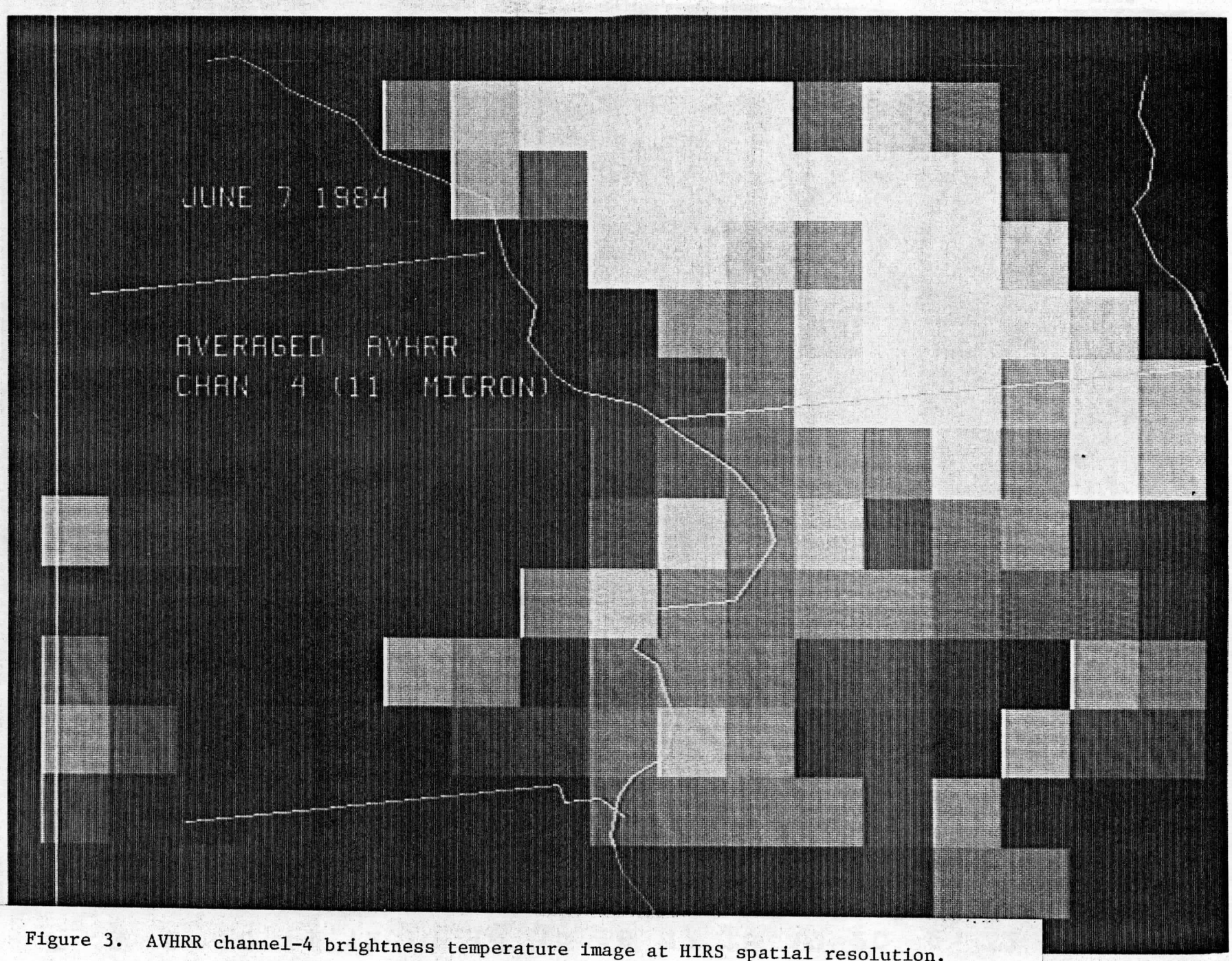

Figure 3. AVHRR channel-4 brightness temperature image at HIRS spatial resolution.

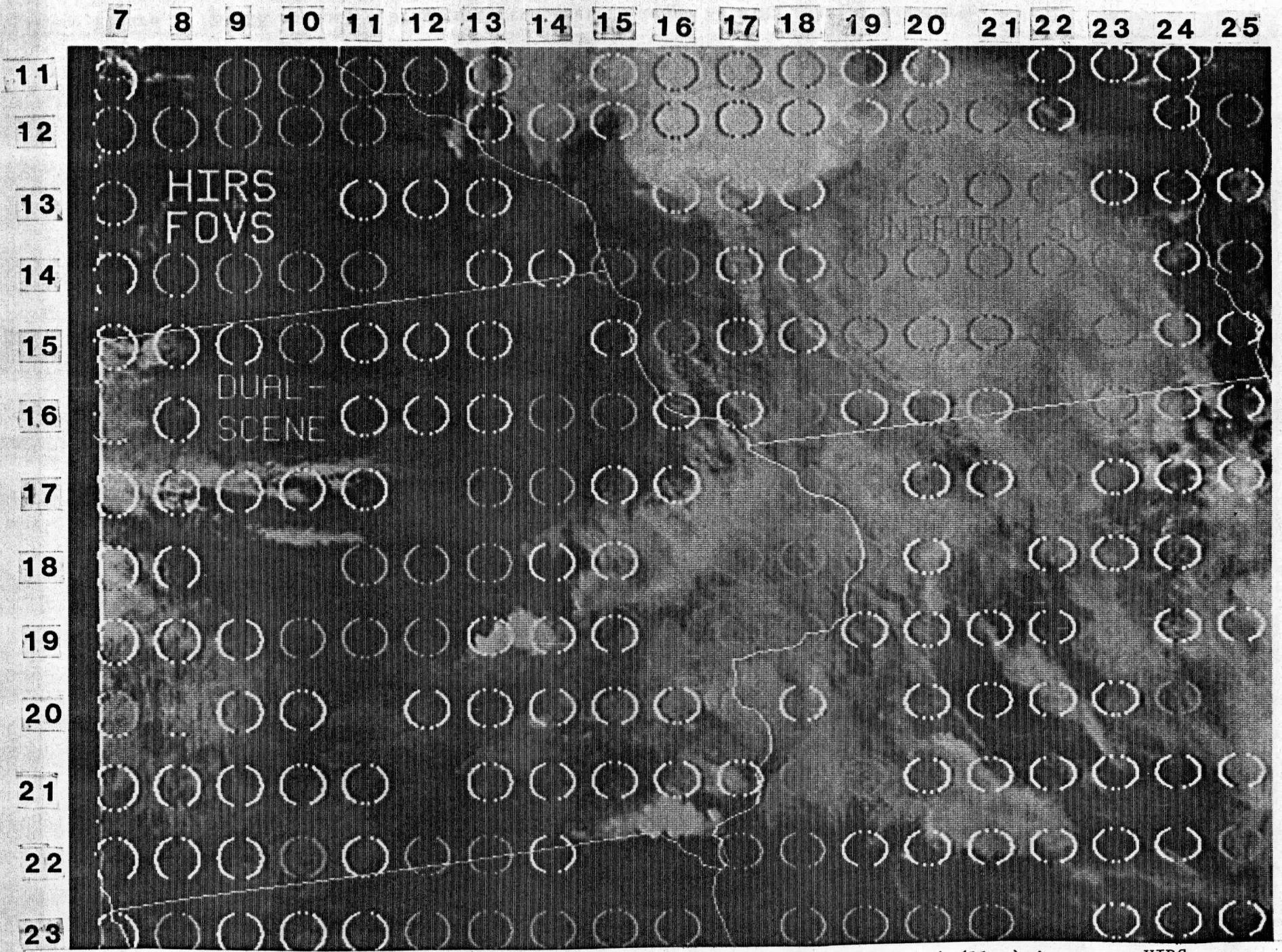

Figure 4. Positions and types of HIRS fields of view superimposed on AVHRR ch-4 (11μm) imagery. HIRS row and FOV numbers, referred to in subsequent figures, are defined at the boundaries. Grey

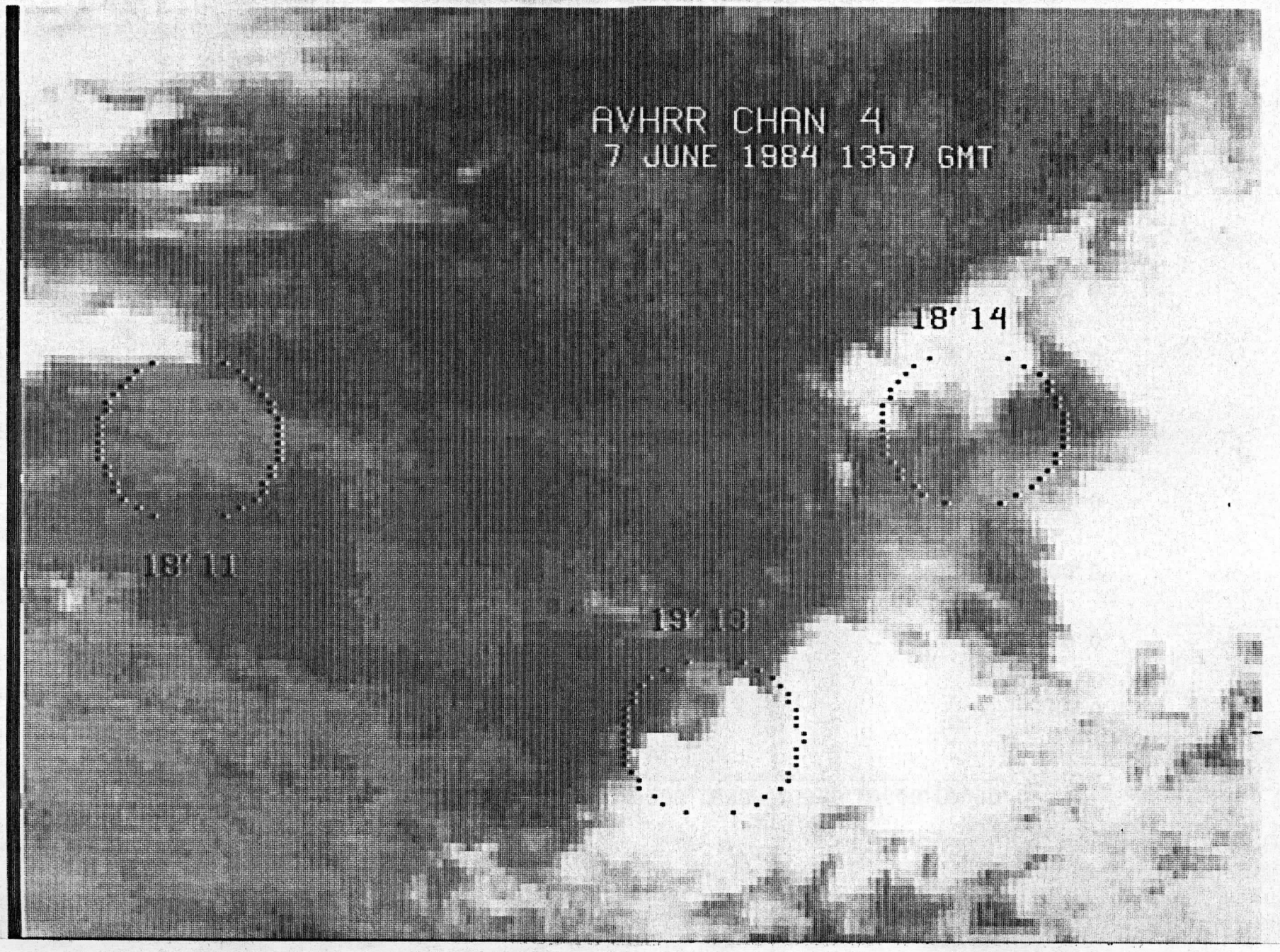

Figure 5. Blow-up of Figure 4 showing three HIRS FOV which were tested. Spot (18'11) passed as uniform scene. The other spots failed as being multiple scene.

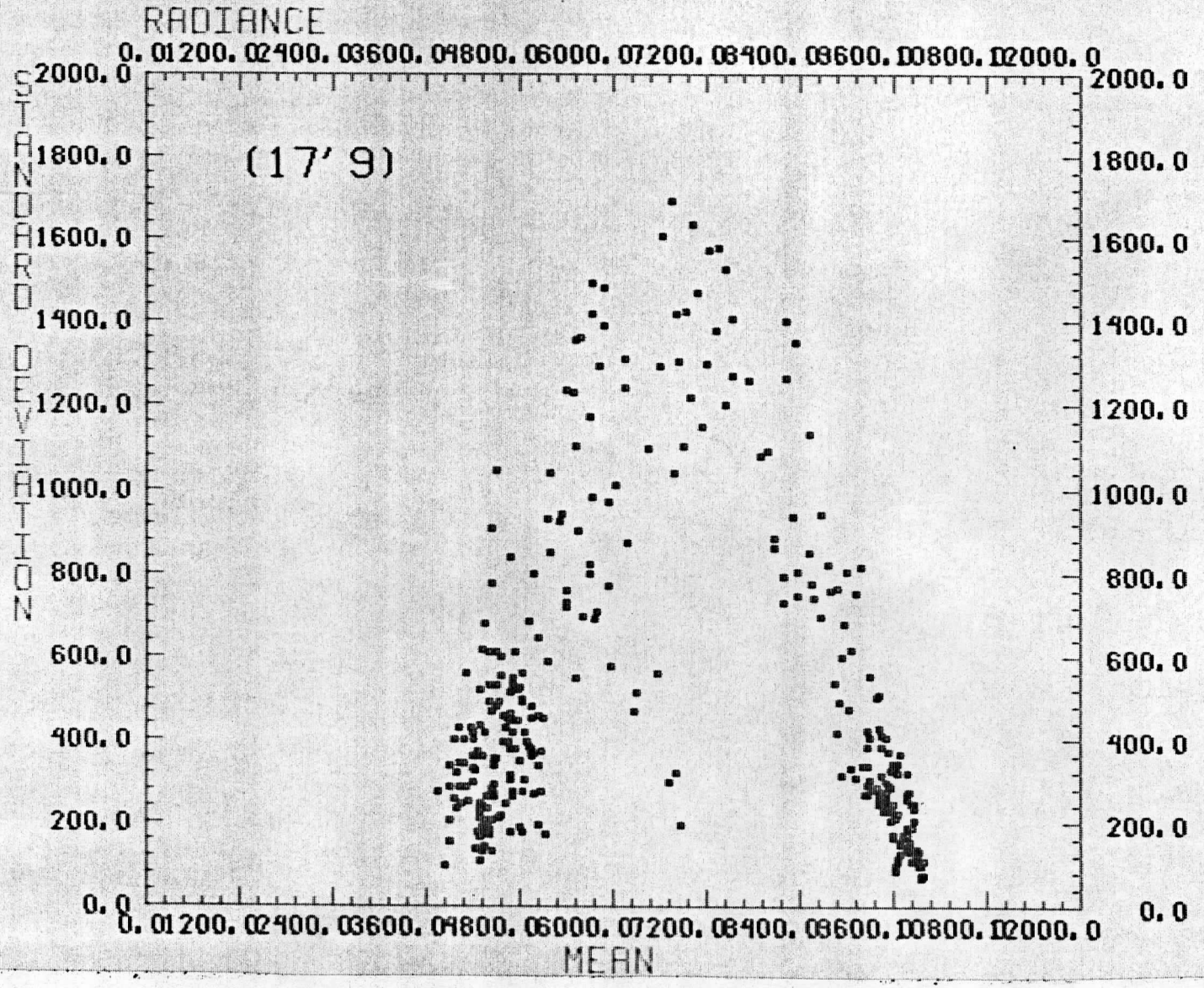

Figure 6. Local mean 11μm radiances and local standard deviations for 3x3 AVHRR pixel arrays which lie within HIRS FOV 17'9 (see Fig. 3). Units are 100 mW m^{-2} SR^{-1} cm.

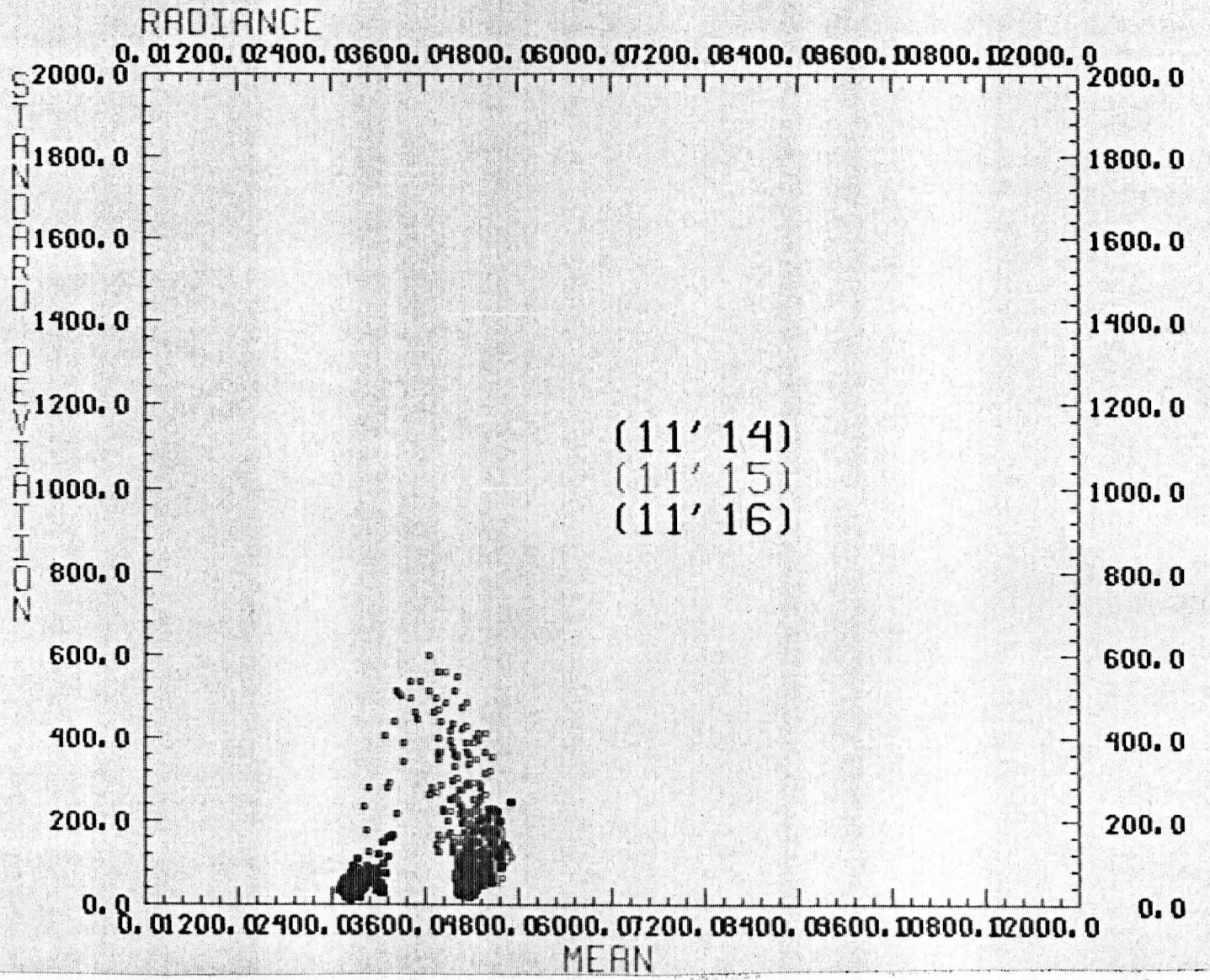

Figure 7. Local mean 11μm radiances and local standard deviations for 3x3 AVHRR pixel arrays which lie within HIRS fields of view 11'14, 11'15 and 11'16. Black points denote the two outer scenes, grey points denote the centre FOV which spans two cloud layers. Units are 100 mW m^{-2} SR^{-1} cm.

PAPERS FROM OTHER CONFERENCES RELEVANT TO ITSC-II

VAS DATA ACQUISITION AND PROCESSING SYSTEM FOR A PERSONAL COMPUTER

Ralph G. Dedecker
Space Science and Engineering Center
1225 West Dayton Street
Madison, Wisconsin 53706 USA

Robert N. Green
NOAA/NESDIS Regional and Mesoscale Meteorology Branch
Colorado State University, Foothills Campus/CIRA
Fort Collins, Colorado 80523 USA

H. Benton Howell
NOAA/NESDIS Development Laboratory
1225 West Dayton Street
Madison, Wisconsin 53706 USA

1.0 MOTIVATION

The microcomputer is the basis for a low-cost interactive video-graphic workstation for meteorological research and operational weather forecasting. A workstation with video-graphic capability is needed for the display of satellite and radar imagery and contour analyses of conventional and satellite surface and vertical sounding observations. The imagery and quantitative data can be accessed from a central computer (e.g., the UW McIDAS, the National Weather Service facility, or a commercial service) using a telephone and modem.

In order to exploit the opportunity for meteorological research and forecast applications of the microcomputer, a menu-driven software system has been developed for the IBM personal computer series. The software, described in this paper, provides three general capabilities:

(a) remote access to a satellite data base via automatic communication,
(b) display and analysis of satellite image products prepared on the main frame, and,
(c) display of temperature and moisture information derived from the VISSR Atmospheric Sounder (VAS).

Future work will generate a software package which will produce a wide variety of meteorological products (e.g., vorticity analyses, vertical cross-sections, isentropic analyses). This is underdevelopment for use in weather service forecast offices and research and educational institutions. Particular emphasis is being given to production of meteorological products from geostationary satellite VAS imaging and sounding system, since it provides high spatial resolution and half-hour interval data useful for local weather analysis and forecasting.

2.0 HARDWARE

In order to minimize the cost, the VAS PC work station was designed to use standard off-the-shelf hardware. The required components are based on the IBM personal computer family. Figure 1 shows a block diagram of the required hardware.

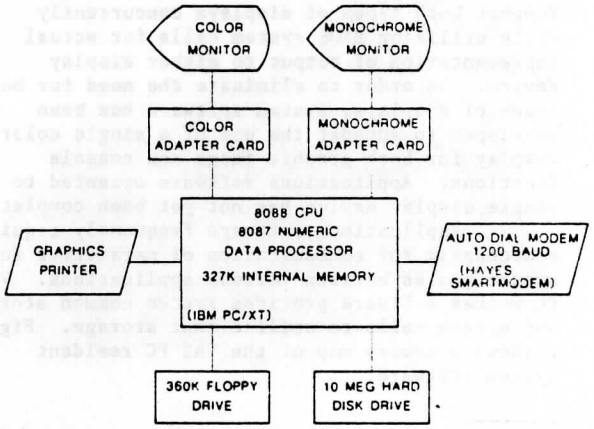

FIGURE 1 HARDWARE REQUIRED FOR THE VAS PC TERMINAL

The IBM PC/XT with a minimum of 328k bytes of memory and a numeric coprocessor (INTEL 8087) is used as the base unit. Current VAS PC software and data bases require approximately 2MB of disk storage space therefore requiring the use of a hard disk. Additional options include the IBM monochrome display card and a monochrome monitor (used as the system console), the IBM color graphics adaptor card and an RGB monitor (used to display graphics and images), an IBM, EPSON, NEC, C.ITOH, or PROWRITER dot matrix printer (used for hard copy of both graphics and text), and a 1200 BAUD Hayes Smartmodem (used to asyncronously acquire data).

Some IBM-compatible computers have been tested in part (such as the COMPAQ) and have been found compatible with the PC VAS software. However, since the software makes extensive use of the IBM PC graphics hardware, care should be taken when selecting an alternate main unit and graphics adapter.

3.0 OPERATING SYSTEM SOFTWARE -- GENERAL

The VAS PC software operates under the standard PC DOS or MS DOS operating system. In addition, resident software has been developed to supplement MS DOS control functions and hardware device drivers where necessary. Of the minimum 328k bytes of memory required for the VAS PC work station, MS DOS and VAS PC terminal resident software utilizes approximately 132k bytes thus making approximately 196k available of applications software. All resident software has been developed using the 8086 assembly language of the native INTEL 8088 microprocessor.

The system software design philosophy has been to use as many of the MS DOS system interfaces as possible so as to help facilitate future software compatibility. The system software implements system calls to MS DOS for system services when possible. When calls to MS DOS are not possible, calls are made to the BIOS (basic input output system ROM). When services cannot be provided via BIOS calls, the system software operates directly on the system hardware.

Standard IBM PC system software does not provide support for more than one display (console device) operation at one time. The VAS PC work station utilizes both a monochrome display for operator console text and menus and a color RGB display for graphics and images. Resident system software has been developed to support both types of displays concurrently while utilizing BIOS system calls for actual implementation of output to either display device. In order to eliminate the need for both types of displays, system software has been developed to support the use of a single color display for both graphic-image and console functions. Applications software oriented to a single display device has not yet been completed.

Applications software frequently requires a mechanism for communication of parameters and system states between various applications. VAS PC system software provides system common storage and system calls to utilize that storage. Figure 2 shows a memory map of the VAS PC resident system software.

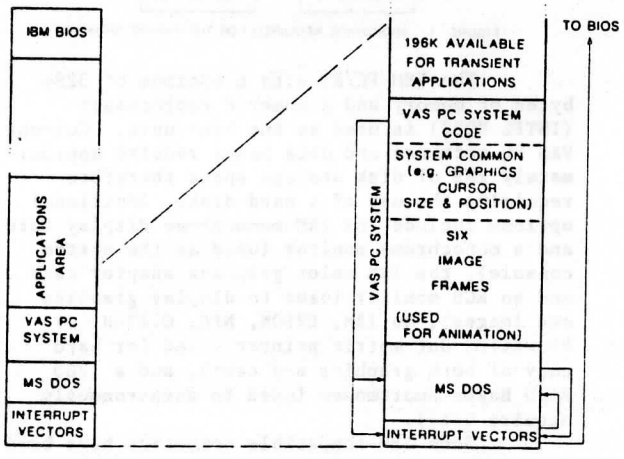

FIGURE 2 MEMORY MAP SHOWING VAS PC RESIDENT SYSTEM SOFTWARE.

3.1 Operating System Software -- Image and Graphic Controls

The VAS PC applications software makes extensive use of graphics and images, and provides mechanisms for saving and restoring graphic and image frames between system common memory and the color display. Three different display resolutions are supported, as well as frame animation and annotation.

The standard IBM graphics display adapter board employs 16k bytes of memory to hold a graphic or image frame. IBM BIOS software provides support for two different display resolutions. When the color display is in the high resolution mode, the 16k bytes of memory allow a 200 rows by 640 columns by 1 bit (black and white) frame. Graphic frames as well as some satellite images are displayed in the high resolution mode (via half toning techniques using a "dither" matrix). When the color display is in the medium resolution mode, the 16k bytes of memory allow a 200 rows by 320 columns by 2 bits frame. Two color palettes are available in this mode, a red, green, yellow palette, and a cyan, magenta, white palette. Graphic frames are displayed in the medium resolution mode. VAS PC system software provides controls for an additional resolution format. When using this low resolution format, a frame can contain 100 rows by 160 columns by 4 bits (16 colors). The 16 colors can be any from the following: black, dark grey, blue, bright blue, green, bright green, cyan, bright cyan, red, bright red, yellow, bright yellow, magenta, bright magenta, light grey, white. Since grey scales are not possible with the standard IBM color graphics adapter, color-coded satellite images are displayed in the low resolution mode. Figure 3 summarizes the three graphics modes available.

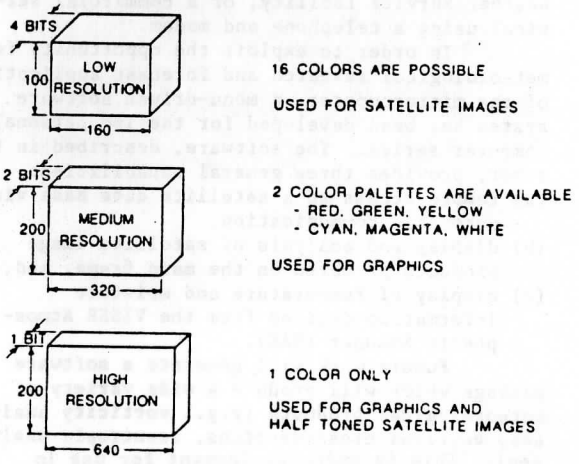

FIGURE 3. THE STANDARD IBM COLOR GRAPHICS ADAPTER GRAPHIC MODES.

Graphic or image frames can be animated via VAS PC system software calls. Storage is provided for up to 6 frames (see figure 2) in any of the three resolutions described above. Each frame requires approximately 16k bytes of resident memory, and more than 6 frames could be allocated at system configuration time. A trade off must be made between total system memory requirements and the number of frames desired.

Animation rates of up to approximately 15 frames per second are achieved by actually moving an image frame (16k bytes) from system common memory to the color adapter display memory.

3.2 Operating System Software -- Non Resident System Utilities

Most of the VAS PC applications software is written in Pascal and FORTRAN. In addition to the resident system services, a number of non-resident utility system routines have been developed to provide system interfaces to the resident system software and system hardware resources.

A group of routines provide a set of low level graphics commands to select the various graphics modes and to provide a set of calls for generating line graphics. A scheme for providing a graphics cursor has been implemented using an exclusive-or function with the color display adapter memory.

Console character display routines provide an ability to generate formatted displays (frequently used with menus) and routines allow keyboard extended character input (function keys) along with character filtering and user feedback.

3.3 Operating System Software -- Program Linkage

The VAS PC work station software includes many more application routines than can be fit into the 196k bytes of memory available for applications. System software has been developed that provide means to invoke, by chaining, various applications from menus or from other applications.

4.0 COMMUNICATIONS

All real time data that is required by the applications programs that are part of the VAS PC software are acquired via a 1200 BAUD asynchronous modem and dial up telephone link. Currently, all real time data are acquired from the IBM 4381 based McIDAS main frame located at the University of Wisconsin Space Science and Engineering Center. Software has been developed on the McIDAS to compress the data sent to the VAS PC system thus reducing transmission time required to transmit such products as satellite images. A number of utility routines have been developed on the VAS PC terminal to allow automated data acquisition.

The VAS PC communications software expects a Hayes Smartmodem to be used as an interface to the McIDAS system, and as such, routines have been developed to use the automatic dialing capabilities of the Hayes modem. Routines are also available to automatically detect key character strings sent from the McIDAS system and to respond to the character strings so that automatic logon and data requests are possible. The VAS PC communications utility routines actually emulate operator keyin requests that are sent to the McIDAS main frame. Utilities also allow local disk file storage of incoming data.

5.0 APPLICATIONS SOFTWARE -- THE MENU SYSTEM

All VAS PC applications software is designed to be invoked from menus. The user generally chooses a menu item (invokes a process) by pressing one of the function keys that are part of the standard IBM PC keyboard. Initially, the user is presented with a main menu. Choosing an item from the main menu, results in the display of another menu providing more specific choices than those available from the main menu. Each menu item, in turn, results in the end process desired being invoked or in the display of a sub menu. Inversely, repetitively pressing the "Esc" key results in returning to the next higher level menu until the main menu is displayed. Current development of the VAS PC terminal applications software provides for three options from the main menu (see Figure 4):

VAS
DATA ACCESS AND PROCESSING SYSTEM

MAIN MENU

KEY	ACTION
F1.	GENERAL McIDAS COMMUNICATIONS
F2.	RETRIEVAL ANALYSIS
F3.	SATELLITE IMAGE ACQUISITION AND ANALYSIS

PLEASE PRESS THE FUNCTION KEY (F1..F3) OF YOUR CHOICE, OR PRESS 'ESC' TO RETURN TO DOS.

FIGURE 4. THE MAIN MENU.

1) General McIDAS communications -- provides a means of a simple general purpose communications with McIDAS and a means for defining and changing the telephone number, user, and project numbers used for communications (see Figure 5).

COMMUNICATIONS CONTROL MENU

KEY	ACTION
F1.	ACQUIRE DATA FROM McIDAS
F2.	CONNECT TO McIDAS AS A SIMPLE TERMINAL
F3.	SEND A TEXT FILE TO McIDAS
F4.	CHANGE THE TELEPHONE NUMBER, USER ID, AND PROJECT NUMBER FOR COMMUNICATIONS WITH McIDAS

PLEASE PRESS THE FUNCTION KEY (F1..F4) OF YOUR CHOICE, OR PRESS 'ESC' TO EXIT

FIGURE 5. THE GENERAL McIDAS COMMUNICATION MENU.

2) Retrieval analysis -- provides a menu of analysis and display routines which are

specifically designed for VAS retrievals processed on the McIDAS. At present, the data used by these routines are collected as ASCII text files and contain temperature, dew point and wind data for standard VAS levels and brightness temperatures for each VAS channel (see Figure 6).

VAS RETRIEVAL ANALYSIS MENU

KEY	ACTION
F1.	INITIALIZE VAS BACKGROUNDS
F2.	CONVERT TEXT TO BINARY FILE
F3.	LOCATE VAS RETRIEVALS
F4.	PLOT RETRIEVAL PARAMETER
F5.	PRINT RETRIEVAL
F6.	ANALYZE RETRIEVALS (BARNES)
F7.	CONTOUR ANALYZED FIELD
F8.	PLOT RETRIEVAL PROFILE
F9.	REVIEW RETRIEVAL FILE

PLEASE PRESS THE FUNCTION KEY (F1..F9) OF YOUR CHOICE, OR PRESS 'ESC' TO EXIT.

FIGURE 6. RETRIEVAL ANALYSIS MENU.

3) Satellite image acquisition/display/analysis -- provides communications mechanisms to acquire and display GOES images (VAS and VISSR) in either high resolution (halftone) or low resolution (color coded) graphics modes, and to display a contour analysis of selected VAS brightness temperatures (see Figure 7).

SATELLITE IMAGE ACQUISITION/DISPLAY/ANALYSIS MENU

KEY	ACTION
F1.	DISPLAY CURRENT FILE OF VAS BRIGHTNESS TEMPERATURES
F2.	ACQUIRE AND DISPLAY VISSR HALFTONE (HI RES) IMAGE
F3.	ACQUIRE AND DISPLAY VISSR COLOR-CODED (LO RES) IMAGE
F4.	DISPLAY CONTOUR ANALYSIS OF CURRENT FILE OF VAS BR. TEMPS.
F5.	ANIMATE/SAVE/RESTORE IMAGES

PLEASE PRESS THE FUNCTION KEY (F1..F5) OF YOUR CHOICE, OR PRESS 'ESC' TO EXIT

FIGURE 7. THE SATELLITE IMAGE ACQUISITION DISPLAY AND ANALYSIS MENU.

5.1 Applications Software - General McIDAS Communications

"Acquire data from McIDAS" --
Upon selection of this option, the contents of a text file are displayed, including: a McIDAS command, file names of locally generated disk files, names of programs to be subsequently invoked, the end-of-data message expected as termination of the data stream and an indicator of display option (e.g., halftone or 16-level image). Prompts are then displayed, allowing each item to be left as is or changed. After the last item is either changed or skipped, the general data acquisition program is initiated. This program automatically dials, logs onto McIDAS, issues the specified command, opens a receive file, receives and stores the incoming data until the end-of-data message is received, logs off McIDAS, closes the receive file and turns control over to the next program to be executed. The next program may be an applications program, e.g., to decode and/or display the data received, or the communications menu program from which this action originated. If communications with McIDAS cannot be established, or if the link is disconnected before the terminating message is received, a message to that effect is displayed, and upon the entry of an "ESC" key, control is returned to the communications menu program.

Connect to McIDAS as a simple terminal" --
This option automatically dials the McIDAS main frame, logs onto McIDAS and then allows the user to communicate with the McIDAS system in the same manner as any other ASCII McIDAS terminal.

"Send a text file to McIDAS" --
This option allows automatic transmission of a text file to the McIDAS main frame in a manner consistent with McIDAS system software.

"Change the communications parameters" --
This option allows specifying the telephone number, user ID, and project number that are stored in a file and are used for automatic dialup and logon parameters with the McIDAS main frame.

5.2 Applications Software -- Retrieval Analysis

"Initialize VAS Backgrounds" --
This program is executed to load graphic images into the six frames of RAM memory which are used by the other programs in this menu. The use of the retrieval analysis programs has concentrated on case study analysis in one geographic area. By generating the geographic background once for the case study region, one increases the speed of the applications routines.

"Convert text to binary file" --
The ASCII text file of VAS data from McIDAS is processed by this routine to filter out possible transmission errors and to create a binary file to be read by the application programs. It is more efficient to read binary files and, thus an increase in execution speed is realized. The resultant file contains all VAS retrievals for a given time period and geographic area formatted one retrieval per record.

"Locate VAS retrievals" --
All retrievals for a given time period are plotted on a background map with a sequence number placed at its latitude-longitude position. The sequence number may be used to access a specific retrieval in other programs. Figure 8

shows an example of the graphics output of this routine.

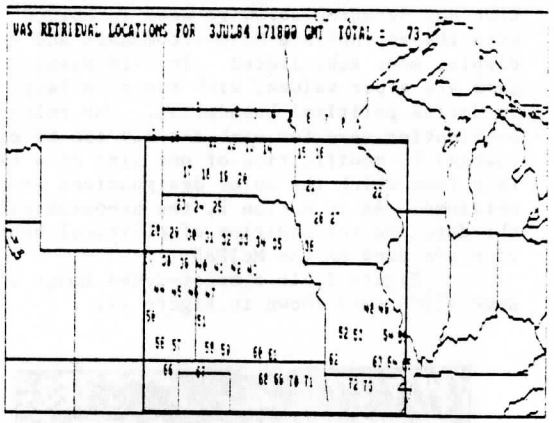

FIGURE 8. EXAMPLE OF "LOCATE VAS RETRIEVALS"

"Plot retrieval parameter" --

A graphic display similar to the previous program's output is generated with the sequence number being replaced by a VAS retrieval parameter chosen by the user from a menu table. A hardcopy of this display may be hand-analyzed.

"Print retrieval" --

The data for the complete retrieval may be displayed in a text format on the monochrome monitor with this program. The retrievals to be displayed are selected by either sequence number or by latitude-longitude box coordinates. A hardcopy of the text is available if the printer is activated by the "Control-Print Screen" command.

"Analyze retrievals (Barnes)" --

A retrieval file can be objectively analyzed with a two-pass Barnes technique. Due to program size limitations, the routine is limited to a file size of 125 observations and an output grid dimension of 16 x 11 one degree longitude-latitude points. The execution time is about two minutes for a typical 60 observation file. The output of this routine is a gridded file which can be used by other programs.

"Contour analyzed field" --

The output file from the analysis program can be displayed in a contoured format in the medium resolution graphic mode. Up to three different fields may be displayed at once with the three different colors available. The contoured field is displayed on a geographic background. Figure 9 presents an example of the contoured product.

"Plot retrieval profile" --

A retrieval can be plotted on a Skew T/log P background. The temperature data is plotted with a solid line, and a dashed line is used for the dew point data. The user has the option of plotting a second retrieval on the same graphic in a contrasting color for comparison analysis. This program also displays information on the monochrome screen showing various computed indices and parameters derived

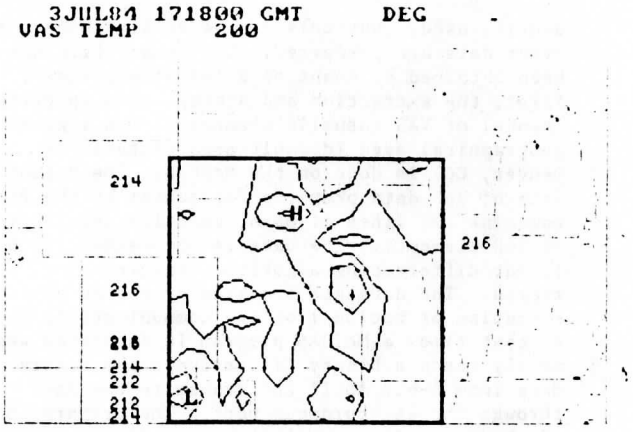

FIGURE 9.

EXAMPLE OF "CONTOUR ANALYZED FIELD"

from the retrieval. Because of sparse availability of wind data for the VAS retrievals, some of the wind-dependent parameters are not useable. Figure 10 gives and example of this routine's graphic output.

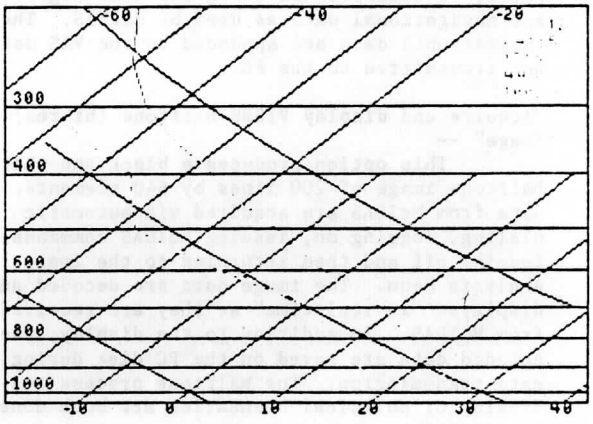

FIGURE 10.

EXAMPLE OF "PLOT RETRIEVAL PROFILE"

"Review retrieval file" --

This program is available to the analyst to quickly scan a given VAS retrieval file. Each retrieval is plotted on the Skew T/log P background, erased and the next plotted as rapidly as possible. The intent of the process is to quickly do a quality control check of a complete file, and to obtain an idea of the make-up of the VAS retrievals.

5.3 Applications Software -- Satellite Image Acquisition, Display and Analysis

"Display current file of VAS brightness temperatures" --

The immediate data source for this display is a binary disk file specified by a "VAS parameter" text file. The name of the file of the latest VAS data acquired from the McIDAS is

usually used, but this can be easily changed if other data are preferred. The binary file has been obtained by means of a two-step process. First, the extraction and storage of a specified channel of VAS (usually channel 8) for a given geographical area (default area centered on Denver, CO) is done on the McIDAS. The McIDAS - file of VAS data prepared for access by the PC contains 100 lines of data, each line consisting of 160 elements. The data is compressed, by a linear differencing algorithm, before being stored. The data are acquired by the PC upon the execution of option 1 of the Communications Menu. At that time, a McIDAS program is initiated which merely reads a binary file,encodes the binary data into 6-bit ASCII and transmits the data through the asynchronous port. The preparation of the data file on McIDAS before PC access minimizes the access time, which is approximately five minutes. After being stored on the PC, in encoded and compressed form, the data are decoded and expanded to its original form. The display program uses the minimum and maximum values of the data to establish the color coding. Ten of 16 available colors are used. The data are plotted line by line in the low resolution mode, after which the political boundaries are plotted. The navigation of the image, i.e. the transformation from earth coordinates to screen coordinates, is accomplished using the same algorithms and navigational data as used by McIDAS. The navigational data are appended to the VAS data and transmitted to the PC.

"Acquire and display VISSR halftone (hi res) image" --

This option produces a black and white halftone image of 200 lines by 640 elements. The data from McIDAS are acquired via automatic dialing, logging on, issuing McIDAS commands, logging off and then returning to the Image Analysis Menu. The image data are decoded and displayed "in real time" as they are received from McIDAS. In addition to the display, the encoded data are saved on the PC disk during the data transmission. The halftone process and the drawing of political boundaries are both done on the McIDAS.

Figure 11 is an example of a halftone image display. The image is a GOES-6 VISSR visible image of hurricane "Josephine" on 12 Oct 1984.

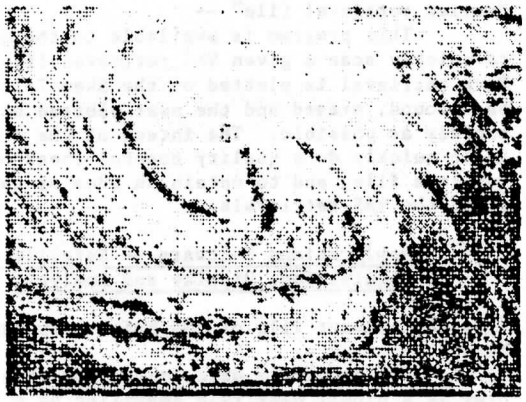

FIGURE 11. VISSR VISIBLE HALFTONE IMAGE OF HURRICANE "JOSEPHINE" (12 OCT 84, 13Z) (IMAGE CENTER 33° N, 71° W)

"Acquire and display VISSR color-coded (low res) image" --

This option uses the same data acquisition and decoding software used in option 2, with the appropriate McIDAS commands and PC display mode substituted. In this display, the data are 4-bit values, with the zero level used to define political boundaries. The color combination used for each display can be easily changed by modification of one line of a text file from which the color designations are obtained. As in option 2, the preparation of the data and the addition of political boundaries are done on the McIDAS.

Figure 12 is a color-coded image of the same VISSR data shown in Figure 11.

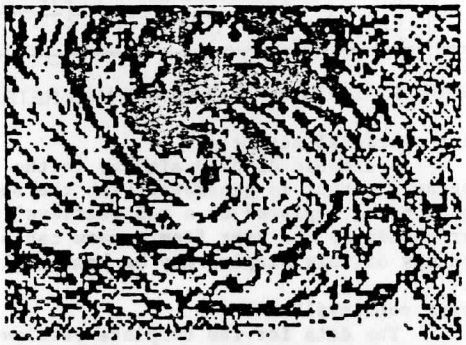

FIGURE 12. VISSR VISIBLE COLOR-CODED IMAGE OF HURRICANE "JOSEPHINE" (12 OCT 84, 13Z) (IMAGE CENTER 33° N, 71° W)

"Display contour analysis of current file of VAS br. temps." --

This option plots a contour analysis of a 20 by 20 grid of values extracted from the same binary file of 100 by 160 points displayed in option 1. The contour interval and smoothing parameters are specified in a text file for easy access and modification. This plot is an example of the medium resolution graphics which can plot in either of two sets (palettes) of 3 colors each. When the plot is completed, control is returned to the Image Analysis Menu.

Figure 13 is an example of a medium-resolution graphics contour analysis of VAS channel 8 (11 μm) brightness temperatures.

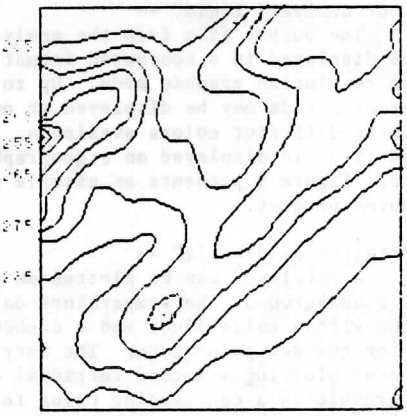

FIGURE 13. CONTOUR ANALYSIS OF VAS CHANNEL 8 (11μm) BRIGHTNESS TEMPERATURES USING MEDIUM RESOLUTION GRAPHICS.

"Animate/save/restore images" --

This option executes a multi-purpose program which is used primarily to prepare and display "movie loops" of satellite images. The most effective display is obtained when all frames are in the same graphics mode (resolution). Of the three modes, the high and medium resolutions are best, because of the longer delay between frames in the low resolution mode. While the animation is in progress, the sequence and dwell times of the frames can be changed. All command definitions are well described, and invalid entries produce only an audible signal, and are subsequently ignored. Upon entry of the "exit" option, control is returned to the Image Analysis Menu.

6.0 SUMMARY

This paper has presented a VAS data acquistion and processing system based on a microcomputer system. The hardware consists of relatively inexpensive, off-the-shelf components which are readily available. Custom designed system software enhances the basic microcomputer operating system to take advantage of special hardware features. An easy-to-use user interface utilizing menus minimizes the computer knowledge required for the operator. The major components of the applications software allow for communications with the McIDAS mainframe computer for VAS data acquisition, analysis of VAS retrieval data, and display and animation of satellite imagery.

7.0 ACKNOWLEDGEMENTS

The work presented in this paper has been funded in part by the NOAA Operational VAS Assessment Program through grants to the NOAA cooperative institutes at the University of Wisconsin at Madison and Colorado State University.

We wish to express our gratitude to the following people for their contributions to the present VAS PC System: Tom Whittaker, UW/SSEC, Fred Nagle, NOAA/NESDIS/Development Laboratory, and to Tony Schreiner, Chris Velden, Gary Wade, and Ray Zehr for helping with preparations for this presentation. Many thanks to Jan Waite for her accurate and expeditious production of the manuscript and to Tony Wendricks for the graphics.

A Low Cost Interactive System for Processing and Displaying Direct-Readout Satellite Soundings

Harold M. Woolf, H.Ben Howell, William L. Smith, W.Paul Menzel

Cooperative Institute for Meteorological Satellite Studies
1225 West Dayton Street
Madison, Wisconsin 53706 USA

1. Introduction

A system to process the NOAA polar-orbiting satellite sounding data has been implemented on an IBM Personal Computer. Based on recent advances in microprocessor technology, this system is low in cost, internationally available, and capable of stand-alone processing of raw satellite bit streams into displays of derived meteorological parameters. The hardware design is based on the IBM PC-XT augmented with commercially available enhancements. It is capable of interactive data processing and color display of satellite imagery and derived quantities. The software has been developed by the Cooperative Institute for Meteorological Satellite Studies (CIMSS) on the University of Wisconsin Man-computer Interactive Data Access System (McIDAS) and adapted to the IBM PC-XT. The radiance measurements from the infrared (HIRS) and microwave (MSU) sensors are ingested, calibrated, earth-located, limb-corrected, amalgamated, and formatted for imaging and sounding-retrieval. Vertical profiles of temperature, humidity, and geopotential height, as well as estimates of surface (skin) temperature, total ozone, and static stability are produced by a combination of statistical and physical algorithms.

2. Hardware and System Software

The basic system consists of an IBM Personal Computer XT, known more familiarly as the "PC-XT." This unit, as purchased from a retail computer dealer, includes the Intel 8088 CPU; 256 Kb of RAM (Random Access Memory); 1 fixed or "hard" disk drive with 10 Mb capacity; 1

flexible or "floppy" disk drive of 360 Kb capacity; and an expansion card containing the disk controller. To this central unit, we have added a monochrome monitor, color monitor, color-graphics card, and printer adapter, all by IBM; an AST Research "Six-Pack-Plus" card containing clock, calendar, serial port, parallel port, and 64 Kb RAM, expandable to 384 Kb; an Intel 8087 numeric co-processor; an Epson FX-80 dot-matrix printer; and a Hayes 1200 bps external modem. An additional 64 Kb of RAM has been installed on the Six-Pack, bringing the total RAM to 384 Kb. We plan to add two more 64 Kb "units" in the near future to bring the system up to 512 Kb.

System software consists of IBM DOS 2.1, the IBM Macro Assembler, and the Microsoft Fortran-77 and Pascal Compilers. DOS and Assembler, although marketed by IBM under their name, are also produced by Microsoft. The compilers have been designed to make use of the high-speed arithmetic capabilities of the 8087 coprocessor. The retail, or list, price of such a configuration is just over $8500; in our university situation, substantial discounts are provided, so that the actual cost is closer to $6500.

3. Applications Software/Purpose of Project

Most of the applications software presently installed on our system has been written in Fortran; some utility routines needed for highly repetitive operations at the byte and/or bit level have been implemented in Pascal or Assembler for the sake of efficiency. The software utilized for satellite sounding data processing was originally developed within the context of the McIDAS system as then -- during the period 1977-1982 -- implemented on the Harris Slash-6 minicomputer. That system was adapted to run in batch mode on the IBM 360/195 or similar computer; our Institute has provided copies of this so-called "TOVS EXPORT PACKAGE" to several research institutions and

government meteorological agencies around the world. Within the last two years, that software, with improvements and enhancements that are continually being developed, has been installed on our new McIDAS system, which is now based on the IBM 4300 series of so-called "super-mini-" computers.

While a 4300-class machine is much less costly than a full-size mainframe, such as the IBM 308x series, it is still far from inexpensive to purchase or lease, and requires fairly costly maintenance support and sophisticated systems-programming support. With the phenomenal rate of increase in "computing power per unit cost" that has characterized the personal, or desktop, computer field in the last year or so, we felt that exploration of the capability and utility of the microcomputer for processing satellite sounding data would be a worthwhile endeavor. Since sounding-radiance data can be obtained from the operational polar-orbiting TIROS-N/NOAA spacecraft by use of relatively simple and inexpensive VHF receiving equipment, it seemed only natural to assess the feasibility of a low-cost data-processing system. The fruits of this research, development, and application effort are being presented at this time.

4. Data Processing Scenario

Before parameters of meteorological interest can be retrieved, the raw satellite data must undergo a rather substantial amount of preliminary processing, which will now be described briefly. We begin with a file of raw TIP data from a line-of-sight satellite overpass, received directly via the VHF beacon or extracted from an HRPT dataset received on S-band. Typically, such a dataset encompasses a period of 8 to 12 minutes; the sounding software has, accordingly, been configured to allow for up to 100 HIRS scan lines, or a period of 10 minutes and 40 seconds.

[SLIDE: orbital tracks]

The first step is to transform this bit stream into a set of "proper" bytes and/or words. This task is accomplished by a program called PRETIP, which is probably the most highly machine-specific component of the entire system. It is here that most of the Assembler and Pascal utilities are employed. When this program was first implemented, entirely in Fortran, it produced the correct answers, but took over three hours to process 10 minutes' data! The current version requires approximately 15 minutes: not quite real-time, but acceptable.

The next step, referred to rather loosely as "ingest," deals with the calibration and navigation, or earth location, of the sounding radiance data. Our program TOVDRI handles this task quite efficiently on the PC-XT, since the 8087 arithmetic coprocessor does the heavy work -- although the basic orbital parameters are provided by NOAA/NESDIS Operations, there is still a considerable amount of "number-crunching" to be done in converting spacecraft time and instrument scan position to geographical locations of individual radiance measurements. Again, a time span of 15 minutes is typical for this portion of the processing.

Programs PRELOC, MSUPRP, and TOVPRE comprise what we term "preprocessing," or the handling of the data prior to attempting retrieval of atmospheric soundings. At this stage, the data may be normalized for view-angle, or "limb-corrected," if that is appropriate for the particular retrieval algorithm that will be applied. The MSU observations are mapped to the HIRS scan pattern to simplify the subsequent joint treatment of the two independent, but quasi-coincident, sets of measurements. Once again, approximately 15 minutes suffices for completion of this task, which results in two output files containing essentially the same data in different

formats: one permits rapid imaging of the data, while the other provides the most efficient access to the radiance measurements for constructing soundings.

While the retrieval of soundings from preprocessed radiances is accomplished with a single program in the IBM 4381 McIDAS and mainframe-EXPORT systems, memory and execution-speed constraints on the PC led us to a further separation of tasks. Program TOVRT1 determines the optimum 3 x 3 field-of-view ensemble for a particular spot, encompassing a geographical area about 75 km square, and outputs a single radiance vector for that area. With a horizontal and vertical spacing of three fov's, the data for 56 spots in 78 lines, in the present case, are reduced to 450 candidates for retrieval.

When a simple statistical algorithm is employed for retrieval of temperature and water vapor from those composite radiance measurements, it is reasonable to attempt to obtain soundings for all 450; this was in fact done, in approximately 8 minutes on the PC-XT, using regression coefficients obtained from Operations. Interactive editing can then be performed to eliminate soundings of questionable quality and/or reliability. We are currently working, however, with a physical retrieval algorithm that is quite computationally intensive; therefore we have the option to reduce the processing burden by additional filtering of the data before attempting retrievals. This is done by first mapping the 3 x 3 output of TOVRT1 onto its own 3 x 3 grid, covering a region of about 225 km square, then selecting the "best" of those nine. At present, this is a very simple filter: the "best" case is that with the highest radiance in the 11 micron window channel -- that is, the one most likely to be clear, or if the data are definitely cloudy, the one least contaminated by cloud. In this manner, the original 450 candidate sounding radiance sets yield 54 cases for actual retrieval attempt.

Finally, we apply program TOVRTZ to those 54 cases: running time is approximately 45 seconds per sounding, and our yield is 44 successful retrievals.

Thus the total processing time for this 7-minute overpass, from preprocessing of the raw TIP data through statistical retrieval, is approximately one hour. Physical retrieval of the low-density dataset adds another 40 minutes, bringing us just about to the time for the next overpass to begin! We are currently working on further improvements to reduce the running time by a factor of two to three. However, even with the present processing speed, satellite soundings over a very large geographical area can be provided by this low-cost system in less time than is normally required for a single conventional balloon sounding. Furthermore, intermediate and final products can be formatted, displayed, and manipulated with the microcomputer-video display system for timely use in weather analysis and forecasting.

The results can be presented in several different ways: a simple printout of the data from the retrieval-output file: computer-generated plots of individual soundings: plots of a single parameter, such as 500mb height, in map form on the printer or the graphics screen: contour analyses of such parameters: and so on. The images that I will now present were generated on the McIDAS system in order to take advantage of the sophisticated photographic hard-copy facilities attached to it: such a system for microcomputers is just entering the marketplace.

Future programs in satellite processing

Improvements to TOVS processing

Larry M. McMillin
National Oceanic and Atmospheric Administration
National Environmental Satellite, Data, and Information Service
Washington, D.C. 20233

When talking about future changes to the operational retrieval system, it is necessary to define a time scale. Although exact dates are not fixed, sometime in the late 80's or early 90's, a new satellite series will be launched. Software for this system will be rewritten rather than modified. Since it will take some time to write the new system and the effort will require the participation of people currently involved in improving the present system, improvements to the present system will halt when the design of the new system starts. Thus, improvements to the present system are essentially limited to tasks that are currently under way, or in some preliminary stage of development. This presentation will be limited to those changes anticipated in the present system.

At the present, the operation is "frozen" to provide a benchmark for switching code from the IBM 360's to the NAS 9000's. Several improvements have passed all the preliminary testing normally required for change and are waiting for the code transfer to be completed this spring. Three of the most significant are an improved water vapor retrieval, an "enhanced" retrieval system, and a new cloud algorithm. At the current time, several versions of physical retrieval algorithms are being evaluated under nearly operational conditions. Two other changes are in a more preliminary stage of evaluation and may be completed soon enough to warrant inclusion in the present system. One involves the use of classification techniques to obtain an initial guess while the second involves the replacement of a cloud test. In terms of systems, the last is a

relatively small change, but shows potential to remove the pronounced tendency for the current system to produce only cloudy soundings in the clear areas behind strong cold fronts.

The complete description of any one of several of these tasks would constitute a lengthy paper in itself, and several of the changes, along with the evaluations that support their consideration, will be described in the literature at the appropriate time. In this presentation, they can only be summarized.

Accuracies of the water vapor retrievals have been improved over the current method by amounts that are 8.8%, 21.6%, 11.9%, 10.1% and 20.1%, respectively, for the latitude zones 60-90N, 30-60N, 30S-30N, 60S-30S and 90S-60S, where the percentages are percentages of the radiosonde amount. These improvements were obtained by following the basic procedure described by Hayden et al. (1981) with modifications to account for the fact that hourly surface observations are not used in the present system. The retrieval system is a standard multilinear regression in which the predictors are atmospheric brightness temperatures and the predictands are dewpoint temperatures. The major differences from the procedure used by Hayden et al. are that the surface transmittances are estimated from the measured radiances and that the atmospheric component of the radiative transfer equation is normalized to an atmospheric radiance by dividing by the quantity $(1-\tau_s)$ where τ_s is the surface transmittance.

The new cloud algorith is a physical retrieval for cloud top temperature. However, the major change is one of philosophy in the cloud parameter. At the time the TOVS system was designed, there was a desire to have a means of determining the retrieval accuracy. The N^* retrievals were expected to be the most variable, and it was expected that the accuracy would be related to cloud top

height and cloud amount. For this reason, a provision was made to output cloud top temperature and cloud amount averaged over the spots used to produce the N^* retrievals as well as several other quality indicators. The concern for a quality indicator has turned out to be unfounded because of improvements in the TOVS instrument over the earlier VTPR. In addition, the cloud height and amounts have frequently been assumed to be averages over all spots, rather than just the few spots used in an N^* retrieval, even though the values are placed with other quality indicators. When the new method is in place, the values will be averaged over all spots so that the output will change from a quality indicator to a meteorological parameter.

The enhanced soundings are soundings produced at a higher resolution. Because of communication constraints, the number of soundings will be kept nearly constant, but the distribution will be changed from one that has a fairly even spacing to one that places more soundings in high gradient areas while keeping the distance allowed between soundings below an adjustable limit. It is anticipated that the limit will be between 100 and 200 KM.

It is possible that the enhanced soundings may differ in accuracy from the accurcies produced now. Changes may occur because present soundings use measurements over a 9x7 array of spots to evaluate consistency and detect soundings that may be erroneous. Areas of consistent sounding errors occur but they seldom, if ever, cover a 9x7 area. Each enhanced sounding is produced from a 3x3 array spot. With a smaller area, it is more difficult to detect errors that may be locally consistent. Changes have been made to attempt to compensate for the fewer spots. Of course, one compensation is that the new system can detect meteorological features that are averaged out by the older system. An earlier attempt to implement the system was unsuccessful because of the effect

of the enhanced resolution on the selection of land/sea coefficients for the microwave instrument near coastlines. The problem has been identified and solved, and another operational test is scheduled for the spring of 1985.

NESDIS is evaluating several physical retrievals as alternatives to the present regression system. Two alternatives are under full test with a third to be tested if resources allow. One of the first two is based on Smith's (1970) iterative approach and the second is the well-known minimum variance approach (see Foster, 1961; Strand & Westwater, 1968; Strand & Westwater, 1968; or Rodgers, 1970).

The third approach is the "one-step" retrieval method discussed by Smith and Woolf (1984). This really differs from a known method such as the minimum information solution in three ways. One is that solutions for water vapor and temperature are made simultaneously. A second is that basis vectors are used in the solution. Finally, the third is that the solution vector for water vapor is the change divided by guess rather than just the change itself. In the test, effects of the several components of the "one-step" method will be evaluated independently. One of the the other goals of the physical retrieval tests is to reduce the number of radiosondes. For a physical retrieval, a few high quality radiosondes, particularly if they coincide with a satellite observation, are more important than having a larger number of less accurate ones.

As mentioned, the evaluation of classification schemes is not as far along in the testing procedure as the items just discussed. Nevertheless, several preliminary studies have been very promising. In this technique, radiance patterns are used to determine a more reliable initial guess. Although several of the papers discuss clustering techniques (see Uddstrom et al., 1985, & Kelly et al., 1976), development is tending toward techniques that provide uniform

spacing of classes, even though some classes, such as those representing fronts, may be sparsely populated. In any event, preliminary results indicate that fine scale structure may be recognized from radiances because of correlations that exist between vertically coarse structure and vertically fine structure, while conventional retrieval methods are constrained to the fine scale structure present in the initial guess.

The last change involves the use of mapped surface temperatures to test for cloudy retrievals behind a cold front. In the test, a cold value relative to the mapped value is interpreted as cloud. As a result, microwave only (or "cloudy") retrievals are produced and since the microwave only retrievals are produced without the information contained in the infrared measurements, they are less accurate. One alternative is to replace the test with a comparison of microwave and infrared window channels. There are difficulties with this approach because the microwave window channel can be lowered by surface water even though it is virtually unaffected by most clouds. Because both window channels are lowered by separate effects, there is a finite probability that a false indication of clear can be generated over a cloudy area with water on the surface. Worse, the probability does not decrease appreciably with the size of the retrieval error so a large error can be passed. In the test, discriminant analysis methods were used to detect standing water in the microwave measurements before the window channels were compared. Although development is needed to define the limits, preliminary results indicate that the approach should work.

In summary, several changes to the present retrieval system are in various stages of the evaluation process. Although it is possible for a problem to be encountered with a potential improvement at any point before it is actually

installed, all the changes appear probable at the moment, with the ones discussed first having the highest probability. As a result of these changes, significant gains in retrieval accuracy are anticipated, particularly for those products other than temperature which have received relatively little attention during the early development of the TOVS processing system.

References

Foster, M., 1961: An application of the Wiener-Kolmogorov Smoothing Theory to matrix inversion. J. Soc. Indust. Appl. Math. 9, 387-392.

Kelly, G.A.M., P.E. Powers, and F.J. Gauntlett, 1976: Temperature and water vapor retrievals from the NOAA-4 satellite in the Southern Hemisphere. Meteorological Observations from Space, Contributions to First Global Experiment Conference Proceedings, COSPAR, Philadelphia, 77-84.

Rodgers, C.D., 1970: Remote sounding of the atmospheric temperature profile in the presence of cloud. Quart. J. Roy. Meteor. Soc., 96, 654-666.

Smith, W.L., 1970: Iterative solution of the radiative transfer equation for temperature and absorbing gas profiles of an atmosphere. Appl. Opt. 9, 1993.

Strand, O.N., and E.R. Westwater, 1968: Statistical Estimation of the Numerical Solution of a Fredholm Integral Equation of the First Kind. J. Assoc. Comp. Mach., 15, 100-114.

Strand, O.N., and E.R. Westwater, 1968: Minimum-RMS Estimation of the Numerical Solution of a Fredholm Integral Equation of the First Kind. SIAM J. Numer. Anal., 5, 287-295.

Uddstrom, M.J., and D.Q. Wark, 1985: "A Classification Scheme for Satellite Temperature Retrievals." To be published in J. Clim. and Appl. Meteor.

SECOND INTERNATIONAL TOVS STUDY CONFERENCE

IGLS, AUSTRIA, 18-22 FEBRUARY 1985

COMMENTS CONCERNING SATELLITE RETRIEVALS AND THE NEED FOR A BASELINE UPPER-AIR NETWORK

(Submitted by the WMO Secretariat)

Summary and Purpose of Document

The report of TOVS-I (August 1983) was reviewed by the CBS Working Group on the Global Observing System at its fourth session (December 1984). The GOS Working Group welcomed the work done by TOVS-I and recognized the value of the recommendations, particularly as regards the more effective utilization of satellite data in the WWW. The GOS Working Group urged that TOVS-II further refine the recommendations concerning evaluations and the calibration of satellite sounding data and that these be brought to the attention of the President of CBS.

The GOS Working Group gave special attention to the recommendations of TOVS-I concerning the organization of a baseline upper-air network which would, as one function, provide data needed for the retrievals of satellite sounding data. The baseline network concept also had been considered by expert groups in WMO and was subsequently endorsed by the WMO Executive Council at its thirty-sixth session (May 1984). Based on a survey conducted in early 1984 and the recommendations of experts, including those of TOVS-I, a concept paper for the baseline network was prepared and reviewed by the CBS Working Group on the Global Observing System. Excerpts from the final report of the fourth session (December 1984) of the GOS Working Group are contained in the Appendix.

ACTION PROPOSED

The TOVS-II is invited:

(a) To review the excerpts of the CBS Working Group on the GOS as contained in the Appendix;

(b) To outline a set of specific proposals which, in the opinion of the TOVS-II participants, would serve to make satellite sounding data of more value to the World Weather Watch, and particularly

(c) To comment on the concept of the baseline network, including making any recommendations on its organization or operation which would enhance the utility of the data in the retrieval of satellite soundings.

Appendix: Excerpts from the final report of the fourth session of the CBS Working Group on the GOS, December 1984

EXCERPTS FROM THE FINAL REPORT OF THE FOURTH SESSION OF THE CBS WORKING GROUP ON THE GOS, DECEMBER 1984

5.1.3 Baseline upper-air networks

5.1.3.1 As part of its consideration of the satellite activities, the Working Group noted that recommendations have been made to initiate a baseline upper-air network to provide data to assist in the calibration of satellite data processing. EC-XXXVI encouraged the establishment of the baseline network and the WMO Secretariat has obtained responses from interested Members on a conceptual design. The Working Group endorsed the need for such a baseline network and expressed its appreciation for the efforts which have been initiated. During its discussion, the Working Group noted that the baseline network would at least in the first stages, concentrate on ocean areas and include, for example, island stations and ASAP equipped ships. Note also was made that as the retrieval of satellite soundings over land areas becomes more reliable, the baseline concept may have to be extended to land areas as well.

5.1.3.2 Note was made that the operation of the baseline network would require certain co-ordination with the over-passage of the satellites and that this would require support from one or more Members to carry out the co-ordination further. While not all soundings needed to be so co-ordinated, those which did would require adjustments to launch schedules and perhaps additional launches. Not all Members operating suitably placed rawinsonde stations would be able to afford these changes. Further, in some instances, change to the equipment or facilities would be required as well. The Working Group noted that such issues are being addressed and that VCP or bi-lateral support had been considered. The Working Group strongly recommended that planning for the baseline networks include, at an early stage, adequate consideration of the funding required including the co-ordinated use of VCP and other AID programmes.

5.1.3.3 The Working Group strongly urged that the detailed planning for the baseline network be carried out as quickly as possible so that Members could be made aware of the overall scope of the programme. It noted in this regard that the first TOVS Study Conference had made recommendations on the technical operation of a baseline network and that a second conference was scheduled for February 1985. The Working Group believed that it would be valuable to consider, as appropriate, the recommendations of the TOVS Study Conference in the planning process.

* * *

7.3.2 The Working Group noted with interest the final report of the First TOVS Study Conference (Igls, Austria, 1983) in which recommendations were made to improve the quality and usefulness of satellite profile data. As noted earlier (see paragraphs 5.1.3.1 to 5.1.3.3), the concept of a baseline network is endorsed and the Working Group recommended that the relevant material contained in Annex VII of its report be presented to TOVS-II (February, 1985). The Working Group further noted that TOVS-I made several recommendations relating to the numerical evaluations of TOVS data and the standardization of the data processing algorithms. The Working Group concurred with the need for such evaluations to be done on a systematic basis and for effort to be put into standardizing the algorithms including intercomparisons with radiosonde data. While recognizing that the TOVS Study Conference is not a formal part of the WWW programme, the Working Group nevertheless recognized the value of the recommendations of the satellite experts particularly as regards the more effective utilization of satellite data in the WWW. The Working Group urged therefore, that TOVS-II be asked to further refine the recommendations of TOVS-I concerning evaluations and calibration and to outline a set of specific proposals which, if the President of CBS agrees, would be submitted to him for his consideration. The Working Group asked that the Chairman bring this matter to the attention of the TOVS-II and the President of CBS. The Working Group further urged that the President of CBS be urged to address the TOVS recommendations to the parts of CBS most concerned and to the President of CIMO as appropriate.

*

* *

ANNEX VII

BACKGROUND PAPER ON THE BASELINE UPPER-AIR SOUNDING NETWORK

Summary and Purpose

The need for baseline upper-air data was presented to EC-XXXVI and accepted by that body. The network needed to provide these data would consist of selected existing upper-air stations on land supplemented by a few new stations in sparse data areas plus selected ASAP-equipped ships. The purpose of the network would be to provide high quality ground-truth data for use in the calibration and processing of satellite soundings. The purpose of this document is to present the concept of a baseline network to the CBS Working Group on the GOS and to propose specific actions.

Background

In August 1983 a survey was made among the WMO Members most concerned with the processing and use of satellite sounding data. Eleven countries were queried on the need for a baseline upper-air (B/UA) network that would support the calibration of the sounding data from satellites. Eight of these Members strongly supported the concept of a B/UA network. Two felt they did not have enough experience in satellite data processing to warrant a reply and one declined to reply. The unanimous opinion of those replying was that there is a definite need for a B/UA network as a sub-set of the GOS upper air network. Annex A is an analysis of the survey results.

The concept of a B/UA network was accepted by EC-XXXVI in two ways. A VCP co-ordinated programme has been established to assist in the installation of new upper-air stations in developing countries which may be required as part of the network. At the same time the BM/UA network concept was included under item 3.1.6.13 of the Executive Council report in the context of arrangements for Operational WWW Systems Evaluations (OWSEs) and the implementation of the ASAP.

Annexes B and C represent suggested criteria for the observations at B/UA stations and the scope of an initial B/UA network.

WMO Members who are involved with the processing of satellite sounding data and/or operate key upper-air stations including ASAP-equipped ships may form a consortium to establish and operate the baseline network. The network, which will be a subset of the GOS, will consist primarily of existing island stations and ASAP-equipped ships. This is the case because satellite sounding data are presently used in oceanic regions. Later, continental stations may be added to the network and the consortium may decide to establish new stations in data sparse areas.

Because of the requirements of the baseline data to be used for the calibration and processing of satellite sounding data, the operation of the stations in the B/UA network will differ from other upper-air stations in three ways:

APPENDIX.

1. Some of the observations (numbers to be determined) will be taken at asynoptic times to match the overhead passage of the satellites.

2. One of the major national centres which process the satellite data likely will act as a network information centre to co-ordinate the activities of the baseline stations taking asynoptic observations.

3. Since it may not be practical to use standardized upper-air equipment at all the network stations it will be necessary to develop data processing techniques which provide highly compatible output data. The development of these techniques will draw heavily on the results of radiosonde intercomparisons conducted by CIMO.

Annexes: A. Analysis of Survey Regarding B/UA Network

B. Criteria for Observations at B/UA Stations

C. List of Possible Stations

Analysis of Survey Regarding B/UA Network

A questionnaire on the need of baseline upper-air network for calibration and verification of satellite data retrievals was sent to a number of Members. Australia, Canada, China, Federal Republic of Germany, France, Japan, Sweden, and the United States agreed with the need for a baseline network of upper-air stations. Norway and the United Kingdom felt they did not have enough experience concerning the processing of satellite sounding data to comment. Australia commented that "The establishment of a bench-mark network is of prime importance to future use of satellite data". Sweden stated "It is our opinion that an upper-air bench-mark network for calibration and comparison is a necessary pre-requisite for any satellite sounding observing system".

Listed below is a summary of the eight replies to the questions in the survey:

1.a In the context of retrieving globally distributed quantitative upper-air data from satellite radiance, is there a requirement to have independent upper-air data for calibration? Yes 8 No 0.

PARAMETER	YES	NO
(a) Wind	6	NOTE 1
(b) Temperature	8	0
(c) Relative Humidity	8	0
(d) Other	NOTE 2	-

NOTE 1 - 1 reply indicated wind was desired but not required
- 1 no comment

NOTE 2 - 4 countries specified ozone
- 1 tropopause height
- 1 cloud height
- 1 aerosol concentration

1.b Does the answer in 1.a depend on the data reduction or retrieval process? Yes 4 No 4

NOTE 1 - The countries answering yes were relating their answer to the type of process they presently use which is:

3 - statistical process
1 - physical reduction

NOTE 2 - The countries answering no felt that there is a need for calibration of upper-air data no matter what retrieval process is used.

1.c Does the answer in 1.a depend on the extent of geographical coverage (local, regional, global) of the satellite radiance being processed? Yes 5 No 2

NOTE 1 - Three countries commented that data is needed for each geographical area (air mass wherein the satellite data is being processed).

NOTE 2 - Two countries commented on the matter of scale. The more detailed the scale of the analysis of satellite data the more stations are needed in the network.

2.1 If calibration is needed, are the current observations from the surface-based GOS adequate? Yes 0 No 8
(Included here are radiosondes, aircraft, rocketsondes, radar winds etc.)

2.b If not adequate, please identify deficiency.

Spacing/areas of globe - three countries commented that there is a lack of data over oceans and in particular the tropic and oceans.

Frequency - four countries commented that soundings are needed coincident with the passage of the satellite.

Data quality/equipment - three countries commented on the lack of precision in much of the present data. One country stated that there is a need for high quality standard equipment.

Other - one country stated a need for measurement of earth radiation.

3. In the context of the answers to 1 and 2, is there a need for baseline upper-air Network? Yes 8

4. If baseline stations are required, what would be their characteristics?

Number and spacing - 50 to 100 stations

Frequency of observations - There was a wide variety of replies to this question ranging from 4 obs/day to 1 obs/week.

Observation coincident with satellite - all countries agreed that this is needed.

Code - some modifications may be needed to standard upper-air codes for these special stations.

Criteria for Observations at B/UA Stations

1. Certain of the upper-air observations should be coincident with the passage of the meteorological satellites. The number of such coincident soundings has yet to be determined. Observations at synoptic times also will be required making suitable adjustments for the satellite - coincident soundings.

2. Inter-network calibration standards and tests should be established to ensure that all B/UA stations operate at a consistent level of performance. The results of CIMO radiosonde intercomparions will be used to assist in establishing the standards and tests.

3. One of the major satellite processing centres should be asked to act as the network control centre. This centre would have the responsibility to monitor the network, conduct inter-network standardization tests and request special observations when necessary: e.g. period after launch of satellite. The centre would also prepare a monthly schedule for each of the network stations.

APPENDIX.

List of Stations

The proposed baseline upper-air (B/UA) network would utilize existing stations whenever possible to minimize the start-up cost of the network. The following list of stations reflects this strategy (10 of the 19 stations are presently in operation) and takes into account the capability of Members to support the stations. There will, however, be a need for external support for stations located in developed countries which cannot be expected to support fully the operating expenses of a B/UA station (4 on the sample list). An appropriate support scheme needs to be developed.

Australia
Cocos Is.(96996)

Cape Verde
Sal (08594) Note 2

Chile
Easter Is. (85469) Note 2

Denmark
Faroe (06011)

Ecuador
Galapagos Is. (84008) Note 2

France
Kerguelen Is. (61998)
New Amsterdam Is. (61996)
Tahiti (91938)

Maldives
Male (43555) Notes 2, 3

New Zealand
Chatham Is. (93986)

Portugal
Azores (08509)

United Kingdom
St. Helena (61901)
Bermuda (78016) Note 1

United States
Adak (70454)
Midway Is. (91066)
Kwajalein, Marshall Is. (91366)
Christmas Is. (91490) Notes, 3,4

Union of Soviet Socialist Republics
Wrangel Is. (21982)

Vanuatu
Vila (91558) Note 5

Note 1 - Station operated by the U.S.
Note 2 - External support will be needed to operate the station as part of B/UA network
Note 3 - No existing upper-air
Note 4 - Surface station operated by New Zealand
Note 5 - Operation of upper-air station funded by U.K. and France and a new agreement is required with Vanuatu

A METHOD FOR MATCHING THE HIRS/2 AND AVHRR PICTURES OF TIROS-N SATELLITES

Tadao Aoki

1. PREFACE

The TIROS-N satellite series carry approximately four kinds of atmospheric surveying instruments which enable a survey of atmospheric verticle temperature distribution, vapour distribution, ground surface temperature, Ozone amount, cloud top height and cloud quantity. HIRS/2 (the second generation of High Resolution Infrared Radiometer Sounder) is the main instrument to measure these various parameters. The size of the HIRS/2 field of view is 17km directly beneath it and 58km at the tip of its scanning range. Therefore, it is not expected that it will be accurate in determining its position by landmark matching as is the case in the stationary orbit type of satellite.

A polar orbital satellite (TIROS-N satellite) is a 3-axis-equilibrium type and its attitude accuracy is approximately 0.12° (directly beneath it about 1.7km). It is usual to first, calculate the orbit and providing that its attitude is correct, then the position of its field of view from its linear angle. However, checking the various parameters for determining the orbit transmitted every day, the values vary widely at a rate of once every 5 to 7 days. As it is one or two days later that we receive information at GTS circuit, there is the possibility that a large orbital calculation error can occur during the delay period. In November 1979, the attitude of TIROS-N changed drastically and at the tip of the scanning field maximum, a 90km error occured.

Considering these facts, something else was needed as a method of determining the field of view, it would be better

if there could be an absolute method of determining the field of view similar to landmark matching. As the field of view of the AVHRR (Advanced Very High Resolution Radiometer) directly beneath it is about 1.1km, the position of its picture can be determined accurately by a method of landmark matching. If the relative position relationships of the pictures of the AVHRR and the HIRS/2 can be determined the position of the field of view of the HIRS/2 can be accurately known.

Here, paying attention to the fact that the 8th channel of the HIRS/2 (the center wave length frequency is about 900cm^{-1}, called the atmospheric window) and the 4th channel of AVHRR (the center wave length frequency is about 900cm^{-1}) have practically the same characteristics, a method to match the two pictures can be developed.

There is another way to effect the matching of AVHRR and HIRS/2. As the field of view of the AVHRR is smaller than that of the HIRS/2, in one field of view of HIRS/2 about 300 to 450 segments of the field of view of AVHRR is contained. The amount of cloud in this field of view of HIRS/2 can be determined, and once the cloud quantity is known the clear day emission amount of each channel of HIRS/2 can be determined to a high degree of accuracy compared to the existing method. (AOKI 1980). From this, accurate readings of verticle temperature vapour distribution etc. can be expected. A method of matching the AVHRR and HIRS/2, in fact, has been developed for this purpose.

The problem, as to which field of view of AVHRR is contained in which field of view of HIRS/2, is not so difficult to solve, if the rotation axis of linear scan of both satellites match perfectly and if the attitude of the satellit is correctly maintained. If within the area which faces the orbital direction directly beneath the satellite, the rotation axis of the AVHRR and HIRS/2 slips about 0.07° in relation to the surface, it becomes a AVHRR 1 line slip. The TIROS-N series satellites pictures were originally AVHRR pictures

and were not designed to investigate cloud quantity in each HIRS/2 field of view, therefore, the field of coincidence of the rotation mirrors of both instruments to a high degree of accuracy could not be expected. This is also true for attitude, as previously explained. However, it is difficult to assume that the amount of slip of the rotation axis of the linear mirrors of the AVHRR and the HIRS/2 would be of a very great degree, on the assumption that the amount of slip is very small from the normal position, a theory has been formulated.

2. ALGORITHM OF HIRS-AVHRR PICTURE MATCHING

2-1 A method of calculating the picture element number of the AVHRR which is comparable to a certain HIRS field of view.

As previously stated, the field of view of the AVHRR is quite small when compared to that of the HIRS/2, from here the term 'picture element' or 'pixcel' will be used and 'HIRS' will be used instead of HIRS/2.

The HIRS scans a 99^{o} range from left to right in the direction of progress of the satellite, at a rate of once in every 6.4 seconds. The number of fields of view to effect observation in one scan is 56 elements. The AVHRR obtains its picture by means of a rotating mirror, this mirror rotates at high speed, one rotation every 1/6th of a second. Its obtain range is controled by a method of detecting the earth edge at every rotation and determining the next image time. The picture obtaining area is 110.8^{o}, this is slightly larger than that of the HIRS and the picture element number is large, being 2048 segments. Pickup is from right to left, the opposite of the HIRS and this factor makes the problems we deal with here more complex. Table 1 shows each characteristic of HIRS, AVHRR scanning.

Our problem is to decide from which picture element numbers to start and at which to finish in a particular AVHRR picture that is contained in the field of view of the HIRS.

From here the first and last picture element numbers of the AVHRR which is contained in the HIRS field of view is shown as N_A, N_B. It would appear to be quite difficult to distinguish the N_A, N_B among all the AVHRR lines, however, this problem can be simplified using an approximation as follows;

One scan of HIRS takes 6.4 seconds, and one scan of AVHRR takes 1/6th of a second, for each line of HIRS there are approximately 38 to 39 lines scanned by AVHRR. We proce with this explanation on the understanding that there is no slip of picture in the linear pixcel direction. In Fig.1 the HIRS lines which probably, 39 AVHRR lines cross, are the lines which are scanning at that time, the preceeding and succeeding lines. If we establish beforehand the N_A, N_B to correspond to 3 X 56 segments of the HIRS field of view and th 39 AVHRR lines, the next 6.4 second scan can be considered as a repeat of the same pattern. As each 6.4 second scan can no be divided by 1/6th second exactly, it is not an exact repeat of the same pattern, however, as the spaces between the lines of the AVHRR are narrow compared to those of the HIRS, not so large an error will occur to approximate the small slip and a repeat of the same pattern. N_A, N_B can, therefore, be give as a function of every line of AVHRR and HIRS, and every fiel of view of HIRS. The number of lines that cross are 3 in Fig There could be a time where 1, 5 or 7 lines cross according t the angle of crossing, however, here we consider that there would not be a large error in matching the angle of AVHRR and HIRS, thus, there would be no more than 5 lines crossing. N_A, N_B are given as functions of relative line number I_A (1 - of AVHRR, the relative line number of I_H (1 - 5) of HIRS and the field of view number J_H (1 - 56) of HIRS, something like $N_A(I_A, I_H, J_H)$, $N_A(I_A, I_H, J_H)$ (I_A=1, ...39, I_H=1, ...5, J_H=1, ...56) and the N_A, N_B of the next 6.4 second scan can be asertained by such relative numbers.

To this point we have disregarded slip of the picture line and pixcel direction, but if the installed direction of the AVHRR and HIRS is not accurate, not only a simple slip of angle, but as shown in Fig.2, a slip occurs in pixcel linear direction. Fig.2 shows the pattern of the picture range obtained within a certain fixed period of time. $H_1H_2H_3H_4$ shows the picture range of HIRS and $A_1A_2A_3A_4$ shows the picture range of AVHRR. The center line of the picture of both HIRS and AVHRR is shown as $C_1'C_2'$ and C_1C_2. The N_A, N_B checked earlier was when there was no slip in pixcel linear direction (the slips are shown here as ΔI, ΔJ) (This is to say that the slips shown as $A_1'A_2'A_3'A_4'$ in Fig.2 which correspond to $A_1A_2A_3A_4$ were moved to a parallel position and the center line was coincided). If this slip is not too large, as N_A, N_B which corresponds to $A_1A_2A_3A_4$, being I_A, substitute $I_A - \Delta I$ to obtain the value of N_A, N_B at $A_1'A_2'A_3'A_4'$ and further make this as $N_A + \Delta J$, $N_B + \Delta J$. (As AVHRR scans from right to left, N_A, N_B is numbered from right to left.)

The N_A, N_B can be calculated at a certain angular degree, disregarding slip in the pixcel line direction. The method to obtain this N_A, N_B is now explained. Imagine the satellite scan as being motionless, its scan line becomes a solid line as shown in Fig.3. At this time make the slip of the AVHRR line from the x-axis as Θ_A and the slip between the HIRS line and the AVHRR line as Θ_{AH}. Here x is at right angles to the direction of progression of the satellite (The direction of progression of the satellite is used as the y-axis). Co-ordinating this motionless scan line to the scan line when the satellite starts to move, it becomes the dotted line shown in the figure. Θ_A is the slip of the AVHRR's scan axis corresponding to the direction of the satellite. Fig.4 shows how Θ_A relates to N_A, N_B which is the quantity showing the relative position correspondence of HIRS and AVHRR. This figure shows

how the picture pattern of the AVHRR for two Θ_A comes about. One obtains the ABCD picture and another obtains the A'B'C'D' picture, the important thing is that in contrast to the field of view of the HRS (oval) is obtained at a certain moment in time (This figure indicates the time when the middle AVHRR line was obtained), the AVHRR line scans, except this middle line, before or after that time. This can cause deformation of the picture.

Next, check the distance PP' from point P which is on the AVHRR scan line to x-axis, that is to say, the y-coordinate of point P. In Fig.5, O' is the satellite, P is the P of Fig.3 and r is the distance of PO'. The upper half disc is the scan face of AVHRR in Fig.3, the lower half disc is the face containing the y-axis. The angle that the two half discs make is Θ_A. If in setting the scan angle of point P as α, PH is a perpendicular line taken down from P to where the two half disc meet and PP' is a perpendicular line taken down from P to the lower half disc (P' corresponds to P' of Fig.3),

$$PH = r \sin\alpha$$

Also as angle $PHP' = \Theta_A$

$$P'H = PH \cos\Theta_A = r \sin\alpha \cos\Theta_A$$

Therefore,

$$PP' = \sqrt{(PH)^2 - (P'H)^2}$$
$$= r \sin\alpha \sin\Theta_A \qquad (1)$$

Here obtain the value of r. If the radius of the earth is set as R_e, the height of the satellite as h, from Fig.6 2 formulae of

$$R_e \cos\beta + r \cos\alpha = R_e + h$$
$$R_e \sin\beta = r \sin\alpha$$

can be obtained. From that

$$r = (R_e + h) \cos\alpha - \left[(R_e + h)^2 \cos^2\alpha - (2R_e + h)h\right]^{\frac{1}{2}} \qquad (2)$$

can be obtained.

If the satellite is moving, the y-coordinate of point P increases further by

$$v\,\delta_A(N-1)$$

Here v is the velocity of the satellite relative to the earth surface, δ_A is the time space of each picture element of the AVHRR and N is the element number of the AVHRR corresponding to point P. Now, we take a point directly beneath the satellite when the HIRS scan starts as the starting point of the coordinates in Fig.3. At the same time, select an AVH line to start the scan as the first AVHRR scan line.

Then, generally the y-coordinate of the Nth picture element at the I_Ath AVHRR line is

$$y_A = r \sin\alpha \sin\theta_A + v\,\delta_A(N-1) + T_A v(I_A-1) \quad (3)$$

Here T_A is the time space of the line and the AVHRR is 1/6th of a second. Also expressing the scan angle as the pixcel number N is

$$\alpha = -\gamma_A + \Delta_A(N-1) \quad (4)$$

Here γ_A is the span angle of the AVHRR and is 55.4° and also Δ_A is the step angle of the AVHRR picture element ($=0.054^\circ$).

Similarly the y-coordinate of each field of view center of the HIRS can be obtained by the following formula.

$$y_H = r \sin\alpha \sin\theta_H + v\,\delta_H(J_H-1) + T_H v I_H \quad (5)$$

Here δ_H is the time interval of each HIRS field of view, also I_H is the HIRS relative line number and the line of Fig.3 is t 0, the line before that is -1, -2 ..... and after that is +1, +2 ..... J_H is the HIRS field of view number and is from 1 to 56. T_H is the time interval of the HIRS line and 6.4 secon scan.

Also θ_H is

$$\theta_H = \theta_A - \theta_{AH} \quad (6)$$

Here θ_H is the angle measured clock-wise from the HIRS line to the AVHRR line when the satellite is motionless as in Fig.3. Similarly θ_A is also the angle of the AVHRR line measured cloc wise from the x-axis.

The scan angle of the J_Hth field of view of the HIRS is given as

$$\alpha = \gamma_H - \Delta_H(J_H - 1) \tag{7}$$

Here γ_H is the span angle ($=44.5^\circ$), Δ_H is the step angle ($=1.8^\circ$). The field of view at that time on the earth surface becomes the oval shown in Fig.7 and the radial b of the short axis is

$$b = r \tan\frac{\eta_H}{2} \tag{8}$$

Here η_H is the angle of the field of view of the HIRS.

Now, set the radial of the long axis as . If the slip θ_A of the fitting angle of the AVHRR and the HIRS is assumed to be very small, then the AVHRR line is almost parallel to the long axis direction. AVHRR line coincided to the long axis

$$n_0 = \frac{\eta_H}{\Delta_A} \tag{9}$$

segments of the AVHRR picture element are contained in this HIRS field of view. This is a constant, independent of the field of view. AVHRR line Δy distant from the long axis contains

$$n = \frac{\Delta x}{a} n_0 \tag{10}$$

segments. Here $\Delta x/a$ can be obtained from the following oval formula

$$\frac{\Delta x}{a} = \left[1 - \frac{(\Delta y)^2}{b^2}\right]^{\frac{1}{2}} \tag{11}$$

Now, calculating formulae to obtain all of the HIRS field of view and the N_A, N_B for the AVHRR relative line numbers are completed. That is, the N_A, N_B of the picture element on the I_Ath relative AVHRR line which is contained in the J_Hth field of view of the I_nth relative HIRS line number is obtained, first by obtaining the scan angle α of the center of the HIRS field of view from (7) and from this, picture element number of the AVHRR N, which coincides to α, is obtained from (4). Next, obtain y_A, y_H from (3) and (5), and calculate

$$\Delta y = |y_A - y_H| \tag{12}$$

When obtaining n from (1) and (10), N_A, N_B is obtained as

$$\left.\begin{aligned} N_A &= N - \frac{n}{2} \\ N_B &= N + \frac{n}{2} \end{aligned}\right\} \tag{13}$$

When $|\Delta y| \geq b$, it shows that the HIRS field of view and its AVHRR line do not cross.

Further, understanding that N_A, N_B is not only a function of I_H, J_H, I_A, but also is a function of Θ_{AH}, Θ_A and the velocity of the satellite relative to the earth surface v,

$$\left.\begin{aligned} N_A &= N_A(I_H, J_H, I_A, \Theta_{AH}, \Theta_A, v) \\ N_B &= N_B(I_H, J_H, I_A, \Theta_{AH}, \Theta_A, v) \end{aligned}\right\} \qquad (14)$$

Figs. 8a, b are the print out of the AVHRR picture element derived by the computer by working out N_A, N_B, and the inner part of the oval, entering its HIRS field of view number. Fig.a illustrate around center of the scan line and fig.b shows the tip part of the scan line. As the figures take the picture element number as the coordinate axis, it becomes an oval stretched towards the line direction. However, the actual shape is rather stretched towards the picture element direction. Fig.9 shows all of the HIRS field of view which was obtained by repeated reduction of the output list after thinning out of the AVHRR picture element in every few segments in Fig.8, and the AVHRR line. In this Fig. as well as in Fig.8 the stretched direction of the oval is the opposite of the actual oval. (It is equivalent to the compressed Fig.1 viewed from the side.)

Here, we do not know the values of Θ_{AH}, Θ_A yet. In the next section we deal with a method of obtaining the values of Θ_A, Θ_{AH} and slip of line - ΔI, pixcel - ΔJ.

Before we deal with this we touch on the subject of earth rotation. Considering that the effect of earth rotation, as shown in Fig.10, is regarded as the appearance of the velocity vector of the satellite relative to the earth surface changed form. The velocity of the satellite relative to the earth surface is almost stationary when there is no earth rotation, because the earth is nearly round and the orbit of th satellite is nearly round. But, when considering rotation, because rotation velocity changes according to the latitude, the effect of rotation differs at every latitude and every position to North or South.

What we consider now is the effect of rotation on the calculation of N_A, N_B, namely, the calculation of the relative position relationship of AVHRR and HIRS. Therefore, if the pickup time of the HIRS field of view and the AVHRR scan line coincide (as the time needed to obtain one AVHRR scanning line is about 0.05 second, the rotation effect of this duration can be neglected), there is no effect caused by the earth rotation. It is only when the pickup time of the HIRS field of view and the AVHRR line do not coincide, the earth rotation takes effect. Now, considering the case when there is no picture slip, for each HIRS field of view, the AVHRR line, which passes around the long axis of the oval of that field of view, is picked up at about the same time as that field of view.

As can be understood from Fig.4, the change of the direction of the satellite track is what Θ_A has changed. Therefore, when looking from the view point of N_A, N_B, adding the rotation velocity is equivalent to v of formula (3) or (6) changed from $|\vec{v}|$ to $|\vec{v}'|$, or Θ_A changed to the altered portion of velocity direction.

The value of N_A, N_B differs when rotation effect is taken into account, according to each latitude belt or each movement North or South of the satellite orbit. However, in an actual calculation, to have a value table of N_A, N_B to express each change in latitude, or each change North or South would lead to the load of calculation required becoming too large. When we neglect the rotation effect, e.g when Θ_A and v are fixed, we need to know what the error will be. For the sake of simplicity, we consider when $\Theta_{AH}=0$. From Fig.4, when we neglect rotation effect, the maximum slip to N_A, N_B is the AVHRR line which is furthest from the long axis of the oval, and its distance is AA' (or BB' ... etc.) as shown in the figure. We now consider, when on the equator, which rotation effect is its maximum, rotation velocity on the equator is 0.464km/sec. and from the long axis of the oval

to the straight line AB, directly beneath the satellite, is approximately 1.5 sec. (Ref. Fig.8a, b or Fig.9) AA' is 0.696km, or as the space between AVHRR picture elements is 0.78km, AA' is barely 1 pixcel segment difference. Further, at the tip of the HIRS scan line, AA' becomes larger than 1.5 sec., but instead, as the picture element spacing becomes larger, the slip of the picture element number is quite similar.

In the above argument, the apparent velocity increase of the satellite has not been dealt with, however, besides the rotation velocity which is one unit smaller compared to the satellite velocity, and because the direction is close to a right angle, its effect is small.

2.3 Deciding the slip amount (ΔI, ΔJ, Θ_{AH}, Θ_A) of the picture of AVHRR and HIRS

The filter characteristic of the AVHRR 4th channel and the HIRS 8th channel is very similar, except that the AVHRR channel filter width is greater than the HIRS channel width. The center wave frequency of the two is in the so called atmospheric window at about 900cm^{-1}. Fig.11 shows a plot of the theoretical relationship between the radiances of both channels computed in a cloud clear area, the correlation can be easily understood.

When N_A, N_B in the previous section is given, the average luminance $\bar{R}_A$ in each HIRS field of view of the AVHRR 4th channel can be calculated. There is a gap between fields of view of the AVHRR, however, because the number of picture elements of the AVHRR is 300 to 450, there must be a good correlation $\bar{R}_A$ to luminance of the HIRS 8th channel R_H, as seen in Fig.11. However, if the correct N_A, N_B is not given, especially when there is cloud in the field of view, $\bar{R}_A$ will become significantly different to R_H. Conversely if the value of N_A, N_B, e.g the values of ΔI, ΔJ, Θ_{AH}, Θ_A, is determined in the order that the correlation with the value of R_H at its best, it shows a picture slip of the HIRS and AVHRR. From such considerations, we here determine the slip which makes

the following quantity minimum. e.g. ΔI, ΔJ, θ_{AH}, θ_A which makes

$$\sigma = \frac{1}{L}\sum_{l=1}^{L}\left[\bar{R}_A(l) - R_H(l)\right]^2 \qquad (15)$$

the minimum, as the slip quantity, will be obtained. l shows the field of view number of HIRS. L is the number of segments of the HIRS field of view used in matching.

First, in order to simplify the treatment, we substitute a variable as follows;

$$\left.\begin{aligned} X_1 &= \Delta I \\ X_2 &= \Delta J \\ X_3 &= \theta_{AH} \\ X_4 &= \theta_A \end{aligned}\right\} \qquad (16)$$

$\bar{R}_A$ is a function of N_A, N_B, namely, it is a function of $X_i (i=1, \ldots 4)$. Expand this around a certain primitive assumption value X^o of X and approximate as

$$\bar{R}_A\,(X_1 \ldots X_4; l) = \bar{R}_A{}^o\,(X_1{}^o, \ldots X_4{}^o; l) + \sum_{i=1}^{4}\frac{\partial \bar{R}_A}{\partial x_i}\,x_i \qquad (17)$$

Here x_i is

$$x_i = X_i{}^o + x_i \qquad (18)$$

Being σ is the minimum, it means that the differential of σ by x_i is 0. From this

$$\frac{\partial \bar{R}_A}{\partial x_m} = 2\sum_{l}^{L}\left[R_A(X^o;\, l) + \sum_{i=1}^{4}\frac{\partial \bar{R}_A}{\partial x_i}\,x_i - R_H(l)\right]\frac{\partial \bar{R}_A}{\partial x_m} = 0,\ m = 1, \ldots 4 \qquad (19)$$

is obtained. Sorting this out, we can write this as

$$y_m = \sum_{i}^{4} k_{mi}\,x_i \qquad (20)$$

Then,

$$y_m = \sum_{l}^{L}\left[R_H(l) - \bar{R}_A(X^o;l)\right]\frac{\partial \bar{R}_A(X^o;l)}{\partial x_m}$$

$$k_{mi} = \sum_{l=1}^{L}\frac{\partial \bar{R}_A(X^o;l)}{\partial x_i}\,\frac{\partial \bar{R}_A(X^o;l)}{\partial x_m} \qquad (21)$$

The differential of $\bar{R}_A$ can be given in the following formula.

$$\frac{\partial \bar{R}_A}{\partial x_i} = \left[\bar{R}_A(X_1{}^o, \ldots X_i{}^o + \delta_i, \ldots X_4{}^o; l) - \bar{R}_A(X_1{}^o, \ldots X_4{}^o; l)\right]/\delta_i \qquad (22)$$

is given appropriately in every i.

Thus, y_m and k_{mi} also become a known quantity. As there are 4 unknown quantities xi and also 4 formula (20) as m=1, ...4, x_i is resolved. However, the answer obtained resolving directly simultaneous equations is known to become unstable as the number of the unknown quantities increase. The reason is because observation errors or calculation errors are contained in y_m or k_{mi} . To resolve this problem is to add an appropriate limit to the answer x_i obtained. Here, we wish to minimize the square sum of the difference (= x) between the primative assumption value (which in this case is 0) and the answer X, then by Twomey (1965) the answer

$$x = k^t(kk^t + \gamma)^{-1}y \tag{23}$$

is obtained. Here, k_{mi} or x_i, y_m of formula (20) is altered to matrix or vector expression such as k, x, y. is a constant given empirically. Here, empirically it is given as

$$\gamma = 10^{-4}\sigma \tag{24}$$

Further, here $X_i = X_i^{\,o} + x_i$ obtained is used as a new primative value and a new X_i is obtained repeatedly. The calculation was repeated until it satisfied the appropriate convergence conditions. Convergence condition was given as follows,

$$\frac{|\sigma^{(n)} - \sigma^{(n-1)}|}{\sigma^{(n-1)}} < 10^{-3} \tag{25}$$

Here, $\sigma^{(n)}$ is σ obtained by a repeat of the nth.

3. VERIFICATION OF THIS METHOD BY SIMULATION

Giving an appropriate value to X_i, (i=1, 4), namely ΔI, ΔJ, Θ_{AH}, Θ_A, calculate R_A and using this make the "observation value" R_H and tried by the method used here as to whether an accurate X_i could be obtained. The following value was given as a certain I_A line, the luminance of the J_A pixcel-th AVHRR.

$$R_A(I_A, J_A) = 100\,[\sin(0.02\pi I_A)\sin(0.1\pi I_A)\cdot \sin(0.003\pi J_A)\sin(0.01\pi J_A) + 1] \tag{26}$$

Next, by the θ_{AH}, θ_A given, obtain N_A, N_B by the ΔI, ΔJ given, calculate an average $\bar{R}_A$ to each HIRS field of view and give R_H by $R_H = 0.9\,\bar{R}_A$ or $R_H = 1.02\,\bar{R}_A$. To the "observation value" R_H of HIRS obtained as such, relate the "observation picture" of AVHRR given at formula (26). The primative value X_i^o is calculated giving 0 to all. The solution values obtained as such and the number of times of repeating until convergence etc. are shown on Table 2. As seen on Table 2, the result obtained is very accurate and restored the value of X_i given at the start.

As previously mentioned, if earth rotation is neglected, an error of about 1 pixcel segment will occur. As we are arguing for a method that is approx. accurate to that degree, the result shown on Table 2 will be sufficient. In this, it shows that accuracy of θ_A is not really good and sensitivity to θ_A is bad. However, this does not mean that the accuracy of N_A, N_B, which we need finally, is bad. As explained, as a part of earth rotation effect, even if the value of θ_A is slightly inaccurate, there is no big influence on the value of N_A, N_B. (That is why, as seen on Table 2, this method is not sensitive against θ_A)

4. CONCLUSION

Taking advantage of the characteristic of the filter of the AVHRR 4th channel, which is a component of the TIROS-N satellite series, and the HIRS 8th channel, we developed a method to determine the relative position relationships of both pictures. By this, in which the HIRS field of view of every picture element of the AVHRR is obtained, can be understood and we now are able to know precisely the position of each field of view. Simultaneously, this enables us to know the cloud quantity of each field of view of HIRS and thus, the accuracy of radiation determination of HIRS will be improved.

Table 1 The characteristics of AVHRR and HIRS/2 scanning.

	HIRS/2	AVHRR
Scan time(sec)	6.4	1/6
Optical FOV(degree)	1.25	0.00745
Step angle(degree)	1.8	0.0541
Cros-track scan(degree)	±49.5	±55.4
Channel number	20	4(5)
Ground FOV(nadir)(km)	17.4	1.1

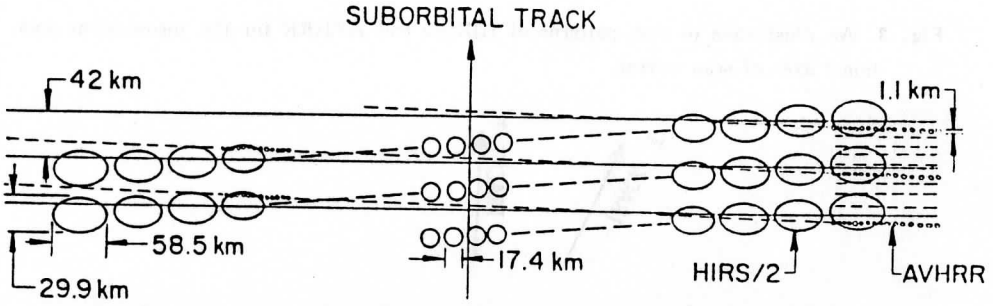

Fig. 1 Scan patterns of HIRS/2 (larger elipses) and AVHRR (smaller elipses).

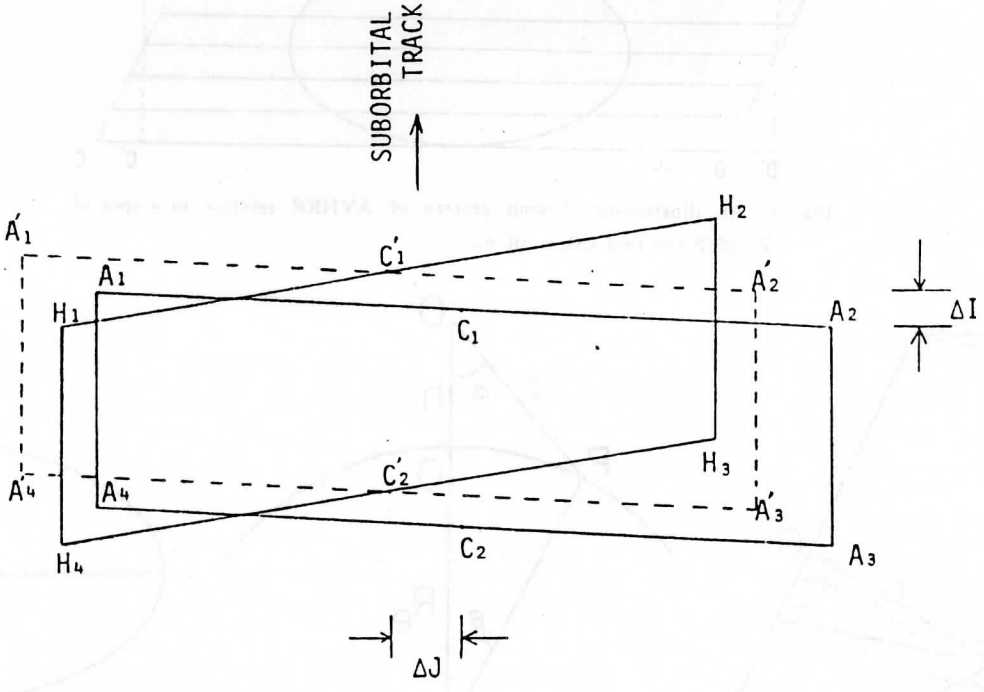

Fig. 2 An illustration of the shifted scan areas of AVHRR ($A_1A_2A_3A_4$) relative to that of HIRS/2 ($H_1H_2H_3H_4$). Unshifted scan area of AVHRR is also shown by $A_1'A_2'$ $A_3'A_4'$.

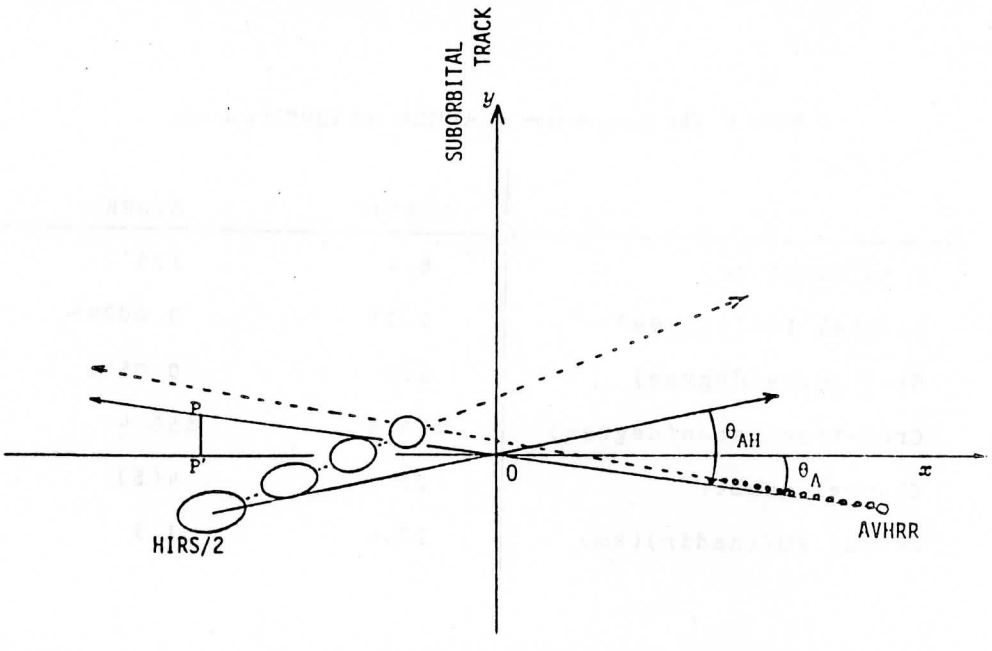

Fig. 3 An illustration of scan patterns of HIRS/2 and AVHRR for the incoincident rotational axes of scan mirror.

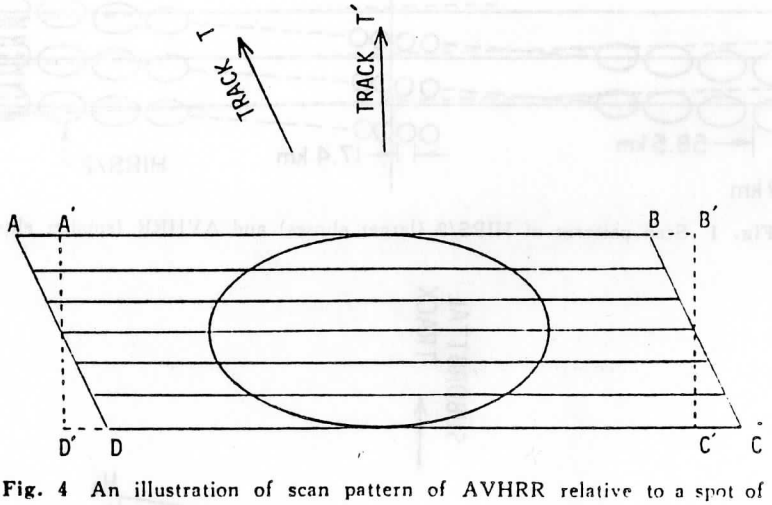

Fig. 4 An illustration of scan pattern of AVHRR relative to a spot of HIRS/2 for two values of θ_A.

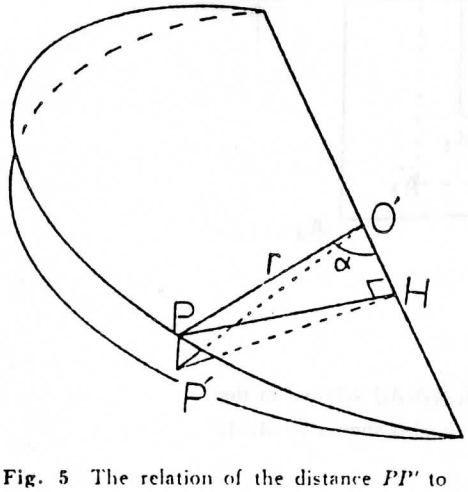

Fig. 5 The relation of the distance PP' to α and θ_A.

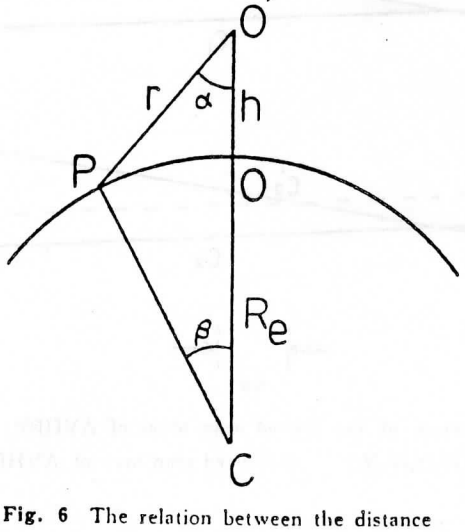

Fig. 6 The relation between the distance and the scan angle α.

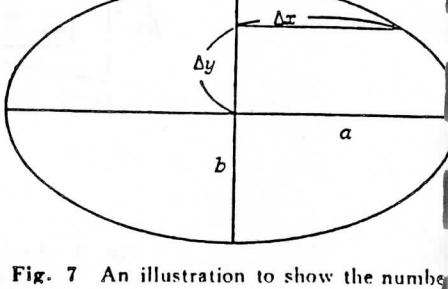

Fig. 7 An illustration to show the numbe of pixcel of an AVHRR line that de viates by Δy from major axis of HIRS /2 sp ot.

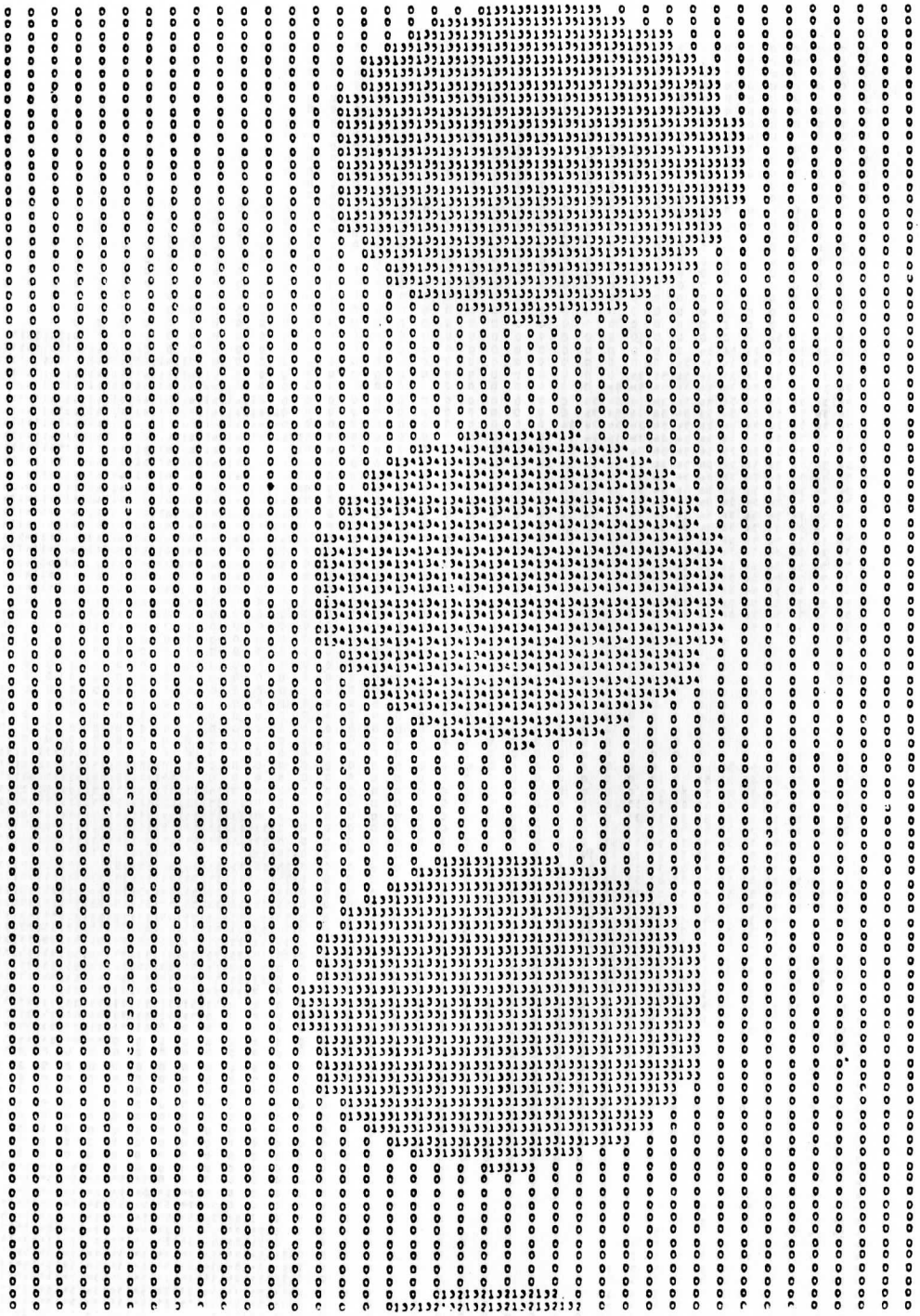

Fig. 8a An illustration of the calculated colocation of AVHRR pixcels and the 34, 35 and 36 th spots of HIRS/2. A case for $\theta_{AH}=\theta_A=0$. The pixcels between N_A and N_B are represented by the numerical numbers 34, 35, 36 or 134, 135, 135 and the other are by 0.

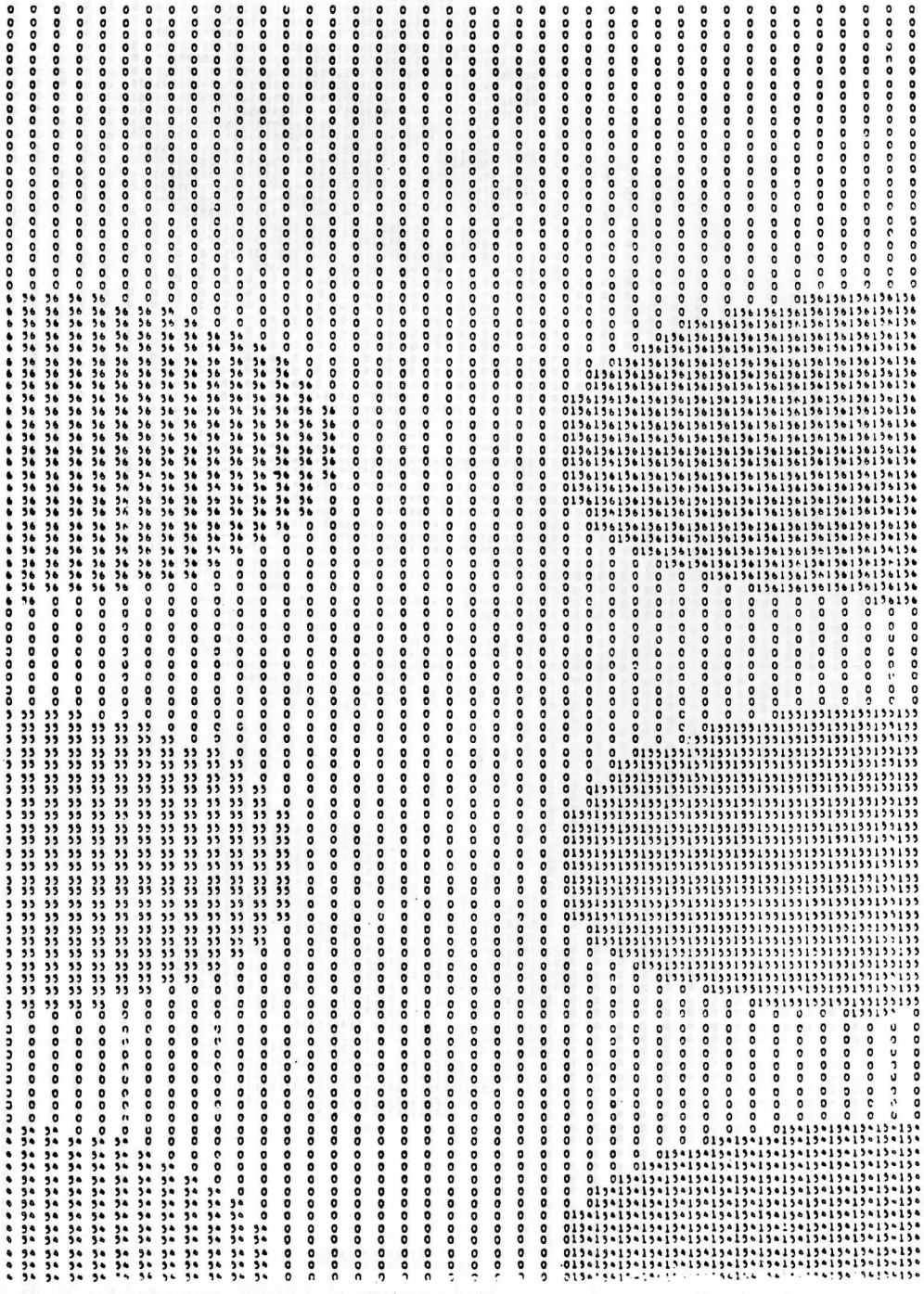

Fig. 8b As in Fig. 8a except for the 54, 55 and 56 th spots of HIRS/2.

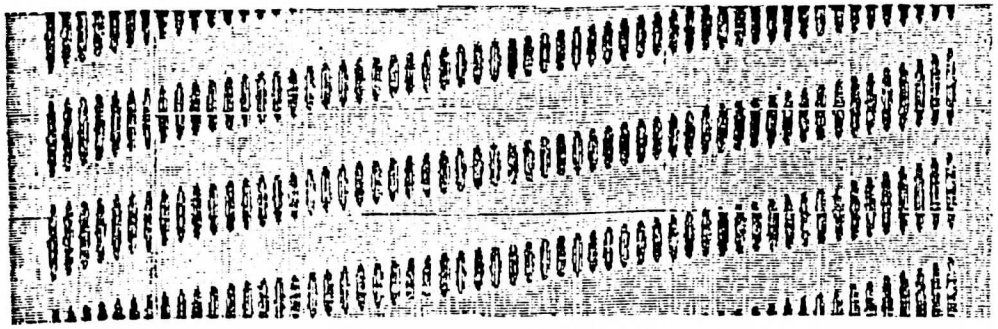

Fig. 9 Illustration of the scan pattern to show the effect of θ_{AH} and θ_A. A case for $\theta_{AH}=\theta_A=0.5$ degree. This is a figure reduced from a computer list such as Fig. 8 except that the every other pixcels of AVHRR are eliminated.

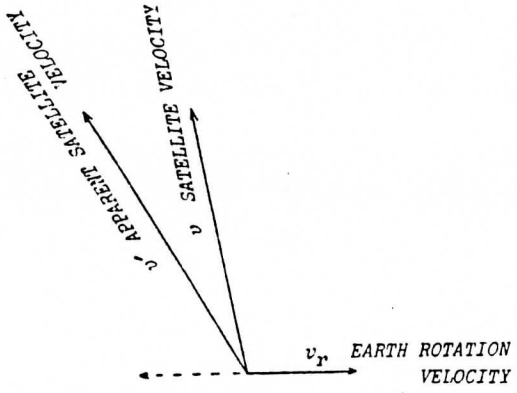

Fig. 10 Illustration of the effects of the earth rotation on the velocity of the satellite relative to the earth surface.

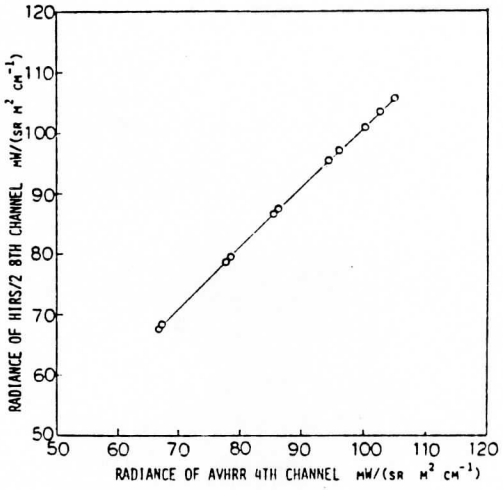

Fig. 11 The theoretical relation ship between the radiances of AVHRR 4th channel and HIRS/2 8th channel.

	ΔJ	ΔI	θ_{AH}	θ_A	n	R_H
example 1	3.0 2.959	3.0 3.186	-0.3 -0.281	-2.0 -2.296	23	$R_H = 0.9\,\bar{F}_A$
example 2	-4.0 -3.790	3.0 3.145	0.2 0.232	6.0 1.519	5	"
example 3	-4.0 -4.046	3.0 2.908	0.2 0.196	6.0 0.802	39	$R_H = 1.02\,\bar{F}_A$
example 4	-5.0 -4.892	-5.0 -5.537	-0.1 -0.083	3.5 3.546	9	"
example 5	3.0 3.058	-2.0 -2.630	-0.3 -0.290	-2.0 -4.216	12	"
example 6	-4.0 -4.042	3.0 2.890	0.3 0.296	5.0 5.309	25	"

Table 2 The comparison between the given (upper row) and the retrieved (lower row) values for ΔJ, ΔI, θ_{AH} and θ_A in the simulation study. The number of the itertion n is also shown.